LCLS-II Final Design Report
DRAFT
December 21, 2014

Contents

	Preface	2
1	Executive Summary	3
2	Project Overview	13
3	Accelerator Parameters & FEL Performance	27
4	Accelerator Layout	53
5	Linac Components	118
6	Cryomodules	204
7	Cryogenic Plant and Distribution	255
8	Undulator Systems	288
9	Photon Transport and Experimental Systems	334
10	Controls and Safety Systems	365
11	Infrastructure and Facility Preparation	409
12	Systems Integration and Availability	437
13	Radialogical Considerations	443
14	Environment, Safety, Health	490
15	Quality Assurance	513
16	LCLS-II R&D Program	518
17	Future Upgrade Opportunities	527
18	Commissioning and Operations	N/A
App. A	LCLS-II Key Parameters	547

Preface

This document is a first draft of the LCLS-II Final Design Report. A final update of this document will be submitted to DOE in support of the LCLS-II CD2/CD3 review, expected in the spring of 2015. The document summarizes the design of the FEL project and provides active links to the detailed information. Most of the links are to documents on the LCLS-II Project site which requires access to the LCLS-II Controlled Documents site to read.

This draft is believed to be largely complete with the exception of Chapter 18: Commissioning and Operations. Most of the figure/table/end note references are believed to be correct and most of the external documentation is believed to be correctly linked. However, there are still missing figures and details to be updated. Most of the missing information is indicated with highlights, typically, yellow for missing information, blue for missing hyperlinks, and green for missing figures. There are also still a large number of formatting errors including figure/table positioning throughout and chapter/page numbering in Chapters 8 and 13.

All comments on the document would be greatly appreciated.

Thanks,

LCLS-II Project Team

1 Executive Summary

TECHNICAL SYNOPSIS

The revised scope of the LCLS-II Project has been aligned with the findings and recommendations of the Basic Energy Sciences Subcommittee report of 25 July 2013, which identified the importance of a high repetition rate X-ray free-electron laser source. The project will construct a 4 GeV continuous-wave (CW) superconducting linear accelerator in the first kilometer of the SLAC linear accelerator tunnel. The linac will provide pulses of electrons at rates of up to 1 MHz to two new undulators in the existing LCLS Undulator Hall. The two undulators will cover the spectral ranges 0.2-1.2 keV and 1-5 keV, respectively, when receiving electrons from the new linac. The existing LCLS linac will continue to operate, providing hard X-rays up to 25 keV. Existing X-ray instruments will be repurposed to exploit these new capabilities. Th Total Project Cost is $965M. The Level-0 Milestone for approval of Critical Decision 4 is Q4FY2021.

1.1 Background

Planning for the LCLS-II Project (LCLS-II) began in 2009, shortly after the LCLS Project demonstrated lasing at 8 keV. Critical Decision 0 (CD-0) for LCLS-II was approved by the Office of Science in May 2010. The project received CD-1 approval in October 2011 and completed all requirements for approval of CD-2 in August 2012. In March 2013 a "continuing resolution" Federal budget appropriation bill was enacted; consequently the LCLS-II Project did not receive line-item approval to start construction. The resultant delay allowed the project to revise its conceptual design in response to most recent recommendations given to the Department of Energy Basic Energy Sciences (BES) Program by the BESAC Subcommittee on Future X-Ray Light Sources [1,2 and see chapter 1.2]. The new conceptual design was reviewed and endorsed by DOE in February 2014, resulting in approval of Critical Decision 1 for the new conceptual design on 22 August 2014. As a result of adoption, with minimal modification, of existing designs and specifications for key systems such as the cryogenic refrigeration plant and accelerator modules, it has been possible for LCLS-II to advance to a level of design maturity to the point of readiness for Critical Decision 3 (CD-3) in spring 2015. The proposed project schedule assumes approval of CD-3 in May 2015, leading to production of first light before the end of 2019.

1.2 BESAC Subpanel Recommendations

The following quotes from the BESAC Subcommittee report [2] summarize the key capabilities that motivate the new LCLS-II design concept:

- "It is considered essential that the new light source have the pulse characteristics and **high repetition rate** necessary to carry out a broad range of coherent "pump probe" experiments, in addition to a sufficiently broad photon energy range (**at least *~0.2 keV to ~5.0 keV***)."
- "It appears that such a new light source that would meet the challenges of the future by *delivering a capability that is beyond that of any existing or planned facility worldwide is now within reach.* **However, *no proposal presented to the BESAC light source subcommittee meets these criteria.*"**
- "The panel recommends that a decision to proceed toward a new light source with revolutionary capabilities be accompanied by a robust R&D effort in accelerator and detector technology that will maximize the cost-efficiency of the facility and fully utilize its unprecedented source characteristics."
- "…the best approach for a light source with the characteristics just enumerated would be a linac-based, seeded, free electron laser (FEL). To meet anticipated high demand for this linear device, the linac should feed multiple independently tunable undulators, each of which could service multiple end-stations. It is considered essential that the new light source have the pulse characteristics and high repetition rate necessary to carry out a broad range of coherent 'pump-probe' experiments, in addition to a sufficiently broad photon energy range (at least ~0.2 keV to ~5.0 keV) and pulse energy necessary to carry out novel 'diffract before destroy' structural determination experiments important to a myriad of molecular systems."

The LCLS facility [3] already produces extremely intense pulses of X-rays spanning 280-10,000 eV. It also produces spatially coherent, short-duration temporally coherent pulses, near the Fourier transform limit in the range of 5-9 keV [4]. LCLS will soon produce similarly short and temporally coherent pulses in the range of 500-1,000 eV [5]. The facility produces sufficiently

high energy per pulse for a wide variety of "diffract before destroy" experiments. However, neither LCLS nor the original LCLS-II concept could provide a sufficiently high repetition rate for the scientific objectives targeted by the BESAC Subcommittee.

SLAC has exerted significant effort in exploring the repetition rate limits of "normal conducting" linacs. A repetition rate of 360 Hz would be relatively easy to achieve, since the SLAC linac was designed to run at this rate. A repetition rate of 1 kHz might be achieved by an extensive modification of all the SLAC linac modulators and klystrons. Repetition rates above 1 kHz require that LCLS-II build a new high repetition rate linac. For this reason LCLS-II will employ a 4 GeVsuperconducting linac producing x-ray pulses a repetition rate approaching 1MHz. LCLS-II will provide up to a thousandfold increase in average brightness compared to LCLS today.

1.3 Capability Gap

The revised Mission Need Statement (MNS) acknowledges the "capability gap" between LCLS performance and the abovementioned capabilities, which the BESAC Subcommittee identified as essential to realize the research potential of future X-ray free-electron lasers.

SLAC has responded to this need in the new configuration of LCLS-II by proposing the addition of a superconducting linac and two variable gap undulators. This combination will greatly expand both the capabilities and capacity of the LCLS complex.

1.4 Mission Need

The revised MNS lists "mission-level assumptions," which anticipate the "key performance parameters" (KPPs) of the project, to be finalized in the approved Critical Decision 2 document, expected in 2015. These mission-level assumptions are:

- A new superconducting linear accelerator
- Expanded spectral reach, from 200 to 20,000 eV
- High repetition rate operations from 200 to 5,000 eV
- Capability to provide "pump" pulses over an extended range of photon energies to a sample, synchronized to LCLS-II X-ray probe pulses with controllable time delay
- Increase of user access through parallel rather than serial beam use

The revised MNS states that, if these assumptions are met,

> "LCLS-II will expand the existing U.S. capacity and capability in X-FEL science and leverage the LCLS investment in a cost effective way. It assures international competitiveness of the U.S. x-ray program for decades to come."

1.5 Key Features of LCLS-II

1.5.1 Superconducting Linear Accelerator

A superconducting linear accelerator operating in "continuous wave" (CW) mode is required to produce x-ray pulses at the high repetition rate cited in the BESAC Subcommittee report. The design of this new accelerator takes full advantage of R&D, technology and engineering designs developed for the International Linear Collider. The LCLS-II linac design also exploits extensive lessons learned in the course of the European XFEL project. This linac will replace the existing SLAC linac in Sectors 0-10 of the accelerator enclosure and klystron gallery. This linac will provide electrons to either (or both) of the new x-ray sources described in sections 1.5.3 and 1.5.4 below.

1.5.2 LCLS ("copper") Linac

The existing LCLS linac, located in sectors 21-30 of the SLAC linac, will not be modified by the LCLS-II project; it will provide high-current, high-energy pulses of electrons at rates up to 120 Hz. It will provide an alternate source of electrons to the new hard x-ray source described below. The 15 GeV electrons of the "copper" linac will make it possible to extend the spectral reach of the hard x-ray source from 5 keV (available using the new SC linac) to 25 keV.

1.5.3 Soft X-ray Source

The new soft X-ray (SXR) undulator source is intended to cover a spectral range of 200-1,200 eV. In particular, the SXR source will cover 250-1,200 eV with 4 GeV electrons from the new SC linac. This source will provide either SASE radiation or narrow-bandwidth radiation (via self-seeding) over its operating range. This source will be installed on the north side of the access aisle in the LCLS Undulator Hall.

1.5.4 Hard X-ray Source

The hard X-ray (HXR) undulator source will be installed on the south side of the aisle in the LCLS Undulator Hall, in place of the existing LCLS undulator. This undulator will receive electrons from either the new superconducting linac or the existing LCLS linac. When fed by the SC linac, it will operate over the spectral range of 1-5 keV at selectable high (approximately 100 kHz) pulse frequencies. When fed by the LCLS "copper" (Cu) linac, the HXR undulator will span 0.28-25 keV, by means of varying both the linac energy and the gap of the undulator.

1.5.5 X-ray Transport and End Stations (XTES)

The project will provide two x-ray beam paths, one for each undulator. These beam paths, shown schematically in Figure 1-1, include the components necessary to filter, attenuate and collimate the x-ray beam.

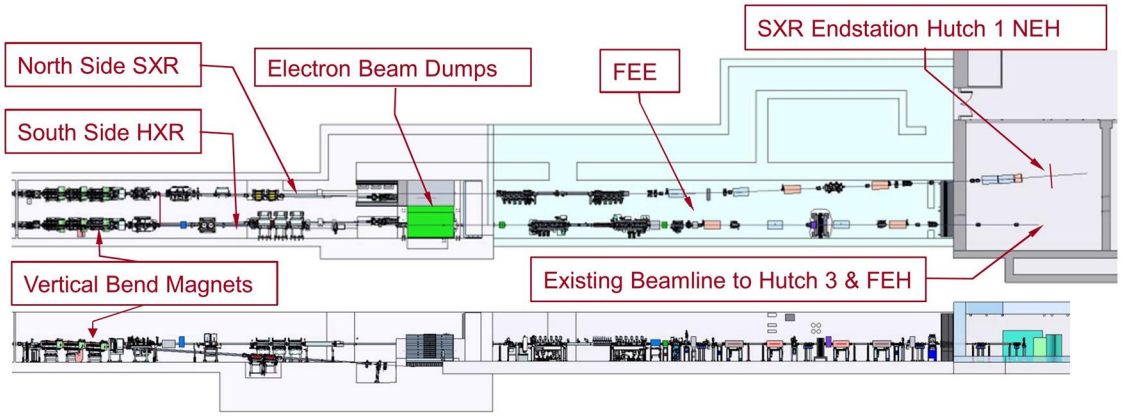

Figure 1-1: Schematic layout of LCLS-II x-ray transport and end stations

The "south side" beam path must transport 1-5 keV photons produced by the new linac in addition to photons up to 24 keV produced by the existing ("copper") LCLS linac. The x-ray beam is deflected horizontally by a pair of mirrors to ensure that gamma rays and very hard spontaneous radiation cannot exit the front end enclosure. Two pairs of mirrors will be provided; one pair will be used to transport 1-5 keV photons and the other pair will be used for harder x-rays. The south x-ray beam path will also provide gas and solid attenuators, non-invasive intensity monitors, imagers and a "K monochromator" that will be used to set the gaps of the new undulators. The south side beam path will incorporate collimators, shutters, diagnostics for imaging, wavefront monitoring and non-invasive pulse energy measurement.

The "north side" x-ray beam path will be dedicated to the new soft x-ray undulator, which will receive electrons from the new north-side undulator and the superconducting linac. This beam path will include attenuators, imagers, non-invasive intensity monitors, and a Kirkpatrick-Baez focusing system. The north-side x-ray beam path is designed to permit later addition of additional deflecting mirrors which will be used to direct x-rays to multiple instruments.

1.5.5.1 Soft x-ray Instruments

Existing LCLS soft x-ray instruments will be "re-purposed" (disassembled and reconfigured reusing original components to the extent possible) for use with the new soft x-ray source provided by LCLS-II. The capabilities of the: Atomic/Molecular/Optical Physics "HFP" end station, the coherent scattering "LAMP" end station and the resonant soft x-ray scattering "REDSOX" end station will be available at the LCLS-II soft x-ray instrument by installing the end station required by each experiment's needs. A concept for a resonant inelastic x-ray scattering (RIXS) instrument has been under development by LCLS scientists for some time, and the layout of the new beam path and end station will permit later implementation of this instrument.

As the soft x-ray research program matures, it is expected that the LCLS Near Experiment Hall will someday be dedicated to soft x-ray research as additional beam paths and end stations

are set up. It is expected that, when this scenario is realized, the capabilities of the x-ray pump/probe (XPP) instrument will be re-created in the Far Experiment Hall, most likely in the X-ray Correlation Spectrometry (XCS) enclosure.

1.5.5.2 Hard X-ray Transport, Optics and Diagnostics

X-rays from the HXR source will be delivered to the existing four hard X-ray instruments (XPP, CXI, XCS, MEC). The high repetition rate of the SC linac is expected to be especially important to the XPP and XCS programs. Two sets of mirrors (one pair for x-rays up to 5 keV and another pair for harder x-rays) are required to cover the full spectrum of the HXR source; the project will provide a pair of mirrors designed for 1-5 keV x-rays.

1.5.5.3 Hard X-ray Instruments

The existing LCLS hard x-ray instruments in Hutches 4-6 will be adapted for use with either the high repetition rate x-ray source or the existing LCLS beam. The Matter in Extreme Conditions (MEC) instrument will most likely operate with harder x-rays from the copper linac.

1.5.6 High Repetition Rate Capability

The new superconducting linac will be capable of producing and accelerating electron bunches at up to 1 MHz and delivering over 1 MW of electron beam power. It is important to recognize that an important figure of merit for x-ray experimenters is the x-ray power delivered to the experiment. Due to considerations such as sample heating and x-ray optics stability, it is anticipated that the maximum practical x-ray power in high repetition rate operation will be approximately 20 watts, regardless of repetition rate. LCLS-II can exceed this x-ray power by a considerable factor, while using less than 120 kW of electron beam power. For this reason the new LCLS-II electron beam dumps will be designed to handle 120 kW.

Other considerations may lead to a limit on linac repetition rate. For example, pump/probe experiments will be limited by the pump laser repetition rate; imaging experiments may be limited by the state-of-the-art in readout of 2-D detectors and data archiving rates. One-dimensional detectors, integrating detectors and electron spectrometers can operate at MHz repetition rates.

LCLS-II will provide a DAQ for basic high-repetition rate detectors (such as a one-dimensional array that can operate at 1 MHz and an integrating 2-D detector). The LCLS-II Project will not undertake the development of fast (1-10 kHz) 2-D detectors. SLAC and other labs working at extending the state-of-the-art in fast readout, and LCLS-II will provide faster detectors to fully exploit LCLS-II capabilities.

1.6 Cost Range

The cost range was subject to an independent cost review as part of the CD-1 approval process. This review confirmed the $750M-$1.2B cost range quoted in the Mission Need Statement. The planned total project cost (TPC) is $965M. Table 1-1 shows the funding profile

assumed in developing the project schedule. The 2015 Omnibus Appropriations bill has authorized full 2015 funding for LCLS-II construction.

Table 1-1. Assumed funding profile from 2010 through 2019 for LCLS-II in units of M$.

Fiscal Year	FY10	FY11	FY12	FY13	FY14	FY15	FY16	FY17	FY18	FY19	FY20	Total
TEC - PED			2.0	5.0	4.0	21.0	15.0					47.0
TEC - Construction			42.5	17.5	71.7	117.7	189.0	185.1	176.0	69.9		869.4
OPC	1.126	9.474	8.0	0.0	10.0	9.3	0.0	0.0	5.9	4.8	0.0	48.6
TPC	**1.126**	**9.474**	**52.5**	**22.5**	**85.7**	**148.0**	**204.0**	**185.1**	**181.9**	**74.7**	**0.0**	**965.0**

1.7 Schedule

The proposed funding profile and schedule for the LCLS-II Project will enable the achievement of "first light" from the new undulator sources during CY2019. The project can be completed on this schedule because it will be executed by a coordinated multi-institutional collaboration as described in the acquisition strategy. Achievement of this schedule is contingent on the following:

- Sufficient funding to support the work plan
- Superconducting RF accelerating modules acquired from two suppliers working in parallel
- Certain key long-lead procurements that can be awarded early in FY2015, after approval of CD-3A
- Reduction of LCLS operation for scientific users by a total of seven months compared to the routine operating schedule (which includes a total of three months of shutdown per year) in order to install all the necessary equipment in the existing LCLS Undulator Hall.

The overview LCLS-II construction schedule is shown in Figure 1-2. Level 1 milestones for Critical Decsion approvals are listed in Table 1-2.

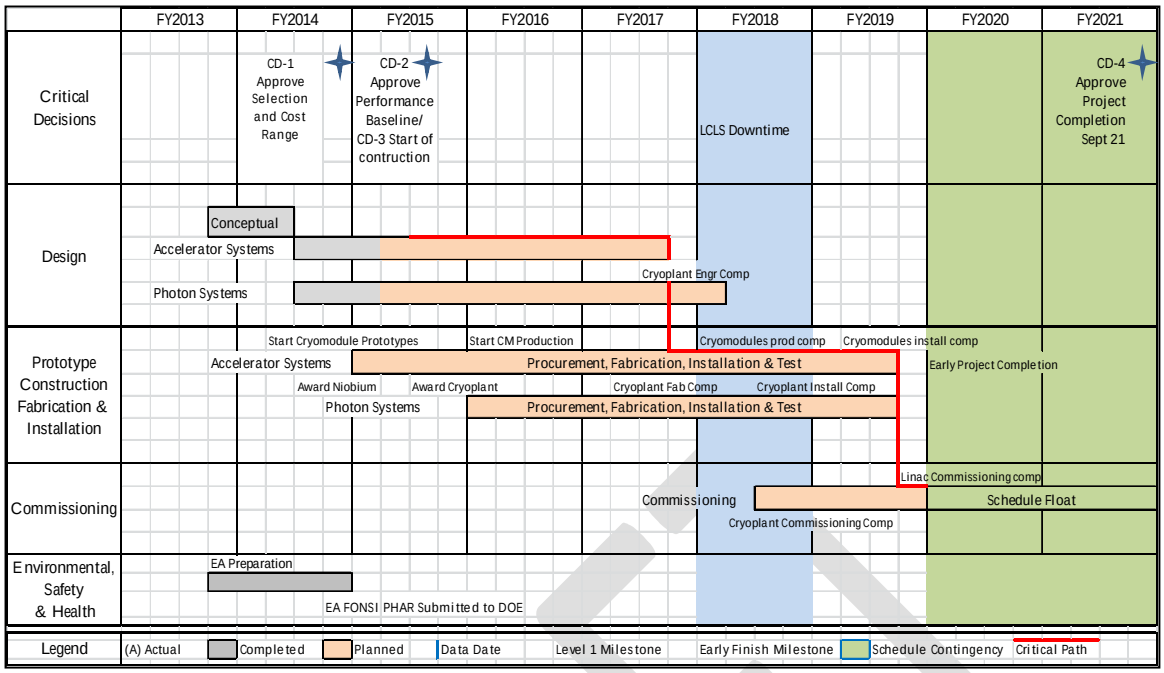

Figure 1-2. Schedule for construction of LCLS-II.

Table 1-2. Proposed Level 0 Milestones for the LCLS-II Project.

Level 1 Milestones	Date
CD-0, approve mission need	4/22/10 (actual)
Revise Mission Need Statement	09/27/2013 (actual)
CD-1, approve alternative selection and cost range	8/22/2014(actual)
CD-3A, approve long lead procurements	September 2014
CD-2, approve performance baseline	June 2015
CD-3, approve start of construction	June 2015
CD-4, approve project completion	September 2021

1.8 Alternatives Analysis

The Department of Energy has considered three alternatives for fulfilling the revised Mission Need Statement considered in creating the acquisition strategy:

- Maintain the status quo: build no new facility and use existing facilities at SLAC or elsewhere in the world.
- Build LCLS-II at SLAC.
- Build a comparable facility in a “green field.”

1.8.1 Status Quo

As observed in the BESAC report [2] and quoted in section 1.3 of this report, the United States lacks key research capabilities that are essential to the mission of the BES program and the Office of Science. Therefore the status quo does not properly support the BES mission. Since no existing or planned FEL facility anywhere in the world can provide high-brightness X-ray pulses at about 100 kHz, as proposed in this conceptual design, the Mission Need cannot be fulfilled by use of any other facility in the world. Construction of a new facility or enhancement of an existing facility is thus required.

1.8.2 Proposed LCLS-II Configuration

The LCLS-II proposal meets the requirements in the BES Subcommittee report. Construction of LCLS-II at SLAC permits: reuse of approximately $400M in existing facilities and infrastructure at SLAC; the $500M invested in the LCLS facility to date; and the experience and expertise of the SLAC/LCLS staff. Since obtaining "first light" at LCLS in April 2009, SLAC and the LCLS staff have shown unprecedented productivity in the form of high-impact groundbreaking scientific output at LCLS. SLAC has, in the four years since LCLS operations began, exceeded every performance goal of the LCLS Project in terms of peak power, femtosecond-scale pump/probe timing capability and peak brightness. SLAC personnel are well-prepared to fully exploit the new capabilities provided by LCLS-II upon its completion. Furthermore, LCLS-II will support a wide range of enhancements to the LCLS facility, as described in Chapter 18 of this report. These enhancements make maximal use of existing SLAC infrastructure, ensuring LCLS can maintain its position at the forefront of x-ray research in the most cost-effective way possible for decades to come.

1.8.3 LCLS-II in a "Green Field"

This option would fulfill the Mission Need. However this option is far more expensive than construction of the proposed LCLS-II configuration. As described in the LCLS-II Acquisition Strategy, construction of a facility equivalent to LCLS-II in a green field would incur approximately $3.5 billion in additional life cycle cost, compared to constructing LCLS-II as described in this report. The additional cost would result from duplicating SLAC facilities, operating them and decommissioning/demolishing them at a future date. It is therefore far more cost-effective to construct the LCLS-II facilities at SLAC.

1.9 Acquisition Strategy

The Acquisition Strategy selects Stanford University, DOE's Managing & Operating contractor for SLAC, to directly manage the LCLS-II acquisition. The acquisition of large research facilities is within the scope of the DOE contract for the management and operations of SLAC and consistent with the general expectation of the responsibilities of DOE M&O contractors.

SLAC will assign responsibility for the design and fabrication of major LCLS-II subsystems to other DOE Laboratories or eventually an NSF Laboratory that possess the expertise and infrastructure to best accomplish these tasks. In particular, Lawrence Berkeley National Laboratory (LBNL) will continue to design and production-engineer the undulators for LCLS-II, and will provide the electron source around which LCLS-II will be designed. Fermi National Accelerator Laboratory (Fermilab) and Thomas Jefferson National Accelerator Facility possess the expertise to design and fabricate cryogenic acceleration modules ("cryomodules"). Argonne National Laboratory will provide undulator vacuum chambers and will develop an alternative undulator design. Argonne will also support FNAL with chemical processing facilities for niobium accelerating structures. In addition, Cornell University will provide development support for improving cryomodule performance.

Most of the assembly, installation, testing, and commissioning of the LCLS-II Project will be performed by the SLAC LCLS-II scientific and technical staff. Much of the subcontracted work to be performed for LCLS-II consists of hardware fabrication. Since a significant fraction of this work requires shutdown of SLAC accelerator facilities, every effort will be made to minimize interruptions to LCLS operation.

1.10 References

[1] Charge to Professor John C. Hemminger, chair of the Basic Energy Sciences Advisory Committee, from William F. Brinkman, January 2013; stored at the BESAC website http://science.energy.gov/~/media/bes/besac/pdf/2013-brinkman-to-hemminger.pdf.

[2] "Report of the BESAC Subcommittee on Future X-ray Light Sources," stored at the BESAC website http://science.energy.gov/~/media/bes/besac/pdf/Reports/Future_Light_Sources_report_BESAC_approved_72513.pdf.

[3] C. Bostedt, et al., "Ultra-fast and ultra-intense x-ray sciences: first results from the Linac Coherent Light Source free-electron laser," J. Phys. B: At. Mol. Opt. Phys. **46** 164003.

[4] J. Amann, et al., "Demonstration of self-seeding in a hard x-ray free-electron laser," Nature Photonics **6**, pp. 693-698 (2012); ISSN: 1749-4885.

[5] Y. Feng, et al., "System Design for Self-Seeding the LCLS at Soft X-ray Energies", Proceedings of the 2012 Free Electron Laser Conference, Nara, Japan, TUOBI01, pp. 205-212, ISBN 978-3-95450-123-6.

2 PROJECT OVERVIEW

TECHNICAL SYNOPSIS

The LCLS-II project is described briefly here in overview. Project scope is described in detail in Chapter 3 and subsequent chapters. Changes in the Project design from the CDR and the status of the technical design are described. Management of schedule, cost and risk is discussed.

2.1 Introduction

As described in the *LCLS-II Project Requirements Document*, LCLSII-1.1-GR-0018, the LCLS-II Project consists of:

- A new high repetition rate (MHz) injector,
- A CW superconducting RF (SCRF) linac that accelerates the beam to 4.0 GeV,
- Re-use of an existing 2.4 km long bypass line from the end of the SCRF linac to the Beam Switch Yard (BSY) after Sector 30 of the SLAC linac,
- Transport lines (one new, one existing) to the LCLS Undulator Hall where two new undulators, the SXR (soft X-ray) and the HXR (hard X-ray), will be installed,
- X-ray transport lines from the undulators through the LCLS Front End Enclosure (FEE) area including X-ray diagnostics, attenuators and mirrors, and
- A new soft X-ray end-station in the LCLS NEH.

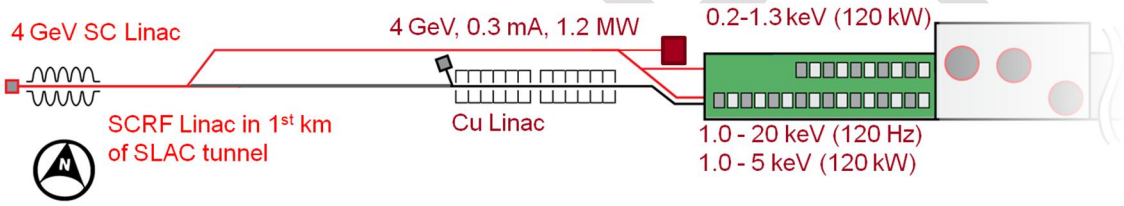

Figure 2-1. Schematic layout of the LCLS-II project scope

The facility is constructed to either deliver high-rate beam from the SCRF linac to both the SXR and HXR undulators, or to deliver the high-rate beam to the SXR undulator and deliver beam from the existing copper (CuRF) linac at 120 Hz to the HXR undulator. As illustrated in Figure 2-2, the SXR undulator is designed to lase in SASE mode over the photon energy range of 0.2 to 1.3 keV when supplied with beam from the SCRF linac. The HXR undulator is designed to lase in SASE mode over the photon energy range of 1.0 keV to 5.0 keV when supplied with beam from the SCRF linac, and over the energy range of 1.0 to 25.0 keV when supplied with beam from the existing CuRF linac. Both undulators will include the option for self-seeding, with SXR self-seeding over the photon energy range of 0.2 to 1.3 keV when fed by the SCRF linac and HXR self-seeding covering the photon energy range from 4.0 to 12.0 keV when supplied beam from the CuRF linac. The HXR self-seeding system is not designed to operate with high power beam from the SCRF linac but may be upgraded to do so as described in Chapters 8 and 17.

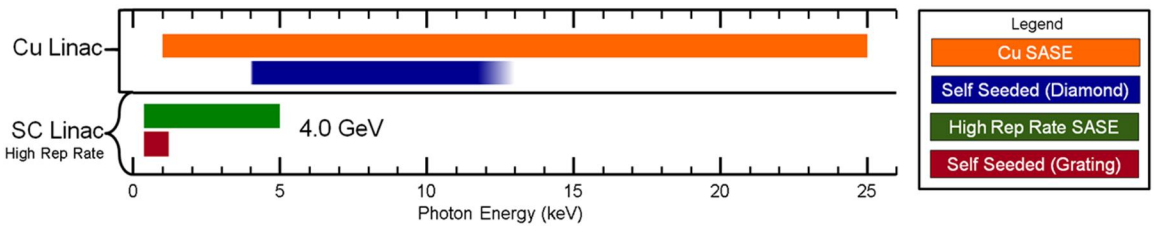

Figure 2-2. Photon energies from the SCRF and CuRF linacs for both SASE and self-seeded operation, assuming 4.0 GeV SCRF electrons and 3-to-15 GeV CuRF electron beams. Self-seeding for photon energies between 1.3 and 4 keV is possible with an upgrade, as described in Chapter. 17.

The critical technologies in the LCLS-II design are the injector which determines the beam emittance for a given bunch charge, the high-Q SCRF linac which accelerates the high rate beam, and the variable strength undulators which enable the large, independent photon tuning range for the SXR and HXR. The injector is described in Chapters 4 and 5, the SCRF cavities and cryomodules are described in Chapter 6, and the undulators are described in Chapter 8. Development programs for these technologies are described in Chapter 16.

The LCLS-II facility will use the existing accelerator tunnels at SLAC. The injector and SCRF linac will be installed in the first km of the existing SLAC linac tunnel after the existing equipment (the SLAC S-band linac) is removed from this portion of the linac tunnel. The layout of the LCLS-II is shown in Figure 2-1. The project parameters and layout are described in greater detail in Chapters 3 and 4, and the infrastructure modifications required to support the LCLS-II are described in Chapter 11.

The LCLS-II project schedule is shown in Figure 2-3. Approval for CD-3, Start of Construction, is anticipated in the third quarter of FY15, allowing procurement and fabrication of components to proceed. The completion of the Project is paced by the procurement, installation and commissioning of the liquid helium cryogenics plant. Installation of components in LCLS operational space will be performed during a 12-month shutdown in FY18. Components can also be installed during annual maintenance shutdowns of LCLS operations. In FY19 the cryogenic systems and SCRF accelerator installation will be complete and commissioning will begin. As commissioning proceeds and operational goals of technical systems are met, those systems are declared operational and transferred to machine operations LCLSII-1.1-PM-0155-R0, LCLSII-1.1-PM-0269-R0. The final system transfer to operations, the soft X-ray end station in the LCLS NEH, is scheduled to occur at the end of 2019.

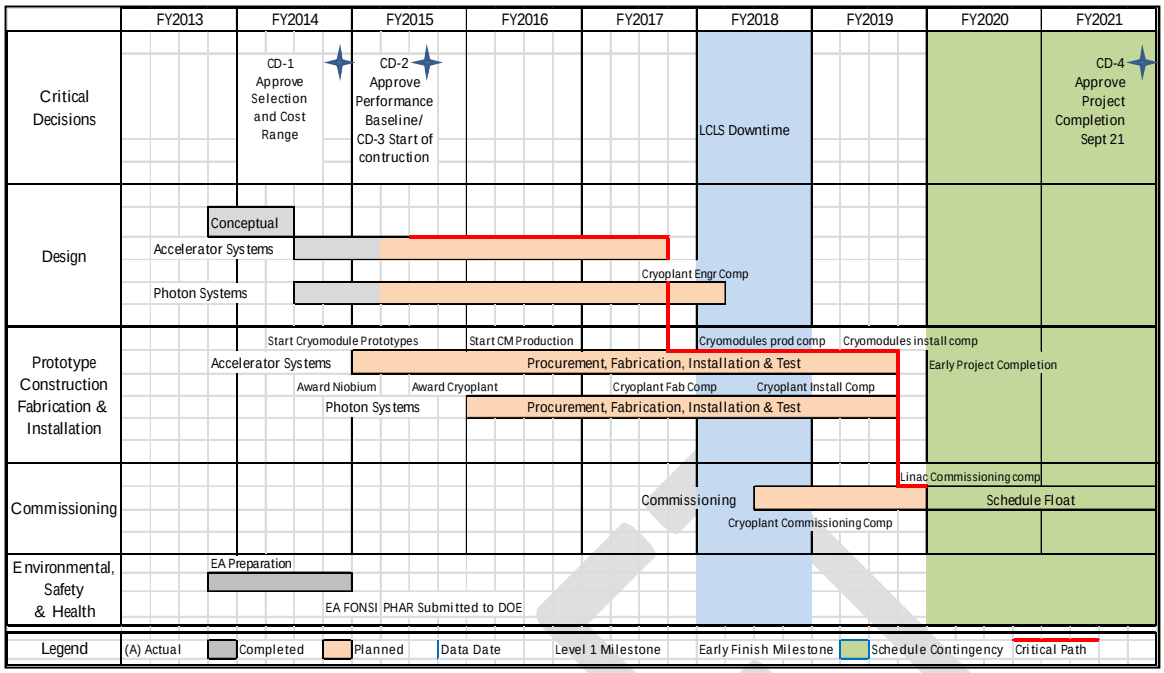

Figure 2-3. The LCLS-II project schedule

2.2 LCLS Scope

The LCLS-II Project will expand and enhance the existing Linac Coherent Light Source (LCLS) facility. The project includes

- Installation of a CW 4 GeV superconducting rf (SCRF) linac and electron source in Sectors 0-10, with a nominal bunch output frequency up to 1 MHz.
- Installation of a helium liquefaction plant, needed for operation of the linac, in the vicinity of Sector 4
- Use of existing transport lines to bypass the middle portion of the SLAC linac and the LCLS linac in Sectors 11-30
- Replacement of the existing LCLS undulator with a hard X-ray variable gap system which maintains self-seeding capability, receiving electrons from either the normal-conducting copper LCLS RF (CuRF) linac or the new SCRF linac
- Installation of a soft X-ray variable gap undulator source with self-seeding capability on the north side of the LCLS undulator hall, receiving electrons from the new SCRF linac
- Installation of a new beam line from the end of the bypass line to the new soft X-ray undulator source, and upgrades to the existing bypass line to the new hard X-ray undulator source
- Installation of new electron beam dumps to contain the new high-power beam

- Installation of X-ray transport, optics and diagnostics for the new soft X-ray undulator to one experiment station in the LCLS Near Experiment Hall (the layout will permit expansion to two stations). The experiment station itself will be one of the existing instruments upgraded for use at high repetition rate.
- Modification of the existing hard X-ray transport and optics to enable use of the new hard X-ray undulator to the existing hard X-ray instruments in the Near- and Far Experiment Halls.

2.3 Machine Operation Modes

LCLS-II systems are designed to support:

- Preservation of all current capabilities of the CuRF linac; LCLS-II is required to preserve the present capabilities of the CuRF linac and all presently foreseen upgrades. No extensions of the properties, parameters, etc. of the electron beam from the CuRF linac are planned within the LCLS-II Project.
- Delivery of electrons from the SCRF linac to the soft X-ray undulator while electrons from the CuRF linac are delivered to the hard X-ray undulator.
- Delivery of SCRF linac electrons to both undulators simultaneously, each undulator receiving a train of evenly spaced bunches, while the CuRF linac is either idle or in operation delivering electrons to a beam dump.
- Controlled or open access to Sectors 0-10 while the CuRF linac is in operation.
- Controlled or open access to the Sector 21 Injector Vault while the SCRF linac is in operation.
- Controlled or open access to End Station A while either linac is in operation, including beam to dumps used in LCLS operation or electrons to undulators.
- Entry to experiment station enclosures when X-ray beams are contained within the Front End Enclosure by safety shutters.
- Parasitic pulse-stealing operation of End Station A test beams (from the CuRF linac) while LCLS facilities are in operation.

2.4 Key Performance Parameters

Table 2-1 provides the Preliminary Threshold and Objective Key Performance Parameters (KPPs) for the LCLS-II Project.

Table 2-1 – Preliminary Threshold and Objective KPPs

Performance Measure	Threshold	Objective
Variable Gap Undulators	2 (SXR & HXR)	2 (SXR & HXR)

Super Conducting Linac Based FEL System		
Super Conducting Linac Energy	3GeV, with systems installed to support 4 GeV operation	≥4 GeV
Super Conducting Linac Repetition Rate	50 kHz	929 kHz
Super Conducting Linac Charge per Bunch	0.02 nC	0.1 nC
Photon Beam Energy Range	250-2,800 eV	200-5,000 eV
High Repetition Rate Capable End Stations	≥ 1	≥ 2
FEL Average Power (10^{-3} BW)	10X spontaneous @ 2.8 keV	>20 W
Normal Conducting Linac Based FEL System		
Normal Conducting Linac Electron Beam Energy	15 GeV	15 GeV
Normal Conducting Linac Repetition Rate	120 Hz	120 Hz
Normal Conducting Linac Charge per Bunch	0.150 nC	0.25 nC
Photon Beam Energy Range	1,000-15,000 eV	1,000-25,000 eV
Low Repetition Rate Capable End Stations	≥ 2	≥ 3
FEL Pulse Energy (10^{-3} BW)	10X spontaneous @ 15 keV	≥2 mJ @15 keV

The Threshold KPPs are the minimum parameters against which the Project's performance is measured when complete. The Objective KPPs describe the technical goals of the Project. If Project performance is sustained and sufficient contingency is available, the Project may use project contingency to attain the Objective KPPs or beyond.

The baseline technical design of the Project includes, as a minimum, all diagnostics required to meet the Threshold KPPs. As the Project progresses, additional diagnostics may be added to the Project scope. The technical design allocates explicit space for additional diagnostics. This approach is described in more detail in *Electron Beam Diagnostics Systems*, LCLSII-2.7-PR-0170. The project parameters and layout are described in greater detail in Chapters 3 and 4.

2.5 Progress since the Conceptual Design

Since the conceptual design was developed, the design of all systems has advanced. A number of design changes have been made as a part of design development. Changes to the accelerator layout are described in Section 4.1.1. Design choices have also made to control Project costs and risks. Scope has also been added to the Project to minimize project dependencies. The major changes are described here.

2.5.1 SSAs replacing vector sum

The initial design for powering the SCRF accelerating cavities involved a klystron powering 48 individual cavities. This design presented a considerable risk to the project and required an R&D program to demonstrate the vector sum design's efficacy. It was also recognized the

system availability would suffer from the klystron single point of failure. The Project took the decision to change this plan to replace the klystron as RF power source with individual solid state amplifiers (SSAs). Each accelerating cavity is powered by its own SSA. This simplifies the RF system and particularly the LLRF system.

2.5.2 Addition of scope to the Project

The scope added to the Project to minimize project dependencies includes the following.

- **Accelerator Equipment Removal:** The Project will disassemble and remove the existing S-band copper linac and associated equipment in the accelerator tunnel from Sector 0 to Sector 10 to make room for the new SCRF accelerator. The Project will remove the equipment and place it in a holding area.
- **Utilities for the new cryoplant:** The new cryogenics plant requires electrical power and cooling water for operations. The Project will design and install these utilities from existing locations in the linac infrastructure.
- **Controls scope additions:** High performance beam containment, machine protection, timing system and beam position monitor systems. Develop high speed electronics and extend systems to meet the requirements of the new 1 MHz high power beam.
- **Linac network and control room server upgrades:** Upgrade linac network switches, servers and control system infrastructure to allow connecting devices to the EPICS control system.

2.6 Design Status

The *LCLS-II Project Final Design Plan* LCLSII-1.1-QA-0065 provides for a phased completion of the final designs for the LCLS-II facility. The plan ensures that designs are sufficiently mature to start procurements and construction, while enabling the most cost-effective schedule for constructing the facility and maximizing the technical capabilities of the facility at CD-4.

The *LCLS-II Project Design and Milestone Review Process* SLAC-I-060-107-002-00-R001 describes requirements and responsibilities for conducting design and milestone reviews. It includes descriptions of the types of reviews, objectives, and topics to be addressed and deliverables to be reviewed. Action items from the reviews are addressed by the responsible engineers, validated by the System Manager and closure tracked by the Quality Assurance Manager. This process is described further in Chapter 15.

2.6.1 Approach to design readiness

Final design readiness at CD-3 recognizes that that not all subsystems will reach final design at the same time. Project-level requirements and interface control points between Accelerator Systems, Cryogenic Systems, Photon Systems and Infrastructure are defined at CD-3, which

ensures that the phased procurements and construction are appropriate for the final design of the LCLS-II. The overall project design will be sufficiently mature to ensure these requirements will be met. Though the design of all subsystems may not be complete, design at CD-3 is sufficiently mature to start phased procurement or construction. This is achieved when the LCLS-II Project Final Design has been successfully reviewed and any incomplete designs carry minimal risk to the successful completion of the project.

Throughout the Project execution phase, focused design reviews are conducted by scientific community peers, external to the Project, to assure the outstanding technical system designs at CD-3 are completed in a timely fashion with sufficient quality to ensure they fully support the baseline performance, cost and schedule requirements. In order to maximize resource utilization, the Project will commence construction with some design efforts ongoing.

A metric for design (or specification for design-build) completion of a system is a cost-weighted average of the design maturity of the scope elements in that system, weighted by the value of the elements. Planned and actual release dates for requirements documents along with planned and actual dates for the preliminary and final design reviews of each element are used to assess design maturity values. Completion of preliminary design is typically assessed at 30% to 50% design maturity for LCLS-II; however some subsystems will be at a higher maturity due to design work during Phase 1 of LCLS-II development or similarity to existing designs. Final Design is assessed as 90% to 100% design maturity.

2.6.2 Summary of LCLS-II Design Status

The Accelerator Systems design is 65% complete. Completing remaining design after CD-3 allows for potential upgrades to diagnostics and controls, using designs developed and proven by SLAC Operations.

- RF Gun – design is a close copy of the existing operating APEX gun
- Injector source components – uses existing and working designs from APEX, including: load lock, magnets, high-level and low-level controls and diagnostics
- Diagnostics components – most are from existing LCLS designs
- Magnets – using existing designs for 93% of magnets
- RF – commercial products
- Beamline – preliminary beamline layout complete
- Dumps – A 240 kW dump is available in the BSY and the design for the 120 kW dump for each undulator is a modification of an existing SLAC design
- Controls – Many systems are similar to current LCLS designs. High performance controls systems to accommodate higher beam power and repetition rate are challenging and need design development.

The Photon Systems design is 65% complete. Completing remaining design after CD-3 allows for coordination with developing designs for LCLS Operations future new instruments.

- Hard and Soft X-ray undulator designs are based on LCLS-II Phase-1 variable gap undulator mechanical and magnetic design and controls. The 1m prototype and the full scale prototype testing have been completed prior to CD-3.
- The vacuum system is a close copy of that used in Phase-1, which has been through full prototype
- LCLS quadrupoles are being re-used and copied
- Phase shifter magnetic design was proven for Phase-1, and is being re-prototyped with minor changes to meet current requirements
- The RFBPM design will have no changes from phase-I prototyped design
- Designs for the Phase-1 interspace supports and movers are reused with minor changes.

Hard X-ray beamline:

- Cooled mirror designs are new to meet current requirements.
- Modifications have been made to the existing gas attenuator design and a new solid attenuator based on an existing design
- The gas energy monitors are being repurposed with upgrades
- The design for the high resolution imager is new, based on an existing design
- The existing in line spectrometer, monochromator, and rapid turnaround diagnostics station are repurposed.

Soft X-ray beamline:

- The gas attenuator design is new, derived from an existing design
- One gas energy monitor is repurposed with upgrades, one is new but similar in design to the one used at LCLS
- The design for the high resolution imager is new, based on an existing design
- The cooled K-B mirror system is new, with the bender design leveraged on an existing design
- The rapid turnaround diagnostics station is derived from an existing design

Cryogenic Systems design is 80% complete. Completing remaining design after CD-3 allows for advancement of project schedule and minimizing cost by starting long duration activities when associate designs are sufficiently mature.

- Cryomodules - Leverages extensive design work for ILC and XFEL and production of XFEL cryomodules, with modest changes to meet LCLS-II requirements
- Cryogenics plant - The existing design for operating plant at JLAB and existing design work by JLAB for FRIB is being leveraged and adapted for LCLS-II requirements

Infrastructure Systems design is 35% complete. Completing remaining design after CD-3 allows for sufficient maturity of the technical systems requirements to ensure appropriate infrastructure is provided.

- Significant portions of the needed infrastructure require no design effort, due to re-use of existing accelerator, undulator, and experimental structures and infrastructure.
- The Cryoplant Building design by an A&E firm is started, with 60% design submittal completed.
- Engineering studies are complete, including noise and vibration studies to understand impact on the cryogenics plant and a structural study for the removal of an FEE wall.
- Technical systems requirements are being documented and controlled in Room Data Sheets, for use by A&E firms for infrastructure design.

2.7 Management of cost and schedule

To build the LCLS-II facility at SLAC, the project will construct main elements described in Section 2.2. The detailed activities to design, fabricate, construct, install and commission the LCLS-II project are described in its Work Breakdown Structure (WBS). Each element (activity) of the WBS has cost, resources (manpower or materials), and linked schedule associated with it. The WBS is the key tool for planning and controlling cost and schedule.

The levels of the WBS reflect a logical breakdown of the work by major system. WBS Level 2 shown in Table 2-2 defines the major LCLS-II systems. Each lower level breaks down the previous level by subsystem and task.

Each LCLS-II system includes related common tasks and activities such as controls, alignment and installation, such that it is a fully integrated system that captures all costs, resources, tasks and activities necessary to complete it. Each system contains progressively lower levels to further define the sub-elements down to the lowest level of the WBS. Contributions from each Partner Lab are segregated at level 3 of the WBS, separated from contributions from other institutions.

Table 2-2. LCLS-II WBS at Level 2

WBS#	LCLS-II Level 2 Systems
1.01	Project Management, Planning & Administration
1.02	Accelerator Systems

1.03	Photon Systems
1.04	Cryogenic Systems
1.05	Infrastructure Systems
1.08	CD, R&D and Commissioning
1.09	Phase 1 Design & Development (completed)

Control Account Managers (CAMs) are assigned control accounts for specific systems and activities and are responsible for ensuring that only budgeted work is authorized, and responsible for controlling expenditures against their accounts. The costs and commitments incurred in these accounts will be transmitted to the LCLS-II Project Office monthly and reported in the monthly LCLS-II Cost Performance Report.

2.8 Risk management

Managing potential risk to the achievement of the project requirements and goals is a key element of the project management process. The LCLS-II Project follows the *SLAC Risk Management Plan* SLAC-I-PMO-005, which is consistent with *Project Management for the Acquisition of Capitol Assets* [DOE O 413.3B], and strives to incorporate "best practices" from other large-scale construction projects around the DOE complex.

The LCLS-II Project *Risk Addendum* LCLSII-1.1-PM-0005 defines a methodology to identify, categorize, and quantify specific risks, determine their consequence and associated probability, and develop mitigation and correction strategies should the risks be realized. It describes the risk thresholds and procedures specific and unique to this project.

The product of the risk management and planning process is a Risk Register listing the various project risks with their classification, probability of occurrence, potential impact on cost and schedule, and mitigation handling strategy. Project risks are centrally managed, but are the result of project-wide risk assessment. Significant technical risks are included in the LCSL-II Risk Registry and are reviewed and updated on a monthly basis by risk owners.

The Project's bottoms-up Detailed Cost Estimate includes the Basis of Estimate information for design maturity and judgment factor. Each System Manager and his or her respective CAMs assess contingency requirements, at the lowest WBS, based on an assessment of risk and uncertainty of (1) design maturity of the component(s) and/or cost estimate, and (2) judgment factors, which considers factors such as the state of the technology, single vendor procurements, and currency and pricing variations. The purpose of the contingency assessment is to provide an overall estimate of the project contingency needs. Bottoms-up contingency assessments are performed when the performance baseline is established and periodically afterward as an independent check to compare actual contingency funds to a contingency assessment.

2.9 LCLS-II design documentation summary

Table 2-3 contains a summary of design documentation organized by system or subsystem. Pertinent Physics Requirements Documents (PRDs), Interface Control Documents (ICDs), Engineering Specification Documents (ESDs), and design reviews completed to date are identified below with links to the applicable report.

Table 2-3. Summary of documentation

System-Subsystem	Physics Requirements	Engineering Spec. and Interface Control Docs.	Conceptual (CDR), Preliminary (PDR), Final Design Reviews (FDR), Plans and Statement of Works (SOW)
Injector (WBS 1.02.02 and 1.02.03)	LCLSII-2.3-PR-0167 LCLSII-2.3-PR-0166 LCLSII-2.3-PR-0165 LCLSII-2.3-PR-0073 LCLSII-2.3-PR-0086 LCLSII-2.3-PR-0085 LCLSII-2.3-PR-0084	LCLSII-2.2-IC-0173 LCLSII-2.5-IC-0056 LCLSII-2.1-IC-0156	
Linac (WBS 1.02.04 and 1.02.05)	LCLSII-2.5-PR-0135 LCLSII-2.4-PR-0110 LCLSII-2.4-PR-0099 LCLSII-2.4-PR-0095 LCLSII-2.4-PR-0091 LCLSII-2.4-PR-0090 LCLSII-2.4-PR-0083 LCLSII-2.4-PR-0069 LCLSII-2.4-PR-0068 LCLSII-2.4-PR-0062 LCLSII-2.4-PR-0060 LCLSII-2.4-PR-0041 LCLSII-2.4-PR-0040 LCLSII-2.4-PR-0039	LCLS-II-2.4-ES-0150 LCLSII-2.5-IC-0056 LCLSII-2.1-IC-0156 LCLSII-3.2-IC-0048 LCLSII-3.5-IC-0116 LCLSII-5.1-IC-0182 LCLSII-5.2-IC-0174 LCLSII-5.2-IC-0183	LCLSII-2.4-SW-0285
Accelerator & Global Controls (WBS 1.02.07)	LCLSII-2.7-PR-0213 LCLSII-2.7-PR-0170 LCLSII-2.7-PR-0176 LCLSII-2.7-PR-0075 LCLSII-2.7-PR-0074 LCLSII-2.7-PR-0066 LCLSII-2.7-PR-0136	LCLSII-2.7-IC-0121 LCLSII-3.5-IC-0115 LCLSII-2.1-IC-0156 LCLSII-2.7-IC-0247 LCLSII-3.2-IC-0048 LCLSII-3.5-IC-0116	

Undulator (WBS 1.03.02, 1.03.03 and 1.03.04)	LCLSII-3.2-PR-0105 LCLSII-3.2-PR-0102 LCLSII-3.2-PR-0101 LCLSII-3.2-PR-0038	LCLS-II-3.2-ES-0049 LCLSII-3.2-FR-0238 LCLSII-3.2-FR-0139 LCLSII-3.2-FR-0104 LCLSII-3.2-IC-0044 LCLSII-3.2-IC-0045 LCLSII-3.2-IC-0046 LCLSII-3.2-IC-0047 LCLSII-3.2-IC-0048	LCLSII-3.2-SW-0103
X-ray Transport and Experimental (WBS 1.03.05)	LCLSII-3.5-PR-0051	LCLSII-3.5-FR-0132 LCLSII-3.5-FR-0067 LCLSII-3.5-IC-0112 LCLSII-3.5-IC-0113 LCLSII-3.5-IC-0117 LCLSII-3.5-IC-0116 LCLSII-5.3-IC-0114	
Cryomodule (WBS 1.04.05 and 1.04.06)	LCLSII-4.1-PR-0146 LCLSII-4.1-PR-0098 LCLSII-4.1-PR-0097	LCLS-II-4.5-ES-0055 LCLSII-4.5-FR-0246 LCLSII-2.5-FR-0053 LCLSII-4.5-IC-0237 LCLSII-2.5-IC-0056	LCLSII-4.5-SW-0236
Cryogenics Plant (WBS 1.02.08)		LCLSII-5.4-IC-0235	
Cryo Distribution (WBS 1.04.09)		LCLSII-4.9-FR-0057 LCLSII-4.9-IC-0058 LCLSII-2.5-IC-0056	
Infrastructure (WBS 1.05.02, 1.05.03 and 1.05.04)		LCLSII-5.1-FR-0142 LCLSII-2.1-IC-0156 LCLSII-2.7-IC-0247 LCLSII-3.2-IC-0047 LCLSII-5.1-IC-0182 LCLSII-5.2-IC-0174 LCLSII-5.2-IC-0183 LCLSII-5.3-IC-0114 LCLSII-5.4-IC-0235	LCLSII-5.2-SW-0120
Radiation Physics (WBS 1.01.02)	LCLSII-2.7-PR-0077 LCLSII-2.4-PR-0107 LCLSII-1.2-PR-0265 LCLSII-1.2-PR-0263 LCLSII-1.2-PR-0261		

	LCLSII-1.2-PR-0260 LCLSII-1.2-PR-0259 LCLSII-2.7-PR-0233 LCLSII-2.7-PR-0232 LCLSII-2.7-PR-0160 LCLSII-2.7-PR-0153 LCLSII-2.7-PR-0100		
R&D and Commissioning(WBS 1.08.01, 1.08.02 and 1.08.03)			LCLSII-8.2-PM-0052
General – Accelerator Physics (WBS 1.01.01)	LCLSII-2.7-PR-0079 LCLSII-2.4-PR-0064 LCLSII-2.1-PR-0234 LCLSII-2.1-PR-0134 LCLSII-1.1-PR-0133		

3 ACCELERATOR PARAMETERS & FEL PERFORMANCE

TECHNICAL SYNOPSIS

This chapter provides an overview of the accelerator parameters and performance that will achieve the requirements described in Chapter 2. The layout of the accelerator systems is described in Chapter 4 and the accelerator components are described in subsequent chapters. The accelerator and FEL parameters will be described in Section 3.1. The limiting accelerator physics issues and performance simulations are described in Sections 3.2 and 3.3, respectively.

3.1 Overview

The LCLS-II has been designed to deliver photons between 200 eV and 5 keV at repetition rates as high as 1 MHz (929 kHz) using a superconducting RF linac (SCRF) linac while still providing pulses at short wavelengths and high X-ray pulse energy over the photon range of 1 to 25 keV using the existing 120 Hz copper RF (CuRF) LCLS linac. To cover the full photon-energy range, the facility will include two variable-strength (gap-tunable) undulators and will also allow the possibility of generating near transform-limited pulses using self-seeding as well as downstream monochromators. The LCLS-II project scope is described in Chapter 2 and a description of its layout can be found in Chapter 4.

The two LCLS-II undulators, referred to as the Soft X-Ray (SXR) undulator and the Hard X-ray (HXR) undulator, will be installed in the existing LCLS Undulator Hall to minimize civil construction and project cost. This limits the maximum undulator length to roughly 150 meters. The beam, undulator, and downstream optics parameters are then chosen to achieve the performance goals described below:

1. Soft X-ray photons from SASE and self-seeding between 0.2 and 1.3 keV at MHz rates, with an average X-ray power of 20 Watts;
2. Hard X-ray photons from SASE between 1.0 and 5.0 keV at MHz rates with an average X-ray power of 20 Watts and with the possibility of a future upgrade to self-seeding operation at energies between 1 and 4 keV;
3. Hard X-ray photons with SASE between 1 and 25 keV and self-seeding between 4 keV and 13 keV at 120 Hz, with performance comparable to or exceeding that of LCLS.

The accelerator and FEL parameters will be described in Section 3.1 while the limiting accelerator physics issues and performance simulations are described in Sections 3.2 and 3.3, respectively. A more complete listing of the accelerator and FEL parameters can be found in Appendix A. They are documented in the *LCLS-II Parameters Physics Requirements Document*, LCLSII-1.1-PR-0133.

3.2 Accelerator and FEL Requirements

A schematic of the LCLS-II facility is shown in Figure 3-1. The electron accelerator will include a new 4 GeV superconducting rf linac (SCRF) and will re-use the existing 15 GeV LCLS copper rf linac (CuRF). The LCLS-II SCRF linac will be composed of superconducting RF cavities in Continuous Wave (CW) operation to accelerate the electron beam to 4 GeV at up to a 1-MHz bunch rate while the existing CuRF linac will continue to operate at a maximum repetition rate of 120 Hz. The layout of the new SCRF linac is similar to that of the LCLS linac. The electron beams are generated in an RF gun and injector that accelerates the electron beam to 100 MeV. Next is a laser heater to reduce the microbunching instability. Three more linac sections, which are separated by the two bunch compressors, form the two-stage bunch

compression system, similar to the LCLS two-stage bunch compressor system. The injector and new SCRF linac will replace the existing SLAC copper linac in sectors 0 through 7, while the remaining copper RF structures in sectors 7-10 will be replaced with a simple beam pipe and FODO focusing lattice (the "extension line").

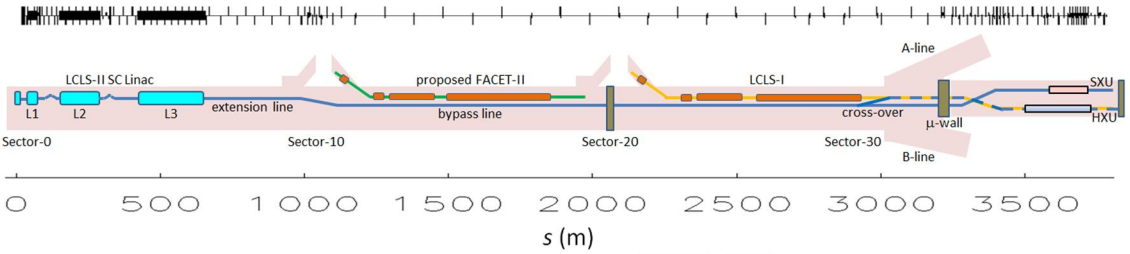

Figure 3-1. Schematic layout of the LCLS-II in the SLAC linac tunnels. The total length of LCLS-II beamline is roughly 5.7 km. Because much of the beamline already exists, only modest modifications will be required for LCLS-II.

At the end of the SCRF linac, the existing PEP-II high-energy ring (HER) Bypass line (suspended from the SLAC tunnel ceiling) will be modified to transport the electron beam from the exit of the extension line in Sector 10 through roughly 1.5 km of linac tunnel. A Beam Spreader will then deflect bunches from the SCRF linac into a high-power beam dump or into one of two possible undulators, a HXR undulator and a SXR undulator, installed in the existing LCLS undulator hall. The CuRF linac joins the beamline to the HXR after the spreader.

3.2.1 HXR and SXR Undulators

The HXR and SXR undulators are described in the *LCLS-II Undulator Systems Requirements PRD*, LCLSII-3.2-PR-0038, as well as in Chapter 8. The SXR undulator can be fed from the SCRF linac, while the HXR undulator can be fed from either the SCRF or the CuRF linacs, although not from both simultaneously. The undulators will be installed in the existing LCLS Undulator Hall. A schematic of the undulator layout appears in Figure 3-2.

Both undulators are variable-gap hybrid permanent-magnet undulators. The HXR undulator has a period of 26 mm, close to that of the existing LCLS undulator, while the SXR undulator has a period of 39 mm. The maximum length of the existing LCLS Undulator Hall is roughly 150 meters. This will allow for the installation of up to 35 segments for the HXR, with each segment being 3.4 meters long followed by an interspace of 1.0 meters for a quadrupole, phase shifter, RF BPM, and *x* and *y* steering coils, To support self-seeding, two of these undulator slots will be reserved for self-seeding monochromators. The self-seeding configuration is described in the *Hard X-ray Self-Seeding (HXRSS) System Requirements PRD*, LCLSII-3.2-PR-0102. The baseline will include 32 HXR segments plus two self-seeding slots, one of which contains the self-seeding monochromator; the other is reserved for a future upgrade.

The SXR undulator can be shorter, and there will be 21 SXR undulator segments plus one empty slot for the self-seeding monochromator, a concept of which is described in the *Soft X-ray Self-Seeding (SXRSS) System Requirements PRD*, LCLSII-3.2-PR-0101. Development of the

SXRSS is ongoing as described in Chapter 8. The last three SXR undulator slots are reserved for the future installation of polarization control undulators, and the space upstream of the SXR undulator may be used for future seeding installations or additional undulators for two-color X-rays or other upgrades. (Some of these upgrade options are described in Chapter 17.)

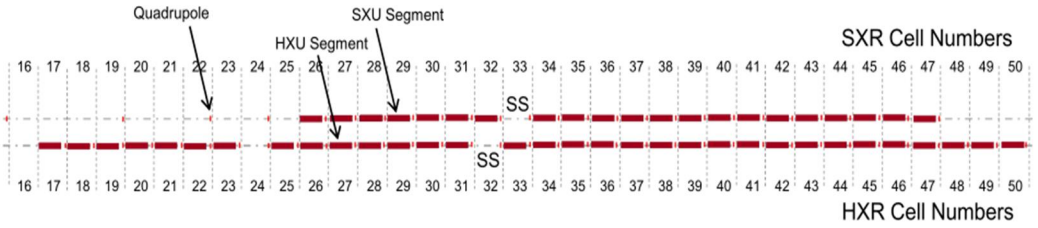

Figure 3-2. Schematic of the undulator layout. The total length represented in this figure is roughly 150 m, and the two undulators are separated horizontally by 2.5 m.

3.2.2 SCRF Linac Requirements

The beam parameters from the SCRF linac, listed in Table 3-1, include performance specifications for the nominal bunch charge of 100 pC as well as the performance ranges and jitter limits. To optimize the FEL performance for a variety of experiments, the LCLS-II is being designed to operate with a wide range of bunch charges ranging from 10 to 300 pC. The maximum repetition rate of the SCRF linac is 0.929 MHz (the injector RF frequency: 1300/7 MHz ≈ 185.7 MHz, divided down to the drive laser oscillator frequency: 185.7/5 MHz ≈ 37.14 MHz, and reduced again to: 37.14/40 MHz ≈ 0.9286 MHz to fill every 40^{th} oscillator cycle). This is consistent with the 1.3 GHz linac, the low-frequency RF gun, and the existing constraints of the SLAC timing system.

The linac is being designed to accelerate 300 μA up to >4GeV for 1.2 MW of beam power, which is sufficient to ultimately generate more than 100 Watts of X-rays in up to ten individual undulator beamlines. The initial LCLS-II configuration will be limited to a maximum power of 250 kW by the downstream beam dump capacity. It only includes sufficient RF power to accelerate 100 uA up to 4 GeV.

The SCRF linac is described in the *LCLS-II Linac Systems Requirements PRD*, LCLSII-2.4-PR-0041, and the *SCRF 1.3 GHz Cryomodule PRD*, LCLSII-4.1-PR-0146. The nominal beam energy is 4.0 GeV, however, as listed in Table 3-1. The installed 1.3 GHz RF cavities (thirty-five 8-cavity cryomodules (CMs)) can accelerate the beam to 4.65 GeV on crest phase, at the 16 MV/m average gradient and with all 280 cavities powered. Achieving 4 GeV beam energy assumes the phasing needed for bunch compression, that roughly 6% of the installed cavities (18 of the 280 cavities) are nominally unpowered to be used as spares if and when they are needed, and that roughly 1% of the installed RF is reserved for the energy feedback systems. The cryogenic system, described in Chapter 7, is designed to cool the 280 cavities with an average Q_0 of 2.7×10^{10} when accelerating the beam to 4 GeV. It is expected that there will be less than 25% variation in the Q_0 of the cavities. The gradient of the individual cavities will be adjusted as to

keep a reasonably constant heat load and to limit field-emission radiation. The cavities will be qualified to operate at 18 MV/m with a $Q_0 > 1x10^{10}$.

Table 3-1. Electron beam operational parameters at SCRF linac end, including rms stability requirements.

Electron Beam Parameters	symbol	nominal	range	units
Final electron energy (operational)	E_f	4.0	2.0-4.14 [1]	GeV
Electron bunch charge (limited by beam power)	Q_b	0.10	0.01-0.3	nC
Max. bunch repetition rate in linac (CW) [2]	f_b	0.62	0-0.93	MHz
Average electron current in linac	I_{av}	0.062	0.001-0.3 [3]	mA
Average electron beam power at linac end (limit)	P_{av}	0.25	0-1.2 [4]	MW
Norm. rms transverse slice emittance at undulator	$\gamma\varepsilon_{\perp\text{-}s}$	0.45	0.2-0.7 [5]	μm
Final peak current (at undulator)	I_{pk}	1000	500-1500	A
Final rms bunch length (at undulator)	σ_{zf}	8.3	0.6-52	μm
Final estimated useable fraction of bunch duration	$\Delta\tau_f/\tau_f$	~50	-	%
Total magnetic compression (cathode to undulator)	C_T	85	25-150	-
Final slice energy spread (rms, with heater)	σ_{Es}	500	125-1500	keV
Estimated RMS Beam Stability Goals:				
Relative rms electron energy stability (at und.)	$(\Delta E/E_f)_{rms}$	< 0.01	-	%
Relative rms peak current stability (at und.)	$(\Delta I/I_{pk})_{rms}$	< 5	-	%
Bunch arrival time stability (rms, at und.)	$(\Delta t_b)_{rms}$	< 20	-	fs
Transverse centroid stability (rms, at und., 100 pC)	$\Delta x_{rms}/\sigma_x$	< 10 [6]	-	%

A schematic of the linac is shown in Figure 3-3. The bunch compression system is designed to be similar to that operating at the LCLS. There is a laser heater at roughly 100 MeV and a two-stage bunch compressor with compression stages at 250 MeV and then 1.6 GeV. The compression system is designed to compress the beams from the injector by roughly a factor of 100. Upstream of the first bunch compressor is a harmonic linearizer that consists of two cryomodules, each containing eight 3.9 GHz SCRF cavities. The 3.9 GHz cryomodules are described in the *SCRF 3.9 GHz Cryomodule PRD*, LCLSII-4.1-PR-0097.

The bunch compressors for the SCRF linac are described in the *LCLS-II BC1 Bunch Compressor PRD*, LCLSII-2.4-PR-0039, and *LCLS-II BC2 Bunch Compressor PRD*, LCLSII-2.4-PR-0040. As illustrated in Figure 3-3, compressing the nominal bunch charge of 100 pC to 1 kA requires running the first portion of the linac at 12 and 21 degrees off-crest in L1 and L2,

1 Upper limit is with all 1.3-GHz RF gradients at 16 MV/m, nominal phasing, and 6% of cavities off.
2 BSY dump steals pulses at a few kHz as a keep-alive and to limit the linac beam power to 250 kW.
3 The average current is limited to 0.1 mA with the present RF amplifiers (0.3 mA with upgrade).
4 The linac is designed for 1.2 MW of beam power although more FEL lines are needed to operate there.
5 The transverse emittance varies with approximately the square-root of the bunch charge.
6 Defined as the rms variation of the position or angle centroid normalized to its rms size.

respectively, along with 65 MV of the 3.9 GHz RF system operating 150 degrees off-crest (decelerating). In this configuration, the maximum beam energy is 4.14 GeV. Other configurations require larger or smaller off-crest phasing, although the beam energy of 4.0 GeV could be maintained even with 30-degree off-crest operation for the bunch compressor system. The bunch compressor system will be capable of generating bunches with peak currents between 500 and 1500 A and also compressing the bunch by roughly a factor of 100. Not all peak currents will be achieved over the full charge range, however.

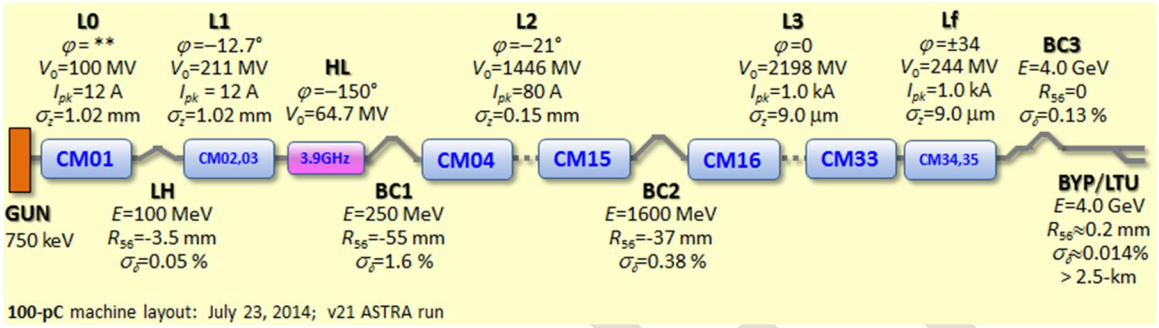

Figure 3-3. Injector, linac, and bunch compression layout used in the start-to-end simulations presented below (100 pC/bunch). Seven L0 phase are shown since the 8th cavity is off.

The performance of the X-ray FEL's depends sensitively on achieving its electron beam parameters. The LCLS-II SCRF linac will use a CW RF gun operating at 185.7 MHz to deliver a high-brightness beam. The LCLS-II transverse beam emittance at the undulators will be a function of the bunch charge. The slice emittances along the core of the beam at the undulators are shown in Figure 3-4 as a function of bunch charge. The projected emittance of 95% of the beam may be increased relative to the slice emittance, but the dilution will be less than 50%. The injector, which is described in the *LCLS-II Injector Systems Requirements PRD*, LCLSII-2.4-PR-0041, must be able to produce beams that allow for 10% slice emittance dilution through the downstream beam transport.

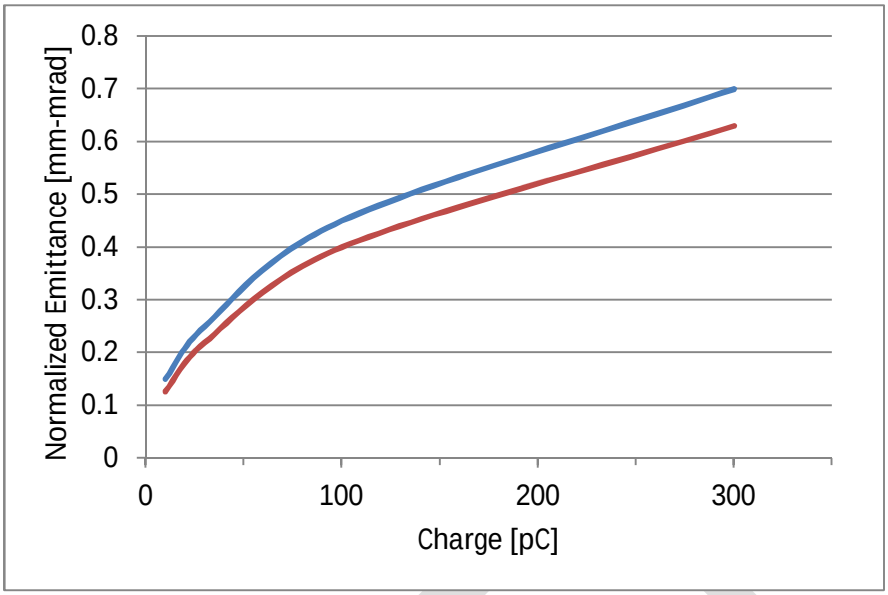

Figure 3-4. Electron slice emittance versus bunch charge at undulators (blue) and injector (red); injector must allow for 10% dilution of slice emittances.

3.2.3 Electron Beam Parameters from the CuRF Linac

The electron beam parameters of the existing CuRF linac, listed in Table 3-2, are based on those of the LCLS. The LCLS-II project requires no modifications to the existing LCLS injector, linac or bunch compressor systems. The beam transport in the Beam Switch Yard (BSY), downstream of the LCLS linac, will be modified as part of an Accelerator Improvement Project (AIP) to allow a connection to the transport line from the LCLS-II SCRF linac. A DC dipole will be used to direct the beam from either the SCRF or the CuRF linac into the transport line to the HXR undulator.

Table 3-2. Electron beam parameters from the CuRF linac in the LCLS-II; the beam from the CuRF linac will be very similar to that produced currently in the LCLS

Electron Beam Parameters	symbol	nominal	range	units
Final electron energy (operational)	E_f	13.6	2.5-15	GeV
Maximum upgrade energy (or reduced duty factor)	E_{max}	17	-	GeV
Electron bunch charge (limited by beam power)	Q_b	0.13	0.02 - 0.30	nC
Bunch repetition rate in linac (CW)	f_b	120	0 - 120	Hz
Normal rms transverse slice emittance (nom. charge)	$\gamma\varepsilon_{\perp\text{-}s}$	0.45	0.2 - 0.7	μm
Final peak current	I_{pk}	3000	500 - 4500	A
Final rms bunch length	σ_{zf}	4.3	0.5-52	μm
Final slice energy spread (rms)	σ_{Es}	1300	500-2000	keV

3.2.4 FEL Performance

The accessible photon wavelengths from the SXR and HXR undulators are plotted in Figure 3-5 versus electron beam energy accessible from the SCRF linac. The undulator parameters are chosen to optimize operation at 4.0 GeV. At the nominal SCRF energy of 4.0 GeV, the SXR beamline can cover the photon energy range of 250 eV to 1.3 keV in either SASE or Self-Seeded mode. To access lower photon energies, such as 200 eV, the linac energy would be decreased to 3.6 GeV. As illustrated in Figure 3-2, a Self-Seeding monochromator will be installed after the first seven undulator segments. The SXR undulator length is >20% longer than that required to saturate in all of these operating modes.

At the nominal SCRF energy of 4.0 GeV, the HXR can cover the photon energy range of 1.5 to 5 keV in SASE mode. For the HXR to access lower photon energies, such as 1 keV, the linac energy would be decreased to 3.3 GeV. Over most of the photon energy range, the HXR undulator length is >20% longer than that required to saturate. However with 100 pC bunch charge, there is little margin at 5 keV, and the photon pulse energy is decreased to a few μJ. In this case, the 20% margin in undulator length can be gained by operating the SCRF linac at the maximum energy of roughly 4.2 GeV or operating at lower bunch charge and thereby lower beam emittance. With 20 pC per bunch, more than 20 μJ of X-rays per pulse are expected.

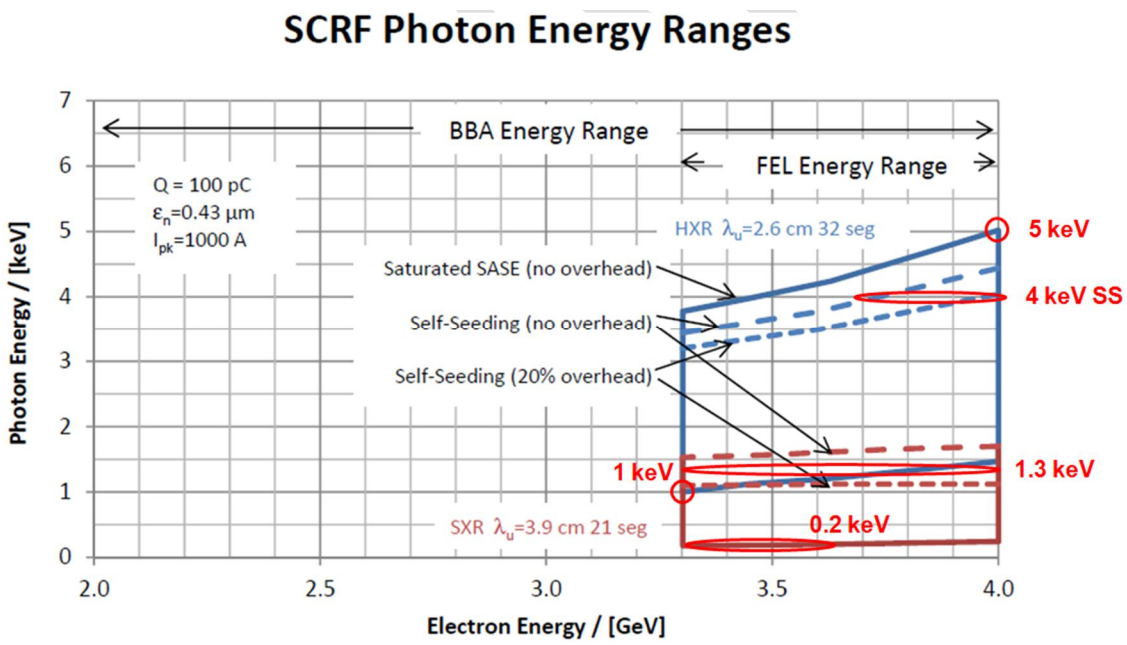

Figure 3-5. Photon Energy versus beam energy from SCRF linac for the HXR (blue) and SXR (red) undulators.

Figure 3-6 and Figure 3-7 illustrate the estimated X-ray pulse energies for the SXR and HXR as a function of the photon energy when fed by the SCRF linac with 100 pC per bunch. Figure 3-6 shows the calculated pulse energy without a post-saturation taper, and Figure 3-7 shows the calculated pulse energies with a post-saturation taper. As is discussed in Section 3.4, current

Start-2-End (S-2-E) simulation results are as much as 50% smaller than the values shown in Figure 3-6 and Figure 3-7. Further optimization is expected to improve the S-2-E performance.

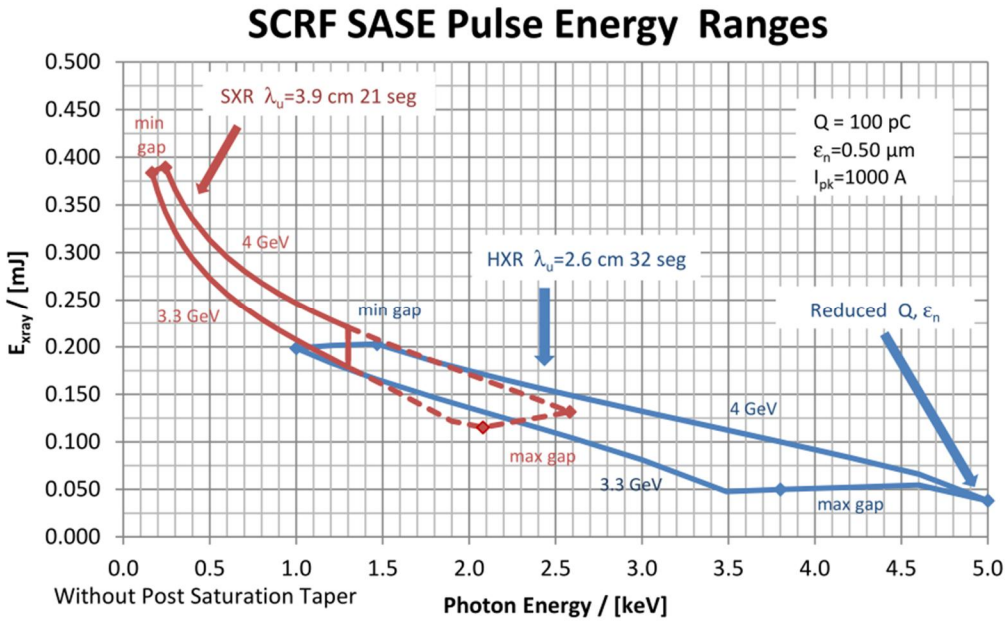

Figure 3-6. **Calculated X-ray pulse energies versus photon energy for the SXR (red) and the HXR (blue) underlators without a post-saturation taper for 100 pC per bunch. The energy per pulse scales roughly with the square root of the bunch charge.**

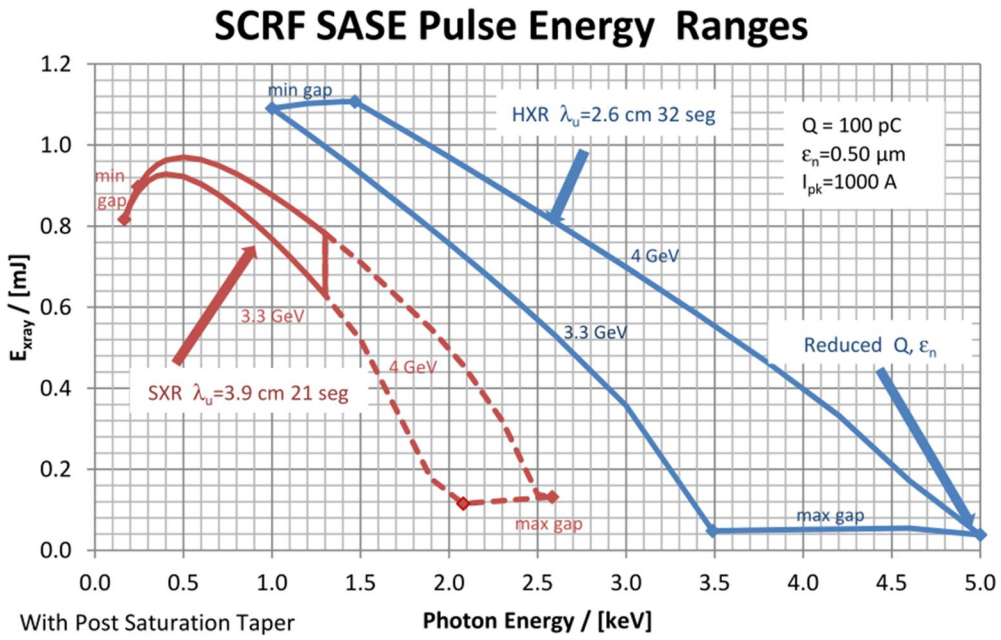

Figure 3-7. **Calculated X-ray pulse energies versus photon energy for the SXR (red) and the HXR (blue) undulators with a post-saturation taper for 100 pC per bunch. The energy per pulse scales roughly with the square root of the bunch charge.**

The tuning range of the HXR FEL, when driven by the existing CuRF linac, is illustrated in Figure 3-8, along with the performance of the LCLS undulator. When fed by the CuRF linac, the

HXR undulator can cover the photon energy range from 1.0 to 25.0 keV in SASE mode. The undulator tolerances will be set to ensure operation at the most stringent wavelength, namely 25 keV. When fed by the CuRF linac, the HXR undulator can also operate in Self-seeded mode for photon energies between 4.0 and 12 keV, as is also illustrated in Figure 3-8. The Self-Seeding monochromator will be installed after the first 14 undulator segments. The HXR undulator length is >20% longer than that required to saturate in all of these CuRF operating modes.

Figure 3-9 illustrates the calculated X-ray pulse energy versus the photon energy for the HXR FEL when fed by the CuRF linac with 130 pC per bunch and compressed to 3 kA (similar to the LCLS operation). Because of the shorter undulator period, the X-ray pulse energy from the HXR FEL will be slightly lower than that of the LCLS at photon energies of a few keV. However, the LCLS-II HXR will be able to generate X-rays over a much wider range of wavelengths than the LCLS.

Finally, when the HXR or SXR undulators are supplied by the SCRF linac, the average X-ray beam power at the experiments is specified to be a minimum of 20W in the *LCLS-II Project Requirements Document GRD*, LCLSII-1.1-GR-0018. The undulators will be able to supply even more X-Ray beam power over most of the operating range, as illustrated in Figure 3-10, and the X-ray transport system is designed to accept up to 200 W of X-rays, as described in the *LCLS-II X-ray Transport and Experimental Systems (XTES) PRD*, LCLSII-3.5-PR-0051. The capability of operating at higher power provides a large margin in achieving the baseline 20 W X-ray power.

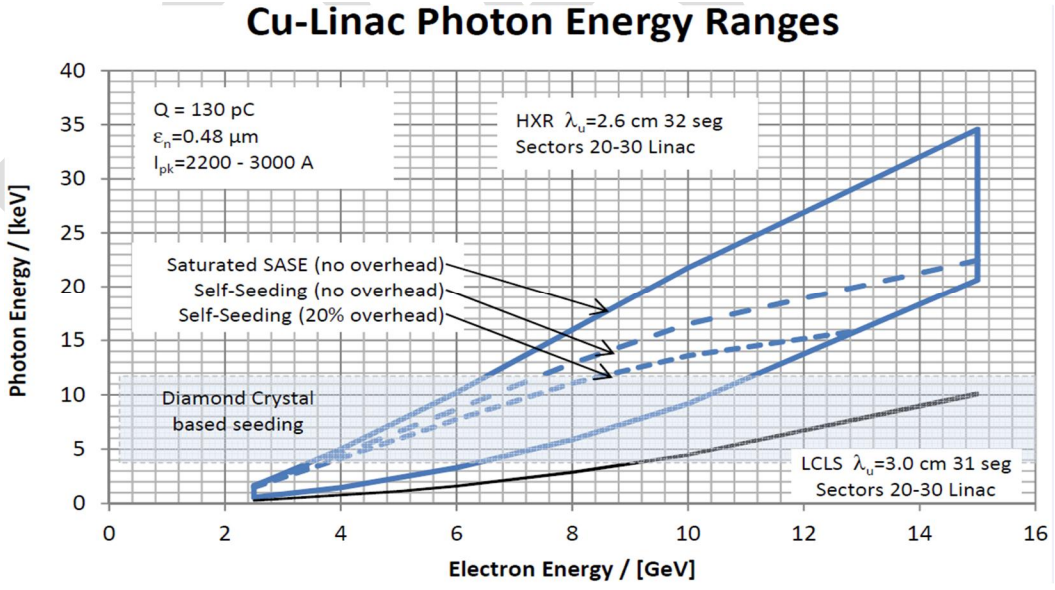

Figure 3-8. Photon Energy versus beam energy from CuRF linac for the HXR (blue) undulator. The performance of the LCLS 30-mm-period undulator is also noted (black).

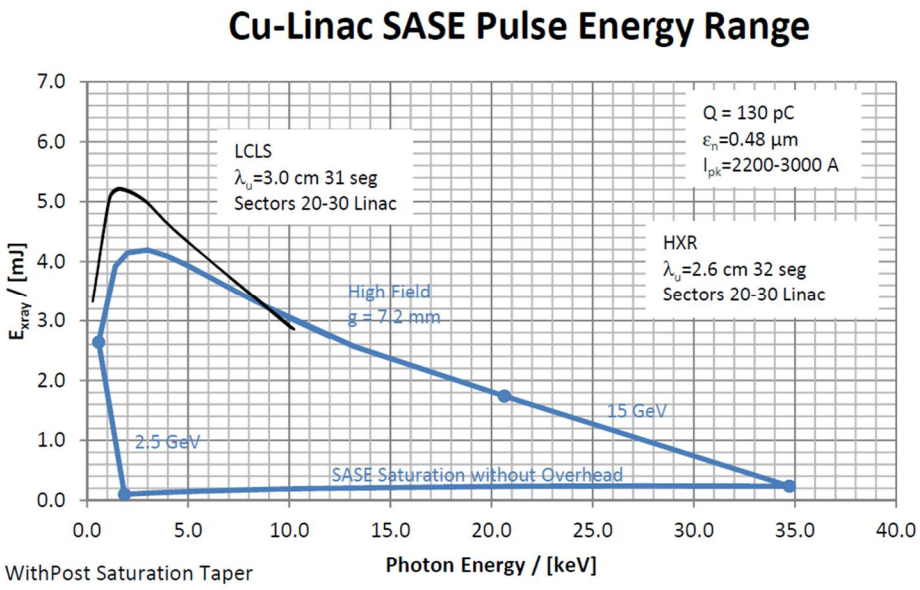

Figure 3-9. **Expected performance — X-ray pulse energy versus photon energy (wavelength) — for HXR (blue) as driven by the existing Cu linac Sectors 20-30 at 120 Hz. The performance of the existing LCLS 30-mm-period undulator is also noted (black). The new HXR undulator would deliver comparable performance over the 1-to-10 keV photon energy range and would also be able to provide X-rays with energies as high as 25 keV.**

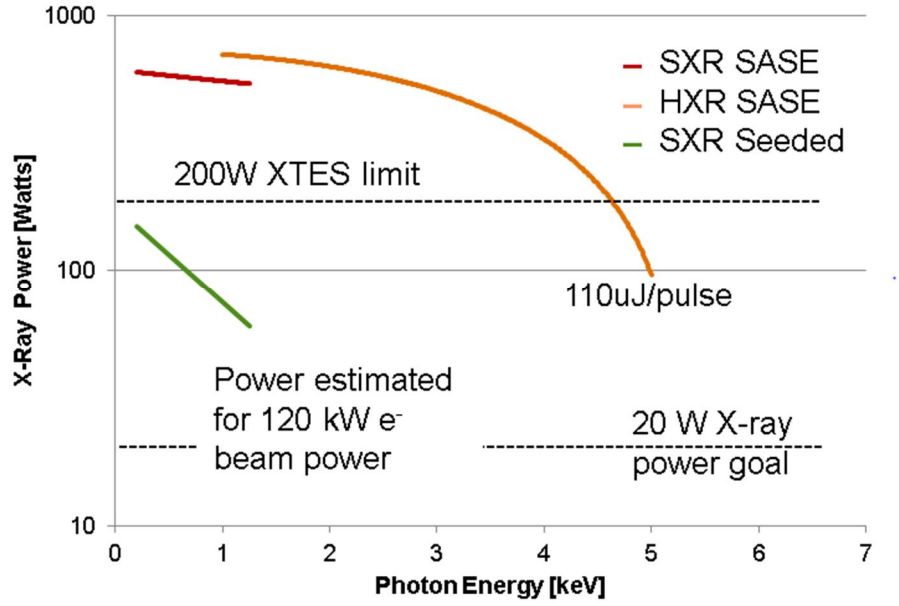

Figure 3-10. Maximum X-ray power from the undulators for the SXR SASE (red), SXR Self-Seeding (green), and HXR SASE (orange) when operating the SCRF linac at 4.0 GeV and 1 MHz.

3.2.5 FEL Operating Modes

The LCLS-II will be flexible in its operating modes consistent with the maximum x-ray beam power, the maximum electron beam power to the BSY and undulator dumps, the maximum repetition rate and the range of bunch charges. As noted above, the HXR can be fed from either the SCRF linac or the CuRF linac, while the SXR can be fed only from the SCRF linac. The BSY Beam Spreader can direct the SCRF linac beam arbitrarily toward either undulator or to the BSY dump. The design does not presently include the capability of delivering different bunch charges or peak currents to the two undulators simultaneously, however. That capability may be developed in the future.

Because of transients induced when changing the beam current profile and timing, the time required to change the rate in the SCRF linac is limited by the damping time of the feedback systems. When operating with a high-repetition-rate beam, we expect that this time will be a fraction of a second. The time needed to switch between the SCRF linac and the CuRF linac will be dominated by the time required to change out the DC magnets and re-establish the electron beam. This should take less than one hour.

The very high average power of the accelerated CW electron beam makes it undesirable to terminate the beam anywhere other than in specially-designed beam dumps. Materials struck by the full-power beam in a persistent manner for more than roughly 100 microseconds may be damaged, possibly leading to a breach of the vacuum chamber. For this reason, several accelerator operating modes are envisioned for initial low-power commissioning, recovery from RF trips, recovery from beam-loss trips, and startup from shut-down periods. These modes are configured to allow machine setup and diagnosis, but are defined at much lower average-power levels to protect the beamline components during these less controlled, more transient startup periods. Beams sent to different destinations may operate in different modes at the same time. For example, it should be possible to tune up low-power beams going to one undulator while simultaneously delivering full-power beams to the other. Examples of possible operating SASE modes are listed in Table 3-3 below.

Table 3-3. Examples of possible operating modes in the LCLS-II.

Configuration	Linac Parameters	SXR	HXR
High rate to SXR and HXR	*SCRF: 4 GeV, 0.929 MHz; 60 pC* *CuRF: off*	50-200 W at 1 keV (120-450 uJ at 460 kHz)	20 W at 3 keV (43 uJ at 460 kHz)
High rate to SXR and medium pulse energy at HXR	*SCRF: 4 GeV, 0.150 MHz; 100 pC* *CuRF: off*	80-200 W at 250 eV (600-1500 uJ at 130 kHz)	20 W at 1.5 keV (2 mJ at 10 kHz)
Medium rate and pulse energy at SXR and HXR	*SCRF: 4 GeV, 0.030 MHz; 100 pC* *CuRF: off*	20 W at 500 eV (2 mJ at 10 kHz)	20 W at 4 keV (2 mJ at 10 kHz)
High rate to SXR and high pulse energy at HXR	*SCRF: 4 GeV, 0.410 MHz; 100 pC* *CuRF: 15 GeV, 120 Hz, 130 pC*	200 W at 250 eV (500 uJ at 400 kHz)	0.5 W at 3 keV (4 mJ at 120 Hz)
High rate to SXR and short wavelength at HXR	*SCRF: 4 GeV, 0.929 MHz; 30 pC* *CuRF: 15 GeV, 120 Hz, 130 pC*	50 - 200 W at 1.2 keV (50-200 uJ at 920 kHz)	0.1 W at 25 keV (500 uJ at 120 Hz)

3.2.6 LCLS-II Availability and Operational Schedule

The LCLS operates for roughly 9 months per year, and it is expected that LCLS-II will be operated in a similar manner. Operation will be 24/7 with a scheduled downtime of roughly five 8-hour shifts every week for machine development, preventative maintenance and upgrades. The availability of the accelerator and X-ray transport systems should be better than 95%, so it should be possible to deliver X-rays during 95% of the scheduled operation.

Engineering will be needed on critical components to maximize the Mean-Time-Between-Failure (MTBF) and minimize the Mean-Time-To-Repair (MTTR). In some places, such as the injector laser systems, redundant systems with hot spares may be required. In others, spare modules or cavities may be used, with an example being the spare 1.3 GHz cavities in the SCRF linac. It is expected that achieving the design availability will take two to three years after the LCLS-II project completion. Details of the planned allocation of the availability requirements can be found in the *LCLS-II Availability Requirements PRD*, LCLSII1.1-PR-0163 and are discussed in Chapter 12.

3.3 Physics Differences between LCLS and LCLS-II

The LCLS-II has been designed based on extensive technical developments in SCRF technology and the progress in understanding X-ray FELs that has been pioneered at the LCLS. The design leverages the work that was completed on CW FEL designs as part of the NLS design in the UK [1] and the NGLS design that was developed at LBNL [2].

In many ways, the physics of the LCLS-II is similar to that of the LCLS, providing confidence in the LCLS-II design. However, it also differs in some significant aspects. Three differences, in particular, impact the LCLS-II performance: First, the CW beam is accelerated in an SCRF linac; second, the SCRF linac can provide high average current and beam power, and, third, the SCRF linac has lower beam energy. These differences and the performance and design implications are discussed below.

3.3.1 SCRF Linac and CW Operation Issues

The SCRF linac operating in CW mode has four impacts. First, the dynamic heat load in the cryomodules (the heat load due to the accelerator voltage) is large. Dealing with this heat load requires a large cryogenic plant (discussed in Chapter 7) and the project has had an intensive effort to improve the cavity Q_0 to reduce the requirements on this cryoplant, as discussed in Chapters 6 and 16.

Second, the electron beam injector has to be qualitatively different from the pulsed RF gun operating at LCLS. Since the FEL performance is critically dependent on the electron beam phase space, a significant effort has been made to develop a high-performance CW injector system. The baseline injector for the LCLS-II is modeled after the APEX RF gun at LBNL [3]. This system has the potential to produce beams with roughly the same transverse phase space as the LCLS gun but with much lower peak current than the LCLS injector, and the longitudinal phase space is

expected to have significant non-linearity which will limit the bunch compression. The baseline injector system, described in Chapters 4 and 5, is designed to provide beams with emittances comparable to those in the LCLS that can be compressed to roughly 1 kA versus 3 to 4 kA in LCLS. Also possible is a DC gun operating at a lower voltage but with a more complicated capture system. As described in Chapter 16, the project is working with Cornell to demonstrate such a DC injector.

Third, the CW RF system with bunches spaced by roughly 1μs offers the potential for much greater stability than the existing LCLS 120 Hz pulsed linac. The RF cavities have a loaded-Q of a few 10^7, corresponding to ~10 ms timescale for fluctuations. Furthermore, beam-based feedback will be able to stabilize the beam energy and transverse position over a very wide range of timescales. The LCLS-II specifications for rms stability (see Table 3-1) are $\Delta E/E < 0.01\%$, $\Delta I/I_{peak} < 5\%$, $\Delta t < 20$ fs, and $\Delta X,Y/\sigma_{X,Y} < 10\%$ without fast beam-based feedback, which is not part of the baseline project but can be installed at a later time to further improve stability.

Lastly, extensive study has been made of the trapped and untrapped HOMs in the SCRF linac [4,5,6]. The potential issues include beam instabilities, component heating, and transient ringing. The RF cavities include two HOM couplers to damp the trapped HOMs to the point where they have little impact on the beam and broadband HOM absorbers at the end of each cryomodule to absorb the broadband power so that it does not contribute significantly to the heat load in each cryomodule. The HOM couplers and absorbers are discussed further in Chapter 6.

Although the HOMs are relatively small, they will cause ringing after transients in the current or trajectory. These can be minimized using procedures to slowly ramp the beam current or trajectory where again, the timescales are set by the Qs which are the order of 10^5 ~ 10^7 corresponding to current ramps that are measured in 10's of ms. While such timescales are not expected to be any limitation for the FEL operation, if desired, the timescales could be shortened using feedforward to anticipate the changes. To further limit the transients in the SCRF linac, it is planned to establish high-repetition-rate beam to the BSY Beam Dump and then adjust the rate to the undulators using the Beam Spreader without changing the beam through the linac.

3.3.2 Beam power issues

The SCRF linac can accelerate significant beam power. The linac is designed to generate 1.2-MW of electron beam although the initial implementation will be limited to 250 kW. This high beam power has a number of implications that are quite different from the LCLS. First, the Machine Protection Systems (MPS) for LCLS-II has to be much more aggressive than LCLS with a response time as short as 100 μs to prevent component damage. Furthermore, because the facility is so large, it is important to have a mid-way abort dump where the beam can be parked before the source is stopped or rate reduced. As described in Chapter 4, the BSY Beam Dump provides this function; the MPS issues are described further in the Machine Protection System Physics Requirements Document.

Second, the beam halo on the high power beam needs to be carefully controlled and this requires a well-designed collimation system. The maximum beam power to each undulator is

limited to 120 kW but, as described in Chapter 8, to achieve a 10-year lifetime, the losses in the undulators must be limited to 12 mW. The LCLS-II includes a multi-stage collimation system in the baseline design which consists of four stages of (x, p_x, y, p_y, ΔE) collimation. If necessary, additional stages can be added and additional collimators can be added to each stage. The collimation systems are described in greater detail in Chapter 4 and the Beam Halo PRD. The collimation simulations are being compared against LCLS experiments to provide confidence in the design [ref].

Third, radiation protection issues must be considered much more carefully. These are discussed in depth in Chapter 13, and many Physics Requirement Documents have been written for all of the impacted sub-systems: *Environmental Radiation Monitoring Requirements*, LCLSII-1.2-PR-0265*; Workplace Radiation Monitoring Requirements*, LCLSII-1.2-PR-0153*; Requirements for Air Ventilation Controls for Radiation Protection of Workers and Public*, LCLSII-1.2-PR-0160*; Radiological Requirements for LCW Systems*, LCLSII-1.2-PR-0211*; Radiation Protection Requirements for the Injector*, LCLSII-1.2-PR-0XXX*; Radiation Protection Requirements for the Halo Collimators*, LCLSII-1.2-PR-0259*; Radiation Protection Requirements for the CEDOG Collimator*, LCLSII-1.2-PR-0260*; Radiation Protection Requirements for the D10 Alternative Location in the Muon Wall*, LCLSII-1.2-PR-0261*; Radiation Protection Requirements for the Beam Transport Hall*, LCLSII-1.2-PR-0263*; Radiation Protection Requirements for DUMP/B Main Dumps*, LCLSII-1.2-PR-0100; and *Radiation Protection Requirements for XTES*, LCLSII-1.2-PR-0122.

The Beam Containment System (BCS) is designed to prevent the electron or X-ray beams from leaving the specified beam channels and possibly impacting personnel while the MPS is designed to prevent damage to the accelerator components. Both are specified in the respective PRDs: *BCS Requirements (Electron Beamlines) Document*, LCLSII-2.4-PR-0107, and *Machine Protection System Physics Requirements Document*, LCLSII-2.4-PR-0XXX. The radiation protection systems are designed to prevent radiation from escaping the accelerator housing including activation of the ground, water or air. In addition, the radiation protection system is designed to handle an accident involving the Maximum Credible Beam (MCB) for both the electrons and photons that can arise if BCS and MPS fail. The MCB for electrons is defined in the *LCLS-II Electron Beam Loss and Maximum Credible Beam Physics Requirements Document*, LCLSII-2.7-PR-0079, while that for the x-ray beam is defined in XX. The facility is being designed for a MCB of 2 MW at the end of the linac and in the undulator hall. Such high electron beam power might also be able to generate very high X-ray powers, and the MCB for X-rays has been calculated to be less than 8 kW at XX.

The radiation protection design will drive a number of changes in operating procedures compared to the LCLS including reduced access to the Beam Transfer Hall which crosses the SLAC Research Yard above ground. These are discussed further in Chapter 13.

3.3.3 Low beam energy and long transport lines

Because the SCRF linac is expensive, the beam energy has been chosen to be as low as that consistent with generating a saturated SASE pulse at 5 keV with the nominal beam parameters. The HXR undulator period of 26mm was chosen to be close to the LCLS period of 30 mm to ensure comparable performance when fed from the CuRF linac. In this case, an electron beam energy of 4 GeV will just saturate in the HXR undulator, assuming an energy spread of 600 keV, an emittance of 0.45 mm-mrad and a peak current of 1 kA.

The low energy section of LCLS-II is similar to LCLS in that the laser heater is located at 100 MeV (versus 135 MeV in LCLS) and BC1 is located at 250 MeV (versus 250 MeV in LCLS). However, the effective acceleration gradient is much lower due to the lower fill factor of the SCRF cryomodules and the inclusion of significant collimation sections. Furthermore, the location of BC2 is at much lower energy of 1.6 GeV (versus 4.5 GeV in LCLS). Finally, the 4 GeV LCLS-II electron beam is transported in a long bypass line around the rest of the existing SLAC linac.

All of these effects will increase the impact of space charge effects and Coherent Synchrotron Radiation (CSR). Space-charge driven micro-bunching in the laser heater region has led to a redesign of the laser heater chicane and optics changes downstream. Transverse and longitudinal space charge effects still appear to be important downstream of BC1, and future optics modifications will focus on moderating these effects. In BC2, the fractional effect and the resulting emittance dilution is much stronger for the same peak current than in LCLS because the energy deviation due to CSR is roughly independent of the beam energy. Finally, at relatively low energy, space charge effects in the long transport lines downstream of the linac cause a significant micro-bunching instability. The present design includes seven small chicanes that locally compensate the R_{56} (longitudinal dispersion) of the bending systems downstream of BC2. While this compensation appears to moderate the micro-bunching instability, additional work will be required to further optimize the design. We are performing experiments on the LCLS operating at ~4 GeV to benchmark the micro-bunching physics and simulation codes [ref].

3.4 Performance simulations

Particle tracking studies have been performed over the full machine — from injector, through the accelerator, and into the FEL — by stringing together results from several computer codes, including *ASTRA* [7] (for the injector), *Elegant* [8] (through the linac), and *Genesis-1.3* [9] (through the FELs) [10,11]. Included in the tracking are 3D space charge forces in the injector (to about 100 MeV), longitudinal wakefields in the linac, CSR in the bends and relevant drift sections, incoherent synchrotron radiation (ISR) in the bends, second-order optics (*e.g.*, chromatic and geometric effects), resistive-wall wakefields in the undulators, and 3D time-dependent FEL simulations. Furthermore, we use high-fidelity beam dynamics simulations from the injector to the undulator using the codes *IMPACT-T* and *IMPACT-Z* [12], which include 3D space charge effects along the entire transport among the other effects listed above, to make detailed analyses of the microbunching instability and final verification of the design.

We describe below the separate simulations for the injector, linac, and the two FELs. A short micro-bunching instability study is described and is followed by a description of full Start-2-End (S-2-E) simulations using *IMPACT* and *Genesis*. The injector, linac, and bunch compressors are shown schematically in Figure 3-3, including RF phase settings for each linac section, cryomodule numbering, chicane locations, and peak current levels along the machine.

At this time, the full S-2-E simulations using *IMPACT* and *Genesis* are yielding X-ray pulse energies that are as much as 50% lower than estimated using the empirical calculations benchmarked against LCLS, although they are still many times greater than needed to meet the baseline specification of 20 Watts. As described in Section 3.2, there are some reasons for this reduction. However, we still expect that the performance will improve with additional optimization. Unfortunately, a full *IMPACT* simulation is time consuming, making the optimization process slow.

3.4.1 Injector Simulations

The LCLS-II injector system consists primarily of a normal conducting electron RF gun, operating in CW mode at 185.7 MHz (1300/7 MHz), a buncher, and an 8-cavity cryomodule operating at 1.3 GHz. The beamline also includes focusing and steering magnets, beam diagnostics, vacuum hardware and a sweeper to minimize dark current. The injector layout, including the laser heater system, is shown in Figure 3-11.

The simulation code used to model the low-energy effects, including space charge and $\beta < 1$ effects, is *ASTRA*, which has been widely used and extensively benchmarked against experiments as well as other simulation codes. The simulations have also been benchmarked against *GPT* [ref] , and both codes have been compared against experimental results from Cornell and LBNL. The initial transverse distribution of the bunch is radially symmetric in transverse position and Gaussian in transverse momenta, as expected in the case of photoemission from a cathode illuminated by a transversely uniform laser. For the longitudinal component, a beam distribution in the range of a few tens of ps and a rise/fall time of 2 ps is assumed for the emission time, whereas a Gaussian distribution is assumed for the longitudinal momentum component. This arrangement provides a factor of three velocity-based bunch length compression over the length of the injector. Detailed parameters of the individual components can be found in the relevant PRDs [13,14].

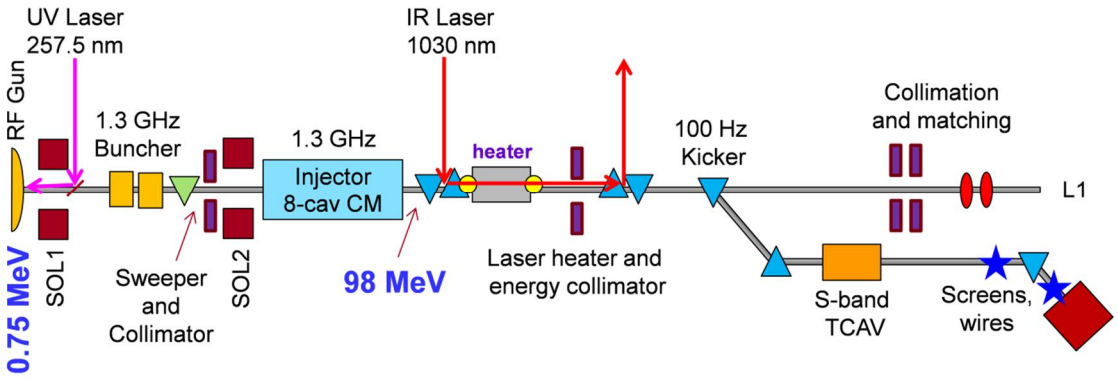

Figure 3-11. Injector layout from RF gun through first 8-cavity cryomodule including the laser heater system and diagnostic section. Parameters can be found in the relevant PRDs.

Figure 3-12 shows the results (as an example) of tracking 0.625 x 10^9 electrons (using 2.5 x 10^5 macro-particles) representing a 100 pC electron bunch through *ASTRA*, which includes space charge forces, up to the exit of the CM01 accelerator section at ~100 MeV, which is expected to be a high enough energy where space charge forces are less important (as is similar in LCLS).

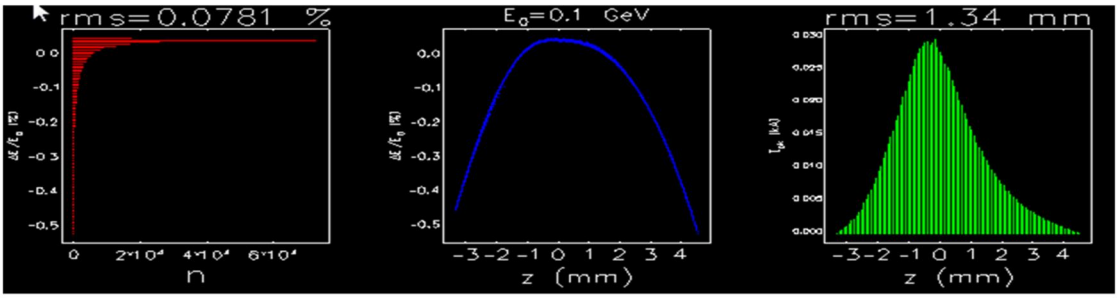

Figure 3-12. Energy distribution (left), longitudinal phase space (center) and current profile (right) for a typical 100 pC electron beam charge injector simulation.

3.4.2 Linac Simulations

The LCLS-II linac layout for a 100 pC bunch charge is shown schematically in Figure 3-3, with the laser heater, the two compressor chicanes (BC1 and BC2), 35 12-m-long, 1.3-GHz RF cryomodules, one 3.9 GHz linearizer RF system, and the final beam switching. The RF phasing, chicane strengths, peak current, energy, and rms energy spread are indicated at each step of the figure.

The macro-particle coordinates from the *ASTRA* run described above are now fed into the linac's next simulation stage, starting from injector output up to the entrance of the HXR undulator. The parameters used for the linac start-to-end simulations (using the computer tracking code *Elegant*) can be found in the relevant PRDs [15]. The accelerator optics functions, from the injector to the HXR dump, are shown in Figure 3-13.

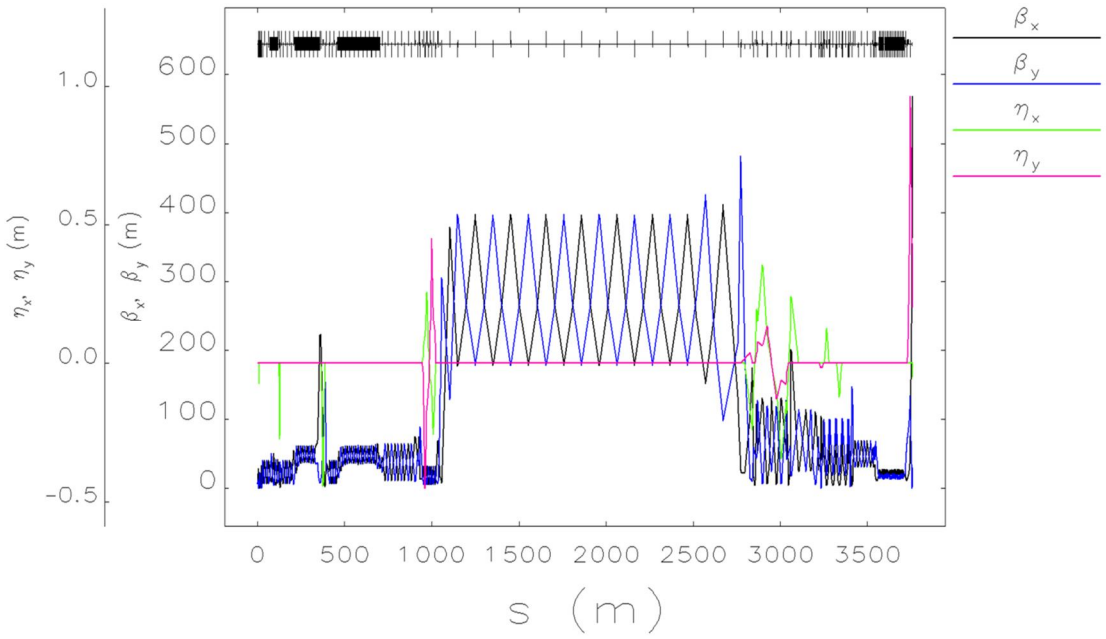

Figure 3-13. Optics across the entire LCLS-II, from the injector to the HXR dump at 4 GeV.

Figure 3-14 shows the evolution of the projected transverse emittances from the injector to the HXR undulator, as well as the slice emittance and slice energy spread, as a function of the electron beam coordinate at the entrance to the HXR undulator at 4 GeV. While the horizontal projected emittance increases slightly around s ~ 300 m, due to CSR effects in the BC2 chicane, and both the x and y projected emittances increase incrementally around s ~ 1000 m at the rolled Dogleg bends, which transport the linac beam up to the bypass line on the tunnel ceiling, the slice emittance is not much impacted. The time-sliced transverse emittance values in the core of the beam are $\gamma\epsilon_{x,y}$ ~ 0.3 μm, while the time-sliced relative energy spread is 0.012 percent (500 keV) rms in the beam core, where the peak current is I ~ 900 A (see Figure 6).

We have performed transport optimizations for various charge distributions that cover most of the LCLS-II operational range. Figure 3-15 shows the electron beam current distribution, longitudinal phase space, and relative energy spread profiles for three such charge distributions at the entrance to the HXR undulator: 20 pC, 100 pC, and 300 pC.

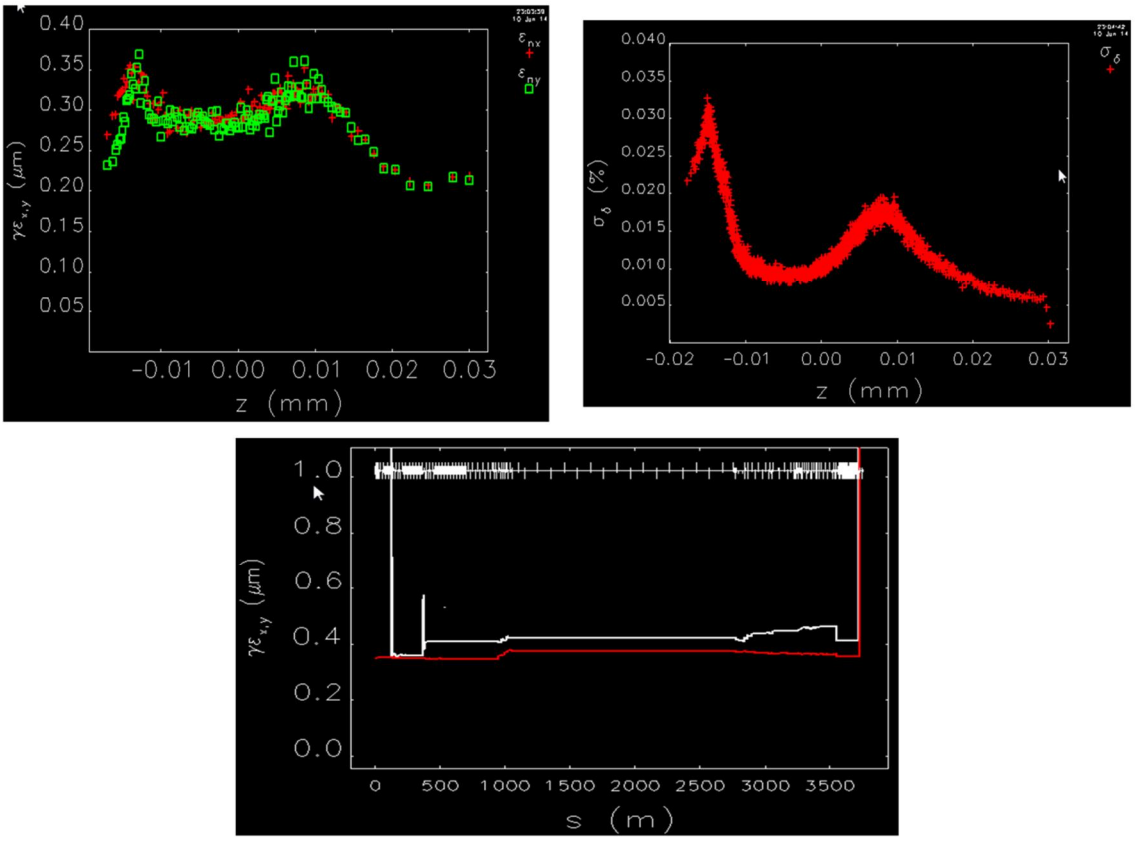

Figure 3-14. The transverse slice emittance (top left) and slice energy spread (top right) at the entrance to the HXR undulator at an electron energy of 4 GeV. The evolution of the transverse projected emittances from the injector to the entrance of the HXR undulator.

Studies have also been made of the error sensitivity in the SCRF linac [16] using the Lucretia code [17], which was developed for the linear collider community. The impact of misalignments in the SCRF linac is small, and the tolerances as specified in the *SCRF 1.3 GHz Cryomodule PRD*, LCLSII-4.1-PR-0146, are relatively loose.

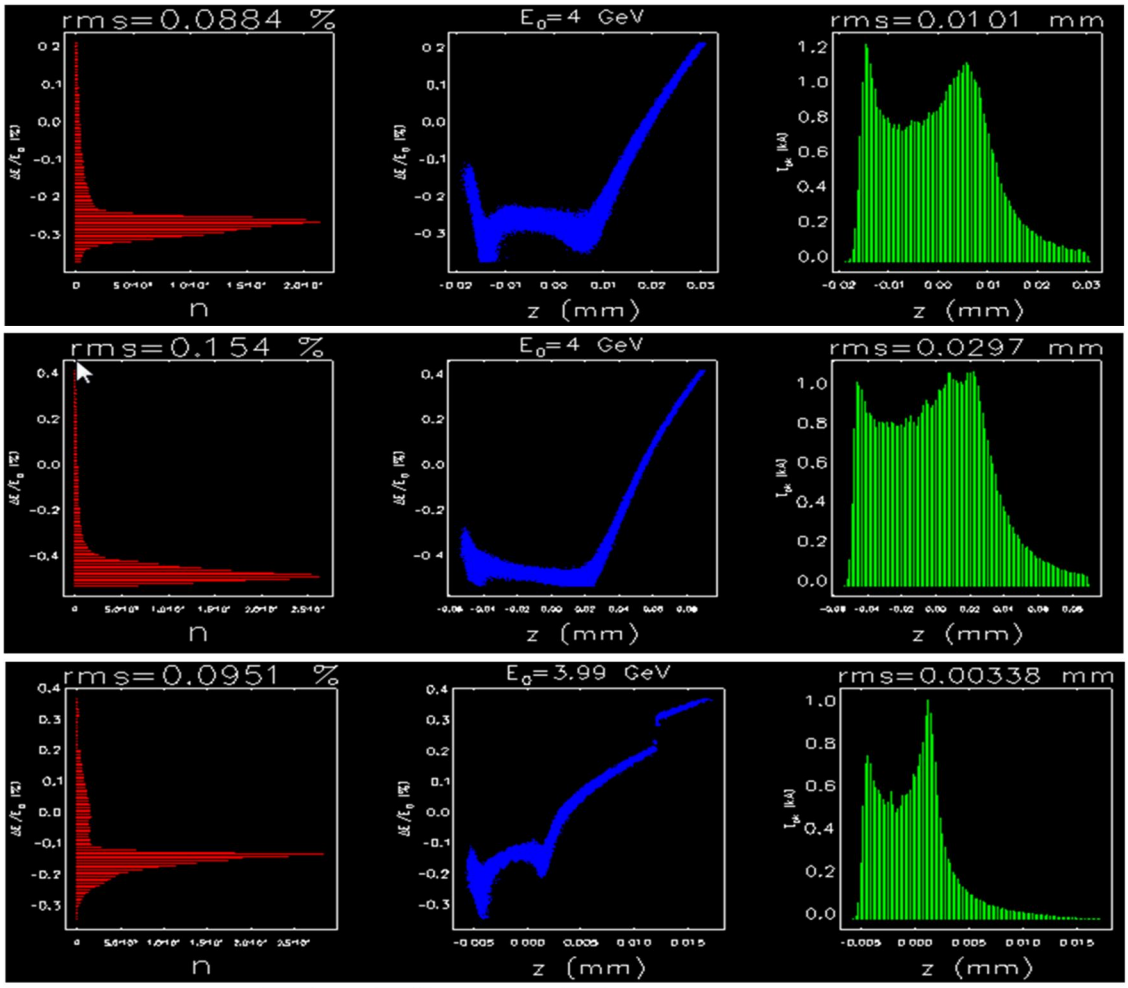

Figure 3-15. The relative energy spread profile (left column), longitudinal phase space (middle column), and peak current distribution (right column) for 100 pC (top row), 300 pC (middle row) and 20 pC (bottom row) charge distributions at the entrance to the HXR undulator.

3.4.3 FEL Simulations

Multiple modes of FEL operation are simulated for both the SXR and HXR undulator beamlines. These modes include, but are not limited to, SASE, self-seeded, high-gain harmonic generation (HGHG), and echo-enabled harmonic generation (EEHG). In addition, we have explored various advanced techniques used to produce narrow bandwidth pulses, including harmonic lasing, pSASE and iSASE. All of the start-to-end FEL simulations include the effects of resistive wall wakefields and spontaneous-undulator radiation-induced energy spread. Below, for illustrative purposes, we discuss the results of SXRSS simulations at E_γ = 1.24 keV photon energy, as the higher end of the tuning range is typically the most difficult for FELs to reach.

The SXRSS system consists of two undulators that are separated by a monochromator and a magnetic chicane. The first undulator consists of seven independently gap-tunable segments, while the second undulator consists of 14 independently gap-tunable segments. The monochromator and chicane occupy the equivalent space of a single undulator segment located

nominally in the N=8 segment position along the strong focusing quadrupole FODO cell strongback. The output macro-particle distribution from the above *Astra* and *Elegant* runs is used to specify the particle distribution used in *Genesis* FEL simulations. This start-to-end particle distribution is matched into the first undulator section with an average beta function $<\beta> = 12$ m. The first undulator section is responsible for generating the seed. The particle and field distributions from *Genesis* are dumped to disk after propagation and amplification in the first undulator section.

The energy of the light produced at this location is E ~ 1 μJ, while the average power along the longitudinal profile of the light is about P_{Avg} ~ 15 MW. The effective source size and location within the seventh undulator can be found by backwards propagation of the full three-dimensional field distribution to the waist position as a function of frequency. At this point, the particle distribution is converted to an *Elegant* macro-particle file and is tracked through a 4-dipole chicane to capture any relevant collective effects. A phenomenological approach is used to model the bandwidth reduction of the seed after transport through the monochromator. The nominal monochromator design's relative bandwidth (1/R = 1/5000) and overall efficiency (~2%) are used to specify a Gaussian filter function that is applied in the frequency domain to each transverse location of the field distribution. The phase of the filter function is defined through Kramers-Kronig relations such that the calculation does not violate causality when the filter is applied to the FEL pulse exiting the seventh undulator section. The monochromatized seed typically has a power P ~ 20 – 30 kW, which is well above the shot noise level of the electron beam (a few hundred Watts). The macro-particle distribution that was tracked through the chicane is then used to specify the electron beam in the seeded undulator section, which interacts with the monochromatized field distribution in a final downstream *Genesis* simulation. These simulations are run to saturation, the results of which can be found in Figure 3-16 for 10 independent iterations.

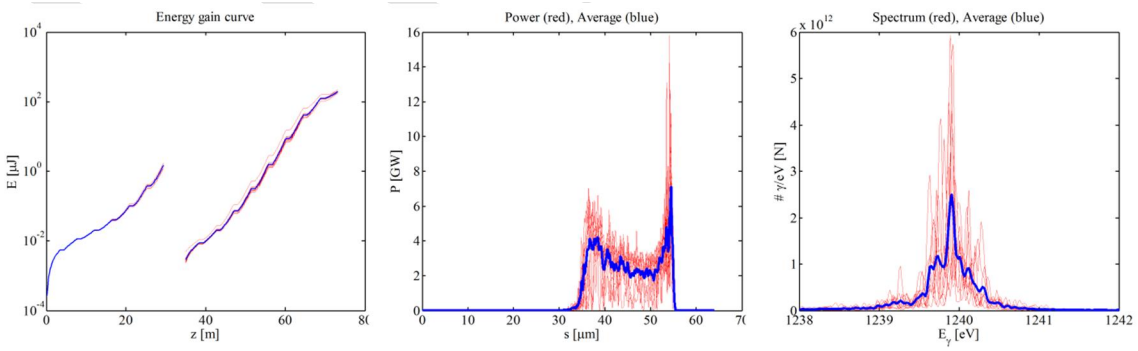

Figure 3-16. The energy gain curve (left), longitudinal power profile (center) and spectrum (right) of 10 independent SXRSS simulations (thin, red lines) and their average (thick, blue line).

The seeded FEL reaches saturation after 16 out of 21 undulator modules with a total average energy E_{avg} ~ 200 μJ and a relative spectral bandwidth of about 1 x 10^{-4}, which is comparable with the monochromator bandwidth, as expected.

3.4.4 Microbunching Simulations

The microbunching instability is modeled using high-fidelity macro-particle simulations using the simulations codes *IMPACT-T* and *IMPACT-Z*, which include three-dimensional space charge and CSR effects (among others). For these simulations, the number of macro-particles used is equal to the real number of electrons. These simulations typically begin with a smooth model of only a short longitudinal section of the electron beam having a flattop current profile and a Gaussian uncorrelated energy spread. This represents only a small fraction of the full 100 pC electron beam. Studies have been made in this manner of the laser heater, BC1, transport through BC2, and transport from the exit of BC2 to the undulators.

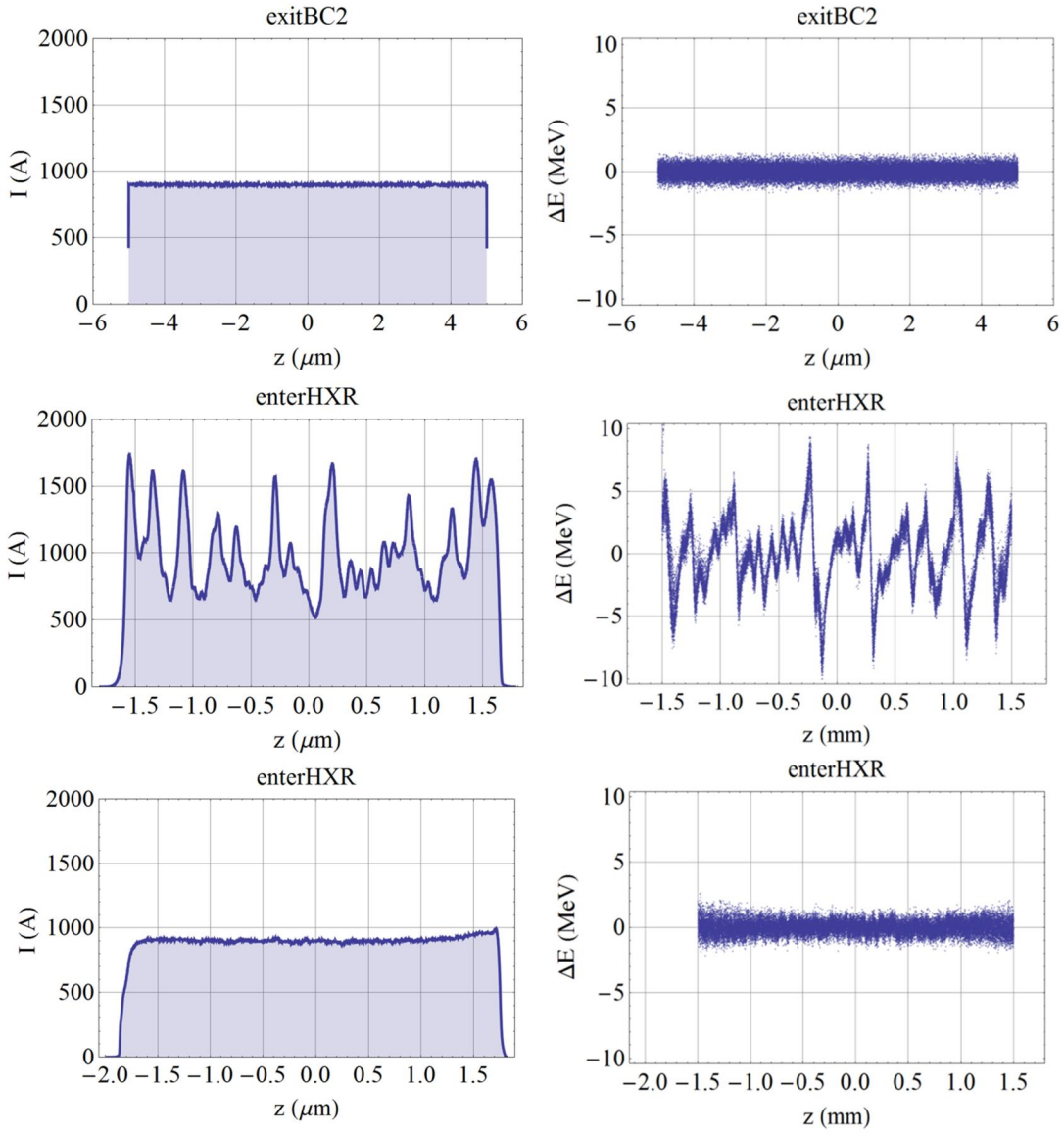

Figure 3-17. Current profile (left column) and energy spread distribution (right column) of an idealized beam tracked in *IMPACT* to model the microbunching instability. The initial distribution after BC2 (top row), the distribution at the HXR undulator entrance showing the effects of the microbunching instability (middle row) and

the same distribution when local R56 compensation chicanes in the Dogleg and LTU sections are included showing the suppression of the instability.

These studies have allowed us to optimize the laser heater and downstream optics, the compression ratios in BC1 and BC2, and the downstream transport. Results have caused the optics about BC1 and BC2 to be improved and the laser heater chicane to be lengthened from ~3 meter to more than 9 meters. Downstream, microbunching on the sub-μm scale develops through the Dogleg and LTU sections between the Muon Shield wall and the FEL beamlines, as can be seen in Figure 3-17. We found that we can suppress the microbunching instability by making the doglegs in the transport isochronous. We accomplished this by placing local R_{56} compensation chicanes near the dogleg bends, as discussed in Chapter 4. We are also investigating the option of performing a final bunch compression at the end of the Bypass line so that the space charge effects through L3 and the most of the transport are greatly reduced.

3.4.5 Full S-2-E Simulations

In addition to these idealized simulations with *IMPACT*, we are currently optimizing full start-to-end (S-2-E) tracking for multiple charge distributions with three-dimensional space charge effects. These studies use *IMPACT-T* from the gun and then transition to *IMPACT-Z* from the injector to the undulator. We use *Genesis* to track through the undulator. These *IMPACT* simulations use a number of macro-particles in the distribution equal to the number of electrons in the beam and are being used to fully verify the space charge effects on the beam and the FELs. In parallel, an experimental study at LCLS using the post-undulator X-band TCAV is being performed to benchmark the *IMPACT* simulation fidelity.

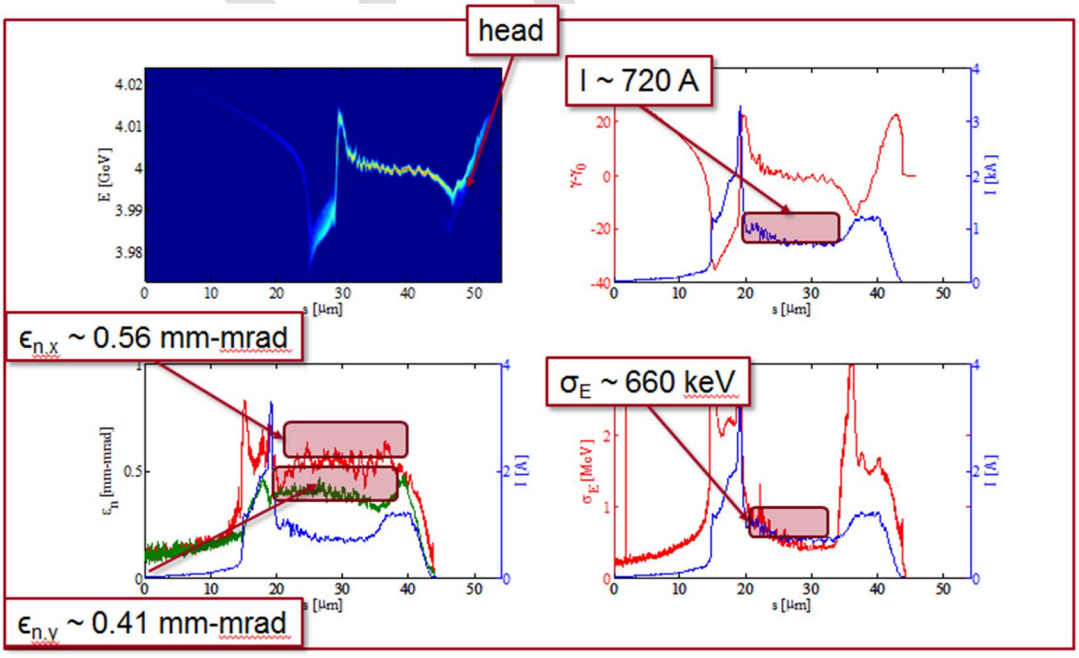

Figure 3-18. Results from IMPACT tracking for 100 pC into HXR undulator; upper left is longitudinal phase space; upper right current profile versus energy; lower left are

X and Y emittances and current profile; lower right is energy spread and current profile.

An example of an *IMPACT* run is shown in Figure 3-18 for 100 pC into the HXR undulator. Microbunching is visible in the longitudinal phase space and results have a lower peak current, larger energy spread and larger emittance than the results from the *Elegant* tracking seen in Figure 3-15. The impact of the poorer phase space has little effect on the spectrum but degrades the output power. Examples of Genesis simulations are shown in Figure 3-19 and Figure 3-20 for 2 and 4 keV photons from the HXR.

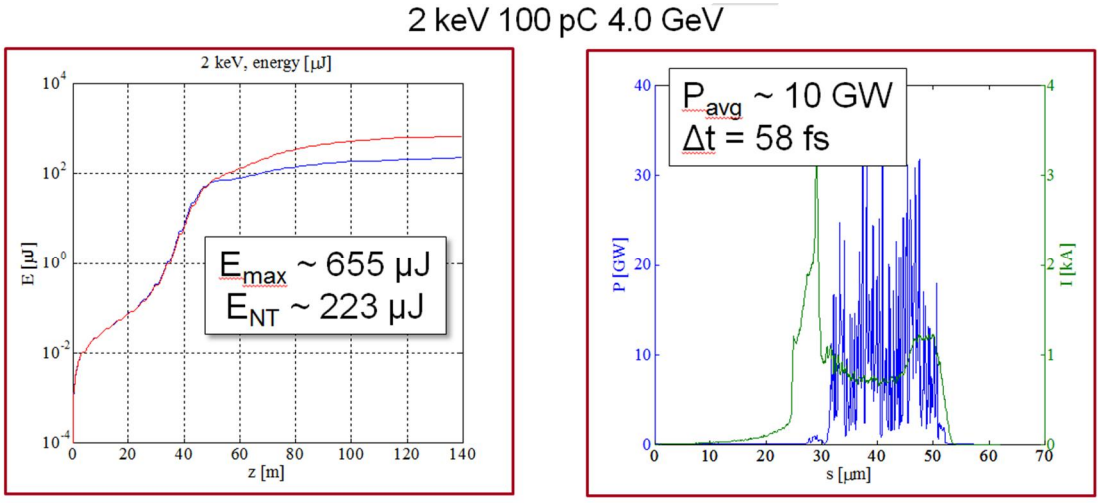

Figure 3-19. Genesis simulation of IMPACT beam in HXR at 2 keV with photon pulse energy (left) for both tapered and untapered undulator configurations; power and current profile versus bunch longitudinal position (right) for the tapered case.

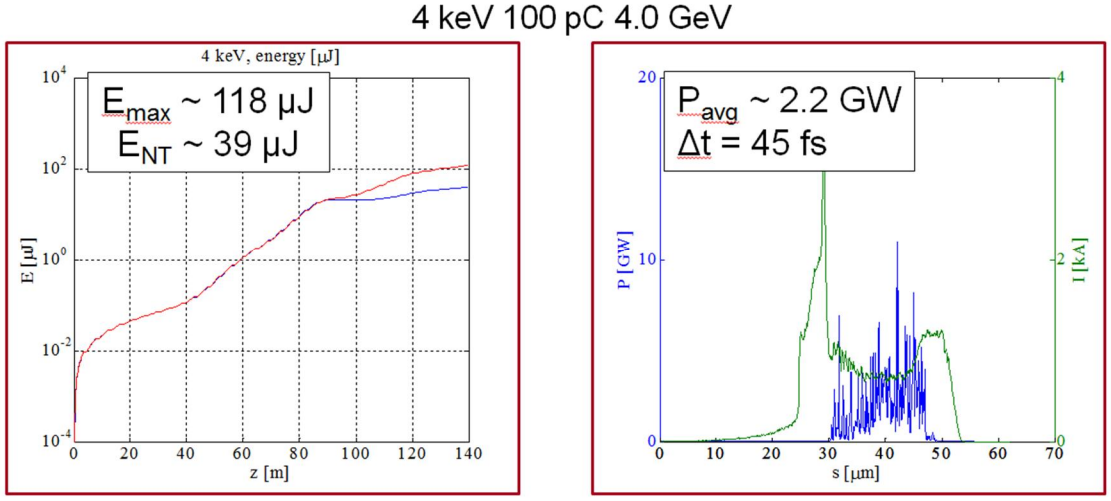

Figure 3-20. Genesis simulation of IMPACT beam in HXR at 4 keV with photon pulse energy (left) for both tapered and untapered undulator configurations; power and current profile versus bunch longitudinal position (right) for the tapered case.

The pulse length is slightly reduced and, at 2 keV, the pulse energy is reduced by about 30% from expectations shown in Figure 3-6 and Figure 3-7. At 4 keV, which is much more sensitive to the beam emittance and energy spread, the reduction of the output pulse energy versus expectation is nearly a factor of four.

As described, the simulations are being optimized to reduce the impact of the space charge effects. Options that will be studies include smoother matching across transitions and delayed bunch compression. Such modifications will have a small cost impact on the design and can be implemented late in the construction cycle. We expect future optimization will significantly improve the results.

3.5 References

1 http://www.newlightsource.org/documents/NLS%20CDR%20Consolidated%20Final.pdf.

2 http://www.lbl.gov/ngls/. ((Do weblink references need text descriptors?))

3 F. Sannibale, et al., Phys. Rev. ST - Accel. and Beams 15 (2012) 103501.

4 K. Bane, et al, "Some Wakefield Effects in the Superconducting RF Cavities of LCLS-II," LCLSII-TN-13-04 (2013).

5 N. Solyak, et al., "HOM's and HOM coupler in 1.3 GHz SCRF Linac," LCLSII-TN-14-04 (2014).

6 K. Bane, et al., "Untrapped HOM Radiation Absorption in the LCLS-II Cryomodules," LCLSII-TN-14-08 (2014).

7. K. Floettmann, ASTRA: A space charge tracking algorithm. User manual available at http://www.desy.de/~mpyflo/Astra documentation.

8. M. Borland, Report No. ANL/APS LS-287, 2000.

9. S. Reiche, Nuclear Instruments and Methods in Physics Research A 429 (1999), pp. 243-248.

10. S. Reiche et. al., Start-To-End Simulation for the LCLS X-ray FEL, Nuclear Instruments and Methods in Physics Research A 483 (2002), 70–74.

11. M. Borland et. al., Start-To-End Jitter Simulations of the Linac Coherent Light Source, In proceedings of PAC-2001, Chicago, IL, USA, June 2001. -

12. J. Qiang et al., J. Comput. Phys. 163, 434 (2000).

13. LCLS-II Gun and Laser Heater Systems, LCLSII-2.2-PR-0085.

14. LCLS-II SCRF Injector System, LCLSII-2.2-PR-0084.

15. Linac Requirements, LCLSII-2.4-PR-0041.

16 A. Saini, et al., "Studies of Misalignment Tolerances for SC Linac of LCLS-II," LCLSII-TN-14-03 (2014).

17 http://www.slac.stanford.edu/accel/ilc/codes/Lucretia/.

4 ACCELERATOR LAYOUT

TECHNICAL SYNOPSIS

This chapter outlines the layout and overall design of the accelerator systems that will achieve the performance and parameters listed in Chapters 2 and 3.

LCLS-II electron accelerator will include a new 4 GeV superconducting linac and will re-use the existing 15 GeV LCLS copper linac. The beams from both linacs will be transported to the existing LCLS Undulator Hall, where two new undulators will be installed. The total length of LCLS-II beamline is roughly 5.7 km; much of the beamline, however, already exists and will require only modest modification for LCLS-II purposes. This chapter will describe the Accelerator layout and overall design, showing how the linac sections and components fit together. The accelerator components themselves are described in further detail in Chapters 5 through 9.

4.1 Accelerator Layout Overview

LCLS-II electron accelerator will include a new 4 GeV superconducting RF linac (SCRF) and will re-use the existing 15 GeV LCLS copper RF linac (CuRF). The overall parameters for the facility are described in Chapters 2 and the electron and photon beam parameters are described in Chapter 3. Additional detail can be found in the *LCLS-II Project Requirements Document*, LCLSII-1.1-GR-0018, and the *LCLS-II Parameters Physics Requirements Document*, LCLSII-1.1-PR-0133.

The LCLS-II SCRF linac will be composed of superconducting RF cavities, in continuous wave (CW) operation, in order to accelerate the electron beam to 4 GeV at up to a 1-MHz bunch rate, while the existing CuRF linac will continue to operate at a maximum repetition rate of 120 Hz. The layout of the new SCRF linac is similar to that of the operating LCLS linac and is illustrated in Figure 0-1. The electron beams are generated in an RF gun and injector that accelerate the electron beam to 100 MeV. The injector and new SCRF linac will replace the existing SLAC copper linac in Sectors 0 through 7, while the remaining copper RF structures in Sectors 7-10 will be replaced with a simple beam pipe and FODO focusing lattice (the "extension line"). The injector is followed by a laser heater to reduce the microbunching instability and three more linac sections that are separated by the two bunch compressors which form the two-stage bunch compression system. The injector layout is described in Section 0 while the SCRF linac is described in Section 4.3.

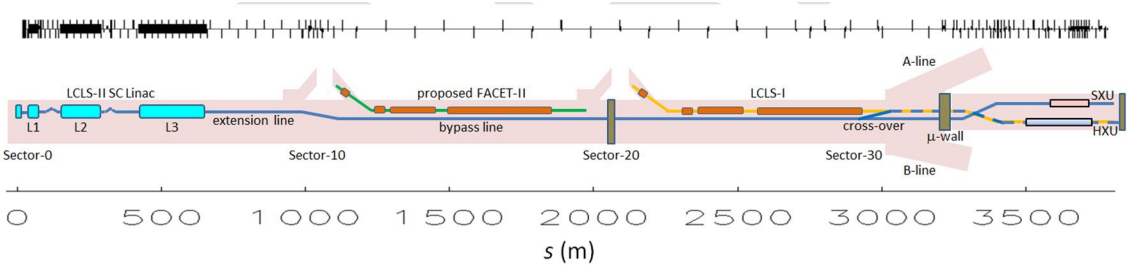

Figure 0-1. Schematic layout of the LCLS-II in the SLAC linac tunnels. The total length of LCLS-II beamline is roughly 5.7 km with both the SCRF and the CuRF linacs however much of the beamline already exists and will require only modest modification for LCLS-II purposes.

At the end of the SCRF extension linac, the existing PEP-II HER Bypass line (suspended from the ceiling of the SLAC tunnel) will be modified to transport the electron beam from the exit of the extension line in Sector 10, through roughly 1.5 km of linac tunnel. A Beam Spreader will then deflect bunches from the SCRF linac into a high power beam dump or one of two possible undulators, a Hard X-ray (HXR) undulator and a Soft X-ray (SXR) undulator, installed in the existing LCLS undulator hall.

In parallel, the existing LCLS copper linac (CuRF) will accelerate electron bunches to energies as high as 15 GeV at a rate of 120 Hz. These bunches can be sent to the HXR undulator when it is not being used by bunches from the SCRF linac or parked on a beam dump upstream of

the merger location. The layout of these transport lines is described in Section 4.4 and the overall layout of the facility is shown in Figure 0-1 with the SCRF linac in blue at far left and the SXU and HXU undulators at far right.

Table 0-1. LCLS-II Beamline regions with location along the SLAC Linac (Z-location), the initial beam energy, and the location of the description in the Final Design Report.

Region	Location Z [m]	Initial Energy [Gev]	Description
Injector	-10.0	0.0	Section 0
Linac 0 (L0)	-7.8	0.001	Section 4.3.3.1
Laser Heater	10.8	0.098	Section 4.3.4
Laser HTR Diagnostic Line	32.2	0.098	Section 4.3.5
Linac 1 (L1)	73.4	0.098	Section 4.3.3.2
Bunch Compressor 1 (BC1)	121.3	0.25 GeV	Section 4.3.6
Linac 2 (L2)	174.5	0.25 GeV	Section 4.3.3.3
Bunch Compressor 2 (BC2)	332.4	1.6 GeV	Section 4.3.7
Linac 3 (L3)	429.8	1.6 GeV	Section 4.3.3.4
L3 Extension	687.7	4.0 GeV	Section 4.3.8
Dogleg to Bypass	951.9	4.0 GeV	Section 4.4.1
Bypass Line	1254.5	4.0 GeV	Section 4.4.2
Beam Spreader	2780.6	4.0 GeV	Section 4.4.3
Beam Switch Yard (BSY) Dumpline	2780.6	4.0 GeV	Section 4.4.4
Linac-to-HXR Undulator (LTUH)	3224.0	4.0 / 15.0 GeV	Section 4.4.5
Linac-to-SXR Undulator (LTUS)	3224.0	4.0 GeV	Section 4.4.6
HXR Undulator	3559.2	4.0 / 15.0 GeV	Chapter 8
SXR Undulator	3559.2	4.0 GeV	Chapter 8
Undulator Dumplines	3717.6	4.0 / 15.0 GeV	Section 4.4.7
Diagnostics and feedback	--	--	Section 4.5.1
Collimation systems	--	--	Section 4.5.2
Magnet and tolerances	--	--	Section 4.5.3

The entire LCLS-II electron beamline is represented as a set of MAD v. 8.52 [1] optics files which are then used to automatically generate a components database for the designers and engineers. The LCLS-II beamline regions are listed in Table 0-1 along with the nominal energy, beginning Z location, and the section where further details are located in this Final Design Report. Each of these regions is usually comprised of multiple individual beamline segments and these are described in the *Beamline Boundaries Physics Requirements Document*, LCLSII-2.1-PR-0134. The individual beamline components are named as documented in *Element naming Convention for MAD Input Files Design Standard,* LCLSII-1.1-TS-0159. The MAD optics files

are also used to generate the Elegant [2] and IMPACT [3] input decks which are used for the Start-2-End beam simulations as well as the FLUKA [4] and MARS15 [5] simulations for the radiation protection studies. The LCLS-II coordinate systems are described in the *LCLS-II Beamline Coordinates Design Standard*, LCLSII-1.1-TS-0034.

The LCLS-II design includes extensive diagnostics to ensure that the accelerator can be tuned to produce the high quality beams that are needed for the FELs. In addition, the new beamlines connected with the SCRF linac will include extensive collimation to allow them to operate with high-power, MW-class electron beams. To avoid unnecessary repetition in the description of each area, Sections 4.5.1 and 4.5.2 presents an overview of the Diagnostic and Collimation systems. Similarly, magnet systems and the associated alignment and jitter tolerances are system-wide and are also described in Section 4.5.3. Other systems that span the accelerator include the Controls and Safety systems, described in Chapter 10, the site infrastructure to LCLS-II, described in Chapter 11, and the Radiation Protection design, described in Chapter 13.

4.1.1 Major Accelerator Layout Changes since CDR

A number of significant modifications have been made to the design since the development of the LCLS-II Conceptual Design Report in February 2014. These include:

1. Updated design of the beamline between RF gun and the first cryomodule, CM01, to allocate space for necessary diagnostics, vacuum control, and the cryomodule end-cap.
2. Lengthening of the laser heater chicane to reduce the microbunching effects.
3. Addition of a betatron collimation stage after the laser heater to remove halo particles at low energy.
4. Addition of four more 3.9 GHz cavities for a total of sixteen to ensure ability to linearize bunch; the division of the 3.9 GHz cavities into two 8-cavity cryomodules instead of three 4-cavity cryomodules; placement of 3.9 GHz cavity couplers on alternate sides of cryomodule to reduce coupler RF deflections; moved location of 3.9-GHz sections to be placed in widest portion of the linac tunnel.
5. Removed betatron collimation stage after the first bunch compressor, BC1, but left space to install collimators at a later time if necessary.
6. Removed parallel diagnostic line (DIAG1) after BC1 and allocated space to install desired diagnostics such as transverse deflecting cavities, OTR screens, and beam stopper, in-line at a later time.
7. Increased space between central bends in BC1 and BC2 chicanes to place additional diagnostics and energy collimator.
8. Allocated space after BC2 for additional in-line diagnostics such as TCAV and OTR screens to be added at a later time as needed.

9. Moved bypass Dogleg to ease cryomodule installation through Sector 10 spur and to allow future installation of CuRF injector in the Sector 11 stub.
10. Removed the BC3 bunch compressor from the Bypass line.
11. Removed Bypass line parallel to the diagnostic line and added diagnostics in-line.
12. Adopted magnetic kicker solution for the Beam Spreader, with an RF deflector as a backup solution if the kicker development proves challenging.
13. Developed isochronous beamline after the Spreader for the SXR and HXR upstream of the Muon Shield wall.
14. Moved the beam switch yard (BSY) dump into the Muon Shield wall to simplify the shielding requirements.
15. Removed the parallel diagnostic beamlines along the HXR and SXR transport lines upstream of the undulators and added necessary diagnostics in-line.
16. Removed collimation systems in HXR and SXR transport lines with direct view of undulators and moved them upstream into the BSY.
17. Elevated the HXR and SXR electron beam dumps and moved them closer together to ease tunnel modifications required for shielding.
18. Optimized optics matching sections throughout; design based on re-use of existing magnets wherever reasonable.
19. Added stoppers and tuning dumps to facilitate operation.
20. Added protection collimators as part of Beam Containment System (BCS).

4.1.2 Documentation and Schedule

A large number of Physics Requirements Documents (PRD's) have been written specifying the overall system. These are listed in Table 0-2.

Many of the systems that are described in this chapter have undergone Preliminary Design Reviews and some have undergone Final Design Reviews or are closely based on systems that have either been though Final Design Review or have been constructed. Examples include the Laser Heater, BC1, BC2, and the HXR LTU, all of which are heavily based on operating systems at LCLS. A list of the design reviews can be found in Table 0-3 and Table 0-4.

Finally, an overall schedule for the accelerator systems is shown in Table 0-5. This schedule shows the major accelerator systems Preliminary Design Review along with the major Final Design Review. It also shows the primary timelines for design, fabrication, and installation of the injector source, the injector, the linac, the transfer lines and dumps, and the controls.

The injector and injector source will be described in Section 0, while the linac is described in Section 4.3, and the transfer lines are described in Section 4.4. Section 4.5 described global systems including the diagnostics, collimation, and magnets and tolerances. The SCRF

cryomodules are described in Chapter 6 while the rest of the accelerator components are described in Chapter 5. The control system is described in Chapter 10.

Table 0-2: Accelerator Systems High-Level Requirements and Specifications.

Document Type	Title	Document Number
Physics Requirements	LCLS-II Parameters	LCLSII-1.1-PR-0133
Physics Requirements	LCLS-II Electron Beam Loss and Maximum Credible Beam	LCLSII-2.7-PR-0079
Physics Requirements	Residual Gas and Beam Stay-Clear Physics Requirements	LCLSII-2.1-PR-0234
Physics Requirements	Beamline Boundaries	LCLSII-2.1-PR-0134
Physics Requirements	Electron Beam Diagnostics Systems	LCLSII-2.7-PR-0170
Physics Requirements	SCRF 1.3 GHz Cryomodule	LCLSII-4.1-PR-0146
Physics Requirements	SCRF 3.9 GHz Cryomodule	LCLSII-4.1-PR-0097
Physics Requirements	RF Power and LLRF Requirements	LCLSII-4.1-PR-0098
Physics Requirements	LCLS-II SCRF Injector System	LCLSII-2.2-PR-0084
Physics Requirements	LCLS-II Gun and Laser Heater Laser Systems	LCLSII-2.2-PR-0085
Physics Requirements	Injector Laser Heater Requirements	LCLSII-2.2-PR-0086
Physics Requirements	Post-LH Diagnostic Beamline Requirements	LCLSII-2.4-PR-0068
Physics Requirements	BC1 Bunch Compressor Chicane Requirements	LCLSII-2.4-PR-0039
Physics Requirements	BC2 Bunch Compressor Chicane Requirements	LCLSII-2.4-PR-0040
Physics Requirements (possible Future)	BC3 Bunch Compressor Chicane Requirements	LCLSII-2.4-PR-0110
Physics Requirements	Linac Requirements	LCLSII-2.4-PR-0041
Physics Requirements	SCRF Electron Linac Extension and Bypass Line Requirements	LCLSII-2.4-PR-0091
Physics Requirements	Beam Spreader	LCLSII-2.4-PR-0090
Physics Requirements	BSY Dumpline and Dump	LCLSII-2.4-PR-0080
Physics Requirements	HXR Post-Spreader and LTU Beamlines	LCLSII-2.4-PR-0340

Physics Requirements	SXR Post-Spreader and LTU Beamlines	LCLSII-2.4-PR-0094
Physics Requirements	Dump Line Requirements	LCLSII-2.5-PR-0135

Table 0-3: Accelerator System Preliminary Design Review Schedule

Component	Date
Accelerator Systems PDR • Injector (Laser, Mechanical and Installation) • Linac • Transfer Lines & Dump • Common Systems o DC Power Supplies o RF o Cable Plant	January 2014
Couplers, PDR/FDR Combined	August 2014
Solid State Amplifiers (SSA)	October 2014
Injector Source (Gun and Load Lock, Injector)	November 2014
Collimators	June 2015
Kicker, Bend and Septum Magnets	June 2015
Magnet Quench Protection System	June 2015
SRF Vacuum Systems	September 2015

Table 0-4: Accelerator System Final Design Review Schedule

Component	Date
Injector Source	April 2016
• Gun	June 2015
• Injector RF Power System	November 2015
• Beamline Components	April 2016
Injector System	October 2016
• Mechanical Integration and Installation	August 2016
• Drive Laser System	October 2016
Linac System • BC1, Mechanical Integration and Installation • BC2, Mechanical Integration and Installation • L1, HL, L2, L3, Mechanical Integration and Installation	August 2016
Couplers, PDR/FDR Combined	August 2014
Transfer Lines and Dump	March 2016
• Bypass, Mechanical Integration and Installation	October 2015
• BSY, Mechanical Integration and Installation	March 2016
• LTU, Mechanical Integration and Installation	November 2015

• Dump, Mechanical Integration and Installation	November 2015
Kicker, Bend and Septum Magnets	November 2015
Collimators	November 2015
Cable Plant - Bypass	November 2015
Power Conversion FDR	June 2016
• DC Power Supplies	
• Quench Protection System	
Solid State Amplifiers (SSA)	August 2016
SRF Vacuum Systems	August 2016
High Power RF	August 2016
Cable Plant	November 2016
Accelerator Systems	December 2016

Table 0-5. Accelerator Systems Production Schedule

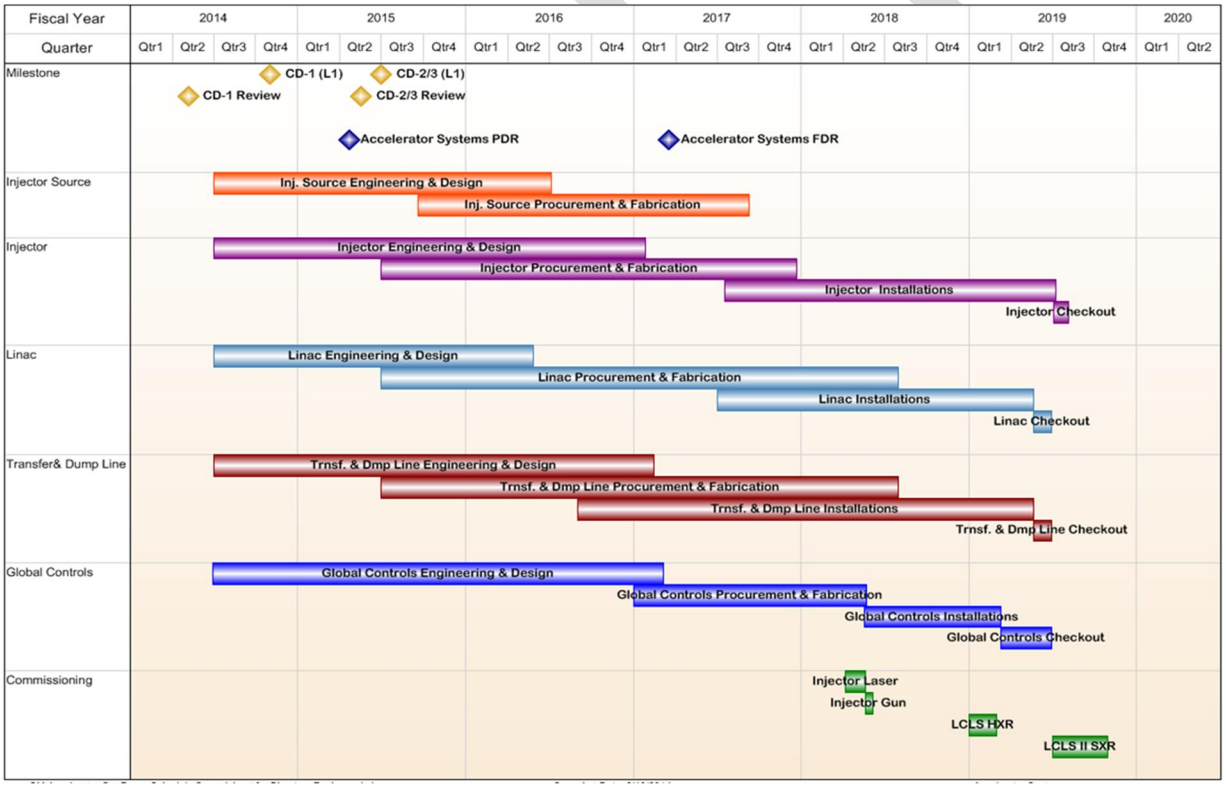

4.1.3 Design Maturity

The LCLS-II Project Final Design Plan LCLSII-1.1-QA-0065 provides for a phased completion of the final designs for the LCLS-II facility. The plan ensures that designs are sufficiently mature to start procurements and construction, while enabling the most cost-effective schedule for constructing the facility and maximizing the technical capabilities of the facility at CD-4. Final design readiness at CD-3 recognizes that that not all subsystems will reach final

design at the same time. Project-level requirements and interface control points between Accelerator Systems, Cryogenic Systems, Photon Systems and Infrastructure are defined at CD-3, which ensures that the phased procurements and construction are appropriate for the final design of the LCLS-II. Chapter 2, Project Overview, contains additional discussion of the approach to design completion. The Accelerator Systems design, described in this Chapter, Chapters 5 and 10, is evaluated to be 65% complete. Completing remaining design after CD-3 allows for potential upgrades to diagnostics and controls, using designs developed and proven by SLAC Operations.

4.2 Injector

The injector consists of a normal conducting CW photo-cathode RF gun operating up to 20 MV/m with a semiconductor cathode for high quantum efficiency (QE), a 1 MHz cathode drive laser, plus an RF buncher, two emittance compensation solenoids and a single standard cryomodule with eight, 9-cell cavities. The cryomodule with 1.3 GHz RF cavities is described in detail in Chapter 6. For CW operation semiconductor cathodes are required with QEs in the few percent range so the average power of the laser at the cathode is less than 1W as opposed to above 1 kW for a metallic cathode. However, semiconductor cathodes require high vacuum conditions in order to exhibit a lifetime on the order of days, and thus the injector also includes a vacuum load lock system to install replacement semiconductor cathodes in a high vacuum environment.

The RF gun is designed to operate reliably at the highest possible CW gradient in order to deliver the brightest beam. The reentrant cavity shape at 186 MHz [6], the seventh sub-harmonic of 1.3 GHz, provides a cavity structure which is large enough to withstand the heat load and operate in CW mode at the required gradients. The long RF wavelength allows for large apertures and thus high vacuum conductivity to accommodate semiconductor cathodes. However, the short accelerator gap of only 4 cm leads to a low exit beam energy of < 800 kV. This low energy requires a long bunch length at the cathode to minimize space charge and therefore an RF buncher to reduce the bunch length at the end of the injector is required. Table 0-6 lists the basic transverse and longitudinal beam quality requirements for a few bunch charge values, including the nominal charge per bunch of 100 pC and the maximum charge per bunch of 300 pC.

Table 0-6: LCLS-II emittance and peak current specifications for the injector

Bunch Charge	95% emittance	Peak Current
20 pC	0.25 μm	5 A
100 pC	0.40 μm	10 A
300 pC	0.60 μm	30 A

4.2.1 Brightness Demonstration

The DC Cornell Energy Recovery Injector injector prototype has previously demonstrated 90% emittance of 0.3 μm at 77 pC/bunch and 1.3 GHz repetition rate [7]. Recent Cornell injector

measurements at all three bunch charges meet the specifications listed in Table 0-6 with a low thermal emittance NaKSb cathode after several improvements, including operating at 400 kV instead of 350 kV and quadrupole corrector coils added to the emittance compensating solenoids. Emittances are approximately 10% larger with a Cs_2Sb cathode. These results are described in more detail in Chapter 16.

The proposed LCLS-II injector beam dynamics are very similar to those of the Cornell DC injector because the gun frequency is sufficiently low that the transit time is much shorter than the RF period, and thus the gun fields appear nearly static to the electrons. However, the time-varying RF fields can operate at higher gradients than a DC field and simulations indicate brighter beams [8] are generated. A prototype gun [9-10] with mature and reliable normal conducting RF technology has been built and is under test at Lawrence Berkeley National Laboratory (see Figure 0-2). To date numerous tests on the prototype RF gun have been completed, including peak field, beam energy, thermal emittance, cathode QE, cathode lifetime and dark current. The gun has operated reliably in CW mode over several days at 19.5 MV/m and 750 kV beam energy. CsTe cathodes have been characterized with QE's over 10% and lifetimes exceeding 30 days. The thermal emittance is approximately 0.75 μm/mm and the dark current measured at the entrance point of the first cryo-module meets the LCLS-II specification of < 400 nA [11]. Additional methods to further suppress dark current will be explored including dry ice cleaning, polishing the cathode iris and a collimator inside the second solenoid. Beam characterization measurements at 30 MeV covering the range of charges in Table 0-6 are planned for summer 2015 after installation and commissioning of downstream accelerator sections, buncher and a transverse deflecting cavity to measure longitudinal phase space and slice emittance.

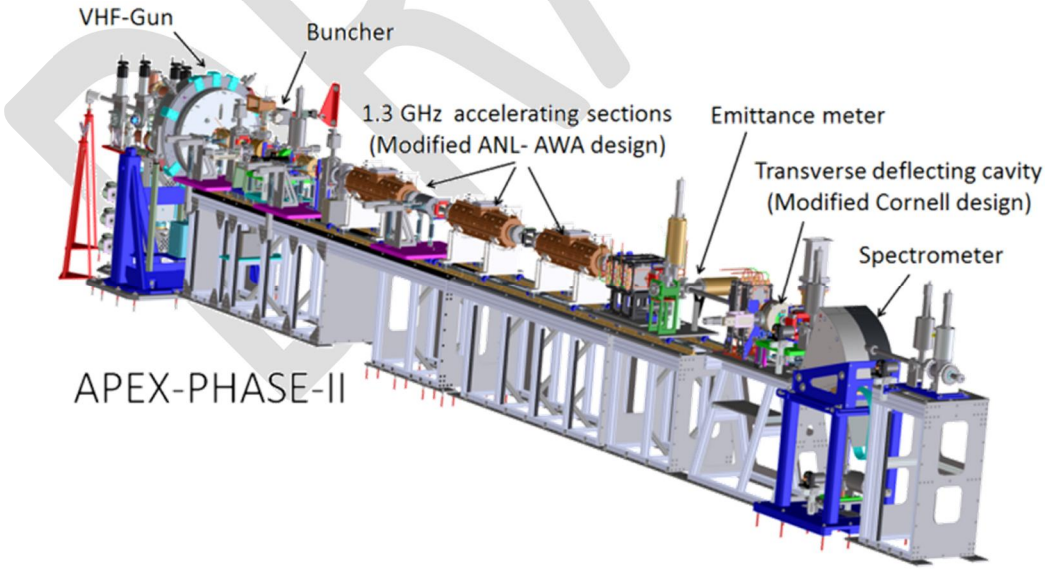

Figure 0-2. Advanced Photo-injector Experiment layout at LBNL

4.2.2 Injector Requirements

Injector requirements are listed in Table 0-7. The injector must deliver a beam of approximately 100 MeV over the range of 10-300 pC charge/bunch and peak currents of 2-50 A with emittance between 0.2 and 0.6 μm at up to 1 MHz repetition rate. These bunches are then further accelerated and compressed in the linac. Detailed injector specifications are available in the *LCLS-II SCRF Injector System Physics Requirements Document*, LCLSII-2.2-PR-0084. The injector source consists of a VHF RF gun, two focusing solenoids and a buncher cavity, along with beam diagnostics and controls as well as vacuum; the layout is illustrated in Figure 0-3. Requirements for these components are documented in: the *LCLS-II VHF-RF Gun Physics Requirement Document*, LCLSII-2.3-PR-0166, the *LCLS-II Injector Buncher Physics Requirements Document*, LCLSII-2.3-PR-0167, and the *LCLS-II Injector Solenoid Physics Requirements Document*, LCLSII-2.3-PR-0165. All of these components are described in detail in Chapter 5. At the end of the injector source, the beam enters linac section L0, which consists of a single standard LCLS-II 1.3 GHz eight 9-cell cavity cryomodule, referred to as CM01. The 1.3 GHz cryomodules are specified in the *SCRF 1.3 GHz Cryomodule Physics Requirements Document*, LCLSII-4.1-PR-0146, and described in greater detail in Chapter 6.

Table 0-7. LCLS-II Injector requirements

Parameter	symbol	nominal	range	units
Electron Energy at gun end	E_{gun}	**750**	500 - 800	keV
Electron Energy at injector end	E_{inj}	**98**	95 - 120	MeV
Bunch Charge	Q_b	**100**	10 - 300	pC
Bunch Repetition Rate in linac	f_b	**0.62**	0 - 0.93	MHz
Dark e^- current in injector	I_D	**0**	0 - 400	nA
Peak e^- current in injector	I_{pk}	**12**	4 - 50	A
Average e^- current in injector	I_{avg}	**0.062**	0.0 - 0.3	mA
Avg. e^- beam power at injector end	P_{av}	**6.1**	0 - 36	kW
Norm. rms slice emittance at injector end	$ge_{\perp\text{-}s}$	**0.4**	0.2 - 0.6	μm
Vacuum Pressure	P_G	**1**	0.1 - 1	nTorr
Cathode quantum efficiency	QE	**2**	0.5 - 10	%
Laser Energy at cathode	E_{laser}	**0.02**	0.0 - 0.3	μJ
Avg. CW RF gradient (powered cavities)	E_{acc}	**16**	-	MV/m

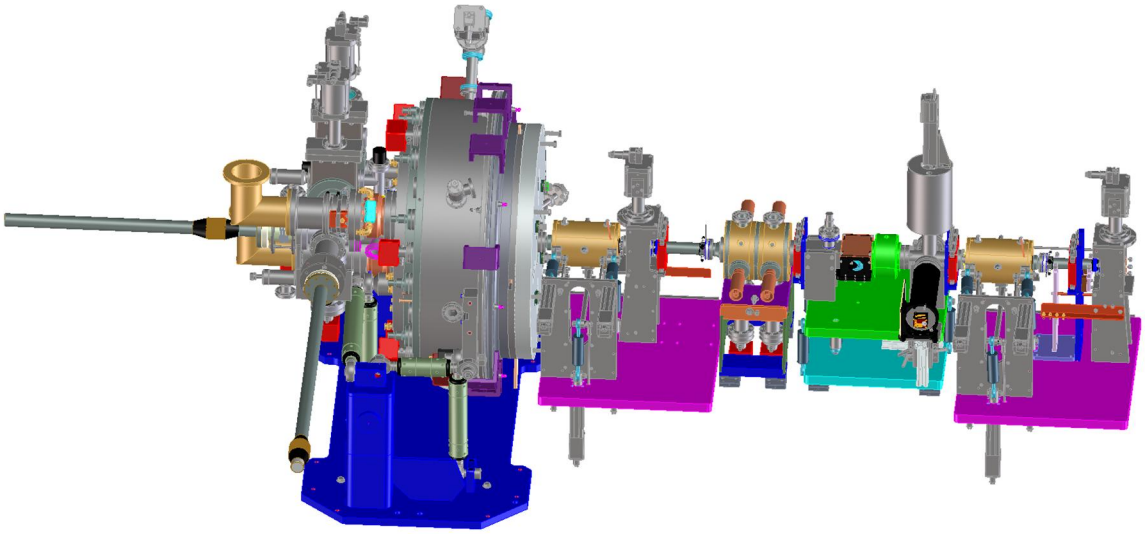

Figure 0-3. Injector source layout showing components from the RF gun to the beginning of the injector linac cryomodule CM01

The cathode specification is QE > 0.5% in the UV, 1/e lifetime >10 days, thermal emittance < 1 μm/mm, time response < 1 ps, and dark current < 1 μA at 20 MV/m. All specifications have been demonstrated with CsTe at LBNL or elsewhere. LCLS-II will implement a standard cathode puck and vacuum transfer case compatible with a vacuum load lock that have been developed at INFN/PITZ and implemented at multiple institutions around the world. These cathodes have survived with minimal performance degradation in the cathode transport suitcase for over one year.

Various alkali-antimonide cathodes are also being developed and tested at LBNL, Cornell, BNL and elsewhere. These cathodes have an advantage of QE >1% in the visible spectrum, which significantly reduces the laser power requirements. However, they require improved vacuum and typically have a shorter lifetime. Thus CsTe is the baseline cathode material, but any cathode compatible with the vacuum load lock system can be tested and implemented as the cathode technology becomes more mature.

The chosen laser wavelength for CsTe is 257.5 nm, which is the fourth harmonic of a 1030-nm fiber oscillator/amplifier laser system. With a cathode QE of 0.5%, only 0.3 W of laser power is required at the cathode. However, assuming UV conversion efficiency of 10% and transport and conditioning efficiency of 10% leads to a laser specification of 30 W. The lasers for the RF gun and the laser heater will be installed in a laser room at the west end of the SLAC linac tunnel.

The laser shape is specified to be a temporal flat top with 20-60 ps pulse length and a uniform, hard-edged transverse profile between 0.2 and 2 mm FWHM. Temporal pulse stacking using birefringent crystals has been demonstrated to be reliable and efficient. Transverse shaping will be realized with an adjustable telescope, hard aperture and relay imaging onto the cathode which is effective but less than 50% efficient. Detailed specifications and description of the laser

system is available in the *LCLS-II Gun and Laser Heater Laser Systems PRD* LCLSII-2.2-PR-0085.

Typical QEs are over an order of magnitude higher than the minimum specified and it is expected that the operating laser power will routinely be more than a factor of 30 less than the worst case specification of 30 W. Commercially available fiber laser oscillator/amplifier systems currently deliver up to 20 W average power. The power levels available from vendors are rapidly rising, typically doubling each year and thus it is expected that the desired power levels will be available commercially before orders need to be placed. For these reasons, the laser technology development is considered low risk despite the specification which is higher than is currently commercially available. Development of alkali-antimonide cathodes will further reduce the laser power requirements by a factor of three or more due to the visible response compared to UV response of CsTe cathodes.

Much of the gun performance has been characterized as described above at LBNL. Although the measured dark current already meets the 400 nA specification at the end of the first cryomodule, there is effort to further reduce the dark current emitted from the gun. Figure 0-4shows the electron beam imaged from the cathode to a downstream screen and the measured dark current at the position of the first cryomodule as a function of beam energy. Since the dark current is predominantly emitted from the edge of the cathode holder, it is expected that much of it can be mitigated through polishing and proper cleaning of the gun cathode nose cone. Alternatively the dark current could be collimated, since the dark current is located at a much larger radius than the photo-current. These techniques will be tested at LBNL. It is also worth noting that an order of magnitude dark current reduction is possible by reducing the beam energy from 750 keV to approximately 650 keV.

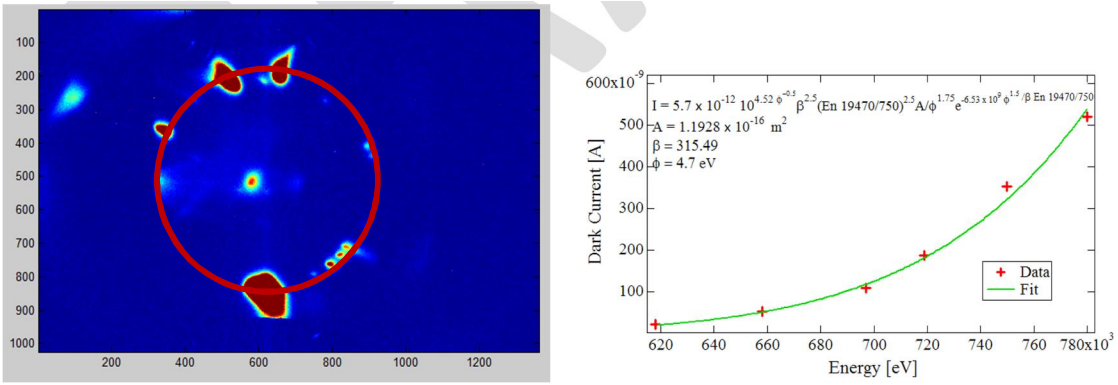

Figure 0-4: Electron beam imaged onto a screen on the left showing dark current surrounding a 1 pC photo-beam in the center. The dark current is predominantly emitted in a circle as represented by the red line which corresponds to the cathode OD. The total dark current as a function of beam energy is shown on the right.

The injector is especially sensitive to field perturbations due to the low beam energy. Field perturbations from RF coupling slots typically cause emittance growth in high brightness

injectors unless they are symmetrized. Simulations with full 3D RF fields indicate approximately 30% emittance increase for the 300 pC case [12] due to the field perturbation from the upstream high-order mode (HOM) coupler of the first RF cavity where the beam energy is only 750 keV. An additional HOM coupler is located at the downstream end of the cavity next to the RF power feed coupler, however, these couplers have a negligible impact due to the significantly higher beam energy of approximately 10 MeV. The impact is smaller at lower charges, where the beam size is reduced and the field perturbation sampled by the beam is smaller. Additional simulations indicate that there are multiple equally effective ways to mitigate this emittance growth as listed below.

1. Add a second HOM coupler at the upstream end of the first RF cavity 180 degrees opposite the first coupler to symmetrize the dipole term.
2. Remove the upstream HOM coupler from the first cavity and add a second HOM at the downstream end where the two couplers and power feed coupler are arranged to symmetrize dipole and quadrupole terms.
3. Remove the upstream HOM coupler from the first cavity and replace it with a coaxial HOM absorber, similar to the absorbers implemented in the Cornell injector [7], which completely removes the coupling hole and resulting field perturbation.

However, modifying the CM01 cryomodule is expensive due to significant engineering modifications as described above and the baseline design for CM01 does not incorporate any changes. Two possible alternatives are to correct the dilution downstream using beam bumps or to create a separate unique capture cavity cryomodule, CM00, with a single RF accelerating 9-cell cavity located between the gun and CM01. A separate injector cryomodule has three additional advantages: creating a warm section between the first two accelerating cavities at approximately 10 MeV where additional diagnostics can be added to tune the injector; enabling optimization of the emittance compensation process by selecting the proper drift distance between the first two accelerating sections; and having a compact cryomodule that can be easily removed for this absolutely critical first rf cavity. This alternate will be considered as a possible upgrade of the injector system.

Like all of the LCLS-II RF cavities, the gun components will be powered with independent sources which will be located in the SLAC Klystron Gallery. Figure 0-5 is a schematic of the gun, injector source, and CM01 which accelerates the beam to 100 MeV. The dual co-axial lines for the 186 MHz RF gun as well as the 1.3 GHz RF feeds for the buncher cavity enter the tunnel through the 1st penetration. The eight waveguides for the eight CM01 cavities enter the tunnel through the following two penetrations.

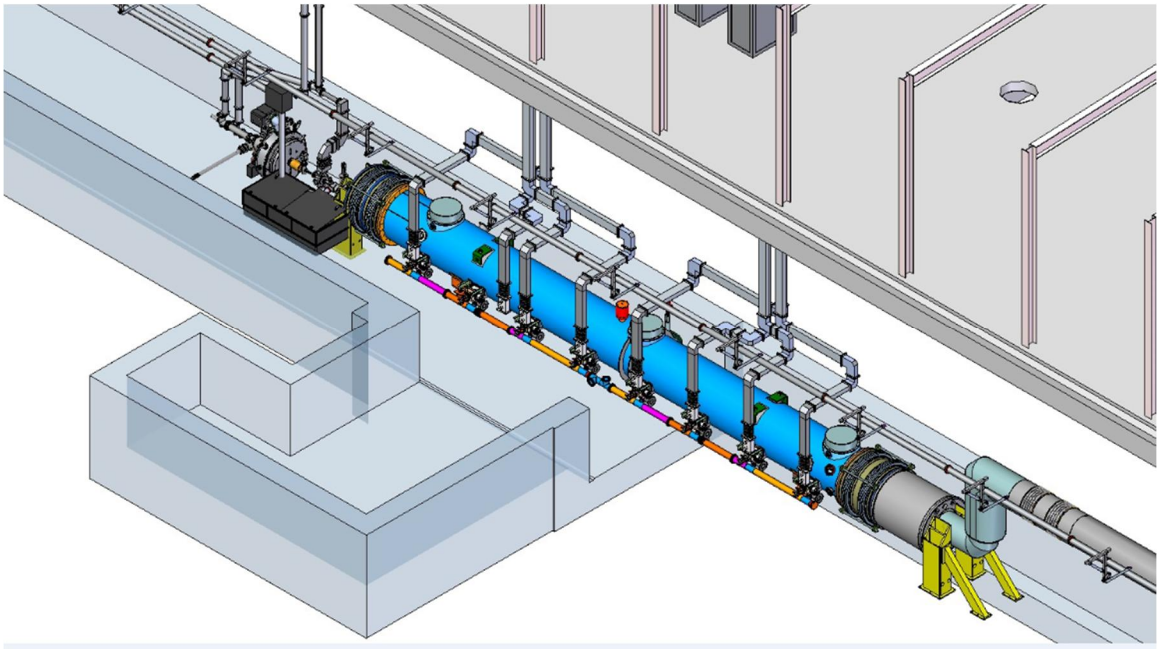

Figure 0-5. **Injector and RF systems layout showing placement of components in the tunnel; the dual laser transport lines (one for the gun and one for the laser heater) are at the left edge; the co-axial 186 MHz waveguide feeds for the RF gun are also at the left side, along with the 1.3 GHz RF feed for the buncher cavity; the eight independent RF feeds for the eight CM01 cavities come through the next two penetrations.**

4.3 Linac Systems

The LCLS-II linac will be composed of superconducting RF cavities, in continuous wave (CW) operation, in order to accelerate the electron beam to 4 GeV at up to a 1-MHz bunch rate. This new SCRF linac will replace the existing SLAC copper linac in Sectors 0 through 7, while the remaining copper RF structures in Sectors 7-10 will be removed and replaced with a simple beam pipe and FODO focusing lattice (the "extension line").. The layout is shown in **Figure** 0-1 with the SCRF linac in blue at far left and is described in more detail in the *Linac Physics Requirements Document*, LCLSII-2.4-PR-0041.

The new superconducting linear accelerator is shown schematically in **Figure** 0-6. It includes a laser heater system (LH), 35 main cryomodules (CM), a 3.9-GHz harmonic linearizer RF section (HL), a first bunch compressor chicane (BC1), a second bunch compressor chicane (BC2), and the four main linac sections labeled L0, L1, L2, and L3. The number of 12-meter-long cryomodules in each main linac section is as follows: one in L0, two in L1, 12 in L2, and 20 in L3 (as listed in Table 0-8). Each of these CMs includes eight 9-cell cavities resonant at 1.3 GHz, while the 3.9-GHz HL section consists of two specialized CMs, each including eight smaller 9-cell cavities. The 1.3 GHz and 3.9 GHz cryomodules are specified in the *SCRF 1.3 GHz Cryomodule Physics Requirements Document*, LCLSII-4.1-PR-0146, and *SCRF 3.9 GHz Cryomodule Physics Requirements Document*, LCLSII-4.1-PR-0097; they are also described in detail in Chapter 6.

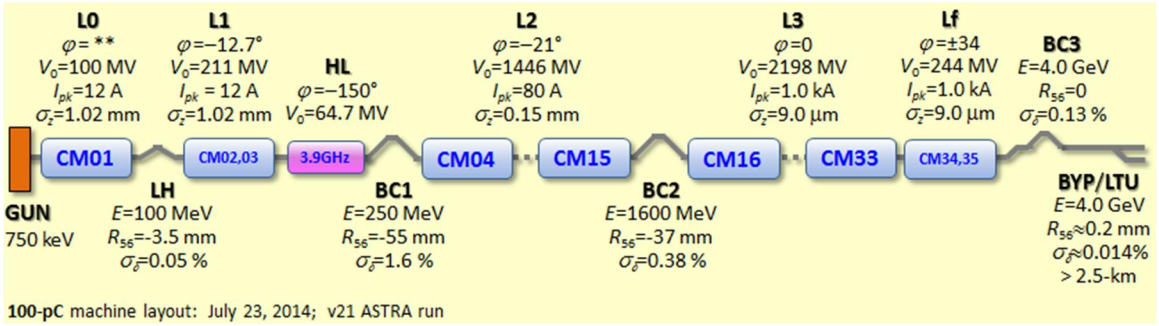

Figure 0-6. Schematic layout of the LCLS-II injector, linac, bunch compressors, and beam transport, with key parameters listed for CW operation with 100 pC per bunch.

The average accelerating gradient over all powered main 1.3 GHz cavities is just under 16 MV/m, with about 6 percent of the cavities unpowered, maintained as reserves in each linac section, or run at low gradient with temporary limitations. The 3.9-GHz HL section has a gradient of 12.5 MV/m with a nominal 64.7 MV (100 pC configuration) on-crest accelerating voltage. Finally, the resistive-wall wakefield of the 2.5-km-long bypass line (LTU) in the linac tunnel helps to remove the remnant energy chirp on the bunch after BC2, allowing the L3 linac section to run on crest phase ($\varphi_3 = 0$). The RF parameters for each linac section in a 100-pC configuration are shown in Table 0-8. Mean RF gradients are defined at crest phase and are averaged over the powered cavities in each linac section.

Table 0-8. Linac RF parameters for CW operation with 100 pC per bunch. Mean RF gradients are at crest phase and averaged over the powered cavities.

Linac Section	V_0 (MV)	φ (deg)	Mean Grad. (MV/m)	No. Cryo Mod's	No. Avail. Cavities	Spare Cavities	Cavities Per Amp.
L0	100	*	16.3	1	8	1	1
L1	211	-12.7	13.6	2	16	1	1
HL	-64.7	-150	12.5	2	16	1	1
L2	1446	-21	15.5	12	96	6	1
L3	2198	0	15.7	18	144	9	1
Lf	244	±34	15.7	2	16	1	1

* The eight L0 cavity phase settings are: 3°, -15°, 0, 0, 0, 0, 15°, 0.

4.3.1 SCRF Linac Requirements

The linac system must accelerate the beam from the injector while compressing the bunch length to achieve the desired peak current. The overall beam parameters for the SCRF linac are listed in the *LCLS-II Parameters Physics Requirements Document*, LCLSII-1.1-PR-0133, and are reproduced in Table 0-9 and Table 0-10.

The linac consists of four SCRF linac sections separated by warm beamlines for the laser heater and bunch compressors. The linac is designed to accelerate up to 300 µA of current at a

gradient of 16 MV/m. The total installed RF voltage is 4.65 GV, but many of the cavities are operated off-crest to achieve bunch compression, and roughly 6% of the cavities are 'spare' and will be used to provide overhead on the gradient.

Table 0-9. LCLS-II SCRF Linac Electron Beam Parameters; from LCLSII-1.1-PR-0133.

Electron Beam Parameters	symbol	nominal	range	units
Final electron energy (operational)	E_f	4.0	2.0 - 4.20	GeV
Maximum upgrade energy (or reduced duty factor)	E_{max}	10	-	GeV
Electron bunch charge (limited by beam power)	Q_b	0.10	0.01 - 0.30	nC
Bunch repetition rate in linac (CW)	f_b	0.620	0 - 0.929	MHz
Average electron beam power at linac end (limit)	P_{av}	0.25	0-1.2	MW
Normal rms transverse slice emittance (nom. charge)	$\gamma\varepsilon_{\perp\text{-}s}$	0.45	0.2 - 0.7	μm
Final peak current	I_{pk}	1000	500 - 1500	A
Final rms bunch length	σ_{zf}	8.3	0.6-52	μm
Final slice energy spread (rms)	σ_{Es}	500	125-1500	keV

Table 0-10 SCRF Linac parameters in the LCLS-II; from LCLSII-1.1-PR-0133.

Linac Parameters	symbol	nominal	range	units
Installed 1.3 GHz RF voltage	V_{13}	4.65	-	GV
Fraction of unpowered cavities (installed spares)	-	6%	-	-
Number of powered 1.3 GHz RF cavities		262	-	-
Average gradient of powered cavities	φ_1, φ_2	<16	14 - 18	MV/m
L1 and L2 RF phase range	φ_1, φ_2	21	15 - 30	Deg.
Energy overhead for feedback	V_{fb}	1.0%	-	-
Installed 3.9 GHz RF voltage	V_{39}	0.080	-	GV
Maximum compressed beam energy	E_{max}	4.14	4.0 – 4.20	GeV
Average cavity Q_0	Q_0	2.7	+/- 20%	10^{10}
Maximum cavity gradient @ Q_0 > 1e10	G_{max}	18	-	MV/m

An example of the RF phase configuration is shown in Table 0-8 for a 100 pC bunch; the detailed phase configuration depends on the bunch charge and the bunch compressor settings. The two bunch compressors, BC1 and BC2, are designed to operate over a wide range of compression (R_{56}) values, which allow a lot of flexibility in optimizing the beam parameters. The linac has been specified to achieve a beam energy in excess of 4.0 GeV across the operating charge range (10 – 300 pC) using 94% of the installed RF cavities; for example, the maximum beam energy in the 'nominal' 100 pC configuration is 4.14 GeV.

The linac is being designed to operate with up to 300 μA of current, and current-sensitive components such as high-order mode (HOM) loads, vacuum chambers, collimators, radiation

protection, etc. are all sized for the full current. However, initially there will only be two undulators and the linac will be limited to 250 kW maximum power (62 µA at 4 GeV), so the RF power will be installed to accelerate 100 µA of electron current.

Since the linac RF operates in CW mode, it could accelerate bunches every RF cycle. The diagnostics and control systems, however, have been designed for a maximum repetition rate of 0.929 MHz. At the maximum initial current of 62 µA, this corresponds to bunches of roughly 70 pC spaced 1.1 µs apart.

High frequency noise in the linac RF systems will cause jitter, changing the final bunch characteristics and affecting the FEL performance. The following final bunch characteristics are affected: 1) the final electron energy, 2) the final peak current, and 3) the arrival time of the bunch in the undulator. We therefore require specific stability tolerances for each RF system (phase and amplitude), bunch charge, drive-laser timing, and bunch compressor chicane strengths (*i.e.*, the main power supply on all four dipole magnets of each main chicane), such that the final machine stability is within some reasonable limits. These limits are chosen as follows: *a*) a final relative electron energy stability of < 0.01 % rms, *b*) a final relative peak current stability of < 4% rms, and *c*) an arrival time of the electron bunch (assumed same as the x-ray pulse timing) of < 20 fs rms.

The component tolerances are chosen such that all errors together will not cause errors more than our final stability goals. This tolerance budgeting is described in more detail in the *Linac Physics Requirements Document*, LCLSII-2.4-PR-0041. The RF system that will meet these requirements is specified in the *RF Power and LLRF Physics Requirements Document*, LCLSII-4.1-PR-0098. Further details of the RF power sources are described in Chapter 5 and the LLRF controls in Chapter 10.

4.3.2 SCRF Linac Layout

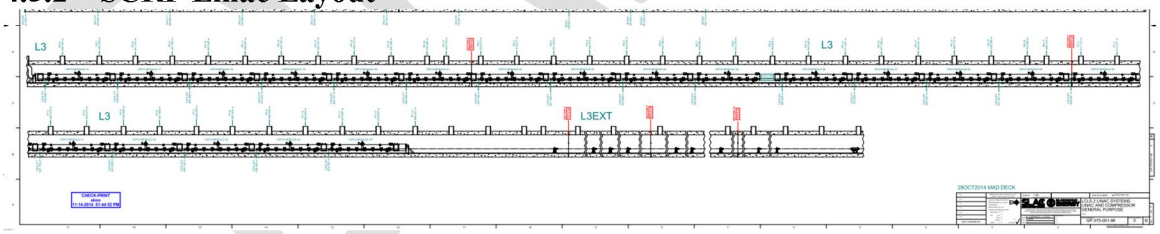

is a schematic showing the location of the cryomodules and warm breaks in the SLAC linac tunnel.

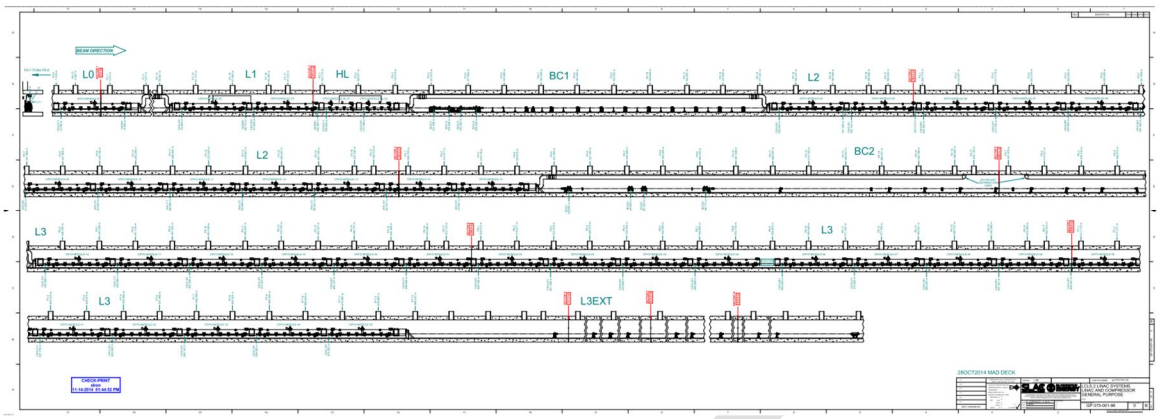

Figure 0-7. Elevation-view of the SCRF linac located in the east end of the SLAC linac tunnel; the linac is broken into four segments by the laser heater and two bunch comrpessors BC1 and BC2; the L3 extension takes the beam from the end of the L3 linac to Sector 10, where the Dogleg will bring the electron beam up and south to match into the pre-existing PEP-II HER Bypass line.

The SCRF linac beamline will be installed close to the tunnel floor and close to the north side of the tunnel wall. The new electron beamline will be roughly 1 meter below and 28 cm to the north of the SLAC CuRF linac. To facilitate the installation, all of the existing CuRF linac components will be first removed; the removal project is described in Chapter 11. After the tunnel is cleared, the cryomodules will be transported at tunnel-level through the Sector 10 spur, across the SCRF linac beamline, and into the linac tunnel. The L3 extension includes an easily removable spool-piece to facilitate the transport from the Sector 10 spur. The location of the new SCRF linac beamline and the planned transport of cryomodules for installation are shown in Figure 0-8.

Installation of the SCRF linacs will begin after the completion of the Sector 0-10 D&D – described in Chapter 11 – which is scheduled to complete in September 2016. All of the SCRF linac hardware will have detailed component reviews as described in Chapter 6 and 7. A mockup cryomodule, illustrated in Figure 4-9, has been constructed at SLAC to optimize the installation process. As indicated in Table 0-3 and Table 0-4, the Linac Installation has had a Preliminary Design Review in January 2015 and will have a Final Design Review in August 2016.

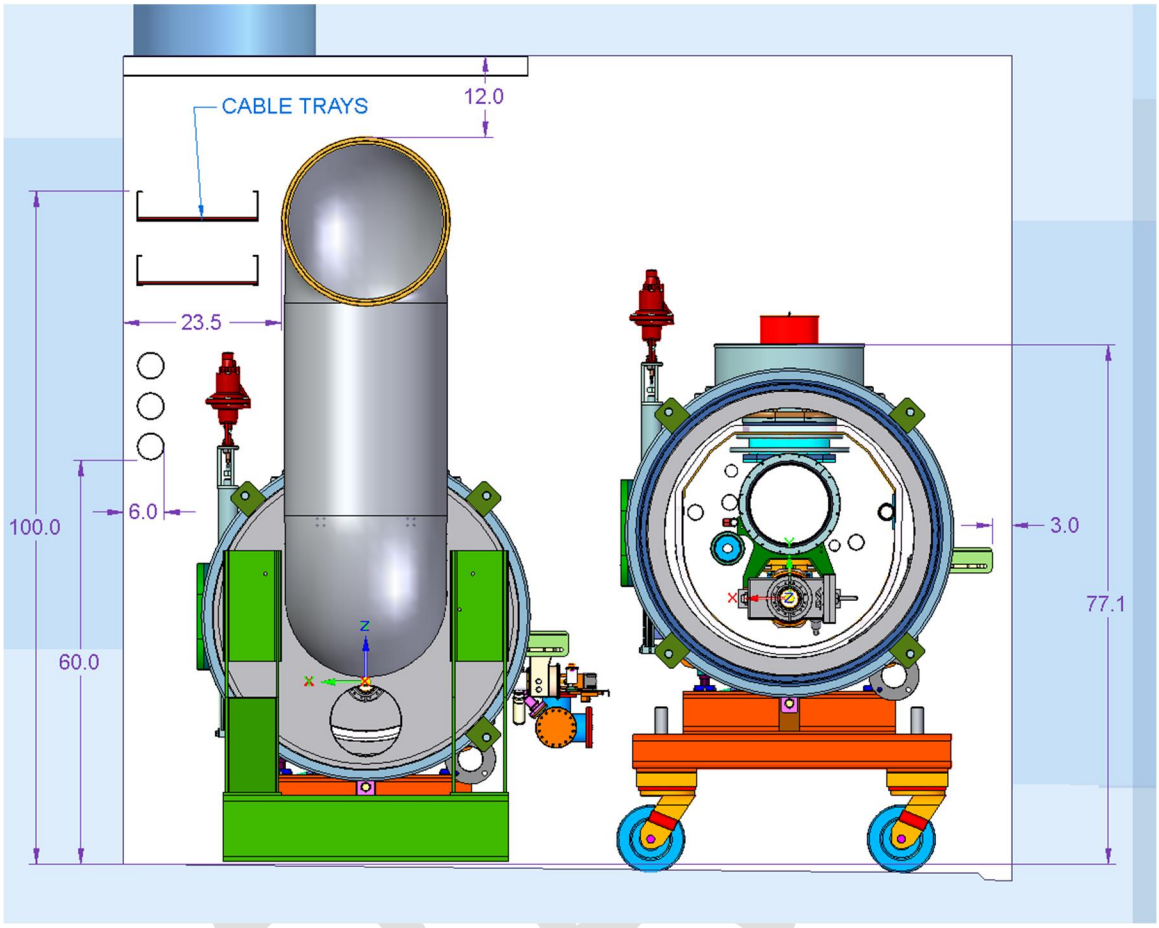

Figure 0-8. **The SCRF linac cryomodules will be installed on the north side of the SLAC linac tunnel. Cryomodules will be brought into the tunnel through the tunnel-level entrance in the Sector 10 spur located on the north side of Sector 10. A 20-meter vacuum chamber spool-piece will be removed from the L3 extension to allow the cryomodules to be rolled to the south side of the tunnel and then moved along the tunnel length for installation.**

Figure 4-9. SLAC tunnel mock-up with cryomodule, couplers, cryo-distribution and racks to understand installation issues.

4.3.3 SCRF Linacs: L0, L1, L2, and L3

The main SCRF linac will be divided into four segments (L0 – L3) by the laser heater and the two bunch compressor sections, BC1 and BC2. The SCRF linac is constructed from 1.3 GHz and 3.9 GHz cryomodules, each containing eight 9-cell RF cavities operating at 2 K, a button BPM located at the end of the cryomodule, and a high-frequency beamline absorber for the un-trapped Higher-Order Modes (HOM); each RF cavity includes two HOM couplers to damp the trapped HOM's. Each 1.3 GHz cryomodule also contain a magnet package with a superconducting quadrupole as well as X and Y dipole correctors. The 1.3 GHz and 3.9 GHz cryomodules are described further in Chapter 6.

The cryomodules in each linac section will be welded together to form a contiguous cryogenic structure. At the entrance and exit of each of the linac segments, an end- or feed-cap will be used to bring the cryogenic fluids into the cryomodules and to brace the cryomodules against the vacuum forces. A drawing of the L1 feed-cap on the 2nd Harmonic Linearizer cryomodule, CMH2, is shown in Figure 0-10; more detail on the cryo-distribution system can be found in Chapter 7.

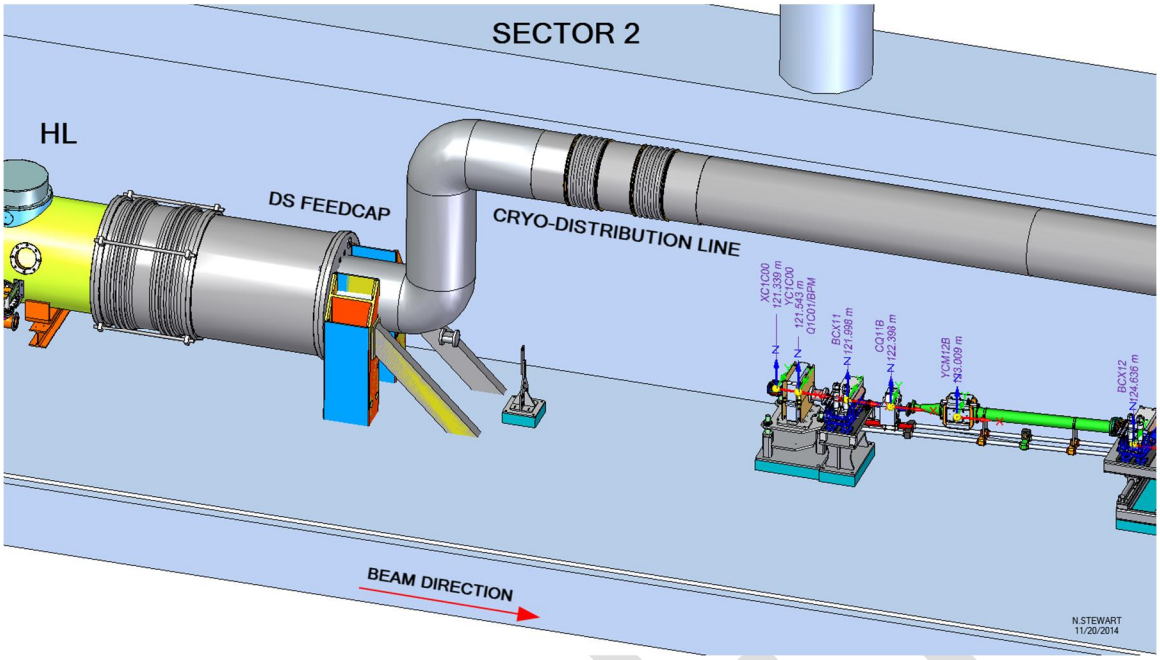

Figure 0-10. L1 endcap and second 3.9 GHz cryomodule, CMH2, in SLAC tunnel illustrating the beginning of the BC1 section and the beamline (without vacuum components) and cryogenic distribution lines exiting the CMH2 cryomodule.

The linac cryogenics will be brought from the cryogenic plant into the SLAC linac tunnel above BC2 (at roughly the 400-meter point along the SLAC linac tunnel). The east feed will then provide cryogenics for CM16 through CM35 while the west feed will provide cryogenics for CM01 through CM15 as well as the two 3.9 GHz harmonic linearizer cryomodules, CMH1 and CMH2.

The RF power for the SCRF linac will be generated aboveground in the SLAC linac galley and then delivered to the RF cavities via WR650 waveguides. Each cavity will be powered by an individual solid-state rf amplifier (SSA) operating at 1.3 GHz or a suitable 3.9 GHz source as appropriate. This provides independent power and phase control of each SCRF cavity, which will allow cavity gradients to be individually stabilized. The waveguides will be brought into the SLAC tunnel through pre-existing penetrations that are located every 20 feet along the linac length. Because the cryomodule placement will not be locked to the penetration positions, each waveguide will need to be customized for the specific cavity. The waveguide connections to the cavity couplers will be made after installing the cryomodule in the tunnel. The RF power systems are described in Chapter 5.

One of the critical issues when operating SCRF systems is ensuring vacuum cleanliness and avoiding particle contamination of the SCRF cavities. General guidelines have been defined for the assembly of the SCRF linac and for the beamline components adjacent to each of the linac segments; these are detailed in Chapter 5. As illustrated in Figure 0-10, all of the warm sections between linac segments, except the gun source region, have 1.3-meter drifts from the end/feed-cap as a mechanical stay-clear to allow the cryo-distribution lines to be bent away from the

beamline, followed by 3-meter sections that will be dedicated to differential pumping and particle trapping. The vacuum requirements and vacuum system for the LCLS-II are described in Chapter 5.

4.3.3.1 The L0 linac

The L0 linac follows the injector source and consists of a single standard 1.3 GHz cryomodule, CM01. It accelerates the beam from 750 keV to roughly 100 MeV (the laser heater is designed to operate over the energy range of 90 – 120 MeV) and is pictured in Figure 0-5.

To capture the beam from the injector source, the linac is operated with the first cavity slightly off-crest and the second and third cavities operated at low gradient. This allows the beam to bunch while completing the emittance compensation matching. The remaining five RF cavities must be operated at close to the nominal gradient of 16 MV/m to achieve the desired beam voltage. The first cavity of the L0 linac is the most critical cavity in the entire SCRF linac and care will be given to understanding the impact of this on the accelerator availability, discussed in Chapter 12.

4.3.3.2 The L1 linac

The L1 linac follows the laser heater and collimation beamline COL0 as shown in **Figure** 0-6. It consists of two 12-m long standard cryomodules (CM02 and CM03) and also two 3.9-GHz cryomodules (CMH1 and CMH2), accelerating the beam from 100 MeV to 250 MeV at an off-crest RF phase in order to chirp the beam for bunch compression in the BC1 chicane, which immediately follows the L1 linac. The optics functions for the L1 linac (including the laser heater section and 3.9-GHz RF sections) are shown in the laser heater section in Figure 0-11. The total length of the L1 cryogenic section is 39.2 meters.

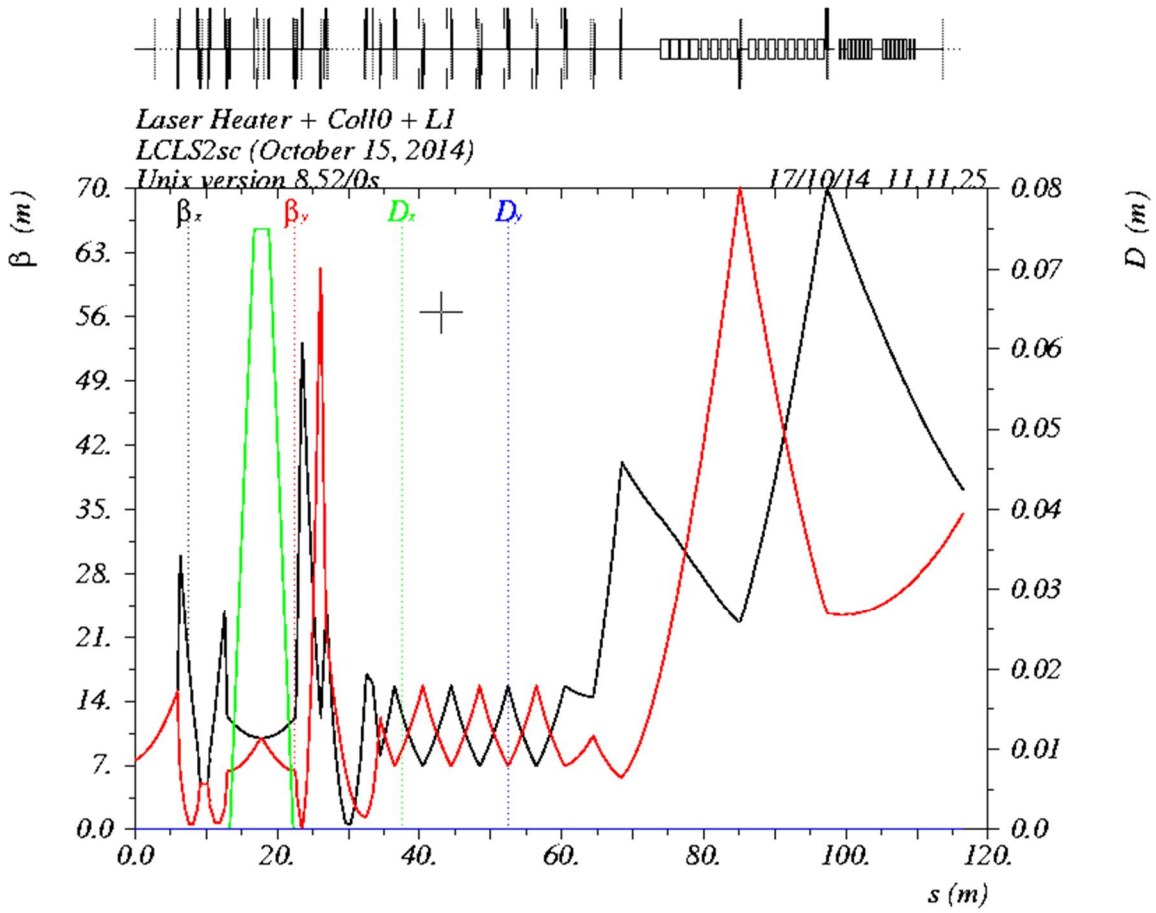

Figure 0-11. Optics functions from the start of the laser heater system to the end of the two 3.9-GHz RF sections. The dispersion (green) in the heater chicane reaches 75 mm and the horizontal and vertical beta functions are equal (~10 m) at the center of the undulator.

The 3.9 GHz cryomodules have couplers exiting both sides of the cryomodule (aisle-side and wall-side) to cancel the RF deflections from the couplers. The L1 linac is positioned so that the 3.9 GHz cryomodules are placed in the widest section of tunnel, close to the injector. Waveguides for the 3.9 GHz couplers close to the housing wall will be pre-installed and routed to the top of the cryomodule to facilitate connection to the RF sources after installation of the cryomodule.

4.3.3.3 The L2 linac

The L2 linac consists of twelve 12-m long standard cryomodules (CM04-CM015), also phased off-crest to chirp the beam appropriately prior to the BC2 bunch compressor chicane, which immediately follows the L2 linac. The L2 linac accelerates the electron beam from 0.25 GeV after BC1, up to 1.6 GeV at BC2. The optics functions for the L2 linac are shown in Figure 0-12. The phase advance per cell is 30 degrees in each plane, and the large variation in the beta functions at the end of L2 is used to match the optics into the BC2 chicane, where the optics are chosen to minimize the CSR-induced emittance growth. The total length of the L2 linac cryogenic section is 149.2 meters.

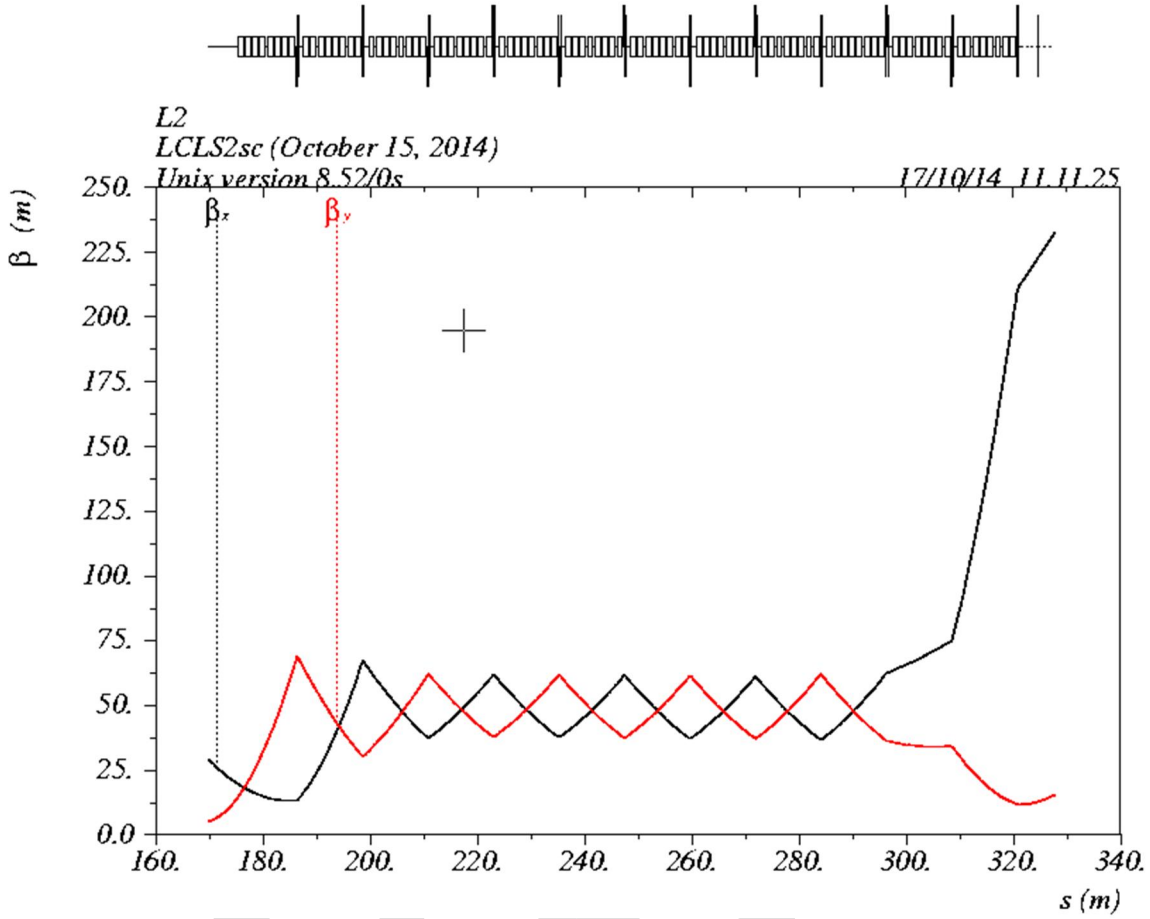

Figure 0-12. Optics functions over the L2 linac, from 250 MeV just after BC1 to 1.6 GeV before BC2. The large variation in the beta functions at the end are used to minimize the CSR-induced emittance growth in the BC2 chicane (just off the plot to the right).

4.3.3.4 The L3 linac

The L3 linac consists of twenty 12-m-long standard cryomodules (CM16-CM035) phased on-crest and accelerating the beam from 1.6 GeV, after BC2, up to 4 GeV. The optics functions for the L3 linac (including the 250-m-long extension line) are shown in Figure 0-13. The phase advance per cell is 30 degrees in each plane in L3. The middle of the L3 linac has a break where additional vacuum supports are placed end-to-end to separate the insulating vacuum into two sections. The cryogenic length of the L3 linac is 249.5 meters.

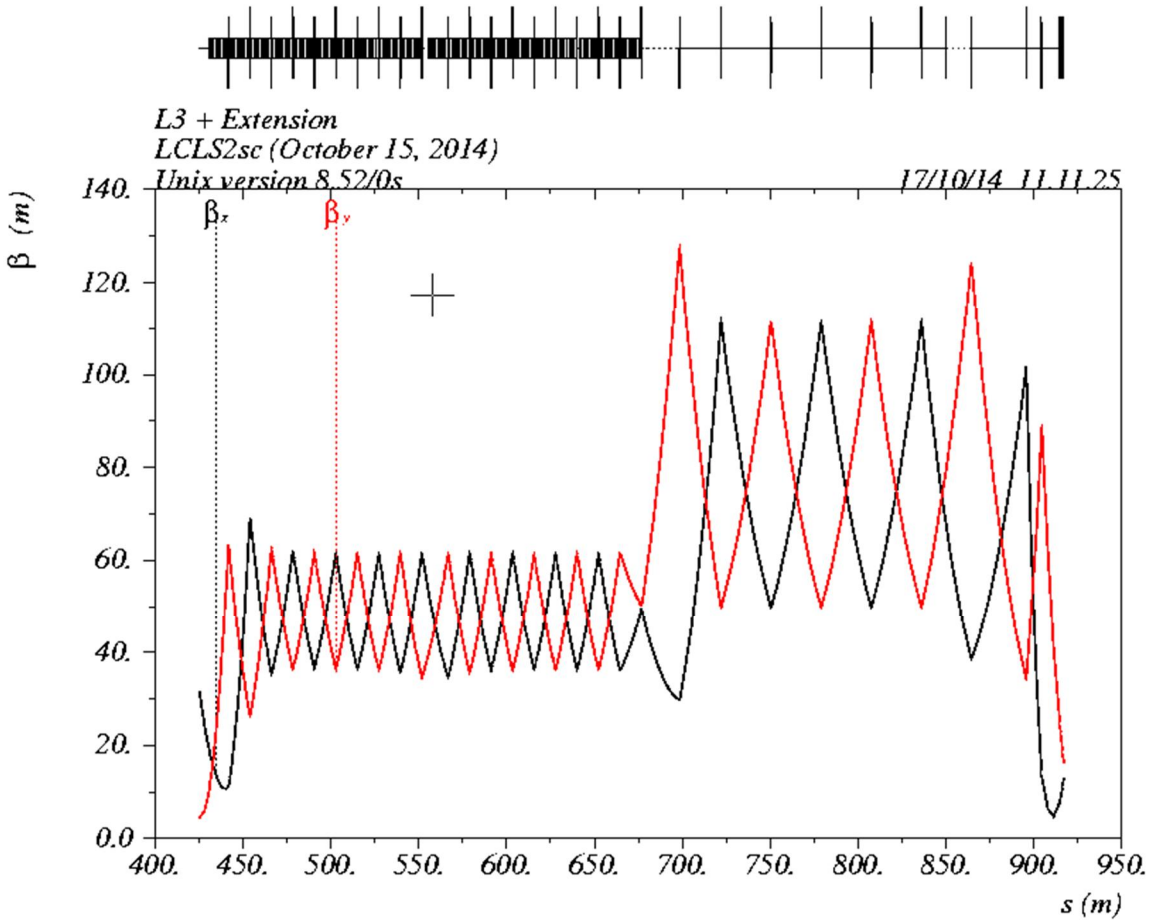

Figure 0-13. Optics functions over the L3 linac, from 1.6 GeV just after BC2 to 4 GeV and through the extension line of sectros 7-10. The phase advance in L3 is about 30 degrees per cell and 45 degrees per cell in the extension line.

4.3.4 Laser Heater, Laser Heater Laser, and COL0 Beamlines

LCLS-II will incorporate a laser-electron-beam heater system (an inverse FEL) in order to generate an uncorrelated energy spread in the electron beam. This produces Laudau damping in the bunch compressor chicanes in order to suppress potential micro-bunching instabilities that may be driven by Coherent Synchrotron Radiation (CSR) in the bunch compressors, and longitudinal space charge (LSC) forces in the linac. The laser heater layout is shown in Figure 0-14 and the beam optics is shown in Figure 0-11. The heater system is located just downstream of the L0 accelerator section at roughly 100 MeV. It is designed to operate with beam between 90 and 120 MeV and is described in more detail in *Injector Laser Heater Physics Requirements Document*, LCLSII-2.2-PR-0086, while the laser system requirements are specified in the *LCLS-II Gun and Laser Heater Laser Systems Physics Requirements Document*, LCLSII-2.2-PR-0085.

Relative to the LCLS laser heater design, the dispersion in the LCLS-II heater has been increased to 75 mm to allow more effective beam energy collimation at this location, which is the first bending section in the accelerator. The R_{56} value of the LH chicane has also been minimized

(< 4 mm), by lengthening the chicane to 9 m, in order to minimize the 'trickle-heating' effect [13].

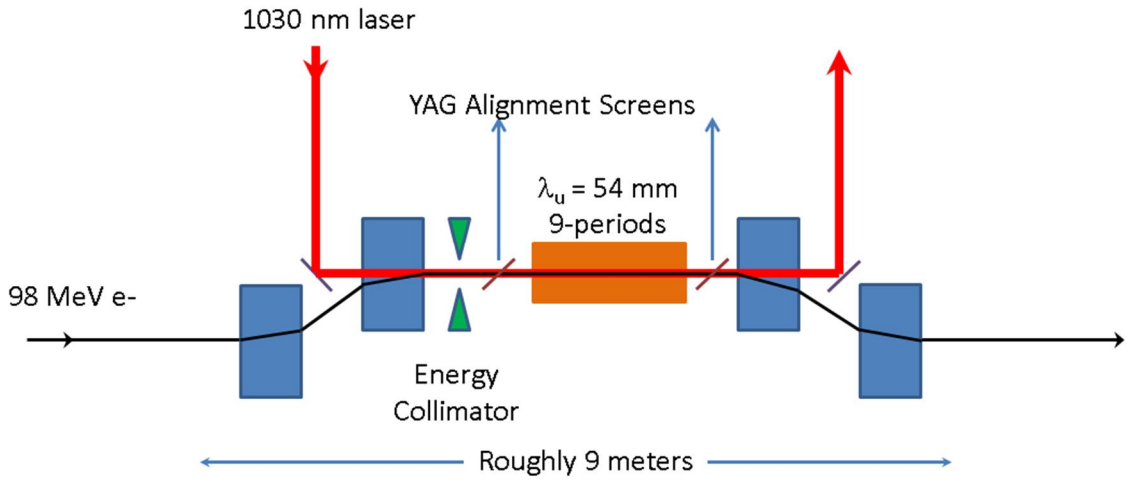

Figure 0-14. Schematic of the laser heater system including an energy collimation and two pop-in screens to align the laser and the electron beam. The length is roughly 9 meters.

The heating requirement for 100 pC at 100 MeV is about 6 keV rms. This slice energy spread is amplified by about a factor of 100 (the total bunch compression factor after the heater), generating 500-600 keV rms slice energy spread in the FEL, which is enough to partially damp the micro-bunching instability but not enough to degrade the FEL performance; as noted in Chapter 3, additional control of the downstream R_{56}'s is also necessary to suppress the micro-bunching effects. Higher (300 pC) and lower (10 pC) bunch charges require more or less energy spread at the heater, but all are aimed at the 500~600 keV energy spread at the FEL. The heater laser system has been specified to provide over 20 keV energy spread at the heater. This will cover all cases of interest, and excess laser power can be used to ease the matching of the laser to the electron beam.

Detailed specifications and description of the laser system is available in the *LCLS-II Gun and Laser Heater Laser Systems PRD* LCLSII-2.2-PR-0085. The choice of 1030-nm for the laser wavelength is primarily dictated by the availability of high-power, high-repetition rate sources (*e.g.*, Yb: glass fibers) while beam energy is determined by the acceleration from the first cryomodule, CM01. The beam energy and laser wavelength determine the laser heater undulator which is described in the *Laser Heater Undulator Physics Requirements Document*, LCLSII-2.2-PR-0324. The heater undulator is an existing undulator that has a period of 5.4 cm and a moderate number of undulator periods (9) so as to broaden the bandwidth of the undulator resonance condition to a few percent. The undulator has a variable gap, allowing the heater to operate with beams between 90 and 120 MeV. Laser and electron beam diagnostics are placed on either side of the undulator to facilitate alignment of the laser and electron beam.

(3D drawing?)

Figure 0-15. Illustration of the installed laser heater and COL0 beamlines with the Post-Laser Heater Diagnostic line beside it.

As noted in Section 4.5.2, the laser heater section also includes the first of four energy and betatron collimation system as described in the *Halo Collimation System Physics Requirements Document*,LCLSII-2.4-PR-0095. The shielding issues associated with the collimators are described in *Radiation Protection Requirements for the Halo Collimators*, LCLSII-1.2-PR-0259. There is an energy collimator before the laser heater undulator, as illustrated in Figure 0-14, to collimate off-energy particles. The laser heater is followed by a periodic lattice, referred to as COL0, with 45-degree phase advance that contains two horizontal and two vertical betatron collimators, where the pairs of collimators are separated by 90 degrees in phase. Additional collimators can be added if necessary to collimate at the 45-degree point in betatron phase as well as at 0 and 90 degrees.

The laser heater installation includes a wire scanner upstream of the laser heater chicane for quadrupole scans of the injector beam emittance and is followed by a kicker-septum pair to extract the beam into the Laser Heater Diagnostic beamline. In addition, there is also a location toward the end of the beamline for an additional wire scanner that could be used for either quadrupole scans or a tomography emittance measurement using the upstream quadrupoles. If installed, the wire scanner would be followed by a stopper that would be used to avoid excess beam loss in the downstream superconducting linacs. The beamline is illustrated in Figure 0-15, which also shows the Post-Laser Heater Diagnostic beamline.

Installation of the Laser Heater will begin after the completion of D&D in Sectors 0-10 D&D – described in Chapter 11 – which is scheduled for September 2016. All Laser Heater hardware will be fully checked out and ready for installation. As indicated in Table 0-3 and Table 0-4, the Laser Heater System has had a Preliminary Design Review in January 2015 and will have a Final Design Review in August 2016 however much of the beamline is very similar to that operating in the LCLS and that designed for the LCLS-II Phase 1 and few uncertainties are expected.

The hardware components for the Laser Heater and COL0 are listed in Table 0-11. Many of the required components, including the laser heater undulator and diagnostics, were constructed as part of LCLS-II Phase 1. The designs for the specific magnets, power supplies, collimators and diagnostics are described in Chapter 5.

Table 0-11. LH and COL0 Hardware Components.

Component	Quantity	Engineering name	Status
Dipole magnet	4	5D3.9	Existing design
Quadrupole magnet	24	1.259Q3.5	Existing design
Dipole corrector ($x + y$)	14	Class-1a	Existing design
Dipole corrector ($x + y$)	5	Class-6	Existing design

Energy collimator	1	-	new
Betatron collimator	4	-	new
Stripline BPM	17	-	Existing design
Bunch length	1	CSR/gap	Existing design
Wire scanners	2	-	Existing design
Undulator	1		Existing magnet
Laser Heater YAG	2		Existing design
1030nm 50W laser	1		(Almost) Commercial

4.3.5 Laser Heater Diagnostic Beamline

The laser heater chicane is immediately followed by an off-axis beam diagnostics line at 100 MeV, described in *Post-LH Diagnostics Beamline Requirements Document*, LCLSII-2.4-PR-0068. This beamline is used to steal electron bunches at up to a 120-Hz rate to allow continuous beam measurements, including transverse projected emittances, beam energy, projected energy spread, and bunch charge. In addition, space is left for horizontal and vertical transverse S-band RF deflectors which will allow time-resolved emittance measurements, time-sliced energy spread, and absolute bunch length and shape measurements. The beam bunches are stolen by a fast kicker (<400 ns rise/fall) operated at up a 120-Hz firing rate and deflected vertically into a magnetic septum where they are directed horizontally off axis into the diagnostic line, a 17.52 meter-long beamline that is 0.5-m displaced and parallel to the main beamline that is optimized to measure the 6D phase space of the electron beam.

The baseline installation will only have transverse emittance and energy spread diagnostics but the beamline has space for horizontal and vertical S-band transverse deflectors, described in the *LCLS-II Diagnostic Beamline Transverse RF Deflectors PRD*, LCLSII-2.2-PR-0322. It is designed to minimize the Panofsky-Wenzel energy spread, induced by the transverse RF deflectors, to allow accurate measurements of the slice-energy spread, bunch length, and transverse slice emittance. A 30-degree spectrometer magnet deflects the beam vertically into a 15-W beam dump; the maximum nominal power is less than 4 W however the beamline will also be used to commission the injector and will receive short bunch trains at low duty cycle. The optics for this beamline are shown in Figure 0-16 and the installation next to the COL0 beamline is shown in Figure 0-15.

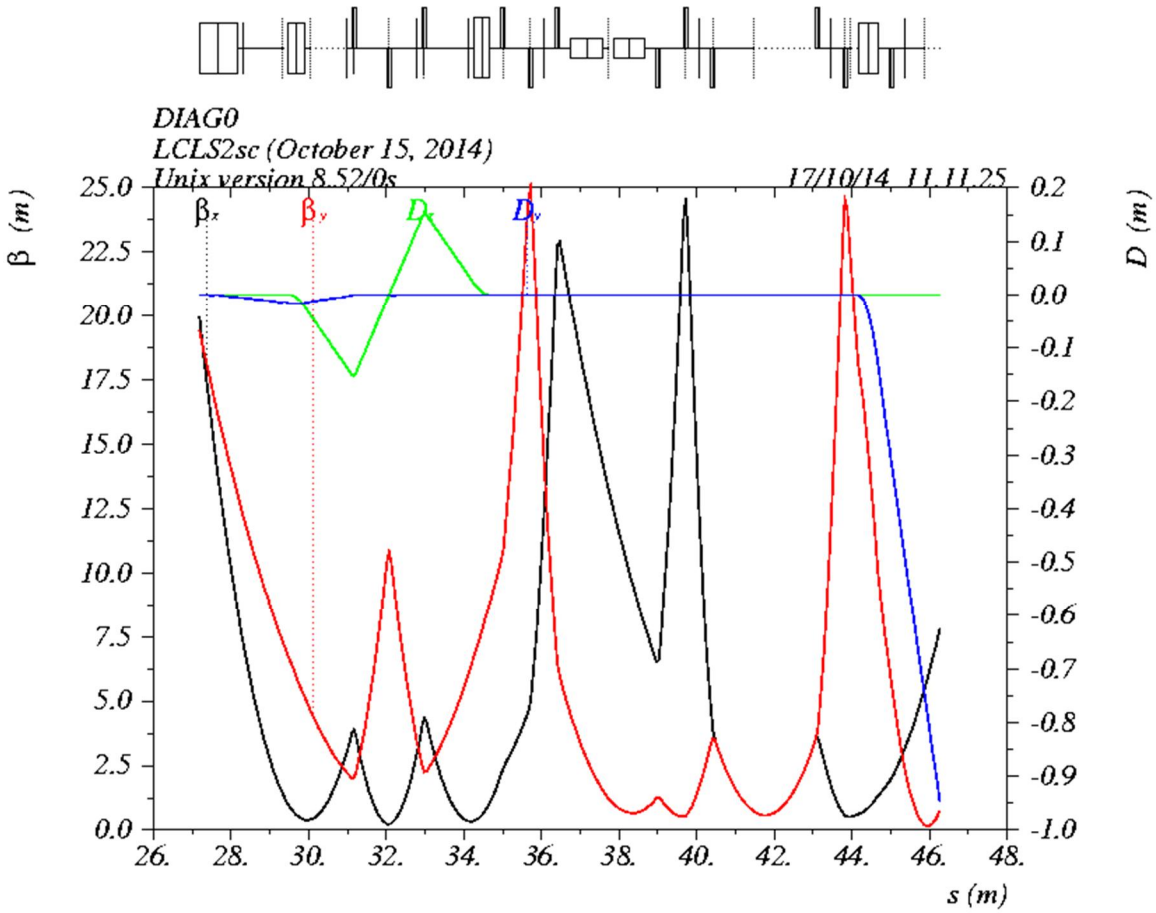

Figure 0-16. Optics functions form the "DIAG0" off-axis diagnostics line: from the post-laser-heater kicker to the off-axis dump. Two RF deflectors are shown, with one a future addition defecting in the vertical plane.

The hardware components for the Laser Heater Diagnostic beamline are listed in Table 0-12. The designs for the specific magnets, power supplies, collimators and diagnostics are described in Chapter 5.

Table 0-12. Laser heater Diagnostic line Hardware Components.

Component	Quantity	Engineering name	Status
Dipole magnet	2	--	New design
Quadrupole magnet	12	1.259Q3.5	Existing design
Kicker	1	--	New Design
Lambertson	1	--	New Design
Dipole corrector ($x + y$)	15	Class-1a	Existing design
Stripline BPM	9	-	Existing design
Wire scanners	1	-	Existing design
Profile monitors	2	OTR	Existing design

Faraday Cup	1	FC	New design

4.3.6 BC1 and COL1 Beamlines

The BC1 System is a warm beamline 61.8 meters in length which starts just downstream of the second 3.9 GHz cryomodule and then ends at the entrance to the L2 linac with CM04. The nominal beam energy is 250 MeV. The beamline consists of four dipole magnets, fifteen quadrupoles, one collimator and beam diagnostics and is illustrated schematically in Figure 0-17.

The beamline has two main functions: 1) compress the longitudinal bunch length by a factor of 3 to 10 in a four dipole chicane and 2) collimate the incoming beam to reduce dark current and trapped field emission. It will also be used to stabilize the beam energy and trajectory at this location along the superconducting linac. The design of the four magnet chicane is very similar to the existing system that is in operation at LCLS while the rest of the beamline will be standard transport line and presents little complication. The requirements for the BC1 bunch compressor are listed in the *BC1 Bunch Compressor Chicane Physics Requirements Document*, LCLSII-2.4-PR-0039, while the requirements of the collimation system are specified in the *Halo Collimation System Physics Requirements Document,*LCLSII-2.4-PR-0095 and the shielding issues associated with the collimators are described in *Radiation Protection Requirements for the Halo Collimators,* LCLSII-1.2-PR-0259.

The BC1 bunch compressor must have an R_{56} that can be varied between 20 and 75 mm. This is done by varying the dipole magnetic field and moving the two center dipoles on a horizontal translation stage. BC1 also includes an energy collimator as illustrated in Figure 0-17 to collimate off-energy particles, a large aperture BPM to measure the energy, and a wire scanner to measure the beam energy spread.

The BC1 compressor is very similar to the operating LCLS BC1 except the chicane magnets are redesigned to have large poles with better field quality and the space between the 2nd and 3rd bends is increased to allow installation of a high power collimator, BPM, and wire scanner. Like the operating LCLS BC1, the compressor would also include two ‘tweaker’ quadrupoles that would allow correction of residual dispersion or emittance dilution from Coherent Synchrotron Radiation (CSR). The compressor is followed by a periodic lattice, referred to as COL1, with 45 degree phase advance that could be upgraded to contain horizontal and vertical betatron collimators where the pairs of collimators are separated by 90 degrees in phase. Interspersed with the collimators, space is allocated for four wire scanners to be installed in the 45-degree lattice to measure the beam emittance after the bunch compressor. In addition, space is left after the BC1 chicane for future X and Y transverse deflecting cavities that would allow accurate measurement of the longitudinal phase space and the slice emittances.

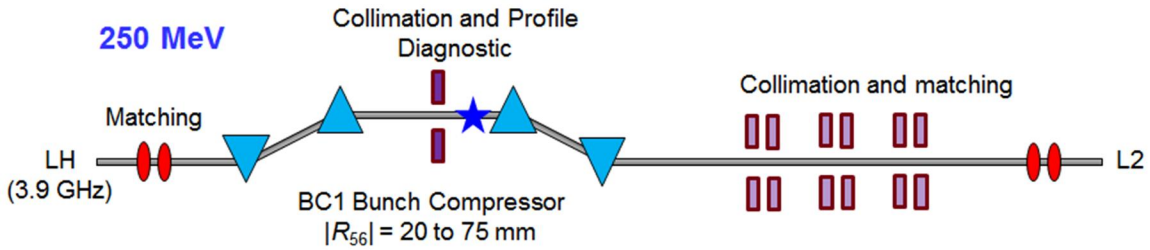

Figure 0-17. Schematic of BC1 from the end of the 3.9-GHz RF section to the start of the L2 linac.

The hardware components for BC1 are listed in Table 0-13. The designs for the specific magnets, power supplies, collimators and diagnostics are described in Chapter 5.

Table 0-13. BC1 Hardware Components.

Component	Quantity	Engineering name	Status
Dipole magnet	4	1.69D6.28	Existing design
Quadrupole magnet	13	1.259Q3.5	Existing design
Trim quadrupole	2	2.362Q3.5	Existing design
Dipole corrector ($x + y$)	2	Class-1a	Existing design
Dipole corrector ($x + y$)	11	Class-6	Existing design
Stripline BPM	13	-	new
Bunch length	2	CSR/gap	Existing design
Wire scanners	1	-	Existing design

Figure 0-18 shows a drawing of the four-dipole BC1 chicane. The center two dipoles, energy collimator and diagnostics are mounted on a translation stage to allow adjustment of the R_{56} through the chicane from 0 to 75 mm. The translation stage is based on the existing translation stage that is in operation at LCLS, with minor modifications to lower the stage to the SCRF linac elevation and lengthen the space between the second and third dipole magnets. The maximum translation of the beamline is 320 mm.

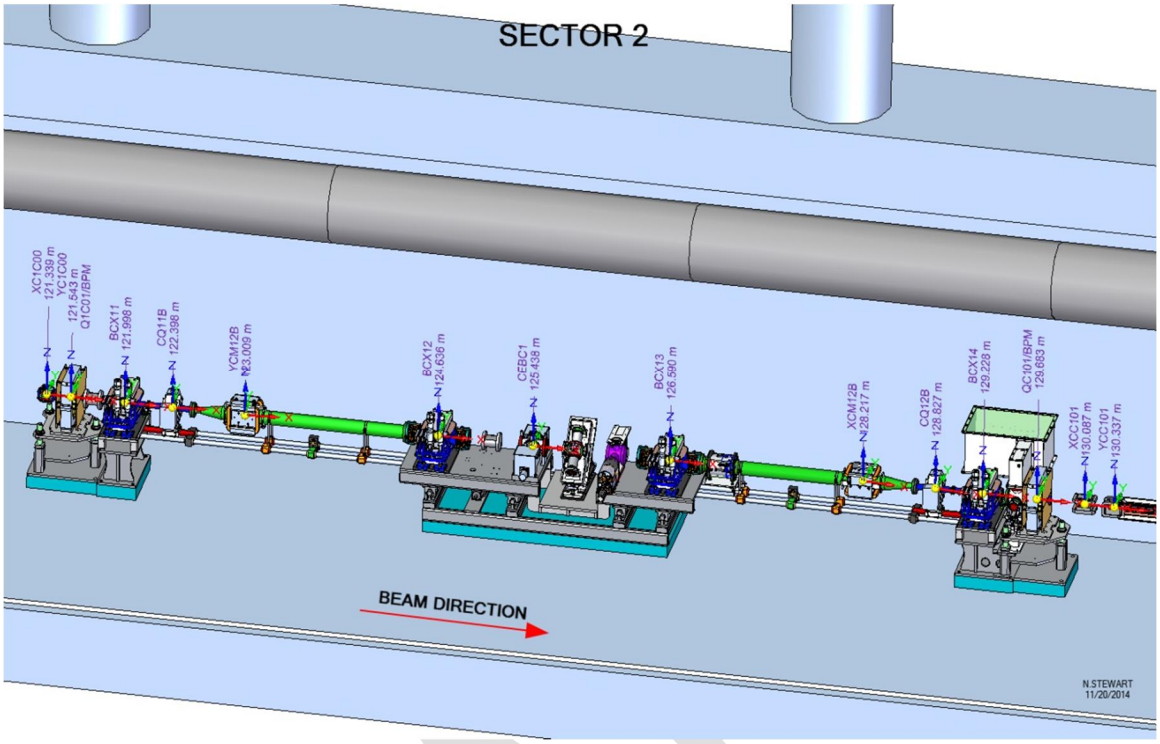

Figure 0-18. Drawing of the BC1 four-magnet chicane showing 4 dipole manets (blue); quadrupoles at entrance and exit; dipole correctors around the large copper beam pipe (green), and the energy collimator and diagnostics between the 2nd and 3rd dipoles on the translation stage; in addition, the CSR bunch length monitor can be seen after the 4th dipole magnet.

The vacuum system through the four-magnet chicane has a large aperture to accommodate ±9% energy bandpass and is designed to minimize the longitudinal impedance as described in the *BC1 Bunch Compressor Chicane Physics Requirements Document*, LCLSII-2.4-PR-0039. The remaining vacuum system is assembled as described in Chapter 5, including the 'particle-free' regions adjacent to the SCRF cryomodules. A CAD drawing of the entire beamline is shown in Figure 0-19. The optics functions are shown in Figure 0-20.

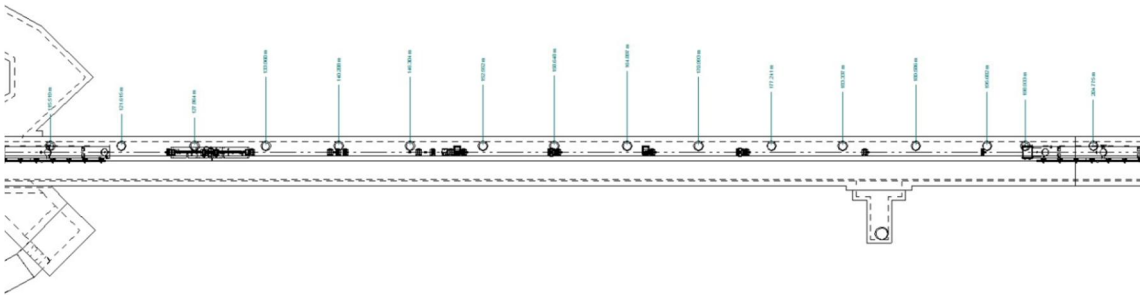

Figure 0-19. Schematic of the 62-meter BC1/COL1 system as laid out in the SLAC linac tunnel.

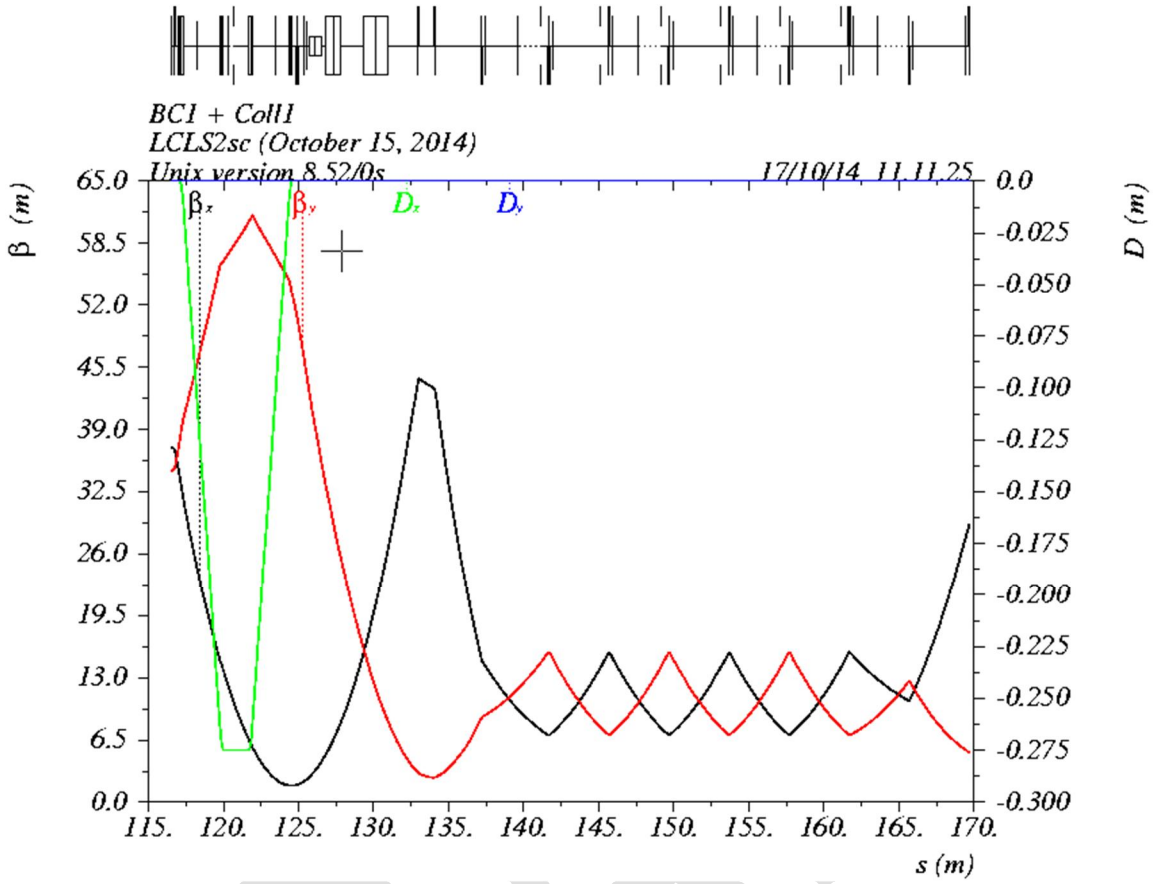

Figure 0-20. Optics functions over the BC1 chicane and collimation section following.

4.3.7 BC2 and COL2 Beamlines

The BC2 system is a warm beamline 106.1 meters in length which starts just downstream of cryomodule CM15 and ends at the beginning of the L3 linac. The nominal beam energy is 1.6 GeV. The beamline consists of four dipole magnets, thirteen quadrupoles, and five collimators and is illustrated schematically in Figure 0-21.

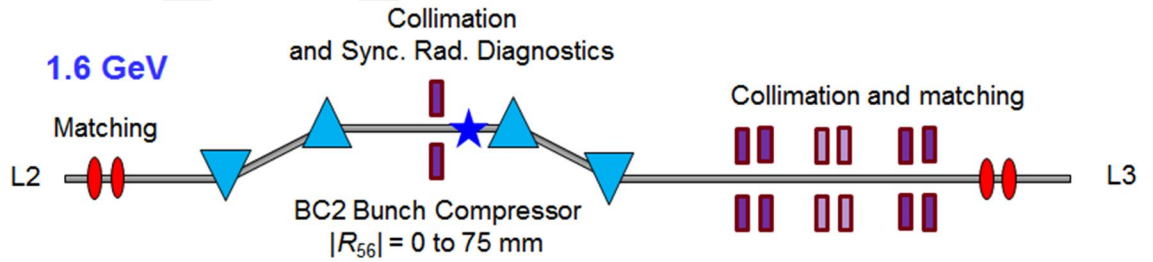

Figure 0-21. Schematic of BC2 and COL2.

The beamline has two main functions: 1) compressing the longitudinal bunch length by a factor of 10 to 30 in a four-dipole chicane, and 2) collimating the incoming beam to reduce dark current and trapped field emission. It will also be used to stabilize the beam energy and trajectory

at this mid-point along the superconducting linac. The design of the four-magnet chicane is very similar to the existing system that is in operation at LCLS, while the rest of the beamline will be standard transport line. The requirements for the BC2 bunch compressor are listed in the *BC2 Bunch Compressor Chicane Physics Requirements Document*, LCLSII-2.4-PR-0040, while the requirements of the collimation system are specified in the *Halo Collimation System Physics Requirements Document*,LCLSII-2.4-PR-0095 and the shielding issues associated with the collimators are described in *Radiation Protection Requirements for the Halo Collimators*, LCLSII-1.2-PR-0259.

The BC2 bunch compressor must have an R_{56} that can be varied between 0 and 75 mm. This is done by varying the dipole magnetic field and moving the two center dipoles on a horizontal translation stage. The translation stage is based on the operating BC2 system at LCLS, but it has been modified for a lower elevation and slightly larger translation. The maximum translation is 630 mm and the BC2 supports will partially occupy the aisle in the linac tunnel; to move cryomodules past BC2, the translation stage will need to be partially disassembled. BC2 also includes an energy collimator, as illustrated in Figure 0-21, to collimate off-energy particles. To minimize the shielding requirements, the maximum power rating of this energy collimator is 10 Watts.

The BC2 compressor is very similar to the operating LCLS BC2, using the same design for the chicane magnets but with the space between the second and third bends increased to allow installation of a high power collimator, BPM, and wire scanner. Like the operating LCLS BC2, the compressor would also include two ‘tweaker’ quadrupoles that would allow correction of residual dispersion or emittance dilution from Coherent Synchrotron Radiation (CSR). In addition, the optics are matched across BC2 to minimize the CSR emittance growth; this yields relatively large incoming beta functions.

The compressor is followed by a periodic lattice, referred to as COL2, with 45-degree phase advance that contains two horizontal and two vertical betatron collimators where the pairs of collimators are separated by 90 degrees in phase. Interspersed with the collimators are four wire scanners that will be used to measure the beam emittance after the bunch compressor.

The hardware components for BC2 are listed in Table 0-14. The designs for the specific magnets, power supplies, collimators and diagnostics are described in Chapter 5.

Table 0-14. BC2 Hardware Components.

Component	Quantity	Engineering name	Status
Dipole magnet	4	1D19.7	Existing design
Quadrupole magnet	11	1.259Q3.5	Existing design
Trim quadrupole	2	2.362Q3.5	Existing design
Dipole corrector ($x + y$)	10	Class-4	Existing design
Energy collimator	1	-	new
Betatron collimator	4	-	new

Stripline BPM	11	-	Existing design
Current mon	1	DCCT	Commercial
Bunch length	1	CSR	Existing design
Wire scanners	5	-	Existing design

Figure **0-22** shows the CAD drawing of the four-dipole chicane. The center two dipoles are mounted on a translation stage to allow adjustment of the R_{56} value through the chicane. The translation stage is based on the existing translation stage that is in operation at LCLS with minor modifications to lower the stage to the SCRF linac elevation.

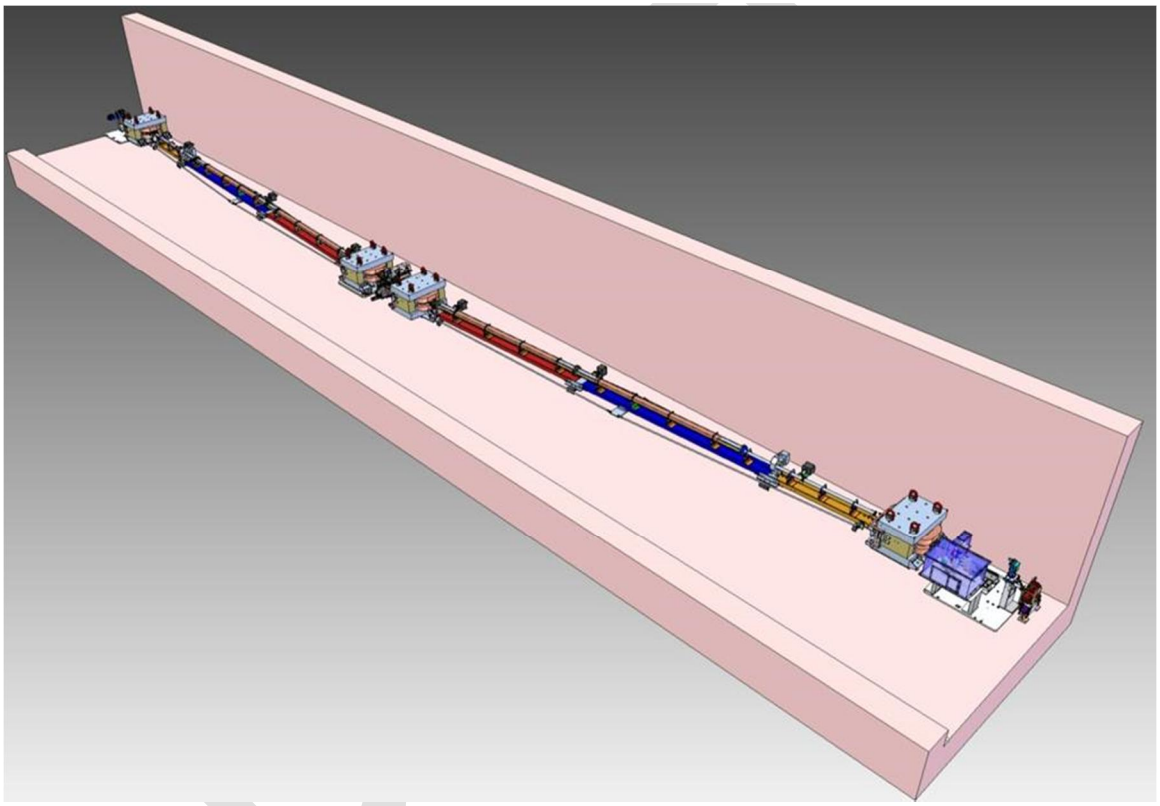

Figure 0-22. Drawing of the BC2 four-magnet chicane which comes out into the linac aisle. The bunch compressor is roughly 20-meters in length and is based on the existing LCLS BC2 design.

The vacuum system through the four-magnet chicane has a large aperture to accommodate ±6% energy bandpass and designed to minimize the longitudinal impedance as described in the *BC2 Bunch Compressor Chicane Physics Requirements Document*, LCLSII-2.4-PR-0040. The remaining vacuum system is assembled as described in Chapter 5, including the 'particle-free' regions adjacent to the SCRF cryomodules. A CAD drawing of the entire beamline is shown in Figure 0-23. The optics functions are shown in Figure 0-24.

(CAD Drawing ???)

Figure 0-23. Schematic of the 106-meter BC2 System as laid out in the SLAC linac tunnel.

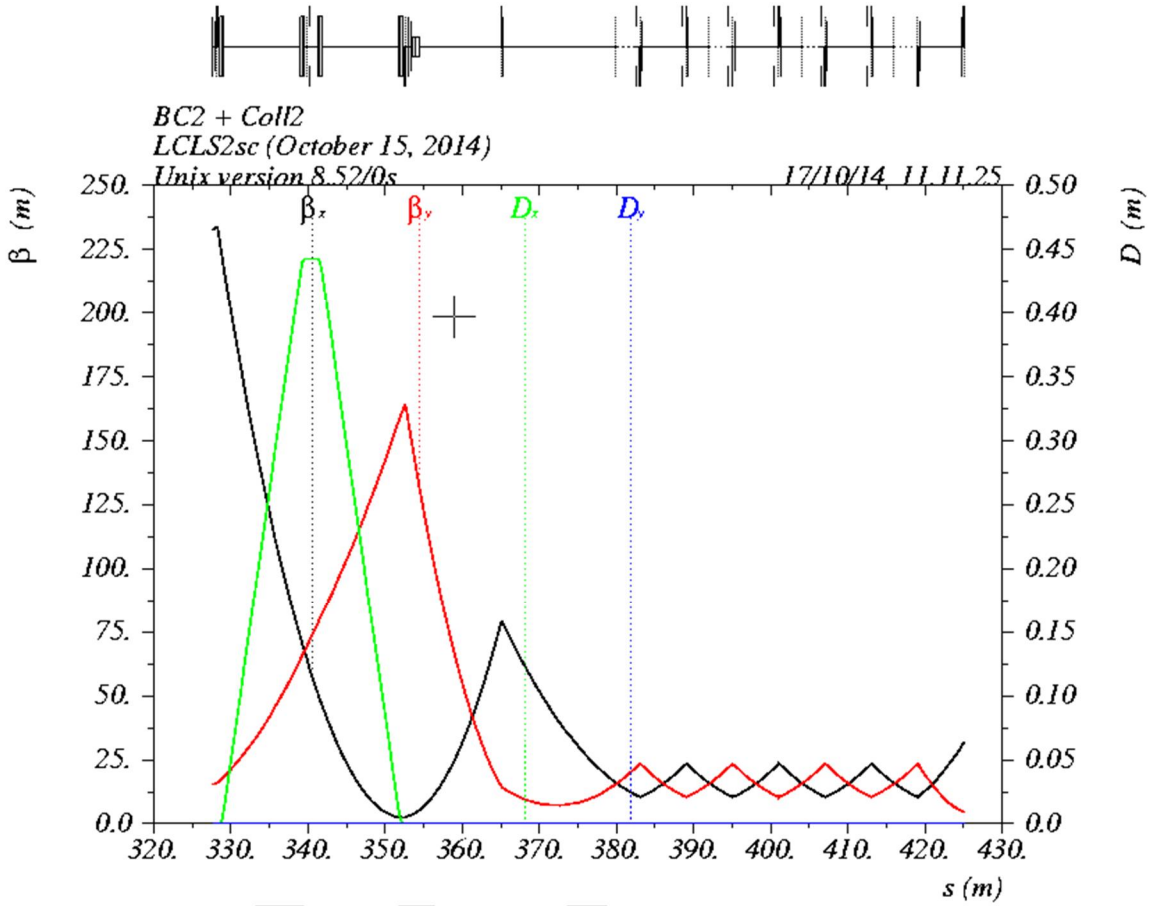

Figure 0-24. Optics functions over the BC2 chicane and collimation section following.

4.3.8 SCRF Linac L3 Extension Line

The L3 extension will transport the beam from the end of the L3 linac to Sector 10 in the SLAC linac. The extension will allow future expansion in the long term with the installation of more cryomodules (up to 6.5 GeV with 19 additional CMs), as described in the *SCRF Electron Linac Extension and Bypass Line Physics Requirements Document*, LCLSII-2.4-PR-0091. The L3 extension also includes a removable spool-piece to allow easy installation of cryomodules from the Sector 10 spur. The L3 extension FODO phase advance is roughly 45 degrees per cell and it is not populated with collimators or diagnostics other than BPMs. The magnets are specified to operate over the beam energy range from 2.0 GeV to 10 GeV. The vacuum chamber will be 2" stainless steel vacuum chamber re-purposed from the existing PEP-II LER Bypass line (the Bypass line not to be used by LCLS-II) and the quadrupoles will be large bore 'wrap-around' quadrupoles re-purposed from Sector 1 of the existing CuRF linac. The BPMs will also be refurbished from the PEP-II LER transport line. The beam optics of the L3 extension line are shown in Figure 0-13.

The hardware components for the L3 Extension are listed in Table 0-15. The designs for the specific magnets, power supplies, collimators and diagnostics are described in Chapter 5. All components in the L3 Extension will be refurbished pre-existing hardware.

Table 0-15. L3 Extension Hardware Components.

Component	Quantity	Engineering name	Status
Quadrupole magnet	7	4.63Q8.0	Existing magnet
Quadrupole magnet	2	1.085Q4.3	Existing magnet
Dipole corrector ($x + y$)	6	Type-4	Existing design
Stripline BPM	8	-	Existing design

4.4 Transfer Lines and Dumps

The transfer lines in LCLS-II will transport the beams from the end of the SCRF linac in Sector 10 around the existing SLAC copper linac and into the BSY at the end of the CuRF linac. Upstream of the BSY, a Beam Spreader will direct the electrons from the SCRF linac to either the HXR or SXR undulators and associated dumps or a high power beam dump in the BSY. An additional transport line connects the existing LCLS CuRF linac to the HXR transport line.

The LCLS-II beamlines were illustrated schematically in Figure 0-1. The total length of transport line exceeds 3.5 km, but much of this is pre-existing and requires only minor modification for LCLS-II purposes. New transport lines include: 1) the Dogleg that brings the beam from the SCRF linac elevation to that of the pre-existing PEP-II HER Bypass line that is used to transport the beams around the existing copper linac, the Beam Spreader and the BSY dump, and 2) the linac-to-undulator (LTU) transport to the Soft X-ray (SXR) undulator and associated dump. The Bypass line, the connection to the LCLS copper linac and the LTU to the HXR undulator and associated dump are all pre-existing.

The SCRF linac is being designed to accelerate up to 1.2 MW of electron beam to facilitate future expansion, even though the initial installation will be limited to roughly 20% of the full capability. Upstream of the Beam Spreader, the SCRF cryomodules, beam collimators, vacuum chamber, Machine Protection System, and Beam Containment Systems are all designed for the full 1.2 MW of beam power. Downstream of the Beam Spreader, each of the SXR and HXR undulators is designed for a maximum of 120 kW and thus the LTU's that transport the beams from the Spreader to the undulators are designed for the lower beam currents. Similarly, the BSY Dump is designed for a maximum beam power of 250 kW (2x120 kW + 10 kW keep-alive). As discussed in Chapter 17, the linac beam power will be increased to support expansion of the site as new undulators beam lines and new dumps are added.

The transport lines will mostly be installed during the long shut down during FY18.

4.4.1 LCLS-II Bypass Dogleg

The Dogleg is a warm beamline roughly 300 meters in length which starts at the end of the L3 Extension, described in Section 4.3.8, and ends after matching into the pre-existing PEP-II HER Bypass line, described in Section 4.4.2. Although the nominal beam energy is 4 GeV, the magnets have been specified to operate over the range of 2.0 GeV to 10.0 GeV. The beamline consists of two dipole magnets, twelve quadrupoles, one energy collimator and beam diagnostics and is illustrated schematically in Figure 0-25.

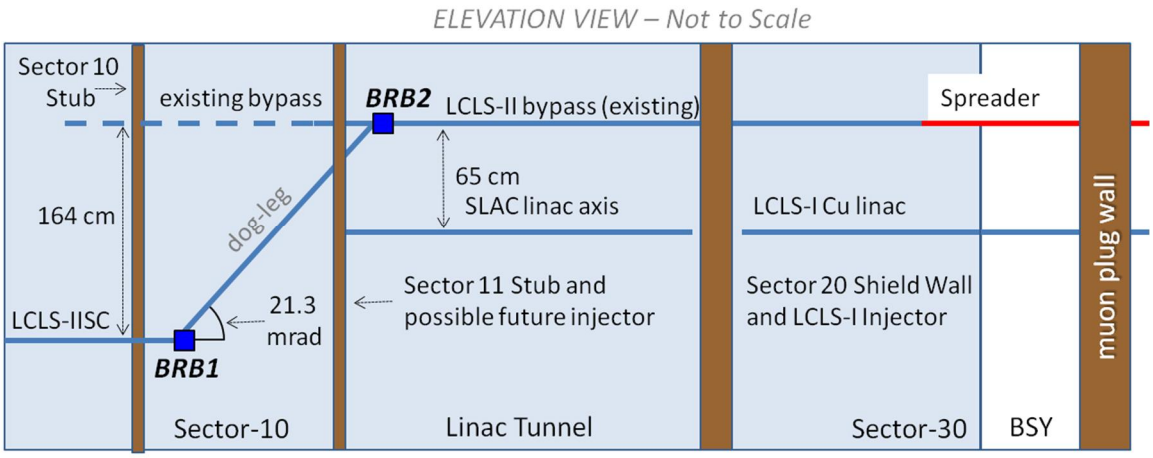

Figure 0-25. Elevation view (not to scale) of LCLS-II bypass line from Sector 10 through the linac tunnel to the Beam Spreader located in Sector 28. The bend angle shown (21.3 mrad) is the vertical projected angle only. The *BRB1* bend is rolled by 60.4° for a net bend of 24.5 mrad, generating both a vertical (21.3 mrad) and horizontal (12.1 mrad) bend angle. The bypass line is shown as 25.570 inches above the SLAC CuRF linac axis, but it is also (not shown in elevation view) 25.610 inches south of the SLAC CuRF linac axis (*i.e.*, above this page).

The dogleg beamline has two main functions: 1) bring the beam from the SCRF linac elevation up to that of the existing PEP-II Bypass line, roughly 165 cm above and 65 cm to the south of the SCRF linac beamline, and 2) measure and collimate the incoming beam energy and energy spread. The Dogleg is the first location at the end of the linac where the beam energy can be measured and collimated. The energy collimator is designed to absorb up to 1 kW of average beam power from off-time particles coming from the gun, and captured field emission current from the linac and the downstream energy measurement would be part of the longitudinal energy feedback. The requirements on the Dogleg beamline are described in the *SCRF Electron Linac Extension and Bypass Line Physics Requirements Document*, LCLSII-2.4-PR-0091 while the requirements of the collimation system are specified in the *Halo Collimation System Physics Requirements Document*,LCLSII-2.4-PR-0095 and the specific shielding issues associated with the Bypass line energy collimator, CEDOG, are described in *Radiation Protection Requirements for the CEDOG Collimator*, LCLSII-1.2-PR-0260.

The Dogleg is placed just downstream of the Sector 10 spur to allow access to the LCLS-II linac tunnel (Sectors 0-10) for cryomodule installation and is sized to allow future installation of

a normal-conducting RF injector in the Sector 11 stub which could connect into the existing SLAC CuRF linac. The beamline optics from the start of the L3 Extension through the Bypass line are shown in Figure 0-26. The focusing along the Dogleg is chosen to cancel the dispersion at the second dipole using four 90-degree FODO cells. The dispersion is relatively large, peaking around 45cm in the vertical plane. The energy collimator, CEDOG, is located at the first high dispersion location, while a wire scanner, WSDOG, is located at the second. The energy collimator, CEDOG, is designed to collimate up to 1 kW of average beam power. This collimator is the primary energy collimator along the beamline and defines the maximum energy aperture for the downstream systems. The shielding and radiological protection issues associated with CEDOG are described in Chapter 13.

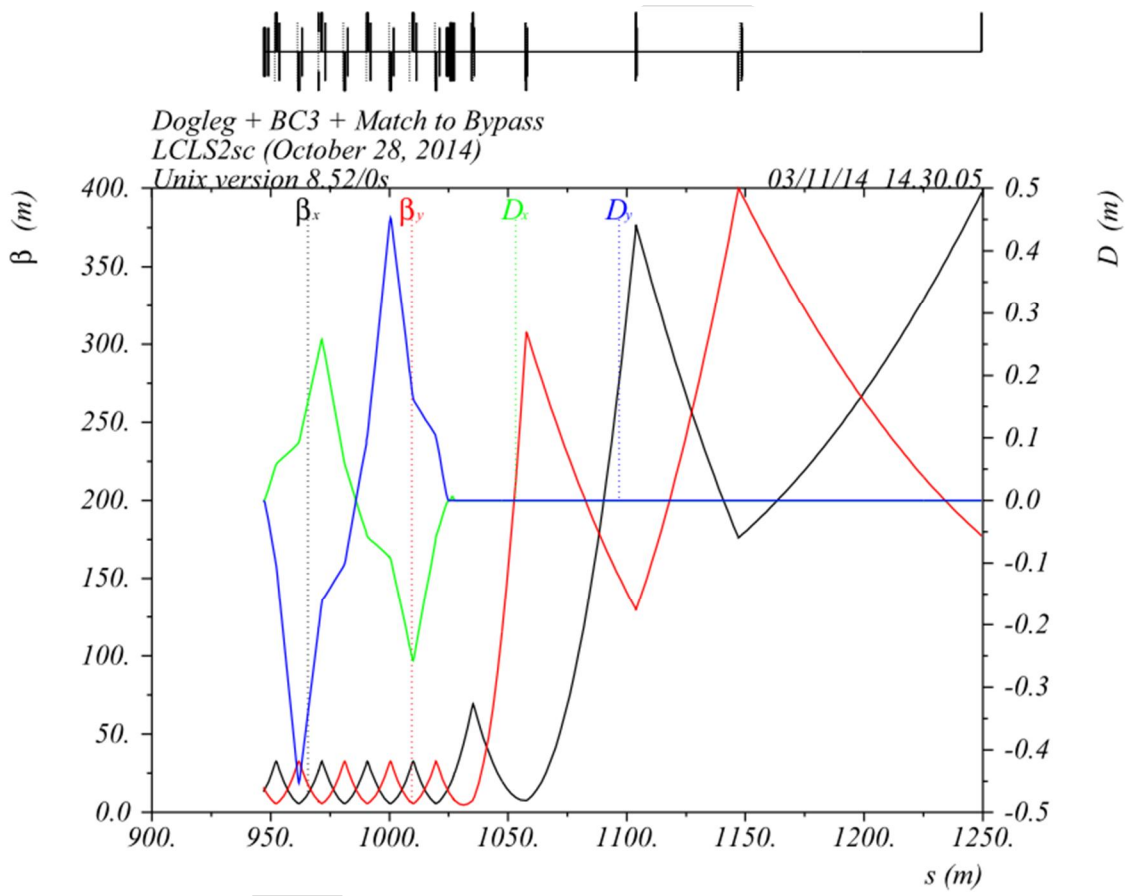

Figure 0-26. The beamline optics functions from the Linac Extension through the Dogleg and the Bypass matching. The Dogleg is located around the 1000-meter mark where the strong focusing quadrupoles are used to match the dispersion. The 101.6-m spacing of the existing bypass line quadrupole magnets can be seen at the end of the matching region.

As described in Chapter 3, one method of suppressing the micro-bunching instability is to compensate the R_{56} of bending systems downstream of BC2. This is performed by adding a weak four-magnet chicane just upstream of BRB1 (the first rolled dipole in the Dogleg) and just

downstream of BRB2 (the second rolled dipole in the Dogleg). These chicanes each introduce roughly 100 microns of R_{56} that compensate that of the dogleg magnets.

The hardware for the Dogleg is listed in Table 0-16. All magnets, BPMs and vacuum chambers in the Dogleg will be refurbished, existing SLAC components except for the new R_{56}-control dipoles. A new wire scanner and new energy collimator will be required. The details of the specific magnets, power supplies, and collimators are described in Chapter 5.

Table 0-16. Dogleg Hardware Components.

Component	Quantity	Engineering name	Status
Dipole magnet	2	1.0D38.37	Existing magnet
Dipole magnet	8	R56	New Design
Quadrupole magnet	1	1.97Q20	Existing magnet
Quadrupole magnet	9	1.97Q10	Existing magnet
Quadrupole magnet	2	2Q4W	Existing magnet
Dipole corrector ($x + y$)	17	Type-4	Existing design
Energy collimator	1	-	new
Stripline BPM	10	-	Existing design
Wire scanner	1	-	Existing design

Figure 0-27 shows a drawing of the beginning of the Dogleg with the rolled BRB1 magnet, which is rolled at 60.4 degrees to elevate the beam to the Bypass line. The vacuum chamber has a relatively large aperture to allow for energy deviations up to ±3%.

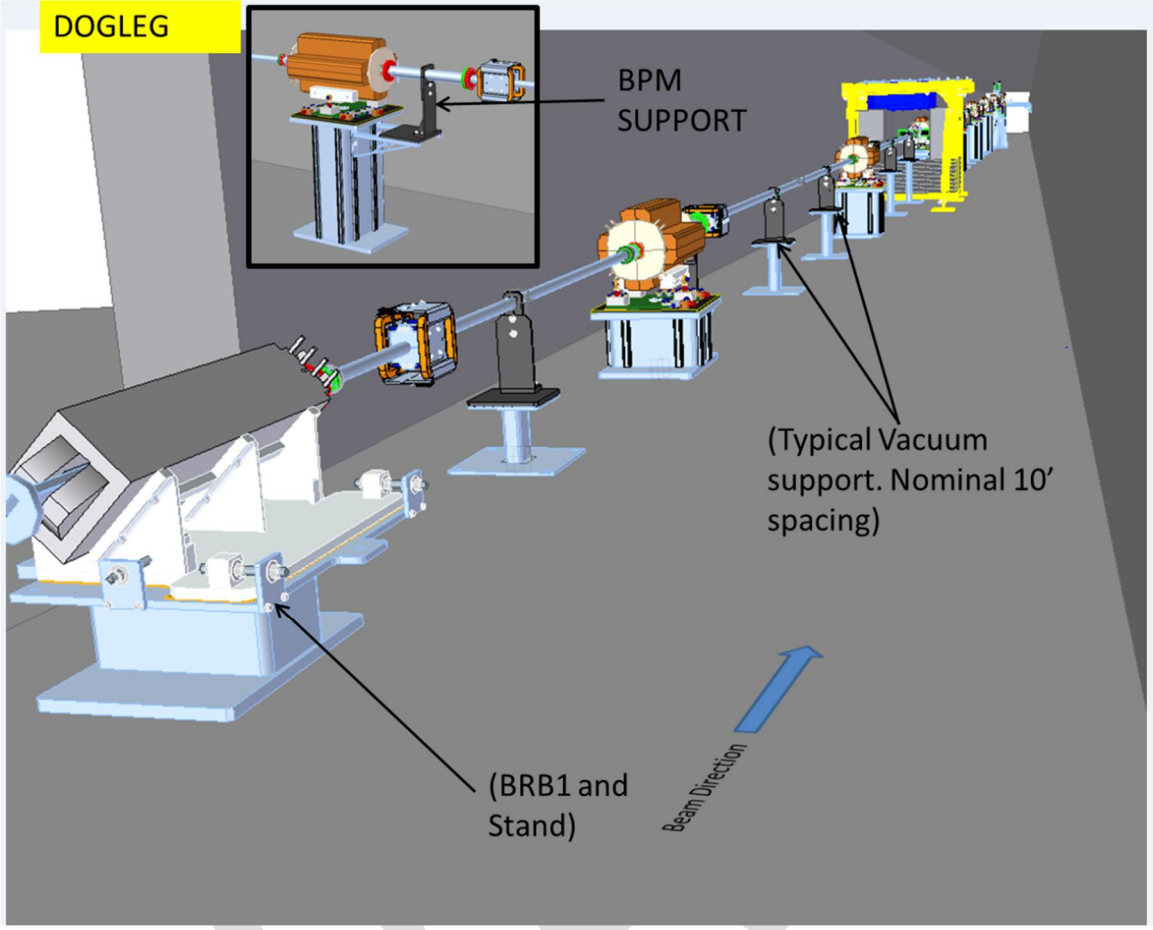

Figure 0-27. CAD drawing showing the beginning of the Dogleg beamline including the rolled BRB1 magnet, the first two quadrupoles, and the structure to support the shielding around the CEDOG collimator.

4.4.2 LCLS-II Bypass Line

The Bypass line is a pre-existing warm beamline roughly 1500 meters in length which starts at the end of the Dogleg, described in Section 4.4.1, and transports the beam to the Beam Spreader, described in Section 4.4.3. The nominal beam energy is 4 GeV however the magnets have been specified to operate over the range of 2.0 GeV to 10 GeV. The beamline consists of a weak focusing FODO lattice with a quadrupole spacing of 101.6 meters. There are 17 quadrupoles, 4 betatron collimators, and a 4-wire emittance diagnostic; the beamline is illustrated schematically in Figure 0-25 while the optics are shown in Figure 0-28.

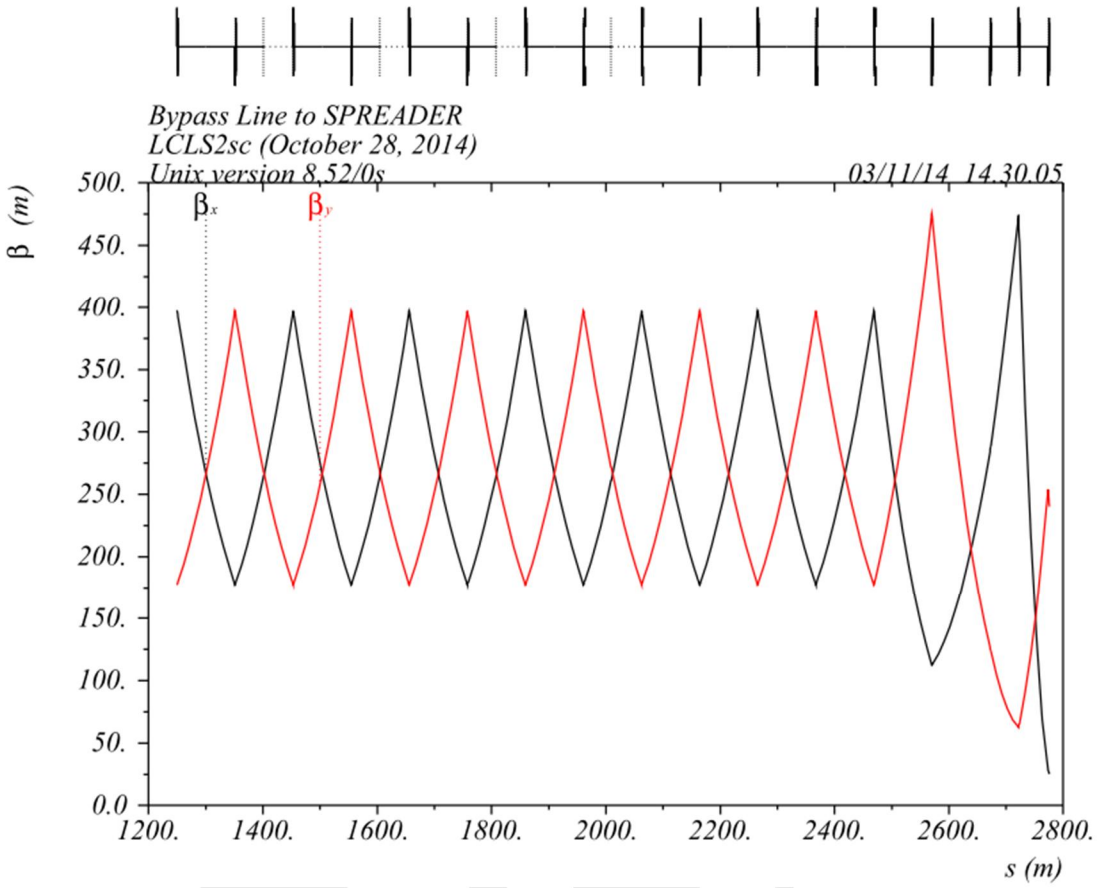

Figure 0-28. The beamline optics functions through the existing Bypass line. The 101.6-m spacing of the existing bypass line quadrupole magnets can be seen at the end of the matching region. Collimators and wires.

The beamline has two main functions: 1) transport the beam from the SCRF linac around the existing copper linac of the LCLS, and, 2) measure and collimate the incoming beam betatron phase space before the beams are sent to the undulators transport lines. The Bypass line was constructed with a similar goal for the PEP-II collider, namely, transport the 9 GeV High Energy Ring beam around the SLAC linac. The existing system will be re-used with minimal modifications. The requirements on the Bypass beamline are described in the *SCRF Electron Linac Extension and Bypass Line Physics Requirements Document*, LCLSII-2.4-PR-0091 while the requirements of the collimation system are specified in the *Halo Collimation System Physics Requirements Document*,LCLSII-2.4-PR-0095 and the shielding issues associated with the collimators are described in *Radiation Protection Requirements for the Halo Collimators*, LCLSII-1.2-PR-0259. The Bypass line includes long drifts and the vacuum chamber may require additional magnetic shielding as described in the *Warm Beamline MuMetal Physics Requirements Document*, LCLSII-2.4-PR-0060. Both X and Y dipole correctors are located at each quadrupole to help correct for deflections due to the earth's magnetic field.

The new hardware for the Bypass line is listed in Table 0-17. The beamlines, magnets, vacuum chamber, BPM's, and supports are pre-existing and will only require minor

modifications. Only the 4 wire scanners and 4 collimators are new hardware. The required hardware components are described in greater detail Chapter 5.

Table 0-17. Bypass Line Hardware Components.

Component	Quantity	Engineering name	Status
Quadrupole magnet	15	2Q4	Installed magnet
Quadrupole magnet	2	2Q4W	Existing magnet
Dipole corrector ($x + y$)	34	Bypass	Existing design
Betatron collimator	4	-	new
Stripline BPM	15	-	Existing design
Wire scanners	4	-	Existing design

The Bypass line components are supported from the SLAC tunnel ceiling. Vibration and component stability have been measured and are acceptable [XX]. The vacuum system is combined with the PEP-II LER Bypass line and will need to be separated. Only minor modifications of the other existing hardware will be required for LCLS-II purposes.

4.4.3 Beam Spreader

The Beam Spreader is located at the end of the Bypass Line in Sector 28 in the SLAC tunnel. It is used to direct the high rate beam from the SCRF linac to the SXR undulator, the HXR undulator or the high power BSY electron beam dump. The spreader system also provides a beam abort function as part of the Machine Protection System so that, if a fault arises downstream, beam can be rapidly directed to a dump before the injector, 3 km further upstream, can be shut off.

The maximum energy that the initial installation of the kicker will support is 4.2 GeV but the system could be upgraded to operate at 6 GeV by lengthening the magnets and reconfiguring the septa. The requirements for the Beam Spreader are described in the *Beam Spreader Physics Requirements Document*, LCLSII-2.4-PR-0090. The requirements for the collimation system are specified in the *Halo Collimation System Physics Requirements Document*, LCLSII-2.4-PR-0095. As documented in *Warm Beamline MuMetal Physics Requirements Document*, LCLSII-2.4-PR-0060, there may be some additional magnetic shielding that is required to limit the operational impact on the adjacent beamline when changing magnetic fields.

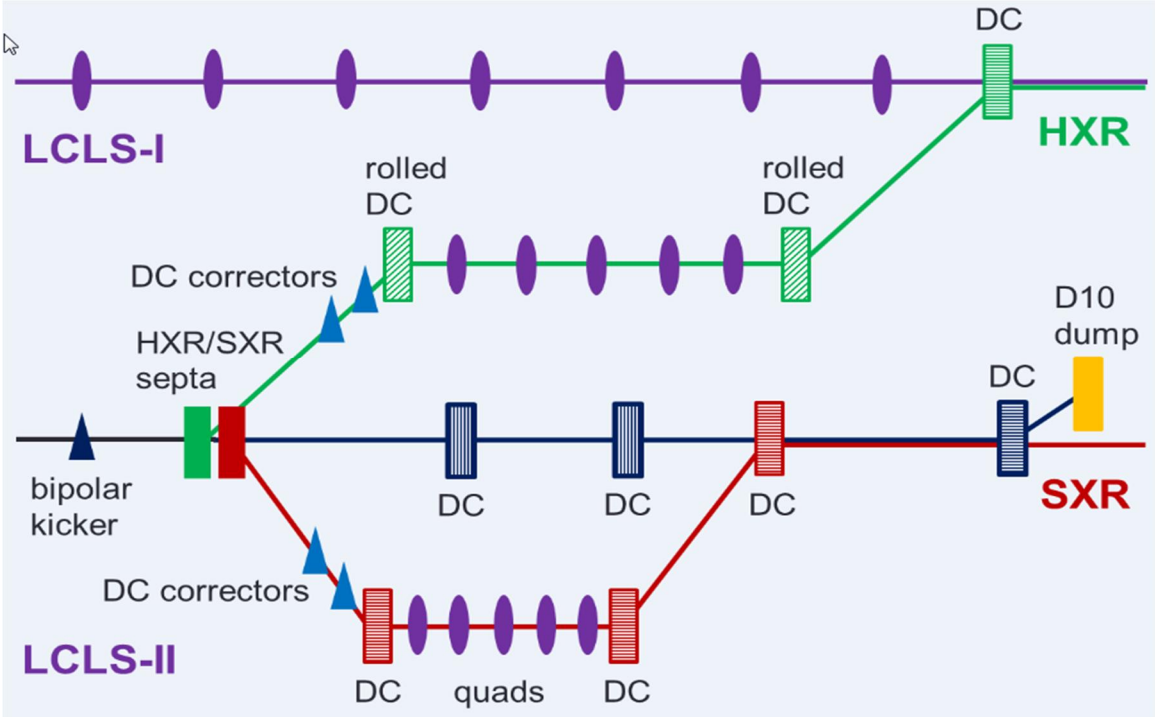

Figure 0-29 **Schematic of the Beam Spreader showing the bipolar kicker and the two lambertson septa used to direct the beams to the SXR (red) and HXR (green) undulators as well as the undeflected beamline (black) running to the BSY Dump (D10).**

The Spreader consists of a bipolar magnetic kicker system that provides a vertical deflection of 0.75 mrad to deflect the beam into one of two Lambertson septa 20-meters away that deflect the beams into the SXR (upward deflection) or the HXR (downward deflection). The kicker pulse length is much less than the 1 μs bunch spacing and allows complete control on the destination of individual bunches.

The expected operational mode is that beam would be established on the BSY dump and then the spreader kicker would be used to direct low rate beam to the SXR and/or HXR undulators. Once the trajectory and FEL performance is optimized, the rate could be increased to nearly the full beam repetition rate while leaving sufficient beam rate on the BSY dump so that the trajectory to the dump could be maintained.

The electron beams directed to the SXR undulator would be deflected to the south by the SXR Lambertson and then returned to the same trajectory with three downstream DC dipole magnets, as shown in Figure 0-29. Nine quadrupoles are used to make the beamline isochronous and these allow adjustment of the R_{56} from ±4mm. Finally, six large-bore quadrupoles are used to match the beam into the Muon Shield wall and the downstream SXR linac-to-undulator (LTU) beamline. The LTU beamline, described in Section 4.4.6, brings the beam through the Beam Transfer Hall to the SXR undulator in the LCLS Undulator Hall. The optics for the Beam Spreader SXR beamline are shown in Figure 0-30.

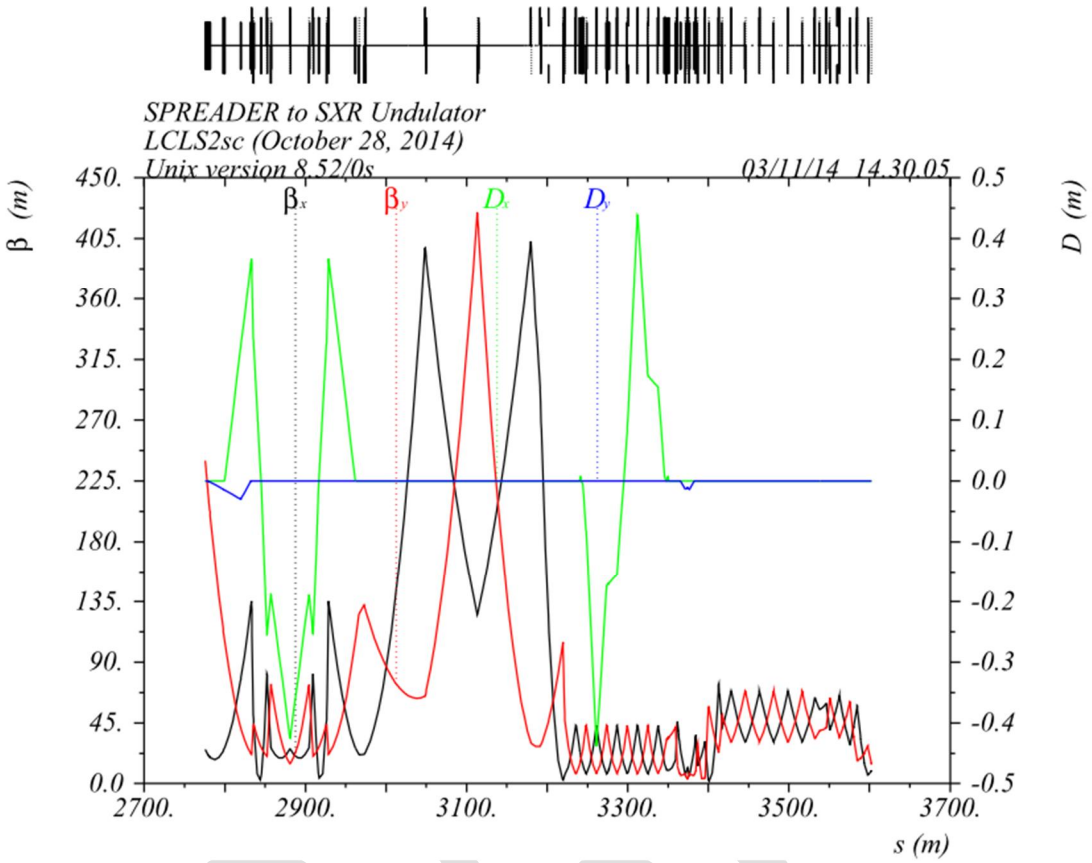

Figure 0-30. SXR beamline optics from the Spreader through the Muon Shield wall and to the SXR undulator; the Muon Shield wall is located at just after the 3200-meter point and the SXR LTU begins at 3234 meters.

Figure 0-31 shows the general layout of the spreader kicker and septa and the downstream separation of the three beamlines. Figure 0-32 illustrates the beamlines roughly 200 meters downstream of the spreader kicker, showing, from right to left, the beamline to the SXR undulator, the beamline to the HXR undulator, the beamline to the BSY dump, and the existing LCLS CuRF linac. This is a complicated region with interleaved beamlines and supports. Detailed CAD models have been developed to avoid interferences and optimize the designs.

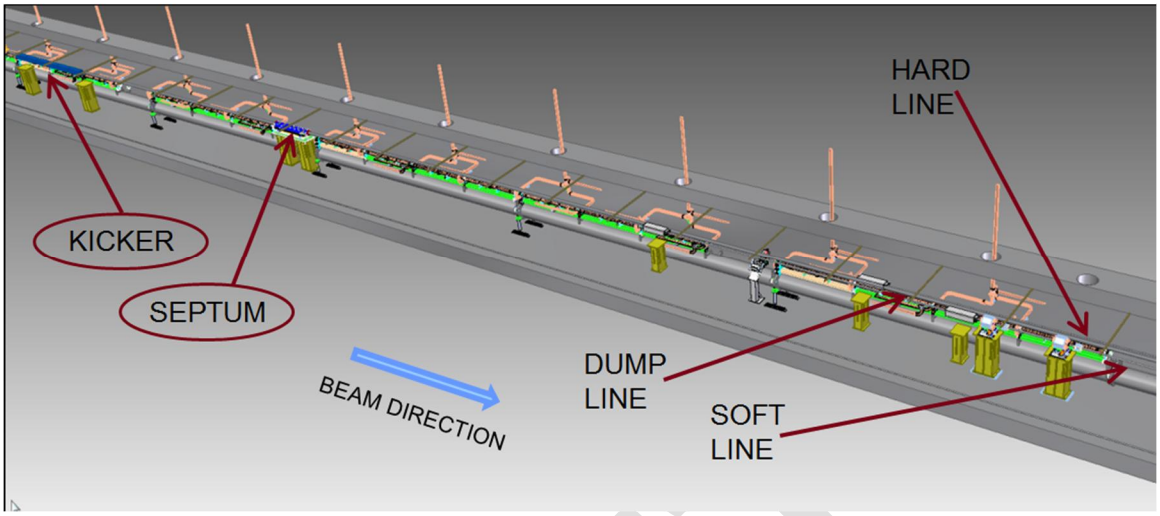

Figure 0-31. Upstream portion of the Beam Spreader layout indicating the kicker, septa, and three downstream beamlines.

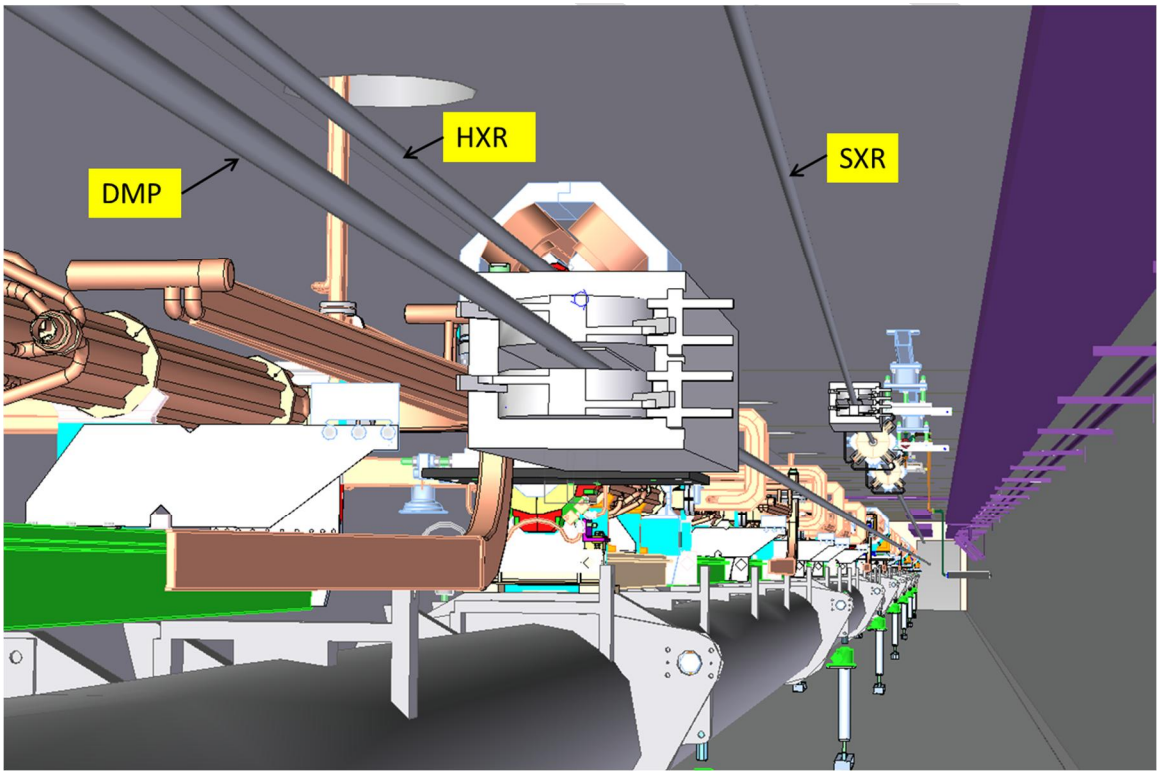

Figure 0-32. The four beamlines roughly 200 meters downstream of the Beam Spreader kicker and septa: the existing LCLS CuRF linac, the spreader line to the SXR, the spreader line to the HXR, and the BSY Dump beamline.

Finally, a new beam channel will need to be constructed through the Muon Shield wall for the beamline to the SXR undulator that is 65 cm above and 65 cm south of the existing LCLS beamline. The Muon Shield wall is a stack of iron blocks that fills the tunnel aperture and extends 55 feet in length as illustrated in Figure 0-35. Figure 0-33 shows the upstream end of the shield

wall where the existing LCLS enters in the lower left. The space for the new beamline to the SXR undulator is indicated with the red dashed line, and the blocks that will have to be re-stacked are indicated with the yellow dashed line.

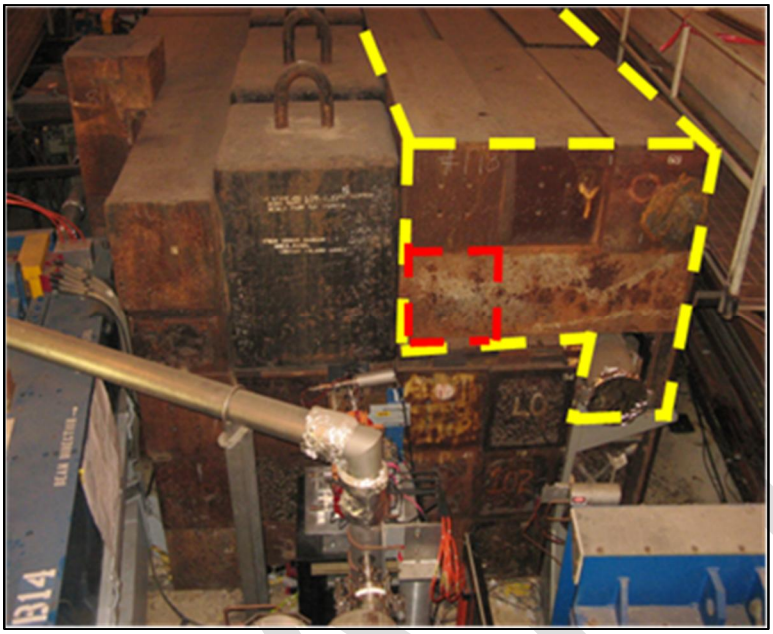

Figure 0-33. Photograph of the Muon Shield wall with red dashes indicating the location of the penetration for the new beamline to the SXR undulator.

In a manner similar to that for the beamline to the SXR, the electron beams directed to the HXR undulator will be deflected to the north by the HXR Lambertson and then further deflected down by 65 cm and to the north by a similar distance to join the existing LCLS beamline using 3 DC dipole magnets. This part of the system is schematically illustrated in Figure 0-29. The final merger dipole magnet that deflects the beam from the SCRF linac onto the LCLS beamline trajectory will be turned off to allow beam from the CuRF linac to reach the HXR undulator.

The beamline consists of two interleaved doglegs, one in the horizontal plane and one rolled by 31.8 degrees. Thirteen quadrupoles are used to match into the existing LCLS beamline while allowing adjustment of the R_{56} over the range of ±1mm. Like the SXR beamline, the existing HXR beamline then enters the Muon Shield wall before the existing HXR linac-to-undulator (LTU) beamline, described in Section 4.4.5, brings the beam through the Beam Transfer Hall to the HXR undulator in the LCLS Undulator Hall. The optics for the Spreader HXR beamline are shown in Figure 0-34.

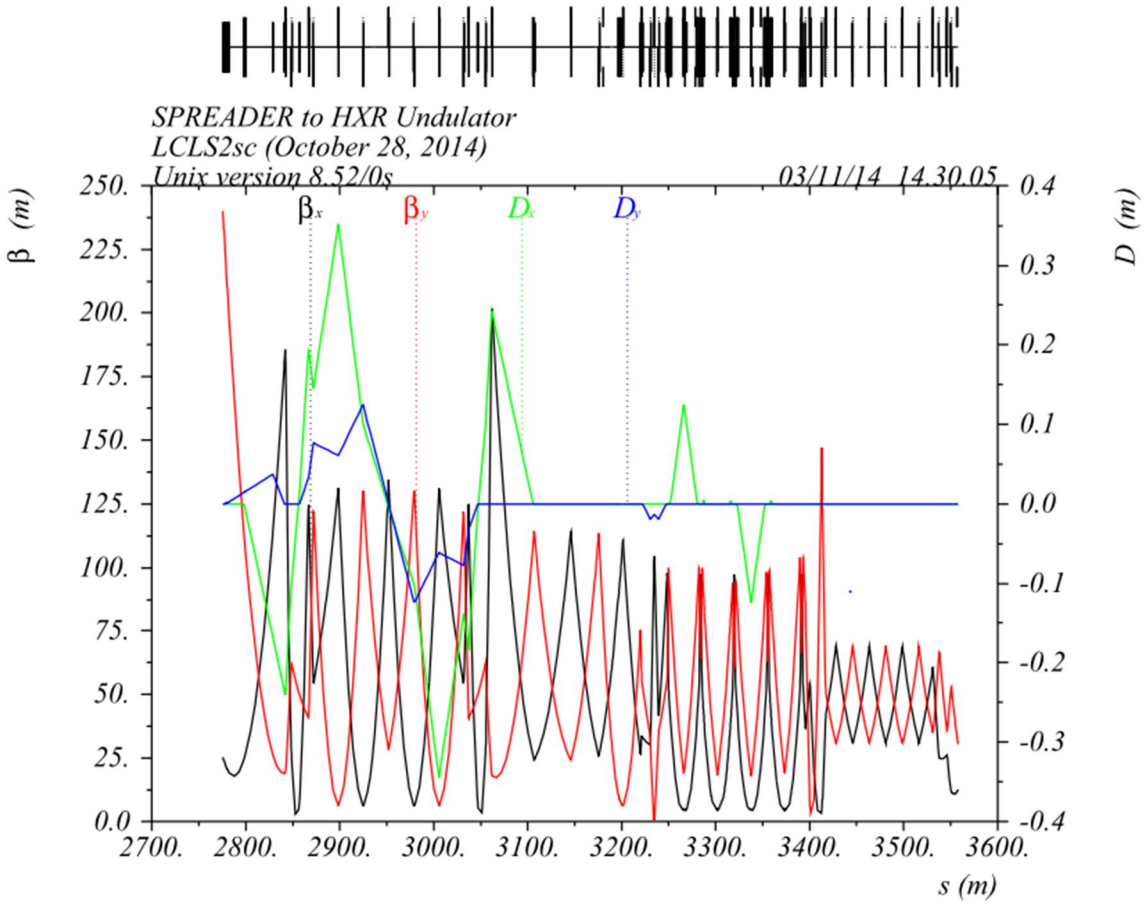

Figure 0-34. HXR Beamline optics from the Spreader through the Muon Shield wall and to the HXR undulator; the Muon Shield wall is located at just after the 3200-meter point and the HXR LTU begins at 3234 meters and ends after the undulator tuning dump, TDUND, at 3573 meters.

Finally, if the spreader kicker is turned off, the electron beam passes through the two septa undeflected and then is directed down and finally to the north into a high power dump located inside the Muon Shield wall. The BSY Dumpline and BSY Dump are described in Section 4.4.4.

Most of the vacuum chambers in the spreader system are standard 1.25" and 2" stainless-steel vacuum chambers. The only exceptions are the spreader kicker chamber, which will be coated ceramic chamber with a 1 cm inside diameter, and the chambers through the spreader septa.

The new hardware components for the Beam Spreader are listed in Table 0-18. The designs for the specific components are described further in Chapter 5. As noted, the baseline design for the spreader kicker is a pulsed magnetic deflector which feeds two Lambertson septa. The primary challenge will be achieving the relative deflection stability requirements of $5x10^{-5}$ while also developing a highly reliable system. The pulsed magnet technology is still in the prototyping phase. If there are unforeseen problems in developing the magnetic kicker, the project can adopt an RF dipole as described in the *Beam Spreader Physics Requirements Document*, LCLSII-2.4-PR-0090.

Table 0-18. Beam Spreader new Hardware Components.

Component	Quantity	Engineering name	Status
Dipole magnet	6	1.0D38.37	New Design
Dipole magnet	4	1.0D22.62	New Design
Quadrupole magnet	19	2Q10	Existing design
Quadrupole magnet	1	50Q3	Existing magnet
Quadrupole magnet	3	0.91Q17.72	Existing magnet
Quadrupole magnet	3	1.085Q4.3	Existing magnet
Quadrupole magnet	6	2Q4W	Existing magnet
Kicker	6	--	New Design
Lambertson	2	--	New Design
Dipole corrector ($x + y$)	27	Class-4	Existing design
Dipole corrector ($x + y$)	8	Bypass	Existing design
Betatron collimator	3	-	new
Stripline BPM	28	-	Existing design

4.4.4 Beam Switch Yard (BSY) Dumpline and Dump

The BSY Dumpline is the beamline that that transports the undeflected beam from the Beam Spreader to the BSY Dump which is located in the Muon Shield wall as illustrated in Figure 0-35. The BSY dump is capable of absorbing the full 250 kW of electron beam power from the linac that is planned in the initial installation. The BSY Dump beamline is roughly 403.4 meters in length and consists of three dipole magnets and two large bore quadrupoles. While the nominal beam energy is 4 GeV, the magnets have been specified to operate over the range of 2.0 GeV to 10.0 GeV. The beamline is illustrated schematically in Figure 0-29.

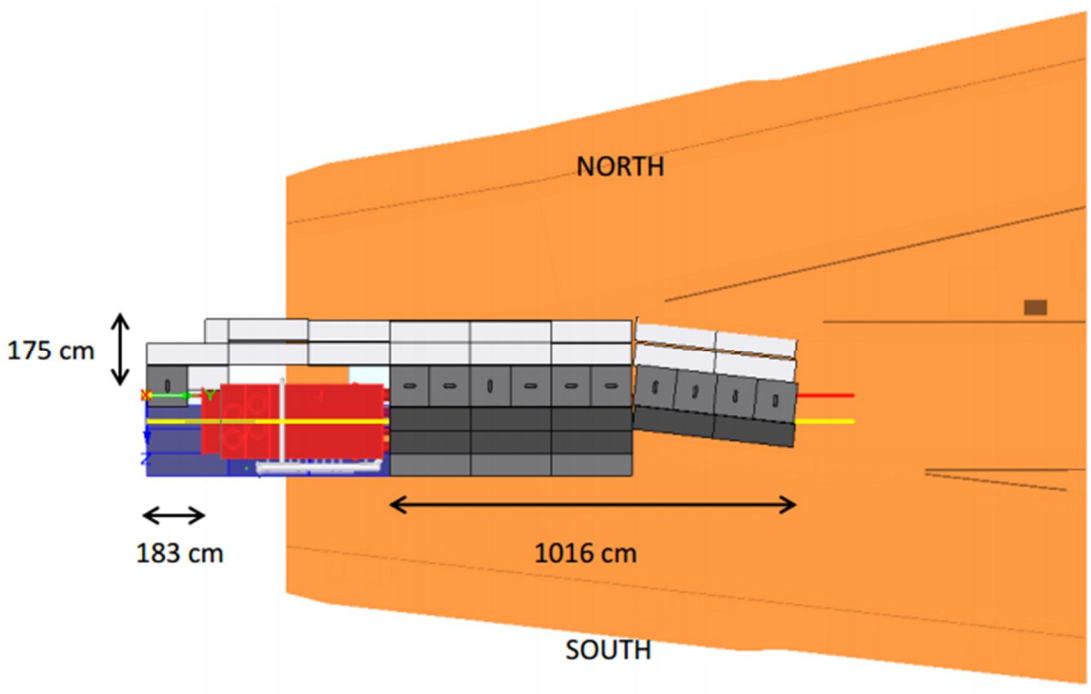

Figure 0-35. Schematic of the BSY Dump dump (red) located in the 55-foot long Muon Shieldi wall (grey) which fills the beginning of the LCLS Beam Transport Hall tunnel.

The beamline has two main functions: 1) absorbing up to 250 kW of electron beam to the BSY Dump, and, 2) measuring the incoming beam energy and energy spread to allow tuning of the SCRF linac. The requirements are described in the *BSY Dumpline and BSY Dump Physics Requirements Document*, LCLSII-2.4-PR-0080, and the shielding issues associated with the dump are described in *Radiation Protection Requirements for the D10 Alternative Location in the Muon Wall*, LCLSII-1.2-PR-0261. The beamline optics for the BSY Dumpline are shown in **Figure** 0-36**.**

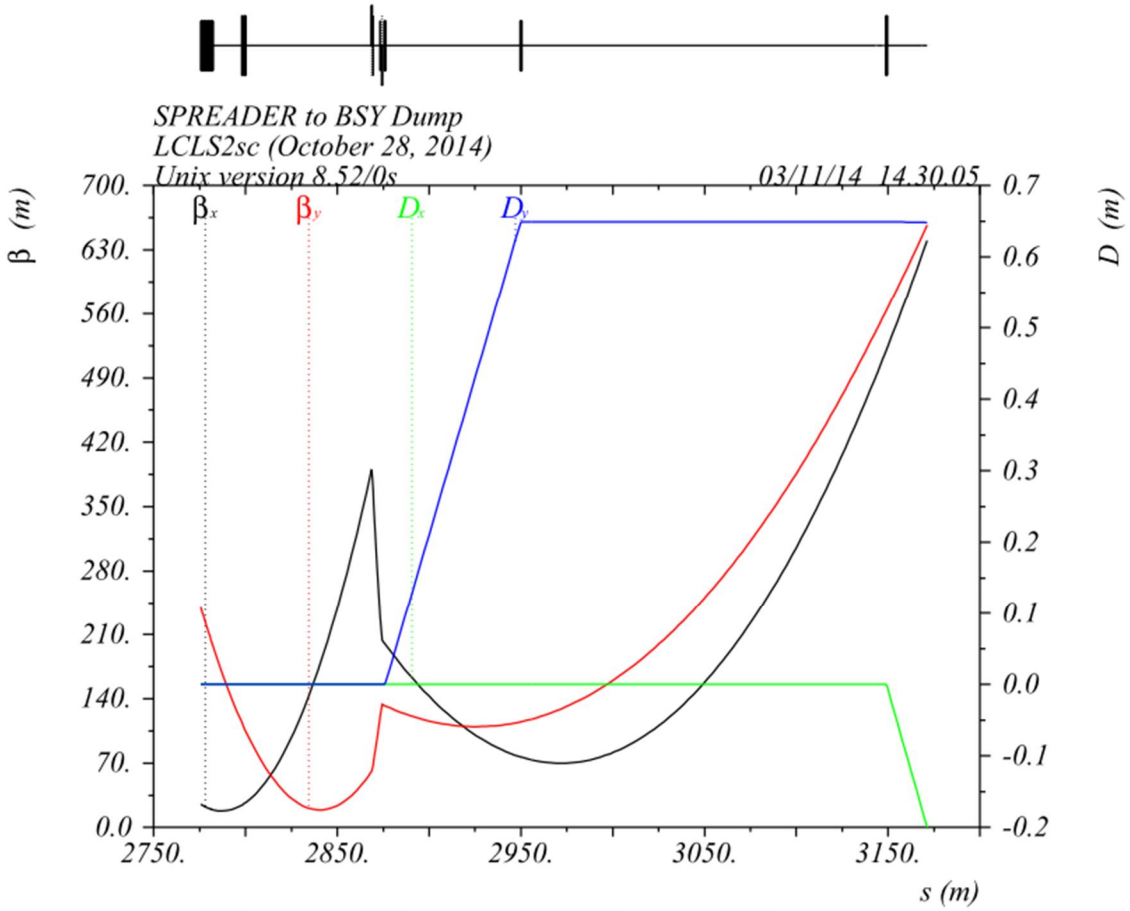

Figure 0-36. BSY Dumpline optics from the Spreader to the Muon Shield wall and the D10 dump.

The vacuum chamber stay-clear is specified to provide the same clearance as in the Dogleg and Bypass line of ±3% in energy and a $15\sigma_{x,y}$ beam with an emittance of 1 mm-mrad and nominally would be constructed of the same 2" stainless steel chamber as in the Bypass line.

Operationally, the SCRF linac will be tuned and stabilized with all beam directed to the BSY Dump before beams are sent at varying rates to the SXR or HXR undulators. Future upgrades of the LCLS-II facility may involve increasing the total electron beam power. In this case, it is expected that new dumps will be added in the BSY region. The BSY region is relatively crowded, with multiple beam lines running through it which may be tuned and changed independently of each other. As documented in *Warm Beamline MuMetal Physics Requirements Document*, LCLSII-2.4-PR-0060, some additional magnetic shielding may be required to limit the operational impact on the adjacent beamline when changing magnetic fields.

The BSY Dump will be a refurbished existing beam dump referred to as D10 that has been located in the middle of the SLAC BSY. The D10 dump will be refurbished and moved to the Muon Shield wall location as part of the effort in modifying the shield wall for the SXR beamline This water-based dump is on a separate cooling circuit that will isolate the radionuclides that will

be produced. The dump is discussed further in Chapter 5 and the radiation protection issues associated with the dump are discussed in Chapter 13.

The hardware components for the BSY Dumpline and Dump are listed in Table 19. These specific components are described in Chapter 5. As noted, the dump itself is constructed from a pre-existing dump referred to as the D10 dump. For the LCLS-II application, the dump will be refurbished and moved into the center of the pre-existing Muon Shield wall.

Table 19. BSY Dumpline Hardware Components.

Component	Quantity	Engineering name	Status
Dipole magnet	3	1.0D38.37	Existing design
Quadrupole magnet	2	3.94Q17	Existing magnet
Dipole corrector ($x + y$)	2	Bypass	Existing design
Stripline BPM	4	-	Existing design
Wire scanner	1	-	Existing design

4.4.5 Hard X-Ray (HXR) Linac-to-Undulator (LTU) Beamline

The Hard X-ray (HXR) LTU beamline will transport the beam from the downstream exit of the Muon Shield wall to the HXR undulator. The beamline is pre-existing and requires only minor modifications, many of which will be completed as part of routine LCLS upgrades. The beamline optics are shown in Figure 0-34.

The beamline has two main functions: 1) bringing the beam from the Muon Shield wall to the HXR undulator, and, 2) measuring and collimating the incoming beam phase space. The HXR LTU consists of a vertical bend that deflects the beam upward by roughly 4.8 mrad, a dogleg that translates the beam to the south by 1.25 meters and then a final transport line that brings the beam into the undulator hall. The beamline is designed to operate over the energy range of 2.5 to 17 GeV and is further described in the *HXR Linac-to-Undulator (LTU) Physics Requires Document*, LCLSII-2.4-PR-0340, while the requirements on the collimation system are specified in the *Halo Collimation System Physics Requirements Document*, LCLSII-2.4-PR-0095. These collimators are designed to collimate small amounts of beam; the beamline is largely above ground and the shielding requirements are described in *Radiation Protection Requirements for the Halo Collimators*, LCLSII-1.2-PR-0259

The existing LCLS LTU has four collimators (CX31, CY32, CX35, CY36) in the straight transport to the undulator. These will be removed (or de-activated) for the LCLS-II because they have been measured to generate significant beam halo that impacts the undulator system. Three additional collimators (CYBX32, CXQT22, CYBX36), possibly upgrades of the four that are removed, will be used for a final collimation stage and will be added to the HXR LTU upstream of the final bending magnet in the HXR LTU before the undulator. If the existing collimators are to be re-used, they will be upgraded as specified in the *Halo Collimation System Physics Requirements Document*, LCLSII-2.4-PR-0095. It should be noted that one additional collimator

(CXQ6), which could also be an upgraded version of one of the four that are to be removed or de-activated, will be installed in the BSY. The two existing energy collimators in the horizontal dogleg will also be upgraded to meet the specifications described in the *Halo Collimation System Physics Requirements Document,*LCLSII-2.4-PR-0095.

The vacuum requirements and the beam stay-clear requirements are listed in *Residual Gas and Beam Stay-Clear Physics Requirements Document*, LCLSII-2.1-PR-0234. No changes are expected to be required to the vacuum system in the HXR LTU.

The existing LTU has wire scanners in the straight transport that will be upgraded as part of normal operations to be 'fast' wire scanners that can work with the high-rate beam from the SCRF linac. The existing LTU also has a single-pulse 120 Hz kicker, BYKICK, that can dump 5 kW beams. This kicker will be de-activated and possibly moved just downstream of Sector 30 of the existing CuRF linac.

As described in Chapter 3, one method of suppressing the micro-bunching instability is to compensate the R_{56} of bending systems downstream of BC2. This is performed by adding three weak, four-magnet chicanes into available space in the LTUH: one after BX32, one before BX35, and one after BX36. These chicanes each introduce roughly 100 microns of R_{56} that compensate that of the dogleg magnets. Further optimization studies will be performed to determine the minimal configuration that will be required.

Upstream of the undulator, an insertable beam stopper, TDUND, will be used to establish the correct beam trajectory and tune the beam emittance. The existing TDUND will be used in its present location.

The project is not installing any additional hardware into the HXR LTU except three new collimators, which may be upgrades of the existing collimators, and the three R_{56}-control four-magnet chicanes. Table 0-20 lists the hardware that will be added; these components are described in Chapter 5.

Table 0-20. Hardware Components added to HXR LTU.

Component	Quantity	Engineering name	Status
Dipole magnet	12	R56	New design
Betatron collimator	3	-	New design

4.4.6 Soft X-ray (SXR) Linac-to-Undulator (LTUS) Beamline

The SXR linac-to-undulator (LTUS) beamline is a warm beamline roughly 335.2 meters in length which transports the beam headed to the SXR undulator from the downstream edge of the Muon Shield wall to the beginning of the undulator system; the undulators are described in Chapter 8. The beamline begins roughly 65 cm above and to the south of the HXR LTU and a dogleg brings the beam over and across (a translation of 1.90 meters) the HXR LTU to end at the same elevation but 2.5 meters to the north of the HXR beamline, as illustrated in Figure 0-37. The SXR LTU beamline crosses the HXR LTU with about a 40.6 cm separation, as illustrated in

Figure 0-38. As documented in *Warm Beamline MuMetal Physics Requirements Document*, LCLSII-2.4-PR-0060, there may be some additional magnetic shielding that is required to limit the operational impact on the adjacent beamline when changing magnetic fields.

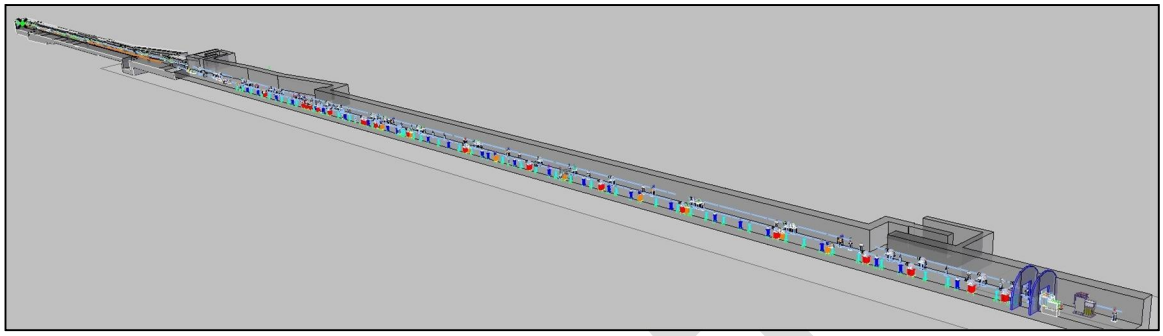

Figure 0-37. Schematic showning the SXR and HXR LTU beamlines from the Muon Shield wall to the Undulator hall.

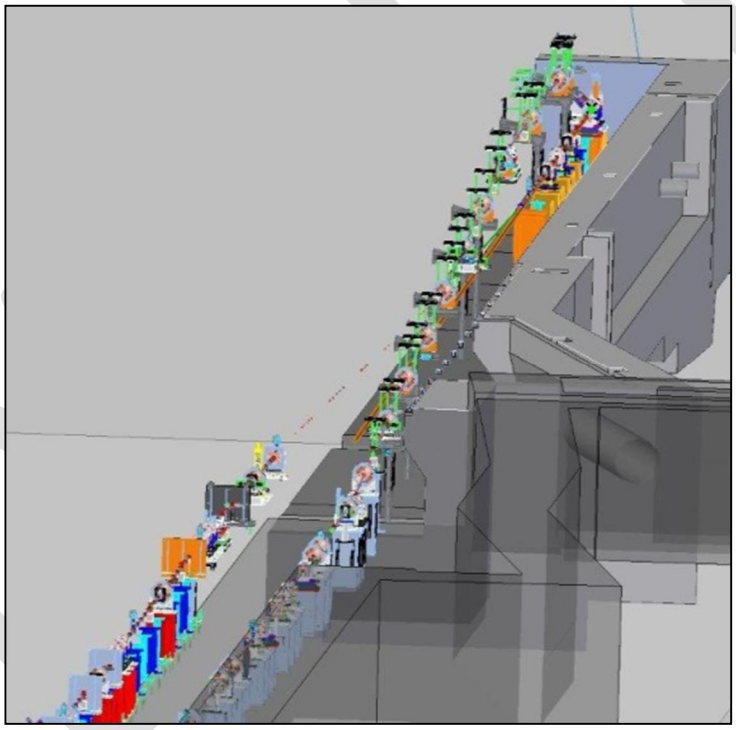

Figure 0-38. Illustration of the SXR and HXR LTU beamlines crossing at a Z location of roughly XX; the beamline separation is 40.6 cm and magnetic shielding may be required between the beamlines to limit the impact of changing magnetic fields as LTU's are tuned for different beam energies.

While the nominal beam energy is 4 GeV, the magnets have been specified to operate over the range of 2.0 GeV to 10.0 GeV. The beamline has two main functions: 1) bringing the SXR-directed beam from the Spreader to the SXR undulator, and, 2) measuring, matching, and collimating the incoming beam upstream of the undulator. The requirements for the beamline are described in the *SXR Linac-to-Undulator (LTU) Physics Requires Document*, LCLSII-2.4-PR-

0079 while the requirements for the collimation system are specified in the *Halo Collimation System Physics Requirements Document*,LCLSII-2.4-PR-0095. The collimators are designed to collimate small amounts of beam; the beamline is largely above ground and the shielding requirements are described in *Radiation Protection Requirements for the Halo Collimators*, LCLSII-1.2-PR-0259.

The LTUS consists of a horizontal dogleg to bring the beam across the LTUH, a vertical arc that deflects the beam upward by roughly 4.8 mrad to correct for the slope of the SLAC linac tunnel, and then a matching and emittance measurement region with 4 emittance wires. The beamline includes a low power tune-up dump, TDUNDB, located just upstream of the SXR undulator that would be used to tune up low-rate beam before sending it through the undulator and to the dump.

The TDUND and TDUNDB tune-up dumps are relatively wide due to the necessary shielding. To minimize the impact on the central aisle, TDUNDB will be staggered 2.8 meters downstream of TDUND. The maximum beam power on TDUNDB will be limited to a maximum beam power of 40 Watts (100 pC at 4 GeV and 100 Hz).

High-rate beams will be brought to the BSY dump before single pulses are sent down the LTUS to TDUNDB to establish the trajectory. The beam emittance and matching will be verified before beams are sent through the undulator to the SXR beam dump. After establishing the clean beam transmission and lasing with the desired characteristics, the beam rate would be slowly increased.

As described in Chapter 3, one method of suppressing the micro-bunching instability is to compensate the R_{56} of bending systems downstream of BC2. In the LTUS, this is performed by adding two weak, four-magnet chicanes: one before BX31B and one after BX32B. These chicanes each introduce roughly 70 microns of R_{56} that compensate that of the dogleg magnets. Further optimization studies will be performed to determine the minimal configuration that will be required.

The hardware components for the LTUS are listed in Table 0-21. The designs for the specific magnets, power supplies, and collimators are described in Chapter 5. The vacuum chamber has a relatively large aperture to allow for ±3% energy deviations and is copper-coated to reduce the resistive wall wakefield.

Table 0-21. LTUS Hardware Components.

Component	Quantity	Engineering name	Status
Dipole magnet	2	1.26D103.3	Existing design
Dipole magnet	2	3D39	Existing design
Dipole magnet	8	R56	New design
Quadrupole magnet	18	1.085Q4.3	Existing magnet
Quadrupole magnet	9	2Q10	Existing magnet

Quadrupole magnet	7	1.259Q3.5	Existing magnet
Dipole corrector ($x + y$)	29	Type-4	Existing design
Dipole corrector ($x + y$)	4	Type4f	Existing design
Energy collimator	2	-	new
Betatron collimator	2	-	new
Stripline BPM	29	-	Existing design
Wire scanners	4	-	Existing design
Tuning stopper	1	TDUNDB	Existing design

4.4.7 Soft and Hard X-ray Dump lines and Dumps

The hard and soft X-ray dump lines and dumps are located at the end of the undulators. Both dump beamlines are very similar, although they will use slightly different components at a detailed level. They consist of: 1) two quadrupoles to match the beam coming from the undulators, 2) a 'soft bend' that gently deflects the beams downward toward the dump pits without generating significant hard synchrotron radiation in the forward direction, and 3) three strong bending magnets that deflect the beams to the beam dumps in the dump pit. The dump bends are followed by a quadrupole pair that matches the dispersion and beta-functions at the dump entrance.

The beamlines have two requirements: 1) safely transporting and absorbing up to 120 kW of electron beam power and 2) diagnosing the electron beam longitudinal phase space. These requirements are described in the *Dump Line Physics Requirements Document*, LCLSII-2.5-PR-0135. The radiation protection issues associated with the undulator beam dumps are described in *Radiation Protection Requirements for DUMP/B Main Dumps*, LCLSII-1.2-PR-0100. The beam optics is shown in Figure 0-39.

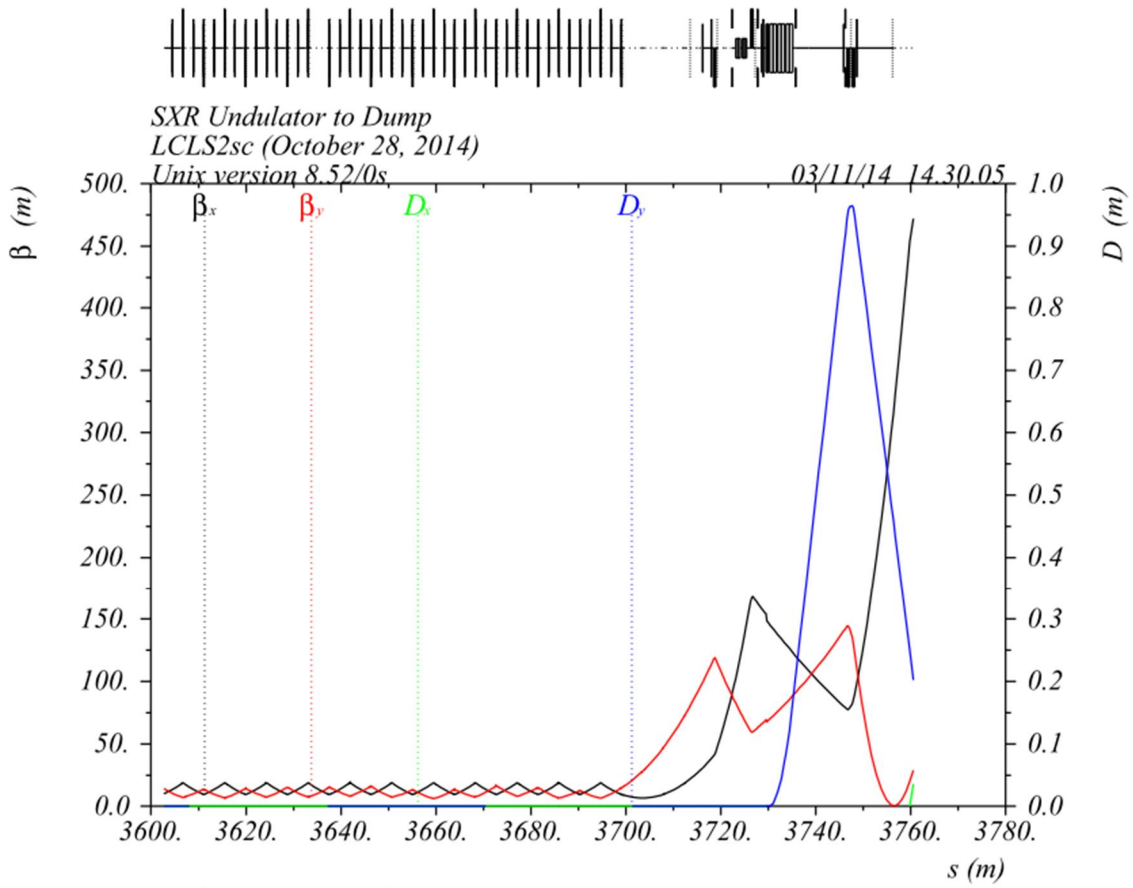

Figure 0-39. SXR Undulator and dumpline optics; the HXR dumpline is very similar with the same component spacing.

The LCLS constructed a dump pit to fit two parallel dump lines and installed a 5 kW dump as part of the original project. The LCLS-II HXR dump will be upgraded for the higher beam power of 120 kW and it will be moved upward and closer towards the center of the dump pit, while the SXR dump will also be designed for 120 kW maximum electron beam power and it will be placed symmetrically. This will reduce the need for external shielding modifications to the facility structure. To accomplish this, the dump bend magnets will be rolled inwards by 10 degrees, decreasing the beam separation from 2.5 meters to 1.88 meters at the dump entrance.

The HXR dump line bends are presently powered in series with the HXR dogleg bending magnets. This configuration will need to be repeated in the LCLS-II HXR but not in the SXR. Because the existing HXR dump bends will be too strong, the design will be modified with either fewer turns in the coils or a larger magnetic gap.

The existing LCLS dump line includes high resolution BPMs to resolve the beam relative energy changes as small as $1x10^{-4}$. The LCLS-II will require that these BPMs resolve energy changes as small as $1x10^{-5}$ and a wire scanner upstream of the dump resolves an energy spread as small as 300 keV ($7x10^{-5}$).

The dump lines must also include at least two high resolution BPMs after the undulator to resolve the undulator beam-based alignment. These will be X-band cavity BPMs based on the same design used for the undulators, with the first located roughly 5 meters downstream of the undulator and the second another 8 meters further downstream.

The existing LCLS dump line includes an X-band transverse deflecting cavity (TCAV) that has been instrumental in understanding the longitudinal phase space. This TCAV will be re-used in the LCLS-II HXR dump line and a similar TCAV is planned for LCLS-II SXR although it will not be included in the initial installation.

The hardware components for the dump lines are listed in Table 0-22. The designs for the specific components are described in Chapter 5. There is no new hardware for the HXR dump line and so the table just lists the new components in the SXR dump line.

Table 0-22. SXR Dumpline Hardware Components.

Component	Quantity	Engineering name	Status
Dipole magnet	1	1.26D18.4	Existing design
Dipole magnet	3	1.69D55.1	Existing design
Quadrupole magnet	2	2Q10	Existing magnet
Quadrupole magnet	2	3.94Q17	Existing magnet
Dipole corrector ($x + y$)	2	Type-4	Existing design
Dipole corrector ($x + y$)	4	Class-5	Existing design
Stripline BPM	3	-	new
Cavity BPM	1	-	new
Wire scanners	1	-	Existing design

The planned dump line installation is shown in Figure 0-40, illustrating the three rolled dump bends and the transport to the beam dumps. The shielding around the dumps is described in Chapter 13. The vacuum chamber has a relatively large aperture to allow for ±3% energy deviations.

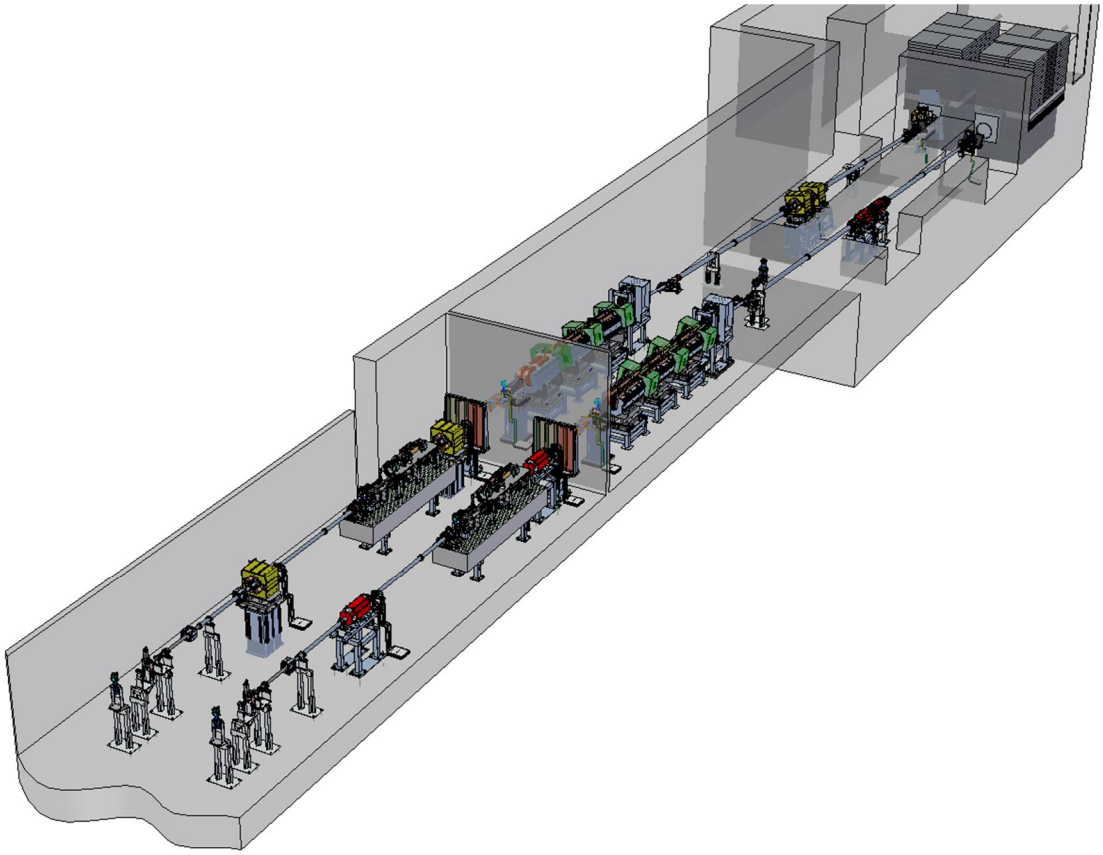

Figure 0-40. Drawing of the SXR and HXR dump lines from the end of the undulators to the 120 kW beam dumps. The dump bend magnets are rolled by about 10-degrees to bring the beams closer to the center of the tunnel to reduce the required shielding.

4.5 Global Systems

There are a number of global systems that are required for the accelerator layout but are not detailed in this chapter. These include the Control and Safety Systems, described in Chapter 10; the Infrastructure and Facility Preparation that is described in Chapter 11; the Systems Integration and Availability Requirements described in Chapter 12; and the Radiation Protection design described in Chapter 13.

There are two global systems that will be described in the subsequent sub-sections rather than be repeated in each sub-section through the rest of this chapter. These include the diagnostic, feedback, and collimation systems, all of which are described below.

4.5.1 Diagnostics and Feedback Systems

Diagnostic systems will be critical to ensure that the LCLS-II produces the high quality beams that are required for the FELs. The Diagnostic systems are described in the *Electron Beam Diagnostics Systems Physics Requirements Document*, LCLSII-2.7-PR-0170. Additional requirements are specified in the *Beam Position Monitor Requirements PRD*, LCLSII-2.7-PR-

0136, the *Single-shot Relative Bunch Length Monitor PRD*, LCLSII-2.7-PR-0074, the *Injector/Linac Wire Scanner System Requirements PRD*, LCLSII-2.4-PR-0099, and the *Injector and Linac Toroids and Faraday Cups PRD*, LCLSII-2.4-PR-0083. Most of the diagnostics in the LCLC-II are designed to operate with the MHz-rate beam, but a parasitic diagnostic beam line will be built after the laser heater which will allow full characterization of bunches extracted at ~100 Hz.

The LCLS-II design includes a beam position monitor (BPM) associated with almost every quadrupole to control the beam trajectory. In addition, there are many BPMs at high-dispersion locations along and after the linac (Laser Heater, BC1, BC2, Dogleg, LTUS, LTUH, and the HXR, SXR, and BSY Dumplines) that are used to measure the beam energy. Wire scanners at these dispersive regions will be used to measure the beam energy spread, while wires in dispersion-free regions will be used to measure the transverse emittance. Emittance measurement locations include the Laser Heater, the Laser Heater Diagnostic Line, BC2, Bypass, and the LTUH and LTUS. Finally, there are bunch length diagnostics in the Laser Heater and after BC1 and BC2.

As described in Chapter 2, the design approach for the LCLS-II has been to include all of the diagnostics required to meet the Threshold Key Performance Parameters as defined in the *LCLS-II Project Requirements Document*, LCLSII-1.1-GR-0018 as part of the baseline project and to allocate explicit space for additional diagnostics that may (or may not) be required to meet the full performance goals so that they can easily be added during commissioning when and if required. This approach is described in more detail in the *Electron Beam Diagnostics Systems Physics Requirements Document*, LCLSII-2.7-PR-0170.

This same approach has been taken for the LCLS-II feedback systems. The accelerator will be commissioned with ‘slow’ feedback systems to stabilize the accelerator. These are software feedbacks that are written as high-level applications. The LCLS-II control system, specified in the *Control System Physics Requirements Document*, LCLSII-2.7-PR-0066, is capable of supporting a high-rate ‘fast’ feedback system that can sample at the full beam repetition rate of 1 MHz (929 kHz). Such a system will be implemented if it is found necessary to stabilize the beam during commissioning, but we expect that it will not be required. The ‘slow’ and ‘fast’ feedback systems are described in the *Longitudinal Beam-Based Feedback Physics Requirements Document*, LCLSII-2.7-PR-0076, and the *Transverse Beam-Based Feedback Physics Requirements Document*, LCLSII-2.7-PR-0075.

4.5.2 Collimation and Beam Stay-Clear

The SCRF linac is being designed to ultimately generate 1.2 MW of electron beam power, although the initial installation will be limited to a maximum beam power of 250 kW. The electron beam power to each undulator will be limited to 120 kW. As indicated in Figure 0-41, extensive collimators will be installed to control unwanted beam losses. The goal is to reduce unwanted beam loss in the SXR and HXR undulators to less than 12 mW on average. The

baseline design includes four stages of (x, p_x, y, p_y, $\Delta E/E$) collimation along the linac and in the BSY with the option of a fifth installation after BC1.

The design of the collimation system is based on the studies done for the future linear colliders, which have more stringent requirements, as well as the experience with the LCLS collimation system. The collimation system is described in the *Halo Collimation System Physics Requirements Document*,LCLSII-2.4-PR-0095, and the adjustable beam halo collimators are described in Chapter 5 while the radiation protection and shielding requirements around the collimators are described in Chapter 13. In general, the collimators are set to limit the beam energy to be within ±2.5% of nominal (except for the bunch compressors where the energy deviations can be much larger) and within $\pm 15\sigma_{x,y}$ in betatron phase space.

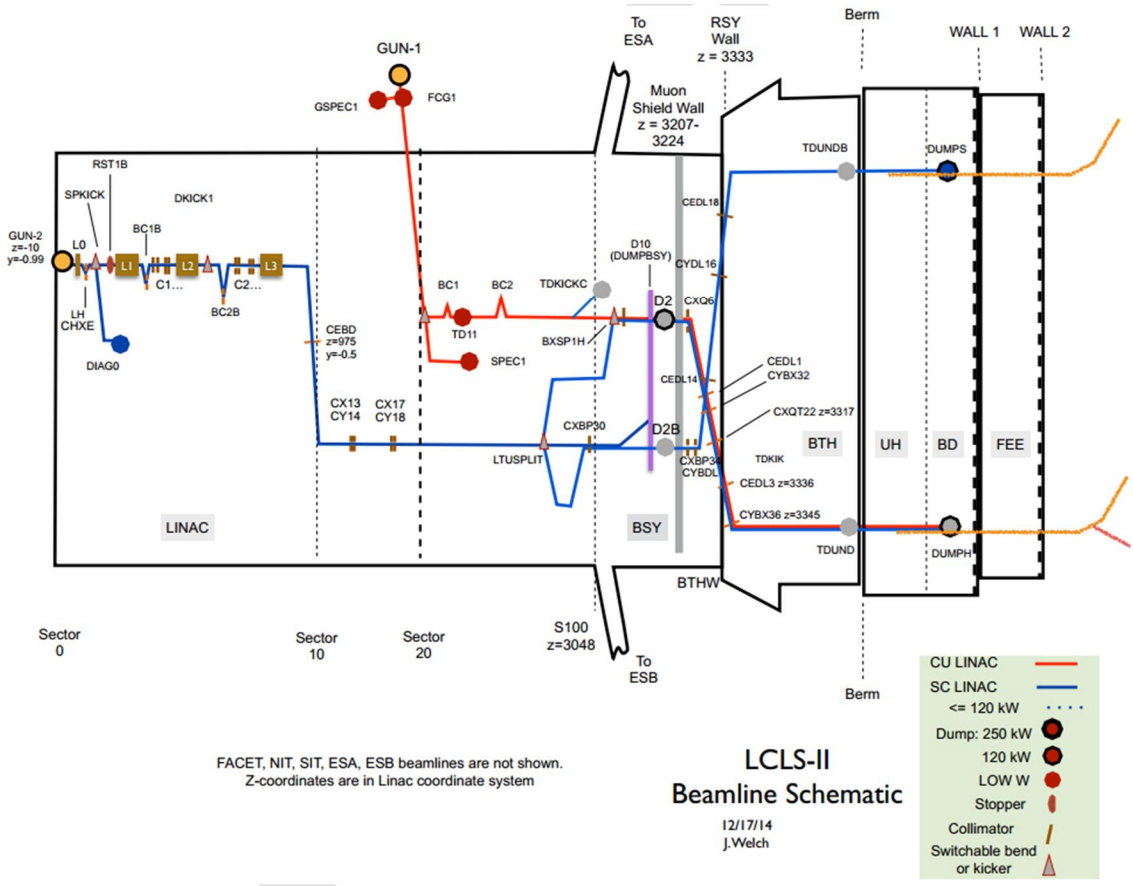

Figure 0-41. Schematic showing beam dumps and collimator locations in the LCLS-II as the beam goes through the linac tunnel and the BSY, across the Research Yard (RSY) into the Undulator Hall (UH) and the Front End Enclosure (FEE). The existing CuRF linac is shown in red while the new SCRF linac is shown in blue. There are 20 collimators between the gun of the SCRF linac and the HXR or SXR undulators to collimate the beam halo in (x, px, y, py, DE/E) and protect the undulators.

In addition to the halo collimators, there will be many fixed protection collimators that are part of the Machine Protection System (MPS) and the beam containment system (BCS) which are described in Chapter 10. These fixed aperture collimators will protect components (and

personnel) from widely errant beams that might arise from severely mistimed bunches or RF setpoint changes due to either component failures or tuning errors.

The Beam Spreader will also provide additional collimation of any off-time bunches because the kicker pulse is relatively narrow compared to the inter-bunch spacing. However, the spreader system is not designed to absorb significant beam power. If there is significant off-time beam power, an additional collimation system will need to be added upstream of the Beam Spreader. If the off-time bunches are coming from the injector, a system at low energy will be most effective; an example of such an off-time collimator is described in the *Injector Dark Current Sweeper Physics Requirements Document*, LCLSII-2.3-PR-0073. If such a system is needed, it would be most likely be installed after the laser heater in the COL0 beamline rather than the injector. Alternately, if most of the off-time beam power is coming from captured linac field emission, a similar but higher power system could be installed in the Bypass line.

In addition to beam collimators, high power dumps are being designed for the end of the undulators and in the BSY and tuning dumps will be placed after the injector, at the end of the CuRF linac, and upstream of the undulators as shown in Figure 0-41. The beam spreader will be used to vary the electron beam rate to the undulators from single-shot pulses to nearly the full repetition rate of 929 kHz while maintaining a keep-alive rate on the BSY dump to ensure that it can be used as a beam abort when necessary.

Finally, the beam stay-clear has been defined to exceed the collimation aperture. The stay-clear is typically set to allow for a $15\sigma_{x,y}$ beam with a 1mm-mrad emittance and a betatron mismatch of 2, ±3% energy deviations, and 2mm steering errors. The stay-clear and vacuum requirements (ignoring the vacuum requirements at the warm-SCRF transitions) are documented in the *Residual Gas and Beam Stay-Clear Physics Requirements Document*, LCLSII-2.1-PR-0234.

4.5.3 Magnet Systems and Component Alignment/Vibration Tolerances

The magnets for LCLS-II are specified in the *LCLS-II Magnets Physics Requirements Document*, LCLSII-2.4-PR-0081. The magnets have been specified to support a 10 GeV beam from the SCRF linac and a 17 GeV beam from the CuRF linac. Most of the required magnets are based on pre-existing designs from either LCLS or other projects at SLAC, as an attempt has been made to re-use existing magnets wherever reasonable. A few new magnets are required, however; these are described in Chapter 5. This process of identifying possible candidate magnets and evaluating their re-use is ongoing.

The magnet power supply and harmonic tolerances are also specified in the *LCLS-II Magnet Physics Requirements Document*, LCLSII-2.4-PR-0081. Magnet harmonic tolerances are specified to limit emittance dilution to the beam and to limit the field variation across the operating aperture. In general, the harmonic tolerances are relatively loose and can be easily met by the specific magnet designs. In dispersive regions, however, the harmonic tolerances can be tight, in some cases requiring specific, modified magnets to meet the required tolerances.

The magnet alignment tolerances are specified in the *Linac Alignment Physics Requirements Document*, LCLSII-2.4-PR-00110. In general, the alignment tolerances for the warm components are similar to those in LCLS; in most of the accelerator, the tolerances are driven by dispersive errors and the relatively large correlated energy spread across the bunch. Beam-based alignment will be used in certain locations such as the undulator to achieve the required alignment. In other locations, global beam bumps can be used to correct the effect of any residual errors.

The alignment tolerances on the SCRF cryomodules are specified in the *SCRF 1.3 GHz Cryomodule Physics Requirements Document*, LCLSII-4.1-PR-0146 and the *SCRF 3.9 GHz Cryomodule Physics Requirements Document*, LCLSII-4.1-PR-0097 based on beam dynamics calculations documented in Ref. [14]. These tolerances are for the alignment of the internal components with respect to the external cryomodule fiducials (when cold) and are expected to be dominated by the internal cryomodule misalignments; the external fiducials should be alignable in the tunnel with an accuracy of 0.1 mm in x and y and 0.2 mm in z, leaving a small contribution to the overall misalignments of the internal components.

Site vibration has two effects on the LCLS-II. First, transverse motion of the quadrupole magnets will lead to transverse beam jitter and, second, the vibration may drive cavity microphonics which will detune the cavities and require additional RF power to stabilize the RF system. Most of the vibration tolerances are similar to those in LCLS. The vibration requirements due to the induced transverse centroid motion are described in *Quadrupole Magnet Vibration Physics Requirements Document*, LCLSII-2.4-PR-0062. Studies of the induced microphonic vibration in the RF cavities show that the effects appear to be insignificant [15].Measurements made along the SLAC linac and the LCLS beamline indicate that, for the most part, the tolerances will be easily achieved. One new addition to the SLAC site will be the high power cryoplant and this is expected to introduce significant vibration around Sector 4 of the SLAC linac. This vibration will impact the BC2 region as well as the SCRF linac cryomodules. Measurements of vibration from the JLAB 4kW cryoplant have been made (LCLSII-4.8-EN-0326), and measurements and modeling are planned for the SLAC site.

If the vibration levels exceed the specifications, multiple remediation paths are available. Possible solutions include direct reduction of the source using vibration isolation techniques or passive vibration isolation of selected components. Finally, the high repetition rate of the acceleration means that fast beam-based feedback will be very effective at suppressing the impact of any transverse vibration and these systems can be implemented as described in Chapter 10.

4.6 References

[1] MAD v. 8.52 reference.

[2] Elegant reference

[3] IMPACT reference

[4] T.T. Böhlen, et al., "The FLUKA Code: Developments and Challenges for High Energy and Medical Applications", *Nuclear Data Sheets* **120**, 211-214 (2014).

[5] N.V. Mokhov and S.I. Striganov, "MARS15 Overview", *Proc. of Hadronic Shower Simulation Workshop*, Fermilab, September 2006, AIP Conf. Proc. 896, pp. 50-60 (2007) and Fermilab-Conf-07/008-AD (2007).

[6] K. Baptiste, et al, *NIM A* **599**, 9 (2009).

[7] C. Gulliford et al., *Phys. Rev. ST Accel. Beams* **16**, 073401 (2013).

[8] I. Bazarov et al., *Phys. Rev. ST Accel. Beams* **14**, 072001 (2011).

[9] F. Sannibale, et al., PRST-AB 15, 103501 (2012).

[10] F. Sannibale, et al., *Proceedings of IPAC2014*, Dresden, Germany MOPRI054, 797 (2014).

[11] J. Schmerge, et al., *Proceedings of FEL2014*, Basel, Switzerland, THP042 (2014).

[12] A. Vivoli, et al., *Proceedings of Linac 2014*, Geneva, Switzerland, THPP060 (2014).

[13] Z. Huang et al, *PRST-AB*, **13**, 020703 (2010).

[14] A. Saini and N. Solyak, LCLSII-TN-14-03 (2014).

[15] C. Adolphsen, private communication (2014).

5 LINAC COMPONENTS

TECHNICAL SYNOPSIS

The LCLS-II linear accelerator is composed of several different sections, from the injector, to the laser heater, L1-linac section, 3.9-GHz linearizer, BC1 compressor, L2-linac, BC2 compressor, L3-linac, extension line, first dog-leg, bypass line, beam spreader, LTUS and LTUH, and (skipping over the HXU and SXU undulators) the main beam dumps, which are also considered part of the linac.

Each of these sections is populated with many new or existing machine components, such as quadrupole focusing magnets, dipole bending magnets, beam position monitors (BPMs), steering coils (correctors), wire-scanners, beam screens, RF accelerating structures, RF deflecting structures, charge monitors, collimators, bunch length monitors, vacuum pumps, power supplies, mechanical supports, etc. This chapter describes many of the main components, by type, within each main machine section. Specifications and brief requirements are referenced for many of these components, referring to project documents such as Physics Requirements Documents (PRDs) and Engineering Specifications Documents (ESDs), which go into much more component detail.

5

5.1 Accelerator Component Overview

The accelerator layout is described in Chapter 4. This chapter will describe the components that make up the beamline systems with the exception of the cryomodules which are described in Chapter 6. The accelerator schematic is shown in Figure 5-1. The high-level systems design requirements, specifications and interfaces for Accelerator Systems are captured in Table 5-1.

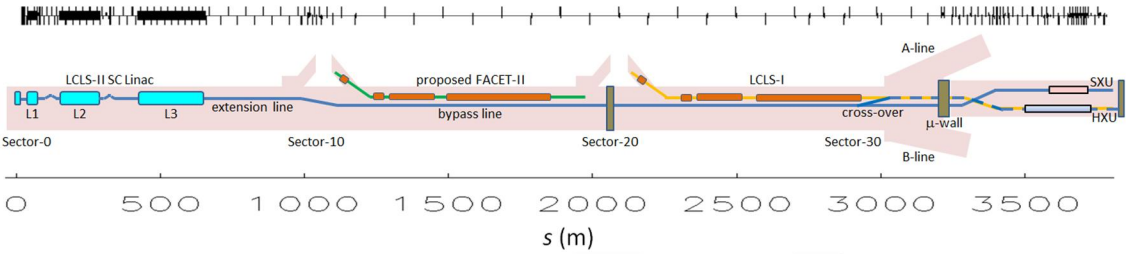

Figure 5-1. LCLS-II beamline schematic illustrating the new SCRF linac (blue) and the existing LCLS CuRF linac (red) as well as the transport lines to the HXR and SXR undulators.

Table 5-1. Accelerator Systems High-Level Requirements and Specifications

Document Type	Title	Document Number
Physics Requirements	LCLS-II Parameters	LCLSII-1.1-PR-0133
Physics Requirements	LCLS-II Electron Beam Loss and Maximum Credible Beam	LCLSII-2.7-PR-0079
Physics Requirements	Electron Beam Diagnostics Systems	LCLSII-2.7-PR-0170
Physics Requirements	RF Power and LLRF Requirements	LCLSII-4.1-PR-0098
Physics Requirements	LCLS-II SCRF Injector System	LCLSII-2.2-PR-0084
Physics Requirements	LCLS-II Gun and Laser Heater Laser Systems	LCLSII-2.2-PR-0085
Physics Requirements	Injector Laser Heater Requirements	LCLSII-2.2-PR-0086
Physics Requirements	Post-LH Diagnostic Beamline Requirements	LCLSII-2.4-PR-0068
Physics Requirements	BC1 Bunch Compressor Chicane Requirements	LCLSII-2.4-PR-0039
Physics Requirements	Post-BC1 Diagnostic Beamline Requirements	LCLSII-2.4-PR-0069
Physics Requirements	BC2 Bunch Compressor Chicane Requirements	LCLSII-2.4-PR-0040
Physics Requirements (Future)	BC3 Bunch Compressor Chicane Requirements	LCLSII-2.4-PR-0110
Physics Requirements	Linac Requirements	LCLSII-2.4-PR-0041
Physics Requirements	SCRF Electron Linac Extension and Bypass Line Requirements	LCLSII-2.4-PR-0091
Physics Requirements	SXR Post-Spreader and LTU	LCLSII-2.4-PR-0094
Physics Requirements	Dump Line Requirements	LCLSII-2.5-PR-0135
Interface Control	Accelerator to Infrastructure Systems	LCLSII-2.1-IC-0156
Interface Control	Accelerator Systems to Cryogenic Systems	LCLSII-2.5-IC-0056

Interface Control	SLAC to LBNL Injector	LCLSII-2.2-IC-0173

Engineering is being performed in accordance with the *LCLS-II Systems Engineering Management Plan*, LCLSII-1.1-PM-0043. The schedule for Preliminary Design Reviews (PDRs) is given in Table 5-2 below. The Final Design Review (FDR) schedule is given in Table 5-3, and Figure 5-2 shows the overall schedule for Accelerator Systems.

Table 5-2: Accelerator System Preliminary Design Review Schedule

Component	Date

Accelerator Systems PDR
• Injector Source Beamline Components & RF Power System
• Injector (Laser, Mechanical and Installation)
• Linac
• Transfer Lines & Dump
• Common Systems
  o DC Power Supplies
  o RF
  o Cable Plant
	January 2014

Couplers, PDR/FDR Combined	August 2014
Solid State Amplifiers (SSA)	October 2014
Injector Source (Gun and Load Lock, Injector)	November 2014
Collimators	June 2015
Kicker, Bend and Septum Magnets	June 2015
Magnet Quench Protection System	June 2015
SRF Vacuum Systems	September 2015

Table 5-3: Accelerator System Final Design Review Schedule

Component	Date
Injector Source	April 2016
• Gun	June 2015
• Injector RF Power System	November 2015
• Beamline Components	April 2016
Injector System	October 2016
• Mechanical Integration and Installation	August 2016
• Drive Laser System	October 2016
Linac System • BC1, Mechanical Integration and Installation • BC2, Mechanical Integration and Installation • L1, HL, L2, L3, Mechanical Integration and Installation	August 2016

Couplers, PDR/FDR Combined	August 2014
Transfer Lines and Dump	March 2016
• Bypass, Mechanical Integration and Installation	October 2015
• BSY, Mechanical Integration and Installation	March 2016
• LTU, Mechanical Integration and Installation	November 2015
• Dump, Mechanical Integration and Installation	November 2015
Kicker, Bend and Septum Magnets	November 2015
Collimators	November 2015
Cable Plant - Bypass	November 2015
Power Conversion FDR	June 2016
• DC Power Supplies	
• Quench Protection System	
Solid State Amplifiers (SSA)	August 2016
SRF Vacuum Systems	August 2016
High Power RF	August 2016
Cable Plant	November 2016
Accelerator Systems	December 2016

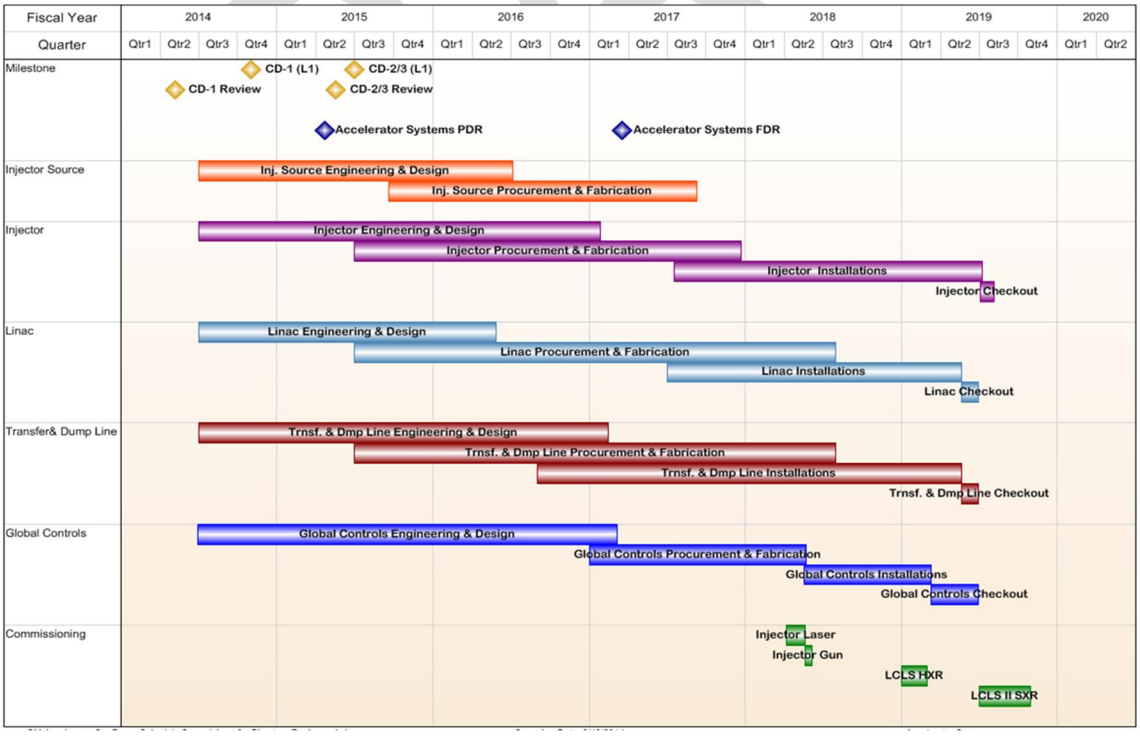

Figure 5-2. Accelerator Systems Production Schedule

5.1.1 Design Maturity

The LCLS-II Project Final Design Plan LCLSII-1.1-QA-0065 provides for a phased completion of the final designs for the LCLS-II facility. The plan ensures that designs are sufficiently mature to start procurements and construction, while enabling the most cost-effective schedule for constructing the facility and maximizing the technical capabilities of the facility at CD-4. Final design readiness at CD-3 recognizes that that not all subsystems will reach final design at the same time. Project-level requirements and interface control points between Accelerator Systems, Cryogenic Systems, Photon Systems and Infrastructure are defined at CD-3, which ensures that the phased procurements and construction are appropriate for the final design of the LCLS-II. Chapter 2, Project Overview, contains additional discussion of the approach to design completion. The Accelerator Systems design, described in Chapter 4, this chapter, and Chapter 10, is evaluated to be 65% complete. Completing remaining design after CD-3 allows for potential upgrades to diagnostics and controls, using designs developed and proven by SLAC Operations.

5.2 Injector Components

The LCLS-II injector will be installed in the existing Linac housing in Sectors 0 and 1. Components include 1) the UV drive laser, 2) the RF photocathode gun (186 MHz), 3) the 1.3 GHz buncher cavity, 4) a dark-current sweeper (pulsed) magnet to reduce the accelerated dark current, 5) a 12-meter-long cryomodule with eight 9-cell L-band cavities (each powered separately), 6) a laser heater system to damp the micro-bunching instability, 7) a pulse-stealing kicker magnet, immediately following the laser heater, used to direct a low power beam (about 100 Hz) into a special off-axis beam diagnostic line, and 8) a short beam collimation and matching section. The diagnostic line allows continual emittance and energy spread measurements at low average power and includes an RF deflecting cavity (S-band), so that these measurements can also be time resolved (*i.e.*, along the bunch length). The LCLS_II injector linac will use mostly standard diagnostic systems.

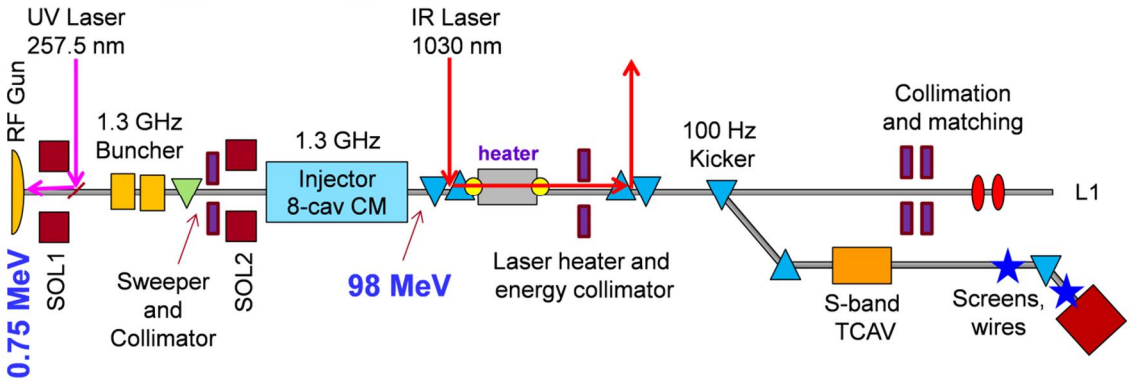

Figure 5-5-3: Injector Layout

5.2.1 Gun and Cathode

The VHF gun developed at LBNL under the Advanced Photoinjector EXperiment (APEX) project has been designed to satisfy the requirements of LCLS-II using reliable and mature mechanical and RF technologies. Requirements can be found in the *VHF-RF Gun PRD*, LCLII-2.3-PR-0166.

The core of the gun is a normal-conducting copper RF cavity resonating at 186 MHz (the seventh sub-harmonic of 1.3 GHz) in the VHF band with a nominal field of 20 MV/m. Figure 5-4 shows a cross section of the VHF cavity with the main components. Tuning is achieved by a mechanical system that slightly pushes or pulls the cavity wall at the beam exit port side. The RF power is supplied through two diametrically opposed, magnetic loop couplers on the cathode back wall of the cavity. APEX has already demonstrated CW operation, design energy, vacuum performance, and the required cathode QE lifetimes with several hundred pC bunches at MHz repetition rate. Experiments to measure the emittance at 100-500 pC charges at 30 MeV beam energies are planned in FY2015.

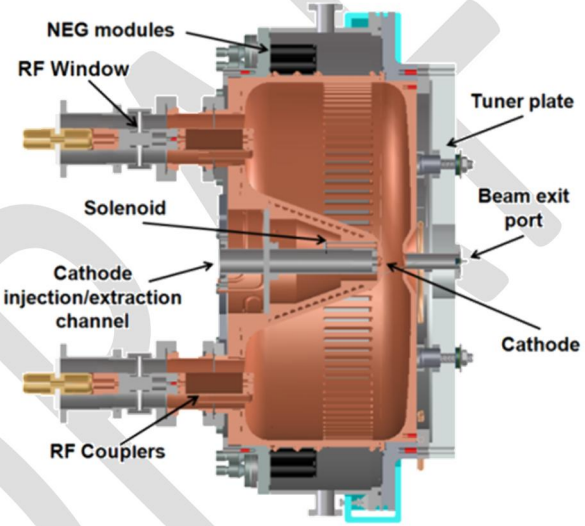

Figure 5-4. VHF cavity cross-section, showing the cavity's main components

The photocathode for the LCLS-II requires high quantum efficiency, low intrinsic emittance, long operating lifetime and prompt response time. The cathode system will consist of a cathode fabrication chamber, a UHV transfer case for storing and transporting the cathodes, and a load lock for inserting and removing cathodes in both the fabrication chamber and the gun. The Cs_2Te cathode has been chosen as the baseline cathode for LCLS-II. This cathode has a long history of use at the FLASH facility, a proven cathode storage and transport system (suitcase), and a load lock for transferring cathodes into and out of the gun under vacuum. The LASA Cs_2Te cathodes still had a quantum efficiency (QE) greater than 10% after a year's storage in the suitcase and are currently being used in APEX beam studies.

. Exchanging cathodes within a transfer case takes about one hour. Exchanging the transfer case requires approximately one shift plus another few days for a bakeout, which is compatible

with operation since it is isolated from the gun. With four cathodes per transfer case and a minimum ten-day lifetime, transfer case exchanges should be required less than once per month. Considering that the Cs_2Te QE is typically 10% and the specification only requires a QE of 0.5%, the laser can compensate for drooping QE for multiple 1/e lifetimes. Therefore, cathode exchanges should be significantly less frequent than once every ten days. Additional lifetime can also be obtained from cathodes by shifting laser position. This is routinely done with DC guns, which operate with the laser off-center due to cathode poisoning from back streaming ions. Thus the same cathode can be reused if necessary by shifting the laser spot and retuning the injector electron beam optics to compensate for the small misalignment. Thus it is expected that cathodes should be very reliable and cathode and transfer case exchanges will be compatible with the LCLS-II user facility schedule.

5.2.2 Buncher

A room temperature, 1.3 GHz CW RF buncher cavity is located between the VHF gun and the injector accelerator in order to initiate the bunch compression in the injector. The cavity, shown in Figure 5-5, is a two-cell scaled version of the 1.5 GHz third harmonic cavities developed for the Advanced Light Source at LBNL. Requirements can be found in the *Buncher Requirements PRD*, LCLII-2.3-PR-0167.

Because of the relatively low electron beam energy at the buncher, the required fields can be achieved in CW mode by reliable and simple room-temperature technology. The buncher cavity RF power source will deliver about 10 kW of CW power. The buncher frequency was chosen to be the same as that in the main linac to satisfy beam dynamics requirements while reducing the RF power system complexity. The buncher cavity design includes two RF coupler ports per cell and two dummy ports rotated 90° from the coupler ports to eliminate dipole and quadrupole field components. The RF coupler design is a coaxial loop style with an integrated RF ceramic window.

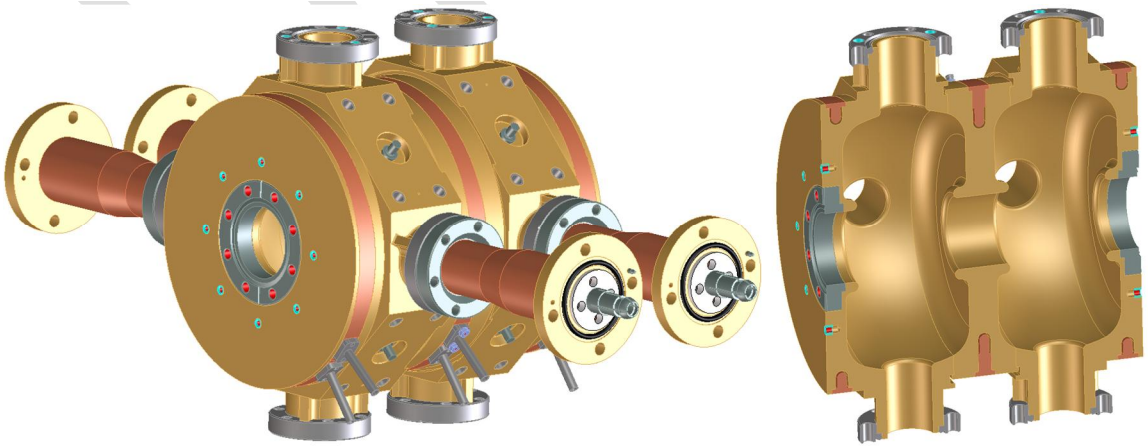

Figure 5-5: CAD drawing of the LCLS-II injector buncher cavity. Left: 3D view. Right: cross section view.

5.2.3 Solenoids

A pair of solenoids, one upstream and one downstream of the buncher, generate the magnetic fields required by the emittance compensation process. Requirements can be found in the Injector *Solenoid PRD*, LCLII-2.3-PR-0165.

The relatively low energy of the beam allows for compact magnets with conventional water-cooling. The fields required for emittance compensation (and for solenoid scans during thermal emittance measurements) are obtained with a magnetic length of about 20 cm and magnetic fields of up to a few kG. Remote-controlled positioning actuators support the magnets and allow for the complete online alignment of the magnets. Each magnet is also equipped with normal and skew quadrupole coils for correcting undesired multipolar components of the magnetic field.

5.3 Laser Systems

The LCLS-II injector laser, called the Drive Laser, illuminates the gun photocathode with UV (257.5 nm) light to generate a high quality electron beam from a photocathode located inside the RF gun. The laser will be located in the Laser Room in the housing upstream of Sector 0 and the UV beam will be transported to the tunnel, as shown in Figure 5-6.

The Drive laser system includes

1) Fiber oscillator and amplifier generating up to 50 W of class IV IR (1030 nm) radiation ,
2) UV Conversion unit producing the fourth harmonic (257.5 nm) of the IR beam.
3) Temporal shaping system (pulse stacker)
4) Spatial shaping and imaging system

In addition to the Drive Laser there is a second laser in the laser room - identical to the first one, called the Heater Laser, that produces IR (1030 nm) beam for the heater. The Heater Laser beam co-propagates with the electron beam through an undulator to add incoherent energy spread to the electron beam through the inverse FEL process in order to minimize the micro-bunching instability downstream without degrading the FEL performance. The Heater Laser system also includes a Transport, Launch and Conditioning system that delivers the beam to the Heater undulator.

Requirements for both lasers are included in the *LCLS-II Gun and Laser Heater Laser Systems PRD*, LCLSII-2.2-PR-0085. Each laser needs to produce up to 50 W in the IR to meet its specifications at the delivery point.

Diagnostics allow all relevant beam parameters to be measured at the required location and are integrated with feedback loops for pointing stability.

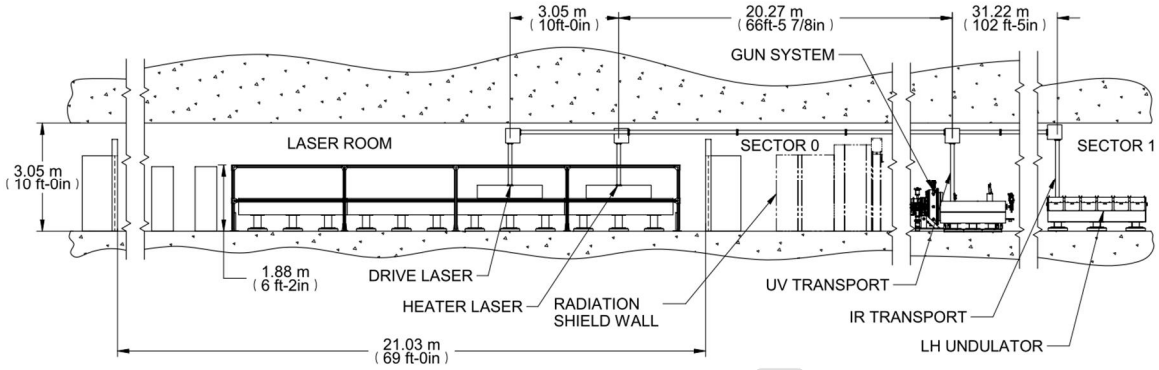

Figure 5-6: Elevation of Laser Room

5.3.1 Laser Room Requirements

The Drive Laser will only operate stably if its environment is well-controlled. The Laser room in Sector 0 has tight specifications in terms of floor vibrations, acoustic level, temperature, and humidity control. The S0 alcove will have sufficient sound proofing to attenuate the klystron and traffic noise to the level of 50dB. The HVAC system will assure a temperature stability of ±0.5°C and a humidity level of 50% with less than 10% of variation. Requirements are included in the *Laser Room RDS*, LCLSII-5.2-RD-0131.

5.3.2 Laser Safety

The Laser Safety System (LSS) will comply with American Standards for the Safe Use of Lasers, ANSI Z136.1 and SLAC ES&H Manual, Chapter 10 - Laser Safety. The LCLS Injector Laser Safety Officer will prepare a detailed system description that will be a part of the Standard Operation procedure (SOP) for this laser facility. The LSS is designed to contain the laser light at all times when unauthorized personnel are present in the Laser Containment Area (LCA). Authorized staff is trained to work safely with both laser hazards and other safety hazards in the room.

5.4 Conventional Magnets

The scope of work for the LCLS-II magnets is to design, engineer, procure, fabricate, test, and deliver conventional DC magnets ready for integration into the overall mechanical installation. There are three main kinds of room temperature DC magnets used in the LCLS-II: 57 dipoles, 278 quadrupoles, and 227 correctors. The subsections below will describe each kind of magnet. The arrangement of magnets, located at the positions given in the MAD (Methodical Accelerator Design) deck, are referred to as the magnetic optical lattice. Each magnet is given a unique name (element name) which is used to identify the magnet and associate it with a particular location with respect to the LCLS-II coordinate system.

Typically, the LCLS-II magnet cores are made from a solid low carbon steel such as 1008 or laminated electrical silicon steel, commonly used in electrical transformers. The magnet

excitation is provided via coils wound from copper or aluminum conductors that are placed around the pole tips and as close to the gap as possible. The conductor may be convectively cooled solid wire or water-cooled hollow conductor, depending on design requirements. The coils are typically insulated either with an applied coating (for the case of solid wire), a textile wrap affixed with epoxy (wet layup), vacuum impregnated with epoxy, or directly potted in a solid matrix of epoxy.

5.4.1 Dipoles

A dipole magnet consists of a core (ferromagnetic steel in most cases), two pole tips having a flat surface and at least one Cu or Al coil oriented such that the field in the gap is transverse to the direction of the electron beam propagation. The styles of dipole magnet used at the LCLS-II are the H-frame, the window frame, the C-frame, and the septum. In some instances the pole tips will have chamfered edges, which reduce the field harmonics and fringe fields generated by the sharp edges of the pole tip. Simply put, the purpose of the dipole magnet is to bend the beam into the desired path. Dipoles are used at LCLS-II in many applications beyond simply directing the beam from one optical path to another. Dipoles are used in the injector as beam energy spectrometers, in which the bending of the electron beam creates dispersion that is analyzed using a profile monitor. Dipole magnets are also used in the bunch compressor chicanes, where the energy dependence of the electron bunch path length through the chicane is exploited to shorten the bunch length. Dipoles arranged in chicanes are also used to move the electron beam "out of the way" to allow overlap of the electron beam with the IR laser of the injector laser heater or to permit insertion of delicate monochromator x-ray optics for the self-seeding instruments in the undulator hall. Often dipoles will be referred to as "bends". The optical analog of a dipole is the prism.

5.4.1.1 LCLS-II Dipole Magnet Performance Requirements

The performance requirements for the LCLS-II dipole magnets are found in the physics requirements document *Magnets,* LCLSII-2.4-PR-0081. Table 5-4 summarizes the most demanding performance requirements for a given magnet design. In some cases all magnets of a given magnet design will have the same performance requirements regardless of where they are used in the LCLS-II magnetic optical lattice. In other cases specific magnets will have more demanding performance requirements than others.

Table 5-4. LCLS-II Dipole Magnet Performance Requirements

Engineering Type	Nominal Dipole Field (kG)	Nominal Beam Energy (GeV)	Nominal Int. Strength (kG-m)	Max Int. Strength (kG-m)	Field Flatness +/- (cm)	b2/b0 @r=1cm	b4/b0 @r=1cm
1.0D22.625	-0.842	4	-0.505	-1.264	0.72	0.001	0.01
1.0D22.625	-0.54	4	-0.324	-0.811	1.19	0.001	0.001

1.0D38.37	3.267	4	3.267	8.167	0.2	0.04	0.1
1.0D38.37	-1.203	4	-1.203	-3.008	2.14	0.0001	0.0001
1.26D103.3	-0.948	4	-2.487	-6.217	0.29	0.01	0.1
1.26D18.43	0.16	4	0.08	0.2	0.16	0.1	10
1.26D18.43	0.16	4	0.08	0.34	0.13	0.01	0.01
1.69D6.28	4.212	0.25	0.859	1.305	1.49	0.0005	0.001
1.69VD55.1	2.059	4	2.99	12.707	0.58	0.001	0.01
1.69VD55.1	2.059	4	2.99	7.474	0.6	0.001	0.01
1D19.7	4.13	1.6	2.269	3.545	0.24	0.01	0.1
1D19.7	-4.13	1.6	-2.269	-3.545	2.19	0.0001	0.0001
3D39	-0.304	4	-0.312	-1.324	0.16	0.01	0.01
4D102.36	0.444	4	1.165	4.95	0.22	0.01	0.01
5D3.9	0.591	0.1	0.074	0.11	0.29	0.01	0.01
0.39SD38.98	1.476	4	1.476	3.689	0.2	0.005	0.01
0.39SD38.98	-0.738	4	-0.738	-1.844	0.19	0.005	0.01
0.79SD14.96	-0.888	0.1	-0.355	-0.533	0.3	0.01	0.01
0.39D38.98	0.874	0.1	0.349	0.524	0.3	0.01	0.01
0.98VD18.7	-3.494	0.1	-1.747	-2.621	1.03	0.001	0.01

Performance requirements listed in Table 5-4 are defined as follows:

- *Engineering Type*: The engineering type designation is used to identify a unique style of magnet. The current SLAC naming convention for a dipole is to use the aperture height (inches) followed by a letter (D for dipole, SD for septum dipole, VD for vertical dipole) and ending with the core length (inches).
- *Nominal Dipole Field*: The required dipole field (magnetic flux density) along the centerline and at the mid-plane of the dipole magnet gap at the nominal beam energy. The units for the dipole B field are kilogauss (kG).
- *Nominal Beam Energy*: The electron beam energy that is used to determine the nominal length integrated dipole field. The units are in gigaelectron volts (GeV).
- *Nominal Integrated Strength:* The required length-integrated dipole field (magnetic flux density) at the nominal beam energy. The units are kilogauss-meters (kG-m).
- *Max Integrated Strength:* The maximum required length-integrated dipole field (magnetic flux density). The units are kilogauss-meters (kG-m).

- *Field Flatness***:** The distance from the magnet center (x or y=0) within which the dipole field value must not vary more than 0.05% of the dipole field value at the magnet center. The units are in centimeters (cm).
- *b2/b0 @r=1cm:* The multipole tolerance at a radius of 1cm, expressed as a ratio of the sextupole harmonic to the dipole harmonic.
- *b4/b0 @r=1cm:* The multipole tolerance at a radius of 1cm, expressed as a ratio of the 10-pole harmonic to the dipole harmonic.

5.4.1.2 LCLS-II Dipole Magnet Designs

A summary of the dipole magnets that will be used for the LCLS-II magnetic optical lattice are given in Table 5-5. A mixture of existing designs created for the LCLS, legacy beamlines at SLAC and new designs will be needed to meet the performance requirements for the LCLS-II. Three of the existing dipole magnet designs were created specifically for the LCLS. Additionally, seven new dipole magnet designs are required, three of which have already been designed during the LCLS-II phase I.

Table 5-5: LCLS-II Dipole Magnets

Magnet Name	Existing or New	LCLS-II Area	Drawing Number
ID19.7	Existing (LCLS)	BC2B	SA-380-325-06
1.0D38.37	Existing (PEPII)	Dogleg, SPD, SPH, SPS	SA-344-100-01
1.0D22.625	Existing (PEPII)	SPH, SPS	SA-344-100-37
3D39	Existing (FFTB)	LTUH, LTUS	SA-235-623-30
1.69VD55.1	Existing (LCLS)	DMPH, DMPS	SA-380-328-01
4D102.36T	Existing (FFTB)	LTUH	SA-380-301-50
5D3.9	Existing (LCLS)	HTR	SA-380-331-12
1.69D6.28T	Existing (LCLS-II)	BC1B	SA-388-320-05
1.26D103.3T	Existing (LCLS-II)	LTUS	SA-388-313-09
1.26D18.43	Existing (LCLS-II)	DMPH, DMPS	SA-388-330-01
0.79SD14.96	New	DIAG0	TBD
0.39D38.98	New	DIAG0	TBD
0.98VD18.7	New	DIAG0	TBD
0.39SD38.98	New	SPH, SPS	TBD

5.4.1.3 New Dipole Magnet Designs for LCLS-II

The LCLS-II will require four new dipole magnet designs:

Two horizontal bend septum type dipoles, one for the injector post laser heater diagnostic line (0.79SD14.96) and the other for the beam spreader in the beam switchyard (0.39SD38.39).

One horizontal bend plane dipole for the post laser heater diagnostic line (0.39D38.39).

One vertical bend dipole for the post laser heater diagnostic line spectrometer (0.98VD18.7).

In addition to the performance requirements found in *Magnets* LCLSII-2.4-PR-0081, additional requirements for the post laser heater diagnostic and beam spreader are found in the physics requirements documents *Post Laser Heater Diagnostic Beamline Requirements* LCLSII-2.4-PR-0068 and *Beam Spreader* LCLSII-2.4-PR-0090.

The 0.79SD14.96 dipole magnet is currently in the conceptual design stage. It will have a solid low carbon steel yoke with water-cooled hollow Cu coils for the main windings. To ease the power supply regulation tolerance this magnet will be strung with the 0.39D38.98 dipole, which is located down beam of the 0.79SD14.96. Therefore, a trim coil will be required for one of the magnets. Mechanical design constraints will dictate which magnet will have a trim coil. The design for the 0.79SD14.96 will be similar to the 0.236D79.64T, which was designed for the LCLS-II phase I linac-to-undulator system. As with the 0.236D79.64T, the 0.79SD14.96 will require that the vacuum chamber be integrated with the magnet yoke due to the 5mm maximum thickness requirement for the septum wall that separates the field-free region from the dipole bend field aperture.

The 0.39D38.39 and 0.98VD18.7 dipole magnets are currently in the conceptual design stage. They will have solid, low-carbon steel yokes with water-cooled hollow Cu coils for the main windings.

The 0.39SD38.98 dipole magnet is currently in the conceptual design stage. It will have a solid low carbon steel yoke with water-cooled hollow Cu coils for the main windings. The magnet will also include a trim coil, as it will be strung on the same power supply of an existing magnet that does not have a trim coil. The design for the 0.39SD38.98 will be similar to the 0.236D79.64T. As with the 0.236D79.64T, the 0.39SD38.98 will require that the vacuum chamber be integrated with the magnet yoke due to the 5mm maximum thickness requirement for the septum wall that separates the field-free region from the dipole bend field aperture.

5.4.1.4 Existing Dipole Magnet Designs for LCLS-II

The current LCLS-II SCRF will be able to use three dipole magnet designs that SLAC created for LCLS phase I: the 1.69D6.28T, 1.26D103.3T, and 1.26D18.43. The 1.69D6.28T dipole magnet was wholly designed at SLAC to meet the performance requirements of the LCLS-II phase I BC1electron bunch compressor chicane. For the current LCLS-II SCRF (phase II), the 1.69D6.28T will satisfy the performance requirements as well. The 1.69D6.28T dipole has a solid, low carbon steel yoke with chamfered pole pieces in an H-frame configuration. The 1.69D6.28T dipole uses water-cooled hollow Cu conductor for the main coil windings, with solid wire Cu conductor for the trim coil windings. Both the main and trim coils are wound with a tapered profile in order to provide clearance for the vacuum chamber and support assembly.

Electrical connections from the main coil bussing to DC power supply cabling is made via Multi-Contact quick connects. A 3D CAD image of the 1.69D6.28T dipole magnet is shown in Figure 5-7. The design data for the 1.69D6.28T dipole is given in Table 5-6.

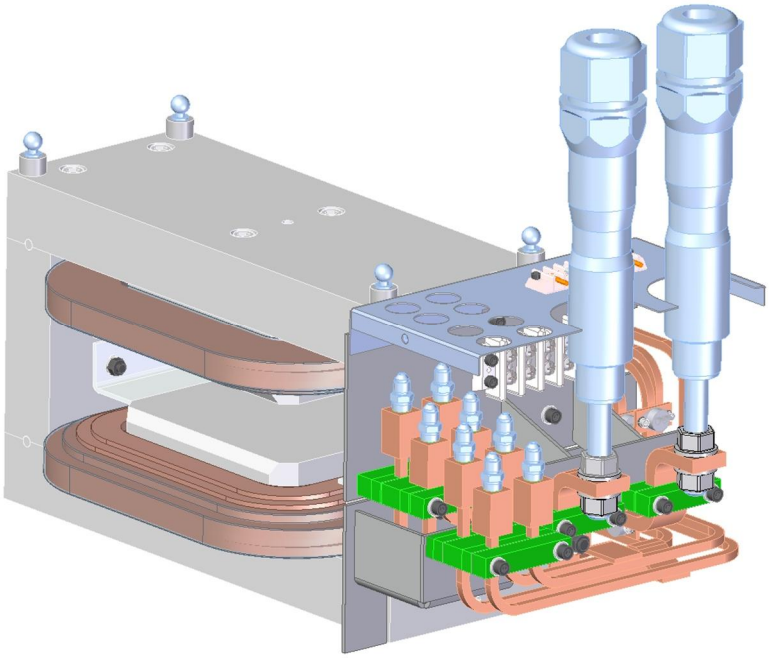

Figure 5-7: 1.69D6.28T 3D CAD Model

Table 5-6: 1.69D6.28T Design Data Sheet

BENDING MAGNET DESIGN DATA SHEET

MAGNET DESIGNATION 1.69D6.28T BEAM ENERGY 0.350 GEV
WHERE USED LCLS II BUNCH COMPRESSOR #1 CHICANE
REQUIRED ∫ Bdl 1.31 (MAX) kG-m. EFFECTIVE LENGTH .203 METER
TRANSPORT REF.NO. RUN ON DATE BEND ANGLE (NOM) 5.391 deg
POISSON RUN NO. D43L160R6 RUN ON DATE 5TH NOV 2012 GAP FLUX 6.453 Kg
CURRENT 379.7 AMPS. TERMINAL VOLTAGE 14.83 VOLTS. MAX. POWER 5.633 KW
PRESSURE DROP 100 PSI. TOTAL COOLANT FLOW 2.04 GPM. IN 4 PARALLEL CIRCUITS
COOLANT TEMPERATURE RISE 10.5 °C. MEAN CONDUCTOR TEMP. 40 °C
MAGNET RESIS. 0.0391 OHMS. GOOD FIELD REGION WIDTH (+/-0.05%) +/- 1.7 IN.
GAP DIMENSIONS: X 7.087 IN. Y 1.693 IN. Z 6.283 IN. MAGNET WEIGHT 269 LB
POLE EXTENSION NO . FLUX LINES PARALLEL TO Y AXIS
CORE STEEL TYPE C1008 SOLID X LAMINATED __ LAM. THICKNESS IN.
TURNS PER MAIN COIL 30 MAIN COILS/MAGNET 2 TOTAL MAIN TURNS 60
MAIN CONDUCTOR MATERIAL Cu (SQUARE) CROSS SECTION 0.236" SQUARE
COIL COND. LENGTH 88.5 FT. COOLANT HOLE DIA. 0.1378 IN. COND. AREA .0395 SQ. IN.
MEAN LENGTH PER TURN 2.48 FT. AMPTURNS/POLE 11391 (MAX)
MAGNET SIZE: WIDTH 23.2 IN. HEIGHT 10.26 IN. OVERALL LENGTH 10.68 IN.
CALCULATED MAGNET INDUCTANCE TBD HENRYS. L/R TIME CONSTANT SEC
TRIM COND. MATERIAL 8 GA Cu, .1348 (SQUARE) TRIM COIL: LENGTH 43 FT. RESIS. 0.048 OHMS
TURNS PER TRIM COIL 15 TRIM COILS/MAGNET 2 TOTAL TRIM TURNS 30
MEAN LENGTH PER TRIM TURN 2.48 FT. TRIM AMPTURNS/POLE 180
DATA SHEET PREPARED BY: CHERRILL SPENCER, 20 DEC 2012
NOTEBOOK PAGES LCLS II BC1 DIPOLE FOLDER
NOTE: TOP ASSY DRAWING NUMBER SA-388-320-05

1.26D103.3T

The 1.26D103.3T dipole magnet was wholly designed to print at SLAC to meet the performance requirements of the LCLS-II phase I LTU electron beam transport optics. For the current LCLS-II phase II (SCRF linac) the 1.26D103.3T will satisfy the performance requirements as well. The 1.26D103.3T dipole has a solid low carbon steel yoke and pole pieces in an H-frame configuration. The 1.26D103.3T dipole uses water-cooled hollow Cu conductor for the main coil windings, with solid wire Cu conductor for the trim coil windings. Electrical connections from the main coil bussing to DC power supply cabling is made via Multi-Contact quick connects. A 3D CAD image of the 1.26D103.3T dipole magnet is shown in Figure 5-8 below. The design data for the 1.26D103.3T dipole is given in Table 5-7 below.

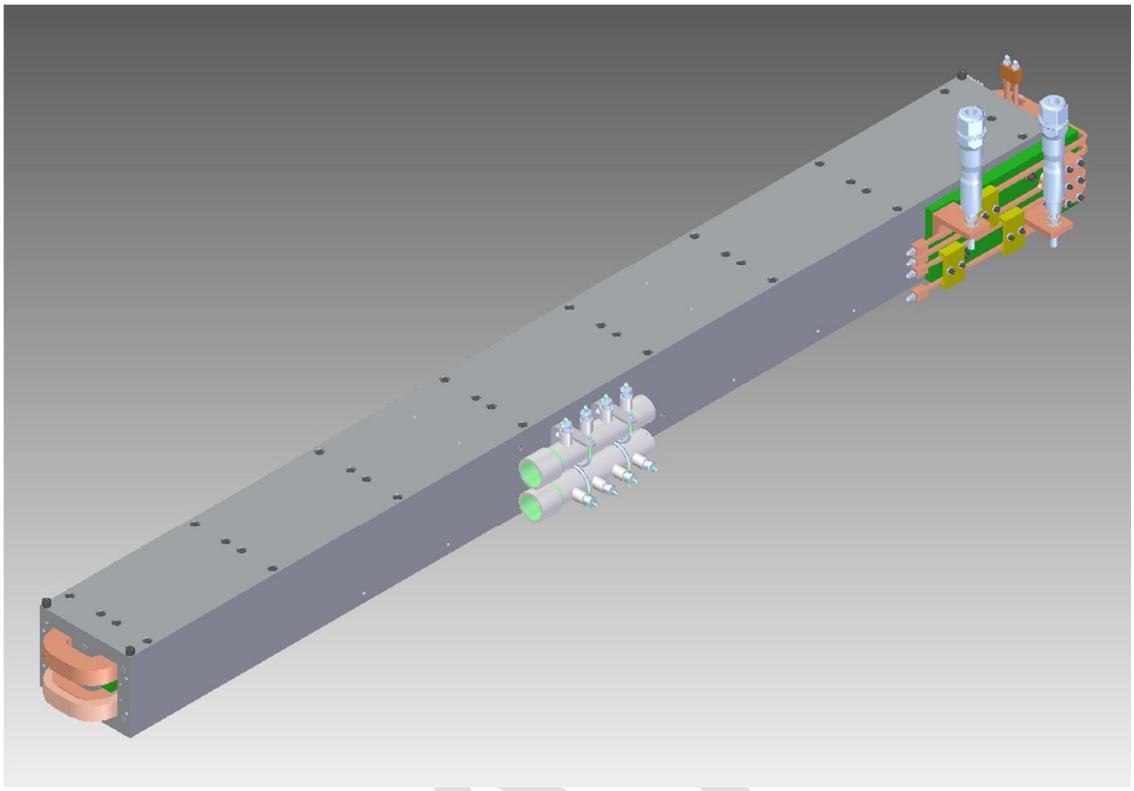

Figure 5-8: 1.26D103.3T 3D CAD Model

Table 5-7: 1.26D103.3T Design Data Sheet

DESIGN DATA SHEET, 17th March 2013 for BX41 and BX42	Units	2 each
OD Bare (square copper)	in	0.340
OD Over Mylar and Glass Tapes, half-lapped	in	0.376
ID Water Passage	in	0.183
Engineering name		**1.26D103.3T**
Steel Length	cm	262.4
Overall magnet length	cm	276.5
Conductor Cross Section	in^2	0.08853
Conductor Weight per Coil	lb	126.98
Conductor Length per Coil	ft	370.1
2h (full gap)	cm	3.2
Good Field Region (+/-0.05%) > +/-0.30cm	cm	+/- 0.8
Beam Energy (maximum)	MeV	13.5 (15)
Sagitta at nominal beam energy (distance from nominal magnet centerline)	cm	0.343
Pole Width	cm	7.62
Integrated strength (Max) [Nom=9.434]	kG-m	10.482
B gap (Max)	kG	3.946
Effective Length	cm	265.6
Amp-Turns (Max, ideal) per main coil	AT	5076.6
Coil-Turns	Turns	20
Layers		4
Turns per layer		5
Core efficiency (at maximum current)	%	99.0%
Real current (Max)	A	253.83
Mean Turn Length	in	222.0
Resistance per Magnet	Ohms	0.0734
Current Density (Max)	A/in^2	2837.9
Voltage Drop Magnet (Max)	V	18.63
Voltage Drop Power Cables (Max)	V	TBD
Total Voltage per string of 8 dipoles (incl 6 BYDs) + cable	V	~227
Power Magnet (Max)	kW	4.728
Number of water circuits per Magnet	EA	4
LCW flow @ 100 delta-psig per circuit	gpm	0.44
Delta water temp ^0C	^0C	10.3
Total LCW per dipole	gpm	1.76

TRIM COIL PARAMETERS		
Trim coil wire #12 square with heavy film insulation, length per coil	ft	252
Coil-turns, in 1 layer,		14
Trim coils resistance	Ohms	0.715
Nominal current (when main coils at max)	Amps	0
Nominal trim voltage	V	0
Trim strength at 6 A : % of dipole max strength	%	1.66

1.26D18.43

The 1.26D18.43 dipole magnet was wholly designed to print at SLAC to meet the performance requirements of the LCLS-II phase I LTU electron beam transport optics. For the current LCLS-II phase II (SCRF linac) the 1.26D18.43 will satisfy the performance requirements as well. The 1.26D18.43 dipole has a solid low carbon steel yoke and pole pieces in an H-frame configuration. The 1.26D18.43 dipole uses solid wire Cu conductor for the main coil windings. A 3D CAD image of the 1.26D18.43 dipole magnet is shown in Figure 5-9 below. The design data for the 1.26D18.43 dipole is given in Table 5-8 below.

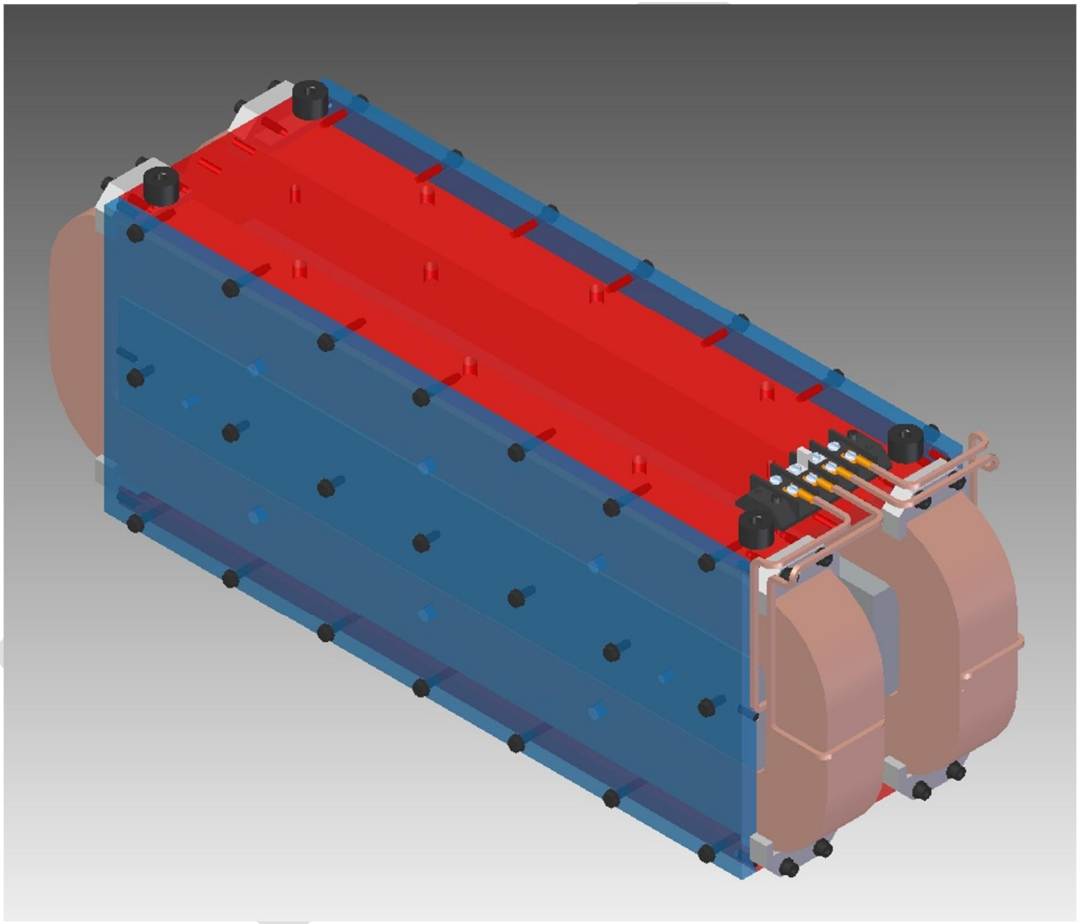

Figure 5-9: 1.26D18.43 3D CAD Model

Table 5-8: 1.26D18.43 Design Data

Parameter	Units	Value
Engineering name		1.26D18.43
Steel Length	in	18.43
Effective length	in	19.69
Overall magnet length	in	22.55
Nominal Conductor Cross Section	in^2	0.01251
Nominal Conductor Weight per Coil	lb	41.3
Conductor Length per Coil	ft	856.0
2h (full gap)	cm	3.2
Good Field Region (> 1.124cm)	cm	1.20
Beam Energy (maximum)	GeV	15.0
Beam Energy (nominal)	GeV	13.5
Pole Width (no chamfers)	cm	7.0
Integrated strength (Max)	kG-m	0.800
B gap (Max)	kG	1.5987
Amp-Turns (Max, ideal)	AT	2080.0
Coil-Turns	Turns	210
Number of Layers		14
Turns per layer		15
Conductor: #9 square AWG, MAX OD	in	0.1205
Nominal Conductor Cross Section	in^2	0.01251
Core efficiency (at maximum current)	%	98%
Real current (Max)	A	9.9
Mean Turn Length	in	49.7
Conductor Length / Coil	ft	870.0
Resistance per Magnet	Ohms	1.13
Current Density (Max)	A/in^2	791.4
Voltage Drop Magnet (Max)	V	11.1
Voltage Drop Power Cables (Max)	V	TBD
Total Voltage per magnet	V	TBD
Power Magnet (Max)	W	110
Power Cables (Max)	W	TBD
Total Power	kW	TBD
Predicted sextupole/dipole, to be <0.0100	At 1cm	0.003
Predicted 10-pole/dipole, to be <0.10	At 1cm	0.00096

5.4.2 Quadrupoles

A quadrupole magnet consists of a core (ferromagnetic steel in most cases), with four pole tips having a hyperbolic surface, each with its own coil (Cu or Al) oriented such that the field in the gap is transverse to the direction of the electron beam propagation. As is the case with the dipole magnet, the pole tips may have chamfers to reduce the field harmonics and fringe fields generated by the sharp edges of the pole tip. The purpose of a quadrupole magnet is to provide focusing of the electron beam. The optical analog to the quadrupole is the lens. However, unlike a lens which provides uniform focusing about the horizontal and vertical planes, a quadrupole will focus the electron beam in one plane and de-focus the beam in the other plane.

5.4.2.1 LCLS-II Quadrupole Magnet Performance Requirements

The performance requirements for the LCLS-II quadrupole magnets are found in the physics requirements document *Magnets* LCLSII-2.4-PR-0081. Table 5-9 summarizes the most demanding performance requirements for a given magnet design. In some cases, all magnets of a given magnet design will have the same performance requirements any place they are used in the LCLS-II magnetic optical lattice. In other cases, specific magnets will have more demanding performance requirements than others.

Table 5-9. LCLS-II Performance Requirements for Quadrupole Magnets

Engineering Type	Pole Tip Field (kG)	Nominal Gradient (kG/m)	Beam Energy (GeV)	Nominal Int. Strength (kG)	Max Int. Strength (kG)	Field flatness +/- (cm)	b2/b1 @r=1cm	b5/b1 @r=1cm
0.91Q17.72	1.29	112.06	4	51.651	219.517	0.081	0.01	1
0.91Q17.72	-0.65	-56.35	4	-25.975	-110.392	0.107	0.01	1
1.085Q4.31	1.4	101.66	4	10.857	27.142	0.098	0.01	1
1.085Q4.31	-1.44	-104.7	4	-11.182	-27.955	0.087	0.01	1
1.259Q3.5	0.86	53.75	4	5.805	24.673	0.069	0.01	1
1.259Q3.5	-0.25	-15.63	0.1	-1.689	-2.533	1	0.005	0.001
1.259Q3.5	-0.25	-15.63	0.1	-1.689	-2.533	1	0.005	0.001
1.26Q12	-2.48	-154.71	4	-49.508	-123.77	0.056	0.01	1
1.26Q12	0.75	46.65	4	14.929	37.324	1.353	0.003	0.001
1.625Q27.3	-0.58	-28.16	4	-20.109	-50.273	1.666	0.01	0.005
1.97Q10	-0.55	-22.03	4	-6.168	-15.42	0.107	0.01	1
1.97Q20	0.58	23.3	4	12.627	31.567	0.082	0.01	1
2.362Q3.5	0	0	1.6	0	2.1	0.52	0.1	0.1
2Q4	0.22	8.09	4	1.006	2.515	0.194	0.01	1
2Q4W	0.8	29.62	4	3.685	9.213	0.137	0.01	1
2Q4W	0.57	21.21	4	2.638	6.595	0.184	0.01	1

3.25Q20	0.65	15.84	4	8.713	37.032	0.056	0.01	1
3.25Q20	-0.67	-16.22	4	-8.92	-22.3	2.961	0.001	0.001
3.94Q17	-1.04	-20.71	4	-8.904	-37.84	2.945	0.001	0.001
4.63Q8.0	1.14	19.36	4	4.802	12.004	0.105	0.03	1
50Q3	-0.19	-17.93	4	-5.137	-19.266	0.094	0.01	1
0.433Q3.1	1.31	238.17	4	20.006	50.015	0.04	0.01	1
0.433Q3.1	0.41	74.82	4	6.285	15.712	0.059	0.01	1

Performance requirements listed in Table 5-9 are defined as follows:

Engineering Type

The engineering type designation is used to identify a unique style of magnet. The current SLAC naming convention for a quadrupole is to use the aperture radius (inches) followed by the letter "Q" and ending with the core length (inches).

Pole Tip Field (kG)

The required B field (magnetic flux density) at the poletip surface at the longitudinal center of the magnet at the nominal beam energy. The units for pole tip field are kilogauss (kG).

Nominal Gradient (kG/m)

The required quadrupole gradient field at the nominal beam energy. The quadrupole gradient field is defined as the pole tip field divided by the aperture radius. The units for nominal gradient field are kilogauss/ meters (kG/m).

Beam Energy (GeV)

The electron beam energy which is used to determine the nominal length integrated quadrupole field. The units for beam energy are in gigaelectron volts (GeV).

Nominal Int. Strength (kG)

The required nominal length integrated quadrupole gradient field at the nominal beam energy. The units for nominal int. strength are kilogauss (kG).

Max Int. Strength (kG)

The maximum required length integrated quadrupole gradient field. The units for nominal int. strength are kilogauss (kG).

Field flatness +/- (cm)

The distance from the magnet center (x,y=0) within which the quadrupole gradient field value must not vary more than 0.05% of the quadrupole gradient field value at the magnet center. The units are in centimeters (cm).

b2/b1 @r=1cm

The multipole tolerance at a radius of 1cm, expressed as a fraction of the sextupole harmonic to the quadrupole harmonic.

b5/b1 @r=1cm

The multipole tolerance at a radius of 1cm, expressed as a fraction of the 12-pole harmonic to the quadrupole harmonic.

5.4.2.2 LCLS-II Quadrupole Magnet Designs

A list of the quadrupole magnets that will be used for the LCLS-II magnetic optical lattice is given in Table 5-10. A mixture of designs created for the LCLS and legacy beamlines at SLAC will be needed to meet the performance requirements for the LCLS-II. Five of the existing quadrupole magnet designs were created specifically for LCLS.

Table 5-10: LCLS-II Quadrupole Magnets

Magnet Name	Existing or New	Area	Drawing Number
1.26Q3.5	Existing (LCLS)	HTR, COL0, DIAG0, BC1B, COL1, LTUH, LTUS	SA-380-309-00
1.26Q12	Existing (LCLS)	SPH, SPS, LTUH, LTUS	SA-380-327-00
2.362Q3.5	Existing (LCLS)	BC1B, BC2B	SA-380-702-28
0.433Q3.1	Existing (LCLS)	HXR, SXR	SA-381-012-00
1.0Q3.1	Existing (SLC)	COL0	SA 237-007-15
1.085Q4.31	Existing (SLC)	EXT	SA-902-675-01R3
4.63Q8.0	Existing (SLC)	EXT	SA-234-007-15R5
1.625Q27.3	Existing (SLC)	Dogleg	AD-235-016-00
1.97Q20	Existing (PEP)	Dogleg	AD-204-211-00
2Q10	Existing (PEPII)	Dogleg	SA-344-113-28
2Q4W	Existing (PEPII)	Dogleg, Bypass, SPS	SA-344-112-08
2Q4	Existing (PEPII)	Bypass	SA-344-112-01
0.91Q17.72	Existing (FFTB)	SPH, LTUH	SA-380-301-00
3.94Q17	Existing (PEPII)	SPD, DMPH, DMPS	SA-342-102-31R4
3.25Q20	Existing (SLC)	DMPH, DMPS	AD-902-614-00
50Q3	Existing (SLC)	SPH	AD-902-673-00

5.4.2.3 LCLS Quadrupole Magnet Designs for LCLS-II

LCLS-II will use four different existing quadrupole magnet designs: the 1.26Q3.5, 1.26Q12, 2.362Q3.5, and 0.433Q3.1. All these quadrupoles were designed to SLAC specifications to meet the performance requirements of the LCLS magnetic optical lattice. They will also be able to satisfy the performance requirements of the current LCLS-II SCRF (phase II).

The 1.26Q3.5 quadrupole magnet was designed to SLAC specification by Everson Tesla Inc. to meet the performance requirements of the LCLS magnetic optical lattice. For the current LCLS-II SCRF (phase II) the 1.26Q3.5 will satisfy the performance requirements as well. The 1.26Q3.5 quadrupole has a solid low carbon steel yoke and pole pieces. The 1.26Q3.5 quadrupole uses solid wire Cu conductor for the main coil windings. A 3D CAD image of the 1.26Q3.5 quadrupole magnet is shown in Figure 5-10.

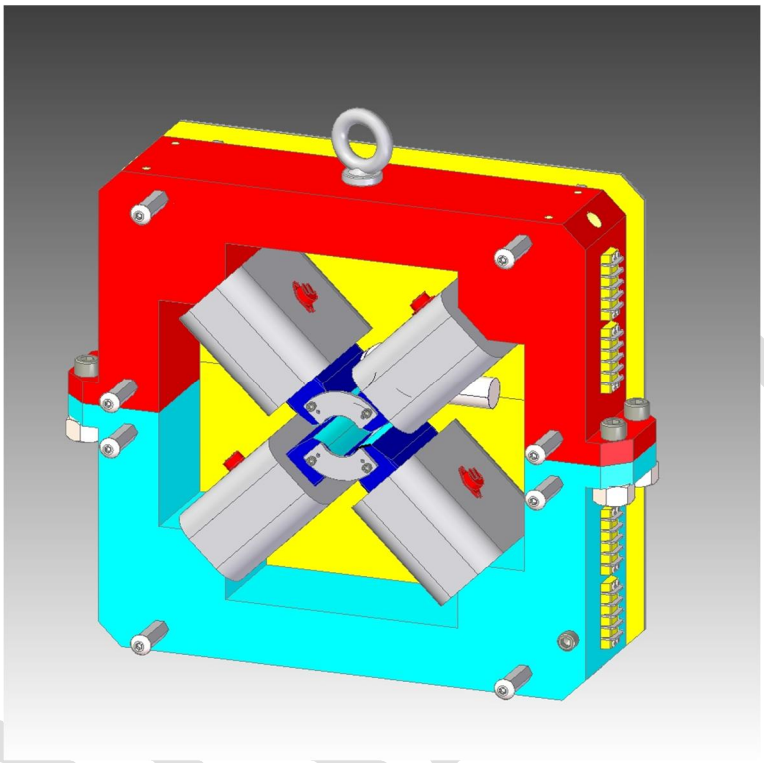

Figure 5-10: CAD Drawing of 1.26Q3.5 Quadrupole Magnet

The 1.26Q12 quadrupole magnet was designed to SLAC specification by Everson Tesla Inc. to meet the performance requirements of the LCLS magnetic optical lattice. For the current LCLS-II SCRF (phase II) the 1.26Q12 will satisfy the performance requirements as well. The 1.26Q12 quadrupole has a solid low carbon steel yoke and pole pieces. The 1.26Q12 quadrupole uses water-cooled hollow Cu conductor for the main coil windings, with solid wire Cu conductor for the trim coil windings. A 3D CAD image of the 1.26Q12 quadrupole magnet is shown in Figure 5-11.

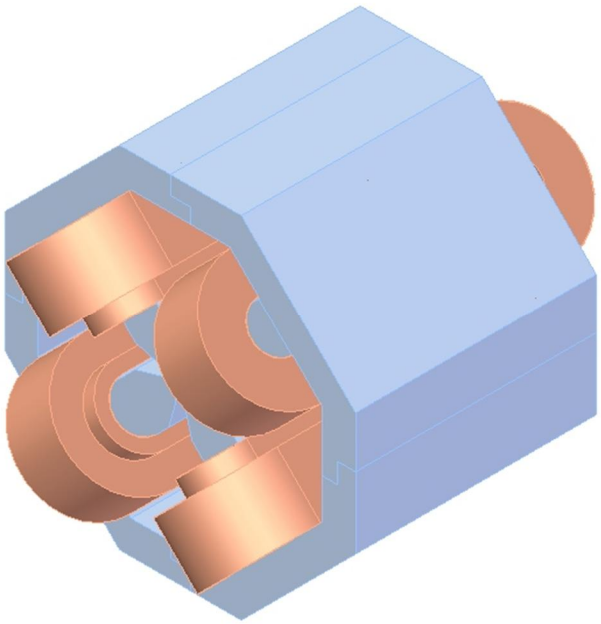

Figure 5-11: CAD Drawing of 1.26Q12 Quadrupole Magnet

The 2.362Q3.5 quadrupole magnet was designed to SLAC specification by Sigma Phi to meet the performance requirements of the LCLS magnetic optical lattice. For the current LCLS-II SCRF (phase II) the 2.362Q3.5 will satisfy the performance requirements as well. The 2.362Q3.5 quadrupole has a solid low carbon steel yoke and pole pieces. The 2.362Q3.5 quadrupole uses solid wire Cu conductor for the main coil windings. A 3D CAD image of the 2.362Q3.5 quadrupole magnet is shown in Figure 5-12.

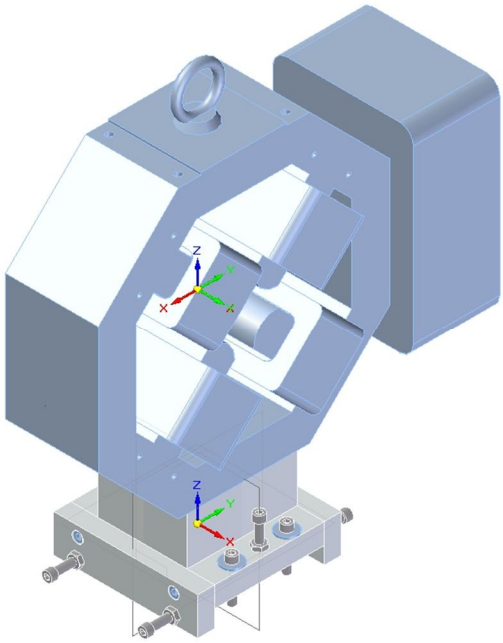

Figure 5-12: CAD Drawing of 2.362Q3.5 Quadrupole Magnet

0.433Q3.1

The 0.433Q3.1 quadrupole magnet was designed to SLAC specification by Everson Tesla Inc. to meet the performance requirements of the LCLS magnetic optical lattice for the undulator region. For the current LCLS-II SCRF (phase II) the 0.433Q3.1will satisfy the performance requirements as well. The 0.433Q3.1 quadrupole has a laminated electrical silicon steel yoke and pole pieces. The 0.433Q3.1 also provides weak vertical and horizontal correction via its trim coil windings which are powered such that they excite a dipole field in the quadrupole gap. The 0.433Q3.1 quadrupole uses solid wire Cu conductor for the main coil windings and corrector trim coil windings. A 3D CAD image of the 0.433Q3.1 quadrupole magnet is shown in Figure 5-13.

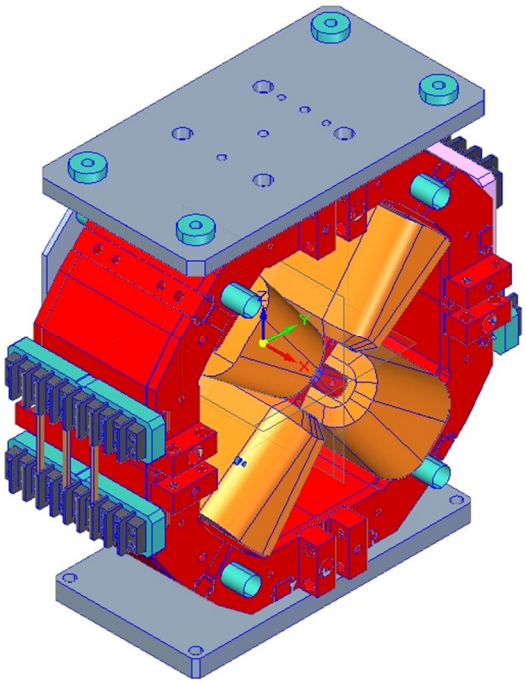

Figure 5-13: CAD Drawing of 0.433Q3.1Quadrupole Magnet

5.4.3 Correctors

A corrector magnet is essentially a weak dipole magnet. A typical corrector magnet consists of a frame (either metallic or non-metallic) which holds two coils oriented such that the field in the gap is transverse to the direction of the electron beam propagation. In most instances, correctors will not have a pole tip as with the typical dipole magnet. In the case of a metallic frame the material may be mild steel or aluminum, with the non-metallic frames being made of G10. All correctors used for LCLS-II are existing designs, listed in Table 5-11. In some cases both vertical and horizontal correctors are combined into a single compact unit. The purpose of a corrector magnet is to correct errors about the ideal electron beam path through the magnetic optical lattice.

Table 5-11: LCLS-II Corrector Magnets

Magnet Name	Area	Drawing Number
TYPE-4	Dogleg, Bypass, LTUH, LTUS	SA-238-004-01
BYPASS	Bypass, SPS	SA-344-115-01
BYPASS#2	Bypass	SA-344-116-01
CLASS-1A	HTR, COL0, DIAG0, BC1B	SA-380-314-42

CLASS-4	BC2B, EXT, SPD, SPH, SPS, LTUH, LTUS, DMPH, DMPS	SA-380-323-01
CLASS-4F	LTUH, LTUS	SA-380-323-01
CLASS-5	LTUH, LTUS, DMPH, DMPS	SA-380-323-11
CLASS-5F	LTUH	SA-380-323-24, 25
CLASS-6	COL0, DIAG0, BC1B, COL1	SA-446-540-14

5.4.3.1 LCLS-II Corrector Magnet Designs

The CLASS-4 corrector magnet is used extensively throughout the LCLS-II magnetic optical lattice. The CLASS-4 corrector design is based off of the TYPE-4 corrector, which was designed for the SLC at SLAC. It has two coils wound from solid wire Cu conductor and a ferromagnetic steel frame which supports the coils and also increases the magnet's efficiency when compared to a corrector with a non-ferromagnetic frame. A 3D CAD image of the CLASS-4 is seen in Figure 5-14.

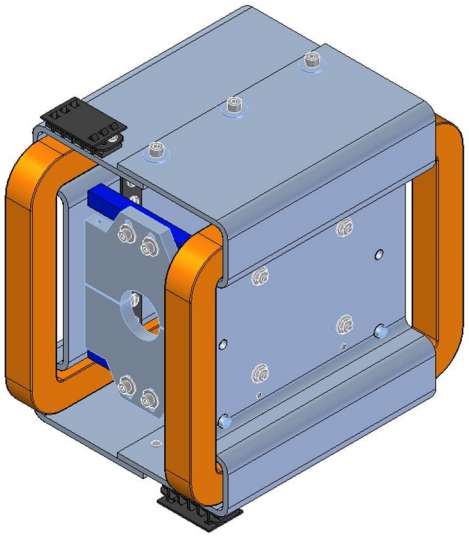

Figure 5-14: CAD Drawing of CLASS-4 Corrector Magnet

The CLASS-5F corrector is a special case of a corrector known as a "feedback" corrector. Unlike the typical corrector such as the CLASS-4 described above, the CLASS-5F lacks a ferromagnetic support frame. The lack of any ferromagnetic material in the corrector frame allows it to be operated in a pulsed mode for fast orbit feedbacks and it does not retain any remnant magnetization as with a ferromagnetic frame corrector. However, because the efficiency is low, the CLASS-5F corrector needs a relatively large number of coil turns. A 3D CAD image of the CLASS-5F is seen in Figure 5-15.

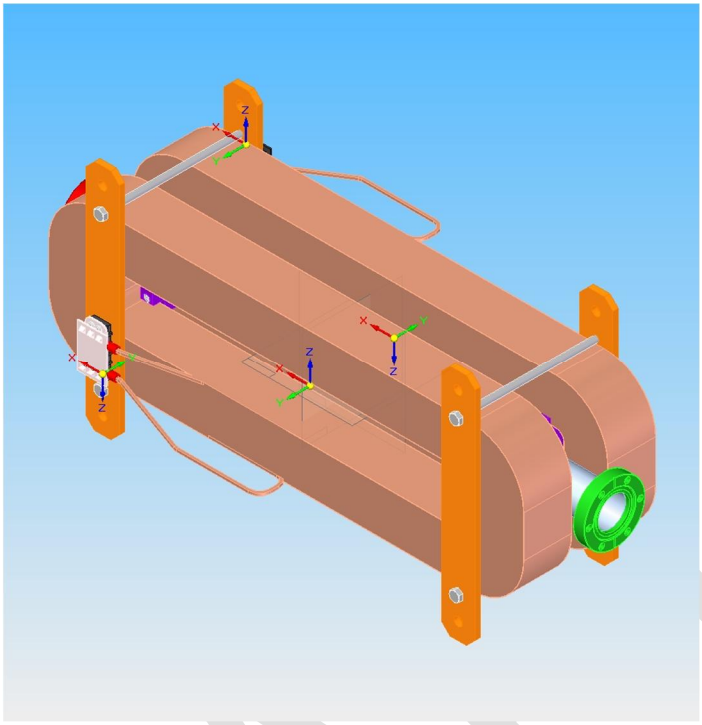

Figure 5-15. Class 5F Corrector 3D CAD Model

5.5 Magnet Power Supplies

5.5.1 Scope

The LCLS-II Magnet Power Supply systems will provide controllable, precise and stable excitation current to dipoles, quadrapoles, correctors and solenoids to generate the magnetic field required to steer the electron beam from the Injector to the Electron Beam Dump. The electron beam requires very tight magnetic field stability tolerances, which translate directly into tight current stability tolerances for the power supplies. The power supplies are designed to power the magnets for a 4 GeV final beam energy plus 15% to standardize the magnets.

5.5.2 Performance Requirements and Parameters

Magnetic field and power supply current performance requirements will be given in two PRDs: *LCLS-II Magnets* and *LCLS-II Steering Corrector Magnets*. The PRDs will tabulate the maximum field and field stability tolerance for each magnet. Tolerance specifications will be given in rms field regulation evaluated over 1 second (short-term) and 10 seconds (long-term), relative to the maximum operating field setting. The power supply relative current tolerance is assumed to be the same as the magnetic field tolerance, which varies between 0.1 and 0.003%.

5.5.3 Design

The magnet power supply systems for LCLS-II will be of similar design to those used at LCLS. Power supply types fall into three main categories: Intermediate, Superconducting and Trim Type power supplies. The power supply type for each magnet is selected based on the current and tolerance requirements.

Intermediate type power supplies, illustrated in Figure 5-16, are provided to magnets that require ≥ 750W power and/or ≤ 0.01% rms relative current stability. Intermediate systems use commercial power supplies controlled by a SLAC-designed PID-based control loop with highly precise and stable current transducers and electronics to regulate current down to 0.001% rms levels. An ESD with additional specifications and details will be released as *LCLS-II Intermediate Magnet Power Supply Specification.*

Superconducting type power supplies are provided to LINAC quadrapoles and correctors. These systems are similar to the Intermediate type power supplies, where commercial power supplies are controlled by a SLAC-designed controller. Additionally, superconducting systems require a quench protection circuit to protect the power supply and magnet from voltage transients. An ESD with additional specifications and details will be released as *LCLS-II Superconducting Magnet Power Supply Specification*.

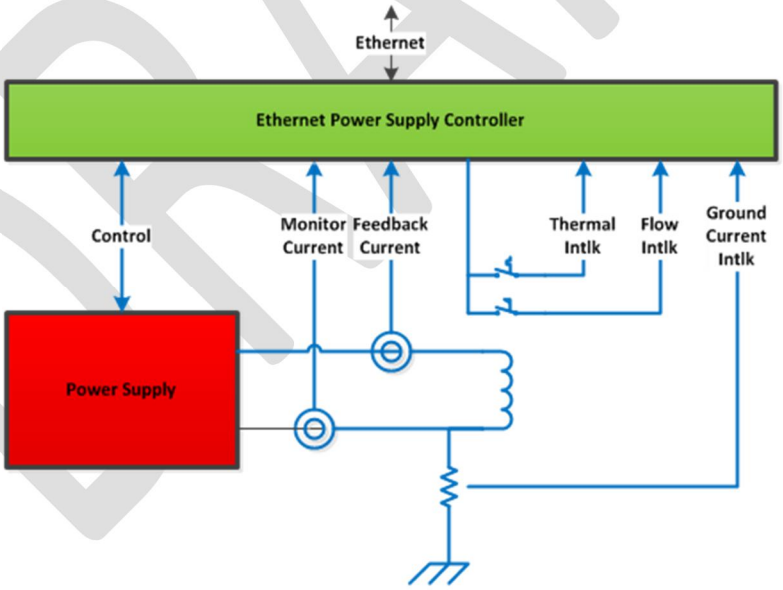

Figure 5-16. Intermediate power supply diagram

Trim Type Power Supplies, illustrated in Figure 5-17, are provided to magnets that require ≤ 40V, ≤ 30A and ≥ 0.01% current stability. The Trim Type Power Supplies are SLAC-designed, crate mounted, modular bipolar power supplies and are available in 1, 2, 6, 12 and 30 ampere

ratings at 40 volts. An ESD with additional specifications and details will be released as *LCLS-II Bipolar Magnet Power Supply Specification.*, SLAC-I-XXX.

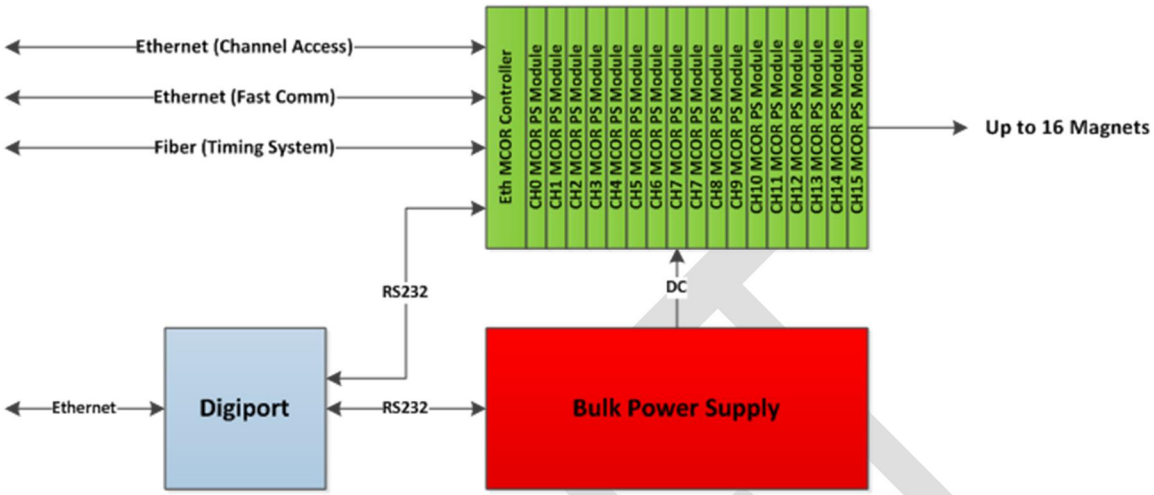

Figure 5-17. Trim Power Supply Diagram

5.6 Beam Spreader

A magnetic kicker is being developed for deployment as a beam spreader for LCLS-II. The kicker will be implemented in conjunction with a set of septum magnets to direct the electron bunches to the Hard X-ray undulator, the soft X-ray undulator, or the BSY high power electron beam dump. The magnetic kicker approach allows for bunch-by-bunch selection of beam destination.

The 4.0 GeV beam requires a 0.75 mrad kick be imparted for diversion into the undulator lines. A positive, negative, or zero strength kick must be selectable on a pulse-by-pulse basis. The zero strength kick steers the beam into the dump. The maximum repetition rate of 929 kHz matches the maximum rate for full beam diversion into the undulator lines. The peak of the kicker's magnetic field must be repeatable to 70 ppm rms. The beampipe aperture is required to be more than 10 mm.

Due to the high repetition rate, it is desirable to have a MOSFET switch to control energy flow to the kicker magnet. Classic strip line kicker designs, containing no magnetic material, require higher voltages to achieve the specified kick field strength. Such voltages may be more than the MOSFET is designed to handle. Therefore we have chosen a ferrite-loaded magnet design to reduce the amount of energy transfer to the magnet for a given kick. With this design, drive voltages can stay below 1 kV, safely in the operating range of commercial MOSFETs.

Two designs are being considered for down selection. The first design is a ferrite loaded transmission line. This design consists of a magnet divided into serial L-C segments to approximate a transmission line. This allows the kicker modulator to be connected outside of the

tunnel via long cables. However, it can be difficult to achieve perfect impedance matching to allow the magnetic field to decay rapidly and not affect subsequent pulses. The second design is the "direct-drive" design. In this design, the magnet is also divided into sections. An electronic driver is mounted directly on each section. There is very little ringing because there are no transmission cables. However, this design requires that the driver be designed to an acceptable level of radiation hardness.

A length-integrated field of 10.5 mT-m is required to achieve the required beam deflection. Given the MOSFET voltage limitation, a reasonable goal for magnet strength is 3.5 mT. Thus, three 1-m sections are required to provide the requisite kick. It is difficult to ensure that the remnant field in the ferrites is identical for pulses of both polarities. The amount of remnant field effects the amplitude of the next pulse, making it more difficult to meet the stringent repeatability requirement. Therefore, the spreader will use separate positive and negative kickers as shown in Figure 5-18.

Figure 5-18: Six 1-m sections making up the beam spreader.

Each 1-m magnet section will contain a ceramic beam pipe to isolate the vacuum and provide uniform beam impedance. The beampipe will be metalized to provide a path for beam image currents. More details are located in the beam spreader engineering note LCLSII-2.5-EN-0350.

5.7 Conventional Supports

Device stands and supports will be similar to those used in LCLS and LCLS-II Phase I. One significant difference is that the beamline center from the Injector to L3 is 0.99 m lower and 0.28m to the north of the original SLAC tunnel beamline position. All stands will comply with *LCLS-II Project Building Inspection Office Codes and Standards of Record*, LCLSII-1.1-TS-0035. In addition, the quadrupole stands will meet vibration tolerances listed in the *Quadrupole Magnet Vibration Requirements PRD*, LCLS-II-2.4-PR-0062.

Engineering specification documents and design reviews will be included in the mechanical design reviews for each area. The Accelerator System Preliminary Design Review, which will include preliminary mechanical design reviews of each area, was held in January 2015. Final design reviews vary per area, and will be described in each area's subchapter following.

5.7.1 Injector Source Supports

The LCLS-II Injector Source support stand designs (see Figure 5-19) are modified versions of the stands used for the Advanced Photoinjector Experiment (APEX) at LBNL. The LCLS-II beamline is approximately 70 cm lower than the APEX beamline, so appropriate changes have been made to the structures to accommodate the reduction in height. The VHF gun is supported by a 6-strut arrangement tied to a base plate and pedestal type strut mounts that allows

independent alignment. The low-energy beamline portion of the Injector Source consists of four separately mounted stations (solenoid 1, buncher, laser mirror box, solenoid 2) that are in turn mounted on a common raft structure. Each of the components on the individual stations has the capability of being independently aligned. The cathode load lock system contains its own series of vertical support posts that will tie directly to the floor.

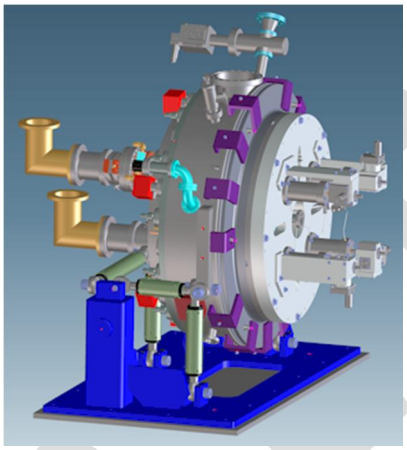

Figure 5-19. Injector Source VHF gun on support stand.

5.7.2 Injector System: HTR, DIAG0, COL0 Supports

The Injector stand design is based on the LCLS-II Phase I support stands, modified to accommodate the lower beamline height. Figure 5-20 shows beamline layout of Heater and Diagnostic section and Table 5-12 shows a list of drawing supports and quantity required for this area. CAD drawings of some of the Injector system supports are shown in Figure 5-21.

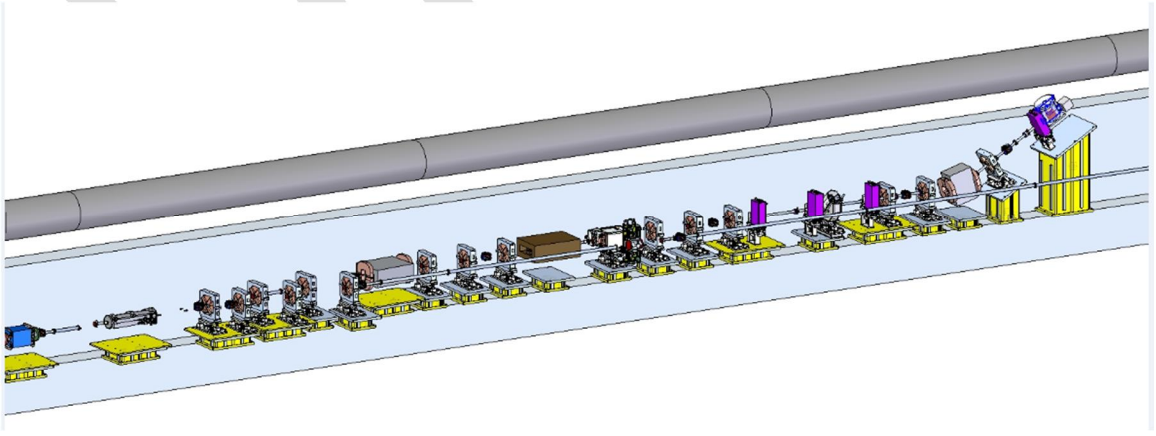

Figure 5-20. Isometric view of HTR, DIAG0 and Part of COL0

Table 5-12: Injector Stands

	Stand Type	Drawing No.	Qty
1	Quad Stand	SA-375-510-11	15
2	Wide Quad Stand	SA-375-510-15	12
3	Inclined Quad Stand 1	SA-375-510-20	1
4	Inclined Quad Stand 2	SA-375-510-25	1
5	Top Plate 1	SA-388-745-62	16
6	Top Plate 2	SA-388-745-22	13
7	Drift Stand	SA-375-510-03	13
8	Table Drift Stand	SA-380-751-78	47

1

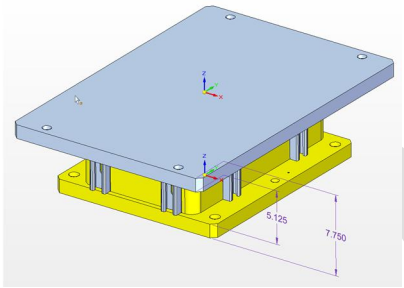

4

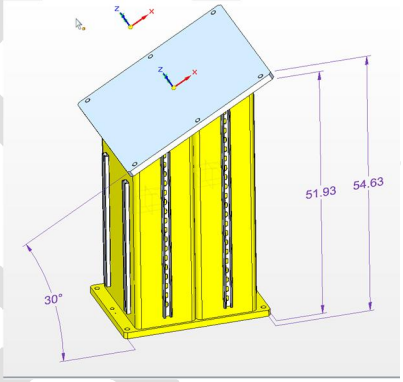

2

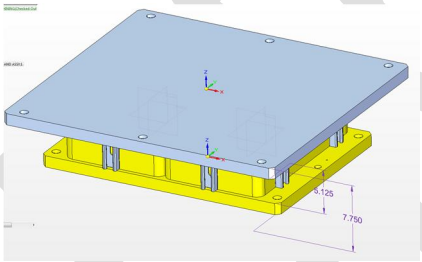

7

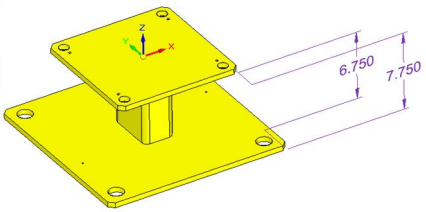

3

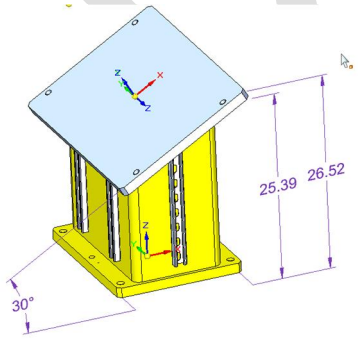

Figure 5-21 3D Models of Injector Supports

5.7.3 L1 to L3

The L1 to L3 area includes the L1, BC1, BC2 and L3 Extension stand and stage designs which are based on the LCLS-II Phase I stands and stages, modified to accommodate the lower beamline height. Figure 5-22 shows isometric view of the first bunch compressor (BC1). Figure 5-23 the isometric and top view of the second bunch compressor (BC2) shows how the chicane bend will move into the aisle way. A new design for a removable support will meet the requirement for a temporary clear route for the cryomodule transportation. Figure 5-24 shows the typical support design (stand and alignment stage) for the L3 extension quads. A list of stands and alignment stages for BC1 and BC2 are shown in Table 5-13.

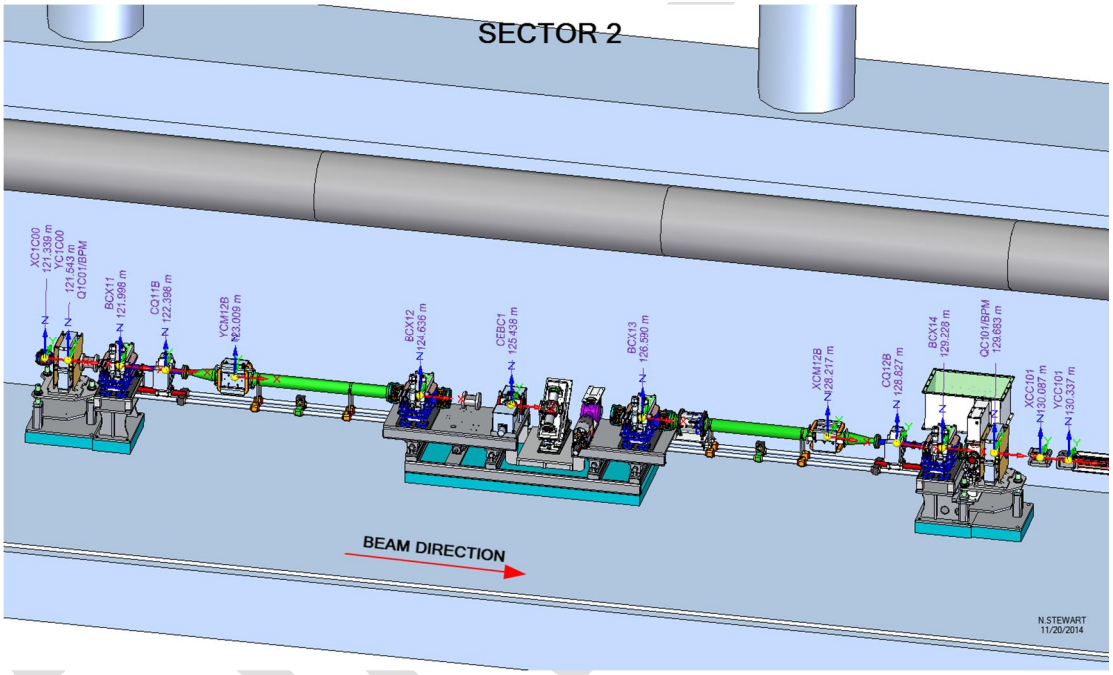

Figure 5-22: Isometric View of First Bunch Compressor

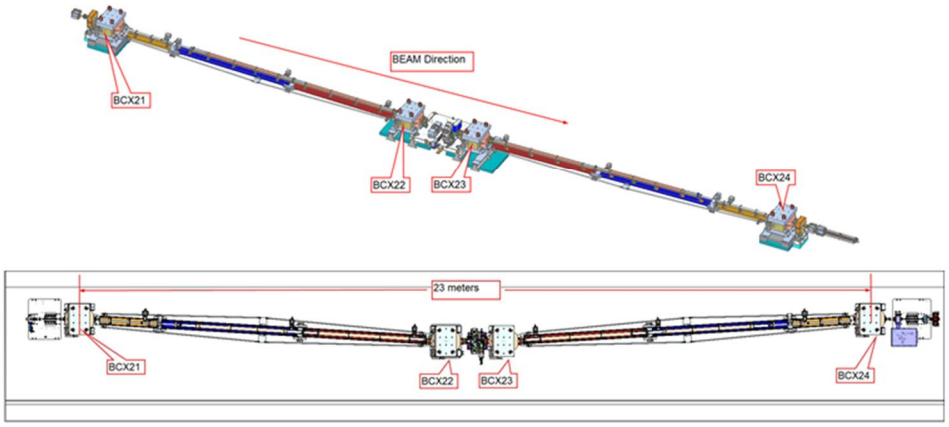

Figure 5-23. Isometric and Top View of Second Bunch Compressor

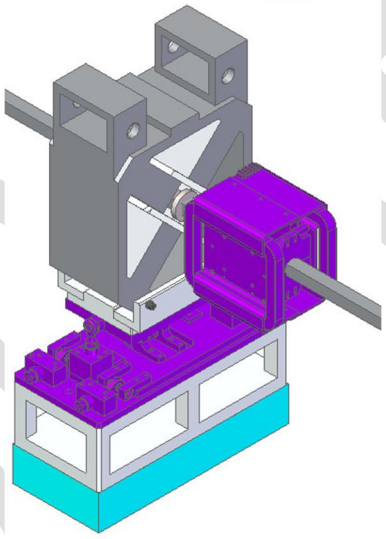

Figure 5-24. Detail View of Typical L3-Extension Quad Support Design

Table 5-13. BC1, BC2 & L3 Extension Stands and Stages

Figure	Stand Type	Drawing Number	Quantity
1	Quad Stand	SA-375-526-50	13
2	BC1 Chicane Table	SA-375-526-02	1
3	BC2 Chicane Table	SA-375-526-XX	1
4	Drift Stand	SA-375-526-40	87
5	Alignment Stage	SA-375-003-50	4

Figure 1

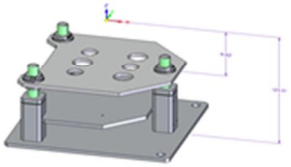

Figure 2

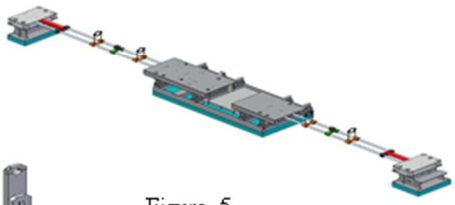

Figure 3

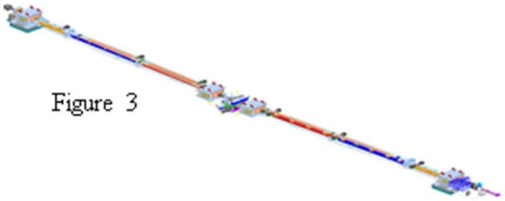

Figure 4

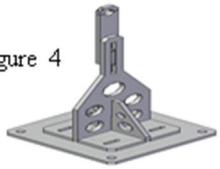

Figure 5

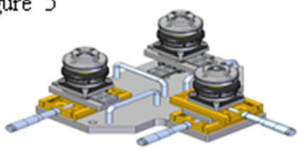

5.7.4 Bypass and Kicker to S30 Supports

The Bypass in LCLS-II is actually made up of two areas defined in the device database, Dogleg and Bypass. The Kicker to Sector 30 area is made up of 3 separate beamlines and areas defined in the device database, the post-spreader Hard X-Ray beamline (SPH), the post-spreader Soft X-Ray beamline (SPS), and the dump beamline (SPD).

5.7.4.1 Beamlines

The Dogleg area of the beamline begins just downstream of the L3 extension area (Z = 952.4m) and ends at the upstream end of the Bypass area (Z = 1153.55m). The first device in this area is a bend magnet (BRB1), which deflects the beamline up until it reaches the second bend magnet (BRB2), where the beamline is deflected to become horizontal again at a height equal to that of the existing PEP-II High Energy line. The beamline will remain at this same height throughout the rest of the Dogleg area.

The Bypass area of the beamline begin downstream of the Dogleg area (Z = 1254.53 m) and ends at the upstream end of the Kicker to Sector 30 area (Z = 2780.07 m). The height of the beamline stays the same throughout the Bypass area.

The Kicker to Sector 30 area begins just downstream of the Bypass area, where a spreader device will be used to split the beamline into three separate and distinct beamlines: SPH, SPS, and SPD. The Kicker to S30 area ends at the wooden door that ends the Linac (Z = 3050.54 m). Each one of the three beamlines follows its own trajectory, and those trajectories result in multiple beamline height changes along the way.

5.7.4.2 Stands

Since the beamline height is changing throughout the Dogleg and Kicker to S30 areas, each stand's height can be different, as seen in Figure 5-25.

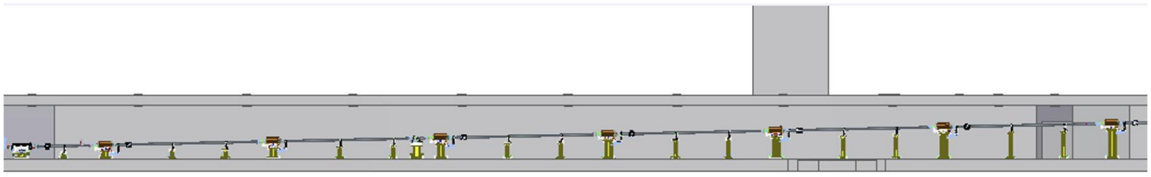

Figure 5-25. Beamline Elevation Change in the Dogleg area of the Bypass

We use the same basic stand design wherever possible, and only adjust the stand height to meet the respective device at its correct beamline height, as shown in Figure 5-26.

Figure 5-26 Typical Stand Design (left), and Stand Height Reduced for QDOG2 (right)

However, there is a point in the Bypass and Kicker-to-S30 regions where the basic stand design no longer is sufficient and additional support is required to accommodate beamline height. In this case, which occurs at the highest beamline elevation, the type of stand design changes and we use additional wall mounting support, as shown in Figure 5-27. This tall stand design will be used through the rest of the Bypass into the Kicker-to-S30 area. In addition, along the way throughout the Bypass and Kicker-to-S30 areas, stands are also used to support the drift tube that spans the gaps between devices in the beamline. These supports may be floor-mounted or ceiling-mounted, as shown in Figure 5-28.

.

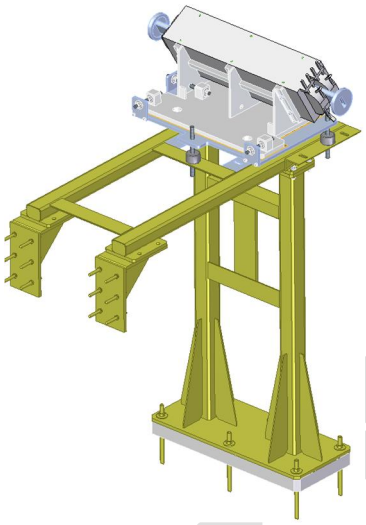

Figure 5-27. Tall Stand Design and Bend Magnet, BRB2

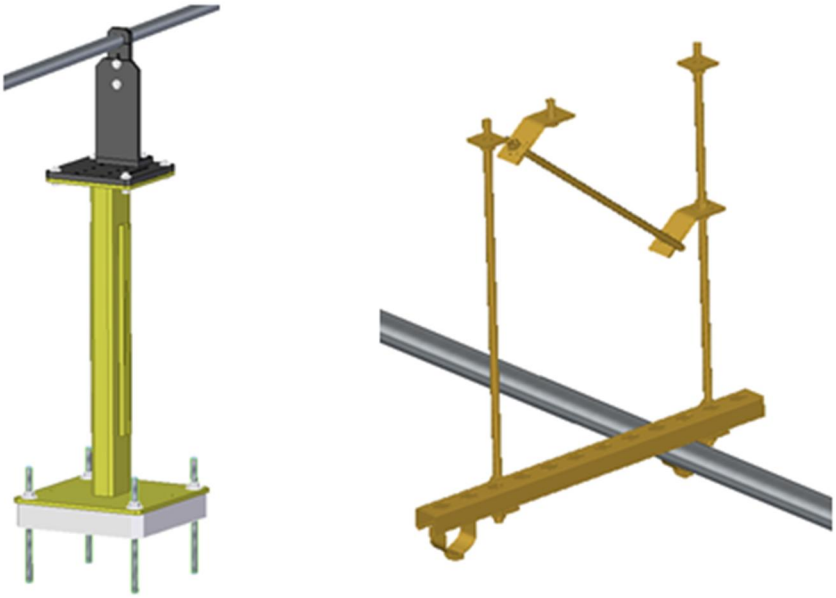

Figure 5-28. Floor-Mounted Drift Support, left, and Ceiling-mounted Drift Support, right

Regardless of stand design used or purpose, we will rely on both hand calculations and FEA simulations to show that the stand and device together, along with the anchors, can withstand applicable seismic forces and meet beamline device vibration tolerance requirements defined in *Project Building Inspection Office Codes and Standards of Record*, LCLSII-1.1-TS-0035 and *Quadrupole Magnet Vibration Requirements PRD*, LCLS-II-2.4-PR-0062.

5.7.4.3 Alignment Stages

The stands exist to support the weight of the device under all applicable loading conditions and get the device to the approximate beamline height. However, being that the stands only get the device close to the correct beamline height, we need alignment stages to provide the remaining positional adjustability for the devices. Figure 5-29 shows the alignment stage used for the Dogleg quadrupoles, which is typical of the stages used for beamline alignment. The alignment stages are mounted to the device in a Ready for Installation (RFI) state before actual installation into the beamline. Eventually the alignment stage (with the device already attached) is secured to the stand, where final adjustments are made for the device height. We are repurposing existing devices and device designs.

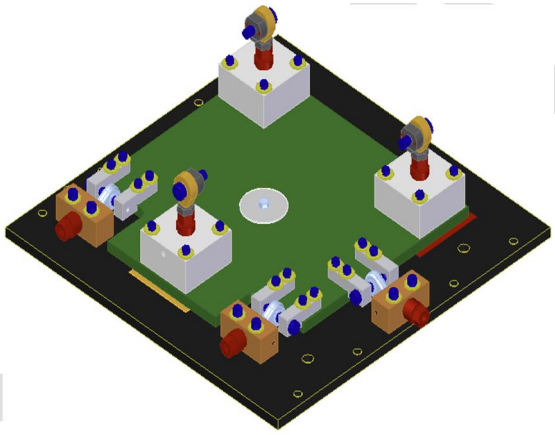

Figure 5-29. Typical Beamline Device Alignment Stage

5.7.5 BSY Supports

The three different beamlines in the BSY each include a different number devices:

- LCLSscD - 2 devices;
- LCLSscH - 30 devices;
- LCLSscS - 19 devices.

Not every device will need an individual support. For example, a set of devices consisting of a quadrupole magnet, BPM and one or more corrector magnets will in most cases require only one support. Also, the drift pipes in every line will need supporting. About 445 m total length of beamline pipe will need to be supported approximately every 10 feet (3m). An alternative design is moving D10 inside the Muon Shield to take advantage of existing shielding. The combined beam pipe length will be about 475 m. Existing LCLS devices upstream of the divergent chamber will be relocated and they will also need new supports in their new location.

BSY devices and beam pipes can be supported in two ways: from the floor and from BSY tunnel south wall. Most devices in BSY will be supported with stands standing on the floor. All magnets will be supported this way. Figure 5-30 shows an example of a support stand.

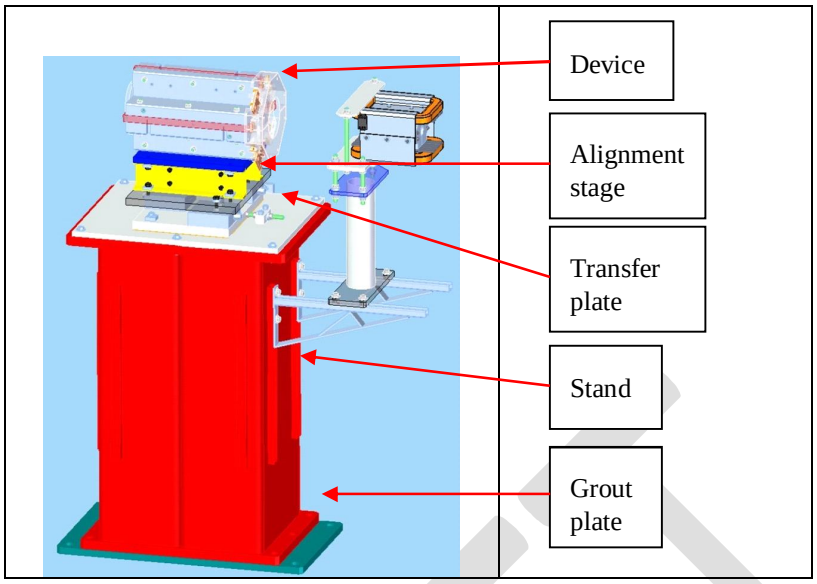

Figure 5-30. Typical BSY Device Support

Supporting from the wall is applicable only for SXR and Dump beam pipes in the BSY sump area upstream of the divergent chamber, which is also a contamination area. Wall supports consist of existing 5/8" anchor pairs every ten feet along the South wall, which will be reused from the old catwalk for the beam pipe support in this area. Most of the South wall in BSY, from SIT tunnel to D10, has such anchors, and Figure 5-31 shows how they can be used to support the beamline.

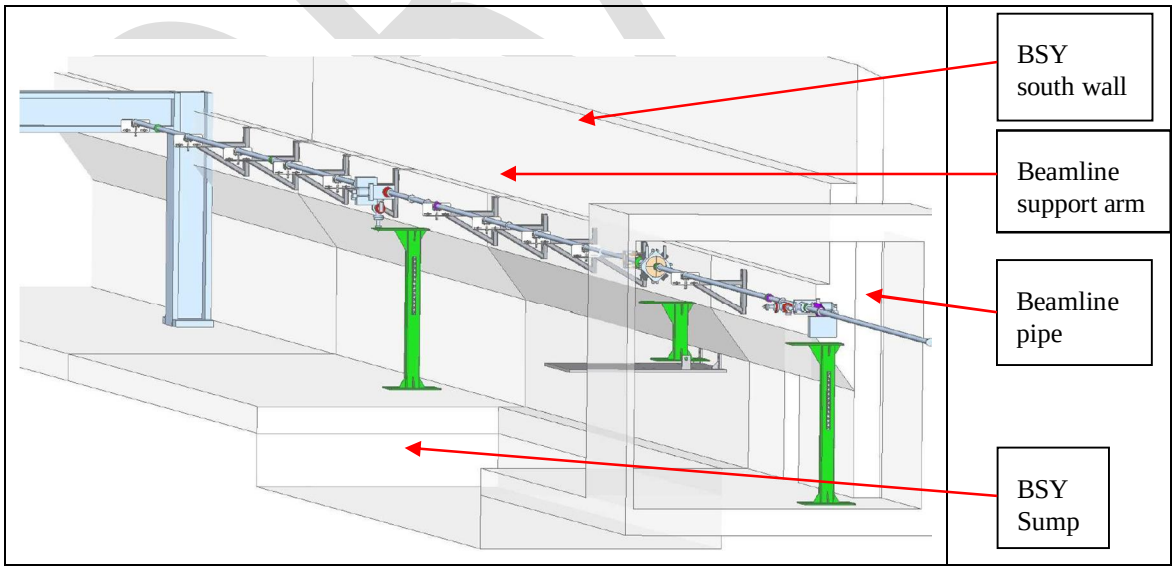

Figure 5-31: BSY Wall Beam Pipe Support

5.7.6 Linac-to-undulator Supports

The LCLS-II LTU Transport Line begins at the BSY down beam face of the 3-3/8” OD Flange right after the MUON shield wall at Linac X=-0.650 m, Z=3224.022 m (LCLS X=-0.650, Z=176.022 m).

Supports in the linac-to-undulator (LTU) line use a combination of existing and new designs.

The LCLS-II magnet stands will be identical in design to the ones found in the LCLS LTU line. See Figure 5-32 for typical component stand designs. The magnet and component alignment stages will also use existing designs from LCLS. Figure 5-33 shows examples of typical alignment stages.

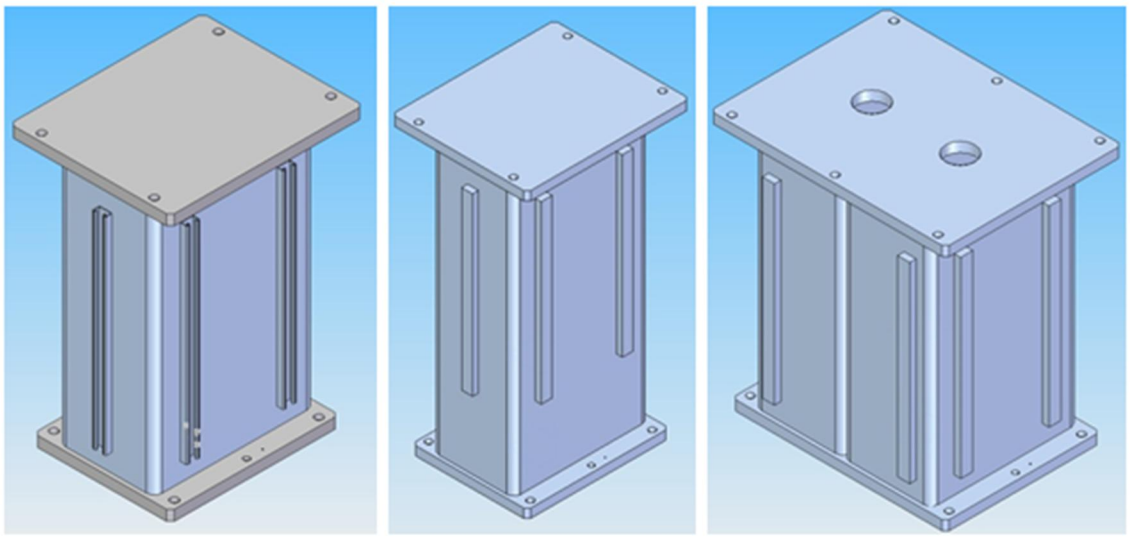

Figure 5-32. Typical LTU magnet and component stands

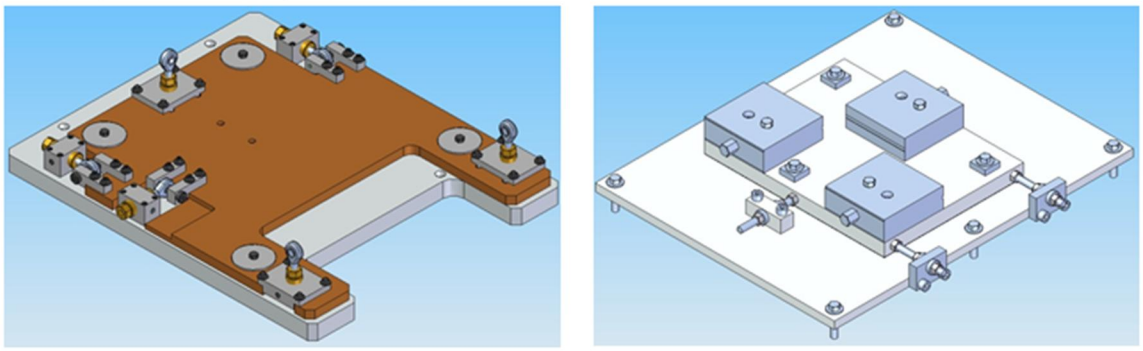

Figure 5-33. Typical LTU alignment stages

The LTU Soft X-ray beamline stand designs are based on the LCLS-II Phase I support stands, modified to accommodate the higher beamline height. Just like the existing LCLS beamline, the LCLS-II Soft X-ray beamline starts at the Muon Shield wall. However, in the BTHW region, it begins above the existing LCLS beamline, crosses over to the north as shown in Figure 5-34 and

becomes parallel at around the BTH west maze. In the BTHW region, special stands are required to support the magnets and components.

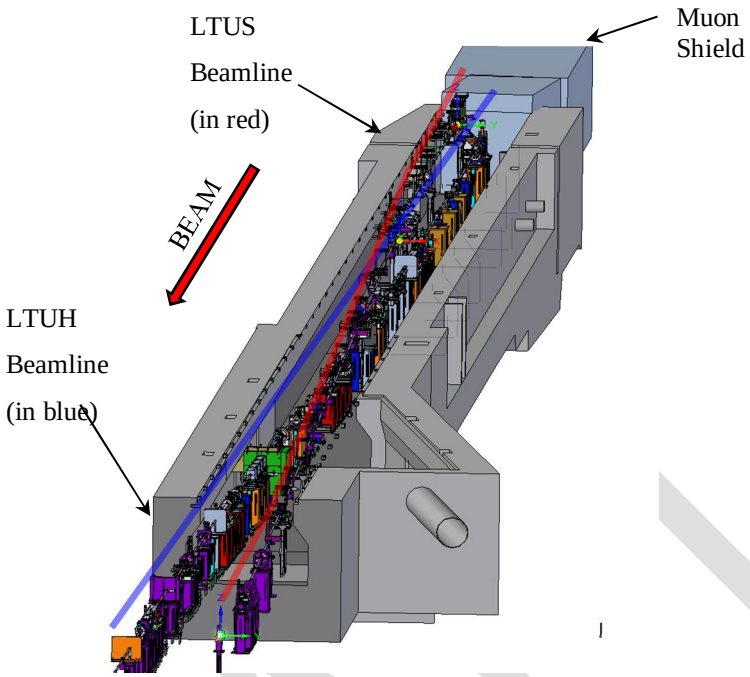

Figure 5-34. ISO view of the LCLS-II LTUS beamline crosses over LTUH beamline at the BTHW

For the new Soft-x-Ray beamline, we have developed a new design for the supports for the quadrupole magnets in the beam transport hall (BTH west) (see Figure 5-35). This design will make component and alignment stage installation easier than it was for beamline components at LCLS. The structure will bolt to the I-beams in the tunnel as part of a four-point support system. It provides low total deflection, low equivalent stress and a random vibration response within specifications, which improves component stability. The new design will address concern for the magnet and component containment during major seismic activity.

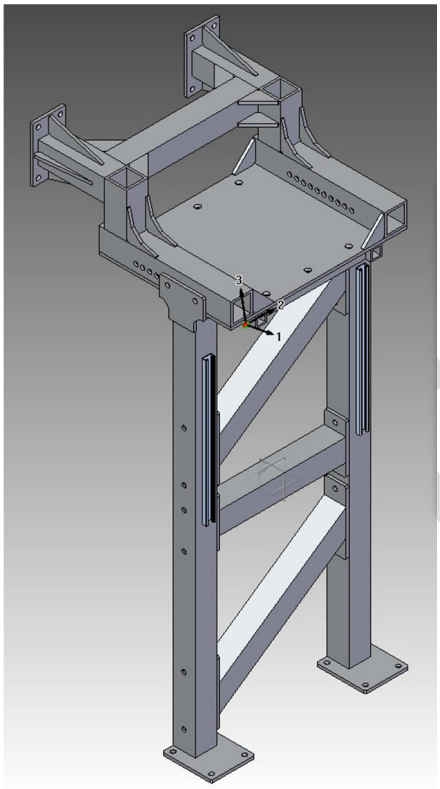

Figure 5-35. Quadrupole Magnet BTH west Design

We also developed a new design to make component and alignment stage installation easier for bend magnets in the BTH west for the new Soft X-ray beamline. . It is similar to the quadrupole magnet supports and will also bolt to the I-Beams as part of a four-point support system. This design has a larger support cradle than the previous design, which enables it to support heavier bend magnets, but also makes the support heavier and more expensive. The new design is shown in Figure 5-36.

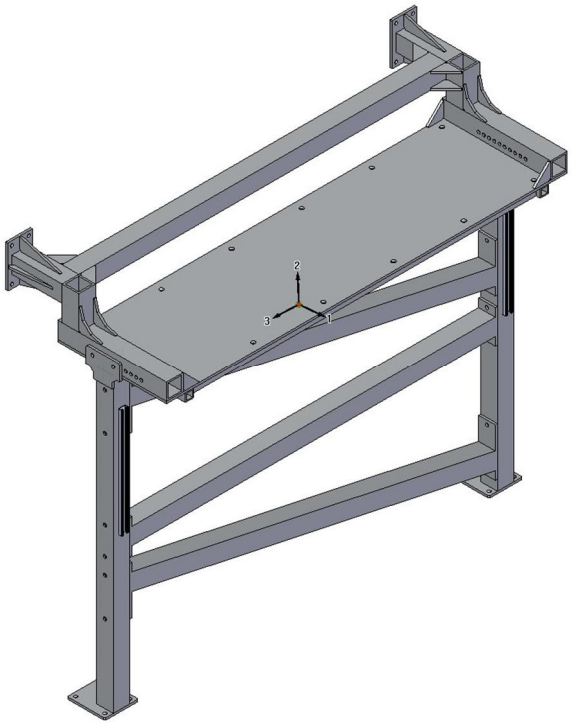

Figure 5-36. Bend Magnet BTH West Support Design

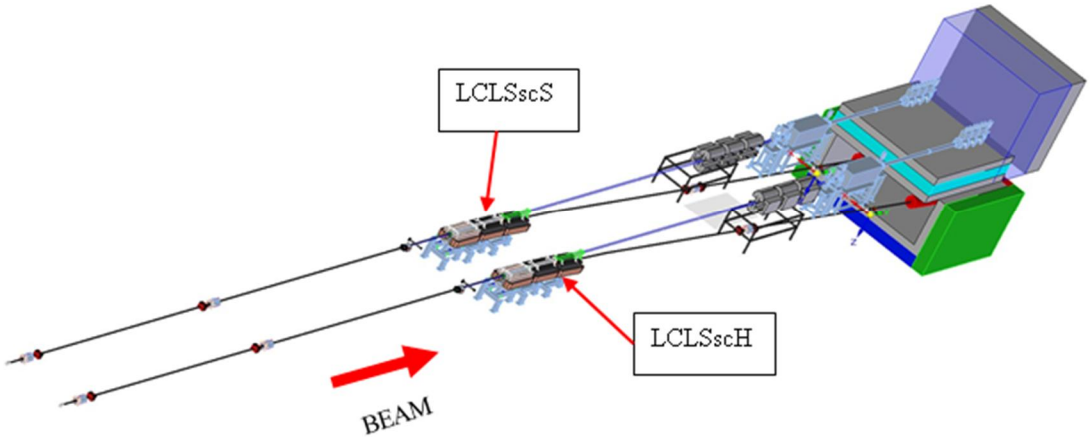

Figure 5-37 Two beamlines ending at EBD

5.7.7 Electron Beam Dump Supports

Two similar beamlines end at the Electron Beam Dump (EBD): the SXR (LCLSscS) on the north side and the HXR (LCLSscH) on the south side (see Figure 5-37). Heavy bend magnets require a different support design than do lightweight devices and beam pipes. Figure 5-38 and Figure 5-39 show different options for supports.

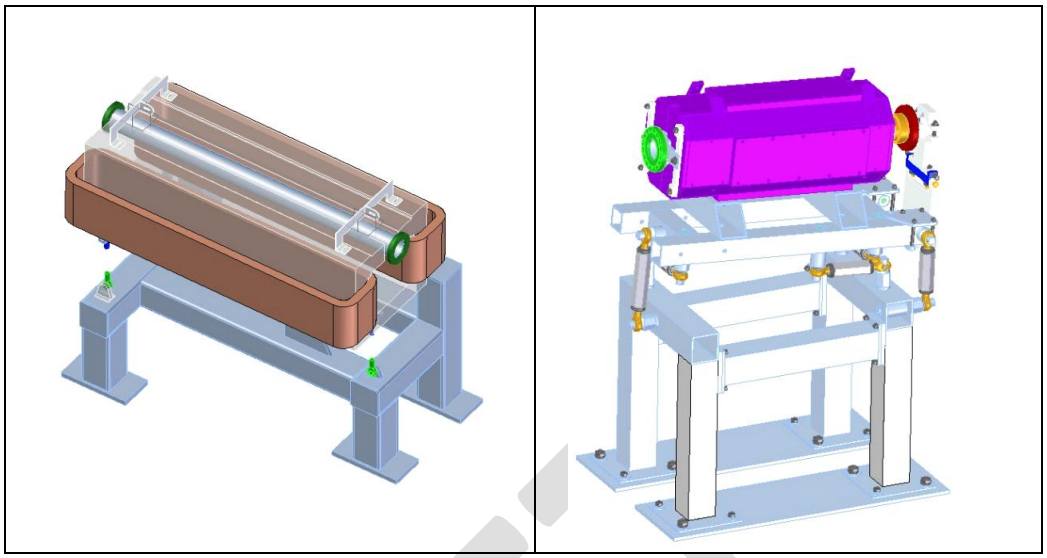

Figure 5-38 EBD heavy supports

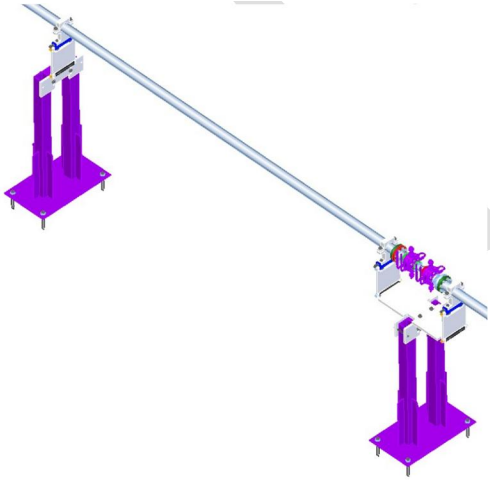

Figure 5-39 EBD light device and beam pipe supports

5.8 Vacuum

The LCLS-II vacuum system consists of multiple independent and interdependent systems, including Beamline vacuum, RF system vacuum, cryogenic system vacuum and support systems vacuum. These systems can be further categorized by region, functional requirements or Project Major System.

- The beamline vacuum system is unique in that it consists of a continuous vacuum environment across multiple Project Major Systems, without physical division, but with widely varying vacuum requirements.
- The RF vacuum system consists of many copies of several physically separated systems, including RF couplers, klystron vacuum, and waveguide vacuum.

- The cryogenic system vacuum consists of several copies of physically and functionally separated vacuum systems including insulating vacuum systems and sub-atmospheric helium vacuum systems.
- Several vacuum subsystems are associated with the Accelerator Subsystem of the LCLS-II. These include 1) the beamline vacuum for the gun, injector, SRF accelerator, diagnostic lines, transport line and dumps, 2) the insulating vacuum system for the cryomodules and for the cryo-distribution system, and 3) the RF coupler vacuum system.
- The linac beamline vacuum system begins at the gun, continues through the SRF accelerator, and then bypasses the existing warm linac, where it is spread into three lines going to the primary dump, SXR and HXR lines in the BSY. For purposes of the vacuum system, these electron beamlines can be characterized as conventional warm electron beamlines, for which SLAC has decades of experience, and cryogenic beamlines, for which SLAC's experience is more limited. All these are designated as UHV beamlines. These beamlines are almost exclusively conductance-limited structures, so that gas loads dominate pressure distributions. An additional characteristic which applies to all of the cryogenic beamline and a portion of the warm electron beamline is that of "particle-free" cleanliness.
- The insulating vacuum systems for cryomodules and cryo-distribution lines are characterized as high vacuum systems with high gas loads. Their principle function is to minimize gaseous heat conduction from the environment to the cryogenic components, which then must be removed by the cryoplant. The challenge to these vacuum systems can be divided into two phases. The initial phase is pumping down from atmosphere to a low enough pressure to initiate cooldown. The second phase is to maintain a low enough vacuum in the event of helium leakage. The driver for the initial pump down is the extremely large surface area due to the multi-layer insulating (MLI) blanket, and the large water vapor load it brings. This requires large pumps and long times to handle the water outgassing. Once cooldown has been achieved, the cryogenic surfaces inside the MLI blanket cryogenically pump the remaining water vapor and all atmospheric gases that leak into the system, adding to the heat load on the cryoplant. During the second phase, the challenge is pumping helium from the helium piping to a low enough vacuum to maintain maximum thermal insulation. In the absence of helium leaks, the cryogenic pumping effect would handle seal permeation and small atmospheric leaks. Experience at SNS and elsewhere has shown that some helium leakage should be expected and therefore helium scavenging pumps are required.
- The RF Coupler vacuum system can be characterized as a warm UHV vacuum system. It also has particle cleanliness requirements due to RF fields, but these are relaxed compared to those of the SRF and communicating beamlines due to the

presence of vacuum windows between the coupler vacuum and the cryogenic beamline. The RF Coupler vacuum system will, however, be treated as "particle-free".

-

5.8.1 Vacuum Pressure Requirements

The pressure requirements listed in the draft ESD presented at the Vacuum System CDR were taken from XFEL drawings and reflect state-of-the-art for SCRF vacuum systems.

Requirements for residual gases included in the *Residual Gas and Beam Stay-Clear PRD*, LCLSII-2.1-PR-0234, are expressed in terms of an effective pressure P_{eff} , and will be converted into nitrogen equivalent pressures to provide one set of traceable requirements .

Pressure requirements for the vacuum system vary along the length of the beamline, as shown in Figure 5-40.

Pressure requirements at the gun are driven by the need for high quantum efficiency of laser photoemission. Of particular concern are residual gases that chemisorb on the target surface. In addition, high fields in the gun require good vacuum for stable operation.

Pressure requirements within the SRF cavities are driven by cryogenic pumping on the cavity surface and the effect of the cryogenic deposits on cavity performance. Pressures as high as $6x10^{-7}$ Torr prior to cool down have yielded acceptable cavity performance.

Pressure requirements in the warm beamlines that communicate with the cryogenic SRF beamline are driven by the need to minimize gas flux to the SRF beamline. By keeping the residual gas pressures at the interface between the warm beamlines and SRF beamlines at or below the vapor pressures of these gases at the 2 K operating temperature of the SRF beamline, the degradation of cavity performance due to cryogenic deposition can be minimized over the extended cryogenic operational periods.

Pressure requirements in the warm beamlines that do not communicate with the SRF beamlines is principally determined by the pressure requirements established in the *Residual Gas and Beam Stay-Clear PRD*, LCLSII-2.1-PR-0234. In some cases the pressure requirements may be set lower for the purpose of extending the lifetime of ion pumps and cold cathode gauges, which degrade quickly at higher pressures.

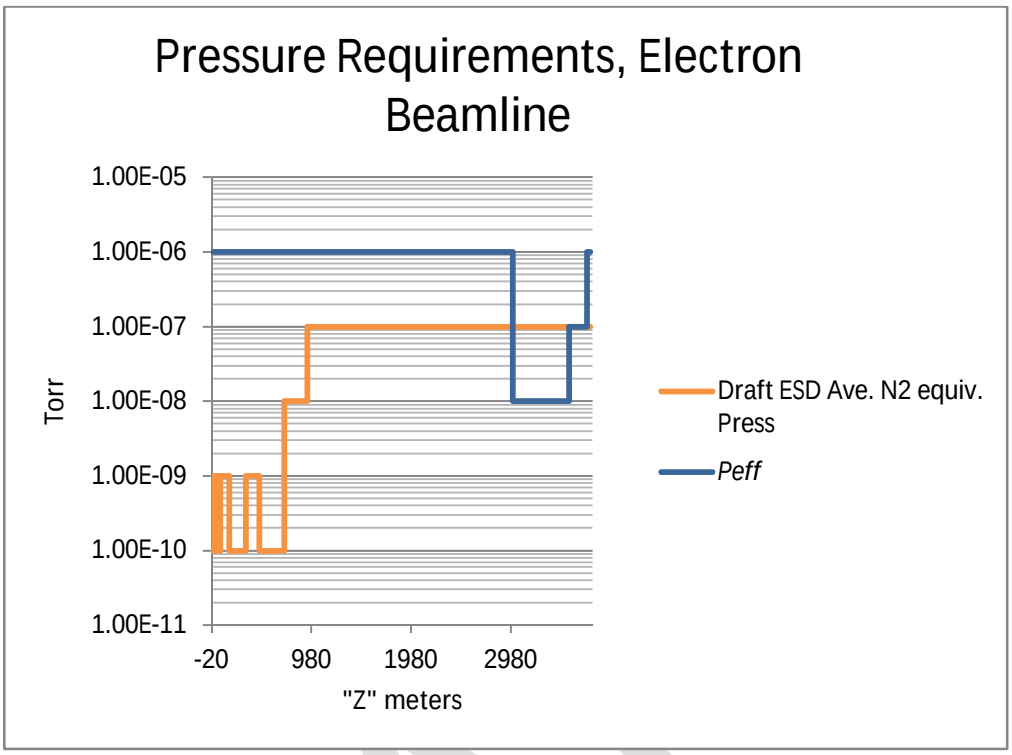

Figure 5-40: Pressure requirements as a function of beamline coordinates. The blue line reflects effective pressure requirements while the other line is based upon functional requirements. Final system design requirements are defined by the lower of the two lines at each "Z" location.

Pressure requirements in the RF couplers are driven by RF breakdown considerations, pump lifetime considerations, and operational considerations. Pressures in the RF coupler system can be used to detect RF breakdown and interlocked to the RF source. Establishing a pressure requirement and operating well below otherwise required pressures will greatly increase the sensitivity of the pressure measurement to small RF breakdown events.

Pressure requirements for the Insulating Vacuum systems are driven by thermal conductivity in the gas, primarily in the space between the layers of the MLI blanket.

5.8.2 Particle Free Transitions

Particulate contamination degrades cavity performance through enhanced field emission [1]. Studies have shown that adopting clean room facilities, processes and protocols similar to those used in semiconductor processing is essential for successful fabrication, assembly and installation of SRF accelerators. The requirement for control of particle contamination extends beyond the SRF cavity in order to preserve the cavity cleanliness throughout the lifetime of the SRF Accelerator. Once an installed cavity is contaminated, methods for recovery of cavity performance are extremely limited. In order reduce the risk of particle contamination of cavities, a particle- free transition zone adjacent to the SRF cryomodules has been defined. This "particle-free" length is at least 20 meters, as described in the LCLS-II Engineering Note: *Particle Free*

Length (LCLSII-4.1-EN-0337). There is not enough distance prior to the first cryomodule, L0B, for a fast sensor and valve, therefore the entire beamline from the Gun to L0B must be a particle-free region. The laser heater beamline, downstream of L0B, will be a particle-free region until the fast valve in DIAG0.

The goal is to design, fabricate and install all components that communicate with the SRF cavity through the vacuum beamline following the same requirements that apply to the SRF cavity. In practice, some compromise of the requirements is necessary to accommodate functional requirements of devices to be installed within this particle- free region.

There are three primary sources of particle contamination within the SRF cavity: environmental sources, contamination created during assembly, and contamination created in vacuum. There are a number of ways in which these particles can be transferred into the SRF cavity, but the primary method for particle transmission is through gas-mediated transfer during pressure transitions, either pump down or venting.

Environmental particle sources will be controlled by adopting clean room practices for cleaning, assembly and installation work. These practices include monitoring and controlling airborne particle counts, gowning protocols to contain human sources of particles, and selection of tools and equipment with low particle generation characteristics.

Contamination during assembly will be controlled through specification of materials, processes and procedures to minimize particle generation. Rigorous testing will be performed during detailed procedure development to qualify materials, processes and procedures.

Particle contamination in vacuum will be controlled through detailed design and testing of in-vacuum components. Components based upon existing designs will be thoroughly reviewed for compatibility with particle-free requirements, revised where feasible to reduce particle generation potential, and evaluated by testing to determine level of risk based upon location with respect to the SRF.

5.8.2.1 Particle Transfer

Once the system has been properly designed, fabricated, and installed, the risk for degradation of cavity performance is primarily due to pressure transitions from atmospheric pressure to medium vacuum or from medium vacuum to atmospheric pressure. Pressure transitions in molecular flow generally do not transfer particles [2].

These risks will be controlled through development of pumping and venting equipment and procedures which will limit the velocity of gas flow throughout the vacuum system that communicates with the SRF. The primary controlling factor is the velocity of gas through the minimum feature or aperture of the system [3]. A flow speed below 2 m/sec will be used to design the venting and pumping procedures. The features to implement this control will be incorporated in the UHV/particle-free service carts dedicated to particle-free vacuum system work.

Any source of mechanical shock or vibration during the venting or pumping process can also increase particle contamination. This factor is controlled by the settling time, since once small particles are suspended in the gas stream, they will be transferred everywhere the gas goes.

LCLS-II will publish an engineering note defining the National Standards to be adhered to in the design, fabrication, assembly, testing and installation of vacuum components to be installed in the particle-free zones.

5.8.3 Vacuum Schematics

Table 5-14 lists the schematics describing the various regions of the beamline, specifying the linac coordinates pertaining to each one. Beamline regions (areas) are as defined in Beamline Boundaries (LCLSII-2.1-PR-0134) whereas the vacuum schematics have slightly different linac coordinate limits.

Table 5-14 Vacuum Schematics

5.8.4 Pumps and Controllers

Table 5-15 lists the various pumps and controllers to be used along the LCLS-II beamline. The LCLS-II electron beamline pumping procedure follows standard SLAC practice, using noble diode sputter ion pumps for the majority of the beamline. These will be augmented with non-evaporable getter (NEG) pumping where pressure requirements are well below $1x10^{-8}$ Torr and the speed of ion pumps drops off. The primary application of NEG augmentation will be in the gun and in the warm beamline regions adjacent to the cryomodules. The cryomodules are primarily cryo-pumped, due to their low operating temperature, and augmented with noble diode ion pumps at each end of a cryomodule string to maintain vacuum prior to cooldown. Noble diode ion pumps are specified to provide the capability to handle noble gases introduced by minute atmospheric or helium leaks.

The RF coupler vacuum systems will be ion pumped, augmented with Ti sublimation pumps or NEG pumps to achieve higher hydrogen pumping speeds. This is motivated by the desire to achieve the lowest possible pressures at the coupler cryogenic window.

Beamline pumping in the Spreader/BSY region will be a combination of historical solutions, including noble diode sputter ion pumps, differential vacuum pump systems, oil free turbo mechanical pumps, and low temperature refrigerated baffles. This complex of pumps is required to facilitate the interconnection between the existing LCLS beamline and the new LCLS-II beamline, while retaining as much of the existing beamline vacuum hardware as possible.

Insulating vacuum systems for the cryomodules and cryo-distribution system will be pumped by turbo mechanical pumps and oil-free mechanical pumps. Capture pump technologies are not suitable due to the expected continuous flow of the noble gas helium. The specified turbo pumps will have high compression ratio for helium and include ceramic or hybrid ceramic/permanent

magnetic bearings to minimize susceptibility to radiation damage. The backing pumps will be selected from either scroll or multi-stage roots pump designs, based upon evaluation of projected lifetime in the radiation environment in which they will be installed. For the initial roughing of the large volumes associated with the insulating vacuum systems, a dry mechanical pump combined with a dry roots blower will be temporarily attached.

Multiple vacuum service carts of two different types will be required to commission and maintain the beamline vacuum. Both versions of the service carts will be equipped with oil-free turbo molecular pumps and backing pumps. One version will be compatible with normal UHV vacuum system operation and will principally be drawn from existing SLAC turbo carts. The second version will be dedicated to particle-free UHV vacuum system use and will have additional features and functionality to achieve particle-free pumping and venting. This will include valves, controllers and filters to prevent turbulent gas flow throughout all stages of pumping and venting. Controllers will be designed to run specific recipes for the various particle-free vacuum regions to optimize pumping and venting cycle times based upon the characteristics of each region.

Table 5-15 Pumps and Controllers

Pump Type	Example	Where Used
Ion Pump, Noble Diode	Gamma 300TV-DI-8S-SC-110-N	Beamline, Coupler Vacuum
Compination Ion Pump + NEG	SAES NexTorr D 300-5	Gun
Titanium Sublimation Pump	Gamma TSP Filament Cartridge in Ambient Sputter Shield	Coupler Vacuum
Turbo Pump	Agilent Twistorr 304 FS ISO 160 w/o water cooling, X3500#10#22	Insulating Vacuum
Dry Backing Pump	Kashiyama NeoDry 15E	Insulating Vacuum
Dry Roughing Pump	Kashiyama MU600	Insulating Vacuum Roughing
Ion Pump HV Power Supply	Gamma Digital MPCe	Beamline, Coupler Vacuum
Turbo Pump Controller	Agilent Twistorr 304 FS AG Rack controller with Profibus, p/n X3506-64003	CryomodulesInsulating Vacuum
Combination Ion Pump++NEG Controller	SAES NEXTorr PS NIOPS-04	Gun

5.8.4.1 Roughing station for the thermal isolation vacuum

The roughing station will consist of an oil-free multi-stage roots pump and roots blower combination equipped with an interface for control system integration. Process cooling water will be required to support the large volumes and gas loads associated with insulating vacuum for the cryomodule and cryo-distribution system. The roughing station will support ultra-dry gas backfill cycles and will pump the insulating vacuum space to a pressure of 0.010 Torr.

5.8.4.2 High Vacuum Pumps for thermal isolation

A turbo pump system with dry backing pump is required to produce and maintain the pressure in the insulating vacuum. This system will consist of a turbo pump with a helium compression ratio of greater than $1x10^8$, and a wear–free, high reliability backing pump. Both pumps will be radiation resistant so they can tolerate the environment of the cryomodules. Isolation valves between the turbo pump and the cryomodule will be electropneumatic, and will include position sensors. An electromagnetic isolation valve will be located in the foreline of the turbo pump. Gauging will be provided to sense foreline pressure, turbo inlet high vacuum, and interconnect vacuum between the electropneumatic valve and the cryomodule manual gate valve.

5.8.4.3 Pumps for the couplers and Particle-free UHV Turbo cart

The coupler vacuum and particle-free UHV beamlines place stringent requirements on the design, equipment selection, fabrication and operation of the pumping systems used to pump down and vent these regions. The turbo pump must be connected to a wear free, particle-free backing pump. All components, including gauging, valves, manifolds and pumps must be cleaned and assembled to meet particle-free zone requirements. Of particular importance is the requirement to control the velocity of gas flow during both venting operations and pump down during any phase when the pressures are above 1 Torr. Valve actuation will be controlled by programmed controllers to eliminate sudden pressure changes.

The turbo pump shall have a nitrogen compression ratio greater than 109 .It shall connect to the system angle valve without the use of hoses or long manifolds. Flanges on the high vacuum side shall be Conflat type with copper gaskets for piping of 0.75” diameter and larger. Smaller piping shall use VCR® fittings with copper gaskets. Any required adjustability or flexibility shall be accommodated in the foreline configuration.

Electropneumatic and electromagnetic valves shall provide isolation in the event of power failures or other faults, consistent with the requirement for preventing sudden pressure changes and controlling gas flow velocity.

5.8.4.4 Pumps for the UHV non-particle-free beamline Turbo cart

UHV non-particle-free beamline turbo pump carts are to be used on beamlines away from the particle-free regions. They are functionally similar to existing SLAC turbo pump carts used to pump down UHV beamlines, with a few specific differences. The turbo pump will be connected to a wear-free, hydrocarbon-free, backing pump. The turbo pump will have an electromagnetic angle valve that isolates the pumped volume from atmospheric pressure in case of a power outage

or any vacuum incident. The turbo pump fore-pump line will have an electromagnetic angle valve that isolates the turbo pump from the backing pump, and a pressure gauge (turbo side).

The turbo pump will have a nitrogen compression ratio above 10^9 .It shall connect to the system angle valve without the use of hoses or long manifolds. Flanges on the high vacuum side shall be Conflat type with copper gaskets for piping of 0.75" and larger. Smaller piping shall use VCR® fittings with copper gaskets. Any required adjustability or flexibility shall be accommodated in the foreline configuration.

5.9 Beam Diagnostic Systems

The electron beam diagnostics for LCLS-II are based on the designs used for LCLS, with modifications for operation at high beam rates. Beam position will be measured with a combination of stripline, cavity, and button (cryo) BPMs, all with FPGA-based processors to provide full-rate (1MHz), real-time measurements. Beam current measurements will be performed by using commercial (DCCT / cavity) devices to calibrate the bunch-charge output on BPMs. High speed wire scanners using an existing SLAC design will allow profile measurements on the full-rate beam. Beam imaging OTR and YAG monitors will be used in the low rate diagnostics lines. Pulse-to-pulse bunch length measurement will be based on mm-wave coherent synchrotron radiation in the bunch compressors, calibrated against low rate measurements using room-temperature, transverse deflection cavities. The CSR radiation detectors will use pyroelectric detectors modified for high average power operation, in addition to mm-wave diodes for some sets of beam parameters in the injector. Beam loss monitoring will be done with a combination of long ion chambers and Cherenkov radiators.

5.9.1 Stripline Beam Position Monitors (BPMs)

5.9.1.1 Introduction

Many BPMs are required throughout the LCLS-II accelerator, from the injector, through the linac, transport lines, off-axis diagnostic lines, FEL undulators, and electron beam dump lines. BPMs are non-invasive measurement devices on the electron beamline that ideally sense the transverse position of each electron bunch with respect to the center of a set of pick-up electrodes and report the beam position (ideally zero) to the control system for each passing electron bunch. Each BPM also reports the estimated bunch charge, although a separate calibration is typically required for absolute charge accuracy. Stripline BPMs offer a low-cost and well-tested option.

5.9.1.2 Position and Charge Requirements

Each BPM is required to read electron beam position (x and y) as well as bunch charge for each passing bunch, with a minimum bunch spacing of 1μs. Operations personnel with control the bunch charge setting, which is variable from 10-300 pC, with 100-pC defined as the nominal LCLS-II operating charge but 10-20 pC as a real option. Position and charge resolution requirements are listed in **Table ?**

5.9.1.3 Installation and Roll Angle

Stripline BPMs can be oriented as shown in Figure 5-41, with a possible roll angle of zero (left), or 45°(right). Most of the BPMs in the existing LCLS are unrolled, but the BPMs in and around bending magnets are rolled by 45° so that the synchrotron radiation and off-energy halo beams do not strike the stripline, possibly damaging it or biasing the position and/or charge measurement. About 10 % of the BPMs are rolled in this manner. However, in LCLS-II, in order to avoid possible confusion where specific BPMs are rolled and others are not, we adopt the strategy in LCLS-II where all stripline BPMs, except a few in the Sector 10 dogleg, are rolled by 45 degrees. The BPM database will include the roll angle for each BPM in order for the control system to process the BPM signals into horizontal and vertical positions as two separate linear combinations of the four strips. With no performance penalty in this rolled configuration, we hope to minimize installation and database entry errors. The roll angle for each stripline BPM is listed in Table 5-16. The eight Sector 10 dogleg BPMs are unrolled ($\Phi = 0$) since the dogleg itself is rolled by 45 degrees.

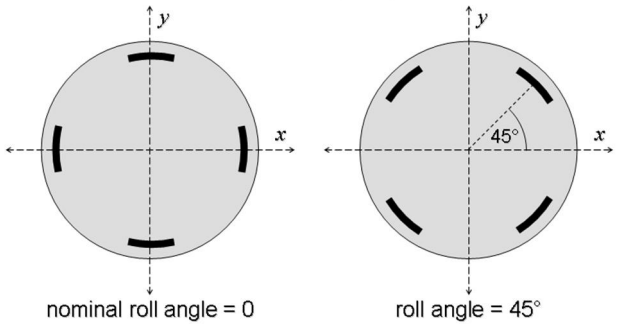

Figure 5-41. BPM striplines are either unrolled (left) or rolled by 45 degrees in the *x-y* plane (right) so that synchrotron radiation and low-energy halo does not strike the stripline.

Several LCLS-II electron transport line sections are guided by rolled bends, defining a beamline section that does not lie purely in the horizontal or vertical planes. In such cases (e.g., the Sector 10 dogleg, the HXR spreader branch, and both main beam dump lines), the installation angle of the BPMs,as well as that of the quadrupole magnets and other components, must be clearly specified. Table 5-16 lists the four beamlines where this stripline BPM installation angle (and the database angle used to untangle the nominal 45-degree roll) must be explicitly noted.

Table 5-16. Stripline BPM installation and database roll angle requirements.

Beamline Description	Area	Installation Roll Angle, (deg)	Database Roll Angle, (deg)
Sector 10 dogleg	Bypass	0	0
HXR Spreader Line	SPH	45	45
SXR Main Dumpline	DMPS	45 + 10	45
HXR Main Dumpline	DMPH	45 – 10	45

All other areas	*all*	45	45

5.9.1.4 Alignment, Drift, and Electrical Offsets

In reality, each BPM will be misaligned to some degree, its position and charge readbacks will drift over time, and even a perfectly aligned BPM will have some small electrical offset. Table 5-17 lists the estimated requirements for these types of errors:

Table 5-17 Estimated BPM transverse alignment, drift, and electrical offset maxima

Accelerator Area	Alignment (mm)	Drift (mm/week)	Offset (mm)
Injector (striplines)	0.2	0.1	0.1
Linac (cold cavities)	0.5	0.2	0.2
Transport/Diagnostic Lines (striplines)	0.2	0.1	0.1
SXR Undulator (cavities)	0.1	0.02	0.10
HXR Undulator (cavities)	0.05	0.01	0.05
Large Aperture (*e.g.*, BC1, BC2, dumps)	0.5	0.2	0.5

5.9.2 X-Band BPM

The following sections and tables which describe the LCLS-II RF BPM design presented are excerpted from the following ESD: *RF Beam Position Monitors*, LCLSII-3.2-ES-0049.

The LCLS-II RF cavity beam position monitors (RFBPMs) provide high-resolution, pulse-by-pulse readback of the beam position in the BTH and the undulator beamline.

The design of the LCLS-II RF cavity BPM will follow in large part the proven, successful .design features of the LCLS undulator BPMs. The changes in the design are based on lessons learned from fabrication and operational experience in LCLS. Table 5-18 lists the differences between LCLS and LCLS-II RF cavity BPMs.

Table 5-18: Differences between LCLS and LCLS-II RF cavity BPMs

	LCLS	LCLS-II	Comments
Nominal frequency	11.384 GHz	11.424 GHz	Better for multibunch
Output	Waveguide	coax	More flexible
Tuning	12 tuning stubs	<= 4 tuners	Lower cost
Down converter	Input 14 dB matching pad Gain switch 28 dB step	<= 3dB I.L. 1 dB step	Improved noise figure and dynamic range
Reference cavity	Single output	2 couplers	Improved mode centering

5.9.2.1 Operating Frequency

The cavity is designed to work in the X-Band frequency range, the same as for LCLS. The choice is dictated by:

- The resolution improves at higher frequency (compared to C-Band or S-Band)
- The dimensions scale with RF wavelength so X-Band frequency takes up the least beamline space
- RF components and technology are available for X-Band operation.

The exact center frequency has been changed from that used at LCLS to coincide with a harmonic of the linac RF to better accommodate future multibunch operation.

5.9.2.2 Number of Coupling Ports

The cavity design, shown in Figure 5-42, will include two symmetric slot coupling ports per measurement plane. This will allow for a calibration tone to be added in the future if desired.

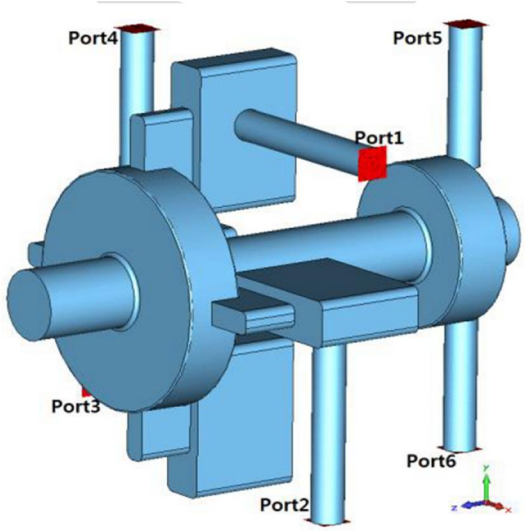

Figure 5-42: Shape of the Internal Cavity Volume

5.9.2.3 BPM Length

In order to prevent mode coupling between the cavities, it is necessary that all cavity volumes be separated by at least four beam pipe diameters. The separation between the dipole and reference cavities is therefore specified as a minimum of 36 mm.

5.9.2.4 Cavity Tuners

The cavity fabrication tolerances are chosen to ensure that the finished cavity will be within ±20 MHz of the nominal frequency. Mechanical tuning “dimples” that deform the cavity wall are to be used to tune the cavities to within ±2 MHz of the nominal frequency. As illustrated in

Figure 5-43, four radial tuners are positioned symmetrically around the dipole cavity and two radial tuners are included on the reference cavity.

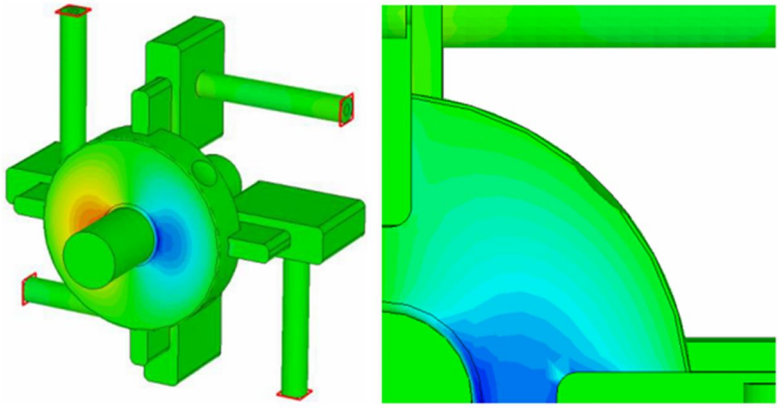

Figure 5-43: Radial Tuner for the Dipole Mode Cavity

5.9.2.5 Cavity Mounting

Proper cavity mounting (see Figure 5-44) is important to ensure that the BPM is rigidly mounted in the correct position.

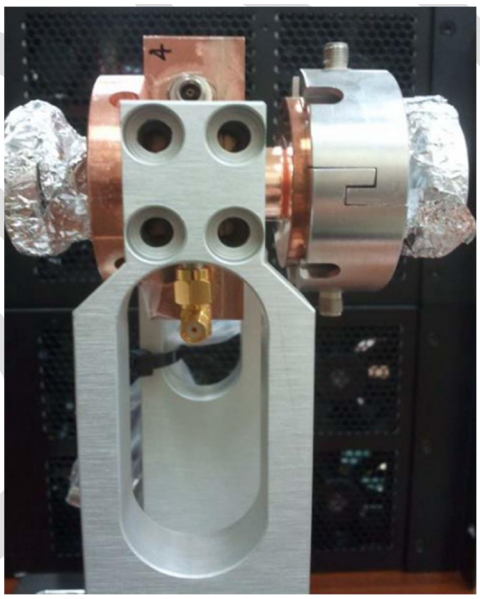

Figure 5-44: Example of a Cavity BPM Holder

5.9.2.6 BPM Receiver

The BPM receiver, described in Figure 5-45 and Table 5-19, is built into a single chassis mounted to the support stand immediately below the cavity BPM support girder. The dimensions of the down converter chassis should not exceed those of a standard 19” rack mount chassis. The present prototype chassis measures 19”x14”x4”. The chassis is connected to the cavity with

flexible coaxial conductor using SMA connectors. The receiver incorporates a down mixer to convert the 11.424 GHz signal to intermediate frequency (IF). The IF is transmitted over longer cables to an upstairs support building where the digitizer electronics are located. The receiver obtains its electrical power from an AC power outlet typically located about 1 meter away, below the interspace table.

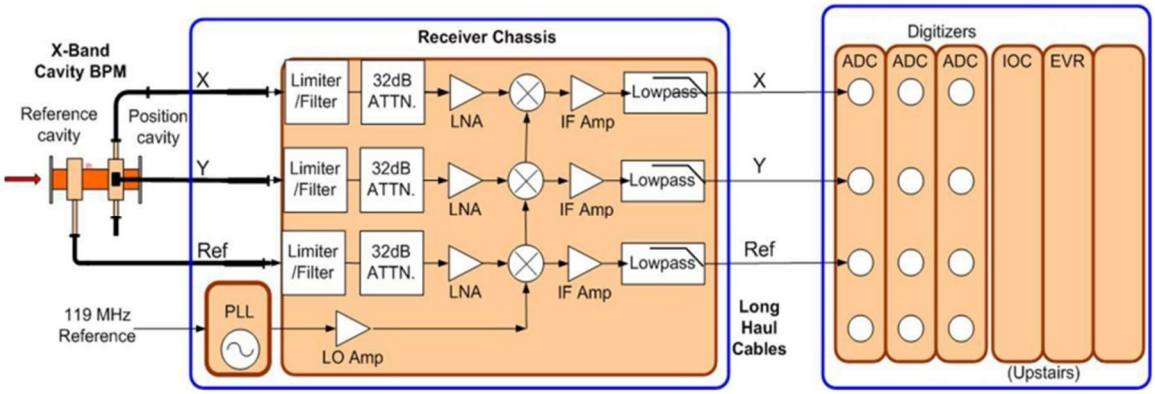

Figure 5-45: BPM Receiver Block Diagram

Table 5-19. BPM Receiver Parameters

Parameter	Specification Limit
Linear Dynamic	~80dB
L_0 Frequency	11.424 GHz
Operational Frequency Band (RF in)	X-Ku
Typical RF Input Frequency	11.424 GHz
Bandwidth at F(RF)	200MHz
IF Bandwidth (119 MSa/s or 238 MSa/s)	30-60MHz
Max Input Power	14dBm
P 1dB Output Power	18dBm
Max L_O to RF rejection	45dB
Max L_O to IF rejection	20dB

5.9.2.7 Power Levels

The x, y and Ref signals coming out of the receiver will have a power level of 13 dBm. Those same signals, at the end of the long haul cables going in to the digitizer, will have a power level of at least 10 dBm.

5.9.3 Current Monitors

The absolute bunch charge measurement for LCLS-II will be based on monitoring the average beam current using integrating current transformers (ICTs). The high-rate single bunch charge measurement will be performed with the sum signal from the beam position measurement systems calibrated against nearby ICTs, since the single bunch charge resolution of BPMs surpasses the one of current transformers. ICTs will be located after each bunch compressor and downstream of the beam spreader in each of the three beam transport lines. A Faraday cup (FC) serving as the beam dump of the diagnostic line DIAG0 will additionally provide an independent absolute charge measurement in the LCLS-II injector area.

Figure 5-46. Bergoz Turbo-ICT

We will use a Bergoz Turbo-ICT, Figure 5-46, which meets the requirements for the relatively low LCLS-II beam current. It will have included a calibration feature by injecting a known current.

Table 5-20 Current Monitor Specifications

Parameter	Specification
ICT	
Beam current range	0.001 – 0.3 mA
Bandwidth	1 kHz
Accuracy	1%
Precision	1%
Faraday Cup	
Rise time	200 ns
Charge range	10 – 300 pC
Accuracy	1%

Precision	2%

The Faraday cup will be constructed to collect at least 99% of the bunch charge and the signal will be split into a picoammeter, to measure the average beam current in comparison to the ICTs, and a charge amplifier, to measure the bunch charge in the low rate diagnostic line.

Details of the current monitor requirements can be found in LCLSII-2.4-PR-0083.

5.9.4 Wire Scanners

The fast wire scanner used for LCLS-II (see will be based upon a prototype design that has been fabricated and tested in the LCLS LTU beamline and is illustrated in Figure 5-47. The requirements can be found in the *Injector/Linac Wire Scanner System Requirements*, LCLSII-2.4-PR-0099.

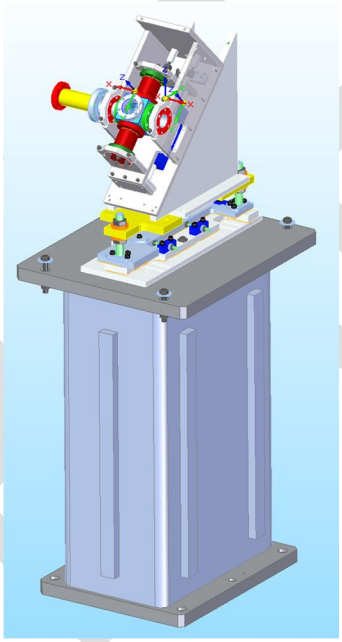

Figure 5-47. Fast Wire Scanner

The LCLS-II wire scanner system is the main diagnostic for projected beam size measurements of the high brightness electron beam for most of the accelerator. This diagnostic is not sensitive to coherent radiation effects from micro-bunching. The system provides profiles, sampled over many bunches, of the transverse beam cross-section projected onto a horizontal or vertical axis depending on the wire orientation. The beam position data acquisition is beam-synchronous, allowing for complete scans in just a few seconds. It can cover a wide range of beam parameters and operating conditions.

The controls software has interfaces for hardware and acquisition control. It provides beam profile data to be displayed or used by higher level applications to determine beam sizes, beam emittance, energy spread, or bunch length.

5.9.4.1 Mechanical Design

The key features of the scanner design are as follows (see Figure 5-48). An external linear motor mounted in a translation stage drives a wire card located inside a pair of opposing bellows. This arrangement eliminates vacuum loads seen by the drive motor. The linear motor is a very compact design and is capable of high forces and high speeds. The device is mounted at 45 degrees so that gravity returns the unit to its home position in the event of a power loss. The 45° orientation also allows for horizontal, vertical and 45° wires to be located within one device. This reduces both cost and the beamline real estate (z length) required to profile the beam in 3 axes. There are hard stops at both ends of the 50 mm travel and radiation hard limit switches set inside those limits.

The wire cards are mounted to a flexure bar that is supported at both ends. This is inherently 100 times stiffer than a cantilever design, eliminating vibration of the wires on the card. Different wire materials and cross-sections can be mounted onto the wire card. The wires are tensioned for position repeatability and to prevent beam interference in case of failure. For the wire scanners located in low rate diagnostic lines, tungsten, a high Z material, is used to provide sufficient beam loss signal for downstream detectors. For all other locations used at high repetition rate, carbon fiber is used.

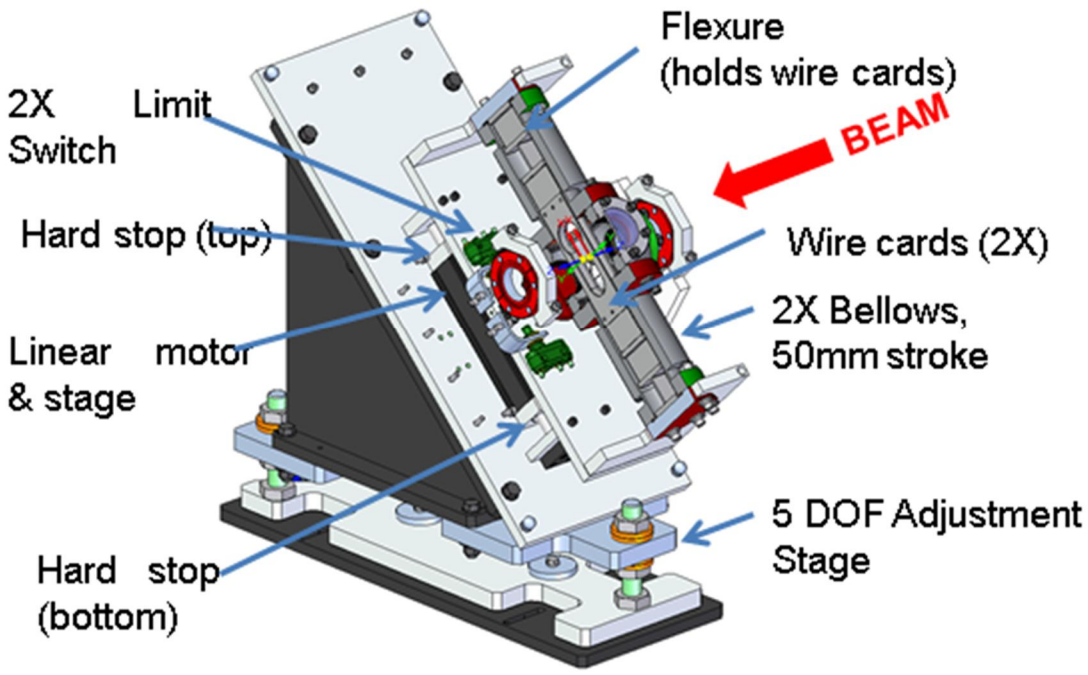

Figure 5-48: Partially exploded view of Wire Scanner with magnetic shields not shown

A magnetic linear encoder is used to report the translation stage position during a scan at beam rate. A differential magnetoresistive sensor detects the magnetic signature of the magnetized scale, producing a sine and cosine signal as it moves along the scale. These analog

signals can then be interpolated internally to produce resolutions of 1 µm. It has excellent dirt immunity and high reliability from proven non-contact sensing technology.

5.9.4.2 Operations

The allowable beam rate for scans (see Table 5-21) will be between 10 Hz and 0.6 MHz depending on operating conditions and wire scanner location. The lower limit of the wire speed is given by considering the smallest beam size at the lowest beam rate. A reasonable sampling of the beam profile of 4 points across 1 sigma beam size of 40 µm requires a maximum horizontal or vertical step size of 10 µm. The stage must translate 14.1 µm in its 45° orientation. The slowest scan speed at 10 Hz then is 141 µm/s. The optimum wire speed at the highest rate of 0.6 MHz and largest nominal beam size of 300 µm would then be 180 m/s, but is not necessary as a lower speed simply provides more samples.

The beam loss detection will be able to detect signals from the least dense projected electron distribution at the extreme case of 10 pC charge, 300 µm beam size, and 40 µm carbon wire. All parts of the wire scanner system installed at the beamline location will have the necessary radiation hardness and mechanical reliability for long term operation with typically multiple scans per day being done.

Each wire scanner or group of wire scanners within an area will have at least two downstream beam loss detectors to measure a beam loss signal proportional to the amount of charge intercepted by the wire. The detector design and readout electronics will have sufficient dynamic range to provide at least a S/N ratio of 10 for the largest beam size at the lowest charge and to not saturate for the smallest beam size at the highest charge. It will be possible to relocate the detectors for placement at optimal loss locations, or in the case of a long fiber loss detector, to vary the signal time integration window.

Table 5-21. Wire Scanner Operating Parameters from PRD

Requirement	Value	Unit
Minimum step size along beam's *x* or *y* axis	4	µm
Minimum step size along direction of wire travel	4-7	µm
Bunch charge range	10 – 300	pC
Minimum wire speed	0.15	mm/sec
Maximum wire speed	350	mm/sec
Minimum beam rate for beam scanning	10	Hz
Maximum beam rate for beam scanning	0.6	MHz
RMS position precision over 500 µm range	3	µm
Absolute reproducibility of wire scanner position	10	µm
Time for full retraction	<1	s
Minimum total scan range	±5	mm

5.9.5 Profile Monitors

LCLS-II profile monitors are based on optical transition radiation (OTR) imagers, yttrium aluminum garnet (YAG) crystals, or phosphors. The following sections and tables, which describe the LCLS-II Profile Monitors, are excerpted from, *LCLS Linac-Injector Profile Monitors* ESD 1.3-1090.

Table 5-22. Profile Monitors

Beamline	Element	Engineering Name	Area	Linac Z (m)
LCLS-IIscS	YAG01	YAG	GUNB	-8.5320
LCLS-IIscS	OTR0H04	OTR	*HTR	14.7961
LCLS-IIscS	YAGH1	DIFFUSE YAG	*HTR	22.4044
LCLS-IIscS	YAGH2	DIFFUSE YAG	*HTR	23.2256
DIAG0	OTRDG01	OTR	*DIAG0	45.7415
DIAG0	OTRDG02	OTR	DIAG0	46.7415
DIAG0	OTRDG03	OTR	*DIAG0	47.7415
DIAG0	OTRDG04	OTR	DIAG0	51.4514
LCLS-IIscS	OTRC011	OTR	*COL0	68.7756
LCLS-IIscS	OTR11B	OTR	*BC1B	126.1379
LCLS-IIscS	OTR21B	OTR	*BC2B	345.6795
LCLS-IIscS	OTR31	OTR	*DOG	1032.7000
LCLS-IIscS	OTRDL18	OTR	*LTUS	3328.8908
LCLS-IIscH	OTR30	OTR	LTUH	3341.4819
LCLS-IIscH	OTR33	OTR	LTUH	3477.2612
LCLS-IIscH	OTRDMP	OTR	*DMPH	3761.2080
LCLS-IIscS	OTRDMPB	OTR	*DMPS	3761.2080

*Deferred Profile Monitors

The purpose of the OTR imaging system is to provide high-resolution measurement of the electron beam profile, preferably at a single shot. It is based on optical imaging using transition radiation produced by electron beams traversing from vacuum into a flat metal surface.

The LCLS OTR imager, shown in Figure 5-49, will be used in all long break sections. It includes a stray-light filter, an OTR screen, an in-vacuum mirror, a vacuum window, and a camera module.

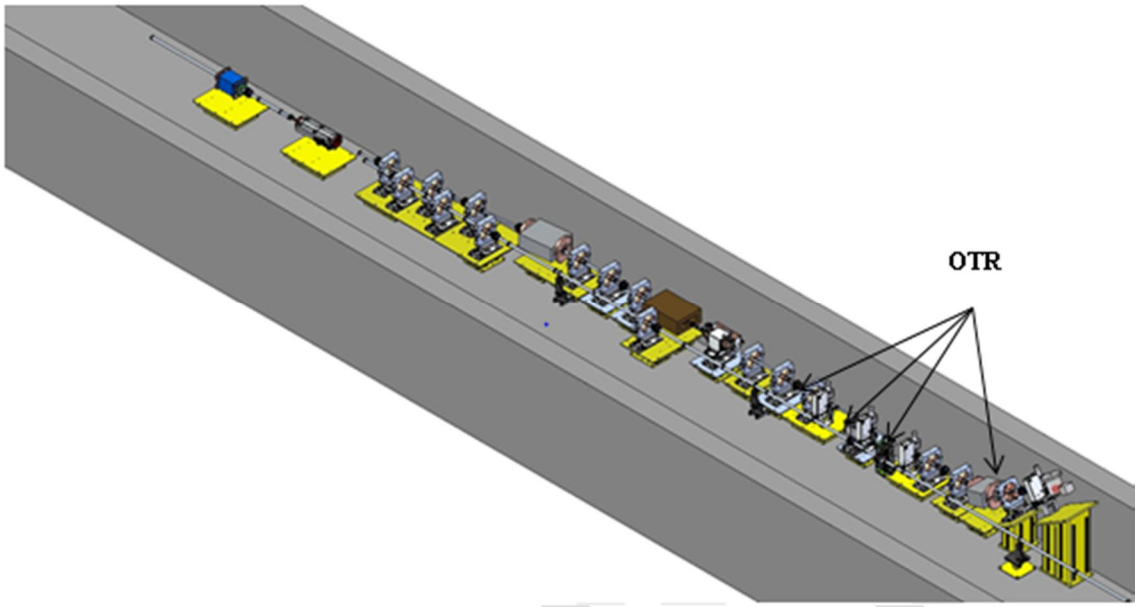

Figure 5-49. OTR Profile Monitors in the Beamline

The basic design of the pneumatic actuator and vacuum chamber will be shared between the OTR, YAG, and phosphor screen profile monitors. The pneumatic actuator will have a pneumatically-driven, linear shaft design. The vacuum chamber will include camera ports and beam axis ports. The motion limits will be defined by damped limit stops and the motion position communicated by limit switches. The profile monitor design will be a radiation hard and modular for ease of servicing.

The OTR uses a 45-degree metal foil or carbon screen that allows the electron beam to pass through with minimal attenuation, while the screen reflects the OTR light toward imaging optics. The vacuum chamber and screen actuator for the OTR will be used for other profile monitor types.

The YAG crystal screen profile monitor is commonly used in many locations in the SLAC linac and other beamlines. This device will use the common profile monitor platform and a crystal/screen design based on SLAC design examples of this type, as shown in Figure 5-50.

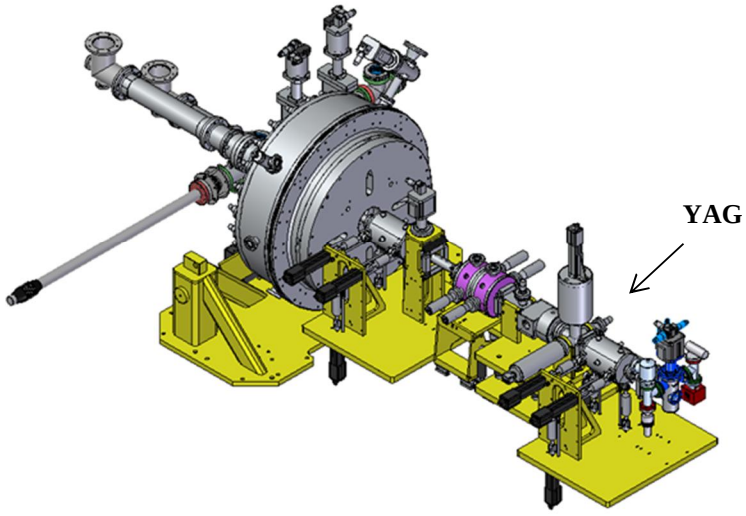

Figure 5-50. YAG Profile Monitor in the Injector Area

The profile monitor is a modular design that has field-replaceable elements. The assembly consists of three modules. The vacuum chamber module illustrates the OTR configuration.

Each profile monitor screen type (OTR, phosphor, and YAG) is compatible with this modular design by using a unique screen mount.

1. Vacuum Chamber Module
2. Vacuum Actuator Module
3. Pneumatic Actuator Module

The vacuum chamber is designed to remain in a fixed beamline position during operation and service. The vacuum actuator is designed to be field-replaceable when the vacuum chamber is vented to air without disturbing device alignment on the beamline. The pneumatic actuator can be removed and replaced in the field without opening the vacuum volume to air. Figure 5-51 illustrates the interface between each module.

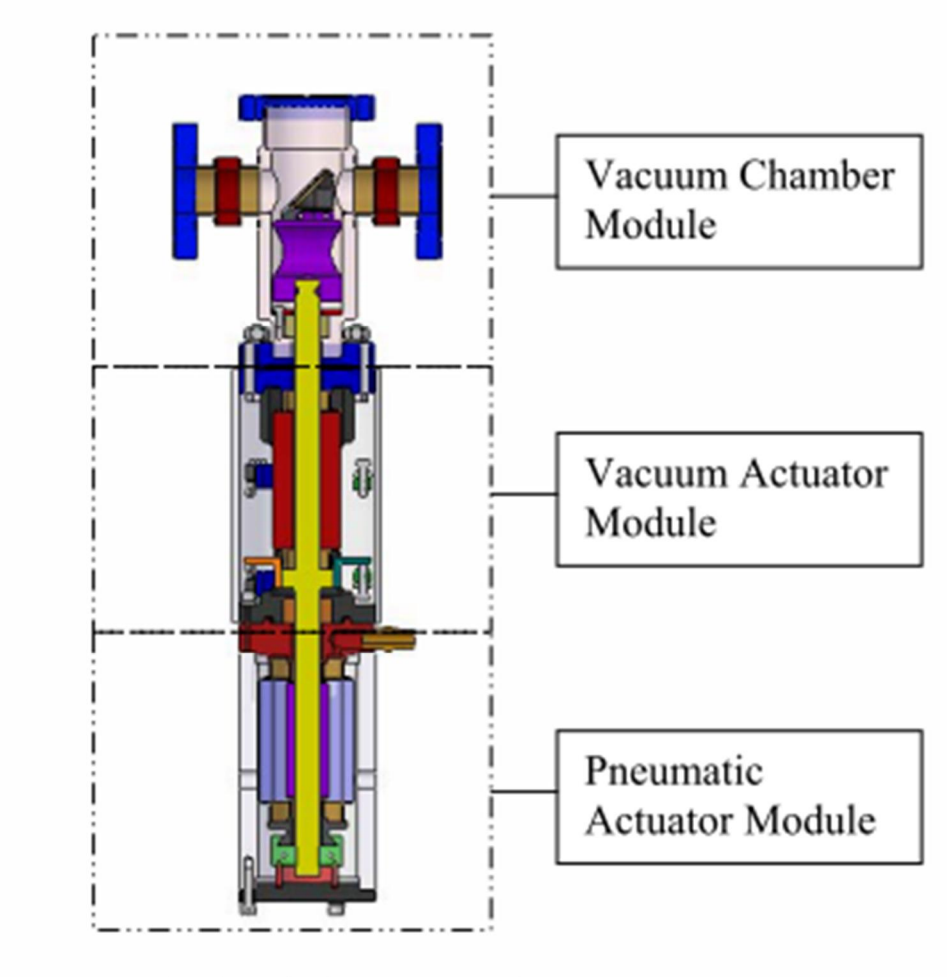

Figure 5-51 OTR Configuration

5.9.5.1 Profile Monitor Screen Design Variants: OTR, Phosphor, YAG

The common platform of the profile monitor is designed to allow the use of different screen materials.

The OTR type monitor uses a thin metal mirror that allows partial transmission of the electron beam while emitting OTR light normal to the beam axis. This light passes through a window transparent to the OTR wavelength and is imaged by a camera through focusing optics, as shown in Figure 5-52 and Figure 5-53.

The metal mirror may be made of titanium or aluminum (see Table 5-23), and has a nominal thickness of 1 µm.

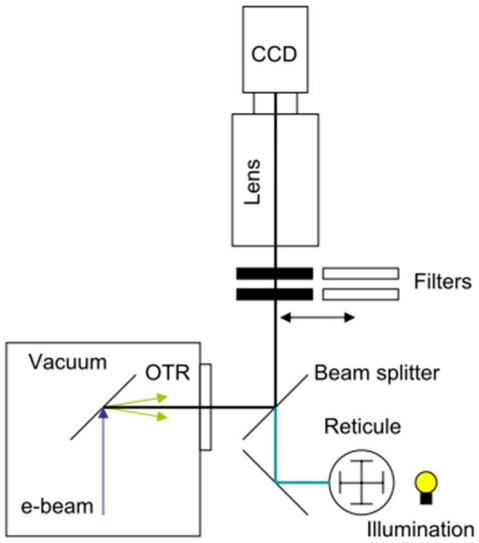

Figure 5-52 Optical Layout of OTR Profile Monitor

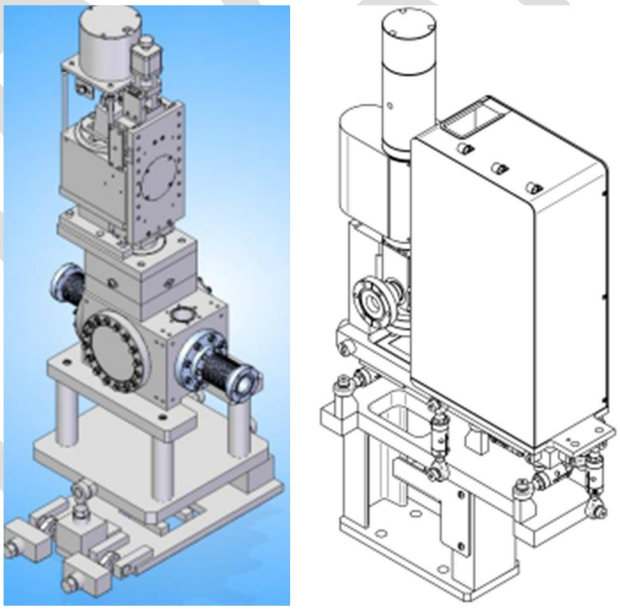

Figure 5-53 Models of OTR Profile Monitor

Table 5-23. OTR Mirror Candidate Material Properties

Material	Z	A	Density (gm/cm^3)	Radiation Length (gm/cm^2)	Radiation Length (cm)
Aluminum	13	26.981538	2.699	24.01	8.9
Titanium	22	47.867	4.54	16.17	3.56

5.9.6 Bunch Length Monitors

Two types of Bunch Length Monitors (BLMs) will be used in the warm sections of the SRF beamline: coherent edge radiation (CER) monitors and coherent synchrotron radiation (CSR) monitors. Requirements can be found in *Single-shot Relative Bunch Length Monitor*,LCLS-2.7-PR-0074.,

5.9.6.1 Coherent Edge Radiation (CER) Bunch Length Monitors

CER BLMs will be used just before the Laser Heater chicane and the BC1 chicane. These Wakefield radiation detectors have ceramic gaps in the beamline, with waveguides located in close proximity to the gap for collecting the Wakefield radiation and transmitting it down the waveguide to the diode detectors. Figure 5-54 shows a drawing of the CER BLM, which will use an existing SLAC design from LCLS.

Figure 5-54. CER BLM Layout Assembly

5.9.6.2 Coherent Synchrotron Radiation (CSR) Bunch Length Monitors

Coherent Synchrotron Radiation (CSR) BLMs (see Figure 5-55) will be used at the end of the bunch compressor chicanes. These detectors use in-vacuum mirrors to reflect the coherent radiation up and out of the beamline to an off-axis mirror that reflects the beam towards the tunnel wall to a detector mounting plate. They will use an existing SLAC design, SA-380-519-40, a device used for LCLS.

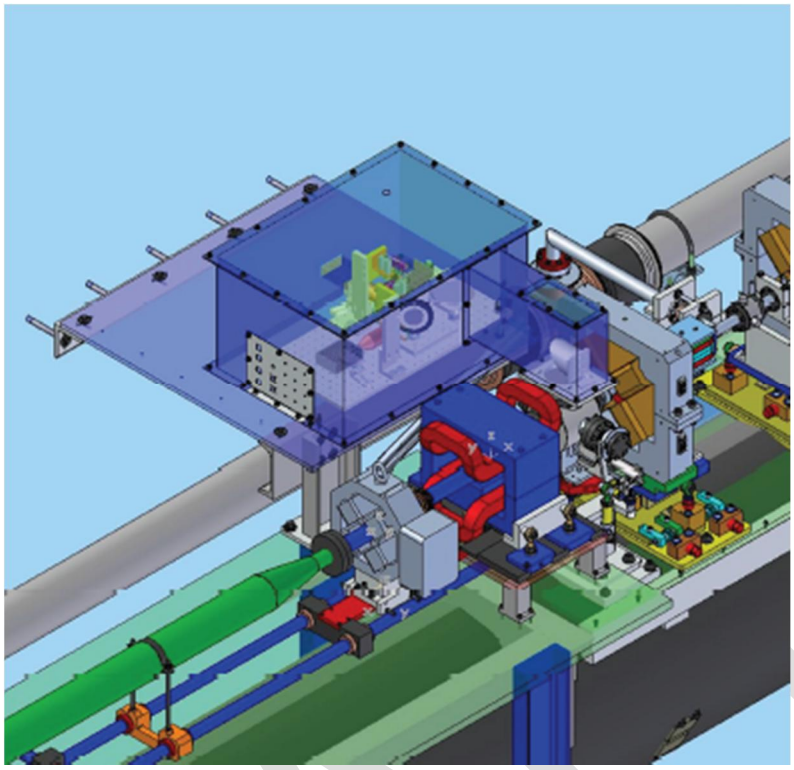

Figure 5-55. CSR Assembly

5.9.7 Transverse Cavities

The post-laser heater diagnostic beamline will include a horizontal RF deflector, located in the off-axis electron beam diagnostic station following the laser heater, to allow time-resolved emittance and energy spread measurements and absolute bunch length measurements. Requirements can be found in *Post-LH Diagnostic Beamline Requirements*, LCLS-2.4-PR-0068.,

Figure 5-56: CSR BLM Vacuum Chamber

The deflecting structure is to be oriented in the diagnostic line with its RF input coupler facing up in order to induce a vertical deflection of the electron beam as shown in Figure 5-57. The input coupler is to be located at the downstream end since the structure is of the backward traveling wave type. The upstream output coupler will be connected to an appropriately rated load with a coupler for independent measurement of the RF phase to the structure.

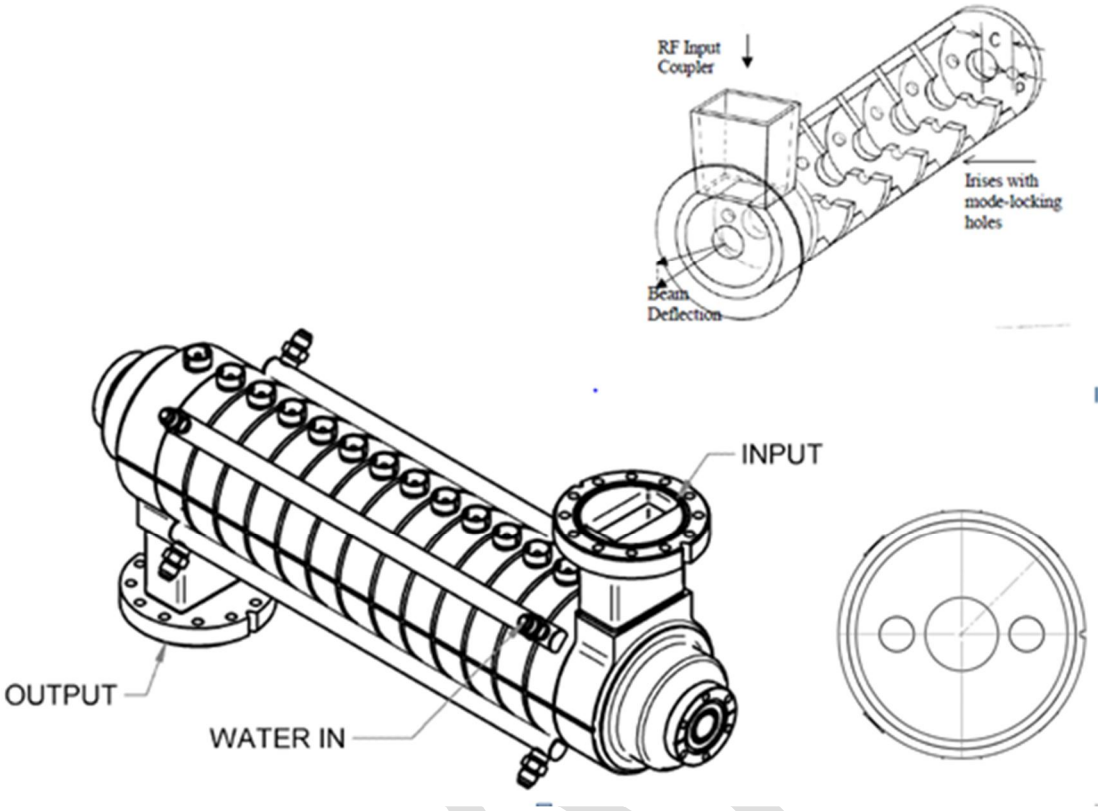

Figure 5-57. Schematic of the LCLS-II 15-cell backward-wave TW S-band transverse deflecting structure (TCAV) and its iris geometry, with polarization locking holes.

The existing device that will be used is SA-388-612-50, an S-band Transverse Deflecting Cavity (TCAV) originally built for LCLS-II Phase I, shown in Figure 5-58. The overall configuration of the structure was based on the design built at SLAC in the 1960s [4]. This design replaces the "disc and cylinder" construction used in previous deflecting cavities with self-aligning diffusion bonded "cups." The RF and mechanical parameters of the structure are summarized in Table 5-24.

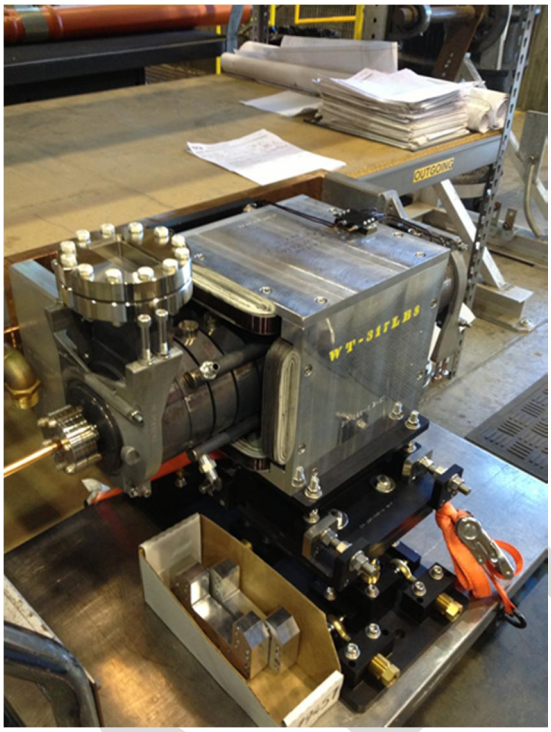

Figure 5-58: Photo of Completed LCLS-II S-band TCAV with steering coils wrapped around it to save beamline space

Table 5-24. : RF and Mechanical Parameters for the Transverse Deflecting Structure

Parameter	Value	Unit
Structure linac location	injector	
Beam energy	135	MeV
Cavity length	0.55	m
RF frequency	2856	MHz
RF phase stability (rms) at all $f > 0.5$ Hz	<0.5	deg-S
Maximum power required	2	MW
Minimum power required	0.5	MW
Maximum deflecting voltage (on crest)	1.4	MV
Minimum deflecting voltage (on crest)	0.7	MV
β_y at deflector center	7	m
Hor. and vert. structure alignment tolerance	400	µm
Longitudinal structure positioning tolerance	5	mm
Roll angle tolerance	2	mrad

5.10 Collimator Systems

LCLS-II uses two systems of electron beam collimators. The Halo Collimation System consists of a number of collimators with adjustable jaw pairs place at strategic locations between

the Laser Heater and just before the final bend magnet at the beginning of the LTU. One group of collimators primarily intercepts electrons that have a large transverse coordinate (halo), while a second group is located to intercept electrons with too large energy deviation from the desired beam. In this manner the five-dimensional phase of the beam can be "cleaned up." Halo collimators will absorb a more or less continuous, low power beam.

The second collimator system is the Protection Collimator System. It is part of the BCS system and consists of a number of collimators with fixed apertures strategically located to confine the electron beam to its approved channel. Normally, protection collimators will not intercept any electron. However, in the event of a mis-steering, mis-wiring, or severe energy change, this system will intercept the electron beam if there is adequate bulk shielding to maintain a safe radiation level in accessible areas. Ray tracing studies are used to determine the best location and sizes for protection collimators.

5.10.1 Halo (Adjustable) Collimators and Shielding

A system of adjustable collimators is needed to remove undesirable electrons from the beam, to both avoid excessive radiation due to beam loss in sensitive areas and reduce activation of accelerator components. Requirements for these collimators can be found in the *PRD Halo Collimator System*, LCLS-2.4-PR-0095.

The halo collimators will reuse an existing SLAC design, SA-380-505-12, a two-jaw collimator used for LCLS, with the exception that jaw material and dimensions will vary by location as indicated in the above-referenced PRD and shown in Figure 5-59.

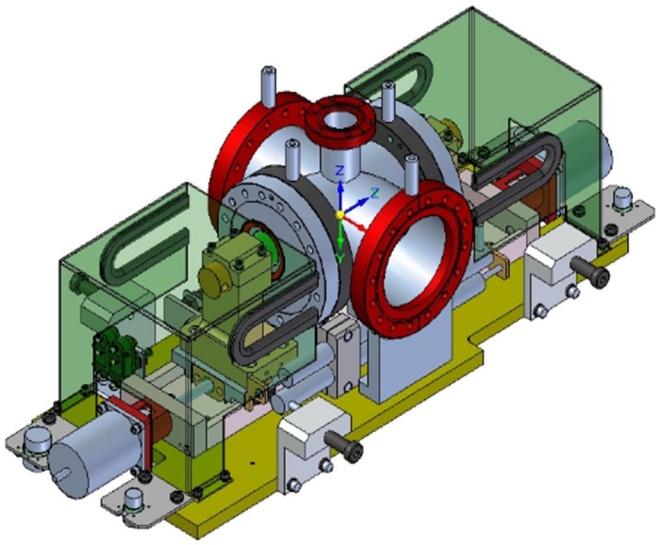

Figure 5-59. Adjustable Collimator assembly with two independently adjustable jaws

5.10.2 Protection Collimators

The LCLSscS and LCLSscH collimators with fixed aperture contain the electron beam within the stay-clear defined by the ray tracing. This ensures that mis-steered electron beams remain contained and do not endanger the equipment. The list of fixed aperture collimators in both LCLSscS (blue) and LCLSscH (red) lines is shown in Table 5-25:

Table 5-25 Fixed Aperture Collimators

No	Element	Type	Beamline	Area	Keyword	Linac Z (m)	Linac Z (ft)
1	PCMUON	MAD	LCLS-IIscH	LTUH	PC	3561.94952	11686.18609
2	PCMUONB	MAD	LCLS-IIscS	LTUS	PC	3564.749489	11695.37234
3	PCTCX	MAD	LCLS-IIscH	DMPH	PC	3727.303752	12228.68685
4	PCTCXB	MAD	LCLS-IIscS	DMPS	PC	3727.303752	12228.68685
5	PCPM0	MAD	LCLS-IIscH	DMPH	PC	3732.705893	12246.41041
6	PCPM0B	MAD	LCLS-IIscS	DMPS	PC	3732.705893	12246.41041
7	PCPM1L	MAD	LCLS-IIscH	DMPH	PC	3740.686355	12272.59303
8	PCPM1LB	MAD	LCLS-IIscS	DMPS	PC	3740.686355	12272.59303
9	PCPM2L	MAD	LCLS-IIscH	DMPH	PC	3751.118717	12306.81994
10	PCPM2LB	MAD	LCLS-IIscS	DMPS	PC	3751.118717	12306.81994

Typical fixed aperture collimators are shown in Figure 5-60 (rectangular aperture) and Figure 5-61 (round aperture).

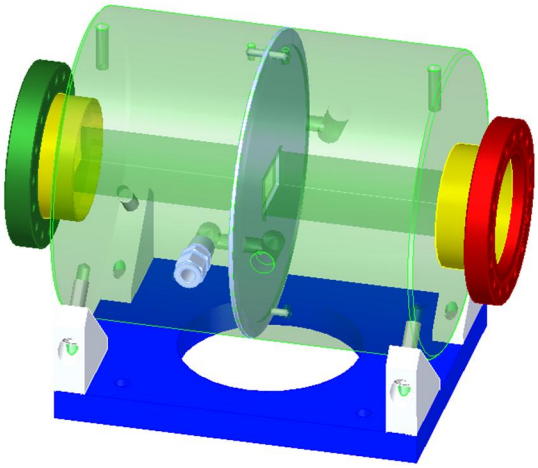

Figure 5-60: Fixed collimator with rectangular aperture used in existing EBD line

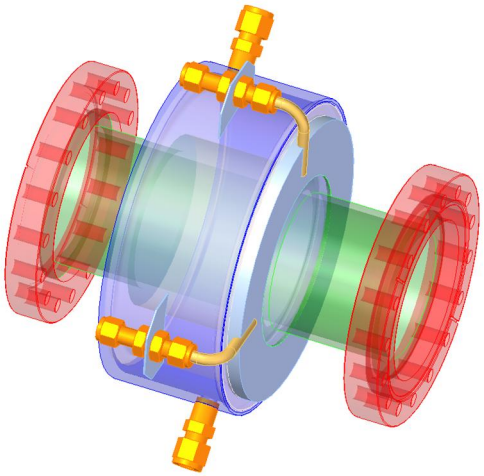

Figure 5-61: fixed collimator with round aperture used in existing EBD line

5.11 Dumps and Stoppers

Beam power absorbing components are defined in PRD LCLSII-2.7-PR-0079. Some important parameters of these devices are shown in Table 5-26. More information about the highlighted devices appears below.

Table 5-26. Beam power absorbed by beam-absorbing components

MAD Symbol	Descripton	Normal Operation [kW]	Performance Requirement [kW]	MCB [kW]
LCLS2scH				
'TD11B'	Insertable Dump	5	5	138
'D2'	Insertable Dump	3.3	5	2000
'TDUND'	Insertable Dump	0.4	0.4	2000
'ENDDMPH'	Fixed Dump	3	119	2000
LCLS2scS				
'STBP33A'	Halo Collimator	0	0	0
'STBP33B'	Halo Collimator	0	0	0
'STBP33C'	Halo Collimator	0	0	0
'TDUNDB'	Insertable Dump	0.4	0.4	2000
'ENDDMPS'	Fixed Dump	4	120	2000
LCLS2scD				
'DUMPBSY'	Fixed Dump	245	300	2000
DIAG0				
FCDG0DU	Insertable Dump	0.001	0.005	0.5
DUMPDG0	Fixed Dump	0.001	0.323	0.5
DIAG1				
FCDG1DU	Insertable Dump	0.003	0.005	1
DUMPDG1	Fixed Dump	0.003	0.825	1

5.11.1 LTU TDUNDs

One diagnostic tune-up dump, TDUND, will be included in each beamline just before the undulator. The TDUNDs beam dumps which should take a beam-power no larger than that at the corresponding tune-up dump of LCLS (TDUND).Table 5-27 shows parameters for the TDUND. A photo of an LCLS TDUND appears in Figure 5-62. LCLS-II TDUNDs will reuse existing designs from LCLS, including the use of tungsten (to break EM showers), lead (to shield the undulators), borated polyethylene (to moderate and absorb neutrons) and outer panels of marble (to shield gammas).

Table 5-27 TDUND Stopper Parameters

Parameter	Value	Unit
Beamline location (in 'LCLS' coordinates)*	512.9874	m
Nominal electron energy	4.3 to 14	GeV
Nominal beam horizontal size range (rms)	0.04 to 0.08	mm
Nominal beam vertical size range (rms)	0.03 to 0.06	mm
Bunch charge range	0.2 to 1	nC
Maximum beam rate via MPS interlock	10	Hz
Max. average beam power	140	W
Field of view for screen (x and y)	±3	mm
Screen resolution (not critical)	0.02	mm
Max. reasonable insertion/extraction time	5	sec

* 'LCLS' coordinates are defined in the LTU with $z = 0$ at station-100.

Figure 5-62: LCLS TDUND

5.11.2 D10

Tune-up dump D10 in BSY was designed as a low power beam dump in the SLAC linear accelerator located in BSY at Linac Z=3175.64 m (upstream face). In LCLS-II, the D10 tune-up dump will be used as high power dump (up to 300kW) in a new location approximately Z=3208m, which is about 2 m downstream of MUON wall face. Figure 5-63 shows the existing and the proposed locations for D10 inside the MUON shield.

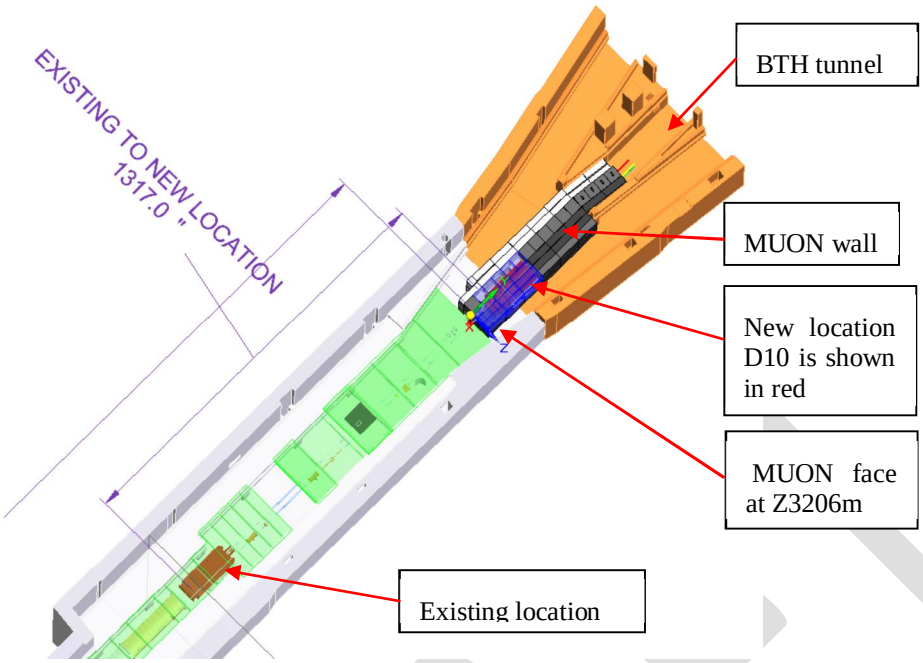

Figure 5-63: Existing D10 location and LCLS-II location inside the MUON wall

Installing D10 inside MUON wall will require some design modifications. Modifications will include, but not be limited to, moving all water fitting outside the MUON shield, eliminating all indium seals, and plugging ports not in use. Figure 5-64 shows the existing D10 design.

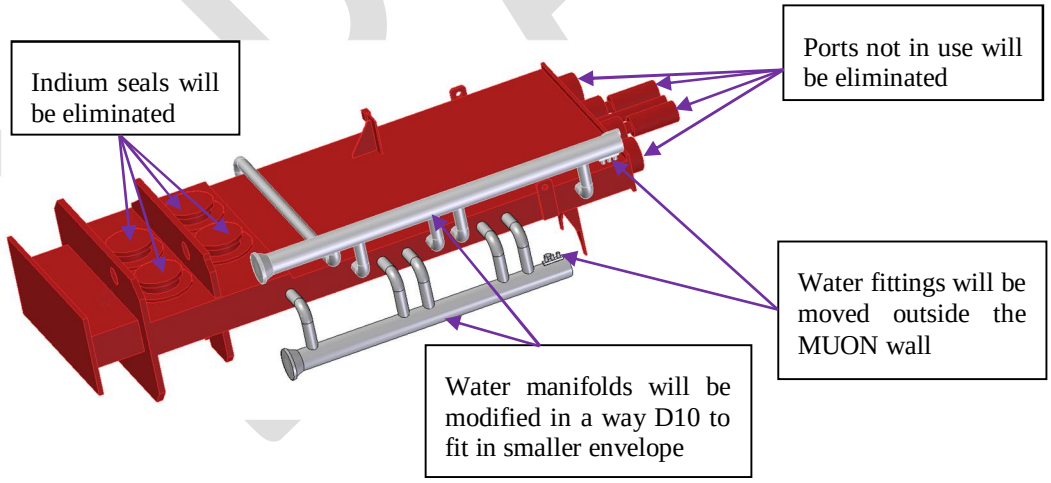

Figure 5-64: Existing D10 design and some of the needed design modifications

5.11.3 Main dumps

The existing EBD will be replaced with two identical dumps installed in the existing pits in the EBD housing, one for the HXR line and one for the SXR line. Both dumps are required to

absorb beam power up to 120kW. Detailed requirements for LCLS-II dumps are given in "LCLSII-2.7-PR-0079-R0" document. Shielding requirements are given in "LCLSII-1.2-PR-0100". General Dump line requirements are given in "LCLSII-2.5-PR-0135-R0". The layout of the EBD lines, per {document title}, is shown in Figure 5-65.

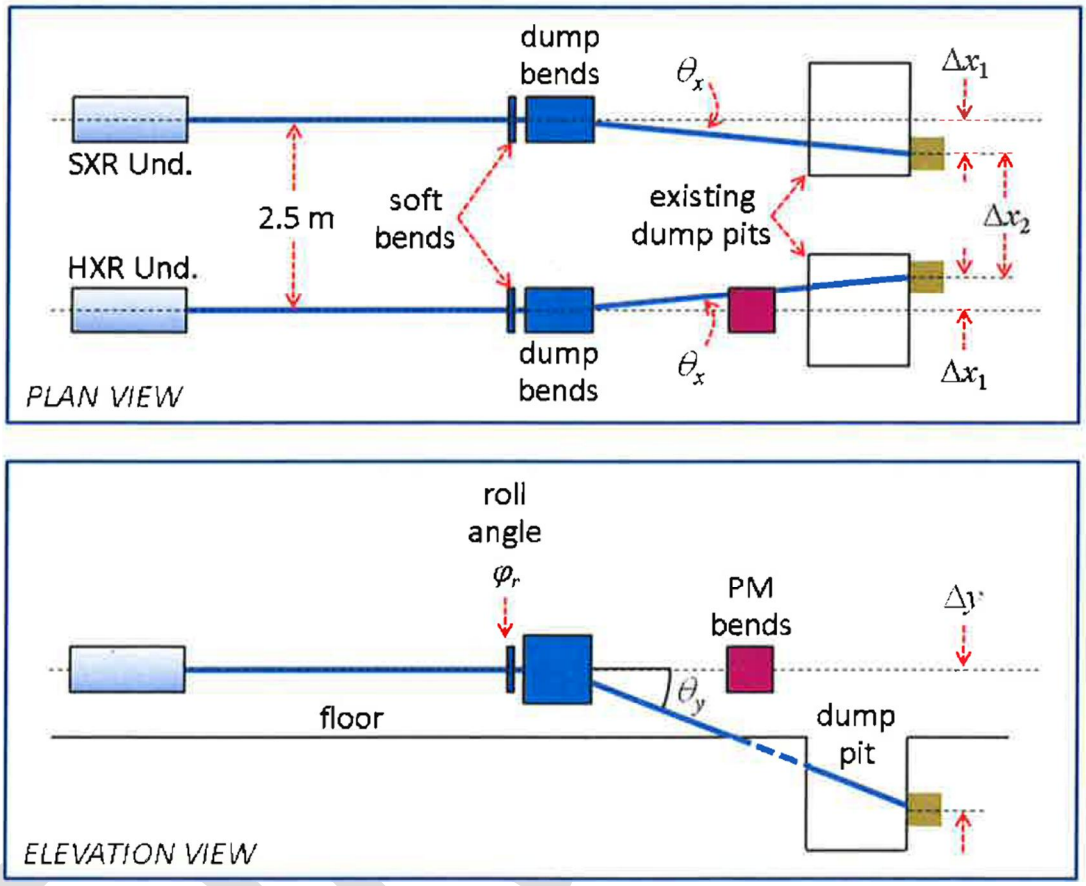

Figure 5-65: LCLS-II Dump lines layout defined in PRD LCLSII-2.5-PR-0135-R0

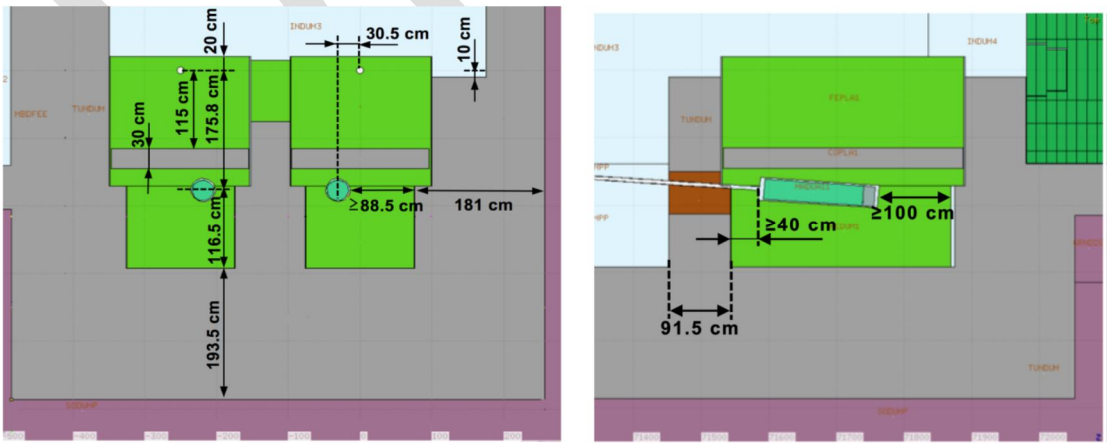

Figure 5-66. Shielding requirements for EBD dump lines

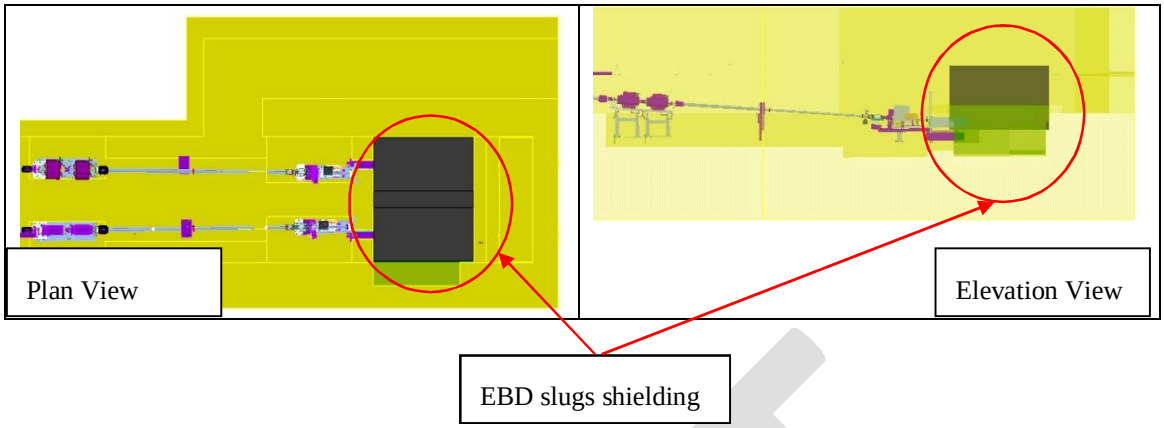

Figure 5-67. Model of EBD lines, pits and shielding

5.11.3 Stoppers in BSY

According to current Mad Deck there are three stoppers in the LCLSscH line and four in LCLSscS line. Stopper names and Linac Z locations are shown in Table 5-28.

Table 5-28: Stoppers in BSY LCLSscH and LCLSscS lines

Name	Beamline	Line	Type	Linac Z
D2	LCLSscH	SPH	INST	3193.238
ST60	LCLSscH	SPH	INST	3194.609
ST61	LCLSscH	SPH	INST	3205.04
STBP32	LCLSscS	SPS	INST	3172.961
STBP33A	LCLSscS	SPS	INST	3180.461
STBP33B	LCLSscS	SPS	INST	3181.96
STBP33C	LCLSscS	SPS	INST	3188.945

5.11.3.1 D2 Stopper

Stopper D2 (also tune-up dump) is an existing BSY device located at Linac Z=3193.24 m. It is water-cooled and rated for 250kW beam power. In LCLS-II it will be used in the SPH line. Figure 5-68 shows the stopper D2 in BSY tunnel.

Figure 5-68: Existing D2 in BSY tunnel

5.11.3.2 Stoppers

There are two redundant PPS stoppers after D2 in the existing LCLS located at Linac Z3194.609m and Z3205.04m, ST60 and ST61. Recently ST61 was replaced with new modified ST61 stopper with external switches and CF flanges. The old design had internal switches and indium seal flanges. In near future ST60 will be replaced with the modified version as well. These stoppers are not considered continuous power absorbers. Figure 5-69 shows photographs of the old and new ST61 stoppers.

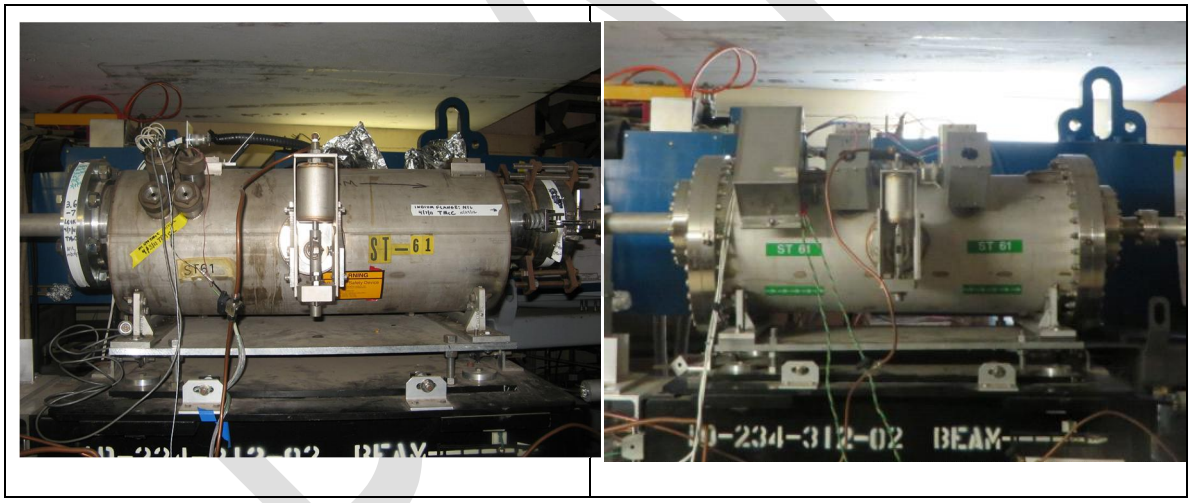

Figure 5-69. Old (left) and new (right) versions of ST61 stopper

There are four PPS stoppers in the SPS LCLS-II line in BSY. All of them will be as the new ST61 new design.

5.12 High Power RF Systems

Several high-power RF systems sustain the electromagnetic fields that accelerate the beam. This begins with the RF high-power sources, or amplifiers, located in the above-ground gallery, continues through the RF waveguide delivery systems, then extends down to the tunnel, and ends

with the fundamental power couplers, which make the final connection through the cryomodule to the accelerator cavities. The low-level RF (LLRF) drive, feedback and controls system, which through this system regulates the cavity fields, is covered in Chapter 10. General requirements of the RF system are given in the Physics Requirements Document *SSA Based RF System and LLRF Requirements*, LCLSII-4.1-PR-0098.

5.12.1 RF Sources

The main high power RF source for the LCLS-II linac will be a 3.8 kW, CW, 1.3 GHz solid state amplifier (SSA). Each of the 280 units required will power one SCRF cavity. This single cavity per source scheme greatly simplifies the LLRF controls, as well as waveguide distribution. The power requirement is set for acceleration of a maximum beam current of 0.1 mA on-crest at a gradient of 16 MV/m, with the fundamental power couplers set for a loaded quality factor of 4.1×10^7. Transmission losses of 6%, allowance for 10 Hz-level residual microphonics detuning (after piezo suppression) and 10% overhead are included in this RF power requirement (of which 1.7 kW becomes beam power at 0.1 mA). The Q_L value is optimal for eventual 0.3 mA operation, which will require the SSAs to be upgraded to 6.8 kW. This value will not be increased for lower current operation in order to retain a reasonably wide cavity bandwidth (31 Hz), at the cost of reflecting considerable power into isolator loads. Actual operational overhead will typically be greater, with beam currents less than 0.1 mA and lower gradients and/or microphonics. Moreover, 6.3% additional cavities are included in the linac to compensate for failed or low gradient cavities. It is assumed that any 'reserve' cavities will be operated so as to lower the overall 2 K cryo-load.

The RF from the SSAs running 'open loop' needs only moderate regulation compared to the closed loop regulation of the cavity fields. Although the cavity bandwidth (BW) is only 31 Hz, the effective BW of the RF station operating in closed loop will be around 70 kHz. The SSAs are specified to have delay-line-like transfer function over this BW. Specifically, the SSAs are to have a small signal, 1 dB bandwidth (two tone measurement) of 1 MHz or wider with a transfer function that is amplitudeflat (< 5%) and phase-linear (< 5° deviation) within 100 kHz of the nominal frequency. The latency through the SSA should be less than 300 ns. Also, the SSA noise figure is to be less than 10 dB, the nominal maximum power is to be achieved with less than 1 dB compression, and the harmonic power output is to be less than -30 dBc.

The AC to RF efficiency goal for the SSAs at the rated power is to be at least 40%, although45% or higher may be possible. The drain voltage should be manually controllable to allow for higher efficiency operation at lower power (e.g. at ~ 2 kW when the beam is off). Although RF isolators will be installed on the waveguide outputs, the SSAs must include self-protection from internal reflections in the RF combiner circuits due to a failed transistor, and continue to operate at reduced power. The SSAs must also protect themselves from overheating.

Each SSA will interface with the global control system via an Ethernet cable, through which various digitized information will be available, including status data, drive power, power supply

voltage and temperatures. Also, four 24V DC permit lines will be provided to interlock on external faults, such as isolator overheating and RF leakage from the waveguides.

Cooling will be provided by low conductivity water (LCW), with a flow rate up to 7 gpm, nominal input and output pressures of 95 psi and 25 psi, respectively, and an inlet temperature of 30 °C. Because they will operate in the open, non-HVAC environment of the SLAC linac gallery, external forced air cooling will not be used to keep dust out of the units. Instead, the SSAs will be essentially air-sealed, and an internal air-to-LCW heat exchanger will be used to remove the heat deposited into the air.

Besides the 1.3 GHz cavities, 16 higher harmonic (3.9 GHz) cavities are included in the linac to linearize the bunch energy spread prior to compression. These cavities are housed in two shorter-length cryomodules. A cavity Q_{ext} of 2.5×10^7 (fixed coupling) was chosen so the loading of a 300 µA beam at the nominal decelerating phase of -165 deg maintains a cavity gradient of 15.5 MV/m. (maximum envisioned). The cavity would also be detuned by 21 Hz to cancel the out-of-phase loading. This gradient, without beam, requires about 700 W to fill the cavity.

The 3.9 GHz cavities will also be individually powered, although small CW S-band klystrons will be used. A 3 kW model, with a gain of 41 dB and an efficiency approaching 30%, is commercially available, although only a fraction of this power is required. This klystron would be powered by an 8.5 kV supply, which may be distributed from a single source to several klystrons.

Details of the L-band SSA can be found in the Engineering Specification Document, *RF Solid State Amplifier (SSA)* LCLSII-2.4-ES-0150-R1. The Physics Requirement Document for the 3.9 GHz Cryomodule is *SCRF 3.9 GHz Cryomodule* LCLSII-4.1-PR-0097.

5.12.2 Waveguide Systems

The RF power produced by the transistors within each SSA rack is combined and output via a standard L-band WR650 waveguide port. At the cryomodule, the input port of the fundamental power coupler is also a WR650 waveguide. For transmission between source and cryomodule, as shown in Figure 5-70, we considered various conduits but settled on a WR650 waveguide. High-power coaxial cables or transmission lines would double the attenuation losses, and they contain spacers made of non-radiation-hard materials. WR770 has lower attenuation, but is too bulky. It does not appear to be necessary to trade some efficiency for space with a half-height WR650 waveguide.

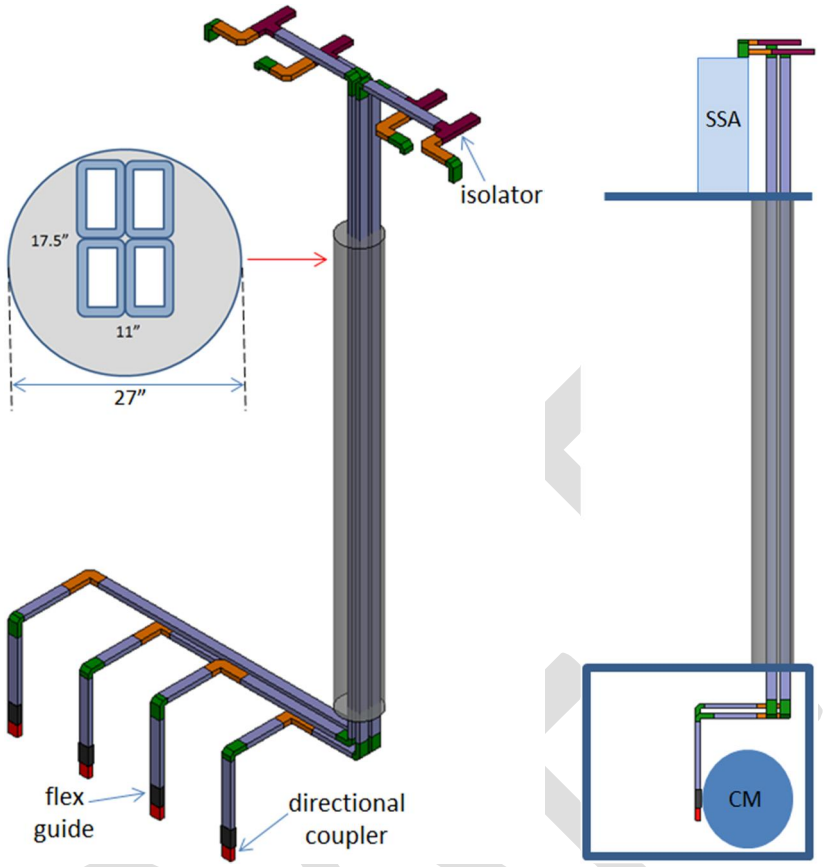

Figure 5-70 Schematics of a typical waveguide layout from SSAs in the gallery through a penetration shaft to fundamental power couplers on the side of a cryomodule. The direction of the longitudinal waveguide runs in the tunnel (shown all one way) will vary, and lengths must be customized.

Having one source per cavity simplifies RF power delivery. No splitters or mechanical phase shifters are needed. Length differences and thermal phase drifts are easily compensated and tracked by the individual LLRF controls. In addition to several bend and straight sections, each waveguide connection will incorporate an isolator, directional coupler and flex waveguide. The water-cooled isolator, which needs to be rated to absorb a full 6.8 kW reflection at any phase with ~30 dB isolation, will be located in the gallery for plumbing convenience and to minimize the heat load in the tunnel. The directional coupler will provide both forward and reflected signals with better than 30 dB directivity, and will connect directly to the cavity coupler input. The short, semi-flexible section then mechanically decouples the long waveguide run from the cryomodule components. The waveguide will be pressurized with dry air to 1-2 psig as part of a non-ionizing radiation protection scheme to detect potential RF leakage from the waveguide. At this pressure, 1/8 inch wall aluminum WR650 is suitable. Special gaskets that provide both an RF seal via a knurled surface, and a gas seal via a molded rubber element, will be used at each flange joint.

The surface-level SLAC Linac gallery has 27-inch diameter penetrations to the tunnel below that are spaced roughly 20 feet apart. With the eight-cavity cryomodule spacing of about 40 feet,

each cryomodule will be powered from waveguide from two penetrations. Thus each penetration must accommodate four waveguides, together with a number of control and monitoring cables. As the 25-foot penetration depth exceeds the maximum length of generally available WR650 sections, the penetrations need to have flanges.

The heating of the aluminum waveguide walls from RF attenuation will be about 26 W/m with 6.8 kW fully reflected, which amounts to about 200 W generated in a penetration per waveguide. Since the penetrations may be plugged at the tops with neutron absorbing material, we plan to cool the waveguides by running air through them.

The two 3.9 GHz cryomodules will have similar waveguide connections between the sources and couplers. In this case, we may be able to recycle the copper WR284 waveguide from the SLAC S-band linac, but fill them with air and change the flanges. The isolators will need to be rated for at least 1.6 kW from beam-generated power

5.12.3 Fundamental Power Couplers

The fundamental power coupler (FPC) is a critical element of the linac, bringing the RF power that accelerates the beam from external waveguides into the interior of the cryomodule to the SCRF cavity beam tube. Although the initial RF sources will provide a maximum of 3.8 kW of power, the couplers need to be capable of handling 6.8 kW for an eventual upgrade to allow 300 μA beam operation. At this power level, they must also accommodate full reflection of the input power at any relative phase.

To benefit from the many years of coupler development and evaluation at DESY, LCLS-II will use DESY's TTF-III coupler design, shown in Figure 5-71. This coupler has a WR650 waveguide input port where the RF couples into a coaxial line with a smaller cross-section to minimize the static heat load. A cylindrical ceramic window inside the "waveguide box" separates the coax vacuum from the waveguide air. A second "cold" window towards the cavity end provides a second level of protection for the beamline vacuum. It too is cylindrical, to avoid buildup of static charge from scattered dark current. A port in the outer conductor allows the intervening region to be pumped. With the room temperature and cavity flanges fixed in position, the three bellows in the coaxial line allow the center conductor to be moved to position the antenna tip for the desired Q_{ext} coupling (i.e., the antenna couples to the evanescent field protruding from the nine-cell cavity's π-mode). The Q_{ext} tuning knob shown in the figure can be motorized for remote adjustment, but the LCLS-II couplers will be set manually. The antenna can be moved over a 15 mm range.

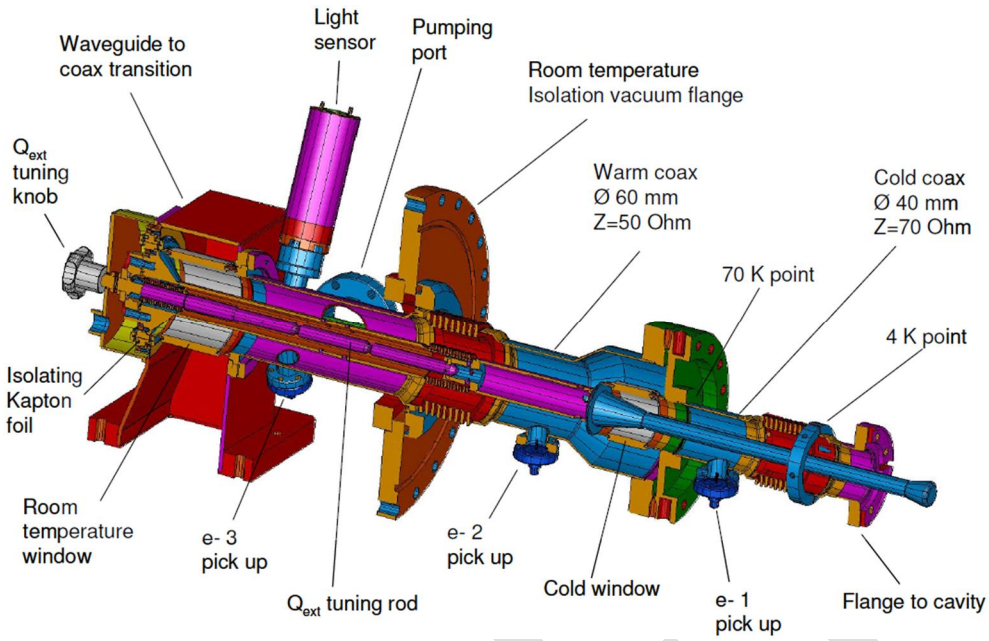

Figure 5-71. TTF-III Coaxial Fundamental Power Coupler

The TTF-III coupler was designed for use in several mA, pulsed linacs, such as XFEL and ILC, and requires two basic changes for LCLS-II. First, the low LCLS-II current requires higher Q_{ext} to efficiently couple power to the beam, from around 3×10^6 for XFEL to 4.1×10^7 for LCLS-II. To this end, the antenna is shortened by cutting 8.5 mm from the flared tip, resulting in a narrower tip as well. This shifts the Q_{ext} range from about $1\times10^6 – 2.0\times10^7$ up to $6\times10^6 – 1.4\times10^8$. As noted above, however, Q_{ext} will not be increased as the beam current is lowered to maintain a reasonable cavity bandwidth.

Further, the average RF power in the power LCLS-II coupler will exceed the coupler rating by about a factor of four. The weak point is the heating of the copper-plated stainless-steel inner conductor between the windows, which would rise to about 700 °C with 6.8 kW of power being fully reflected. The 30 µm thickness of the copper plating was originally chosen as a compromise between the inner conductor heating and the static heat loss it causes. With CW operation, the static load is much smaller in relative terms, so the plating thickness can be increased with only a minor increase in the total heat load. A copper plating thickness of 150 µm was chosen to keep the peak temperature below about 450 °C, the temperature at which the couplers are baked. Testing so far has shown this to be effective.

A related change, currently being finalized, is an improvement of the thermal anchoring of the 70 flange (see “70 K point” in Figure 5-71) to the 70 K supply line though an aluminum plate and copper braids (not shown in the figure). This flange has been found to get considerably warmer than expected during CW operation, approaching room temperature. The connection to this flange is being modified to reduce the temperature drop across the contract areas. This modification is largely peripheral to the design of the coupler itself.

An improvement to the design initiated at SLAC for the ILC program involves how the top of the waveguide box seals around the top of the coaxial endcap assembly. It was found that uneven contact due to imperfect alignment can lead to arcing at this joint. A change from a stainless-Kapton-stainless "capacitor ring" interface to a plug-compatible stainless-copper-stainless "flex seal" solved the problem. This sacrifices the ability to bias the center conductor for multipacting suppression, but the "capacitor ring" could be reinstalled if need be, and multipacting is very unlikely to be a problem at low power (the first multipacting band appears around 50 kW).

The fundamental power couplers for the sixteen 3.9 GHz cavities will be of a similar coaxial configuration, except that they will have fixed coupling and the warm window will be flat instead of cylindrical, and located at the interface of the waveguide box to the WR284 S-band waveguide. They will also be adapted for higher average power and increased Q_{ext} compared to the FLASH 3.9 GHz cryomodule couplers. Their coupling specification is $Q_{ext} = 2.5\times10^{7}$, and unlike the 1.3 GHz cavities, they will be oriented to exit from alternating sides of the cryomodule, changing cavity-to-cavity, to minimize transverse RF kicks.

The couplers for the fundamental and harmonic cavities are referenced in the Physics Requirement Documents, *SCRF 1.3 GHz Cryomodule*; LCLSII-4.1-PR-0146 and *SCRF 3.9 GHz Cryomodule* LCLSII-4.1-PR-0097. Details of the 1.3 GHz coupler can be found in the Engineering Specification Document, *Fundamental Power Coupler* LCLSII-4.5-ES-0055.

5.13 References

1 "A Cleaning Facility to Prepare Partcile Free UHV Components", K. Zapfe, U. Hahn, M. Hesse, H. Remde, Deutsches Elektronen Synchrontron DESY, Hamburg, Germany.

2 "Particle Free Pump Down and Venting of UHV Vacuum Systems", K. Zapfe and J . Wojtkiewicz, DESY, SRF 2007.

3 J. Martingnac, et al., "Particle Contamination in Vacuum Systems", *Proceedings of the 1995 Workshop on RF Superconductivity*, city, country (1995).

4 G.A. Loew and O.H. Altenmueller, *Design and Applications of the RF Structures at SLAC*, SLAC -PUB 135, 1965.

6 CRYOMODULES

TECHNICAL SYNOPSIS

The LCLS-II main linac cryomodule is based on the existing XFEL design, using TESLA-style superconducting accelerating cavities, and with minimal modifications to accommodate CW operation and LCLS-II beam parameters. Cryomodules contain superconducting cavities together with cryogen distribution lines and thermal shielding, and are assembled in a small number of strings without breaks between individual cryomodules. At the downstream end of each 1.3 GHz cryomodule are focusing and steering magnets and a beam position monitor. Beam line higher-order-mode (HOM) absorbers are located in the cold sections between cryomodules. The cavity tuners, HOM couplers, and fundamental power couplers are also developed from existing designs. Cryogenic bypass lines are required only in the short warm sections of the linac.

The linac contains 280 accelerating cavities operating at 1.3 GHz and 16 superconducting cavities operating at the third harmonic frequency of 3.9 GHz. They are assembled in 35 cryomodules containing 1.3 GHz accelerating cavities, and two cryomodules containing 3.9 GHz linearizing cavities. The average accelerating gradient of approximately 16 MV/m is a conservative requirement in terms of present-day cavity capabilities. The accelerating cavities utilize recent advances in nitrogen doping to obtain an average unloaded quality factor Q_0 of $2.7x10^{10}$ at an operating temperature of 2 K and nominal accelerating gradient of 16 MV/m, resulting in a 2 K heat load that allows the use of a single cryoplant design based on the CEBAF CHL-II helium plant. Harmonic cavities are used to linearize the correlated energy spread in the electron bunches, and are based on the 3.9 GHz design successfully implemented at FLASH.

The 1.3 GHz cryomodules and the 3.9 GHz cryomodules contain eight RF cavities each. Active control of the cavity resonant frequency is provided by an end-lever tuner with motor and piezo-driven components. Each RF cavity is independently powered through a fundamental power coupler with variable Q_{ext} connectedvia air-filled waveguide to a solid state amplifier at 1.3 GHz or a klystron at 3.9 GHz.

Cryogenic circuits provide 2 K liquid helium to the cavities, with provisions for rapid cooldown of cavities in an individual cryomodule. as well as a nominally 5 K thermal intercept circuit, and a nominally 45 K thermal radiation shield and thermal intercept circuit. Cryogenic heat load is dominated by dynamic RF heating of approximately 10 W per cavity, for the 1.3 GHz cavities. For 4 GeV beam operation, the estimated heat load at 2 K is 3.5 kW including uncertainty factors and overheads, and is within the cryoplant design capacity of 4 kW at 2 K, allowing for an overcapacity margin.

1
2
3
4
5
6

6.1 Scope, Schedule and Partner Lab Roles

An XFEL-style cryomodule (also similar to a TESLA/ILC style 3+), with minimal changes for CW operation, has been selected for the LCLS-II main linac in order to provide efficient and low-risk cryomodule design, production, and operation, consistent with space constraints in the existing SLAC tunnel. The cryogenic linac consists of strings of as many as 20 cryomodules cooled in series with internal cryogenic piping connected from one cryomodule to the next, and unsegmented insulating vacuum extending over up to 12 cryomodules. Thirty-five 1.3 GHz cryomodules will be assembled at Fermilab and JLAB: one prototype and 16 production cryomodules at Fermilab and one prototype and 17 production cryomodules at JLAB. In addition, two 3.9 GHz cryomodules will be assembled at Fermilab. These require 3.9 GHz harmonic cavities for preparing the longitudinal bunch distribution for magnetic compression, based on the successful FLASH design, and are synergistic with the 1.3 GHz cryomodules and cryogenic distribution systems. A risk-based design methodology has been employed to optimize long-term reliability and maintainability of the systems, and all production cryomodules of a given frequency are identical in design and final assembled state. Prototype 1.3 GHz cryomodules are different from production units in cavity and tuner configuration details. Existing assembly and test facilities at JLAB and Fermilab are used, with minimal modifications. After assembly the first 50% of the cryomodules undergo acceptance testing at Fermilab and JLAB before shipping overland to SLAC. Each laboratory is responsible for developing complete documentation and controls for the work performed at the respective laboratories. Once completed and delivered to SLAC, the cryomodules from Fermilab and JLAB are identical in all ways.

The major cryomodule features for both 1.3 GHz and 3.9 GHz cryomodules are:

- Un-segmented “monolithic” cryogenic linac sections with insulating vacuum and cryogenics piping connected directly from one cryomodule to the next
- Cooling circuits at 45 K, 5 K, and 2 K (nominal temperatures)
- Capability for control of cavity cooldown rate within a single cryomodule
- Magnetic shielding to provide very low residual field (<5 mG) at the cavities

Each of the thirty-five 1.3 GHz cryomodules has these components:

- Eight TESLA-style 1.3 GHz accelerating cavities with average $Q_0 = 2.7 \times 10^{10}$ at $E_{acc} = 16$ MV/m
- Superferric 2 K conduction-cooled quadrupole and dipole (H,V) corrector package at the downstream end
- Button-type beam position monitor (BPM) at the downstream end
- Electro-mechanical cavity tuner (end-lever tuner) with stepper motor (slow) and piezo (fast) control mechanisms
- Adjustable coaxial fundamental power coupler (modified TTF input coupler)

- Higher order mode (HOM) couplers on cavities
- Beamline HOM absorber mounted in the beampipe at the downstream end

Each of the two 3.9 GHz cryomodules has these components:

- Eight 3.9 GHz cavities with average $Q_0 = 2.5 \times 10^9$ at $E_{acc} = 15.5$ MV/m
- Cold electro-mechanical end-lever cavity tuner with stepper motor (slow) and piezo (fast) control mechanisms
- Fixed coaxial fundamental power coupler ($Q_{ext} = 2.5 \times 10^7$)
- Higher order mode (HOM) couplers on cavities
- Button-type beam position monitor (BPM) at the downstream end

Engineering, design, procurement, assembly, test, and shipping of cryomodules is accomplished by the LCLS-II collaboration of Fermilab and JLAB (partner labs) working with SLAC. R&D activities include contributions from Cornell University. ANL participate with Fermilab in processing of superconducting cavities. Procurements are made through one laboratory, with delivery to other partner Labs as needed for production. Early procurements have been made for the niobium and niobium-titanium materials needed for cavity fabrication, in order to meet the cavity production schedule.

Cavity production includes a high-temperature nitrogen doping procedure, in order to achieve high quality factor. Members of the cryomodule teams at Fermilab, JLAB, and Cornell are involved in developing the required procedures for production, as discussed in Chapter 16. Test facilities for high-Q cavity development are based on existing superconducting RF infrastructure at partner Labs, including both vertical and horizontal cryostats, with developments to address LCLS-II needs. At Fermilab and JLAB, upgrades of facilities for testing of completed cryomodules are included in the Project.

Changes to XFEL designs to accommodate CW operations include cavity tanks with a larger chimney allowing a greater heat flow to the two-phase helium pipe, and also dual helium input pipes to each cavity helium tank. Each cryomodule has a JT valve for producing 2 K helium from the supply line, and cryogenic circuits to allow controlled cooldown of individual cryomodules. The fundamental power couplers have increased copper plating thickness on the inner conductor between the windows to limit its temperature rise, and a shorter antenna to shift the Q_{ext} range higher. The fundamental power couplers also have adjustable coupling capability, but will not be adjusted during operation. Tuners are end-lever type, with motor control and piezo stacks to provide slow and fast tuning capability optimized for CW operation.

The two prototype 1.3 GHz cryomodules will be assembled from existing cavities and modified tuners and therefore differ somewhat from LCLS-II production cryomodules. One prototype cryomodule is to be built and tested by Fermilab and one by JLAB. Prototype testing begins in 2015, and assembly of production cryomodules begins in 2016. The 3.9 GHz

cryomodule production will be done exclusively at Fermilab, dovetailing with completion of 1.3 GHz cryomodule design, assembly and test activities.

Each partner laboratory is responsible for incoming inspection of all components. Equivalent processes are in place to qualify all components to agreed-upon criteria. Non-conforming components are managed with a graded approach, including participation of representatives from SLAC, Fermilab, and JLAB when appropriate. The major roles and responsibilities are divided amongst participating labs as follows:

SLAC

- Fundamental power couplers for 1.3 GHz cryomodules
- Utilities and civil construction
- Controls interfaces
- Coordination and integration

Fermilab

- Cryomodule engineering and design
- Participation in the high-Q_0 R&D program
- Preparation of ILC cavities for the prototype cryomodules
- Vertical testing of production cavities
- Prototype and production cryomodule testing
- Delivery of one prototype and sixteen production 1.3 GHz cryomodules to SLAC
- Delivery of two 3.9 GHz cryomodules to SLAC

JLAB

- Participation in the high-Q_0 R&D program
- Preparation of ILC cavities for the prototype cryomodules
- Vertical testing of production cavities
- Prototype and production cryomodule testing
- Delivery of one prototype and seventeen production 1.3 GHz cryomodules to SLAC

Cornell

- Participation in the high-Q_0 R&D program

ANL

- Support of Fermilab cavity surface processing with joint superconducting RF cleaning facility
- Support of Fermilab cryomodule engineering and design

The cryomodule design interfaces strongly with the design of low-level RF controls, fundamental power couplers, and high-Q_0 R&D results; each of these are described in detail elsewhere in this document, in Section 10.6, Section 5.12, and Section 16.2, respectively.

High-level systems design requirements, specifications, and interfaces for the cryomodules are captured in the documents shown in Table 6-1. Systems functional requirements flow down from physics requirements, which in turn describe how a system needs to perform and what criteria the system needs to meet to satisfy the *Global Requirements Document* LCLSII-1.1-GR-0018. All of these documents have a formal approval procedure, controlled by the project, and are accessed from the LCLS-II Controlled Documents Site. In addition, this site is a repository for Engineering Notes documenting theoretical, computational, and experimental details of designs.

Table 6-1. Cryomodules systems-level requirements and specifications, and related technical notes

Document Type	Title	Document Number
Physics Requirements	LCLS-II Parameters	LCLSII-1.1-PR-0133
Physics Requirements	Linac Requirements	LCLSII-2.4-PR-0041
Physics Requirements	Availability	LCLSII-1.1-PR-0163
Physics Requirements	SCRF 1.3 GHz cryomodules	LCLSII-4.1-PR-0146
Physics Requirements	3.9 GHz cryomodules	LCLSII-4.1-PR-0097
Physics Requirements	RF power and LLRF requirements	LCLSII-4.1-PR-0098
Physics Requirements	Magnets	LCLSII-2.4-PR-0081
Physics Requirements	Steering Correctors	LCLSII-2.4-PR-0082
Physics Requirements	Beam Position Monitor	LCLSII-2.4-PR-0136
Functional Requirements Specifications	1.3 GHz Superconducting RF Cryomodule	LCLSII-4.5-FR-0053
Functional Requirements Specifications	3.9 GHz Superconducting RF Cryomodule	LCLSII-4.1-FR-0096
Interface Control	Cryogenic Distribution System	LCLSII-4.9-IC-0058
Interface Control	Accelerator Systems to Cryogenic Systems	LCLSII-2.5-IC-0056
Interface Control	Electron Beam Controls To Accelerator Systems, Cryogenic Systems, Photon Systems, and Infrastructure Systems	LCLSII-2.7-IC-0266
Interface Control	1.3 GHz Cryomodule interface requirements	LCLSII-2.5-IC-0312
Project Management Note	High-Q_0 R&D Plan	LCLSII-2.6-PM-0052
Engineering Note	LCLS-II Cryogenic Heat Load	LCLSII-4.5-EN-0179
Engineering Note	Operating temperature	LCLSII-4.5-EN-0185
Engineering Note	Cryomodule design methodology	LCLSII-4.5-EN-0186
Engineering Note	High-Q development plan and choice of Q_0	LCLSII-4.5-EN-0216
Engineering Note	Gradient optimization	LCLSII-4.5-EN-0217

Engineering Note	N-doping process – physics and technique	LCLSII-4.5-EN-0218
Engineering Note	Peak detuning and Q_{ext}	LCLSII-4.5-EN-0219
Engineering Note	Power sources and distribution configurations	LCLSII-4.5-EN-0220
Engineering Note	Tuner electro-mechanical design	LCLSII-4.5-EN-0221
Engineering Note	Magnetic Shielding: Requirements and Possible Solutions	LCLSII-4.5-EN-0222
Engineering Note	Monte Carlo Linac Evaluation and Optimization	LCLSII-4.5-EN-0223
Engineering Note	Horizontal tests of dressed cavities	LCLSII-4.5-EN-0224
Engineering Note	A Study of Magnetic Shielding Performance of a Fermilab International Linear Collider Superconducting RF Cavity Cryomodule	LCLSII-4.5-EN-0310
Engineering Note	Vibration Measurements at the JLAB Cryoplant and Linac	LCLSII-4.8-EN-0326
Engineering Note	Cryomodule Seismic Design Criteria	LCLSII-4.5-EN-0226
Engineering Note	Pressure System Requirements per ES&H Manual Chapter 14	LCLSII-1.2-EN-0020
Engineering Note	Cryogenic and Oxygen Deficiency Hazards Requirements per ES&H Manual Chapter 36	LCLSII-1.2-EN-0063
Engineering Note	LCLS-II Commitments via Environmental Assessment	LCLSII-1.2-EN-0250

The schedule for major design reviews is given in Table 6-2. Figure 6-1 shows the overall schedule for cryogenic plant and distribution systems.

Table 6-2. Cryomodules Design Review Schedule.

System	Component	Review	Date
Cryogenics Systems	Cryogenics Systems	Preliminary Design Review	August 2014
Cryomodules	1.3 GHz Prototype Cryomodule & Dressed Cavity	Final Design Review	January 2015
	1.3 GHz Production Cryomodule	Final Design Review	April 2015
	3.9 GHz Cryomodule	Final Design Review	June 2016

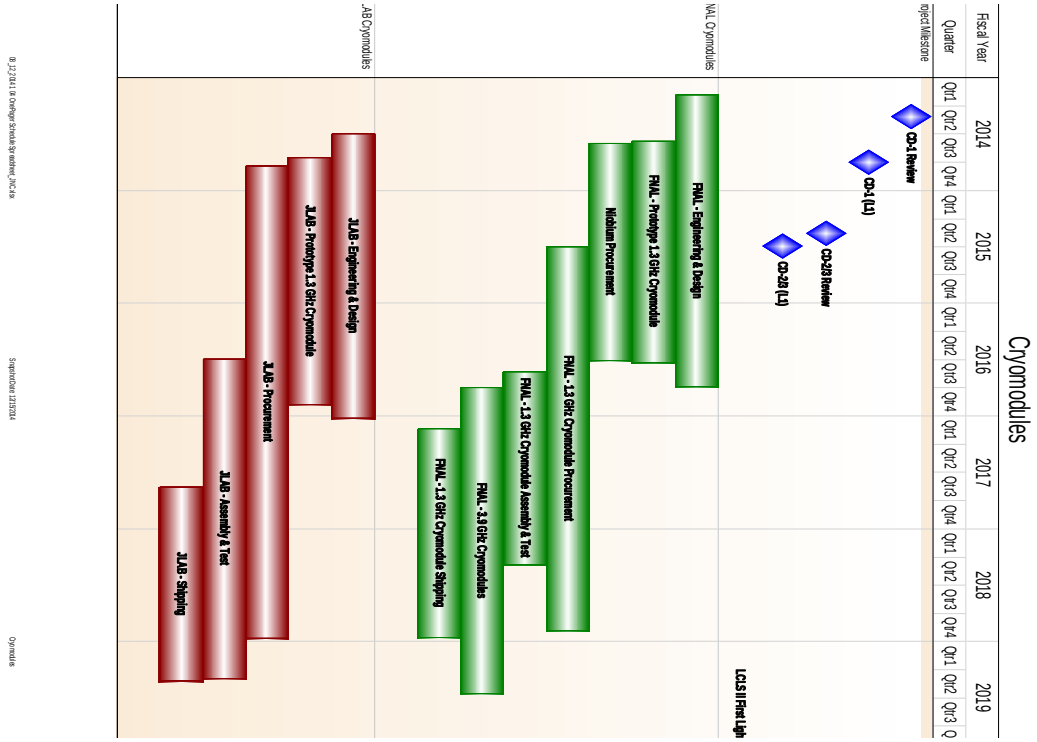

Figure 6-1. Cryomodule Production Schedule

6.1.1 Design Maturity

The LCLS-II Project Final Design Plan LCLSII-1.1-QA-0065 provides for a phased completion of the final designs for the LCLS-II facility. The plan ensures that designs are sufficiently mature to start procurements and construction, while enabling the most cost-effective schedule for constructing the facility and maximizing the technical capabilities of the facility at CD-4. Final design readiness at CD-3 recognizes that that not all subsystems will reach final design at the same time. Project-level requirements and interface control points between Accelerator Systems, Cryogenic Systems, Photon Systems and Infrastructure are defined at CD-3, which ensures that the phased procurements and construction are appropriate for the final design of the LCLS-II. Chapter 2, Project Overview, contains additional discussion of the approach to design completion. The Cryogenic Systems design, described in this chapter and Chapter 7, is evaluated to be 80% complete. Completing remaining design after CD-3 allows for advancement of project schedule and minimizing cost by starting long duration activities when associate designs are sufficiently mature.

6.2 Design of 1.3 GHz Cryomodule Design

6.2.1 Requirements

Each 1.3 GHz cryomodule contains eight 1.3 GHz 9-cell TESLA-type cavities, a combined quadrupole and X and Y dipole correctors, a BPM, and in the interconnect region a beamline HOM absorber, as described in *SCRF 1.3 GHz Cryomodule Physics Requirements Document* LCLSII-4.1-PR-0146. The cryomodules are designed to operate the cavities at 2 K, transfer heat

to the cryogenic fluids with a cavity Q_0 of $2.7x10^{10}$ at 16 MV/m in CW mode, and also absorb additional beam induced heat. The linac provides installed redundancy of approximately 6% of the cavities, and they may be powered at lower gradient to reduce the total heatload. The cavities are qualified at a voltage of at least 18 MV/m CW without quench or onset of significant field emission. RF cavity phase and amplitude stability tolerances are a function of location along the LCLS-II, as specified in the *Linac Requirements* PRD LCLSII-2.4-PR-0041. Each cavity package includes two HOM couplers that damp the deleterious trapped monopole and dipole HOMs to reduce the loaded Q value below $\sim 1x10^{6}$. The quadrupoles and dipole correctors are sized to allow up to 10 GeV beam operation, for a possible future upgrade. Physics requirements for the quadrupoles, steering magnets, and BPMs are summarized in the respective sections below.

The 1.3 GHz superconducting RF Cryomodule functional requirements, documented in LCLSII-4.5-FR-0053, are divided into sections covering the following topics: operational, mechanical, cryogenic, beam tube, insulating vacuum, coupler vacuum, tuner, magnets, coupler, magnetic shielding, beam line absorber and beam position monitor. The 1.3 GHz Cryomodule interface requirements are documented in LCLSII-2.5-IC-0312.

Engineering for the 1.3 GHz cryomodule is being performed at Fermilab and began prior to the LCLS-II Project. The engineering is being performed in accordance with the Fermilab Engineering Manual, which is consistent with the engineering process documented for the project in the *LCLS–II Systems Engineering Management Plan* LCLSII-1.1-PM-0043. Table 6-3 lists the 1.3 GHz cryomodule engineering design reviews.

Table 6-3. 1.3 GHz Cryomodule Engineering Review Schedule

Review	Type	Date
Fundamental power coupler modification	Engineering Peer Review	Feb 07, 2014
Fundamental power coupler	Final Design Review	Aug 29, 2014
Prototype 1.3 GHz cryomodule dressed cavity design	Engineering Peer Review	Apr 15, 2014
Niobium pre-procurement	Engineering Peer Review	Apr 17, 2014
Niobium	Procurement Readiness Review	May 16, 2014
Prototype 1.3 GHz cryomodule	Engineering Peer Review	Jun 06, 2014
Cryogenic Systems	Preliminary Design Review, Integrated Safety Review	Aug 13-15, 2014
Prototype 1.3 GHz cryomodule	Final Design Review	Jan, 2015
Production 1.3 GHz cryomodule	Final Design Review	Apr, 2015
1.3 GHz cryomodule production readiness		Jun, 2016

Superconducting RF (SRF) cavities have pressure code compliance complications due to materials, welding and testing issues. In order to ensure an equivalent level of safety to the ASME pressure code as required by 10 CFR 851, specific guidelines have been developed for SRF cavities. The LCLS-II SRF cavities are designed and tested in accordance with Dressed Niobium

SRF Cavity Pressure Safety, Fermilab ES&H Manual Chapter 5031.6. The LCLS-II Project has reviewed and accepted this approach as documented in LCLSII-1.2-EN-0020.

The LCLS-II Project is built in an area that experiences seismic activity. As a result, special design requirements have been developed and are specified in *Cryomodule Seismic Design Criteria*, LCLSII-4.5-EN-0226. The criteria are established to ensure life-safety, and for moderate earthquakes to also minimize non-structural damage.

The heat load presented to the 2 K cryogenic system is dominated by the dynamic losses in the SRF cavities. The dynamic losses are characterized by the unloaded quality factor, Q_0. An average quality factor of 2.7×10^{10} has been established which allows the cold linac to be cooled by an existing cryogenic plant design. An R&D plan, *High-Q_0 R&D Plan* LCLSII-8.2-PM-0052, was performed to verify the cavity processing recipe and to understand any cryomodule design changes that were required to best be able to achieve the required Q_0 in the installed linac.

Procurement requirements for the LCLS-II Project have been formalized in the *Procurement Plan*, LCLSII-1.1-PM-0032. This document states the thresholds that trigger the requirements for an advanced procurement plan as well as a procurement readiness review. Based on this plan, a 1.3 GHz cryomodule components procurement plan, LCLSII-4.1-PM-0229, has been developed. This plan defines how cryomodule procurement responsibilities are divided between Fermilab and JLAB.. Components are delivered directly to both labs from the vendors. Technical representatives for each procurement have been established at both labs in order to ensure consistent QA and QC.

6.2.2 Prototype Cryomodules

Fermilab and JLAB will each build a prototype 1.3 GHz cryomodule, prior to the production run of the remaining 33 cryomodules. The primary purposes of the prototypes are to: 1) test the cryomodule design modifications as soon as possible, 2) prove out the JLAB infrastructure modifications; and 3) develop procedures and travelers, train staff, etc. The cryomodule schedule is advanced by using existing cavities and couplers, which are long lead time items. Note that tests of these prototypes come too late to incorporate design modifications into the production cryomodule design, but they can affect the assembly procedures used.

The prototype cryomodules take advantage of 16 existing Fermilab ILC 9-cell cavities, which were purchased largely with the 2009 Americas Recovery and Reinvestment Act funding. These cavities are slightly different from the LCLS-II cavities, in that they have beam tubes of equal lengths, which has implications for the tuner design and results in differences between the prototype and production cryomodule dressed cavity details. Functionality of the prototype cryomodules, however, is the same as that of production cryomodules as they will be used in the LCLS-II linac.

The XFEL-style end-lever tuner, which nominally requires a longer beam tube, has been redesigned to fit the prototype cryomodule cavities, and to permit access through ports that will be added to the cryostat. Existing ILC power couplers (16 cold parts, and a fraction of the warm

parts, with the remaining warm parts being purchased) are being modified for CW operation for use in these prototypes. The vast majority of the cryomechanical design for the prototype cryomodule is identical to that of the production cryomodule.

6.2.3 Cryomodule Mechanical and Cryogenics Design

6.2.3.1 Cryomodule Design Introduction

An XFEL-style cryomodule (very similar to a TESLA/ILC type 3+ cryomodule), modified for CW operation, was selected as a baseline concept in order to provide as efficient and quick a start as possible for cryomodule design and production. In a string configuration, they provide an un-segmented, "monolithic" cryogenic linac with insulating vacuum and piping connected from one cryomodule to the next.

The RF cavities are welded into titanium helium vessels, which are filled with 2 K saturated liquid helium, surrounding the RF cavities. Each cryomodule includes eight RF cavities, one superferric (cold) quadrupole combined with a corrector magnet package consisting of horizontal and vertical dipole correctors, and a cold beam position monitor. The LCLS-II cryomodules are 12.22 m long. Each dressed cavity incorporates a cold, electro-mechanical, end-lever tuner of the design used by XFEL, and an adjustable coaxial coupler. A CAD model of the LCLS-II cryomodule with various internal lines and other features labeled is shown in Figure 6-2. Like the TESLA/ILC dressed cavities, the maximum allowable working pressures are be 4 bar cold, 2 bar warm for the helium vessels and associated piping, and 20 bar for other piping.

Several significant differences from the XFEL (or Type 3+) design are necessary to meet LCLS-II requirements. Heat loads greater than 10 W per cavity at 2 K, with eight cavities per cryomodule, as opposed to 1-2 W per cavity for XFEL, result in some thermal and helium flow considerations which force changes from the XFEL design. Changes include increasing sizes of some pipes to allow conduction of the heat from the cavities through the superfluid helium, limiting the length of the 2 K 2-phase bath, omitting the 5 K radiation shield, using modified input and HOM couplers and coupler cooling, and adding special cool-down features which help to expel magnetic flux through the superconducting transition. A typical cross-section of the cryomodule modified for LCLS-II is shown in Figure 6-3, with cryogenic lines as labeled in Figure 6-2 CW operation imposes tight constraints on cavity frequency in order to minimize RF power source requirements, and microphonics and cavity frequency variation with pressure are modeled and minimized, as is the magnetic shielding configuration to enable high-Q_0 performance of the cavities described inSection 6.2.11.

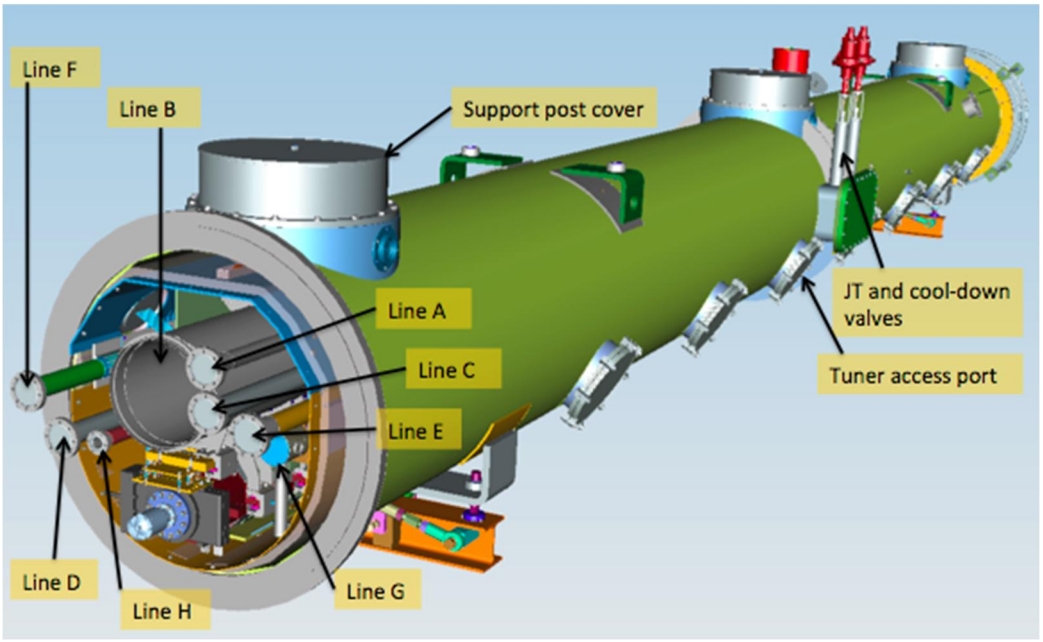

Figure 6-2. Cryomodule assembly, showing cryogenic lines: Line A (sub-cooled helium supply), Line B (gas return pipe), Line C (low temperature intercept supply), Line D (low temperature intercept return), Line E (high temperature shield supply), Line F (high temperature shield return), Line G (two-phase helium), and Line H (warm-up / cool-down).

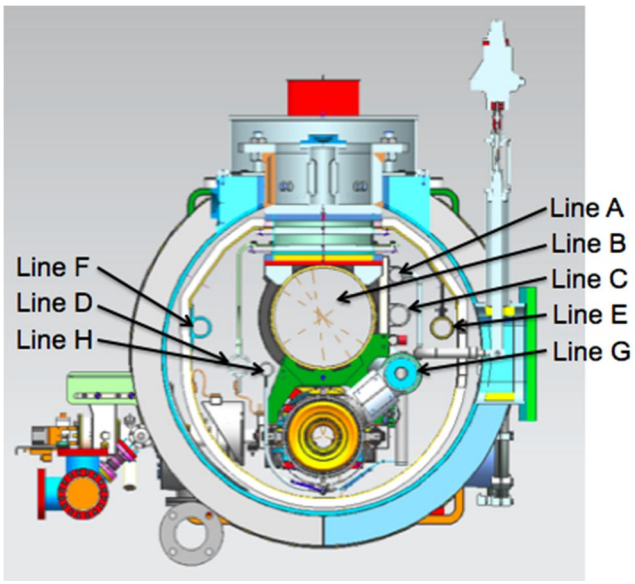

Figure 6-3. Cryomodule cross section, showing cryogenic lines as identified in Figure 6-2 The tuner access ports shown horizontal here will be at an angle for easier access.

Both the relatively large per-cryomodule heat load of 80 W or more at 2 K and the 0.5% SLAC tunnel slope make it desirable to control the 2 K liquid level by increasing in the diameter of the 2-phase pipe (Line G in the above cryomodule figures). Division of the 2 K liquid units at the one-per-cryomodule level is also desirable in order to adequately control helium mass flow

and helium inventory in each cryomodule. The 2-phase pipe size increases to 95 mm ID, compared to 69 mm ID for the ILC cryomodule. Similarly the "chimney" from each helium vessel to the 2-phase pipe is increased to 95 mm ID, compared to 55 mm for XFEL/ILC. The influence of the slope of the SLAC tunnel on liquid level in this larger 2-phase line is illustrated in Figure 6-4.

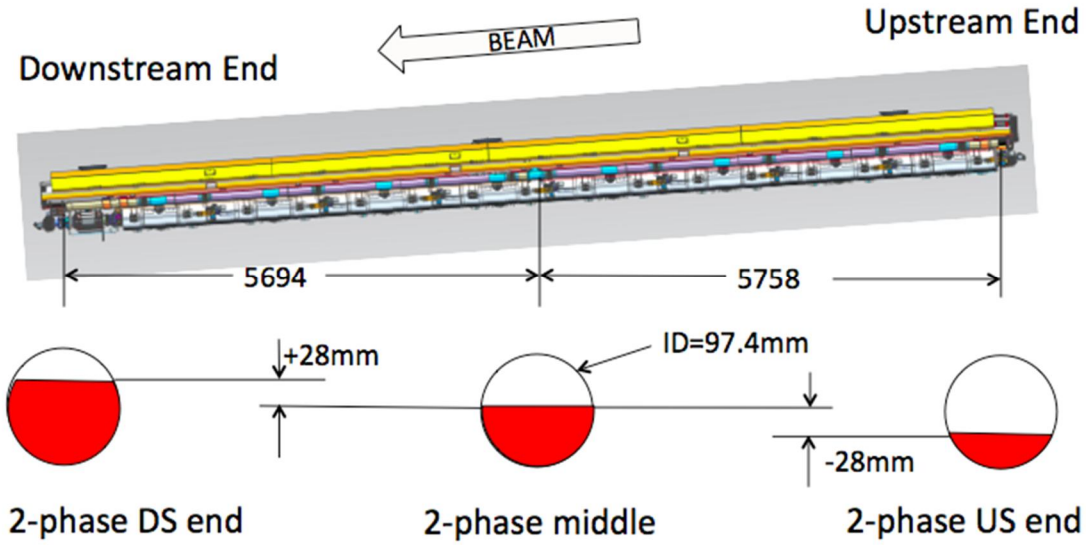

Figure 6-4. Liquid levels in the 2-phase pipe with 0.5% SLAC tunnel slope, with pipe sized to accommodate liquid levels both downstream (DS) and upstream (US).

Each dressed cavity contains about 27 liters of liquid helium, for a total of 214 liters for the eight cavities in a cryomodule. The cryogen pipes contain another 134 liquid liters equivalent helium mass, so a cryomodule total inventory is about 348 liquid liters. Thus, the 37 cryomodules in the linac contain in total about 13,000 liquid liters equivalent mass of helium. This amount of liquid helium is not very large compared to other large cryogenic systems for accelerators, less than the amount required at the Tevatron or CEBAF.

6.2.3.2 Cryo-mechanical safety and code compliance

Emergency venting has been carefully analyzed to assess influence on line sizes, cryomodule features, and Oxygen Deficiency Hazards (ODH). Large flow rates may be generated by loss of insulating or beam pipe vacuum, and the helium space surrounding the RF cavities is only rated for a 4 bar maximum differential pressure. Accommodating these large flow rates can affect pipe sizing in the cryomodule. Similarly, emergency venting for the long runs of thermal shield and intercept supply and return lines, which run continuously through the cryomodules in each half of the linac, may have an influence on line diameters beyond that required for steady-state operation. Pipes are sized consistent with the design goal of not incorporating helium vent valves in each cryomodule, but rather constraining those only to distribution end boxes, for the sake of cryomodule design simplicity and in order to more easily to duct vented helium out of the tunnel so as to reduce the ODH risk.

Pressure vessels and piping must meet DOE, SLAC, and partner laboratory standards. The Fermilab ES&H manual, section 5000, includes standards for cryogenic system safety, pressure vessels, SRF dressed cavities, vacuum vessels, oxygen deficiency hazards (ODH), and more. SLAC, Fermilab, and JLAB will agree upon a common set of standards based on these, as well as standards used at other partner labs. The baseline is to use Fermilab safety requirements. The helium vessel around the cavity is the pressure containment vessel, and hence must meet SRF pressure vessel standards, and the piping must also meet pressure piping standards.

Seismic analysis is also required for the location at SLAC. Fermilab is presently doing mechanical analyses of a cryomodule assembly under various acceleration and/or oscillatory modes as required by SLAC. These are also needed for design for shipping.

6.2.3.3 Q_0 preservation requirements

In order to produce manageable heat loads at 2 Kelvin within existing cryogenic plant size, LCLS-II requires a high cavity unloaded quality factor of Q_0 of 2.7×10^{10} or greater, on average. Preservation of this high-Q_0 requires that the superconducting niobium cavities include minimal trapped magnetic flux, which can be achieved by using magnetic shielding that keeps the ambient fields at the cavity below 5 mG. Magnetic field reduction may include active external coils (see Section6.2.11), although this is not currently in the baseline design. The helium vessel "chimney" has been slightly offset to place it over a cavity iris, rather than equator, to help mitigate the effects of the interruption in magnetic shielding at the chimney.

RF cavity tests as part of the high-Q_0 R&D program have shown that a large temperature gradient across the cavity diameter during cool-down can sweep out trapped magnetic flux, even in the presence of tens-of-mG residual magnetic field at the cavities. Optimal cool-down flow rates for most effectively sweeping out the trapped magnetic flux are under study in horizontal test cryostats. The need for relatively high flow rates in the helium vessels to produce the desired large temperature gradients requires that cryomodules are cooled individually. Figure 6-5 shows the presence of a cool-down valve in each cryomodule in addition to the separate JT valve for liquid level control in each cryomodule.

Horizontal tests at Cornell have shown that uniform cooling of the bimetallic joints at each end of the cavity does provide important suppression of thermally induced currents which generate internal magnetic fields that result in harmful trapped flux. Thus, the design for symmetrically located dual cool-down supply ports and a (nearly) centrally located "chimney" connecting to the 2-phase pipe on each cavity (shown in Figure 6-6) have been shown to be good choices for high-Q_0 preservation.

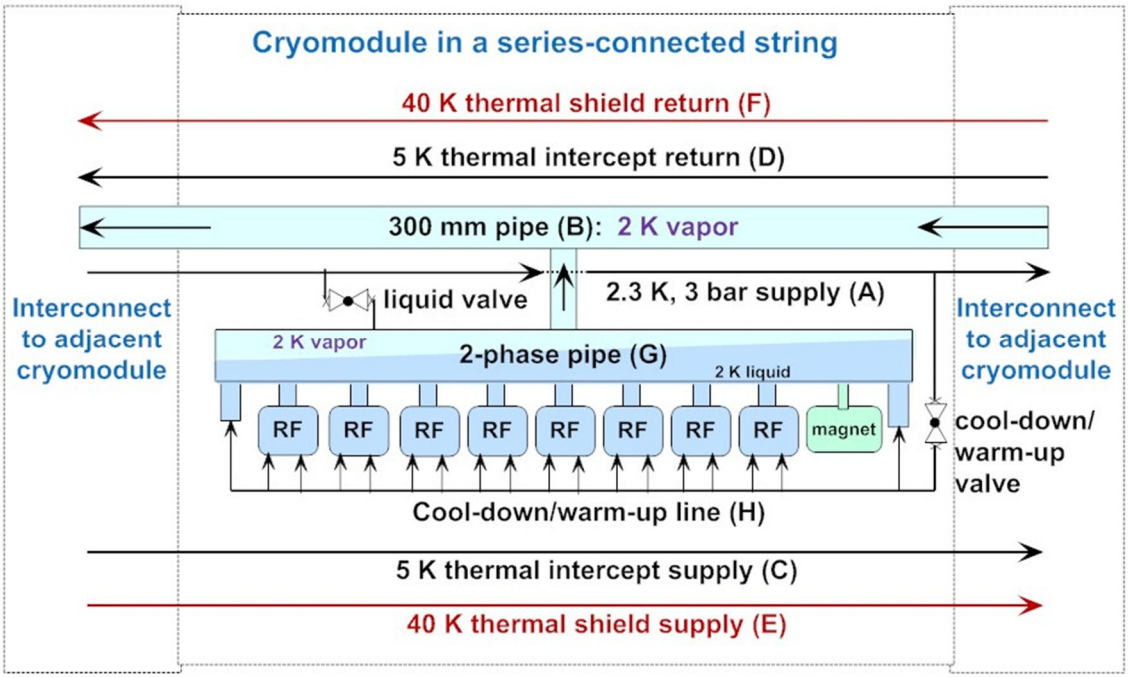

Figure 6-5. Cryomodule helium flow schematic

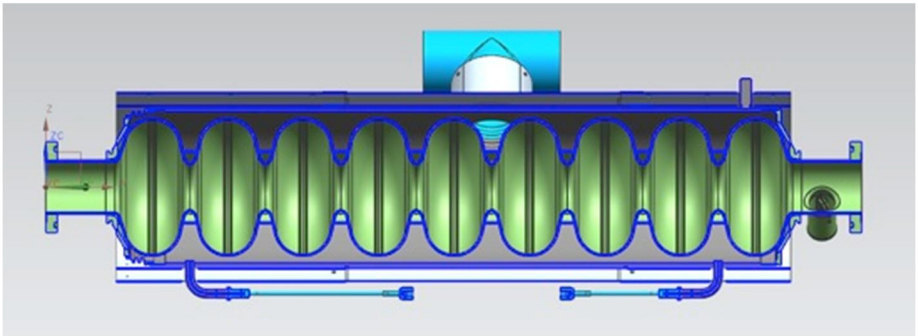

Figure 6-6. Helium vessel design with two cool-down supply ports and a (nearly) centrally located connection to the 2-phase line for symmetric cooldown.

6.2.3.4 Tuner access ports

The Fermilab end lever tuner for the prototype cryomodules is designed to allow access to critical components after the cryomodule is warmed up and vented, via access ports on the cryomodule. Spallation Neutron Source (SNS) cryomodules successfully incorporated such access ports, which proved to be useful, and the Cornell energy recovery linac (ERL) injector cryomodule also includes tuner access ports. The ports on the LCLS-II cryomodules allow access to the tuner motor, drive mechanism, and piezos without pulling the cavity string out of cryostat. These ports must be on the opposite side from the input couplers. Although this is the wall side in the SLAC tunnel, the SLAC and Fermilab cryomodule models plus tunnel mockups indicate that these ports provide practical access. Ports also allow access during tests on the cryomodule test stand.

The ports do not enable access to XFEL-type end-lever tuner parts, as will be used in the production cryomodules, and these access ports are only useful for the Fermilab tuner. The two prototype cryomodules incorporate the Fermilab tuners and short-ended ILC cavities, and include access ports which mitigate the risk of problems with the new tuner design.

6.2.3.5 Pipe sizes

LCLS-II cryomodule pipes are sized not only for steady-state flow conditions but also for cool-down, warm-up, and emergency venting flow rates. Line sizes for the cryomodule are shown in Table 6-4.

Table 6-4. Cryogenic lines in the cryomodules.

Line	Description	Pipe ID [mm]	Design Pressure [bar]	Operating Temperature [K]
A	Helium Supply	54.8	20	2.3
B	Helium Gas Return	300	4	2
C	Low Temperature Intercept Supply	54.8	20	5
D	Low Temperature Intercept Return	50.8	20	5
E	High Temperature Shield Supply	54.8	20	40
F	High Temperature Shield Return	52.5	20	40
G	Two Phase Pipe	97.4	4	2
H	Cooldown Line	38.9	4	5

The helium circuits in the cryomodule and distribution system are analyzed together. Analyses of each circuit have been done to ensure the circuit can accommodate the necessary heat loads and flow rates defined in engineering note LCLSII-4.5-EN-0179. The operating modes include a “fast” cooldown, where a large flow of helium is supplied to a number of cryomodules through the cooldown valve that has been added to each cryomodule. Emergency venting of each line has been analyzed to determine the location of rupture disks and relief valves to protect the circuit in failure scenarios such as loss of beam-line vacuum or loss of insulating vacuum.

6.2.3.6 Cryomodule alignment

Upon cooldown, the LCLS-II cryomodules must retain the cavity alignment within required RMS error of 0.5 mm transversely and laterally as described in the *SCRF 1.3 GHz Cryomodule Physics Requirements Document* LCLSII-4.1-PR-0146 and also provide external reference fiducials (see Figure 6-7) to permit proper positioning of the internal cavity strings and magnets in the linac. Each cryomodule includes alignment socket locations at each end and in the middle.

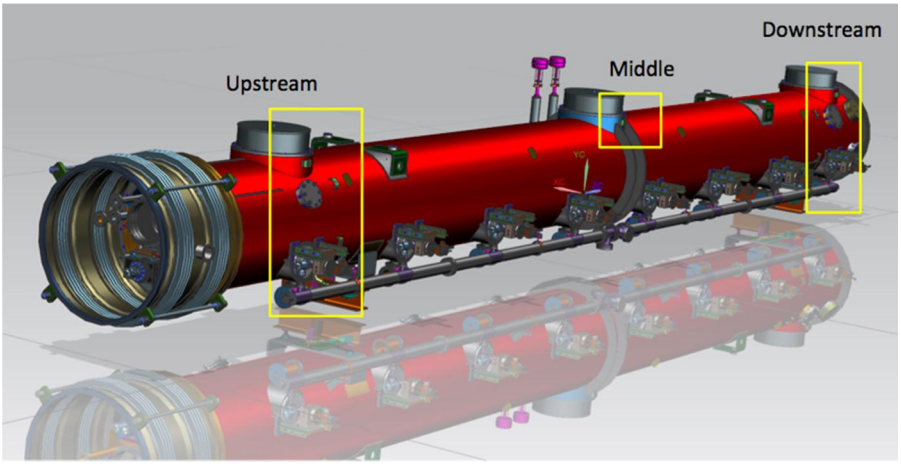

Figure 6-7. Alignment socket locations for cryomodule alignment

6.2.4 Cavity Design

The TESLA 9-cell superconducting cavity is the baseline design for LCLS-II. This cavity design was introduced in the early 1990s [1] with the main goal of achieving a high gradient that would lower the cost of very long linacs operated in the TeV energy regime. The TESLA cavity was designed to achieve a low peak surface electric field to accelerating field ratio in order to reduce field emission, a primary gradient-limiting mechanism devised two decades ago. Since then, significant progress has been made in overcoming the field emission limit as well as other limits, such as quench limit and high field Q-slope limit [2, 3]. Significant experience in TESLA cavities has been accumulated at DESY, in the TESLA Test Facility (TTF) which later became FLASH. Currently, 800 9-cell TESLA cavities are being industrially produced for the European XFEL project. The TESLA cavity has also been adopted for the ILC, which has driven development of high-gradient SRF cavities and other SRF components and systems and associated infrastructures. A major achievement in SRF cavity development is the realization of repeatable and reliable cavity processing procedures, leading to the demonstration of 45% (75%) production yield for gradients > 35 MV/m and $Q_0 > 8\times10^9$ for single pass (two pass) processing and vertical qualification testing. By the time of publication of the ILC Technical Design Report (TDR) in June 2013 [4], a global SRF expertise and infrastructure was established. U.S. industry, amongst others, is qualified to manufacture the 9-cell ILC cavities, and SRF facilities at JLAB, Fermilab/ANL are qualified to process and test full-scale 9-cell cavities with throughput considered to be appropriate for LCLS-II. The high-Q_0 surface process adopted for LCLS-II is described in Chapter 16.

The TESLA/ILC cavity is shown in Figure 6-8. It operates in π mode at a resonant frequency of 1300 MHz, and consists of nine accelerating cells between two end group sections. One end group has a port for coupling RF power into the structure, and the other end has a port for a field sampling probe used to measure the cavity field. Each end group also has a higher order mode (HOM) coupler structure with a probe port for extracting HOM power which can also be used for diagnostics. The main parameters of a TESLA 9-cell cavity are given in Table 6-5.

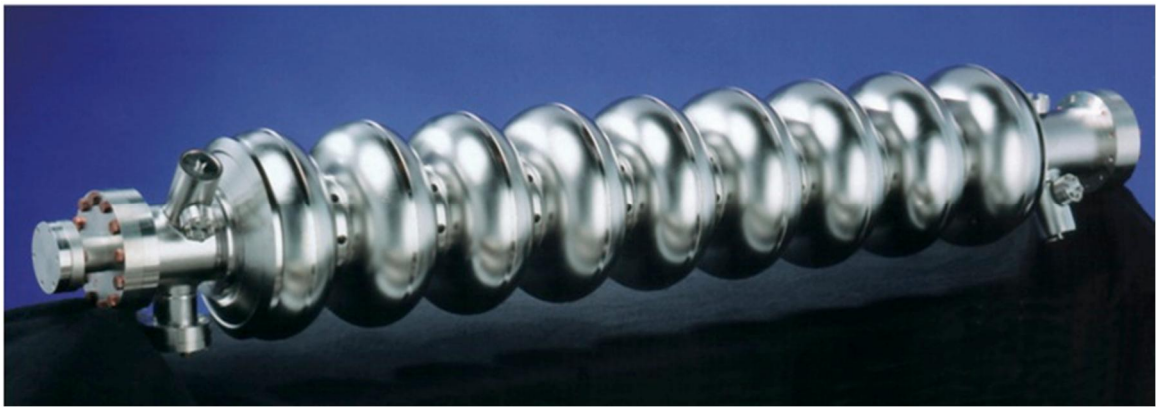

Figure 6-8. LCLS-II baseline cavity: TESLA style 9-cell niobium cavity.

Table 6-5. TESLA Cavity Detailed Parameters.

Parameter	Value
Type of accelerating structure	Standing wave
Accelerating mode	TM010, π-mode
Type of cavity-cell shape	Tesla - type
Number of cells	9
Total length	1247 mm
Effective length	1038 mm
Iris diameter	70 mm
Beam pipe diameter	78 mm
Cell to cell coupling	1.87%
R/Q (r/Q)	1036 Ω (998 Ω/m)
Geometry constant	270 Ω
Lorentz detuning	≤1.5 Hz/(MV/m)^2
B_{peak}/E_{acc}	4.26 mT/(MV/m)
Δf/ΔL	315 kHz/mm
Number of HOM couplers	2
Q_{ext} for high-impedance HOM	< 10^6

With the recent development of advanced surface processing and cleaning procedures, field emission in the gradient range of 14-16 MV/m needed for LCLS-II operations is not expected to be a limitation. The captured current is expected to be less than 1 nA per cryomodule, and this current will mostly be swept out of the beam pipe by the quadrupole magnets.

Considering that LCLS-II cavities are operated in CW mode, as opposed to the pulsed mode at XFEL or ILC, the heating at the end groups and HOM pickup probe requires careful mitigation. The feedthroughs are described in Section 6.2.6; and the F-shaped part of the HOM assembly, which is integral to the cavity design, is unchanged.

Niobium with a RRR ≥ 300 is used to fabricate the cavities, with impurity requirements as shown in Table 6-6.

Table 6-6. Typical Properties of High-Purity Niobium Used in XFEL/ILC Cavities.

Element	Impurity content in ppm (wt)	Property affected by impurity	Requirement
Ta	≤500	RRR	≥300
W	≤70	Grain size	≈50 μm
Ti	≤50	Yield strength	>50 MPa
Fe	≤30	Tensile strength	100 MPa
Mo	≤50	Elongation at break	30%
Ni	≤30	Vickers hardness	
H	≤2	HV 10	≤50
N	≤10		
O	≤10		
C	≤10		

Use of the existing TESLA cavity design allows LCLS-II to benefit from extensive development and widespread experience with this technology. Additionally, incorporating recent advances in nitrogen-doping processing of the cavities increases Q_0, allowing cost-effective operation at a temperature of 2 K and lowering the overall cost for the cryogenic systems. The doping process involves adding a small partial pressure (~mTorr) of nitrogen added to the furnace for few minutes at the end of the standard 800°C degassing cycle in ultra-high vacuum, and is described in engineering notes *N-doping Process – Physics and Technique* LCLSII-4.5-EN-0218 and *High-Q Development Plan and Choice of Q_0* LCLSII-4.5-EN-0216. Following the bake in a nitrogen atmosphere, a light electropolish is applied and only a few microns of the cavity surface are removed. Doping of the surface with nitrogen interstitials in this way effectively reduces the residual resistance and the Q_0 approaches that given by the BCS limit. Cavities produced in the high-Q_0 R&D program yield an average Q_0 of 3.4×10^{10} at 16 MV/m (see Chapter 16) indicating that the design Q_0 of 2.7×10^{10} at 2 K is attainable.

6.2.5 Cavity Tuner

The functional requirements for the LCLS-II 1.3 GHz cavity tuner are presented in Table 6-7. The Fermilab-designed tuner for the prototype cryomodules is a modified version of the Saclay-I compound lever mechanical tuner design [5], and is shown schematically in Figure 6-9, and as a 3D model in Figure 6-10. Details are given in the engineering note *Tuner Electro-Mechanical Design* LCLSII-4.5-EN-0221. Production cryomodules are planned to use the Saclay-I tuner design.

Table 6-7. Tuner Functional Requirements Specifications.

Parameter	Value
Slow Tuner maximum range	1.3mm/ 420kHz
Slow tuning sensitivity	1-2 Hz/step
Fast (Piezo) Tuner maximum range	1kHz/3□m
Fast (Piezo) Tuner tuning resolution	1Hz/3nm
Fast Tuner response bandwidth	5kHz
Minimum tuner stiffness	30N/□m
Minimum tuner mechanical resonance	5kHz
Tuner operating condition	Insulating vacuum, T=20-60K
Slow Tuner motor/actuator spindle rotations expected over 20 years	1000
Fast/piezo Tuner lifetime	$5x10^9$ pulses

The tuner allows the resonant frequency of each cavity to be precisely tuned to the desired frequency by applying an axial force across the cavity. The Fermilab tuner has two key design characteristics different from the Saclay I tuner: 1) the active elements of the tuner (motor and piezo) can be replaced through a designated port in the cryomodule wall, and 2) the piezo stroke is directly translated to the cavity flange, which is important for dynamic control of the narrow-band cavity.

A tuner is mounted on each cavity on the end opposite the power coupler. A stepper motor drives a lead-screw through a planetary gearbox, providing slow or “static” tuning. As the lead-screw turns, it applies a force between the helium vessel and the cavity beam tube flange via a compound lever with ratio of 1:20. The operation of the tuner is shown schematically in Figure 6-9. As the motor operates it applies pressure to the cavity, changing its length. The 1.3 mm maximum stroke of the slow tuner provides the required static tuning range of 440 kHz.

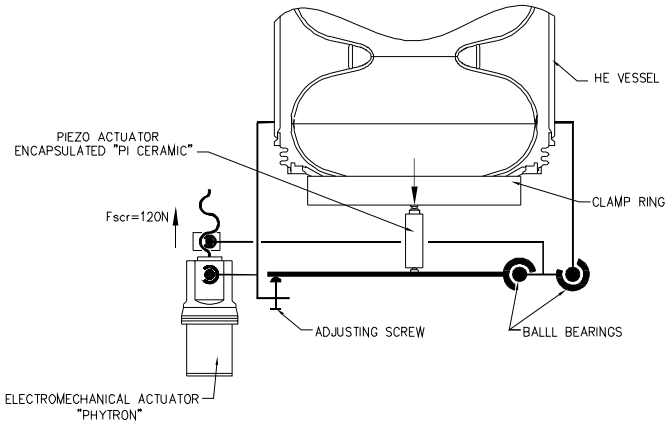

Figure 6-9. Fermilab tuner design schematic.

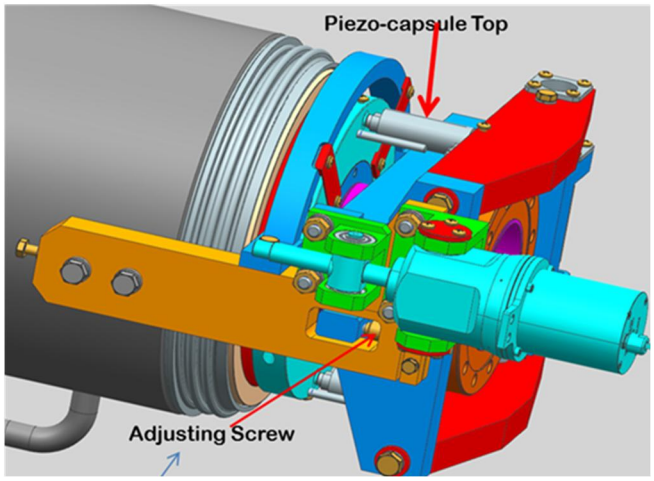

Figure 6-10. 3-D model of the Fermilab tuner.

Prototypes of the Fermilab tuner have been procured and are under test. A photograph of one of the prototype tuners is shown in Figure 6-11.

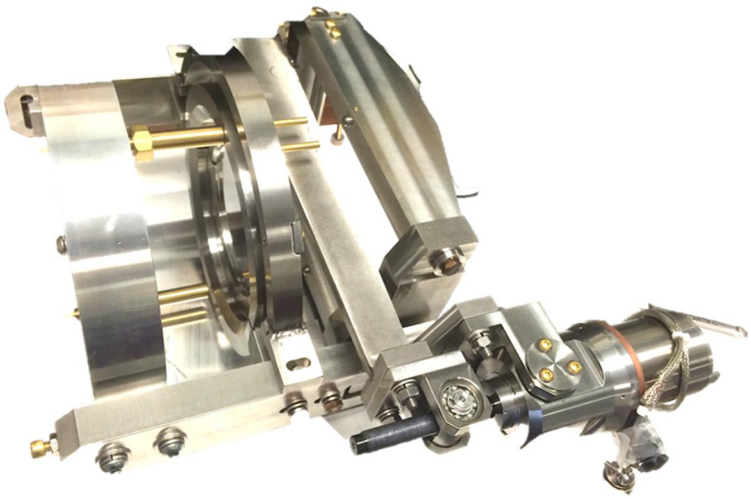

Figure 6-11. Photograph of a prototype Fermilab Tuner.

The slow actuator for the tuner consists of an integrated vacuum rated stepper-motor/planetary-gearbox/lead-screw assembly manufactured to specifications provided by Fermilab. The reliability of the actuator has been confirmed by extensive cold testing in the Fermilab HTS for 5000 spindle rotations, the equivalent of more than five times the expected lifetime at LCLS-II, and for pulsed operation with incremental movements of the spindle.

Dynamic or "fine" tuning is provided by encapsulated piezo actuators in the top and bottom linkages that transmit the force from the lever to the beam tube flange. A 3D model of the piezo actuator assembly is shown in Figure 6-12 (left), together with the piezo actuator itself (right). Each encapsulated piezo actuator is assembled from two piezo-stacks glued together, each $10x10x18mm^3$. Using two actuators provides redundancy in the event of single-piezo failure. The piezo elements are encapsulated to minimize shear forces, which might lead to damage. In the

expected operating temperature range, 10-20 K, individual piezo actuators at maximum operating piezo voltage of 120 V provide a stroke of ~6-7 μm, corresponding to a cavity dynamic tuning range of ~2-3 kHz. To achieve the required dynamic tuning range of 1 kHz, the piezo-stack can be driven with a reduced voltage of ~40-60V on each piezo actuator, which significantly increases the lifetime of the fast tuner.

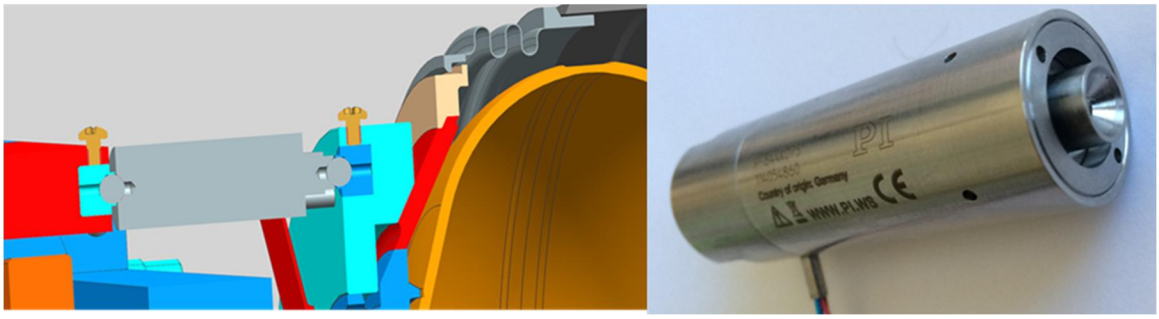

Figure 6-12. 3-D model of encapsulated piezo-stack assembly, shown in gray, on the Fermilab tuner (left). Photograph of the encapsulated piezo stack (right).

6.2.6 Cavity Endgroups

Cavity endgroups contain two HOM couplers (one per side), a port for the fundamental power coupler and a port for pick-up antenna (field probe), as shown in Figure 6-13.

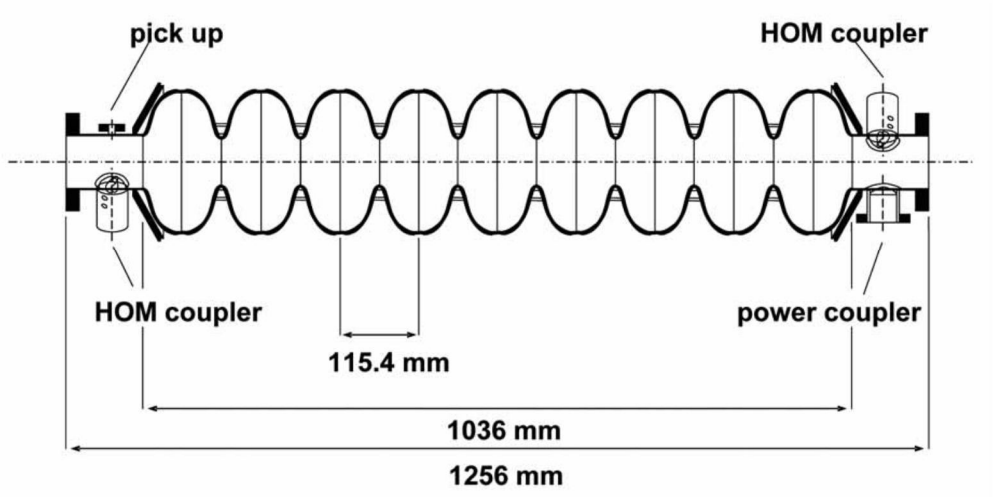

Figure 6-13. TESLA-style niobium 9-cell cavity with end-groups, containing the couplers and pickup ports. The endgroups are conductively cooled from the cavity, which is immersed in liquid helium, and HOM feed-throughs and power coupler are also cooled by thermal straps (not shown).

6.2.6.1 HOM coupler

The spectrum of the electron bunch reaches very high frequencies of up to 15 THz due to the short length (σ_z = 9 μm) of the accelerated bunches. Two types of devices, HOM couplers and beam pipe absorbers, manage this power and minimize its dissipation in the 2 K environment. Monopole and dipole modes below the cut-off frequency of the interconnecting beam tubes (the

non-propagating part of the spectrum) are damped by the cavity HOM couplers [6] of which two are attached to each cavity, one at either end, roughly 90 deg rotated in azimuth.

A modified DESY HOM coupler design has been determined to be suitable for LCLS-II. This design [7] provides damping with $Q_{ext} < 10^6$ for all monopole and dipole higher order modes that are trapped in a cavity, and is proven for pulsed operation up to 40 MV/m. For CW operation, heat transfer from the coupling antenna, which sits at a node of the fundamental mode, to the 2 K cavity was improved, and thermal straps were added between the antenna feedthrough and the 2 K supply line. The HOM feedthrough thermal conduction from the center pin has been improved by JLAB with sapphire ceramics, a molybdenum pin and copper heat sink. DESY developed a similar improved feedthrough design for CW applications in XFEL, as shown in Figure 6-14. Two versions of feedthroughs developed by DESY/Kyocera and JLAB are shown in Figure 6-15. Both feedthrough designs were tested in the Horizontal Test Stand (HTS) at Fermilab and meet requirements for LCLS-II, and beyond with accelerating gradient up to 23 MV/m.

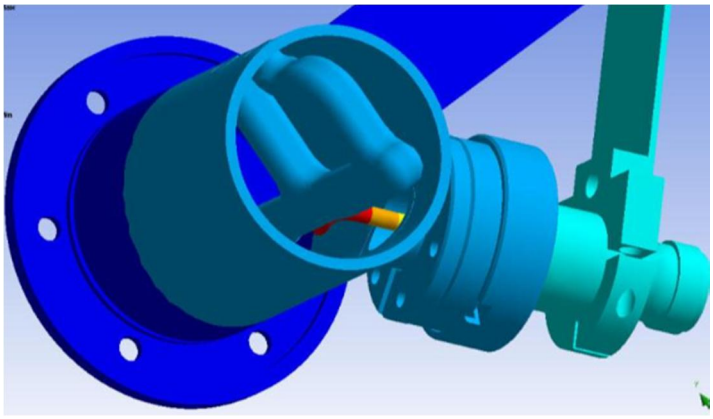

Figure 6-14. 3D model of the 1.3 GHz cavity HOM coupler

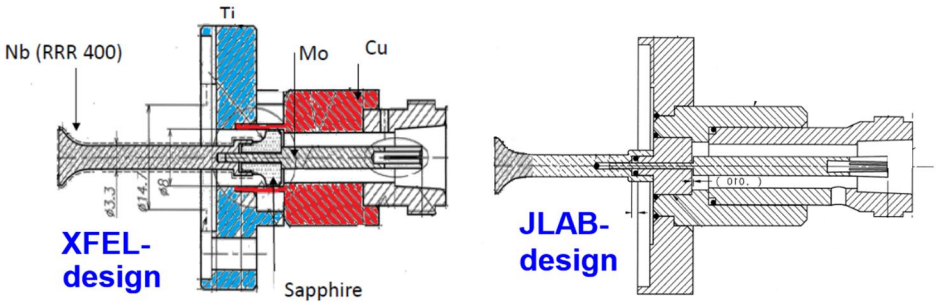

Figure 6-15. Two HOM feedthrough designs; DESY/XFEL (left) and JLAB (right), with a molybdenum pin and sapphire ceramics for CW operations.

6.2.6.2 Fundamental power coupler

The LCLS-II fundamental power coupler is based on the TTF3 coupler developed by DESY **[8]**. The coupler and the high-power RF system are described in Section 5.11.

6.2.7 Superferric Magnet Package

Each 1.3 GHz cryomodule contains a superferric magnet package. The magnet package generates the quadrupole field for beam focusing, and dipole fields to correct the beam orbit in the vertical and horizontal planes. The magnet specifications are shown in Table 6-8.

The superconducting magnet package for LCLS-II is based on a doublet quadrupole with dipole corrector design, using the latest experience and results obtained from the magnet design, fabrication, and tests for ILC, ASTA, Project-X, and the KEK SRF cryomodule test facility [9, 10, 11, 12, 13, 14, 15]. The magnet package is mounted at the end of a cryomodule for easy access and installation (Figure 6-16). The magnet is splittable in the vertical plane to facilitate mounting around the beam pipe [13], is conduction-cooled, and does not have a helium vessel. As such, it does not need to be attached in the cleanroom, thus reducing the possibility of contamination. This design also allows for accurate magnet positioning inside the cryomodule by eliminating the positional uncertainty between and cold mass and the liquid helium vessel after cool-down. Cooling for magnet and current leads is provided by high-purity aluminum straps.

The magnet concept and performance has been demonstrated in tests of ILC magnets [13-16] at ASTA [10], and a version that was built as part of a Fermilab-KEK collaboration is currently being tested in a cryomodule at KEK [13]. The magnetic field analysis shows that the magnet yoke is not saturated (<1.5 T) and there is a linear dependence between the operating current and the integrated gradient. Table 6-9 lists the magnet package parameters.

Table 6-8. Linac quadrupole and corrector dipole magnet specifications.

Parameter	Unit	Value
Integrated peak gradient at 10 GeV	T	2.0
Integrated minimal gradient at 0.4 GeV	T	0.05
Aperture	mm	78
Magnet effective length	mm	230
Peak gradient	T/m	8.7
Quadrupole field non-linearity at 10 mm diameter	%	0.5
Dipole trim coils integrated strength	T-m	0.005
Magnetic center offset in the cryomodule	mm	0.5
Thermal sink temperature	K	2.2

Table 6-9. Magnet Package Parameters

Parameter	Unit	Value
Magnet physical length	mm	340
Magnet width/height	mm	322/220
Pole tip radius	mm	45
Peak operating current	A	≤ 50
Number of quadrupole coils		4
Number of dipole coils		8
Type of superconducting coils		Racetracks
NbTi superconductor diameter	mm	0.5
Quadrupole inductance	mH	82
Liquid helium temperature	K	2.2
Quantity required		35

The quadrupole is assembled from two half-cores having racetrack superconducting coils on the magnet poles. The magnet halves are tightened to each other by end plate bolts. The magnet core is assembled from 1.5-mm-thick, laser-cut laminations fabricated from low carbon steel. The half-core is pressed in a horizontal press and welded to sidebars and end plates, forming a rigid mechanical structure. The magnet package has four racetrack type coils, each wound into an aluminum channel. This channel is used for the coil epoxy vacuum impregnation, forming a closed mold. Each coil has a quadrupole, and vertical dipole and horizontal dipole sections that are spliced at the magnet downstream end, forming the quadrupole and dipole windings.

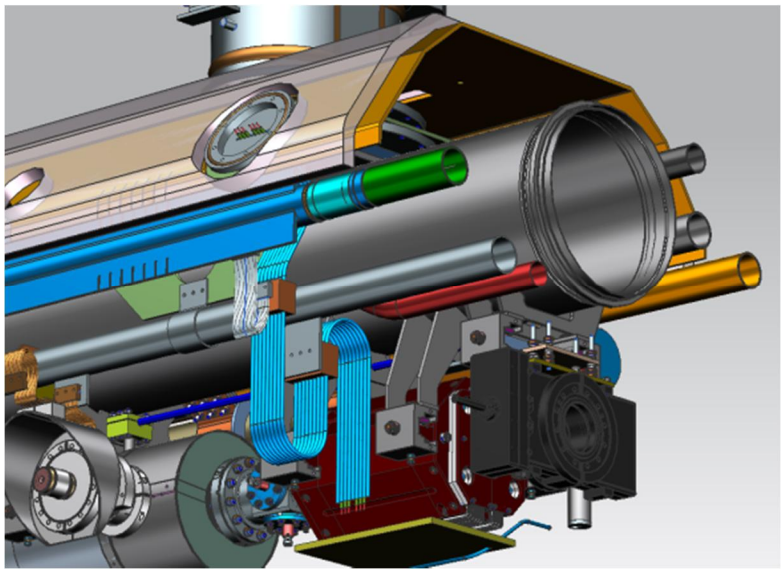

Figure 6-16. 3D model of the magnet package inside the cryomodule

The required quadrupole current changes by a factor of 40 as the beam energy increases along the linac. At lower currents, a degaussing procedure is used to eliminate the iron yoke residual

magnetization, and the superconductor persistent currents. The magnet is self-protected by induced eddy currents in the coil aluminum case and an external dump resistor permanently connected to the magnet current leads. This substantially reduces the magnet system cost and increases the system reliability. The magnet is installed in the cryomodule using standard SRF cavity supports which provide magnet positioning with specified tolerances. Figure 6-17 shows the magnet package installation in the KEK Cryomodule.

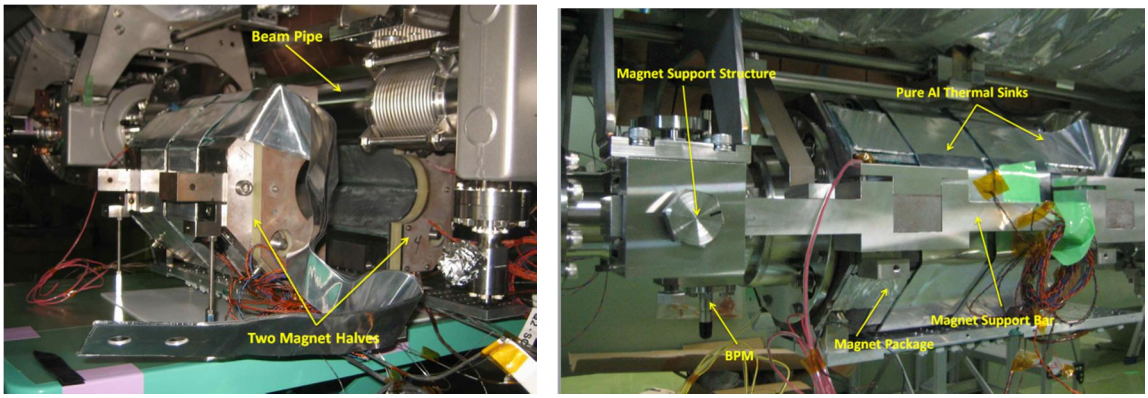

Figure 6-17. Magnet package before (left) and after (right) installation in the KEK cryomodule.

6.2.8 Cold Beam Position Monitor

Button Beam Position Monitors (BPMs) are installed in every cryomodule and are attached with alignment pins to the quadrupole/corrector magnet described in Section6.2.7. As part of the beamline vacuum enclosure, they are cooled by virtue of thermal conductance along the beampipe connected to cryogenic elements. These BPMs are used to monitor the beam orbit and provide transverse beam position data for beam steering with the corrector magnets. Since the cold BPMs are the only beam diagnostic instruments in the cryogenic sections of the linac, and are buried inside the cryomodules, high reliability is essential. The LCLS-II linac can operate in a variety of regimes including single shot operation with bunch charge as low as 10 pC. A resolution of < 100 μm at 10 pC is sufficient to preserve the low emittance during single shot operations; for other modes of operation, a better resolution may be obtained with multi-bunch averaging.

A button BPM pickup meets these requirements in a compact, simple mechanical design, that is reliable and easy to clean. The existence of a large button, cold BPM from the European XFEL proves that this design has been successfully integrated into a cryomodule. This BPM can meet the resolution requirements for LCLS-II for a signal processing scheme in the 1.5 GHz – 2.3 GHz frequency band [17]. The possibility of using a simpler but reduced performance processing scheme, downmixing ~1 GHz button signals to an intermediate frequency that is digitized by a standard controls digitizer, is still an option [18].

The BPM beam pipe walls, as with other non-superconducting beampipe components in the cryomodules, are copper plated in order to increase the thermal conductivity and lower the ohmic losses. The thickness of the plating is chosen to be 15–20 μmto ensure a minimum copper layer

of few µm (larger than a skin depth in the copper) when taking into account thickness variations during plating. The residual resistance ratio (RRR) of a copper film obtained by electrolytic deposition can vary from 10 to 100 depending on technology and further thermal processing [19].

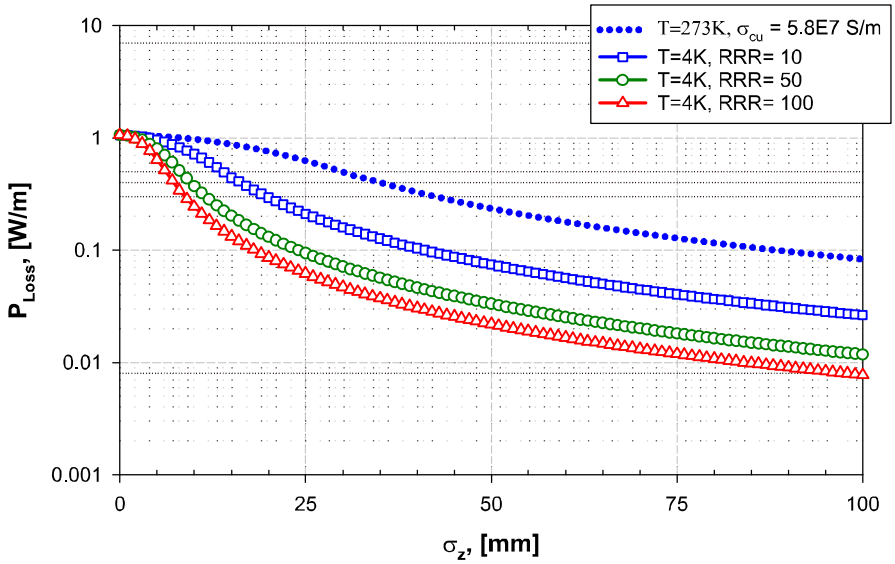

Figure 6-18. Resistive loss in the copper wall vacuum pipe at 4 K (shapes) and 273K (dotted) for the normal skin effect regime, and for different values of residual resistance ratio (RRR), as a function of bunch length.

The ohmic losses generated by the beam passing through the button BPM are a function of the operating temperature, the RRR of the copper coating, and the bunch length. Losses can be evaluated analytically by resistive wakefield theory using either normal skin effect (NSE) or anomalous skin effect (ASE) approximations [20, 21]. Due to uncertainty in RRR, both NSE and ASE regimes are probable for the LCLS-II conditions. The results of resistive losses calculation using the NSE approach are shown in Figure 6-18 for copper plating with different RRR values and the most worse case of LCLS-II linac operation, with 25 µm RMS longitudinal bunch length (σ_z), 300 pC bunch charge, and 1 MHz bunch rate. A similar calculation in the ASE regime is shown in Figure 6-19, in comparision with the NSE regime for copper coating with typical RRR of 50. The ASE regime predicts a maximum 0.3 W/m resistive loss in the copper-coated beam pipe. The length of the BPM is 180 mm, which translates to about a 50 mW heat load transferred to the 4 K thermal anchors in the cryomodule.

In addition to resistive loss, the beam passing through the button BPM generates wakefields and only a fraction of the total power lost by a bunch is radiated to the pickup ports [18]. A simulation of total power loss for the maximum bunch charge of 300 pC and 1 MHz repetition rate of the LCLS-II linac is illustrated in Figure 6-20. Extrapolating, this fraction would be below 20-25 % for σ_z in the range of tens of microns. Thus, the BPM produces another 80 mW of RF power radiated to the beam pipe and absorbed mostly by the HOM absorber and partially by other elements in the cryomodule.

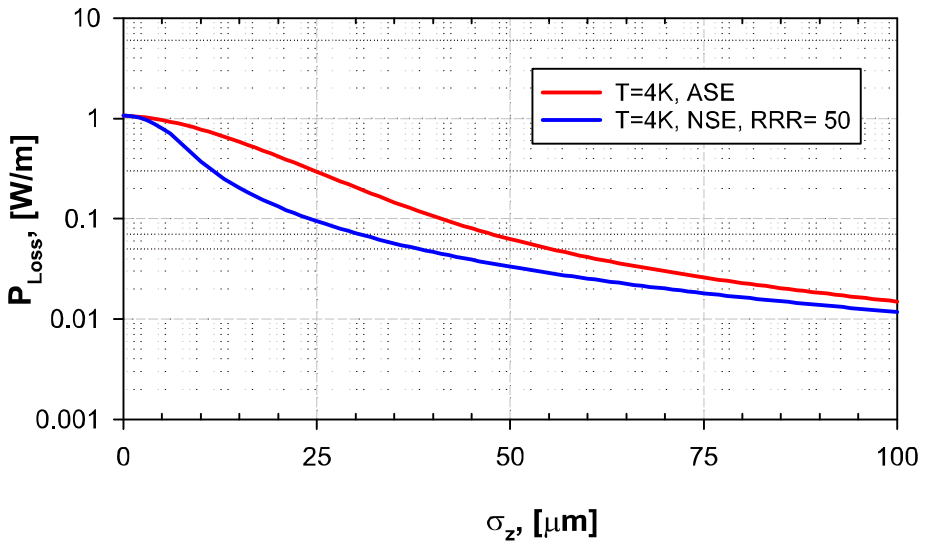

Figure 6-19. Resistive loss in the copper wall pipe at 4 K for normal skin effect (NSE, blue) and anomalous skin effect (ASE, red), residual resistance ratio (RRR) 100, as a function of bunch length.

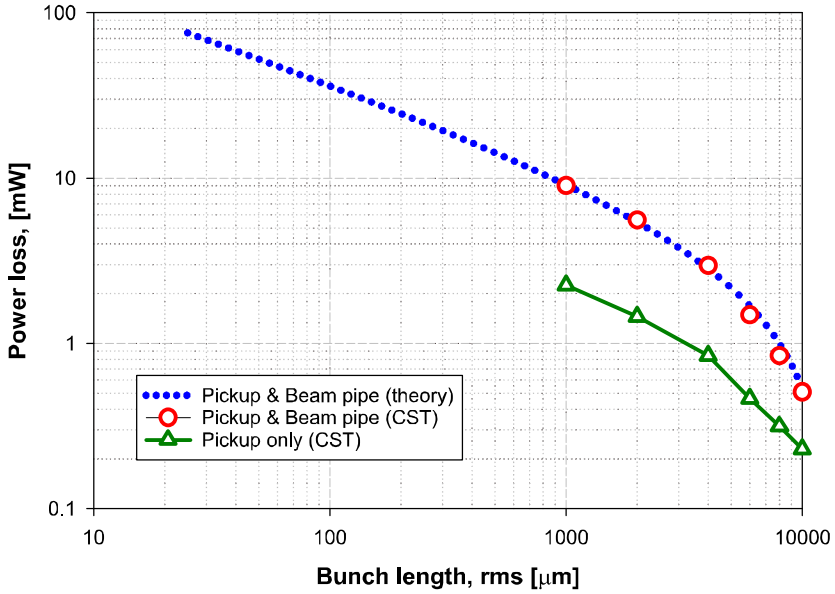

Figure 6-20. Full (blue and red) and pickup only (green) power losses generated by the 300 pC and 1MHz rate electron bunches passing through the 20 mm diameter button BPM, calculated and simulated with CST Particle Studio.

DESY studied the possibility of overheating in the BPM button during CW operation. They performed a detailed thermal analysis for the XFEL maximum beam load (30 Hz repetition rate, 4.5MHz bunch repetition, 1 nC), which corresponds to 78.7 mW total loss at the BPM [22]. This value is the same for the maximum LCLS-II parameters. A maximum button temperature of 11.4 K is found, assuming all beam generated loss is absorbed by the buttons only. In reality this value is overestimated by factor of at least ten since the majority of the power loss is radiated to the

beam pipe as wakefields, and other power is transferred through RF cables as the pickup signal. Thus, the expected rise of the copper button temperature is a few degrees Kelvin or less.

6.2.9 HOM Absorber

The equilibrium HOM power generated per cryomodule by a beam of 300 pC charge per bunch and repetition rate of 1 MHz is 7.7, 10.7, 1and 3.8 W in the L1, L2, L3 linac sections respectively. Wakefields in the transition regions, where beam enters each linac section, increase losses in the first few cavities. The largest increase is seen at the entrance to the L3 section, where the first two cryomodules experience 29.5 and 14.5 W, respectively, compared to 13.8 W for the remaining cryomodules.

A beamline HOM absorber developed by DESY, shown in Figure 6-21, has been adopted for LCLS-II. A large portion (>80%) of the propagating HOM power is dissipated in beam pipe absorbers installed between between cryomodules, which transfer heat to the ~45 K cryogenic lines . Non-superconducting beamline components in a cryomodule are copper plated to minimize resistive losses: more than half of the HOM power would be dissipated at 2 K if bellows and pipes were not copper-plated.

The absorber power handling capability of 100 W covers the whole range of LCLS-II operating parameters. Even at this high power, good heat conductivity of the chosen ceramic keeps the temperature gradient across the ceramic ring below 140 K, which is a safe limit. Several tests have confirmed that this gradient does not change the mechanical and RF properties of the absorber. An absorber prototype was installed in a FLASH cryomodule and tested in a cold environment with beam to demonstrate performance and to prove that simulations accurately predict HOM losses in the absorber [23]. The beam line absorber is a heavy device (~40 lbs) and is held by a support to avoid mechanical deformation of the beam line.

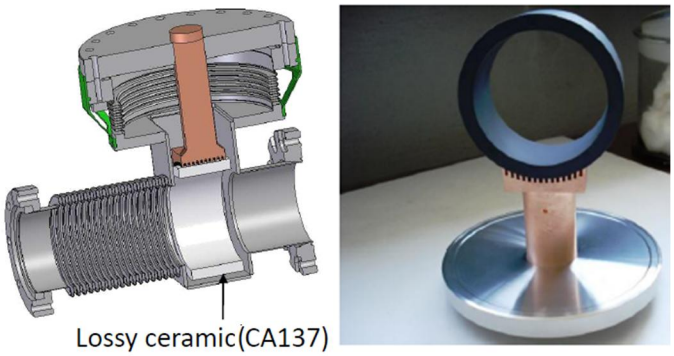

Figure 6-21. Layout of the beam pipe absorber: 3D model showing the lossy ceramic installed next to a bellows and with copper thermal sink to the warm (approximatley 70 K) thermal intercept (left); photograph of the lossy ceramic mounted on copper heat strap (right).

6.2.10 Cryomodule Vacuum System

The LCLS-II cryomodule includes three distinct vacuum volumes: insulating vacuum, beamline (including cavity) vacuum, and the vacuum space between the warm and cold window on each fundamental power coupler. Figure 6-22indicates these regions within a cryomodule. The insulating vacuum serves to minimize convective heat transfer to the cavity helium vessel and gas conduction in the multi-layer insulation (MLI). The insulating vacuum is maintained by a turbo pump which is backed by a dry scroll pump. The turbo pump is connected to a gate valve through a 4" port on the flexible bellows interconnection section. For initial pump-down, a separate roughing pump line with a Roots blower and a cold trap is used. Several backfills with dry nitrogen effectively purge the water in the MLI layers. The turbo pump is turned on once the pressure reaches 10^{-2} Torr. When the pressure reaches 10^{-4} Torr, the turbo pump is valved out and cool-down can begin. In linac strings with multiple cryomodules, cold cathode and convection gauges are installed on alternate modules, to monitor the pressure when cold or during pumping down, respectively.

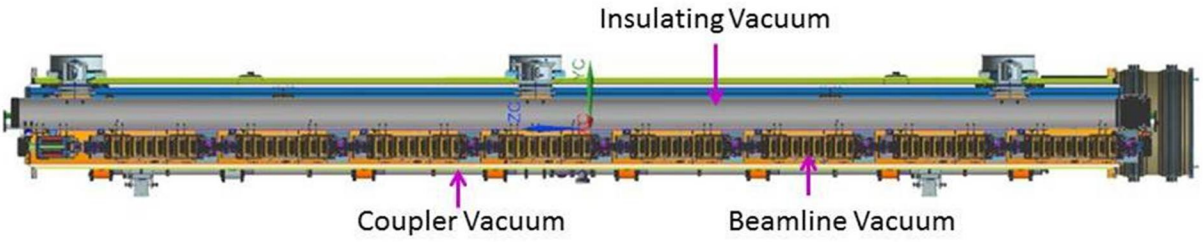

Figure 6-22. Vacuum subsystems of the cryomodule

The beamline vacuum subsystem includes two pump stations, one at each end of a cryomodule. Each station contains an ion pump and a cold cathode gauge. In order to minimize the risk of particulate and gas contamination of the cavities, special care is given to the pumpdown and venting procedures. The pump station is equipped with oil free pumps, flow controllers and diffusers to avoid strong turbulence of the gas flow, and particle filters to clean the dry nitrogen for venting.

The RF power input coupler attached to each cavity has two ceramic windows, one at a temperature of ~70 K and one at room temperature. This design enables complete closure of the cavity in the clean room by mounting the coupler up to the first window, thus preventing any contamination of the cavity RF surface during subsequent assembly of the module. The space between the fundamental power coupler cold and warm windows is kept under vacuum, which is separate from the cavity vacuum. During RF operations, there may be vacuum activity in this space due to gas being released from the waveguide or potentially from arcing on the windows. The coupler vacuum volumes are pumped through a right angle valve to a vacuum manifold, which is equipped with an ion pump and a titanium sublimation pump. On the end of this manifold, there are ports to connect a wide range gauge and a roughing pump station. The right angle valve on each coupler provides the possibility of connecting a separate pumping line in case of a leak in a coupler. Figure 6-23shows the fundamental power coupler vacuum system.

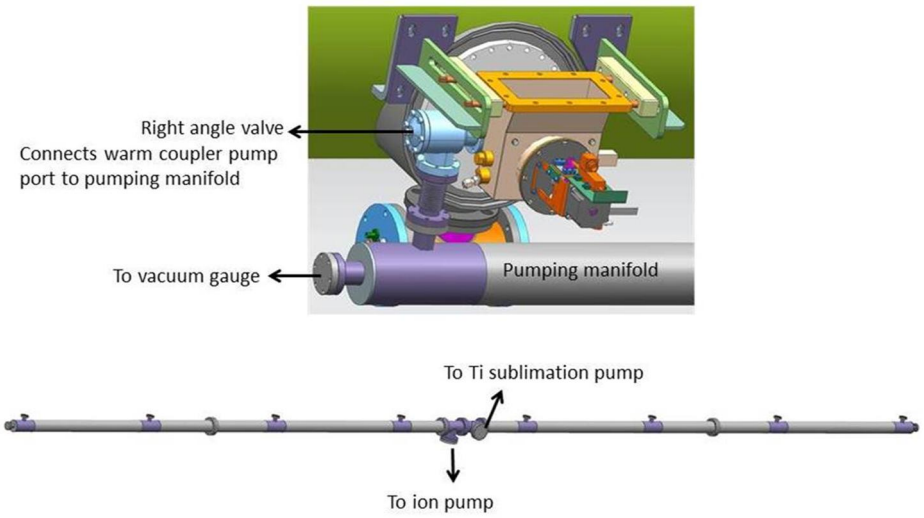

Figure 6-23. Cryomodule fundamental power coupler vacuum subsystem

To avoid cavity contamination from particles, all vacuum beamline components in the cavity string are cleaned in a class 100 or better clean room to remove particles, and components are installed into the machine in local clean rooms. This preparation is in addition to standard UHV procedures.

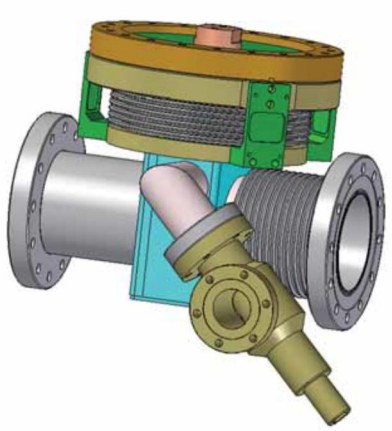

Figure 6-24. Cryomodule beamline interconnection, including HOM absorber and pumping port.

The beamline vacuum in the cryomodule consists of eight cavities connected to each other via copper-coated bellows, a beam pipe inside the superconducting quadrupole, a beam position monitor, and a module interconnection including baemline HOM absorber and pumping port.These are assembled in a class 10 clean room and closed off by all-metal gate valves at both ends. The quadrupole beam pipe and BPM are also copper-coated to reduce heating from propagating wakefields excited by the beam. Vacuum sealing is provided by aluminum gaskets between NbTi and stainless steel flanges. After assembly, the complete string is evacuated and then removed to add the tuners, thermal and magnetic shielding and thermal straps. Finally it is inserted into the cryomodule vacuum vessel. The beamline interconnection between the accelerator modules consists of a 300 mm long section that incorporates an HOM absorber, a

bellows and a vacuum pumping port, as shown in Figure 6-24.. The cryomodule vacuum sub-systems parameters are summarized in Table 6-10.

Table 6-10. Summary of the cryomodule vacuum subsystems

			Beamline vacuum	**Insulating vacuum**	**Warm coupler vacuum**
Pressure (Torr)	Cold		$1x\ 10^{-10}$	$1x\ 10^{-6}$	$1x\ 10^{-9}$
	Prior to cool-down		$1x\ 10^{-8}$	$1x\ 10^{-4}$	$1x\ 10^{-7}$
Characteristics			Particle free pump-down/venting	Roughing pump for the multi-layer insulation.	Outgassing during RF operation
Pumps		Roughing	Turbo, with particle free setup	Roots blower, then Turbo	Turbo
		In operation	Ion pump	Turbo, in case of a leak	Ion pump and Ti sublimation pump

6.2.11 High-Q_0 preservation: Magnetic Shielding and Cooldown

High-Q_0 niobium cavities produced by nitrogen-doping have special requirements with respect to their environment at the 9.2 K transition between the normal and the superconducting states [24]. In particular, they tend to be more sensitive to the detrimental effects of magnetic flux trapping than non-doped cavities. Niobium is a Type II superconductor and unlike a Type I superconductor does not expel all of the flux that it encloses when it undergoes superconducting transition into the Meissner state. In fact, under certain conditions, as much as 100% of the flux can be trapped [25]. Each quantum of trapped flux is associated with a core region of normal conducting niobium that, while quite small, increases RF power dissipation. Less flux trapping translates to lower helium refrigerator load, and thus the LCLS-II cryomodules are designed to minimize residual magnetic field at the cavities.

6.2.11.1 Sources of Magnetic Flux

There are two principle sources of magnetic flux in a cryomodule: 1) ambient magnetic field and 2) thermocurrent-driven magnetic field. The ambient field is determined by the local magnetic environment around the cryomodule and by the presence of any magnetized components within the cryomodule itself. The Earth's magnetic field is typically on the order of 50 μT. Thermocurrent-driven field occurs during cooldown of the cryomodule when large thermal gradients are present [26]. Current caused by Seebek effect voltage exists in the bi-metallic cavity and the helium vessel. At temperatures above 9.2 K, current flows along the length of the cavity and returns through the helium vessel with a somewhat radially symmetric pattern. For this case, even though the thermocurrent can be quite large, the radial symmetry of current density prevents the presence of significant magnetic flux in the SRF layer at the inside surface of the cavity. This is the usual case for a vertical test of a cavity. However, for the case of a horizontally oriented cryomodule, it is usual for the bottom side of the cavity to become superconducting as helium is

introduced from the bottom of the cavity helium tank. This is a strong symmetry-breaking perturbation, and leads to magnetic fields in the cavity superconducting surface layer.

6.2.11.2 Mitigation of Magnetic Flux Trapping

The magnetic flux can be reduced to a level which maintains the LCLS-II Q_0 requirement if the remanent field at the cavity is attenuated below 0.05 μT. The traditional way to lower ambient flux in cryomodules is to attenuate the magnetic field with passive magnetic shielding using a combination of low and high magnetic permeability materials [27]. In order to augment this effect sufficiently to reach our tight tolerance, thorough demagnetization of all magnetic materials present in the cryomodule is necessary. The inherent inefficiency of long, thin cylindrical shields may be compensated by the implementation of active field cancellation in the direction parallel to the cavity axis.

Neither passive shielding nor active cancellation help with thermocurrent flux. Here the current is minimized by minimizing the thermal gradient that drives it, as described in Section 6.2.3.

6.2.11.3 Flux Expulsion

It has been demonstrated that nearly all flux, up to 20 μT, can be expelled from a cavity if there is a sufficiently large spatial thermal gradient present at 9.2 K [28]. It is evident that the best situation is to have a minimal longitudinal thermal gradient driving thermocurrent while at the same time achieving a large transverse (vertical) thermal gradient, as described in Section 6.2.3. Providing these conditions is an important part of the cryomodule and cryogenics design described in Section 6.2.3.

6.2.11.4 Minimization of Trapped Flux

The LCLS-II cryomodule magnetic shielding design combines all available flux mitigation techniques while arranging cooldown dynamics to minimize thermocurrent and maximize flux expulsion. The combined two layers of magnetic shielding and possible active cancelation design is shown in Figure 6-25.

Both finite element modeling and laboratory measurements on a Fermilab ILC cryomodule indicate that, with the shielding and compensation arrangement of Figure 6-25, a magnetic field amplitude of $3x10^{-7}$ T, averaged over the active one meter active length of each cavity in a cryomodule, is achievable [29].

The arrangement of helium inputs and outlets for the cavity helium vessel has been selected to be approximately symmetric about the center cell of the cavity. This is aimed to minimize thermal gradients along the length of the cavity, and lead to minimized flux from thermocurrents. Nitrogen-doped cavities with helium vessels have met the LCLS-II performance specification during horizontal cryostat tests at both Fermilab and Cornell University, verifying the design.

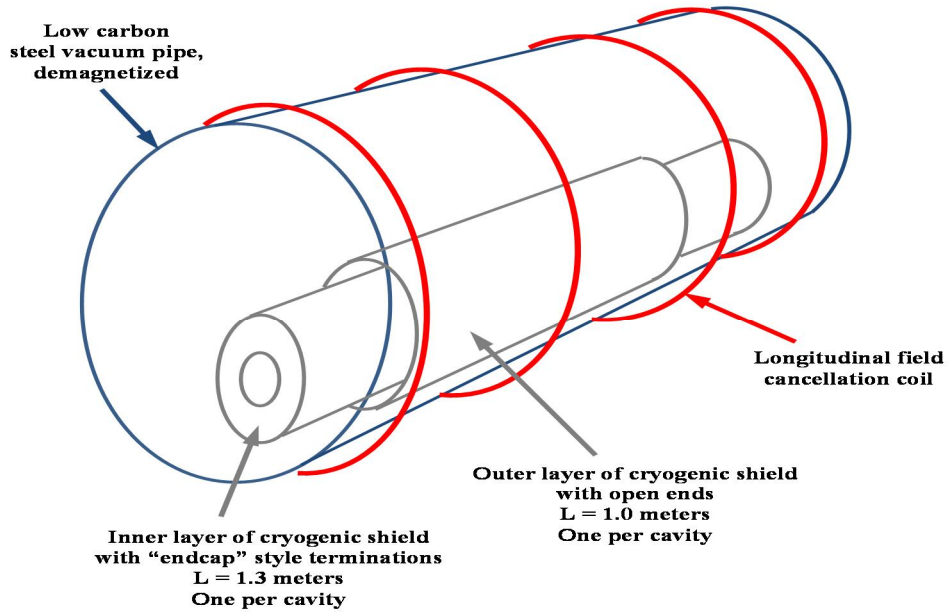

Figure 6-25. Schematic diagram of the LCLS-II magnetic shield and possible active cancellation coil arrangement (one cavity section is shown)

6.3 Design of 3.9 GHz Cryomodules

6.3.1 Requirements

Space charge effects limit the maximum obtainable charge density from the photocathode, and thus the minimum bunch length. For LCLS-II, a 300 pC bunch has a length of approximately 1 mm at the exit on the injector. Sinusoidal variation in the RF voltage over this distance leads to a correlated energy variation, or "chirp," in the uncompressed bunch and, after bunch compression, to an asymmetric bunch profile. Applying a voltage at a harmonic $\omega_1 = 3\omega_0$ of the fundamental RF frequency ω0 results in an integrated voltage that is approximately linear over the bunch length, removing the curvature of the beam distribution in longitudinal phase space, and facilitating more efficient bunch compression and controlled bunch charge distribution [30]. Linearization of the longitudinal phase space of electron bunches in a superconducting RF linac has proven to enhance beam quality and simplify operation, as evidenced by the performance of the harmonic linearizer cryomodule, ACC39, at the FLASH facility at DESY [31, 32].

Such a harmonic linearizer operating at 3.9 GHz, three times the frequency of the LCLS-II main linac, is installed just before the first bunch compressor BC1 (see Chapter 4). The harmonic linearizer section consists of two cryomodules, each containing eight cavities. Table 6-11 provides the basic parameters.

The accelerating structures utilize superconducting RF cavities packaged in cryomodules based on the design first developed at Fermilab for the FLASH ACC39 module now in operation at DESY. Refinements in the design for similar cryomodules being built for the European XFEL are also incorporated. The LCLS-II 3.9 GHz cryomodule design thus builds on experience at

Fermilab, DESY, and LASA (Milano) on design and operation of existing and proposed 3.9 GHz systems [33]. Since other designs are for a pulsed linac, the LCLS-II system is modified to support operation in the CW mode.

Table 6-11. 3.9 GHz RF Parameters.

Parameter	Nominal	Minimum	Maximum	Units
RF frequency	3900	-	-	MHz
Operating temperature	2	-	-	K
3.9 GHz voltage (two cavities in reserve)	55		75	MV
Average operating gradient (two cavities in reserve)	11.4	-	15.5	MV/m
Beam to RF Phase	-165	-90	-180	deg
Cavity Q_0	2.5×10^9	1.5×10^9	-	-
Cavity length (L)	0.346	-	-	m
R/Q (r/Q)	750 (2168)			Ω (Ω/m)
Geometry constant (G)	275			Ω
Coarse (slow) tuner range	750			kHz
Fine (fast) tuner range	~1			kHz
HOM damped Q value (monopole and dipole)	$\leq10^6$			-
Lorentz detuning	≤0.6			$Hz/(MV/m)^2$
Cavity alignment requirements (RMS)	0.5			mm
Peak detune (with piezo tuner control)	30			Hz
Required cavity field amplitude stability†	0.01			% (rms)
Required cavity field phase stability†	0.01			deg (rms)
Q_{ext} *(fixed)*	2.5×10^7	-	-	-
RF beam power per cavity (@300 μA)	1.2			kW
RF power needed per cavity (with overhead)	0.7			kW
Cavity dynamic load	10			W

6.3.2 Cryomodule Mechanical and Cryogenics Design

The cryomodules incorporate Fermilab DESY/FLASH 3.9 GHz dressed cavities, with some modifications, to create what is essentially a shortened LCLS-II 1.3 GHz cryomodule. A four-cavity, 3.9 GHz, pulsed-operation 3.9 GHz linearizer cryomodule designed and built at Fermilab and operating in FLASH at DESY is shown in Figure 6-26.

Figure 6-26. 3.9 GHz cryomodule built at Fermilab and installed in the FLASH facility at DESY

The choice of two cryomodules, each containing eight cavities, is largely driven by optimizing factors such as required total voltage, reasonable cavity string/cryomodule assembly, length of cryomodule, and number of interconnects. Fundamental power couplers are mounted in a scheme identical to that used for a similar cryomdoule designed for XFEL. In order to minimize transverse kicks, input couplers are located on either side of the cryomodules, with cavity pairs oriented as shown in Figure 6-27. As a result, RF feeds and warm coupler vacuum lines are required on both sides of the cryomodule. The cavities are powered powered individually using 3 kW klystrons and operated in pairs to compensate for coupler kicks. HOM couplers are of the now-proven single-post Formteil design and are described below. A BPM will be located at the downstream end of each cryomodule, but no quadrupole or correctors, and there will not a beamline absorber between the cryomodules.

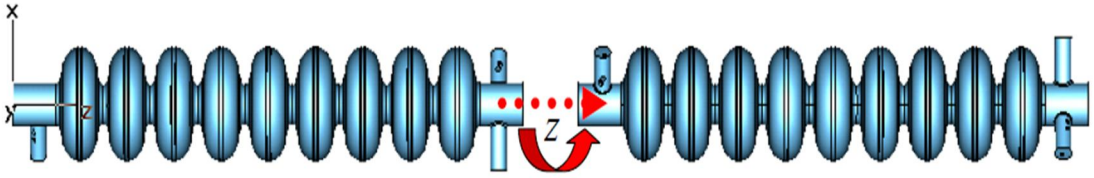

Figure 6-27. Orientation of pairs of 3.9 GHz cavities to minimize transverse kicks to the beam by the fundamental power couplers.

The longitudinal distribution of the cavities within each cryomodule is yet to be exactly determined but is not as tightly constrained to be an integer number of half-wavelengths as for the 1.3 GHz cryomodules. The diameter and interfaces at each end of a cryomodule are identical to the 1.3 GHz cryomodules for contiguous interconnection of an identical cooling scheme with closed two-phase and cool-down pipes, JT valve and cool-down valve, pipe sizes, thermal shielding, and interconnects. The beam pipe and bellows between cavities and at the ends of the cryomodules have a nominal diameter of 40 mm and are copper-plated so as to reduce heating due to HOMs and evanescent fundamental mode fields. Other differences from the 1.3 GHz cryomodules are that the 3.9 GHz cryomodules have no magnets, smaller cavity helium vessels,

modified connections to the support structure, shorter coupler-to-coupler spacing, and magnetic shielding modified for the different helium vessel size and configuration. An image from the CAD design model for the 3.9 GHz cryomodule is shown in Figure 6-28.

The total predicted heat load under nominal conditions is approximately 10 W per cavity and is dominated by cavity dynamic heating. Typical Q_0 for the 3.9 GHz cavities without nitrogen doping is 2.0×10^9, and some improvement with nitrogen doping similar to that for 1.3 GHz cavities is assumed to produce a Q_0 of 2.5×10^9. The overall heat load for each 3.9 GHz cryomodule is predicted to be comparable to that for each 1.3 GHz cryomodule, approximately 80 Watts dissipated at 2 K.

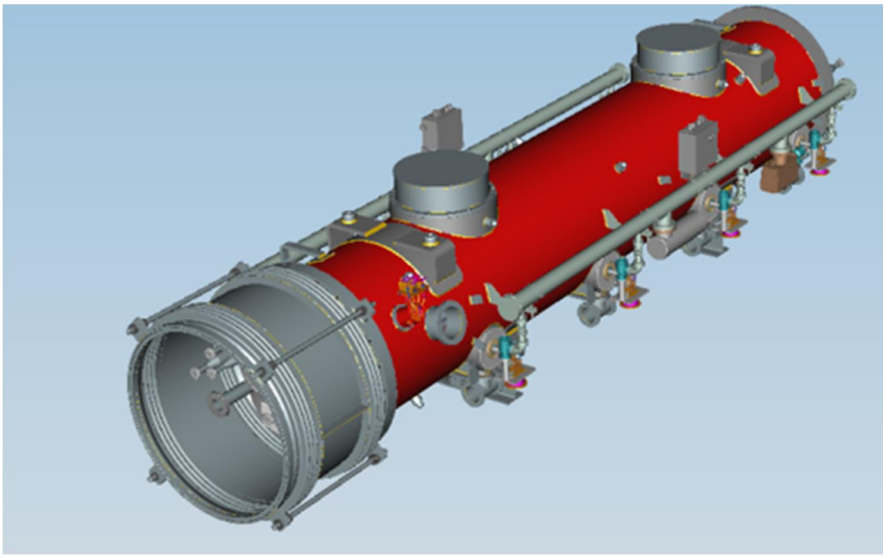

Figure 6-28. LCLS-II 3.9 GHz cryomodule CAD design model

6.3.3 3.9 GHz Cavity

The 3.9 GHz cavities for LCLS-II are essentially a scaled version of the TESLA-style 1.3 GHz cavities, and are based on the cavities already in operation at FLASH and now in fabrication for XFEL, as shown in Figure 6-29. Existing cavities routinely operate at 19 MV/m at FLASH and have been tested to over 20 MV/m in both pulsed and quasi-CW modes.

Some modification is needed, as the cavities cannot be an exact scaling of the 1.3 GHz versions. There is a need to enlarge the beam tube and iris diameter in the end cells so as to have sufficient coupling to the input coupler. The minimum aperture required is 30 mm. The coupler longitudinal position from the end cell also cannot be scaled exactly, but needs to be further away because of mechanical design constraints associated with the helium vessel and port flanges. End groups include HOM couplers, described in Section6.3.5 Thermal heating is significantly higher than for 1.3 GHz cavities, and for CW operation this requires some modification to the helium vessel similar to that foreseen for the 1.3 GHz counterparts – i.e. a larger diameter 2-phase 'chimney' and pipe. Cavity processing utilizes electro-polishing in lieu of Buffered Chemical Polishing (BCP) which was previously employed. Otherwise, standard treatment and pre-test processing protocols are followed.

Figure 6-29. 3.9 GHz cavity.

All production cavities are tested vertically prior to dressing, and acceptance requires measured gradient and Q_0 in vertical test of at least 15% above specification. The first four dressed cavities are tested horizontally, with approximately 20% of the remaining cavities to undergo such testing.

A modest development effort aimed at improving the Q_0 value by means of nitrogen doping is envisioned prior to cavity production. Such work is expected to provide some modest enhancement, thereby reducing the heat load per cavity. As the losses due to BCS superconducting current scales with frequency squared, these cavities already have a factor of nine increase in power loss compared to their 1.3 GHz counterparts.

6.3.4 Cavity Tuner

The 3.9 GHz cavity tuner is a compound lever mechanical design, similar to the 1.3 GHz cavity tuner discussed in Section 6.2.5 and shown in Figure 6-10 and Figure 6-11. The tuner allows the resonant frequency of each cavity to be precisely controlled to generate the required voltage and phase to linearize the energy variation along a bunch. Tuning range is ~750 kHz for the slow tuner, and ~1 kHz for the fast tuner.

6.3.5 Endgroups

The 3.9 GHz cavity end-groups have a 40mm diameter beam-pipe and include two HOM couplers, one per side, a 30mm diameter port for the power coupler on the downstream end, and a port for the field probe on the upstream end, as shown in Figure 6-30. The design, position and orientation of HOM couplers are chosen to reach optimum coupling with HOM modes and minimization of power leakage from the fundamental mode (the leakage of the 3.9 GHz mode into each HOM coupler contributes an external Q-value greater than 10^{11}).

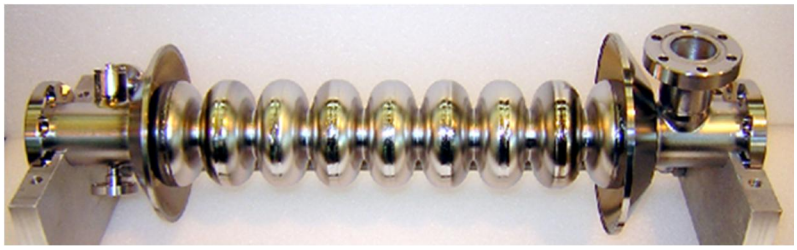

Figure 6-30. 3.9 GHz 9-cell cavity, showing end-groups.

6.3.5.1 HOM coupler

Dressed cavity tests demonstrated that the accelerating gradient in existing pulsed 3.9 GHz cavities was limited by thermal quench on the HOM antenna tip. The limit depends on the choice of HOM coupler and feedthrough with a niobium antenna (seeFigure 6-31): all cavities with the two-leg trimmed HOM coupler design reach 12-19 MV/m, and those with the one-leg design reach 21-22 MV/m, in CW operation [34]. The one-leg design is chosen as the baseline for LCLS-II cavity.

The HOM coupler feedthrough design, based on a re-optimized JLAB feedthrough with sapphire insulators, provides good thermal conductivity and passband up to 10 GHz. Several cold thermal cycles, with subsequent vacuum leak checks, were performed to ensure reliable feedthoughs.

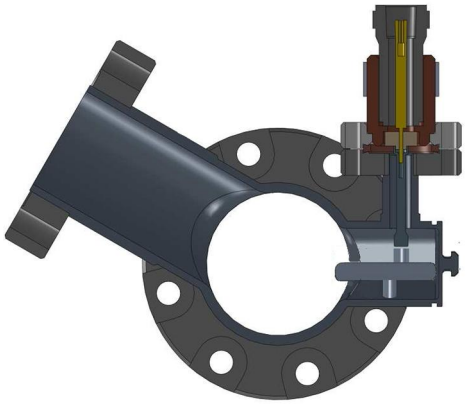

Figure 6-31. One-leg HOM coupler with feedthrough.

The HOM damping performance of the cavity was studied both in simulations and measurements. Results for a cavity with two baseline HOM couplers are presented in Figure 6-32. All trapped modes are damped at the level $Q_{ext} < 10^6$, meeting the LCLS-II specification.

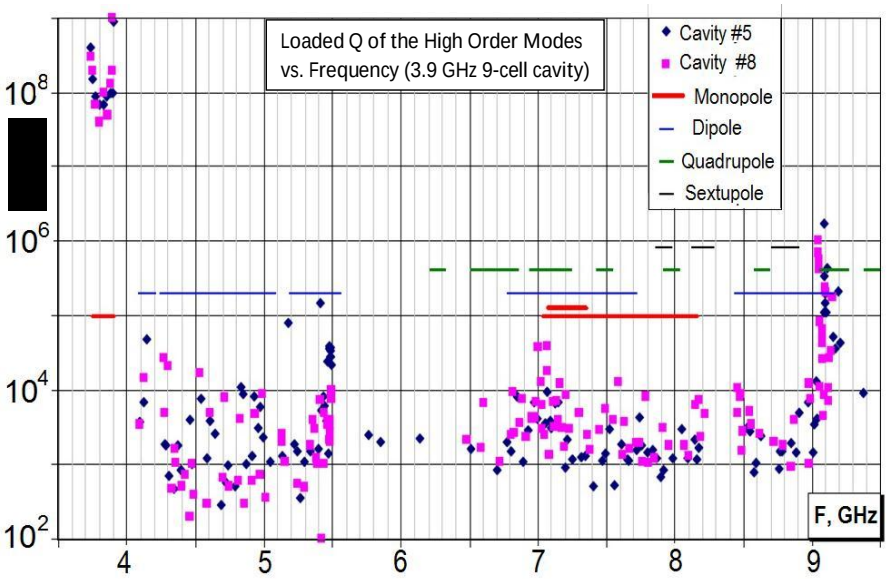

Figure 6-32. Cold measurements of Q_{ext} for all trapped modes in two 3.9 GHz 9-cell cavities: Cavity #5 has the two-leg HOM coupler design; cavity #8 has the one-leg design chosen for LCLS-II.

6.3.5.2 Power coupler

The main coupler for the 3.9 GHz cavity is designed for 2 kW CW power in traveling wave mode. This power mostly comes from the beam, and power from the generator does not exceed 0.7 kW. The coupler is a 50 Ohm coaxial line with a 30mm outer diameter. The coupler consists of three sections: a cold section, assembled on the cavity in a clean room and closed by a cold ceramic window; a warm section; and a waveguide section with a pillbox waveguide warm window. The cold cylindrical windows are based on TTF3 coupler ceramics (see Chapter 5). The warm window is adapted from a window design developed for a commercially available 80kW Klystron. The general view of the coupler is shown in Figure 6-33. Two bellows in the inner conductor and two in the outer conductors in the warm part accommodate thermal shrinkage and cavity misalignment during cooldown and warm-up cycles. All stainless steel surfaces, including the bellows, are copper-plated to reduce HOM heating. The thickness of the copper plating on the inner conductor in the warm part is increased for LCLS-II to 100 µm to reduce the maximum temperature on the bellows. The coupler antenna is made out of pure copper; all the outer conductors are plated with 10 µm of copper. A relatively short bellows with 10 convolutions helps maintain a maximum temperature inside the coupler of less than 350 K for the design power of 2 kW in CW mode (seeFigure 6-34). The coupler has fixed coupling, and nominal Q_{ext} of $2.5x10^7$.

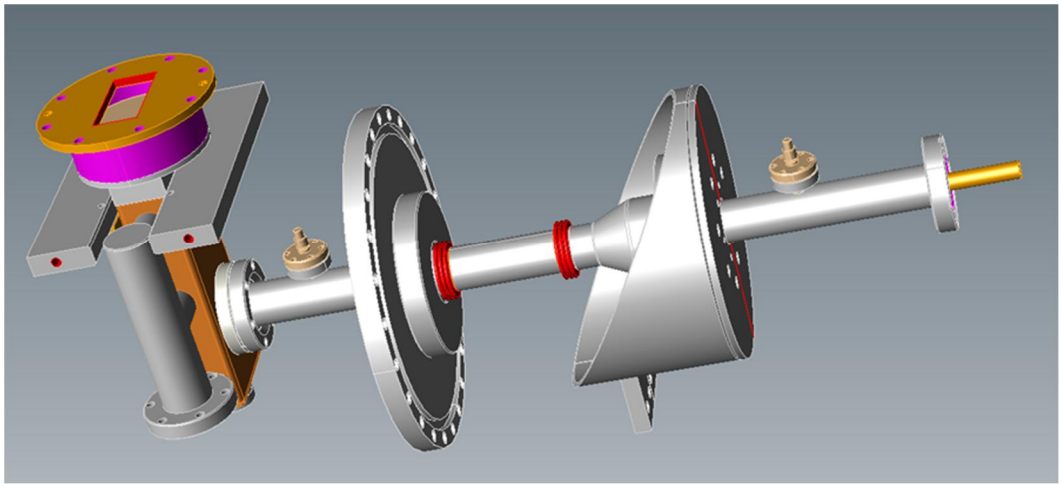

Figure 6-33. Model of the 3.9 GHz coupler for 2 kW CW operation.

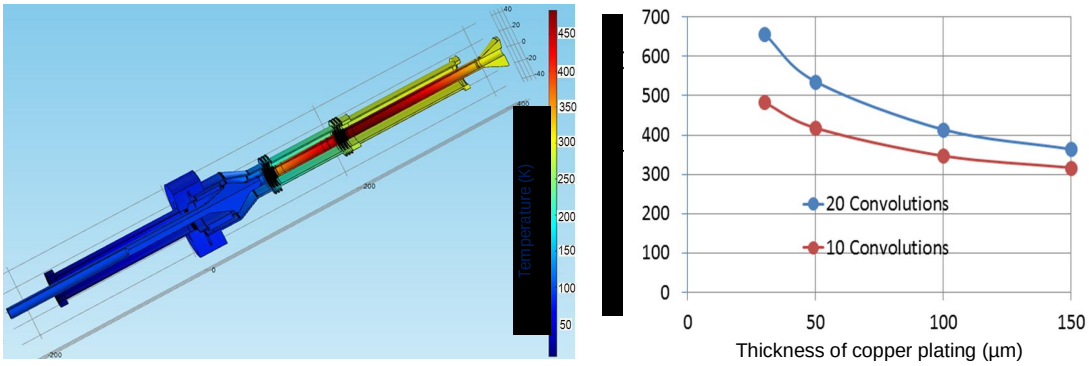

Figure 6-34. Model and thermal simulation of the 3.9 GHz fundamental power coupler for 2 kW CW power in a traveling wave (left). Dependence of the coupler maximum temperature (K) on the copper plating thickness (microns) on the inner conductor (right).

6.3.6 Vacuum Chamber

The vacuum considerations for the 3.9 GHz cryomodules are similar to those for the 1.3 GHz cryomodules, described in Section6.2.10. The 3.9 GHz cryomodule includes three distinct vacuum volumes: insulating vacuum, beamline (cavity) vacuum, and a vacuum volume between the warm and cold window on each fundamental power coupler. The beamline vacuum in the cryomodule consists of eight cavities connected to each other via copper coated bellows, a beam pipe to accommodate a beam position monitor, and a module interconnection section.

6.3.7 Magnetic Shielding

As described in Section 6.2.11, the LCLS-II cryomodules are designed to minimize residual magnetic field at the cavities by combined shielding and active cancelation. The magnetic hygiene for the 3.9 GHz cryomodules is similar to that for the 1.3 GHz cryomodules, as shown schematically in Figure 6-25 in Section 6.2.11.4.

6.4 Cryomodule Heat Loads

6.4.1 Introduction, assumptions and inputs

A more complete description of predicted and design heat loads (where "predicted" means best estimate and "design" includes an additional engineering design margin for uncertainty) for various modes of LCLS-II linac operation can be found in the engineering note *LCLS-II Cryogenic Heat Load* LCLSII-4.5-EN-0179. Sources include analyses and measurements on similar cryomodules. Parameters come from the LCLS-II Conceptual Design Report, with the differences for the current baseline design being the addition of two 8-cavity 3.9 GHz cryomodules, all accelerating cavities powered with correspondingly lower gradient, and beam current reduced from 0.3 mA to 0.1 mA. Heat load estimates come from cryogenic system (transfer lines, end boxes, etc.) heat measurements, current lead measurements and analyses, input coupler predictions scaled from measurements on existing couplers, HOM and wakefield analyses, RF cavity dynamic heating calculations based on Q_0 and gradient, and the TESLA design report. Sources for this information are listed in LCLSII-4.5-EN-0179.

6.4.2 Analysis

Heat loads are tabulated, added together, and multiplied by appropriate uncertainty factors in spreadsheets, which are referenced and summarized in LCLSII-4.5-EN-0179. Some highlights are presented here. A summary of 1.3 GHz and 3.9 GHz cryomodule static heat load without margin is presented in Table 6-12.

Table 6-12. Estimated Cryomodule Static Heat Load

	High temperature thermal shield	**Low temperature thermal intercepts**	**2.0 K level**
Cryomodule static heat load [W]	100.0	12.0	6.0

Reports of measured static heat load values for XFEL-style cryomodules were used to reach the above conclusion, which is a best estimate, with no margin added.

Dynamic heat loads include RF heating in the cavity, input coupler heat, HOM couplers and absorbers, magnet current leads, and other sources like dark current. The RF load is based on cavity gradient, cavity Q_0, cavity R/Q, cavity length, and fraction of cavities powered, assumed here to be 100%. For all 280 1.3 GHz cavities operating at 15 MV/m providing the required beam energy of 4 GeV, with $Q_0 = 2.7 \times 10^{10}$, the RF heat load to 2.0 K is 8.7 Watts per cavity. Parameters in this analysis come from the LCLS-II Conceptual Design Report except for the assumption of 100% of cavities powered and correspondingly reduced gradients.

Input coupler heat is scaled from TTF coupler data, resulting in dynamic heating of 0.03 W, 0.24 W, and 12.2 W per coupler for the 2 K, 5 K, and 45 K levels, respectively. Static heat is included in overall cryomodule static heat measurements, so only dynamic heating for the input coupler is added in the heat load analysis.

HOM coupler cables generate some heat when removing the beam-induced HOM loads. This is a dynamic heat load which is scaled from the TESLA design report estimate by the number of cavities per cryomodule. The result is only 0.18 W per cryomodule.

Power deposition from HOMs and wakefields induced by the beam goes partly to the 2 K structures (cavities, beam pipe, beam pipe bellows) and partly to warmer regions such as HOM absorbers (intercepted at 45 K) located at each cryomodule interconnect and warm beam pipe outside of cryogenic sections of the accelerator. Estimates for total power deposition and fraction intercepted by the 2 K structures and by the 45 K absorbers come from analyses and simulations provided by accelerator physicists and are detailed in LCLSII-4.5-EN-0179. We estimate that 20% of HOM heating goes to the 2 K level.

LCLS-II magnet current leads, like those used at XFEL, are conductively cooled bronze leads based on the CERN LHC corrector current lead design. Since same current lead design is incorporated into the single spoke resonator cryomodule for the Fermilab PXIE project test linac at Fermilab, extensive analysis and testing have already been performed. Heat loads are scaled for our magnet current and number of leads from conclusions of the studies for PXIE.

An arbitrary small level of 1% of cavity dynamic heat, or approximately 0.7 W per cryomodule, is included to represent dark current, beam-induced heat in the cold beam tube bellows, and other sources of heat not yet explicitly taken into account.

Cryogenic distribution system heat loads were provided by cryogenic system designers, based on measurements for similar cryogenic valve boxes, end boxes, and transfer lines in Fermilab and CERN cryogenic systems.

Various sources of uncertainty arise. Static heat loads always show some variability due to measurement difficulties, assumptions made in analyses, and variations in assemblies. Dynamic heat loads depend on various analytical assumptions.

The major contributor to uncertainty in dynamic heat load is the unloaded quality factor. The nominal $Q_0 = 2.7 \times 10^{10}$ originated from a study to determine the unloaded Q required assuming existing cryoplant capacity of 18 kW total at 4.5 K-equivalent. Removing cavity dynamic heat consumes approximately 2/3 of total cryogenic power, thus a 10% change in Q_0 from the assumed average value implies approximately a 7% change in cryogenic power. However, HOM and wakefield heating and fraction intercepted by the 45 K HOM absorber present another significant dynamic heat uncertainty.

Our present analysis utilizes a final factor of 1.3 for static heat load uncertainty and a factor of 1.1 for dynamic. These multipliers are taken on the best-estimate totals of static and dynamic heat, respectively, with static heat including non-cryomodule heat loads from the distribution system.

6.4.3 Heat load results

A summary of predicted heat loads for steady-state CW operation *without* uncertainty margins at each temperature level are presented in Table 6-13. "Predicted" means best estimate without extra margins. A summary of heat loads for steady-state CW operation *with* uncertainty margins at each temperature level are presented in Table 6-14. For this case, calculations included a multiplier of 1.3 for static and 1.1 for dynamic heat to provide maximum expected heat loads.

Table 6-13. Summary of Base Predicted Heat Loads for Steady-State CW Operation, without uncertainty factors. 'Upstream' means the upstream portion of the linac fed by one of the two distribution lines from the cryoplant.

Predicted Heat Loads (base, no margin)	High Temperature Thermal Shield	Low Temperature Thermal Intercepts	2.0 K level
Upstream Static heat, [kW]	4.05	0.39	0.25
Downstream Static heat, [kW]	3.00	0.32	0.18
Upstream Dynamic heat, [kW]	1.04	0.05	1.23
Downstream Dynamic heat, [kW]	1.34	0.10	1.47
Total Upstream heat, [kW]	5.09	0.44	1.49
Total Downstream heat, [kW]	4.35	0.42	1.66
Total heat for LCLS–II linac, [kW]	9.44	0.86	3.14

Table 6-14. Summary of Maximum Expected Heat Loads Including Uncertainty Factor for Steady-state CW Operation

Maximum Expected Heat Loads (with uncertainty factor)	High Temperature Thermal Shield	Low Temperature Thermal Intercepts	2.0 K level
Upstream Static heat, [kW]	5.27	0.50	0.33
Downstream Static heat, [kW]	3.91	0.41	0.24
Upstream Dynamic heat, [kW]	1.14	0.06	1.36
Downstream Dynamic heat, [kW]	1.48	0.11	1.62
Total Upstream heat, [kW]	6.41	0.56	1.69
Total Downstream heat, [kW]	5.38	0.52	1.86
Total heat for LCLS–II linac, [kW]	11.80	1.08	3.54

The estimated heat load at 2 K is 3.5 kW including uncertainty factors and overheads, which is within the cryoplant design capacity of 4 kW at 2 K, allowing for an overcapacity margin.

6.5 Cavity Preparation and Testing

6.5.1 1.3 GHz Cavity Procurement

The preparation process includes procurement of cavity materials, procurement of dressed cavities, fully processed and assembled and ready for vertical acceptance testing. It should be

noted that this cavity procurement strategy follows closely the model established for the XFEL cryomodule assembly.

The niobium and niobium-titanium materials are purchased, inspected and then supplied to the cavity vendors. A key part of the inspection process includes eddy current scanning of the high residual resistance ratio (RRR) niobium sheets. In order to comply with 10CFR851, the various materials are appropriately marked and serialized to ensure traceability.

The cavity fabrication is divided into three parts: 1) mechanical fabrication and initial tuning, 2) cavity processing, including initial electropolishing and nitrogen doping, and 3) final assembly, including tuning, high pressure rinsing, cavity dressing, warm RF measurements, pressure testing and leak checking. The nitrogen doping process employed to attain high-Q_0 values requires the use of a furnace capable of 800°C and nitrogen injection. Electropolishing is necessary to prepare the surface before heat treatment and remove the damage layer after baking to uncover the final doped surface conditions. More details concerning the doping process can be found in *High-Q Development Plan and Choice of Q_0* LCLSII-4.5-EN-0216.

A dressed cavity consists of the cavity assembly with an integral helium vessel, the two-phase header tee, supply line connections, a pair of HOM probe feedthrough assemblies, one field probe feedthrough assembly, a beamline coupling feedthrough flange on the fundamental power coupler end of the cavity, a pumping flange assembly that includes a right angle valve and burst disk for the opposite beamline port, and a blank-off flange on the fundamental power coupler port. The components that close the various ports on the cavity are provided to the cavity vendors. The dressed cavity assembly is shipped and essentially ready for vertical testing.

6.5.2 Cavity Receipt and Preparation for Testing

The cavity preparation process includes receipt inspection, confirmation of vacuum and pressure integrity, verification of warm RF properties including cavity frequency and external coupling, and attachment to a vertical test stand. Once complete, the dressed cavity assembly is ready for vertical testing. A subset of cavities are prepared for horizontal testing in a test cryostat in order to monitor the quality of clean room assembly processes and provide feedback to the assembly teams. The horizontal testing configuration mimics the final cryomodule assembly and includes a successfully tested, dressed cavity with one of two options: 1) critically-coupled, with power supplied via a coaxial cable, or 2) over-coupled, with power supplied via a fundamental power coupler assembly.

6.5.3 1.3 GHz Cavity Testing

The main acceptance testing method is vertical testing of fully dressed cavities with critical coupling in order to confirm that the accelerating gradient and cavity quality factor meet requirements. Consideration for margin above nominal operating gradient and quality factor is taken into account. The full suite of RF parameters measurements include cavity frequency, pass-band frequencies and HOM coupling. Measurements are made to characterize important features such field emission level, residual resistance and local magnetic field in the test apparatus. A

subset of cavities are tested in a horizontal cryostat, with the capability to test either critically-coupled or over-coupled depending on the requirements of the specific test. When testing critically-coupled cavities, the test parameters are identical to those used in vertical testing. When testing over-coupled cavities, additional testing is required to evaluate the performance of the attached fundamental power coupler assembly. Measurements of field emission levels, residual resistance and local magnetic field are planned.

6.6 Cryomodules and String Assembly

6.6.1 1.3 GHz cryomodules

The assembly process for 1.3 GHz cryomodules is very similar to that developed for the XFEL cryomodule. The production of XFEL cryomodules is in a mature state, producing about one cryomodule per week at the facility in Saclay, France [35]. The Fermilab and JLAB production facilities include several major work stations: clean room (two work stations included), cold mass 1, cold mass 2, insertion, and final assembly (includes preparation for shipping). There is also a test facility for acceptance testing at both labs. shows the JLAB cryomodule production facility schematic; similar facilities for cryomodule assembly exist at Fermilab.

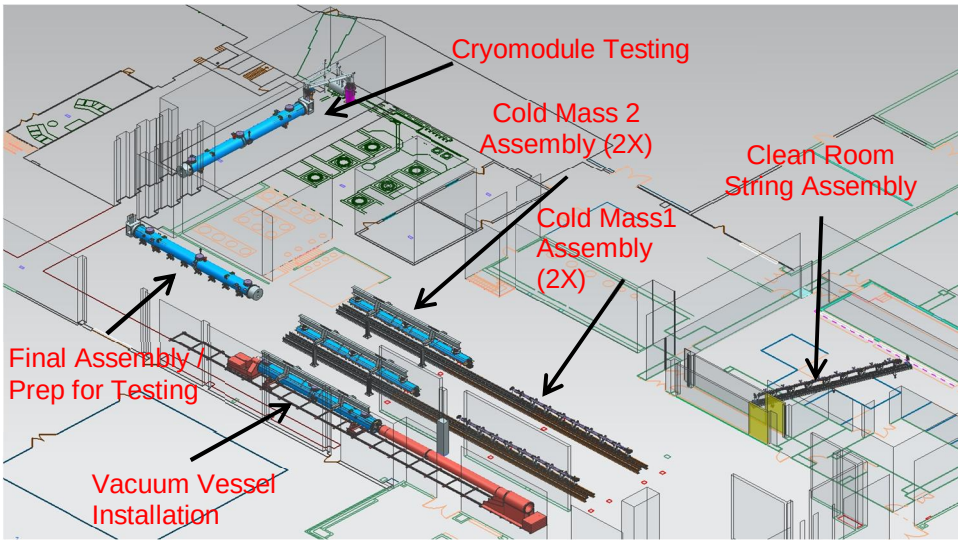

Figure 6-35. JLAB cryomodule production facility

6.6.1.1 Clean Room String Assembly

Installation of the fundamental power coupler and the cavity string assembly are in many ways the most critical assembly stages of the cryomodule assembly. It is here that qualified cavities are integrated with the magnet package drift tube, beam position monitor, fundamental power couplers, isolation valves and interconnecting bellows. The work is completed in ISO 4 clean rooms under very strict particulate and contamination control procedures. The assembly includes many bolted connections and utilizes sophisticated tooling to ensure proper mechanical assembly tolerances while minimizing the opportunity for contamination. Specialized ultra-high

vacuum equipment along with high purity gases are used for vacuum pumping, venting, and leak checking. Figure 6-36shows a model of the cavity string assembly.

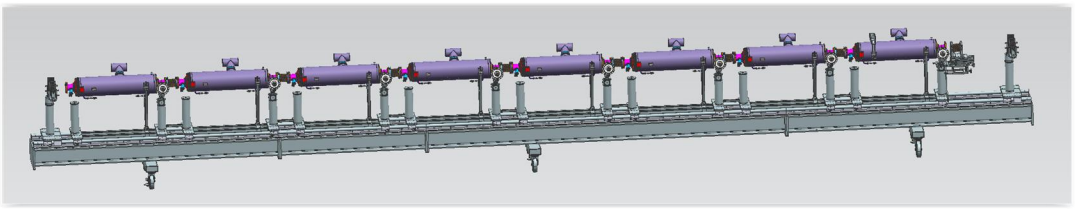

Figure 6-36. Cavity string assembly model

6.6.1.2 Cold Mass 1 workstation

Once completed, the cavity string is moved out of the clean room and into the Cold Mass 1 work station. In this work station the following components are installed, requiring multiple critical adjustments.

- Cavity frequency tuners, requiring the preset of cavity/tuner to ensure the cavity is always tuned in tension. This is done to avoid hysteresis in the mechanical tuner when operations include going from tension to compression.
- Magnetic shielding,
- Instrumentation including temperature sensors, heaters and liquid level sensors
- Invar tie rods, set to maintain the relative position of the cavities in the cryomodule
- The HOM ports are tuned to minimize the fundamental mode leakage
- Two-phase cryogenic line, which is completed with orbital welding. During this assembly phase the weld connections to the 2 phase cryogenic line are leak checked.

6.6.1.3 Cold Mass 2 workstation

The second cold mass assembly station work includes the installation of a large part of the cryostat components and transfer of the cold mass from the string tooling to the gas return pipe. Cryostat components include the cooldown lines, thermal straps, thermal shield, instrumentation, and multi-layer insulation. In this work station the split magnet package is installed around the drift tube and current leads are installed. The connection of the two-phase line to the gas return pipe is made and the cold mass is mounted on the gas return pipe. The cryogenic piping is leak checked , and pressure tested. It is at this stage that the cavity and other cold mass components are aligned using a laser tracker. Figure 6-37 shows the cold mass 2 work station at Fermilab.

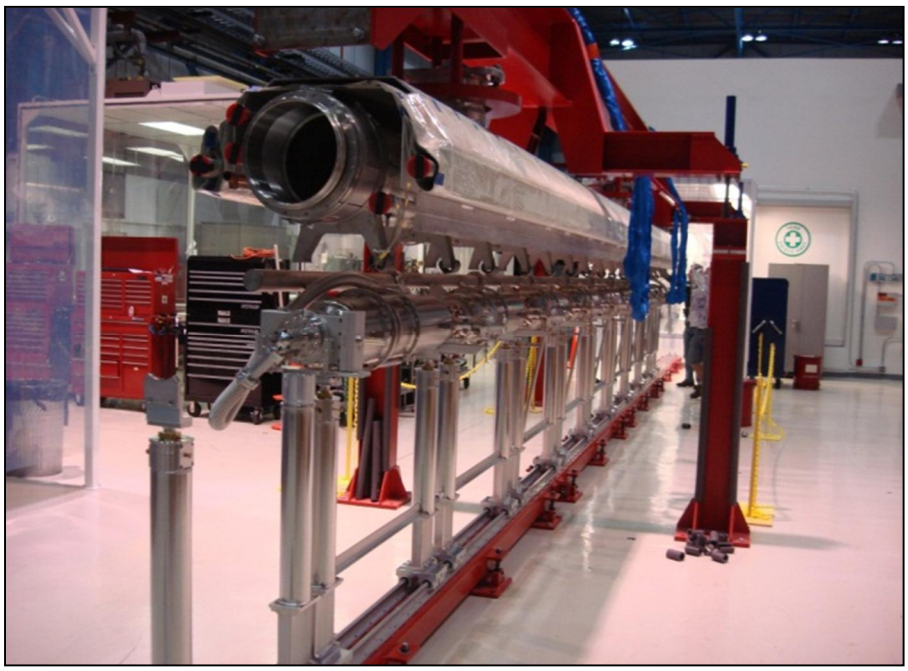

Figure 6-37. Cold mass 2 workstation, at Fermilab, with the "4-poster" assembly fixture (red frame) around the cold mass (ILC example)

6.6.1.4 Cold Mass Insertion

The cold mass is lifted off the "4 poster" assembly fixture (seeFigure 6-37) and installed, along with the vacuum vessel, on the massive cantilever tool. The vacuum vessel is slid/positioned over the cold mass and the cold mass support is transferred to the vacuum vessel using three support posts. Alignment and fiducalization takes place here, providing the references needed or positioning the cryomodule when installed in the SLAC tunnel. Figure 6-38 shows a layout of this workstation.

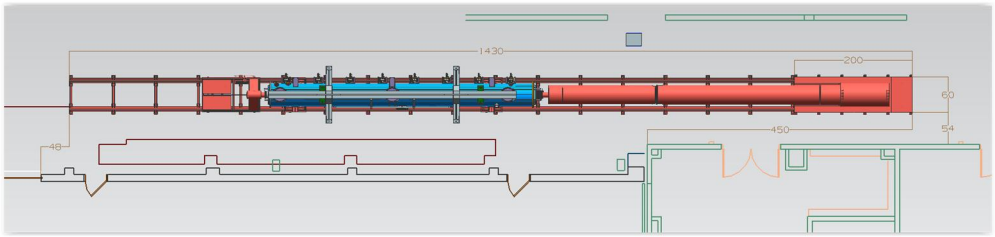

Figure 6-38. Layout of the cold mass insertion workstation. The cryomodule is shown in blue to the left, the long cantilever supporting the cold mass shown in red to the right.

6.6.1.5 Final assembly

This stage requires a significant amount of the overall work including terminating all instrumentation at the vacuum vessel, installing the warm part of the FPC, closing up all ports around the FPC and posts, and final leak checking of the vacuum vessel. The closure of the ports

on the vacuum vessel is a labor-intensive step. Once this is completed the cryomodule is ready for preparation for testing or shipping as appropriate.

6.6.2 3.9 GHz Cryomodules

The 3.9 GHz cryomodule assembly process is similar to that for the 1.3 GHz cryomodules described above, with the exception of the magnet which is not included in the 3.9 GHz cryomodules (although space is allocated in case they are needed). The two 3.9 GHz cryomodules are assembled at Fermilab.

6.7 Cryomodule Testing

Cryomodule acceptance testing is performed at Fermilab and JLAB on cryomodules after the final assembly is completed. Acceptance testing is designed to measure cryomodule performance to qualify cryomodules prior to shipping to SLAC. In addition to qualifying cryomodules, acceptance testing is the opportunity to learn about and provide feedback into the production process. The project baseline plan includes testing the first 50% of the cryomodules produced at both partner labs. This strategy allows for early feedback into the production process when it is most likely needed and also provides the experience necessary to develop confidence that the cryomodule performance is routinely consistent with eliminating the need for qualifying the cryomodules prior to shipping. That is to say, cryomodules are so reliable that acceptance testing adds little value. Testing processes include the following.

- Verifying instrumentation with special emphasis on interlock instrumentation.
- Measuring cavity performance, including quality factor, limiting accelerating gradient, RF coupling coefficients, and the onset of field emission gradient.
- Testing cavity tuner characteristics for range and resolution.
- Evaluating fundamental power coupler operating parameters and limitations for heating and vacuum degradation, if any.
- Measuring cryogenic performance including static and dynamic heat loads to the 2, 5, and 45 K circuits.
- Testing vacuum performance of the beamline, insulating, and fundamental power coupler systems.
- Qualifying the magnet package.

Figure 6-39 shows two models of the JLAB cryomodule test facility. Testing of cryomodules at Fermilab and JLAB are the rate limiting phase during production. As such, it is important to carefully specify the details of the test programs and develop personnel training procedures. The prototype cryomodules have additional instrumentation installed to support more extensive performance characterization. The schedule for testing the prototype cryomodules has some float, as the schedule for the first production cryomodule test is well past that of the prototype.

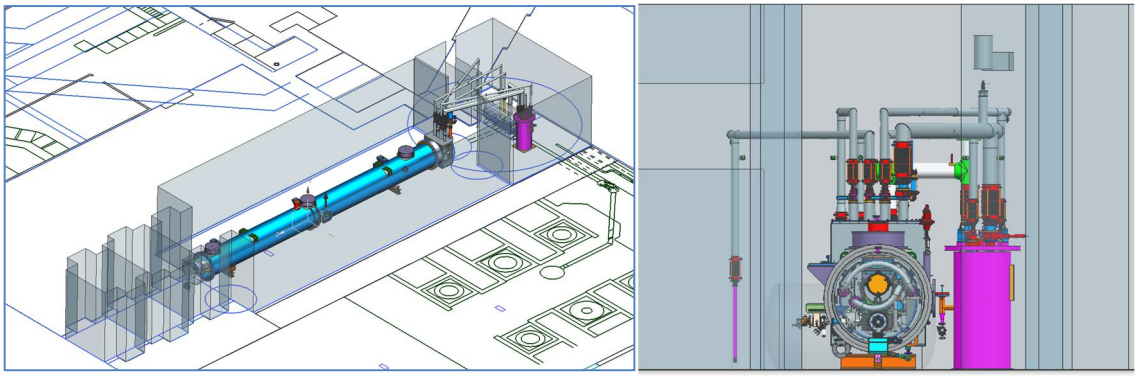

Figure 6-39. The JLAB cryomodule test facility. View of the cryomodule inside the shielded enclosure (left); cross section of the cryomdule under test (right)

6.8 Cryomodule Shipping and Installation

Fermilab and JLAB will be responsible for shipping cryomodules to SLAC after assembly and test. A dedicated shipping fixture, modeled after the existing XFEL fixture, will be designed and tested. Testing will include a shipping test of dead weight to simulate a production cryomodule, and one of the prototype cryomodules. Cryomodules are shipped to SLAC where they are accepted, stored until the tunnel is ready, and integrated in strings. We do not expect to store completed cryomodules at the producing labs. Three fixtures each for Fermilab and JLAB will be produced to support this plan. SLAC is responsible for the unloading of cryomodules as well as the acceptance inspections at SLAC. SLAC will remove shipping covers and return the fixtures and covers to Fermilab and JLAB.

Instrumentation is included during shipping to monitor acceleration, vacuum, and position of the cryomodules throughout the shipping process.

6.9 References

1 D. Proch, "The TESLA Cavity: Design Considerations and RF Properties", *Proc. of the Sixth Workshop on RF Superconductivity, CEBAF*, Newport News, Virginia, Oct. 4-8, 1993.
2 B. Aune et al., *Phys. Rev. ST Accel. Beams* **3,** 092001 (2000).
3 A. Yamamoto et al., "Advances in Superconducting RF Technology for the ILC", *Proc. 2012 Applied Superconductivity Conference*, Portland, OR, October 7-12, 2012.
4 "The International Linear Collider Technical Design Report," SLAC-R-1004, ISBN 978-3-935702-77-5 (2013).
5 C.Pagani "TTF Tuner Development: Saclay and INFN-Blade" *2005 ILC Workshop*, Snowmass, Colorado (2005).
6 N.Baboi, "Studies of High Order Modes in Accelerating Structures for Linear Collider", Dissertation, DESY (2001).
7 J.Sekutowicz, "Higher Order Mode Coupler for TESLA", TESLA preprint 1994-07. http://flash.desy.de/sites2009/site_vuvfel/content/e403/e1644/e1446/e1448/infoboxContent1690/tesla2000-39.pdf (2009).
8 W.D. Moeller, "High Power Coupler for TESLA Test Facility", http://tesla.desy.de/new_pages/TDR_CD/PartII/chapter02/references/Moeller99.pdf (1999).
9 F. Toral et al., "Design and fabrication study on the TESLA500 superconducting magnets," *IEEE Trans. Applied Superconductivity* **12,** 282 (2002).

10 F. Toral, et al., "Magnetization Effects on the Superconducting Combined Magnet Prototype for XFEL," *IEEE Trans. Applied Superconductivity* **19**, 1136 (2009).
11 C.M. Spencer, et al., "Measuring the Magnetic Center Behavior and Field Quality of an ILC Superconducting Combined Quadrupole-Dipole Prototype," *IEEE Trans. Applied Superconductivity* **20**, 1964 (2010).
12 V.S. Kashikhin, et al., "Superconducting Magnets for SCRF Cryomodules at Front End of Linear Accelerators," *Proceedings of IPAC'10*, 379, Kyoto, Japan(2010)
13 G.V. Velev et al., "A Fast Continuous Magnetic Field Measurement System Based on Digital Signal Processors," *IEEE Trans. Applied Superconductivity* **16**, 1374 (2006).
14 F. Toral, et al., "Final Design and Prototyping of the Superconducting Magnet Package for the Linear Accelerator of the European XFEL," *IEEE Trans. Applied Superconductivity* **24**, 4000706 (2014).
15 V.S. Kashikhin, et al., "Superconducting Splittable Quadrupole Magnet for Linear accelerators," *IEEE Trans. Applied Superconductivity*. **22**, 4002904 (2012).
16 N. Andreev, et al., "Conduction Cooling Test of a Splittable Quadrupole for ILC Cryomodules," *IEEE Trans. Applied Superconductivity*. **23**, 3500305 (2013).
17 D.M. Treyer et al., "Design and Beam Test Results of Button BPMs for the European XFEL," DESY Report DESY-2041-01447 (2013).
18 A. Lunin et al., "Development of a Button BPM for the LCLS-II Project," *TUPF18, IBIC14*, Monterey, CA (2014).
19 M. Fouaidy et al., "RRR of Copper Coating and Low Temperature Electrical Resistivity of Material for TTF Couplers", *TUP65, SRF* Ithaca, NY (2005).
20 .K. Bane, "The Short-Range Resistive Wall Wakefields", SLAC-PUB-95-7074(1995).
21 B. Podobedov et al., "Resistive wall wakefields in the extreme anomalous skin effect regime," *Phys. Rev. ST Accel. Beams* **12**, 044401 (2009).
22 D. Lipka et al., "Button BPM Development for the European XFEL," *MOPD19, DIPAC2011*, Hamburg, Germany(2011).
23 J. Sekutowicz et al., "Beam Tests of HOM Absorber at FLASH", *THPEC022, IPAC'10*, Kyoto, Japan (2010).
24 A. Grassellino, "Nitrogen and Argon Doping of Niobium for Superconducting Radio Frequency Cavities: a Pathway to Highly Efficient Accelerating Structures," http://iopscience.iop.org/0953-2048/26/10/102001/metrics (2013).
25 H. Padamsee, J. Knobloch, T. Hays *RF Superconductivity for Accelerators*,173, J. Wiley & Sons: New York (1998).
26 A. Crawford, "A Study of Thermocurrent Induced Magnetic Fields in ILC Cavities," http://arxiv.org/abs/1403.7996(2014).
27 D. Edwards, "TeSLA Test Facility Design Report," http://tesla.desy.de/TTF_Report/CDR/pdf/cdr_chap4.pdf, 157 (1995).
28 A. Romanenko, "Ultra-High Quality Factors in Superconducting Niobium Cavities in Ambient Magnetic Fields up to 190 mGauss", http://arxiv.org/abs/1410.7877 (2014).
29 A. Crawford, "A Study of Magnetic Shielding Performance of a Fermilab International Linear Collider superconducting RF Cavity Cryomodule,, http://arxiv.org/abs/1409.0828 (2014).
30 K. Flöttmann, T. Limberg, and P. Piot, "Generation of Ultrashort Electron Bunches by Cancellation of Nonlinear Distortions in the Longitudinal Phase Space," TESLA-FEL Report No. TESLA-FEL 2001-06(2001).
31 H. Edwards et al., "3.9 GHz Cavity Module for Linear Bunch Compression at FLASH", *Proc. Linear Accelerator Conference LINAC2010*, MO304, Tsukuba, Japan (2010).
32 E. Vogel, et al., "Test and Commissioning of the Third Harmonic RF System for FLASH", *Proc. IPAC'10*, THPD003, Kyoto, Japan (2010).
33 P. Pierini et al., "Status of the European XFEL 3.9 GHz System", *Proc. IPAC'12*, WEPPC009, New Orleans, USA (2012).
34 Khabiboulline, et al., "New HOM Coupler Design for 3.9 GHz Superconducting Cavities at Fermilab", *Proc. PAC 07*, WEPMN098, Albuquerque, USA (2007).
35 C. Madec et al,. "The challenges to Assemble 100 Cryomodules for E-XFEL," *Proc. SRF2013*, Paris, France (2013).

7 CRYOGENIC PLANT AND DISTRIBUTION

TECHNICAL SYNOPSIS

The LCLS-II cryogenic plant and distribution systems designs are based on existing technology, and major requirements are demonstrated at the CHL-II facility installed at CEBAF. Two major subsystems are involved, along with the associated auxiliary systems: the cryogenic plant, and the cryogenic distribution system. The cryogenic plant consists of warm recirculation compressors with associated cooling, oil-removal systems and dryers, cold boxes with heat exchangers, cold compressors, and ancillary support equipment. The cryogenic distribution system consists of the distribution box, vacuum insulated cryogenic transfer lines, feed caps and end caps on cryomodule strings, needed to feed and return the cryogens to the linac components. The systems are closed and supply cold helium at appropriate temperatures and pressures to the cryomodules, recirculating through the refrigerator. Cryogenic bypasses span the warm linac beamline elements, at the laser heater and bunch compressors. Several operating conditions are planned for, including rapid cooldown of the cavities within a single cryomodule to maximize magnetic flux expulsion.

The integrated systems convert compressed, ambient-temperature helium into superfluid, and deliver superfluid helium, cooled to 2.0 K by expansion at each cryomodule, to the accelerator cavities. Operation at 2.0 K allows achieving the efficiency of a high cavity quality factor while using existing technology demonstrated by the CEBAF CHL-II cryogenic plant. In addition, the systems serve cryogens to a nominally 5 K thermal intercept circuit, and a nominally 45 K thermal radiation shield and thermal intercept circuit.

The cryoplant is located approximately mid-way along the length of superconducting linac components, in a dedicated building north of the linac. From this central location, the distribution system feeds two arms, one running upstream and one downstream along the linac.

The refrigeration capacity of the cryogenic plant is approximately 18 kW at 4.5 K equivalent, 4 kW at 2.0 K, and is within the current capabilities of single 4.5 K and 2 K cold box designs. The capacity accommodates the cryogenic heat load estimate of 3.5 kW at 2 K, based on an average cavity quality factor Q_0 of 2.7×10^{10}, operating all cavities at a voltage of 15 MV/m, and with uncertainty factors associated with static and dynamic heat load estimates.

1
2
3
4
5
6
7

7.1 Scope, Schedule and Partner Lab Roles

The LCLS-II cryogenic systems are designed to support controlled cooldown of cryomodules and provide sufficient cooling capacity at appropriate temperature levels to enable operation of the superconducting cavities and other cryogenic components within their respective operational conditions, as described in Chapter 6. Figure 7-1shows the cryogenic systems schematic layout. The three major subsystems are the cryogenic plant, its associated auxiliary systems, and the cryogenic distribution system. Cryogenic plant and distribution systems designs are based on existing technology, and the cryoplant requirements have been demonstrated at the Central Helium Liquifier (CHL-II) facility installed at CEBAF.

The major refrigerator components of the cryogenic plant, that is, the warm and cold compressors, the 4.5 K cold box, 2 K cold box, and ancillary equipment, are located external and adjacent to the linac and klystron gallery. The 4.5K cold box has a refrigeration capacity of approximately 18 kW at 4.5 K equivalent that provides the required cooling capacity for the cryomodules for operating at 2 K, the low temperature thermal intercepts that are held at a nominal temperature of 5 K, and the high temperature thermal shield and thermal intercept that operates at a nominal temperature of 45 K.

The interface boxes and distribution boxes are located in the klystron gallery. Cryogenic transfer lines pass from the distribution boxes into and along the accelerator enclosure. The connections to the distribution boxes are from the interface between the cryogenic plant (cryoplant or CP) and the cryogenic distribution systems (CDS).

The cryogenic distribution system supplies cryogens to two lines, one running upstream and one downstream from the cryoplant, and returns cryogens to the cryoplant, which is centrally located with respect to the superconducting linac. The heat loads are approximately equal in each string. Under normal operation, the plant cools both cryomodule strings. Cryogenic bypasses allow for warm accelerator beamline sections between the cryomodule strings. Three bypasses are planned: one for a laser heater and two for bunch compressors. The scope of this work extends to the interface with the distribution box

Partner Lab roles are divided between the cryoplant and cryogenic distribution systems such that JLAB has responsibility for the cryoplant, and Fermilab has responsibility for the CDS. Cryoplant components are specified and procured by JLAB and delivered to SLAC, Cryogenic distribution systems components are designed and procured by Fermilab and delivered to SLAC. Both Fermilab and JLAB provide civil infrastructure requirements and specifications to SLAC, and both manage installations and commissioning of their respective systems.

Cryoplant production involves significant interaction with vendors in developing the design-to-specification systems. JLAB is responsible for procurements and for technical interactions with vendors. Early procurement is required for the 4.5 K cold box in order to meet the project schedule.

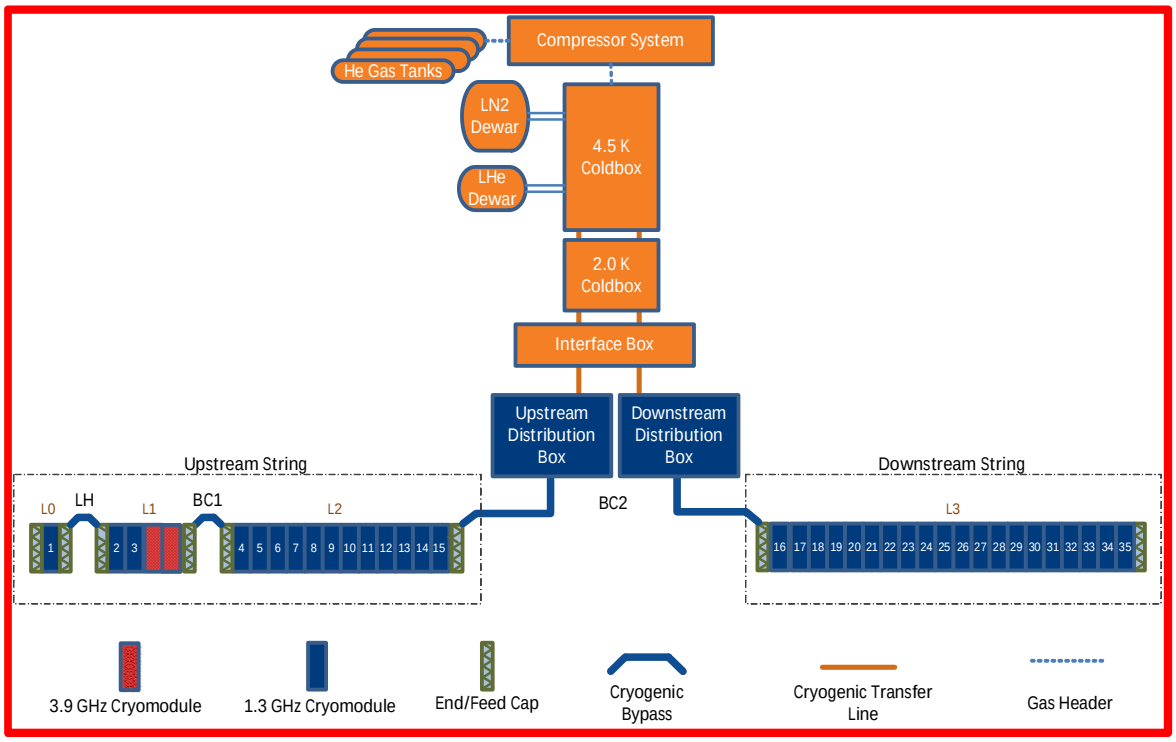

Figure 7-1. LCLS-II cryogenics systems schematic layout. The refrigeration system is located centrally along the linac,and distributes cryogenic cold helium upstream and downstream. Cryoplant systems components are shown in orange, cryogenic distribution systems in blue.

Major roles and responsibilities are:

SLAC

- Utilities and civil construction
- Controls interfaces
- Coordination and integration

JLAB

- Cryoplant design specification and procurement
- Warm recirculation compressors
- Helium purification systems
- Helium gas storage
- Liquid nitrogen storage
- Liquid helium storage
- 4.5 K cold box

- 2 K cold box
- Interface box
- Plant control PLC and instrumentation
- Installation and commissioning of the cryoplant

Fermilab

- Cryogenics distribution systems design and procurement
- Distribution boxes
- Vacuum insulated cryogenic transfer lines
- Cryomodule feed caps
- Cryomodule end caps
- Cryogenic bypass lines
- Installation and commissioning of the cryogenics distribution systems

High-level systems design requirements, specifications, and interfaces are captured in the documents listed in Table 7-1. The schedule for major design reviews is given in Table 7-2. Figure 7-2 shows the overall schedule for cryogenic plant and distribution systems.

Table 7-1. Cryogenic plant and distribution systems-level requirements and specifications, and related technical notes

Document Type	Title	Document Number
Engineering Note	Cryogenic Heat Load	LCLSII-4.5-EN-0179
Functional Requirements	Cryogenic Plant	LCLSII-4.8-FR-0244
Functional Requirements	Cryogenic Distribution System	LCLSII-4.9-FR-0057
Physics Requirements	Availability	LCLSII-1.1-PR-0163
Interface Control	Accelerator to Cryogenics	LCLSII-2.5-IC-0056
Interface Control	Cryogenic Distribution System	LCLSII-4.9-IC-0058
Interface Control	Cryoplant to Infrastructure Systems	LCLSII-5.4-IC-0235
Interface Control	Electron Beam Controls To Accelerator Systems, Cryogenic Systems, Photon Systems, and Infrastructure Systems	LCLSII-2.7-IC-0266
Engineering Note	Cryoplant design, segmentation and upgrade options	LCLSII-4.5-EN-0187
Engineering Note	Cryogenic Plant Seismic Design Criteria	LCLSII-4.8-EN-0227

Engineering Note	Cryogenic Plant Construction and Operation Noise Assessment	LCLSII-5.4-EN-0215
Engineering Note	Pressure System Requirements per ES&H Manual Chapter 14	LCLSII-1.2-EN-0020
Engineering Note	Cryogenic and Oxygen Deficiency Hazards Requirements per ES&H Manual Chapter 36	LCLSII-1.2-EN-0063
Engineering Note	LCLS-II Commitments via Environmental Assessment	LCLSII-1.2-EN-0250
Engineering Note	Cryogenic System Process	LCLSII-4.1-EN-0327
Engineering Note	Cryogenic System Operating Temperature	LCLSII-4.5-EN-0185
Engineering Note	Gradient Optimization	LCLSII-4.5-EN-0217
Engineering Note	Cryogenic Distribution Seismic Design Criteria	LCLSII-4.9-EN-0225
Engineering Note	Cryomodule Design Heat Flux for Vacuum Failures	LCLSII-4.5-EN-0214
Engineering Note	Cryoplant Margin, Operability and Maintainability	LCLSII-4.8-EN-0336

Table 7-2. Cryogenic Plant and Distribution System-Level Design Review and Specifications Schedule.

System	Component	Review	Date
Cryogenics Systems	Cryogenics Systems	Preliminary Design Review	August 2014
Cryogenic Plant	4.5K Cold Box	Specification Release	September 2014
	2K Cold Compressors	Specification Release	October 2014
	Warm Helium Compressors	Specification Release	January 2015
Cryogenic Distribution	Distribution (Tunnel and Surface Components)	Preliminary Design Review	January 2015
	Distribution (Tunnel and Surface Components)	Final Design Review	July 2015

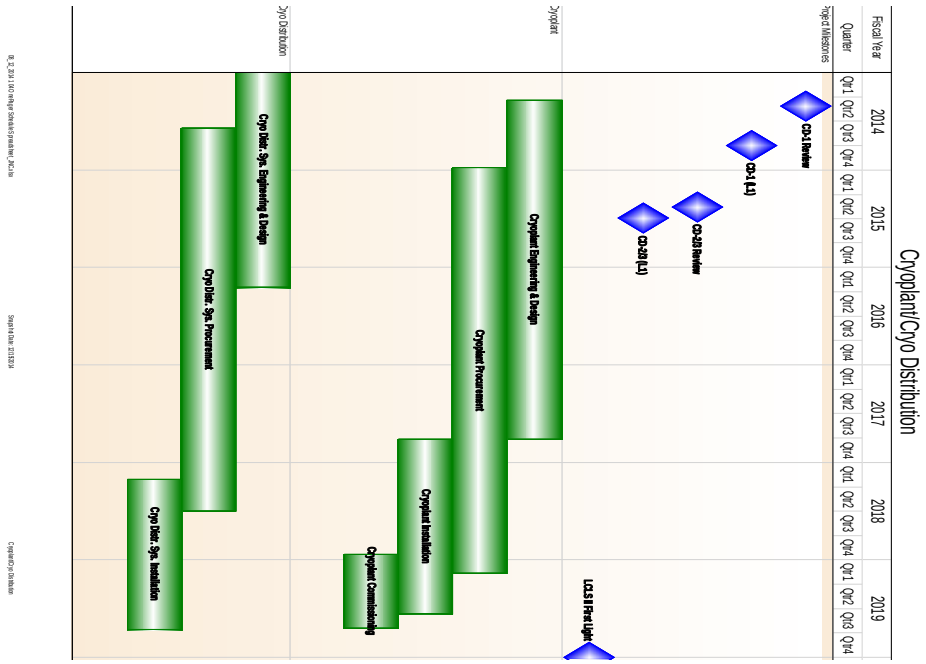

Figure 7-2. Cryogenic Plant and Distribution Systems Production Schedule

7.1.1 Design Maturity

The LCLS-II Project Final Design Plan LCLSII-1.1-QA-0065 provides for a phased completion of the final designs for the LCLS-II facility. The plan ensures that designs are sufficiently mature to start procurements and construction, while enabling the most cost-effective schedule for constructing the facility and maximizing the technical capabilities of the facility at CD-4. Final design readiness at CD-3 recognizes that that not all subsystems will reach final design at the same time. Project-level requirements and interface control points between Accelerator Systems, Cryogenic Systems, Photon Systems and Infrastructure are defined at CD-3, which ensures that the phased procurements and construction are appropriate for the final design of the LCLS-II. Chapter 2, Project Overview, contains additional discussion of the approach to design completion. The Cryogenic Systems design, described in this chapter and Chapter 6, is evaluated to be 80% complete. Completing remaining design after CD-3 allows for advancement of project schedule and minimizing cost by starting long duration activities when associate designs are sufficiently mature.

7.2 Requirements

The linac cryogenic system consists of three major subsystems: the cryogenic plant, the cryogenic distribution system, and the associated auxiliary systems. The system is expected to operate for 20 years, with an estimated continuous operation of two to five years without a scheduled shutdown. Scheduled maintenance shutdown is nominally six weeks in duration. The expected availability of the cryogenic system is 98.6%, after optimization with operating experience.

The cryogenic heat load estimate is discussed in Section 6.4 and also documented in *Cryogenic Heat Load* LCLSII-4.5-EN-0179. It includes 30% and 10% uncertainty factors associated with static and dynamic heat load estimates, and a summary of the heat loads can be found in Table 7-3. The required plant capacity is within that of existing designs for single cold boxes at 4.5 K and 2 K. As a result, the baseline design is similar to the CEBAF CHL-II, with refrigeration capacity of approximately 18 kW at 4.5 K equivalent.

Table 7-3. LCLS-II cryogenic systems heat loads, including uncertainty factors.

Maximum Expected Heat Loads (with uncertainty factor)	High Temperature Thermal Shield	Low Temperature Thermal Intercepts	2.0 K level
Upstream Static heat, [kW]	5.27	0.50	0.33
Downstream Static heat, [kW]	3.91	0.41	0.24
Upstream Dynamic heat, [kW]	1.14	0.06	1.36
Downstream Dynamic heat, [kW]	1.48	0.11	1.62
Total Upstream heat, [kW]	6.41	0.56	1.69
Total Downstream heat, [kW]	5.38	0.52	1.86
Total heat for LCLS–II linac, [kW]	11.80	1.08	3.54

7.2.1 Functional Requirements

The cryogenic plant consists of warm recirculation compressors with associated cooling, oil-removal systems, and dryers and cold boxes with ancillary support equipment. The system converts compressed, ambient-temperature helium into superfluid helium. The cryogenic distribution system consists of distribution boxes, cryogenic transfer lines, feed and end caps, and cryogenic bypasses that span warm linac beamline sections. The auxiliary system consists of warm helium gas-storage tanks, interconnecting piping between the various systems and components, a liquid nitrogen (LN_2) storage-dewar system, liquid helium (LHe) storage dewar, a purifier system, an instrument air system, cold box chilled water system, and associated cryogenic safety systems. The cryogenic system is located in the center of the linac to balance the load, as shown inFigure 7-1. This allows the plant to cool the upstream cryomodule string independent of the downstream string.

The cryogenic system as a whole is required to perform the following functions:

- Provide sufficient cooling at appropriate temperature levels to enable operation of the SRF cavities and other cryogenic components within their respective operational conditions.
- Ensure that the system shall support controlled cooldown of cryomodules.
- Ensure that the system and its components comply with the SLAC ES&H manual.
- Provide for proper protection of process fluids from contamination.

Details of the functional requirements can be found in the *Cryogenic Plant Functional Requirements Specification Document* LCLSII-4.8-FR-0244 and the *Cryogenic Distribution System Functional Requirements Specification Document* LCLSII-4.9-FR-0057. Systems requirements and design are also discussed in documents listed inTable 7-1.

7.2.2 Helium Refrigerator Description

The linac refrigeration system consists of two integrated sections: a 4.5 K cold box and a 2 K sub-atmospheric cold box. A reduction in helium vapor pressure necessary to reach superfluid temperatures is achieved by using only cold compression, as shown in Figure 7-2Table 7-2. This full cold compressor cycle has been implemented at CEBAF and SNS, and is planned for FRIB.

Operating costs for the cryogenic system are significant. It is thus desirable to make the cryogenic system as efficient as is practically possible during normal operation, as well as at expected lower capacity operating conditions. Turn-down capability of the helium flow through the cold compressors is limited at a constant pressure ratio due to the surge line associated with the hydrodynamics of the compressor wheel. Two methods can be used to turn down the flow while avoiding the surge line: reducing the suction pressure in the warm vacuum compressor of the hybrid cycle, or adding another cold compressor stage in the full cold compressor cycle. For LCLS-II, an additional fifth stage of cold compressor is provided.

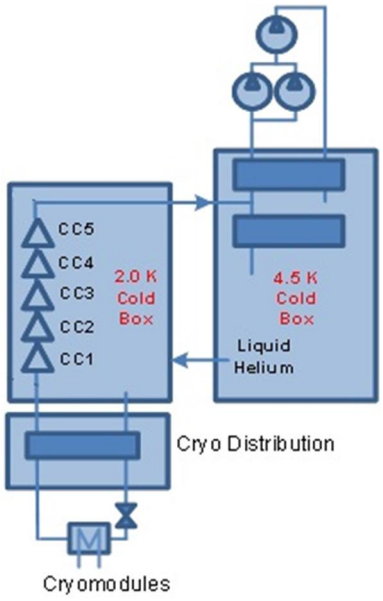

Figure 7-3. Full cold compressor 2 K refrigeration cycle adopted by LCLS-II

The design cryogenic plant capacity is given in Table 7-4, consistent with the existing cryogenic plant used by the JLAB 12 GeV upgrade project. Since cryogenic plants of this type are custom-designed, the use of an existing design offers saves time and money by compressing the vendor engineering and design phase. As a result, the baseline configuration for the LCLS-II cryogenic plant consists of the combined JLAB 4.5 K and 2 K cold boxes, shown in Figure 7-3.

Table 7-4. Cryogenic plant design capacity

Thermal load temperature	System design capacity
2 K	4.0 kW
5K to 8K	1.3 kW
40K to 55K	14 kW

7.2.3 Cryogenic Systems Operating Conditions

The cryogenic system is designed to operate as efficiently as is practical over a wide range of operating requirements. Efficiency is particularly important for operating conditions that are expected to last for extended periods of time. Operating conditions for the cryogenic systems are specified in *Cryogenic Heat Load*, LCLSII-4.5-EN-0179, and include the following:

7.2.3.1 Full linac 2.0 K CW maximum heat load operation

This represents the normal 2.0 K CW linac operation with beam, and is based on estimated heat loads with uncertainty factors. There is no mode with only one of the linac strings at 2.0 K. Either both of the linac strings are pumped down to sub-atmospheric pressure, or neither is pumped down.

7.2.3.2 Full linac 2.0 K CW nominal heat load operation

This represents the nominal 2.0 K CW operation of the linac at the estimated heat load and with no uncertainty factors applied.

7.2.3.3 Full linac 4.5 K standby

This represents the 4.5K linac standby operation. The cryogenic system must allow operation of one or both strings at 4.5 K. When one string is not at 4.5 K, the cryogenic system must allow positive isolation while at 300 K or during cooldown from 300 K to 4.5 K.

7.2.3.4 Linac cooldown to 80 K or warmup to 300 K.

This represents the cooldown or warmup of the linac between 300 K and approximately 80 K. This mode allows full linac warmup or cooldown without the use of turbines. The cryogenic distribution system mixes warm shield supply flow (at 80K and its nominal pressure) with 300 K gas to achieve the required temperature level. Return flow to the cold box during cooldown or warmup bypasses the low pressure flow around heat exchangers up to discrete temperature inlet points. The cryogenic plant recovers refrigeration for return flow below 200 K. This mode considers warmup or cooldown of both strings simultaneously.

7.2.3.5 One cryomodule warmup above transition (to as much as 40 K) and recooling.

During warmup, the linac 2.0 K circuits must be pressurized to positive pressure, and cold compressors are bypassed. Liquid helium in cryomodules remains below 4 K and stratified under positive pressure. The removal of liquid helium from the cryomodule to be warmed up requires

use of electric heaters. This results in a slow boil-off rate, with 4.5 K vapor being added to the 300 mm pipe. Subsequent warmup above saturation temperature with the sub-cooled helium supply line cold requires an electric heater on the supply line from the cooldown valve, slow flow taken and warmed via the cooldown line for that one cryomodule. The second string is in the same state as the string containing the cryomodule being cycled through transition.

7.2.3.6 One string cold at 4.5 K while the other string is warmed up or cooled down.

This mode maintains one string at 4.5 K while the other string is warmed up to 300 K or cooled down to 4.5 K. The cryogenic system must allow operation of one string at 4.5 K while the other string is under a controlled warmup or cooldown between 300 K and 4.5 K.

7.2.3.7 Cooldown from 80 K to 4.5 K

This mode completes cooldown and fill of a linac string to 4.5 K. The cryogenic system must allow operation of one string in this mode while the other string is held at either 300 K or 4.5 K.

7.2.3.8 Fast Cryomodule Cooldown from 40 K

This mode allows for a fast cooldown of a cryomodule through superconducting transition in order to reset the magnetic field trapped in the cavities to a lower level. The cryogenic system must allow operation of one string in this mode while the other string is held at either 300 K or 4.5 K.

7.2.4 Warm Helium Compressors

The 4.5 K helium refrigerator plant's compressors consist of multi-stage, oil-flooded screw compressor skid assemblies to compress ambient temperature helium gas from 1 atmosphere to the inlet service pressure required for the 4.5 K refrigerator operation. The estimated power use is 3.6 MW for the steady state plant operation. The compressor skids are grouped into low, medium and high pressure piping manifolds. Trace oil contained within the helium gas is removed from the supply process flow into the 4.5 K cold box to less than 1 ppb_v.

7.2.5 Gas Management and Storage Systems

The supply and return gas piping manifold from the compressor system to refrigerator is controlled by a gas management system — a series of valves that transfer helium gas into and out of the cryogenic system from gas storage tanks, and compressor bypass valves that control pressures within the cold box and the LHe stored in the linac cryomodules. The gas management system can also recover the liquid and store it in gaseous form during a plant warmup to ambient temperature. To accomplish this, five 4,000 scf gaseous helium storage tanks and one 10,000 liquid liter helium dewar are provided. The LHe dewar provides a refrigeration capacity buffer to stabilize the refrigeration supply between the refrigerator and the linac, and also enables performance testing of the refrigeration system prior to connection to the linac.

7.2.6 LN2 Precooling System

Liquid nitrogen is supplied by one double-walled, vacuum-insulated 31,000-gallon horizontal dewar with a maximum allowable working pressure of 250 psi. External to the dewar, an ambient air vaporizer is used to provide pressurized nitrogen gas supply to the facility. The dewar and vaporizer are located outdoors. Liquid nitrogen is fed to the facility by a single-circuit, vacuum-insulated transfer line. The transfer line is insulated with multilayer super-insulation to minimize heat flux.

7.2.7 Vacuum Systems

Utility and guard vacuum systems support the operation of the refrigerators. The insulating vacuum systems are comprised of diffusion / mechanical vacuum pump systems for the 4.5 K and 2 K cold boxes. Each is equipped with local controls for the pumps and their associated isolation valves and instrumentation to maintain the cold box insulating vacuum to 10^{-6} Torr. In the event of a power failure, the system automatically shuts down and isolates the system from the cold box to maintain the insulating vacuum. Local and remote monitoring instrumentation is provided for determining the system performance and status.

A guard vacuum system is provided to guard relief devices and other boundaries that are part of the subatmospheric system, to minimize air contamination into the 2 K systems during normal operation.

Portable and fixed utility vacuum pumps, along with LN2 cooled traps, are used to decontaminate piping that has been opened to air during maintenance or repair. Typical use of the utility pumps include three evacuations of the process volumes with back fills of pure helium gas. LN2 cooled traps provide visual indication of the effectiveness of the moisture contamination removal and protection of the utility pump oil from degradation.

7.2.8 Cryogenic Distribution System

The cryogenic distribution system connects the cryoplant to the cryomodule strings, and consists of the equipment needed to supply and return the cryogens via vacuum-insulated pipelines to the linac components needing these services throughout the entire linac. This equipment includes distribution boxes, cryogenic transfer lines, feed and end caps, and cryogenic bypasses to facilitate warm linac beamline elements.

7.2.9 Utilities

The cryogenic plant warm helium compressors carry a high inductive electrical load due to the motor drive of the compressors. The electric substation that provides power to the cryogenic plants must be sized to provide the magnetization start current to the largest compressor motor during the time when all other motors are running, and the starting applied voltage at the motor does not drop to less than 80% of nominal voltage rating. Although the cryogenic plant is only expected to use 3.6 MW of electric power during nominal operation, the substations are substantially larger due to the high percentage of inductive load and voltage drop during starting.

The demonstrated successful and recommended substation electrical power for the cryogenic systems is 7.5 MW.

7.3 Cryogenic Plant Design

7.3.1 Cryogenic Cycle and Cryoplant Operating Modes

JLAB modeled the cryoplant performance of its 12 GeV cryogenic plant, and developed a similar model based on LCLS-II requirements. The purpose of the model is to establish and validate that the plant design performance, as specified in

Table 7-5 –through Table 7-10, can be achieved by a single combination of cryogenic equipment. The cycle establishes the extreme operational boundaries of the plant between full maximum liquefaction and refrigeration. Within these two boundary operating conditions, the plant can provide a full domain of refrigeration load combinations between partial liquefaction and various temperature refrigeration requirements of activities such as load cooldown, warmup and steady state operation. Cryoplant design and commissioning experience for the JLAB 12 GeV plant is documented in [1, 2].

Additional operating conditions set the performance expectations of the cryogenic plant for various temperatures between the extreme conditions of maximum refrigeration and liquefaction modes. An included 4.5 K standby capability establishes the requirement for operation above 2 K, where the cryogenic plant can maintain 4.5 K liquid in the cryomodules during extended periods without beam to substantially reduce utility requirements as compared to 2 K operation. A total of six cryogenic plant operating modes have been validated by the cycle study and are presented in the following sections. These modes form the basis for the 4.5 K cold box specification.

The piping and instrumentation diagrams for the cryoplant are listed in Table 7-11.

7.3.1.1 Mode 1: Maximum 4.5K Cold Box Design Capacity

This mode is the design mode for the 4.5 K plant. It defines the turbines flow coefficients and the compressors sizes. The loads are the estimated loads including uncertainty factors.

Table 7-5. Mode 1, maximum 4.5 K cold box design capacity

		Supply		*Return*		
Load	***w*** **[g/s]**	**p [atm]**	**T [K]**	**p [atm]**	**T [K]**	**q [kW]**
Warm Shield	≤136	≥3.5	≤35	≥2.5	≤55	≥14
Cold Intercept	≤37	≥3.25	5.5	1.29	7.50	≥1.29
4-K Refrigeration						
4-K Liquefaction	≥15	≥3.2	4.5	1.10	300.0	
Sub-Atmospheric	≥200	≥3.2	4.5	1.20	30.0	

7.3.1.2 Mode 2: Nominal Turn Down

This mode is the continuous 2 K CW operation mode, at estimated heat load with no uncertainty factors applied.

Table 7-6. Mode 2, nominal turn down

		Supply		*Return*		
Load	***w*** **[g/s]**	**p [atm]**	**T [K]**	**p [atm]**	**T [K]**	**q [kW]**
Warm Shield	≤94	≥3.5	≤35	≥2.5	≤55	≥9.8
Cold Intercept	≤27	≥3.2	5.5	1.29	7.50	≥0.86
4-K Refrigeration						
4-K Liquefaction						
Sub-Atmospheric	≥157	≥3.2	4.5	1.20	30.0	

7.3.1.3 Mode 3: Maximum Liquefaction

In this mode we use the turbines flow coefficients obtained in the maximum capacity mode to size the turbines wheels and the brake coolers.

Table 7-7. Mode 3, maximum liquefaction

		Supply		***Return***		
Load	***w*** **[g/s]**	**p [atm]**	**T [K]**	**p [atm]**	**T [K]**	**q [kW]**
Warm Shield	≤144	≥3.3	≤44	≥2.3	≤56.5	≥9.4
Cold Intercept	≤20	≥3.2	≤5.8	≥1.23	≤10.8	≥0.86
4-K Refrigeration						
4-K Liquefaction	≥140	≥3.2	4.5	1.10	300.0	
Sub-Atmospheric						

7.3.1.4 Mode 4: Maximum Refrigeration

This mode is used to match the compressors flow capacity to the different loads. It is also used to size the heat exchangers.

Table 7-8. Mode 4, maximum refrigeration

		Supply		*Return*		
Load	***w*** **[g/s]**	**p [atm]**	**T [K]**	**p [atm]**	**T [K]**	**q [kW]**
Warm Shield	≤136	≥3.5	≤35	≥2.5	≤55	≥14.16
Cold Intercept	≤31	≥3.2	≤5.3	≥1.23	≤8.8	≥1.29
4-K Refrigeration	≤481	≥3.2	≤4.5	≥1.23	≤4.45	≥9
4-K Liquefaction						
Sub-Atmospheric						

7.3.1.5 Mode 5: Maximum Fill

This mode is designed to provide maximum capacity for the plant to fill all headers and cryomodules once the minimum operating pressure is achieved.

Table 7-9. Mode 5, maximum fill

		Supply		*Return*		
Load	***w*** **[g/s]**	**p [atm]**	**T [K]**	**p [atm]**	**T [K]**	**q [kW]**
Warm Shield	≤135	≥3.7	≤35	≥2.7	≤55	≥14.16
Cold Intercept	≤35	≥3.2	≤5.3	≥1.23	≤7.8	≥1.29
4-K Refrigeration						
4-K Liquefaction	≥45	≥3.2	4.5	1.10	300.0	
Sub-Atmospheric	≥157	≥3.2	4.5	1.20	30.0	

7.3.1.6 Mode 6: 4.5K Standby

This mode consists of maintaining the cryomodules at 4.5 K to minimize cost of operation when the beam is down.

Table 7-10. Mode 6, 4 K standby

		Supply		***Return***		
Load	***w*** **[g/s]**	**p [atm]**	**T [K]**	**p [atm]**	**T [K]**	**q [kW]**
Warm Shield	≤79	≥3.7	≤35	≥2.7	≤55	≥9.1
Cold Intercept	≤20	≥3.2	≤5.3	≥1.23	≤7.5	≥0.7
4-K Refrigeration	≤23	≥3.2	≤4.5	≥1.23	≤4.5	≥0.4
4-K Liquefaction						
Sub-Atmospheric						

Notes for

Table 7-5 through Table 7-10:

[1] Shield load pressure drop shall be 1.0 atm for all modes.

[2] 4.5-K refrigeration load return condition is saturated vapor at the specified pressure.

[3] Mode-6 (Stand-by) shall be designed for minimum number equipment operation (both the of compressors and turbines) and with at least 40% of the Mode-1 compressors off.

[4] ≤ indicated listed value is a maximum allowed/required.

≥ indicated listed value is a minimum allowed/required.

Table 7-11. Piping and Instrumentation Diagrams (P&ID) for the Cryoplant

P&ID Title	JLAB Drawing Number
LCLSII Warm Helium Compressor System	79120-0002
LCLSII Low Pressure Compressor	79120-0003
LCLSII Medium Pressure Compressor	79120-0004
LCLSII High Pressure Compressor	79120-0005
LCLSII Oil Removal System	79120-0700
LCLSII Oil Management System	79120-0701
LCLSII Gaseous Helium Storage	79720-0000
LCLSII LHe Storage Dewar System P&ID	79720-0120
LCLSII LN2 Storage Dewar P&ID	79720-0200
LCLSII He Gas Distribution System P&ID	79320-0000

7.3.2 Cryogenic Circuit Configuration

The cryogenic system contains six cryogenic circuits, as shown in the process flow diagram in Figure 7-3. Each cryomodule contains these same lines, as well as the cryogenic transfer lines described in chapter 6 and in Section 7.4. Cryomodules also have additional lines, described in Section 6.2.

Line A (sub-cooled helium supply) supplies supercritical helium to cryo-modules. Supercritical helium gas exits the 4.5K cold box at approximately 3.2 atm and 4.5 K. The Line A supercritical gas gets sub-cooled to approximately 2.5 K in a counter-flow 2-4 K heat exchanger by the sub-atmospheric (0.031 mbar) saturated helium gas exiting from the cryo-modules and then expands via a JT valve for the initial cooling and filling of the superconducting cavities LHe tanks.

Line B (gas return pipe) serves as return header that routes the boil off helium gas from the cryo-modules at 0.031 atm and 2K to the suction of the cold compressor.

Lines C (low temperature intercept supply) and D (low temperature intercept return) provide the supply and return helium gas flow, respectively, for cooling the low temperature intercepts at a nominal temperature of 5.5K. Line C delivers helium gas at 3.2 atm and 5.5 K and Line D returns the flow back to the 4.5K cold box at 1.3 atm and 7.5K

Lines E (high temperature shield supply) and F (high temperature shield return) provide the cooling for the thermal radiation shields. The thermal shield circuit is fed by the 4.5 K cold box at 3.7 atm and 35K via Line E. After cooling the radiation shield of all the cryomodules the helium gas returns to the 4.5K cold box via Line F at 2.7 atm and 55K.

Figure 7-4 also shows the two bypass headers, high pressure and low pressure, connecting the main compressor with the cryogenic distribution system bypassing the 4.5K cold box. These headers connect the main compressor discharge to the supply Lines A, C, and E and the main

compressor suction to the return lines B, D, and F. These headers assist in the initial controlled cooldown (for mixing 300K gas with the 4.5K cold box stream) and warmup or during cooldown of one linac string while keeping the other string cold. These high pressure and low pressure headers are also connected to the recovery and purifier compressor system discharge and suction, respectively.

Process flow diagrams for the various linac operating conditions have been studied and documented in *Cryogenic System Process* LCLSII-4.1-EN-0327.

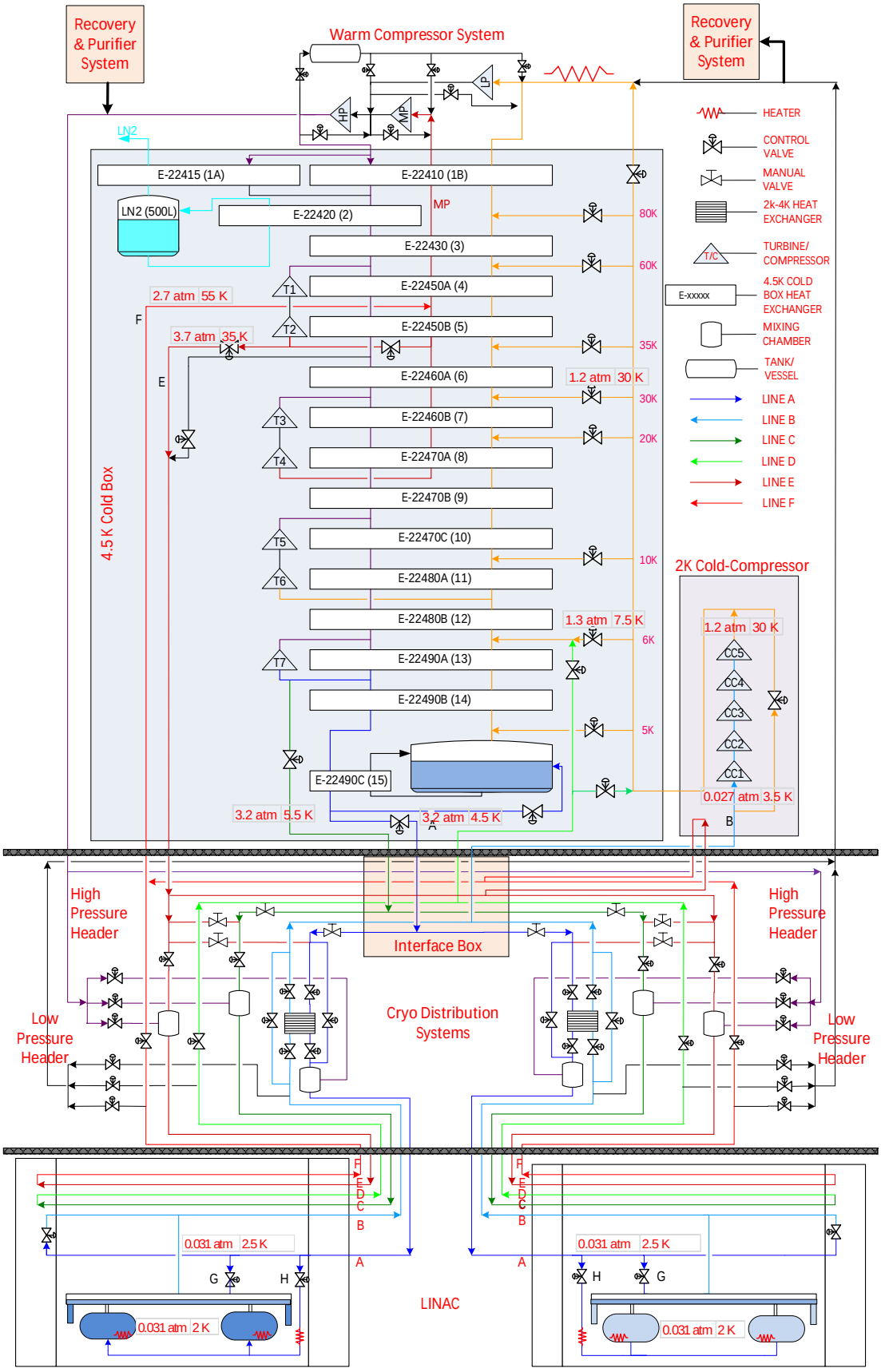

Figure 7-4. Cryogenic systems circuits

7.3.3 Warm Recirculation Compressors

The Warm Recirculation Compressors system consists of equipment needed to compress helium gas service for the 4.5 K cold box. The system includes five oil flooded screw compressor skids and a common three stage filtration oil removal system. The design of the compressors are for continuous operation with a 20 year expected life. Each skid contains 250 gallons of oil which is injected into the gas compressor to cool and seal the compressor mechanical screws during compression of the gas. Major components of the compressor skids consist of an 3600 rpm electric motor to drive the gas compressor, a discharge gas heat exchanger to cool the compressed gas, an oil heat exchanger to cool injection oil, a discharge gas bulk oil separator, an oil injection pump and a locally mounted control panel.

The compressor skids are a proven design, completed for the Jefferson Lab's 12 GeV upgrade. A photograph of the JLAB compressors is shown is Figure 7-5.

Figure 7-5. Warm recirculation compressors at JLAB

The three low pressure compressors are equipped with 800 hp motor drives. A single medium pressure compressor and a high pressure compressor are equipped with 1000 and 2500 hp motors, respectively. Both the motor and compressor are configured for ease of maintenance or removal. Main inlet and outlet process line valves provide positive safety isolation.

The gas and oil heat exchangers use 3,000 gallons per minute of cooling water with a temperature rise of 15 degrees F. When in operation, the compressors consume 3.7 MW of electric power at 4160 V. During reduced refrigeration loading at 4.5 K, the compressors only consume 1.7 MW of power. All electrical power feeds to the compressor are underground. Helium gas and cooling water piping are located within a piping trench which is common to all compressors.

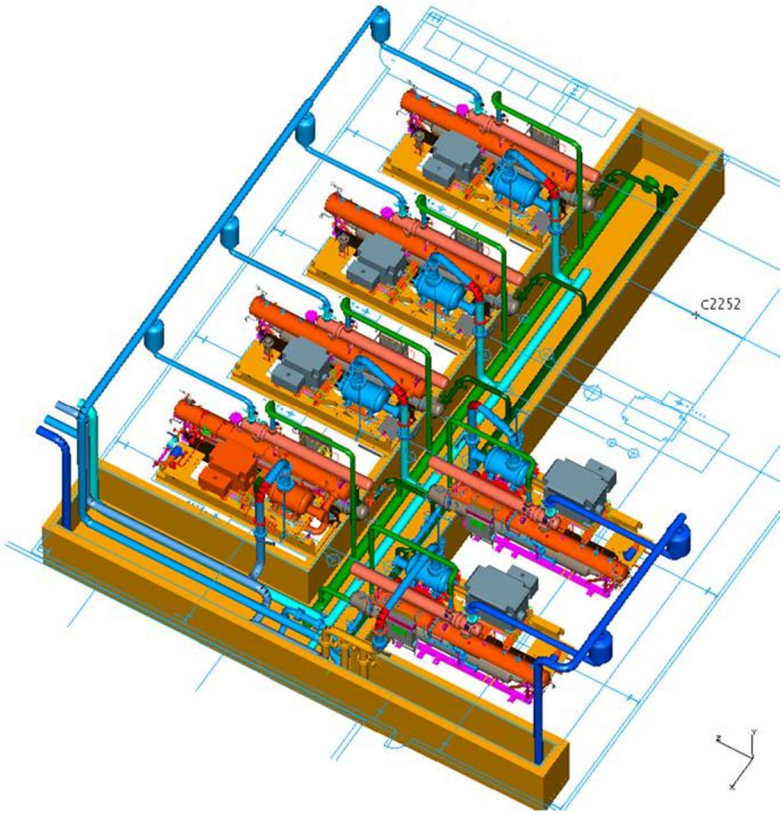

Figure 7-6. Typical Helium Compressor Room Layout with piping trench, water, and helium piping (example shown includes option spare 6th compressor)

An overview of the compressor skid equipment layout is shown in Figure 7-6. The compressors are a source of both heat and noise. The noise level between compressor skids is expected to be 104 dBA. Four 20,000 scfm compressor roof fans, combined with large wall mounted noise abatement air intake louvers, remove the heat generated by the compressor skids.

Each compressor skid is equipped with a locally mounted control panel programmed to perform the functions of safety monitoring and operation of the compressor skid. The control panel works in coordination with the motor safety system of the motor control center. The safety alarms and automated shutdowns include high discharge temperature and pressure, low oil injection pressure, low suction temperature and pressure, high motor amperage, motor voltage imbalance, and motor short circuit protection. Other machine controls include compressor start/stop, slide valve load/unload, and emergency system shutdown. The PLC control system interfaces with LCLS-II accelerator controls directly via Ethernet.

For oil inventory management, each compressor skid is equipped with oil fill, drain, and inter-skid oil inventory balancing valves. All skids use UCON 170X synthetic processed oil. Compressor major maintenance is required every 74,000 hours.

7.3.4 4.5 K Cold Box

A 4.5 K cold box provides the refrigeration of the compressed gas from room temperature to 4.5 K. The cold box consists of two large evacuated vessels containing the cryogenic heat exchangers and piping, see Figure 7-7. The upper temperature cold box vessel contains large helium gas and liquid nitrogen heat exchangers which use liquid nitrogen to cool the helium gas to 80 K. At full refrigeration plant capacity the liquid nitrogen consumption is expected to be 140 gallons per hour. The upper temperature cold box section also contains two parallel charcoal adsorber vessels which remove trace air contamination from the helium gas to less than 1 ppm_v. Since the upper cold box uses liquid nitrogen, which is vaporized and released into the atmosphere, the cold box is located out-of-doors to minimize the possibility of oxygen deficiency hazard. Figure 7-8 shows the outside upper temperature 4.5 K cold box on the right with the warm recirculating warm helium compressor oil removal vessels on the left. Appendix B of the *4.5 K Cold Box Technical Specification*, LCLSII-4.8-CT-0284, presents the reference design schematic.

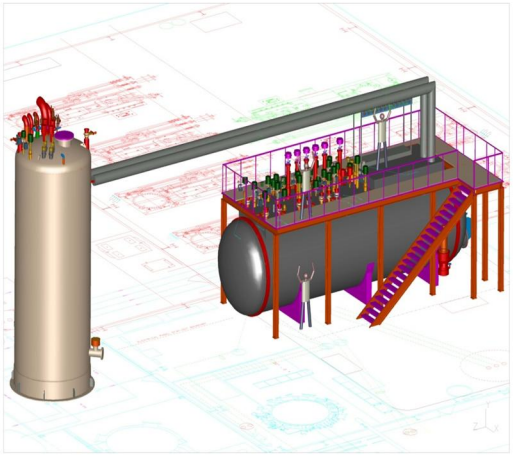

Figure 7-7. Model of the 4.5K cold box upper and lower vessel sections

Figure 7-8. Upper temperature 4.5K cold box at JLAB (on right)

The upper cold box 80 K helium gas is then fed to a lower horizontally-mounted cold box with multiple serially-connected turbine-expanders to lower the helium gas temperature from 80 K to the three temperatures required by the accelerator cryomodules: nominally 35 K, 5.2 K, and 4.5 K. Each of these supply temperature levels are returned to the 4.5 K cold box for refrigeration recovery at 55 K, 7.5 K, and 30 K, respectively. The lower 4.5 K cold box installed at JLAB is shown in Figure 7-9.

Figure 7-9. Two views of the lower 4.5K cold box section and internal piping installed at JLAB

The lower 4.5 K cold box is provided with an upper platform to access valving and the control hardware of the cold box. An instrumentation rack is mounted on the platform with controls panels for the cold box turbine control, and Allen-Bradley PLC control. The control interface for remote supervisory control and system monitoring is Ethernet-based. All safety and control loop control programming associated with the 4.5 K cold box is provided within the PLC control hardware. The cold box safety and operational controls are designed to be standalone and with full local plant operation capability. The lower temperature cold box equipment as installed at JLAB, inclusive of control racks, panels, and valving, is shown in Figure 7-10**Error! Reference source not found.**.

Figure 7-10. Top of lower 4.5 K cold box equipment and instrument rack at JLAB

7.3.5 2.0 K Cold Box

The 2.0 K Cold Box is designed to provide vacuum pumping over the liquid helium within the cryomodule to maintain a constant operating pressure of 0.030 bar. The cold box is designed as a single, horizontally-mounted, evacuated vessel consisting of five stages of centrifugal cold compressors in series. A five-stage design was chosen over a four-stage design to reduce the pressure ratio across each stage. This allows an enhanced flow turn-down of the cold compressors without adding heat or flow bypassing of the cold compressors, which would otherwise require full 4.5 K load on the refrigeration system regardless of the actual 2 K refrigeration load. Each cold compressor stage consists of an externally accessible water cooled variable speed motor drive and magnetic bearings, which have demonstrated extreme reliability in other similar cryogenic plants over the past 20 years. The cold compressors are capable of pumping up to 200 g/s of 4 K helium gas from a subatmospheric cryomodule pressure of 0.030 bar to 1.2 bar at 30 K. A typical five-stage vertical 2 K cold box assembly is shown in Figure 7-11.

A typical single liquid nitrogen cooled cold compressor stage and compressor wheel is shown in Figure 7-12. The 2 K cold box system controls are modeled after the five-stage cold compressor system control developed by JLAB and successfully operated since 1999. The control design approach provides cryomodule pressure regulation within 100 microbar with large time duration, while reducing overall plant power consumption when reducing 2 K refrigeration capacity due to decreased refrigeration load.

The 2 K cold box is equipped with bypass valving, which allows shutdown of the cold compressors while bypassing the cryomodule return flow to the 4.5 K cold box at 4.5 K and 1 bar. This operating mode of the cold compressors allows the 4.5 K cold box to maintain 4.5 K helium within the cryomodules during extended periods without beam and provides utility cost savings up to 46% compared to operation at 2.0 K.

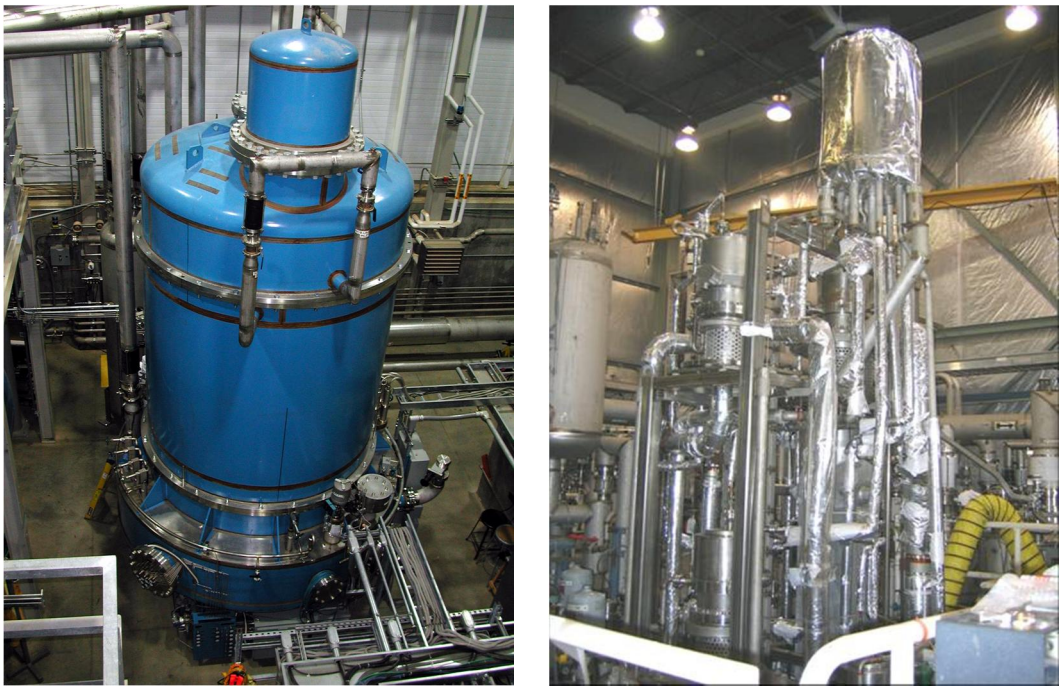

Figure 7-11. Vertical 2K Cold box and internal assembly

The 2 K cold box control system includes variable speed control of each cold compressor stage up to 38,000 rpm. It also includes magnetic bearing control panels to suspend and maintain the cold compressor drive shaft and wheel position within a tolerance of 1 mil. Other design features include cold compressor inlet flow straighteners to ensure equal distribution of flow entry into the compressor, and interstage volume design criteria to eliminate pressure instability coupling between stages during operation.

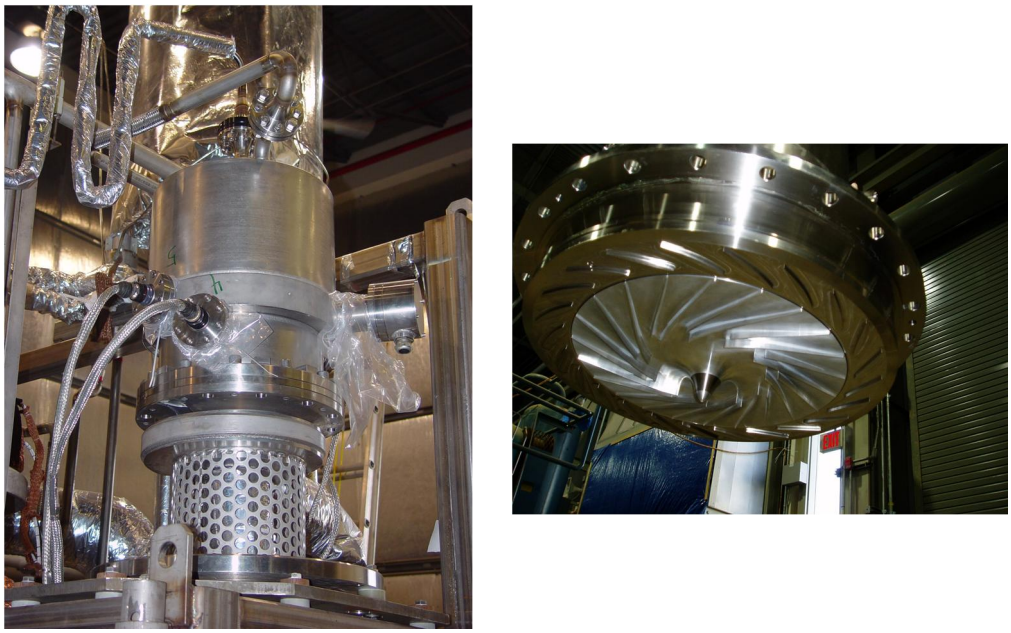

Figure 7-12. Typical LN2 cooled cold centrifugal compressor and centrifugal wheel

7.3.6 Ancillary Equipment

A number of supporting systems are required for the cryogenic plant. These include helium gas storage, helium purification and recovery, motor control center, guard vacuum system, instrument air system, liquid nitrogen storage, and liquid helium storage.

The helium gas storage system consists of 5, 4,000 scf vessels. Each vessel can hold helium gas up to 16 bar (equivalent to 2400 liters of liquid helium). The helium gas storage system is interconnected to the refrigeration system to supply helium gas into the refrigeration system as the gas is converted to liquid or to recover excess gas from vaporized liquid. A gas storage system is shown in Figure 7-13.

Figure 7-13. Gaseous helium storage vessels at JLAB

A helium purification and gas recovery compressor system provides less than 1 ppm_v of air and water contamination. The purification capacity is rated at 18 g/s. The system is a key contributor to maintaining a contamination free system for extended multi year continuous operation.

In addition, a 10,000 liquid helium dewar provides additional storage capability beyond the capacity of the gaseous helium storage vessels. The total liquid helium inventory of the accelerator cryomodules is estimated to be 15,000 liters.

A 4160V, 3-phase motor control center is provided for the warm helium recirculating compressor drive motors. The motor starters of the center provide the starting, stopping and motor safety controls. The motor control center is a double-ended, class 1 center consisting of three 800 hp, one 1000 hp, and one 2500 hp starters. The 2500 hp starter is a electronic reduced-voltage design. A spare 2500 hp starter space is provided for a future spare 2500 hp compressor.

A guard vacuum system provides a vacuum utility which services an intercept space between two concentric flange seals on sub-atmospheric refrigeration piping. The vacuum between the seals is designed to intercept possible air leakage past the first outer seal, which would otherwise enter and contaminate the sub-atmospheric process line. The system consists of two primary vacuum pumps and one spare vacuum pump.

7.4 Cryogenic Distribution Systems Design

The cryogenic distribution system (CDS) consists of the equipment needed to feed and return the cryogens, via vacuum insulated cryogenic pipes, to the linac components needing these services throughout the entire linac. This includes distribution boxes, cryogenic transfer lines, feed caps, end caps and cryogenic bypasses. A simplified cryogenic system (cryoplant, CDS, and linac cryomodules) diagram is shown in Figure 7-1 in Section 7.1, with cryogenic distribution systems shown in blue connecting the linac to the cryoplant.

The CDS interfaces to the cryogenic plant (CP) via set of removable, vacuum-insulated cryogenic transfer lines installed between distribution boxes (CDS scope) and the interface box (CP scope). The CDS also interfaces to the CP via a set of warm helium headers used to return warm gas during transient operating modes such as purification, cooldown, and warmup.

The CDS distributes cryogens from the CP to the linac cryomodules via cryogenic transfer lines with feedcaps connected to the string of cryomodules in the linac tunnel. The cryogens flow through each linac cryogenic string: upstream to L0, L1, L2 and downstream to L3. At the end of each string, the flows are rerouted through endcaps back through the cryomodules, transfer lines and the distribution boxes to the CP [3].

Reference design piping and instrumentation diagrams (P&IDs) for the cryogenic distribution system is provided in *CDS DB 2K Heat Exchanger Engineering Specification* LCLSII-4.9-EN-0296 and [4]. Based on theses P&IDs, valve and instrument lists are provided in the *CDS Valve List* LCLSII-4.9-EN-0254.

A Failure Mode and Effects Analysis was performed and documented in *CDS Failure Mode and Effects Analysis* LCSLII-4.9-EN-0255. This analysis of reasonable postulated equipment failure or operator error for each component assures that any failures result in a safe condition or are mitigated appropriately. Pneumatic control valves on supply lines usually close upon loss of control pneumatics or electrical signal, whereas return valves open on such events, allowing helium gas return to the CP and its helium compressor system.

General system failure modes or upsets resulting from external sources, including power outages, were addressed in a "What-if Analysis" and are documented in *CDS What-If Analysis* LCLSII-4.9-EN-0253. The control system is equipped with an uninterruptable power supply system to provide continuous electrical conditioning, controls hardware protection and backup power.

7.4.1 Surface Components - Distribution Boxes

The CDS has two distribution boxes. Each distribution box is dedicated to a string of cryomodules, upstream and downstream. This architecture provides flexibility for positive isolation of each string of cryomodules from the CP during installation, commissioning, operation and maintenance, including repairs.

Connection between the distribution boxes and the interface box is accomplished via removable, vacuum-insulated cryogenic transfer tubes ("U-tubes"), while the connection to the tunnel component is accomplished via welded cryogenic transfer line. To streamline installation, commissioning and operation of the CDS, each distribution box has vacuum break between its vacuum vessel and the tunnel transfer line.

The inlet to each distribution box accepts U-tube connections to the interface box. Both U-tubes and the interface boxes are in the CP scope. The design of the U-tubes is identical to those used for the JLAB's 12GeV cryoplant, specifically the low pressure helium return from the linac.

The distribution boxes are located in the Klystron Gallery above new penetrations to the tunnel and centered on bunch compressor 2 (BC2). A cartoon rendering of the distribution boxes (large cylindrical shapes), and interface boxes (large rectangular shapes), is shown in Figure 7-14.

Each distribution box is a vacuum vessel that contains cryogenic control valves, low pressure JT heat-exchanger, mixing chambers, interconnect piping, and safety relief devices. The size of the distribution box is driven by desire to maintain position of the JT heat exchangers in a vertical orientation as well as the large outer diameter of the gas helium return line. The mechanical design of the distribution boxes uses thermal radiation shields and intercepts to minimize heat leak to process lines, specifically the sub-cooled helium supply and gas helium return.

A reference design piping and instrumentation diagram for the upstream distribution box is provided in *CDS Distribution Box Flow Schematic* LCLSII-4.9-EN-0305. The downstream distribution box is identical to the upstream box.

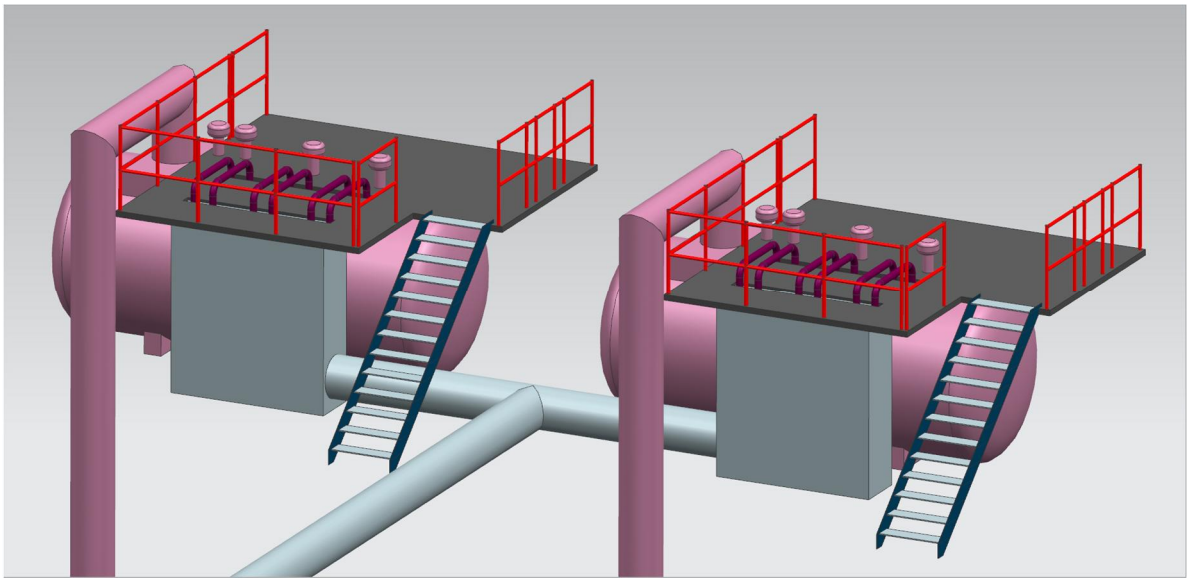

Figure 7-14. Distribution boxes site layout

Required CDS operating modes are defined in the *Cryogenic Distribution System Functional Requirements Specification* LCLSII-4.9-FR-0057. The approach to satisfy these requirements is documented in *CDS Cryomodule Cooldown Method* LCLSII-4.9-EN-0290. The design allows for independent cooldown and warmup of each linac string. Controlled cooldown and warmup of the

cryomodule strings requires mixing warm and cold helium gas from the CP, described in *CDS DB Mixing Chamber Cooldown Rate Control* LCLSII-4.9-EN-0291.

7.4.2 Tunnel components

7.4.2.1 General Layout

The CDS tunnel cryogenic components have three cryogenic bypass transfer lines that route cryogenic services around warm components along the beam line, hence are named cryogenic bypass. Three cryogenic bypasses are installed along the linac: a 75-meter cryogenic bypass around the laser heater (LH), a 65-meter bypass around the first bunch compressor (BC1) and a 110-meter bypass around the second bunch compressor (BC2). These bypasses, including six feed caps and two end caps, are shown in Figure 7-15. Each bypass has a vacuum break located at the midpoint. Expansion and contraction of the bypass inner lines is compensated by feed cap vertical expansion joints described in *CDS DB Site Layout* LCLSII-4.9-EN-0293.

Bypasses are connected to the feed caps, which cryogenically terminates a cryomodule string, at both ends. End caps are located at the end of a string of cryomodules and functions as cryogenic turnarounds for each process circuit. Connection to the distribution boxes is accomplished via two vertical transfer lines that enter the tunnel at the midpoint of the BC2 bypass through two 36-inch diameter access shafts.

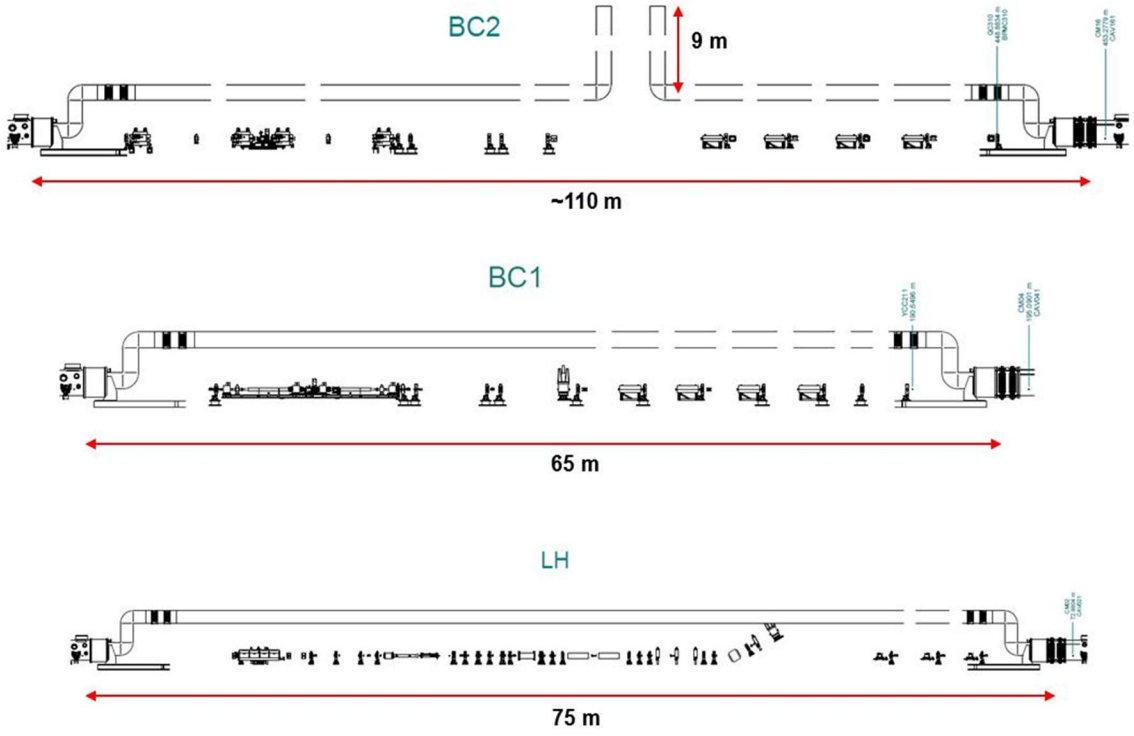

Figure 7-15. Cryogenic bypass tansfer lines, shown above the electron beamline warm components in three locations: bunch compressor 2, bunch compressor 1, and laser heater.

7.4.2.2 Cryogenic Bypasses

Figure 7-16 shows a cross section of the CDS cryogenic bypass transfer line, a 24 inch outer diameter compound vacuum insulated cryogenic transfer line that contains the six cryogenic circuits described in Section 7.3.2: Line A (sub-cooled helium supply), Line B (gas return pipe), Line C (low temperature intercept supply), Line D (low temperature intercept return), Line E (high temperature shield supply) and Line F (high temperature shield return).

Line A supplies supercritical helium to cryomodules at approximately 2.6 K and pressure of about 3 bar for initial cooling and filing of the superconducting cavities. Line B serves as return header that routes boil off helium gas from cryomodules to the suction of the CP's cold compressors. This header operates at pressures below atmosphere. Lines C and D are carrying cooling services for low temperature intercepts, while Lines E and F service thermal radiation shields. To reduce thermal radiation heat load to the process lines, a thermal shield surrounds all the lines and is trace-cooled by Line F.

Additionally, each line in wrapped with multiple layers of double-sided, aluminized Mylar and thermal spacers. Table 7-12 shows nominal operating parameters and line sizes for the various circuits. In certain areas the size of the process circuits is reduced due to space constraints. This is mainly in transitions between the feed cap and main overhead transfer lines, where space constraints limit the possible line sizes.

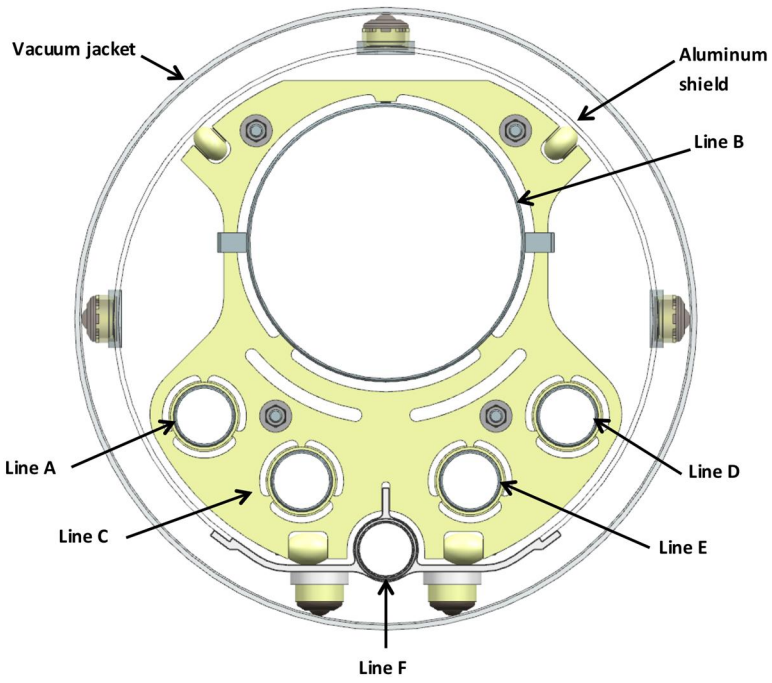

Figure 7-16. Cryogenic bypass transfer line cross section

Table 7-12. Cryogenic distribution systems nominal line sizes and operating parameters

Operating Parameters/Line	A	B	C	D	E	F
Pressure, [bar]	3	0.031	3	2.8	3.7	2.7
Temperature, K	2.6	2.00	4.5	5.5	35	55
Nominal size, DN [mm]	40	300	50	50	50	50

The thermal shield is cooled by the high temperature shield supply circuit, which consists of a 6061-T6 aluminum extrusion supported by a pair of roller ball transfers spaced every ten feet. The ball transfers allow the shield circuit to move as the circuit contracts during cooldown. The aluminum sheet is segmented every ten feet to reduce mechanical stresses during cooldown. Ball transfers are located at 90 degree positions spaced every ten feet to guide and support the shield within the vacuum jacket. The ball transfers are housed in G-10 cups to minimize thermal conduction to the process lines.

The helium circuits are supported with a double spider assembly with wheels that allow independent movement by rolling on top of the aluminum shield extrusion. The support assembly consists of two G-10 spiders tied together with threaded rods and G-10 tubes. Line B is rigidly attached to the support assembly while the other helium circuits slide within G-10 tubes that are part of the support assembly. A support assembly is spaced every ten feet along the length of the transfer line. With this design, each circuit and shield can move independently during warmup and cooldown of the cryogenic system.

A bypass transfer line is supported from the tunnel ceiling by sliding supports mounted to the ceiling. Sliding supports are required to compensate for movements of the outer vacuum jacket in the event of a rupture of a cryogenic circuit. Support systems are adjustable in three axes for ease of installation and meet seismic design criteria as outlined in the SLAC seismic design specification [5].

7.4.2.3 Feed Cap with Vertical Expansion joint

Thermal movements during cooldown and warmup are compensated in the feed cap vertical expansion joint with braided flex hoses oriented in a direction perpendicular to the bypass transfer line and offset from the CM transfer line. Each expansion joint is designed for a total movement of approximately four inches. Each circuit flex hose is installed with a 2-inch offset under the room temperature conditions. As each circuit cools down, it contracts and the flex hose passes the neutral position to a minus-2-inch offset The expansion module is designed to allow for independent cooldown of each circuit. The feed cap side of the expansion joint has a vacuum break.

The diameter of Line B is reduced to 8-inch pipe within the expansion module and reduced further to 6-inch pipe as it enters the feed cap. Tunnel height constraints limit the diameter and length of the braided flex hose for the required thermal movement. Pressure drop calculations documented in *CDS Gas Return Pipe Pressure Drop Analysis* LCLSII-4.9-EN-0292 and [6]

verify that the calculated pressure drop was within the limits required by the *CDS Functional Requirements Specifications Document* LCLSII-4.9-FR-0057.

The expansion joint vacuum jacket includes a bellows to allow for thermal movement of the bypass vacuum jacket in case of an internal process line rupture. To counteract pressure forces, the vacuum jacket of the bypass and vertical expansion joint are anchored to the civil structures. Figure 7-17 shows a vertical expansion joint.

The anchors are mounted to the tunnel ceiling. Vacuum breaks are located at the feed caps and at the midpoint of the bypass transfer line (see *CDS Vacuum Break Analysis* LCLSII-4.9-EN-0299 and [7]). The vacuum breaks define segmented insulating vacuum circuits. This simplifies vacuum leak detection, which in turn streamlines installation, commissioning, operations and repairs.

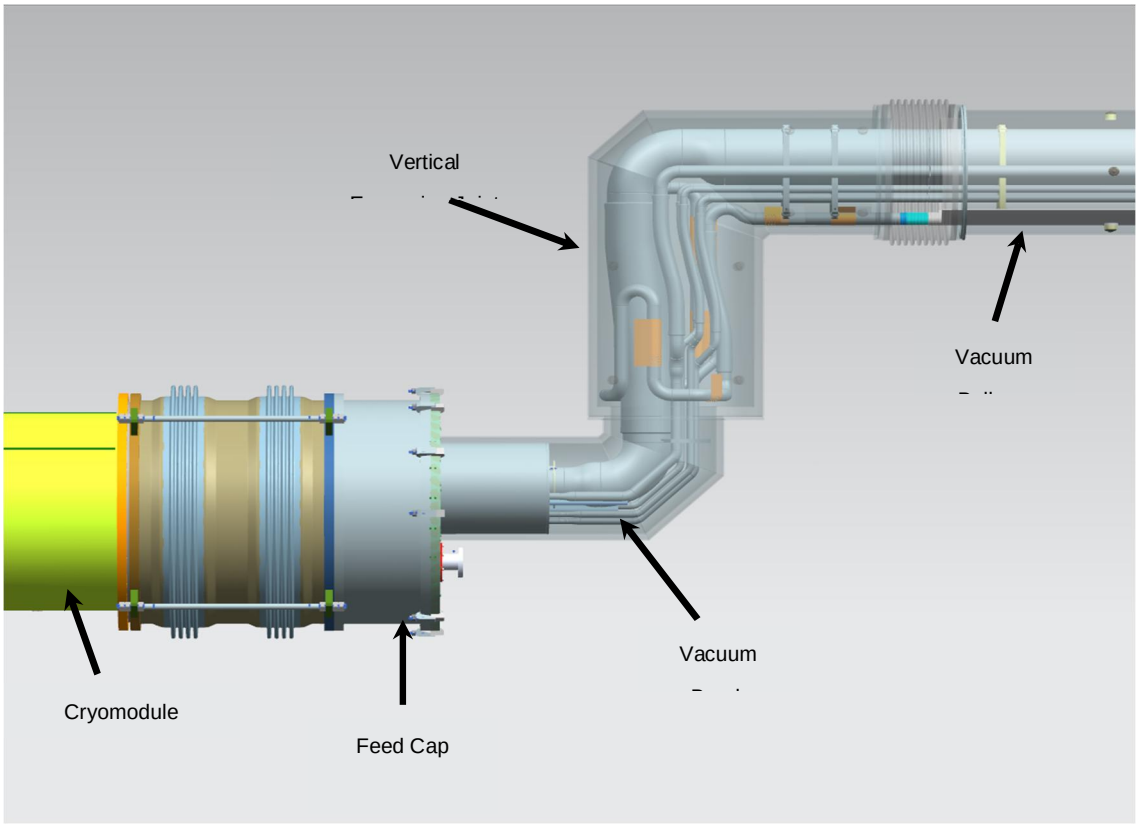

Figure 7-17. Detail of cryogenic transfer line, showing vertical expansion joint

7.4.2.4 Vertical Transfer Line

The cryogenic transfer line for each string (upstream and downstream) enters the tunnel from the Klystron Gallery through two 36-inch diameter penetrations located at the midpoint of the BC2 bypass region. The vertical transfer lines extend to the Klystron Gallery where they connect to the distribution box, which in turn connects to the cryoplant. The penetrations are 25 feet in length and were added specifically for these transfer lines.

The thermal compensation scheme for the vertical transfer lines utilizes braided flex hoses similar to those used in the half-bypass expansion modules. The braided flex hoses are installed in the vertical section above the elbow at the penetration. Due to the relatively short distance from the bypass anchor, the flex hoses only need to compensate for a total travel of 2.5 inches. Similarly, braided flex hoses are located in the elbow at the surface to compensate for the thermal contraction in the vertical run through the penetration, which in this case is only 1.5 inches. Another vacuum break is located directly above the braided flexes and functions as an anchor for the flex hoses, and further segmenting the insulating vacuum.

7.4.3 Feed Caps and End Caps

The LCLS-II CDS includes six feed caps: downstream of CM01, 3.9 GHz CM02, and CM15, and upstream of CM02, CM04, and CM16, and and two end caps: upstream of CM01 and downstream of CM35. Each feed cap within the CDS provides an interface between the supply transfer line and a given cryomodule string. Helium flows into cryomodules through Lines A, C, and E, and returns through Lines B, D, and F (see Section 7.4.2.2). The feed caps and end caps provide anchoring of each process circuit, which translates the pressures forces to the external support structures. They also anchor all cryogenic circuits within the cryomodules and transfer pressure forces from the cryomodule to the floor of the tunnel. To achieve this, each feed cap has a bolt-on structural steel beam assembly that can withstand these loads and minimize deflection of the feed cap end plate. A structural analysis of this support assembly has found that all vacuum loading stresses and deflection in the end plate are below the allowable limits for the existing design [8].

Feed caps and end caps house instruments, control and relief valves necessary for CDS operation. All temperature sensors are surface-mounted to reduce the likelihood of leaks. Sizing of reliefs for each CDS circuit is outlined in a separate note [7].

7.4.3.1 Injector End and Feed Cap

Figure 7-18. Injector feed cap, end view (left) and side view (right)Figure 7-18 shows the feed cap used at the downstream end of the injector cryomodule. The end cap on the other end of the injector cryomodule is constrained by the warm injection region upstream of the linac, which limits the maximum longitudinal dimension for the end cap at the injector cryomodule to 670 mm (see *CDS Cryomodule Cooldown Method* LCLSII-4.9-EN-0290). As a result, this end cap must be custom-designed to specifically reduce the longitudinal distance, but since the standard cryomodule vacuum bellows is 850 mm in length the injector cryomodule must also be modified from the standard design used for all other cryomodules. In addition to a shortened vacuum bellows, some of the internal components of the injector cryomodule require modification, including the Line B bellows (see Section 7.4.2.2), and all interconnect lengths. The Line B bellows is offset from the Line B centerline in the cryomodule to align with centerline of the Line B bellows in the feed cap, to balance the forces on the anchor in the injector cryomodule. The interconnect region of the injector end cap-to-cryomodule interface is also modified to accommodate the reduced longitudinal distance.

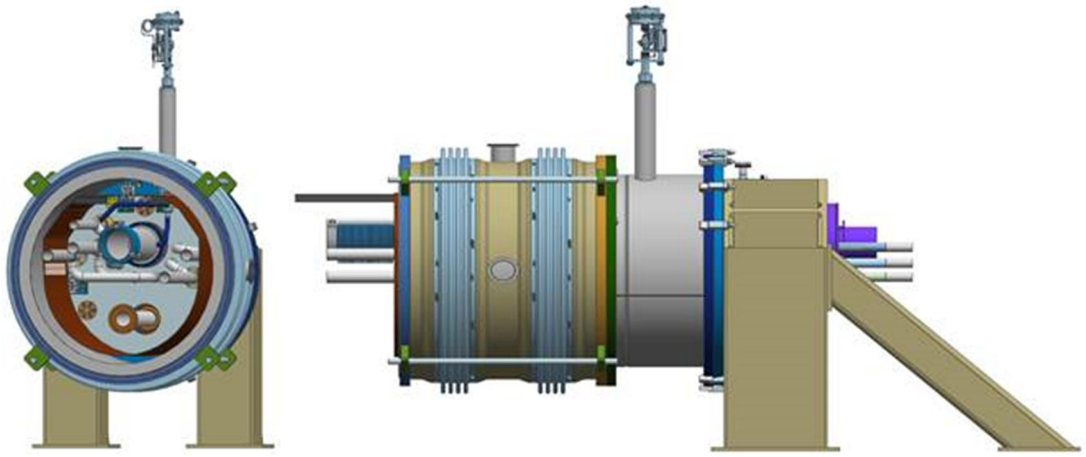

Figure 7-18. Injector feed cap, end view (left) and side view (right)

7.5 References

1 "Commissioning of Helium Compression System for the 12GeV Refrigerator," CEC-2013 .

2 "Commissioning of Helium Refrigeration System at JLAB for 12GeV Upgrade," CEC-2013.

3 LCLS-II CDS Design and Tunnel Site Layout, Fermilab Team Center Engineering Note #ED0001999, 2014.

4 LCLS-II CDS Transfer Line Vacuum Jacket Relieving Requirements and Pressure Rating, Fermilab Team Center Engineering Note #ED0002018, 2014.

5 "Seismic Design Specification for Buildings, Structures, Equipment, and Systems," SLAC-I-720-0A24E-001-R004 (2014).

6 LCLS-II CDS Relief System Analysis, Fermilab Team Center Engineering Note #ED0001995, 2014

7 LCLS-II CDS Tunnel Schematic, Fermilab Team Center Engineering Note #ED0001997, 2014

8 LCLS-II CDS Thermal and Mechanical Analysis of the Endcap and Feedcap, Fermilab Team Center Engineering Note #ED0002005, 2014.

8 Undulator Systems

TECHNICAL SYNOPSIS

The LCLS-II project includes two new undulator systems: one for generating hard X-rays, HXR, (1,000 – 25,000 eV) and the other one for generating soft X-ray, SXR, (200 – 1,300 eV). Each undulator line is comprised of individual undulator segments separated by 1.0-m-long break sections. Each undulator segment will be a variable gap, permanent-magnet planar hybrid device with a nominal minimum gap height of 7.2 mm and a total nominal length of 3.4 m. The HXR undulator line will be made up of 32 individual undulator segments, each with 130 26- mm-long periods. The SXR undulator is made up of 21 individual undulator segments, each with 87 39-mm-long periods. The poles will be made of vanadium permendur and the magnet blocks of a grade of NdFeB with a high intrinsic coercivity for better resistance to radiation-induced demagnetization. The electron beam will be focused by two separated function Focusing-Drift-Defocusing-Drift (FODO) lattices, using electromagnetic quadrupoles placed between the undulator segments. These focusing or defocusing lenses (quadrupoles) will share the drift spaces (break sections) between the undulator segments with electron beam position monitors, phase shifters, beam loss monitors, and X-ray collimators. The two undulator beam lines are designed to receive electron beams from the new 2 – 4 GeV superconducting linac at high repetition rates, up to 1MHz. The SXR line is optimized for the energy from 200 to1,300 eV. The HXR line is operate from 1 to 5 keV with the electron beam from the superconducting linac at up to 1MHz. The HXR line will also be able to receive electron bunches from the existing 2.5 – 15 GeV LCLS linac reaching photon energies up to 25 keV at a rate up to 120 Hz.

Provision will be made for magnetic tuning of the undulator segments. Tolerances have been developed that will set the magnetic tuning requirements for the individual undulator segments. Diagnostics for the electron beam will include beam position monitors and beam loss monitors after each undulator segment, and at the ends of the undulator line.

LCLS-II will use a similar undulator alignment strategy as is being used in the current LCLS system, even though there are system differences, such as variable gap, large undulator size, and a smaller available range of electron energies with the superconducting linac, which require special considerations. The electron beam trajectory must be straight to within a few microns at 13.6 GeV over a distance of about 10 m to limit phase errors between electron and photon beams. It is shown here that this specification can be achieved with beam-based techniques.

Self-seeding schemes similar to what is used currently in the LCLS beam line are included to produce nearly transform-limited pulses, minimal jitter in X-ray wavelength and potentially higher spectral brightness by one-to-two orders of magnitude when taken to full saturation..

8

8.1 Scope, Schedule, Status, Partner lab roles

8.1.1 Scope

The LCLS-II undulator systems will deliver two variable gap undulators in the existing LCLS Undulator Hall. On the south side of the hall the existing fixed gap undulator will be replaced with variable gap system to generate hard X-rays, HXR. This undulator will be optimized with the superconducting linac operating from 2 to 4 GeV for the photon energy range of 1 to 5 keV, and with the Cu linac operating from 2-15 GeV) for the photon energy range of 1 to 25 keV. On the north side of the hall a new soft X-ray, SXR, variable gap undulator system will be installed. Both undulators are shown in Figure 8-1. The undulator systems extend from just downstream of the tune-up-dumps at the west end of the Undulator Hall to after the last undulators at the east end.

The length of the HXR undulator hall will be filled with 32 3.4-m-long undulator segments. The period of the HXR undulator is 26mm. There is a short drift section before the first undulator and two gaps in the regular 4.4-m-long cells that are set aside for self-seeding sections. In one of these cells the proven exiting HXR self-seeding system will be installed.

The SXR line will have 21 3.4-m-long undulator segments. The period of the SXR undulator is 39mm. This line will also have repeating 4.4-m-long cells. The last three cells at the east end are reserved for the future addition of polarizing after burners similar to the DELTA polarizing undulator being developed for LCLS [1]. There is one cell set aside for soft X-ray self-seeding. The existing SXR self-seeding system will be upgraded to operate at the high rep-rates the superconducting linac can deliver. There will be a drift section with a sparse lattice of quadrupole magnets between the tune-up-dump and the first undulator segment. This drift section is being laid out to facilitate future addition of undulator segments.

The critical interfaces of the undulator system are to the Electron Systems that bound it at the up and downstream ends, to Global Controls system, which is responsible for controlling the undulator systems, and to Infrastructure, which is responsible for the Undulator Hall and delivery of utilities to agreed interfaces are defined in Interface Control Documents and Room Data Sheets, see Table 8-1.

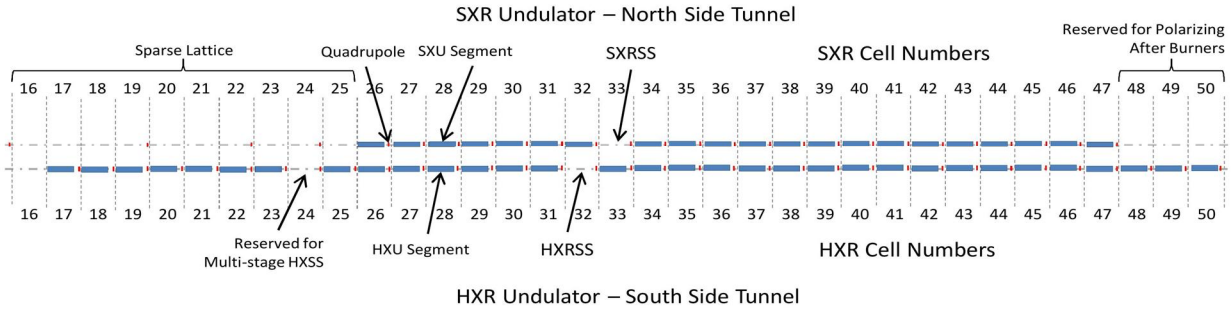

Figure 8-1. Schematic Layout of the SXR and HXR Undulators in the tunnel.

8.1.2 Final Design Schedule

Undulator system activities are integrated into the LCLS-II P6 project schedule under work breakdown structures (WBS) 1.03.02, 1.03.03 and 1.03.04. SLAC is responsible for all the vacuum and interspace system in WBS 1.03.02, and LBNL is responsible for the HXR undulator magnet segments in WBS 1.03.03 and SXR undulator magnet segments in WBS 1.03.04.

The Undulator schedule is composed of three main phases: Engineering and Design, System Procurement and Fabrication, and Integration and Installation. Individual activities for each component or subsystem fall within one of these phases. The undulator systems schedule is summarized in Figure 8-2. The system Preliminary Design Review (PDR) is scheduled for March of 2015 and the Final Design Review (FDR) for July 2016. The PDR for both the HXR and SXR undulator magnetic segments was in October of 2014 and the FDR the segments is schedule for January of 2016. The schedule is well advanced and progressing as planned. Where relevant, we direct the reader to further supporting documentation containing more information about the undulator systems. Tables 8-1 through Table 8-3 contain lists of all currently available, relevant documents.

Table 8-1. Undulator system requirements documents.

Title	Document Number
Undulator System PRD	LCLSII-3.2-PR-0038
Undulator Phase Shifter PRD	LCLSII-3.2-PR-0105
LCLS-II Parameters PRD	LCLSII-1.1-PR-0133
Beam Position Monitor Requirements PRD	LCLSII-2.4-PR-0136
Hard X-ray Self-Seeding (HXRSS) System Requirements PRD	LCLSII-3.2-PR-0102
Soft X-ray Self-Seeding (SXRSS) System Requirements PRD	LCLSII-3.2-PR-0101

Undulator Segment Functional Requirements FRD	LCLSII-3.2-FR-0139
Undulator Phase Shifter FRD	LCLSII-3.2-FR-0238
Magnetic Measurement Facility Requirements FRD	LCLSII-3.2-FR-0104

Table 8-2. Interface Control Documents and Room Data sheets between Undulator systems and other areas of LCLS-II.

Title	Document Number
Undulator to Infrastructure ICD	LCLSII-3.2-IC-0047
Undulator to Electron Systems ICD	LCLSII-3.2-IC-0048
Undulator System to Global Controls, Power Conversion, and Cable Plant ICD	LCLSII-3.2-IC-0045
Undulator System Devices to Motion Control ICD	LCLSII-3.2-IC-0137
Undulator to Metrology Monument System ICD	LCLSII-3.2-IC-0046
Undulator Vacuum Chamber to Undulator Systems ICD	LCLSII-3.2-IC-0190
Undulator Hall RDS	LCLSII-3.2-RD-0012

Table 8-3. Engineering Specification and Statement of Work Documents of undulator systems.

Title	Document Number
Undulator Segments, SXR and HXR	See list section 8.3
RF Beam Position Monitor	LCLSII-3.2-ES-0049
Undulator Interspace Support and Alignment	LCLSII-3.2-ES-0157
Undulator Beam Loss Monitor	LCLSII-3.2-ES-0180
0.433Q3.1 Quadrupole Magnet	LCLS-II-3.2-ES-0317
Undulator Phase Shifter	LCLSII-3.2-SW-0103
Commissioning Two Magnetic Benches	LCLSII-3.2-SW-0242
Kugler Bench Delivery and Install in B033	LCLS-II-3.2-SW-0172

Unload and Move Kugler Bench MB6500	LCLSII-3.2-SW-0171

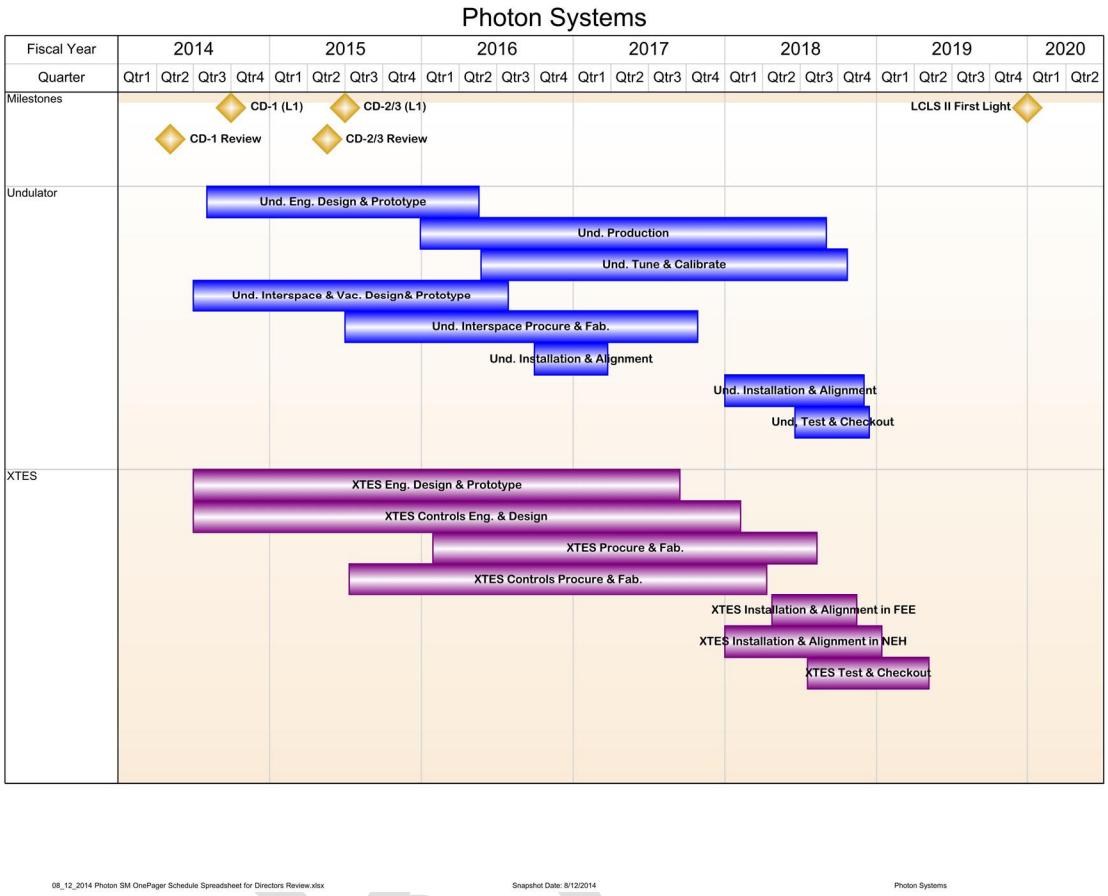

Figure 8-2. Photon Schedule Outline - Update with Undulator specific schedule

There are eight components to the undulator system: the Hard X-ray (HXR) and Soft X-ray (SXR) Undulators, Phase Shifter, Quadrupole Magnets, RF Beam Position Monitor, Beam Loss Monitor, Vacuum Systems, and Interspace Support Stands & Alignment. Figure 8-3 provides a layout of the undulator system, showing all elements of the sub-systems.

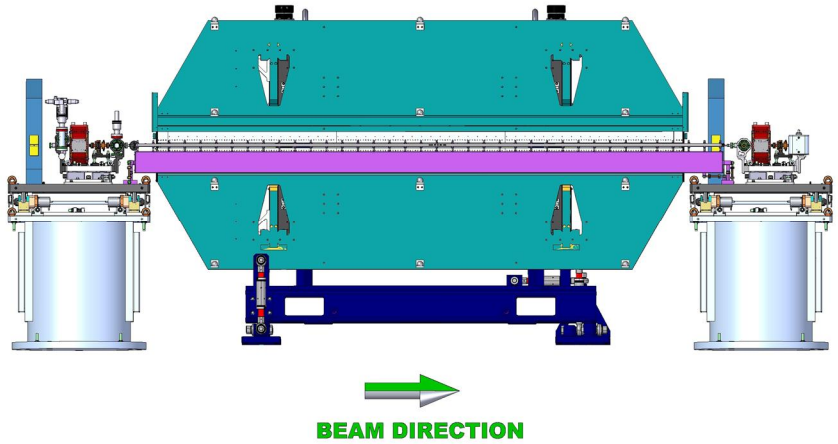

Figure 8-3. Complete undulator cell drawing (Update figure showing the crrent undulator and labeling all the elements)

8.1.3 Design Maturity

The LCLS-II Project Final Design Plan LCLSII-1.1-QA-0065 provides for a phased completion of the final designs for the LCLS-II facility. The plan ensures that designs are sufficiently mature to start procurements and construction, while enabling the most cost-effective schedule for constructing the facility and maximizing the technical capabilities of the facility at CD-4. Final design readiness at CD-3 recognizes that that not all subsystems will reach final design at the same time. Project-level requirements and interface control points between Accelerator Systems, Cryogenic Systems, Photon Systems and Infrastructure are defined at CD-3, which ensures that the phased procurements and construction are appropriate for the final design of the LCLS-II. Chapter 2, Project Overview, contains additional discussion of the approach to design completion. The Photon Systems design, described in this chapter and Chapters 9, is evaluated to be 65% complete. Completing remaining design after CD-3 allows for coordination with developing designs for LCLS Operations upgrades to instruments.

8.1.4 Test Facilities

The LCLS-II undulators will be measured and tuned at both the SLAC Magnetic Measurement Facility (MMF) and an equivalent one at LBNL. The HXR undulators will have the majority of the tuning done at LBNL. The remainder of the tuning, and all final data sets and fiducialization will be done at SLAC. All the SXR tuning, final data sets, and fiducialization will be done at SLAC. In addition, several studies will take place at SLAC. The magnetic deflection parameter, K value, of the undulators at different gap settings and at different temperatures will be mapped. The effect of the Earth's magnetic field in the undulator gap will be determined, and the correction scheme will be verified. We will conduct various transportation tests, frame deformation tests, and storage temperature tests, to ensure that the methods we use to store and handle the undulators do not change their calibration.

In preparation for undulator testing and calibration, the SLAC MMF is undergoing a construction build-out and an equivalent facility set up at LBNL to allow for undulator tuning and calibration testing in assembly-line fashion, see *Magnetic Measurements Facility Requirements*, LCLSII-3.2-FR-0104 and section 8.4.2 below. These activities span the time period from October 2014 through December 2015.

8.1.5 Undulator Segments

The preliminary design review (PDR) for the undulator segments for the Soft X-ray and Hard X-ray undulators took place in October 2014 at LBNL.[2] The review committee in attendance, James Rank (Brookhaven Nat. Lab.), Alexander Temnykh (Cornell University) and Andrew Ringwall (SLAC), solidly agreed that the design of the undulator segments were well advanced of a preliminary design and that the program is well positioned to being near production-level capability. The committee concluded that the program should move forward with development and testing of the proposed prototype undulator. The first prototype undulator will be delivered in November 2015, with testing shortly following and lasting through July 2016. The Final Design Review (FDR) is set for February 2016, with final design drawings to be released in March 2016.

For a description of the physics requirements for undulator segments, see section 8.2.1; for a description of the engineering design of the prototype, see section 8.3.

8.1.6 Phase Shifters

The *Undulator Phase Shifter PRD*, LCLSII-3.2-PR-0105, was released in April 2014 with PDR following in May 2014. The *Undulator Phase Shifter FRS*, LCLSII-3.2-FR-0238 and the statement of work, Undulator Phase Shifter, LCLSII-3.2-SW-0103, were released in October 2014. The request for proposal (RFP) for the prototype went out in December of 2014, with delivery of proposals a month later. Down-selection and award took place in February 2015. The vendor's prototype engineering design review is due in June 2015 with final delivery set for November 2015. The final design review is to take place in December 2015.

8.1.7 Quadrupole Magnet

Quadrupole magnet designs will be based on the current systems used in the LCLS. The design release is scheduled for August 2015, and shortly thereafter in September a subcontract will be awarded to a manufacturer, with the first production batch of eight quadrupoles delivered to SLAC in November 2015. Magnet testing will occur from November 2015 through April 2016. Subsequent orders of the remaining quadrupoles will arrive in January and March 2016, with each batch undergoing six months of testing once it arrives.

8.1.8 RF Beam Position Monitor

The Beam Position Monitor Requirements PRD, LCLSII-2.4-PR-0136, was released in March 2014 and the RF Beam Position Monitor ESD, LCLSII-3.2-ES-0049, in May 2014. Prototype testing and design down-select took place May 2014 through February 2015. The final design review is scheduled for early April 2015 with the final design released at month's end.

8.1.9 Beam Loss Monitor

The PRD was released in April 2014, with the preliminary design review occurring shortly thereafter, in May. The Undulator Beam Loss Monitor (BLM), LCLSII-3.2-ES-0180, was finalized in November 2014. RFP and subsequent contract award for a prototype instrument took place in January 2015. The prototype BLM will be received in March, with testing thereafter. The FDR is scheduled for September with the release of final drawings the following month, October 2015.

8.1.10 Vacuum Systems

Vacuum systems are divided into three sub-systems: the interspace vacuum system, the drift vacuum system and the undulator vacuum chamber. For a description of the overall physics requirements for vacuum systems, see section 8.2.10; for a description of the engineering designs of each vacuum system, see sections 8.5.3.

Interspace Vacuum System: PDR for the interspace vacuum took place in May 2014 with contract award going out in November 2014, and a prototype was delivered shortly thereafter. Testing will be on-going through March 2015, with the FDR scheduled to occur in May 2015.

Drift Section Vacuum System: The preliminary design of the drift section vacuum was completed in April 2014 and shortly thereafter, the PDR took place. FDR is scheduled for May 2015, and final drawings for the drift section will be released in July 2015.

Undulator Vacuum Chamber System: The undulator vacuum chamber PRD was released in April 2014, with the preliminary design released in September 2014. The Memorandum Purchase Order and award contract subsequently followed, with PDR taking place in October. Contract award for the prototype chamber was awarded in December and then the prototype is to be fabricated and tested by April 2015. The FDR is scheduled for May 2015.

8.1.11 Interspace Support Stands & Alignment

The PRD for interspace stands was released in April 2014 with preliminary designs released in February 2015 and PDR following thereafter. Issuance of the statement of work (SOW) and contract quickly followed in March and the prototype stands expected for delivery in May 2015. The FDR will be held in January 2016 with final drawings issued in March 2016.

8.1.12 Soft X-ray & Hard X-ray Self-seeding Systems

Soft X-ray Self-seeding System The physics requirements document for the soft X-ray self-seeding system was released June 2014 with the conception design review currently scheduled

one year later in June 2015, along with release of the engineering design document in the same month. Upon implementing suggested changes to the system design from the concept design review, PDR will follow in November 2015 and shortly thereafter will be the FDR (February 2016). Final release of drawings will also take place in February 2016.

Hard X-ray Self-seeding System No major re-design effort will take place with the hard X-ray self-seeding system as the plan is to use the HXRSS currently used by LCLS. Possibly, new parts will be purchased to update and/or to upgrade performance of the system. We note that installation of the current HXRSS is scheduled for April 2018.

8.2 Requirements

The detailed requirements of the LCLS-II undulator system are given in the *Undulator System PRD* LCLSII-3.2-PR-0038. This section will give a brief summary of the main system aspects, beginning with a list of basic undulator parameters in Table 8-4.

The LCLS-II undulator system is comprised of two independent undulators, the hard X-ray undulator (HXR) and the soft X-ray undulator (SXR). Each undulator is comprised of individual undulator segments (32 HXU and 21 SXU) separated by break sections (or interspaces), that will provide space for placing interspace components, i.e., a quadrupole, an RF beam position monitor, a phase shifter, a collimator and a beam loss monitor, plus various vacuum components. In addition, there will be one undulator quadrupole and two RF beam position monitors (RFBPMs) after the last segment, and also two RFBPMs upstream of the first undulator segments.

Upstream of the SXR undulator magnetic segments, there will be space for up to nine additional cells to enable future upgrades to the undulator line. These cells will initially be sparsely populated with beam optics elements, requiring only four additional undulator system-type quadrupoles.

Table 8-4: Basic undulator parameters

Parameter	SXR Values	HXR Values
Number of undulator segments	21	32
Number of quadrupoles	22+4[1]	34
Number of RF beam position monitors	22+3	34+3
Number of Phase Shifters	20	31
Number of beam loss monitors	21	32
Break section length	1.00 m	1.00 m
Total magnetic undulator length	71.25 m	108.8 m
Total undulator length, including interspaces	95.80 m	144.20 m

[1] Added counts are components located before and/or after the regular undulator segment lattice.

8.2.1 Undulator Segments

The undulator segments will be planar, variable strength permanent magnets. The wiggle plane basic parameters of the undulator segments are listed in Table 8-5.

Table 8-5. Basic undulator segment parameters

Parameter	SXU Values	HXU Values
Undulator period length (λ_u)	39 mm	26 mm
Segment length	3.4 m	3.4 m
Number of effective periods per segment (N_p)	87	130
Number of poles per segment	174	260
Minimum operating gap	7.2 mm	7.2 mm
Maximum K_{eff} (at minimum operational gap)	>5.48	>2.44
Maximum operational gap height	22 mm	20 mm
Minimum operational *K* values	1.24	0.44

8.2.2 Break Section Components

Each break section contains components such as quadrupoles, radio frequency cavity beam position monitors, phase shifters, radiation collimator, and beam loss monitors, that are necessary for controlling and monitoring the electron beam as well as monitoring radiation levels

These components will be mounted on a common support that can be precisely positioned by remote control. Motion ranges and component stability during motion are listed in the *Undulator System PRD* LCLSII-3.2-PR-0038. As mentioned above, some of the interspace components are also required upstream and downstream of each undulator. Only those components between undulator segments and those directly preceding the first undulator segment and following the last undulator segment require motion control.

8.2.3 Quadrupoles

The quadrupole requirements are defined in *Undulator System PRD* LCLSII-3.2-PR-0038. In both undulator lines they will be air-cooled electro-magnets with laminated cores and three separate coil circuits: 1) Quadrupole, 2) Horizontal Dipole Corrector, and 3) Vertical Dipole Corrector. They will be mounted together with the other break section components on a remotely adjustable table, with a motion range of ±1.0 mm in both transverse directions. The maximum integrated quadrupole gradient will be ±4.0 T, the maximum field integral range of the correctors will be ±0.5 mTm.

Both LCLS-II undulator lines (HXR and SXR) use a FODO lattice to focus the electron beam and keep the average beta function constant along the undulator. Both FODO lattices have the same cell length of 4.4 m but can have different focal lengths. The average beta function required

for optimum FEL gain is roughly proportional to electron energy for a given gap and undulator period. At a constant (but small) strength of focusing quadrupole magnets, the beta function will be proportional to electron beam energy. Also, the beam-based-alignment algorithm (see below) favors a constant quadrupole gradient. Therefore, at LCLS-II, as was the case at LCLS, the FODO lattice will operate at a constant gradient. The integrated quadrupole gradients (IG) can be independently chosen for each undulator line but will be kept invariant with energy changes in support of electron beam base alignment (BBA). The integrated quadrupole gradient needs to be below about 2.5 T for superconducting linac operation, while for Cu linac operation higher gradients can be used with restrictions on the low electron energy end of the operating range.

8.2.4 Phase Shifters

As the electrons travel through an undulator segment, their phase in the pondermotive well of the X-ray radiation field slips by exactly one X-ray wavelength for every undulator period travelled. As the gap of the undulator or the electron beam energy is changed, the radiation wavelength will adjust itself to maintain this condition. As the electron and X-ray beams transverse the field-free space in the interspace sections the electrons' phase change will be a function of the gap of the previous undulator and, therefore, be mismatched for most gaps. This needs to be corrected by phase shifter devices, installed in each break section between undulator segments. Requirements for the phase shifters are specified in a separate *Undulator Phase Shifter PRD* LCLSII-3.2-PR-0105.

8.2.5 Beam Position Monitors

The capability to precisely measure the transverse position of each individual electron bunch to sub-micron precision is essential for the application of electron BBA. The RF Beam Position Monitors (RFBPMs) used for LCLS demonstrated resolution of better than 250 nm. A similar design is has been developed for LCLS-II. Alignment can take advantage of the fact that the RFBPM body has circular shape and that the mechanical center of the device coincides with the center of the circular body shape that can be observed when the device is installed. It is important that an RFBPM is installed next to every undulator quadrupole. Two RFBPMs also need to be installed before the first and after the last undulator segment, as well as one RFBPM in each dump line.

8.2.6 Ambient Field Correctors

Small magnetic fields present in the undulator hall, other than those intentionally created by the beam steering magnets, can modify the electron beam trajectory. The dominant sources are the Earth's magnetic field and magnetic components such as vacuum pumps, motors and magnetized steel pieces. The amount of trajectory errors that these fields will generate will depend on the locations of those magnetic components and on the gap height of the undulator segment. In the case of the Earth field, extra field components will be distributed more or less homogenously along the vacuum chamber and will deflect the electron beam onto a circular

trajectory. A detailed description of the ambient field correctors are given in the *Undulator System PRD* LCLSII-3.2-PR-0038.

8.2.7 Beam Loss Monitors

Protecting the magnetic material from demagnetization due to radiation generated by the electron beam is very important for a continuous and reliable operation of the facility. Beam Loss Monitors (BLMs) that are integrated in the facility's Machine Protection System (MPS) are instrumental in protecting the undulators. The MPS is designed to prevent the electron beam from entering the undulator hall if radiation levels, as detected by the BLMs, exceed a threshold. The devices can be constructed very similarly to those used to protect the LCLS undulator, i.e., a quartz Čerenkov radiator, monitored with a photomultiplier. The shape of the radiator needs to be improved to reduce the sensitivity gradient that the existing BLMs exhibit [3].

A data acquisition system must be set up for continuous integration of the BLM signals. An upstream wire monitor can be used, at low repetition rates to calibrate the trip points of the BLMs. There is an ongoing program on LCLS to determine the appropriate trip points.

8.2.8 Temperature and Position Stability

It is important that the local undulator temperature stays stable to within a ±0.1 K. A temperature gradient over the length of the undulator is acceptable as long as the temperature at any given point is stable. The temperature of each undulator segment needs to be monitored redundantly. Each of the two strongbacks (magnet arrays) of each undulator segment needs to be equipped with three independent temperature sensors, each with an accuracy of ±0.1 K after calibration. The total long-term drift shall stay within a ±0.05 K range. In addition, each of the two jaws (magnet arrays) of each phase shifter needs to be equipped with a sensor of the same resolution and long-term drift stability as the undulator segment temperature sensors. Additional temperature sensors are needed to monitor each of the vertical support pillars for the undulator, the break section support, phase shifter, quadrupole, and the ambient air at each undulator segment.

The gap height settings of the undulator segments and the phase shifters need to be monitored with absolute linear encoders with a repeatability of better than 1 µm, while for the phase shifter, a single encoder for gap height will be sufficient. The undulator segments require gap height and mid-plane position encoders on both ends of each device.

X-ray FELs demand that the positions of undulator components be stable to less than 1 µm per day. A <1µm precistion wire position monitor (WPM) system has been developed and incorporated into the LCLS undulator line [4]. Provisions are to be made for the future installation of an adapted version of the existing system for the LCLS-II HXR beamline, and a second system will be installed on the LCLS-II SXR beamline.

8.2.9 Radiation Damage Issues

Undulator segments at LCLS are being removed from the beamline and re-measured at the MMF on an on-going basis. These measurements show a reduction in $\Delta K/K$ at a rate of about 0.01% over 4 years. At the same time, radiation levels are integrated along the undulator line showing a steady dose rate during beam operation at 120 Hz with up to 250 pC bunch charge. Due to the high repetition rate planned for LCLS-II, there will be up to 1000 times more electrons per second in the LCLS-II beam than there are in the LCLS beam.

Several measures will be implemented to protect the undulator magnet material from damage. They consist of:

- A complete collimator system upstream of the final bends in the LTU to limit the five-dimensional phase space (x, x', y, y', E), such that electrons that pass the collimator system will not be able to get lost in the undulator vacuum pipe if the undulator system components are set correctly.
- A MPS based on the BLMs and RFBPMs to prohibit beam operation at high radiation doses or with trajectory amplitudes outside a ±1 mm envelope.
- Radiation monitors along both undulator systems consisting of Radiation-Sensing Field-Effect Transistors, RADFETs, and Čerenkov detectors of higher sensitivity that the BLMs. The RADFETs measure the integrated dose and can be read remotely. The high-sensitivity Čerenkov detectors will be used while tuning the linac to minimize the halo electrons.

8.2.10 Vacuum System

The LCLS-II undulator vacuum system needs to be operated at a pressure better than 10^{-6} Torr in order to keep bremsstrahlung and emittance growth to a minimum. To achieve this, an ion pump needs to be installed in each interspace section. The pump speed inside the narrow segment chamber is expected to be limited by the conductance in the vacuum system. The mechanical vacuum chamber requirements are dominated by wakefield considerations. The interaction between the electron beam and the vacuum chamber generates longitudinal and transverse wakefields (characterized through the vacuum chamber impedance) that can reduce FEL gain and need to be kept small. There are three main contributors to the vacuum chamber impedance:

- electrical surface conductivity
- surface roughness
- geometric shape of the beam channel

The surface roughness slope needs to be monitored by surface scans performed on small chamber samples during the vacuum chamber fabrication process. The goal is to keep the contribution from surface roughness and geometric shape small compared to the unavoidable contribution from the resistive wall conductivity. One component of the latter, AC conductivity

[5], can be reduced by the choice of aluminum as surface material. The same requirements apply for the vacuum systems of both the SXU and HXU.

.

8.2.11 Undulator Hall

The undulator hall temperature and floor stability are a concern. As discussed in section 8.2.8 it is important that the local undulator temperature stays reasonably stable. Floor stability is very important since component position monitoring will not be available. Random movement of quadrupoles by 8 µm (rms) will reduce FEL output by about 40%, requiring another application of Beam Based Alignment, BBA. The stability requirements are given in *Undulator System PRD* LCLSII-3.2-PR-0038.

8.2.12 Undulator Magnetic Tuning

In order for the SASE process to produce optimum gain, four tuning considerations need to be satisfied for each operational gap:

1. Control of the undulator parameter, K_{eff}
2. Phase shake reduction throughout each segment
3. Reduction of the overall phase error across each segment
4. Reduction of the first and second integrals of the horizontal and vertical field components

Table 8-6 lists specific parameter requirements needed to address the above concerns.

Table 8-6. Basic Undulator Segment Tuning Requirements

Parameter	SXU Values	HXU Values	Unit
Undulator parameter tolerance $\Delta K_{eff}/K_{eff}$	$\pm 3.0\times10^{-4}$	$\pm 1.5\times10^{-4}$	
Horizontal K sextupole $\left\|\frac{1}{2}\left(1/K_{eff}\right)\ \partial^2 K_{eff}/\partial x^2\right\|$	$<6.8\times10^{-4}$	$<3.4\times10^{-4}$	$1/mm^2$
Phase shake (rms) over L_{cell}	±5.0	±4.0	deg Xray
Cell phase error	±10.0	±5.0	deg Xray
First field integral of B_y per cell (abs)	<40	<40	µTm
Second field integral of B_y per cell (abs)	<150	<150	μTm^2
First field integral of B_x per cell (abs)	<40	<40	µTm
Second field integral of B_x per cell (abs)	<50	<50	μTm^2

The phase errors are based on the segment cell length, L_{cell}, which is defined as the length of a line along the magnetic segment axis over which the total phase slippage is πN_p for the tuning gap height, when centered longitudinally at the segment center. N_p is the number of segment

poles per strongback. A consequence of the field integral tolerances in Table 8-6 lists specific parameter requirements needed to address the above concerns.

Table 8-6 is that differences between environmental field components (Earth field, etc.) in the undulator hall and those in the magnet measurement facility need to be smaller than 0.1 G, which is very likely not going to be the case without ambient field correctors. The undulator parameter and the phase shake are determined over the segment core, i.e., without considering the end sections.

8.2.13 Alignment Strategy Overview

During initial installation of the components, the quadrupole magnets will be aligned to a straight line within a local error of 100 µm (rms) and a walk-off amplitude of less than 250 µm. Both the quadrupoles and the undulator jaws will be equipped with tooling balls that are fiducialized to the magnetic axis of the devices. For the undulator, this fiducialization will be done at the tuning gap. The detailed alignment tolerances are listed in *Undulator System PRD* LCLSII-3.2-PR-0038.

The undulators, which will be installed independently of the quadrupole magnets, will then be aligned in the tunnel such that their magnetic axes are centered between the magnetic axes of the neighboring quadrupoles. This procedure has been successfully applied several times for the LCLS undulator segments since operations began. Using laser trackers, a precision of about 50 µm (rms) can be achieved.

The LCLS alignment strategy [6] has been very successful in producing a straight electron beam trajectory sufficient for high FEL gain using a BBA procedure based on variable electron energies. LCLS-II will use a quite similar strategy, even though there are system differences, such as variable gap and large undulator size, which require special considerations.

The vacuum chamber, which needs to be centered on the electron beam, will be supported off the adjacent quadrupole support movers and aligned relative to the quadrupole centers during the initial alignment procedure. The BBA procedure will move the quadrupole positions in order to straighten the electron beam trajectory. The vacuum chamber will move with the quadrupoles. The position of the undulator segment strongbacks will need to be adjusted to stay centered on the vacuum chamber.

8.3 Undulator prototype and production plans

The collection of Engineering Notes, listed in Table 8-7, thoroughly documents the design details and analysis of the LCLS-II undulators. The following two sub-sections will give an overview of the mechanical and magnetic design with reference to specific Engineering Notes for details.

Table 8-7. LBNL Undulator Design Engineering Notes

Title	Engineering Note

Magnetic Material Specification	LC0100 - #10620
Vacoflux 50 Pole Annealing Specification	LC0100 - #10698
Demagnetization of Permanent Magnet Block	LC0100 - #10700
Pole Chamfer Effect on End	LC0100 - #10725
LCLS-II Mechanical System Procurement Scope	LC0100 - #10792
Mechanical System Assembly Tolerances	LC0101 - #10800
Magnetic Field Loss Due To Clearance between Pole And Permanent Magnet	LC0100 - #10817
Magnetic Gap Interference Analysis	LC0100 - #10853
Flexure Mount Plate Pre-Production Tests	LC0101 - #10863
Results of Magnet Measurement and Tuning for the LCLS-II Magnet Module Prototype	LC0107 - #10903
Magnet Measurement Bench Installation	LC0107 - #10912
Magnet Module Assembly – Pole and Magnet Location and Spacing	LC0103 - #10915
Study of Possible Demagnetization During HXU-32 Assembly	LC0100 - #10916
Hard X-Ray Undulator Moving Plates	LC1111 - #10929
Prototype Gap Drive System Test Results	LC0102 - #10932
End Design For HXU-32	LC0100 - #10938
Hybrid Undulator Error Signature and Tuning Analysis	LC0103 - #10939
Magnetic Tuner For HXU-32	LC0100 - #10944
Analysis of Initial Errors in the HXU-32 Magnet Module Prototype	LC0107 - #10957
Undulator Transport Analysis	LC0100 - #10965
Work on Undulator without LOTO	LC0100 - #10966
Kugler Magnetic Measurement Bench Acceptance Tests	LC0107 - #10974
HXR Magnetic Design	LC0103 - #10988
Gap Drive Compensating Spring Design Concept	LC0102 - #10989
SXR Magnetic Design	LC0104 - #10994
LCLS-II Long Lead Production Basis Of Estimate	LC0100 - #10996
Nook Roller Nut Mounting Block Analysis	LC0102 - #11005
Monorail Carriage Lubrication	LC0102 - #11006

Drive Linear Slide Analysis	LC0102 - #11007
Flexure Plate Analysis	LC0102 - #11008
Pole Flexure Analysis For SXR	LC0109 - #11012
Flexure Mount Plate Pre-Production Tests	LC0102 - #11013
Monorail Carriage Deflection (Yaw) Test	LC0102 - #11014
Frame Analysis	LC0102 - #11018
Tightness of Pole Flexure Bolt with Respect to Temperature Change (SXR)	LC0109 - #11020
Undulator Seismic and Model Analysis	LC0102 - #11023
Measurement Apparatus 5-point	LC0107 - #11027
Improved Sorting Procedure For The LCLS-II Undulators	LC0107 - #11028
Magnet Module Load Deflection Simulation	LC0109 - #11037
Pole Flexure Cyclic Load Test	LC0103 - #11038
Gap Drive System Deflection Test	LC0107 - #11028

8.3.1 Undulator mechanical design

The undulator mechanical design, including the frame, strongbacks, drives, encoders and alignment jacks, is common to both the HXR and SXR. The magnetic designs share the same design concept, but differ in details due to the different period lengths. Figure 8-4 shows an overview of the undulator design with labels for reference in the discussion below.

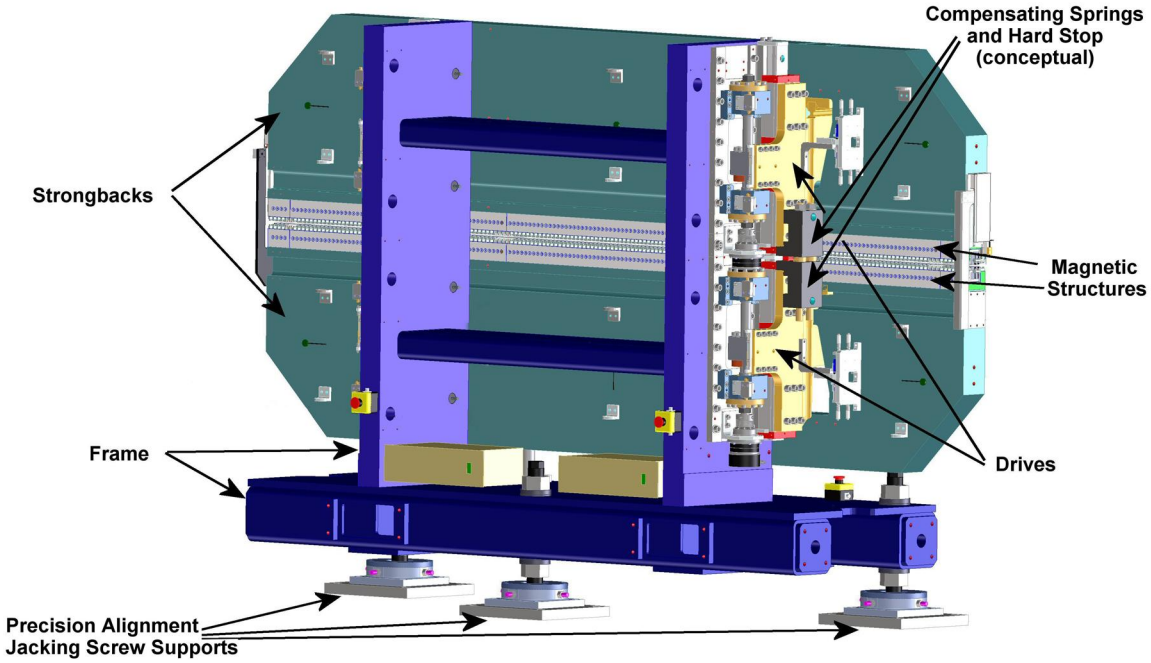

Figure 8-4. Overview of undulator design.

The frame is a welded steel structure. It is supported on two base plates via a set of three jacks that allow for leveling and alignment. The only machined surfaces are the mounting pads for the drives. Engineering Note LC0102 - #11018 documents analysis of the frame.

A set of four drives are used to adjust the magnetic gap. Each drive consists of a harmonic drive servo motor which drives a monorail and roller carriage via a roller screw. Flex plates connect the drive systems to the magnetic structure. Figure 8-5 shows a drive system and flexplace assembly. Engineering Notes LC0102 - #10932, LC0102 - #11005, LC0102 - #11006, LC0102 - #11007, LC0102 - #11014 and 11043 document design details analysis and tests of the gap system.

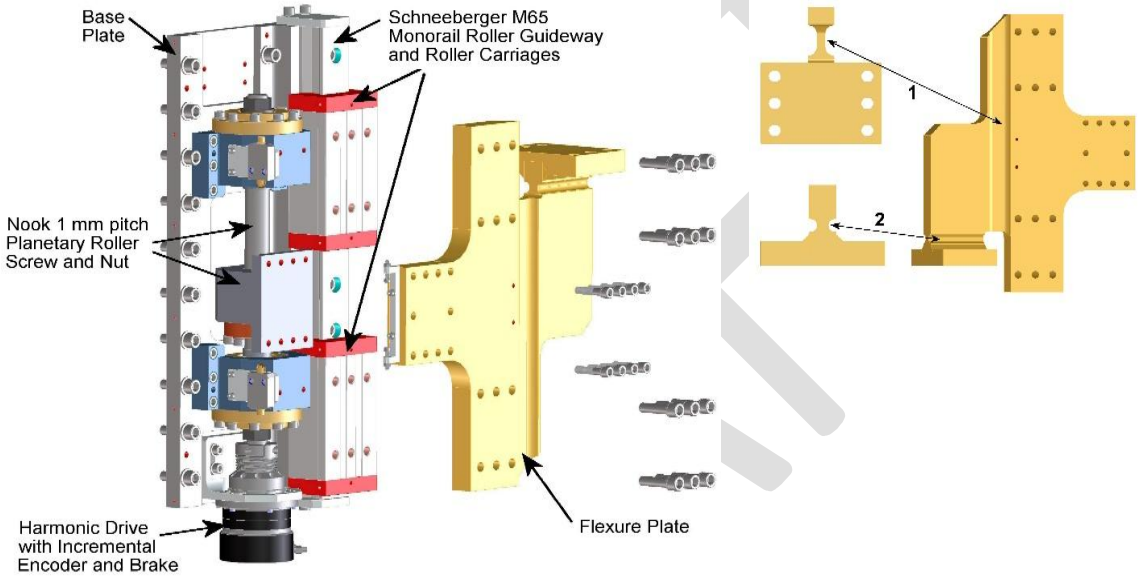

Figure 8-5. Drive system and flexure plate strongback mount.

The magnetic strongback is machined from 6061 aluminum. Its function is to support the magnetic structure and minimize the deflection due to attractive magnetic forces between the upper and lower magnetic structures. The flexure plate that connects the drives to the strongback allows for differential thermal expansion between the aluminum strongback and the steel frame and pitch of the strongback. The intention is to control motion so that upstream and downstream gap motion is synchronous. However, a motor fault or control system error will result in pitch rotation of a strongback, resulting in elongation between the upstream and downstream mounts and rotation of the mounting surface. The flexure region 1, as illustrated in Figure 8-5, allows for elongation. Flexure region 2 allows for rotation. Engineering Notes LC0101 - #10863, LC0102 - #11008, LC0102 - #11013, LC0109 - #11020 and LC0109 - #11037 document the design details, analysis and tests of flex plates and strongbacks.

The magnetic gap read-back is provided by absolute linear encoders attached to each end of the strongback pairs. A system of eight limit switches prevents contact between the magnetic

structure and the vacuum chamber. Four switches are attached to both the upper and the lower magnetic structures, two upstream and two downstream. The switches are engaged with direct contact of the vacuum chamber. A linear transducer attached to the upper strongback is in contact with the vacuum chamber to maintain relative position between the magnetic structure and the chamber. Tilt limit switches are used to protect the flexure plates from failure due to over rotation, and an additional set of switches on each drive prevent over-travel. Figure 8-6 shows the system of encoders, transducer and limit switches. Engineering Note LC0100 - #10853 documents an analysis of potential gap interference, which informs the design of the gap interlock system.

Figure 8-6 also shows the compensating spring system. The magnetic attractive force between the top and bottom magnetic structures is a strong nonlinear function of gap. The constant gravitational force acts in the same direction as the magnetic force for the top magnetic structure, but is opposite for the lower structure. The gap for which the gravitational force will overcome the magnetic force on the lower structure is about 13.5 mm for HXR and 21 mm for SXR. This force reversal has the potential for an undesirable mechanical backlash in the gap control within the important operating gap range. A set of compensating springs attached to upper and lower flexure plates will prevent this possibility. The spring system will be nonlinear and is designed to approximately cancel the attractive magnet force in the gap range from the minimum gap of 7.2 mm to about 30 mm, which is beyond the operating gap range of 20 mm for HXR and 22 mm for SXR. The springs incorporated into the system housing will act as a hard-stop to limit the minimum magnetic gap. Engineering Note LC0102 - #10989 documents the design details and analysis of the compensating springs and hard stops.

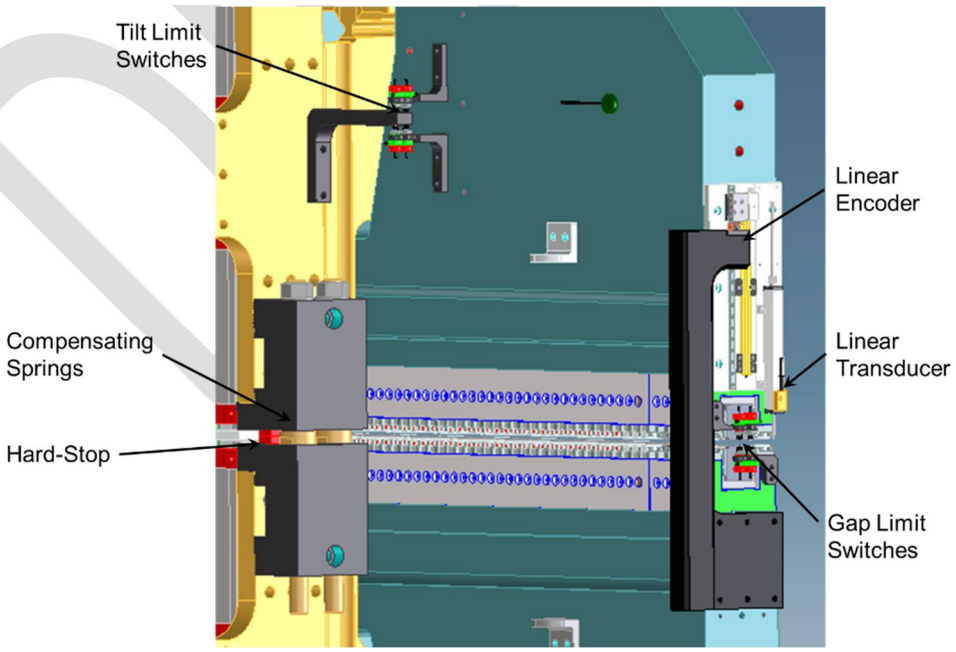

Figure 8-6. Limit switches, compensating springs, linear encoder and transducer.

8.3.2 Undulator Magnetic Design

The magnetic structures for both HXR and SXR are hybrid designs consisting of vanadium permendur poles energized by NdFeB permanent magnets. Each top and bottom magnetic structure is composed of three periodic magnetic modules and two end modules, as illustrated in Figure 8-7. The magnetic length is approximately 3.4 m, but the exact length as well as the length and configuration of the magnetic modules is different for HXR and SXR to accommodate the different period lengths.

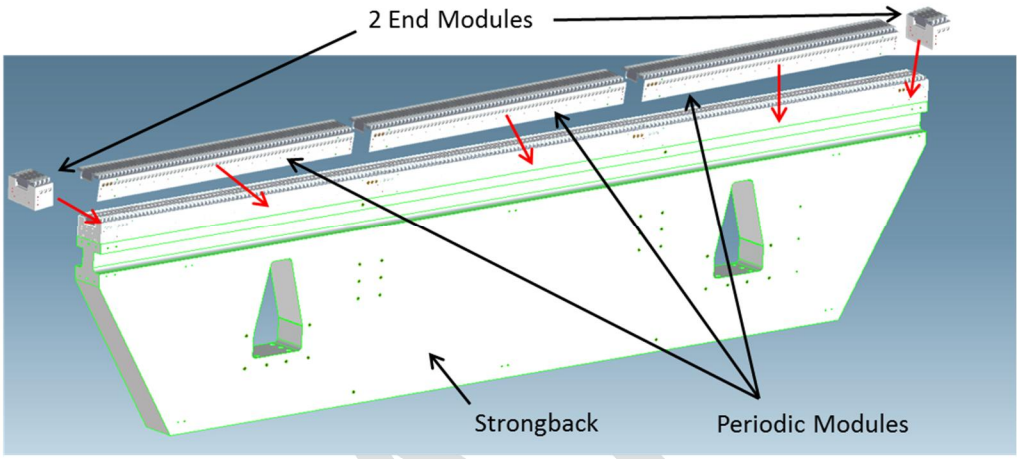

Figure 8-7. Magnetic structure.

Figure 8-8 shows a closer view of magnetic structure details and illustrates mechanisms incorporated into the design for vertical field tuning. Poles and magnets are mounted to module keepers, made of 7075 aluminum to match the thermal expansion characteristics of the strongbacks. Pole mounts include flexures to allow for magnetic tuning via vertical pole position adjustment. The pole mount flexures are made of 316 stainless steel and are attached to the poles with adhesive and a retention screw. Poles are precisely located along the beam direction by pins to maintain precise periodic spacing. Magnets are clamped within the slots between poles. Each pole location within the module has the provision for adding a pair of magnetic tuners, which provide an additional means for magnetic tuning by increasing or decreasing the magnetic excitation of the adjacent pole. The tuners consist of cylindrical magnets magnetized perpendicular to their axes. The tuner pair can be counter-rotated to vary the strength of the magnetic excitation. Engineering Notes LC0100 - #10620, LC0100 - #10698, LC0100 - #10700, LC0100 - #10725, LC0100 - #10817, C0103 - #10915, LC0100 - #10916, LC0103 - #10939, LC0100 - #10944, LC0103 - #10988, LC0104 - #10994 and LC0109 - #11012 document design details and analysis of the magnetic designs for HXR and SXR.

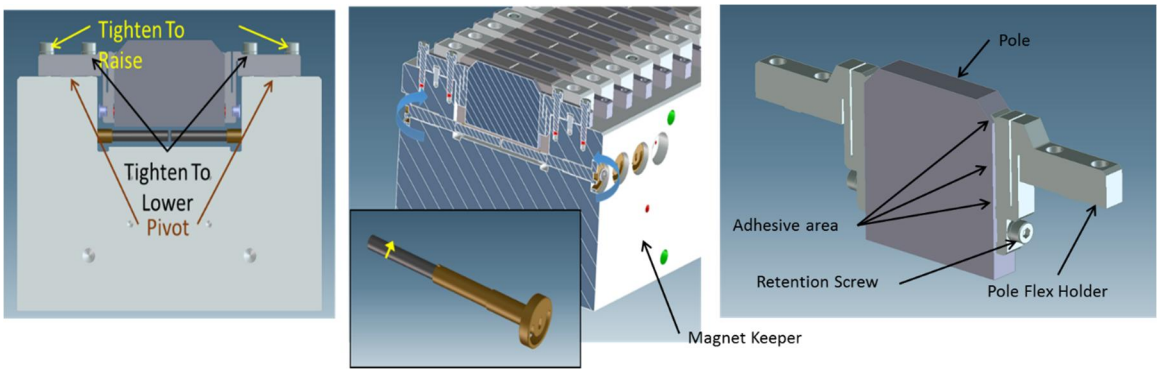

Figure 8-8. Pole and magnet tuner configuration.

The magnetic structure is designed to produce a vertical field, which will produce horizontally polarized light. However, small horizontal fields will, in general, also be present due to magnetic errors. Figure 8-9 illustrates mechanisms incorporated into the design to tune out first and second horizontal field integral excursions. Horizontal field tuning is accomplished with a combination of pole canting and the optional introduction of small magnet slugs within the clamps holding the primary periodic magnets.

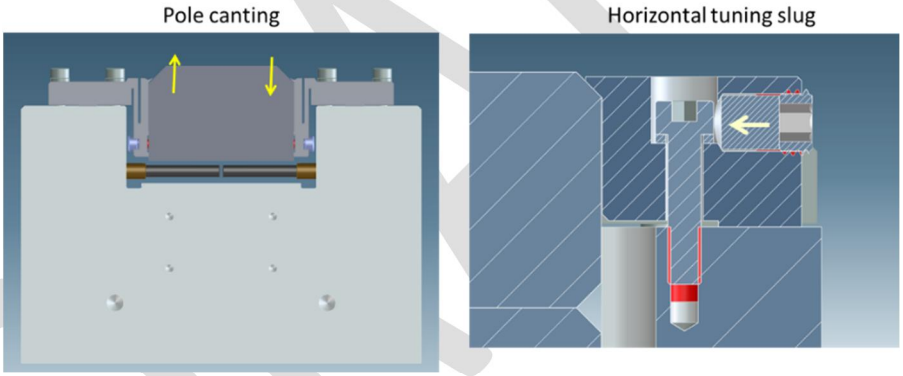

Figure 8-9. Horizontal tuning via pole canting and horizontal magnet slugs.

The magnetic design was analyzed with Opera 3D, see Engineering Notes: HXR Magnetic Design, LC0103 - #10988 and SXR Magnetic Design, LC0104 - #10994. The periodic portion of the magnetic structure was modeled as a quarter period with symmetry planes at the horizontal and vertical mid-planes, as illustrated in Figure 8-10. The following features are common to both the HXR and SXR:

- The poles incorporate 5-mm corner chamfers to increase the magnetic flux in the central region.
- The magnet blocks incorporate 3-mm corner chamfers for clamping the blocks into the module keepers. The chamfers are incorporated at all four corners to maintain symmetry to allow rotation as part of magnet sorting.
- The magnet blocks incorporate a 1-mm edge chamfer to minimize potential for demagnetization. The magnet edges adjacent to poles and closest to the magnetic gap

are a region of high reverse fields. Chamfers are incorporated on top and bottom edges to maintain symmetry for magnet sorting.

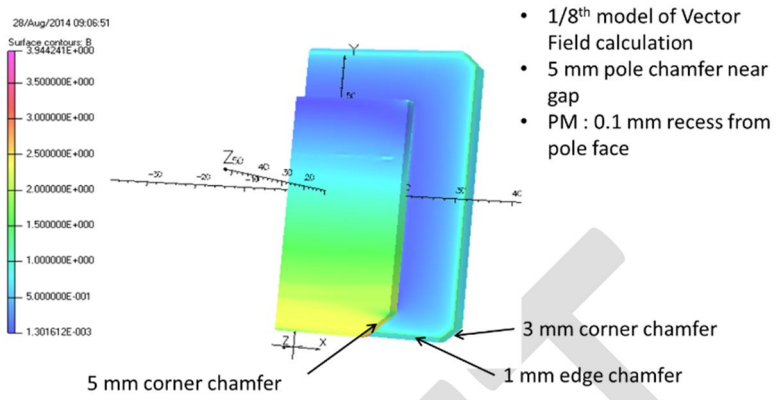

Figure 8-10. Magnetic model.

The results of periodic magnetic field calculations are summarized in Table 8-8.

Table 8-8. Calculated results of periodic magnet field calculations for HXR and SXR.

Parameter	HXR		SXR	
	Result	Requirement	Result	Requirement
B_{eff} [T]	1.036	1.010	1.518	1.490
Field Roll-Off*	9.5×10-5	3.4×10-4	1.7×10-4	6.8×10-4

*Corresponds to sextupole: $[(1/2)(1/B_{eff})(\partial^2 B_{eff}/\partial x^2)]$

The magnet volume with the highest reverse fields, and thus the greatest potential for demagnetization, is at the interface between the pole and magnet at the corner chamfer, as illustrated in Figure 8-11. The highest reverse field is 22.2 kOe and 25.3 kOe for HXR and SXR, respectively. In both cases, calculations show that demagnetization will not occur for temperatures up to 40º C. Engineering Notes LC0100 - #10700, LC0100 - #10817, LC0103 - #10988 and LC0104 - #10994 document the design details and analysis of demagnetization potential.

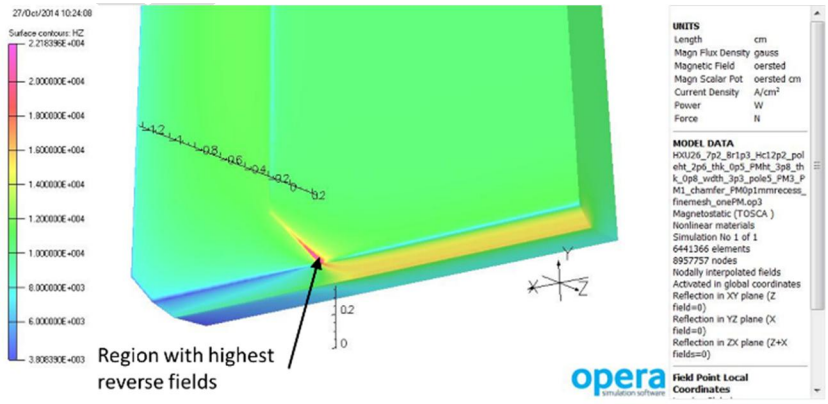

Figure 8-11. Region with greatest potential for demagnetization.

The magnetic termination of the magnetic structure must taper the periodic field in a controlled way to minimize trajectory kick and offset at the entrance and exit. The magnetic end designs for HXR and SXR are based upon an ideal series of normalized pole scalar potentials: 0, ±0.25, ±0.75, ±1.0. In general, this ideal scalar potential series cannot be maintained for a range of gaps with a hybrid design, due to the variation in magnetic capacitance between the poles and horizontal mid-plane and variation in differential pole saturation as a function of gap. The design goal is to minimize this variation within the operating gap range. The end design incorporates poles that are identical to periodic poles and adjusts magnet heights to achieve the desired field taper. Figure 8-12 illustrates the magnetic model of the magnetic end design. Engineering Notes LC0100 - #10938, LC0103 - #10988, and LC0104 - #10994 document the design details and analysis of the magnetic end terminations.

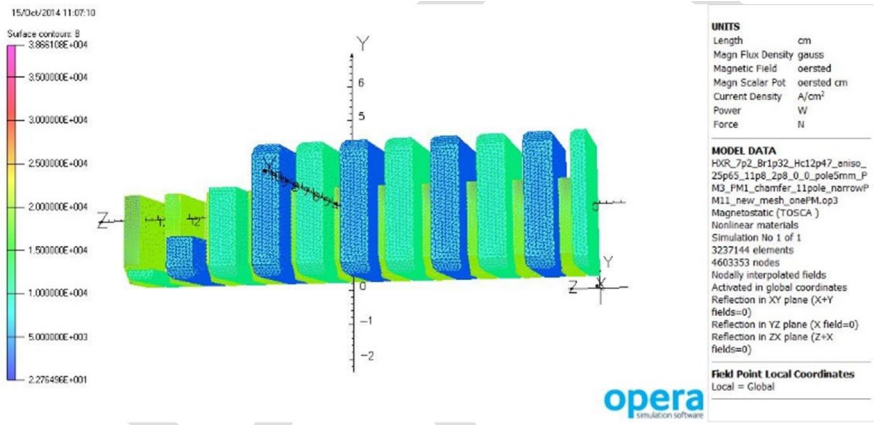

Figure 8-12. Magnetic model of end design.

Figure 8-13 shows the calculated total shift values over the 20 mm and 22 mm operating gap range for HXR and SXR, respectively. Total shift incorporates the entrance kick slope projected over the full 3.4 m length plus the entrance and exit offsets. The calculated values are within the required range of 100 μTm^2. In practice, values can be further reduced with the introduction of pole height and rotor tuning.

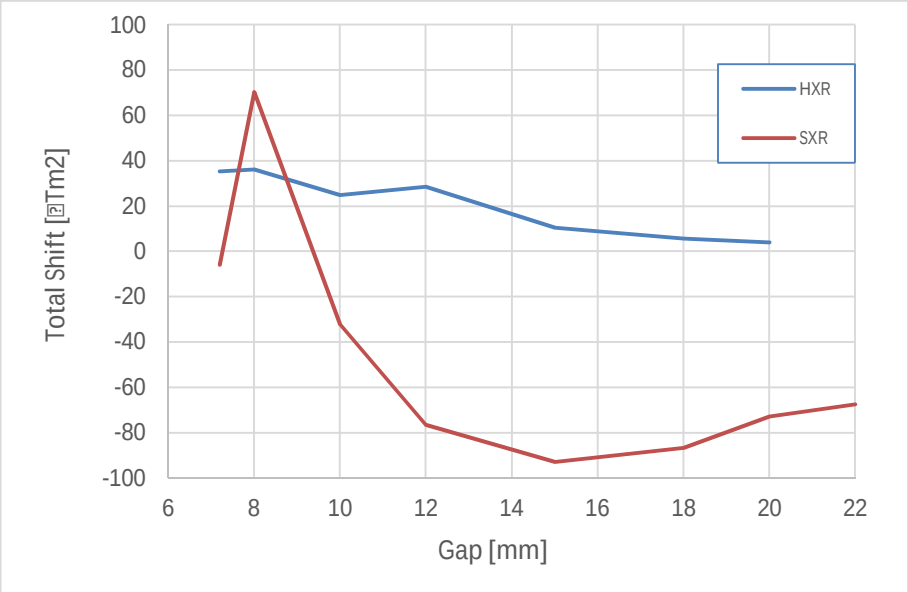

Figure 8-13. Calculated total shift values for HXR.

8.3.2 Undulator Production Plans

The overall project schedule requires a peak undulator delivery rate of one undulator segment per week over a time span of approximately 16 months. The undulator mechanical system – as described in section 8.3.1 – will be procured as a complete, fully assembled and aligned unit from a qualified vendor. In a similar manner, the fully assembled and pre-aligned magnet modules – consisting of the poles, flexures, magnets, and the module keeper – will be procured from a separate qualified vendor. Two independent magnet vendors and two mechanical structure vendors will be qualified and engaged for the LCLS-II project. Suppliers will be qualified by building a prototype undulator unit.

LBNL will integrate the magnetic modules with the mechanical structure. In order to satisfy production rate requirements, LBNL has to develop three assembly lines. Integration work flow is planned in discrete steps and includes following activities: 1) Mechanical system QA/QC, 2) Magnetic system QA/QC, 3) Undulator assembly, 4) Magnetic Tuning, and 5) Shipping to SLAC. LBNL has developed a specific QA process for LCLS-II as well as a manufacturing plan with rigid configuration control.

8.4 Undulator Magnetic Measurements and Tuning

Most of the magnetic measurement and tuning techniques that were used for LCLS can be applied to LCLS-II. Many new challenges, however, must still be overcome. These include the effects of the Earth's magnetic field and difficulty fiducializing large undulators. A summary of the current status and potential challenges follows.

8.4.1 Undulator Tuning

The undulator tuning for LCLS-II will be similar to LCLS, but the variable strength of the undulators will require a much more extensive set of measurements. There will also be differences in the shimming techniques used. Finally, the lack of a magnetic shield on the undulators will require measurement and correction of the background magnetic fields.

The principles of undulator tuning have been documented in a technical note [7]. The note shows how most quantities of interest are calculated and which adjustments to the undulator magnetic field must be made to change these quantities. The principles outlined are the same for LCLS-II as they are for LCLS.

The implementation of shims for LCLS-II will be different compared to LCLS. In LCLS, the gap was fixed and the poles were fixed. All correction fields were made by adding magnetic material, which altered the undulator field. LCLS-II will incorporate: 1) individually positionable poles that will allow for field corrections to be made by changing vertical position and angle of each pole and 2) optionally insertable permanent magnet rotor pairs above top poles and below bottom poles to allow for individual pole energization refinement. These two "knobs" have different gap dependencies, which, when appropriately combined, are intended to cancel the net error fields from all sources over the entire range of gap motion. The effect of pole motions and rotor pair strength and orientation will be measured and parameterized. These parameterizations will be used in a computer program to determine the necessary adjustments to correct the trajectories and phase. The computer algorithm to determine the shim strengths for LCLS undulators is given in [8].

For adjustable gap undulators, the shimming to correct trajectories, phase shake and, field integrals is first done at a tuning gap near the minimum gap. The tuning gap is chosen to minimize the phase errors caused by undulator jaw deformations due to magnetic forces. By choosing a tuning gap near the minimum gap, the undulator field errors are corrected when the effect of the field errors is the largest. As the gap is increased, the effect of both the field errors and the correction fields is reduced. If the field errors and corrections do not track each other as the gap is changed, then additional corrections will be made per the above algorithm, to accommodate the range of gap motion. Additional powered dipole coils on the beam pipe will make corrections to the trajectories over a large distance for distributed errors, such as compensating external fields whose effect may change as the gap is changed.

8.4.2 Magnetic Measurement Systems

A number of different systems are used to measure undulators in the Magnet Measurement Facility (MMF) [9][10].For example, Hall probes carried by a precision bench are used to determine trajectories, phase errors, *K* value [11]. The average trajectories are checked using coils that are one period long. This check ensures that errors like the planar Hall effect are small. Hall probes are, however, unsuitable for accurate determination of the overall field integrals. A long coil system gives the first and second field integrals [12][13]. The undulators are aligned relative

to the bench using a capacitive sensor system and a cam mover system [14]. A temperature measurement system accurately gives the undulator temperature [15][16]. Fiducialization is done using a combination of Hall probe measurements in special high-gradient magnets attached to or mounted near the undulator and either a Coordinate Measuring Machine (CMM) or a laser tracker to locate relevant tooling balls [17][18]. The CMM is also used to do extensive mechanical measurements on the undulator, or various parts thereof. For LCLS, the CMM was also used to measure the girder that holds the undulator [19].

The MMF has some capability to repair damaged undulators. A permanent magnet block magnetizer is used to repair radiation damage. Measurement systems must check the blocks before and after magnetization. A Helmholtz coil system is used to measure the magnetic moment of the blocks. A Hall probe mapping system is used to localize radiation damage in magnet blocks.

The MMF also has a system to accurately fiducialize quadrupoles, which is required for the quadrupoles between undulator segments. The fiducialization is done by a vibrating wire system built onto a coordinate measuring machine [20,21, 22, 23].

The MMF has several calibration systems. A large electromagnet is used to calibrate Hall probes. A chiller keeps the probe at room temperature in the magnet. The temperature of the undulators is measured with thermistors. The thermistors are calibrated in a water bath using a reference thermometer [24]. The reference thermometer can be inserted in any thermistor mount to check the measurement in place. The magnets used to fiducialize the undulators need to be calibrated to determine a point with given magnetic field relative to tooling balls [25]. A special fixture allowing magnet flips is used for this purpose.

The MMF employs a number of secondary measurement systems to constantly check for errors. The undulator benches have reference magnets which are measured by the Hall probe and in which an NMR probe can be inserted to constantly monitor Hall probe accuracy. Survey crews use alignment scopes to check for significant fiducialization errors and hand-held reference thermometers to verify temperature. Most importantly, reference magnets (undulator or quadrupole) are used to continuously monitor the repeatability of the whole measurement process.

A reference undulator was measured many times during the tuning of the LCLS undulators. These data sets give estimates of the random errors in the tuned undulators [26]. The measured trajectories in the reference undulator were stable and straight to within ±2 μm (at 13.6 GeV). Changes in the phase errors were less than ±2 degrees between data sets. The phase advance in the cell varied by less than ±2 degrees between data sets. The rms variation between data sets of the first integral of B_x was 10 μTm, and the rms variation of the second integral of B_x is 17 μTm². The rms variation of the first integral of B_y was 7 μTm, and the rms variation of the second integral of B_y was 12 μTm². The rms variation of the x-position of the fiducialized beam axis was 35 μm in the final production run. This corresponds to an rms uncertainty in the K value of

$\Delta K/K$=2.7×10^{-5}. The rms variation of the *y*-position of the fiducialized beam axis was 4 μm in the final LCLS production run.

The MMF presently has all equipment necessary to measure and tune LCLS undulators. A laboratory with temperature controlled to ±0.1°C contains two undulator measurement benches, a high-precision, 7-meter Kugler bench and a less precise Dover bench. For LCLS-II the Dover bench will be replaced with a second high-precision measurement bench and at LBNL an equivalent facility has been developed to accommodate the production run schedule.

8.4.3 Earth's Magnetic Field

The LCLS undulators were measured in the same orientation as they will have in the tunnel [27] [28]. This was done to minimize background field errors. In addition, the LCLS undulators have magnetic shields to reduce the effect of the difference of the background field in the tunnel compared to that in the MMF.

Magnetic shields are not planned for the LCLS-II undulators because of their variable gap design. This makes background fields a much larger problem. The undulators will continue to be measured in the same orientation as they will have in the tunnel. This will minimize the effect of the external horizontal field, especially as the gap is opened.

Without a magnetic shield on the undulators, further effort to deal with external fields is required. Trim coils will be in incorporated into the four corners of undulator beam pipe over its full length. A large Helmholtz coil will be built to apply external fields to a small number of undulators in order to characterize the resulting field in the gap and also the necessary current in the trim windings, in order to correct it. A map of the magnetic field in the tunnel will be made. The difference between the tunnel field and the field in the MMF, along with the characterization from the test undulator in the large Helmholtz coil, will determine how to set the current in the trim windings for each undulator position in the tunnel. A portable system to measure field integrals will be used in the tunnel to check the final field integrals. A portable vibrating wire system for making these measurements in the tunnel is under development [29]. Moving coil measurements as done in the MMF could alternately be performed.

8.4.4 Fiducializing Large Undulators

The LCLS undulators were fiducialized in a three-step process [30][31]. First, the Hall probe was positioned to move along the desired beam axis. The distance the Hall probe was required to move from the beam axis to a zero field point in fiducialization magnets at each end of the undulator was recorded. Second, the distance from the zero field point to tooling balls on the fiducialization magnet was determined using a special calibration fixture. Third, the distance from the tooling balls on the fiducialization magnets to tooling balls on the undulator was determined with a CMM.

Since the LCLS-II undulators are large, the final step of measuring tooling ball positions will not be possible with a CMM. Other measuring instruments, such as laser trackers, are accurate to

approximately 50 micrometers and will be used instead of the CMM. A touch probe system which will effectively turn the measurement bench into a CMM is also under development.

8.4.5 Throughput

The throughput of the MMF for LCLS undulators was approximately one undulator segment every two weeks. This included time to come to thermal equilibrium, mechanical measurements on the CMM, mechanical straightening of the gap centerline with checks on the CMM, rough tuning on the Dover bench, fine tuning on the Kugler bench, making a final data set on the Kugler bench, fiducialization on the Kugler bench, fiducialization on the CMM, and final mechanical measurements on the CMM. All this work was done in parallel at the CMM, Dover bench, Kugler bench, and at a separate stand for mechanical work, such as applying shims and gap straightening.

LCLS-II undulators will require all the steps mentioned above. In addition, LCLS-II undulators will have an adjustable gap. This will require a larger tuning effort and a more extensive final data set. Field integral corrections as a function of gap must be determined. Three measurement benches will be employed, one at LBNL and two at SLAC. All final data sets will be done on the same bench for each undulator line in order to minimize errors.

8.5 Interspace and vacuum systems

8.5.1 Interspace Assemblies

The interspace sections reside between undulators and contain beam diagnostics components, magnets, and the interspace vacuum system. These assemblies sit atop a pedestal support and cam positioning system, allowing remote adjustment of the populated girder. The interspace girder also supports two adjacent undulator vacuum chambers, i.e. a single vacuum chamber is supported by successive interspace assemblies.

8.5.1.1 Assembly variations

All interspace sections have similar component layouts, though discrete assemblies exist to serve distinct purposes. As such, there are five unique interspace sections within the undulator system. In addition, each interspace section has two configurations; the assemblies are mirrored about the center aisle to serve either the HXR Undulator or SXR Undulator line. The three main interspace assembly types are detailed below. Additionally, the first and last interspace assemblies on each line have unique configurations due to their limited component population. A fully populated interspace assembly is shown in Figure 8-14 in its installed configuration.

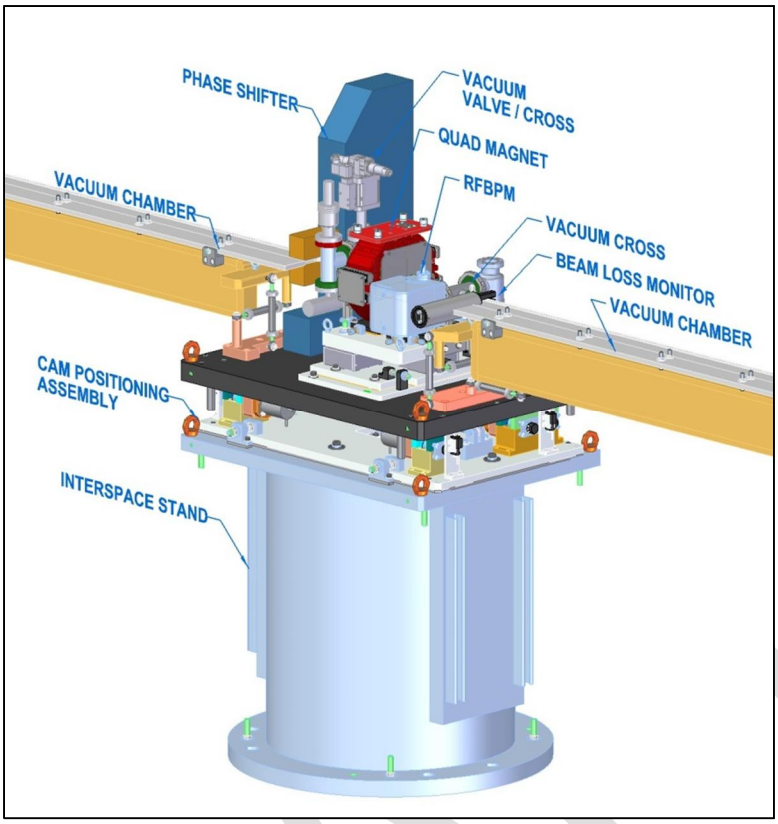

Figure 8-14. Populated interspace section. Undulators removed from view for clarity.

8.5.1.2 Isolation Section

The Isolation interspace section is located at regularly-spaced intervals throughout the undulator line. It includes a pneumatic gate valve to isolate a section of undulators, facilitating maintenance needs. The Isolation interspace section is shown in Figure 8-15. The assembly components, beginning at the upstream end and moving downstream, are:

- Phase shifter magnet assembly
- Isolation (gate) valve with cold cathode/Pirani gauge pair attached
- Quadrupole magnet with vacuum spool
- Beam position monitor
- Vacuum cross with cold cathode/Pirani gauge pair and ion pump attached

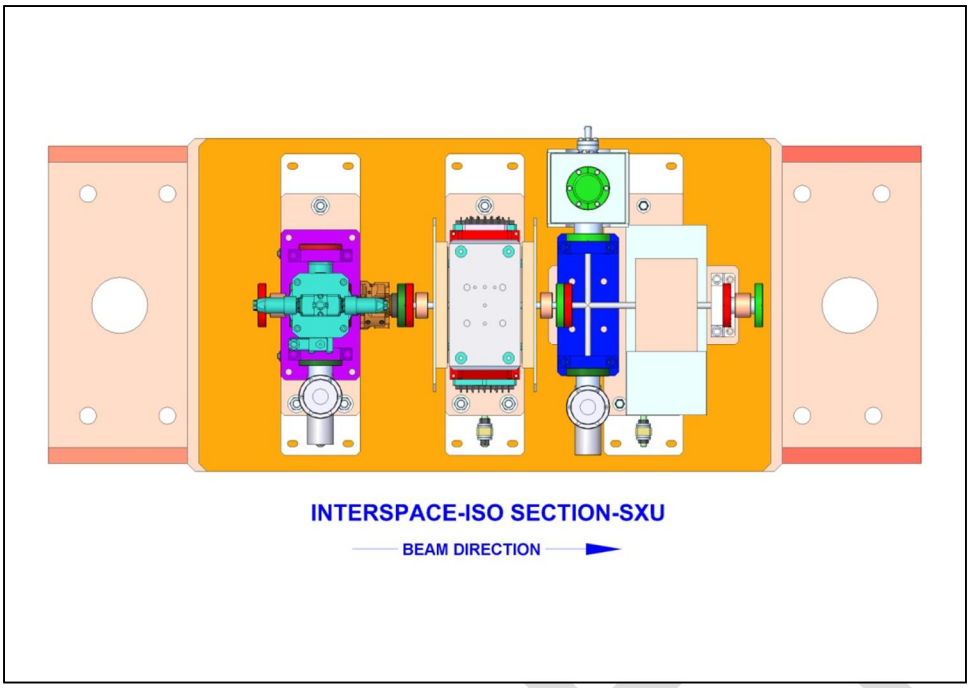

Figure 8-15. *Isolation* interspace section, for the HXR and SXR lines are identical

8.5.1.3 Pumpout Section

The Pumpout interspace section is located at regularly-spaced intervals throughout the undulator line. It includes a manual right angle gate valve with a connection flange for a turbo pump cart, which allows venting and evacuating the isolated undulator section. The Pumpout sections are located at the midpoint of each isolated HXR and SXR section. The Pumpout interspace section is shown in Figure 8-16. The assembly components, beginning at the upstream end and moving downstream, are:

- Phase shifter magnet assembly
- Vacuum cross with right angle valve attached
- Quadrupole magnet with vacuum spool
- Beam position monitor
- Vacuum cross with cold cathode/Pirani gauge pair, ion pump, and right angle valve attached

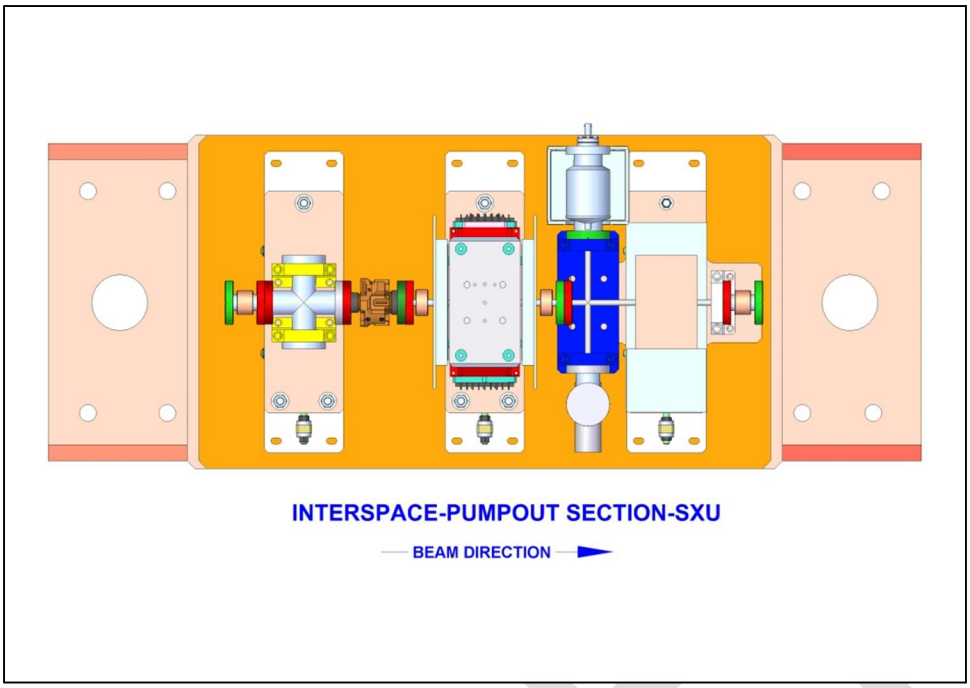

Figure 8-16. *Pumpout* interspace section, for the HXR and SXR lines are identical

8.5.1.4 Standard Section

The Standard interspace section is used as the default interspace where an Isolation or Pumpout section isn't required. The Standard interspace section is shown in Figure 8-17. The assembly components, beginning at the upstream end and moving downstream, are:

- Phase shifter magnet assembly
- Quadrupole magnet with vacuum spool
- Beam position monitor
- Vacuum cross with ion pump attached

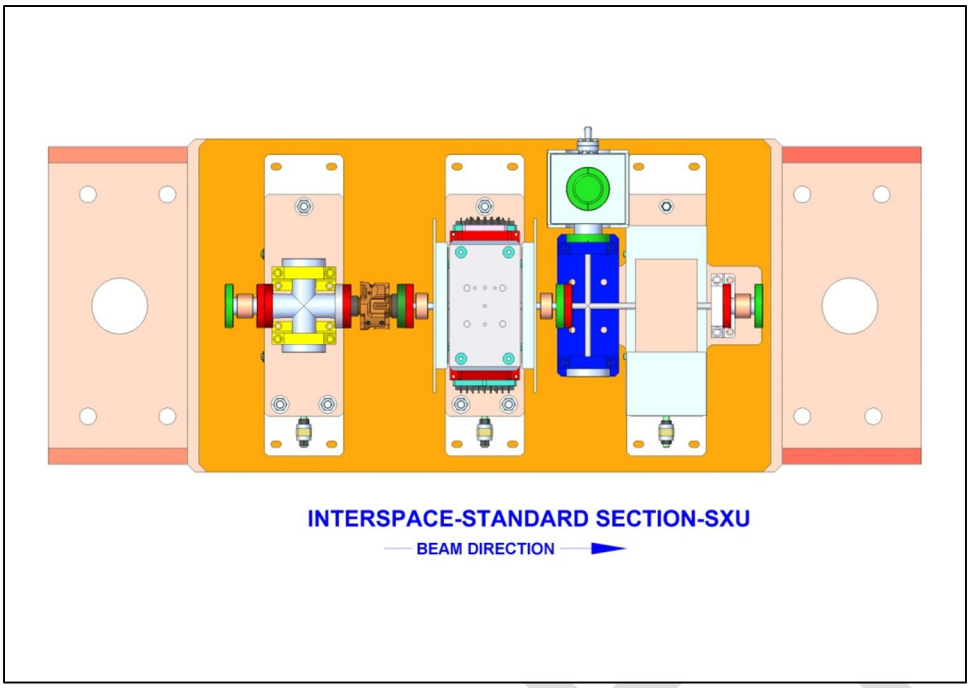

Figure 8-17. *Standard* interspace section, for the HXR and SXR lines are identical

8.5.2 Supports

A support stand weldment, seen in Figure 8-18, is used in conjunction with a cam positioning system to support each undulator interspace assembly. The pedestal design is adapted from LCLS, with a round tube sandwiched by top and base plates. Studs are included at the top and bottom plates to provide an electrical grounding location.

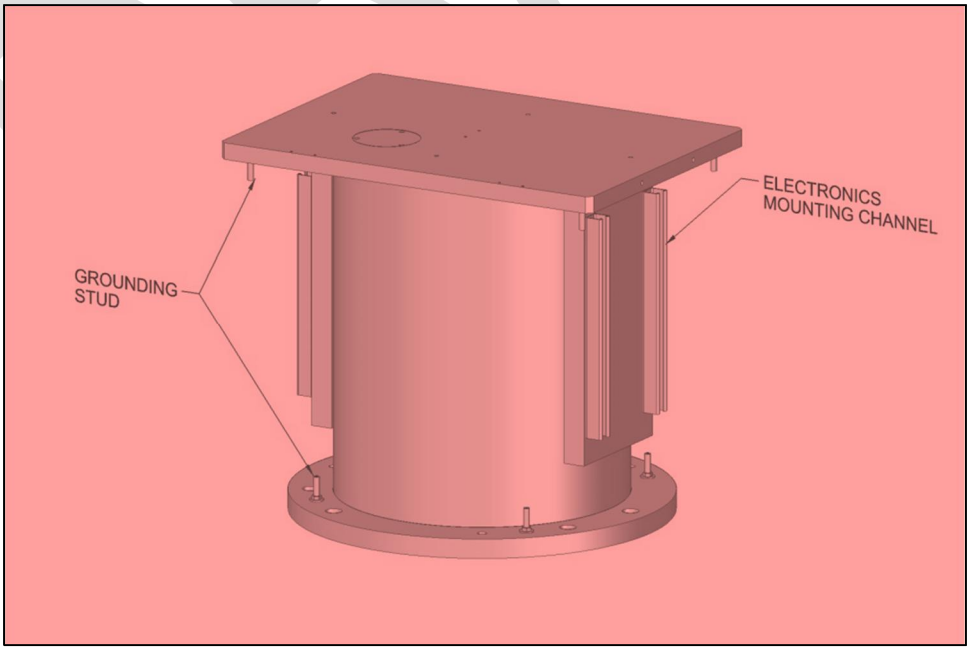

Figure 8-18. Interspace support stand weldment

8.5.2.1 Support stand

Thermal stability is paramount in order to provide a stable mechanical environment for the system quadrupole and BPM devices. Accordingly, the stand may be filled with sand to provide additional thermal mass and vibration damping capabilities. In addition, the support stand includes two channels to attach low-power interspace component electronics.

8.5.2.2 Cam positioning system

The LCLS-II cam positioning system consists of a five-camshaft configuration with five contact points between the interspace stand and component assembly base plate. The contact points include a flat, a standard (narrow) vee, and a split (wide) vee, constraining five degrees of freedom (DOF). This system provides vertical (y) and horizontal (x) motion control and is capable of small pitch adjustments about the x-axis. Roll (about z-axis) and yaw (about y-axis) DOF adjustments are not anticipated but are achievable with the five-cam system. A z-restraint constrains the interspace component assembly in the longitudinal (z) direction.

On the SXR line the sparse lattice components upstream of the undulator segments do not require remote adjustment. Consequently these locations will include a solid pedestal riser in place of the cam positioning system.

8.5.2.3 Component stages

The quadrupole and RFBPM components require precision alignment, necessitating individual adjustment stages, as shown in Figure 8-19. The composite stage wedges provide precise vertical, pitch, and roll adjustment. Individual stages are used to provide precise horizontal, longitudinal, and yaw adjustments. Precision shims may be placed beneath individual component stages if relative vertical alignment is required between the components.

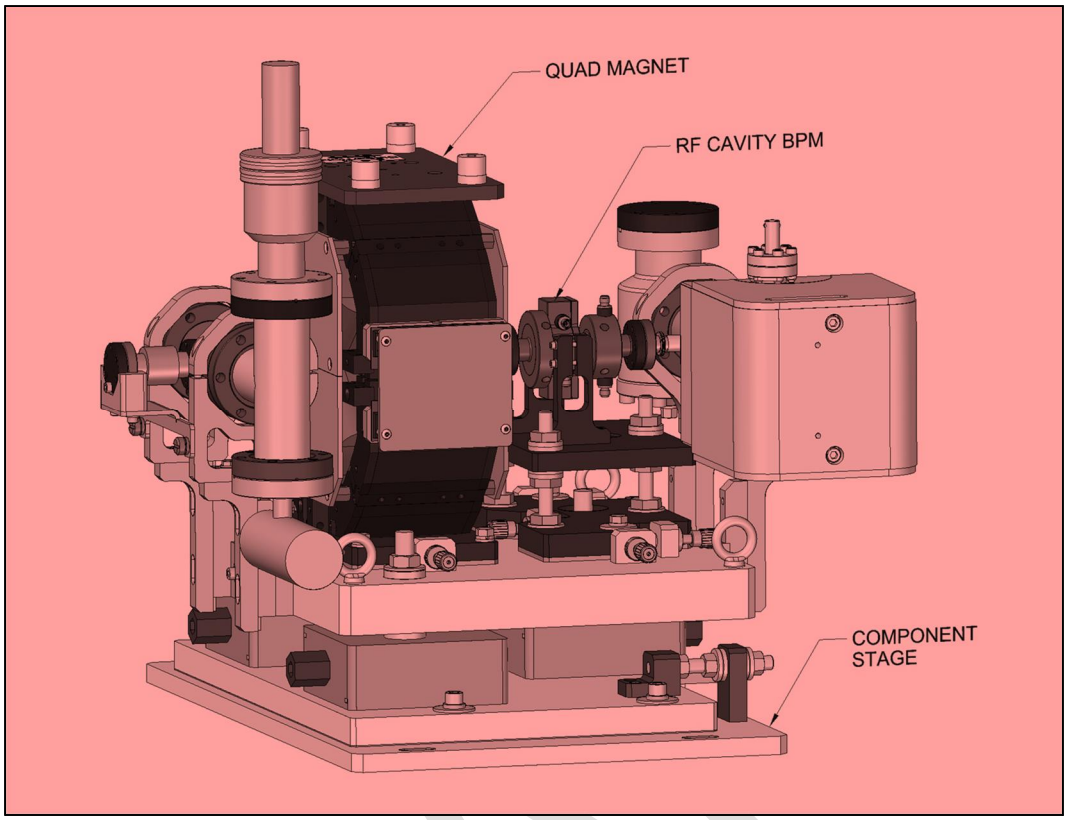

Figure 8-19. Populated Component Stage for either HXR or SXR systems

8.5.3 Vacuum System

The LCLS-II undulator vacuum system, shown in Figure 8-1, is comprised of 4.4-m-long cells on both HXR and SXR lines. Each cell consists of an undulator vacuum chamber and an interspace vacuum system. The LCLS-II undulator vacuum system must operate at a pressure better than 10^{-6} Torr in order to minimize bremsstrahlung

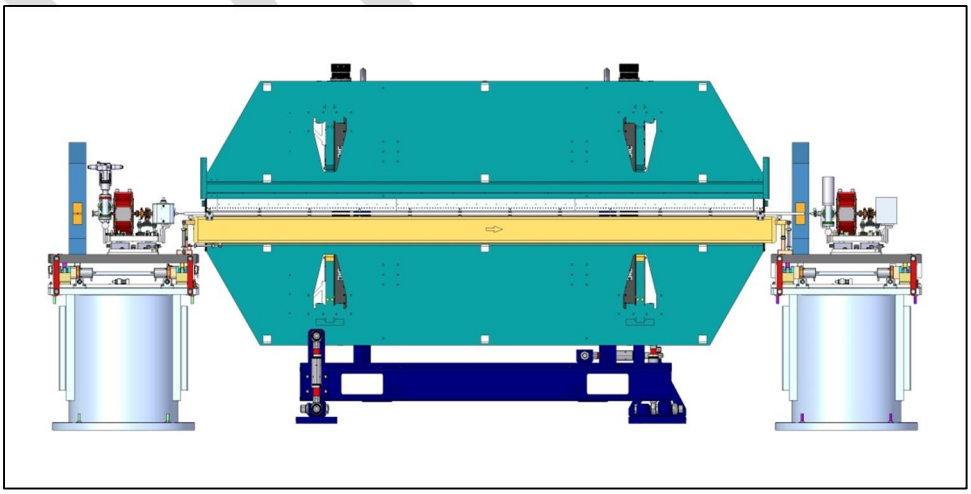

Figure 8-20 - Typical undulator/interspace layout. The vacuum chamber through the undulator is supported from the up and down stream interspace component mounting plate on a kinematic type mount. (Update with current undulator design from LBNL)

8.5.3.1 Undulator Vacuum Chamber

The vacuum chamber shall be produced from a 6063-T6 alloy aluminum extrusion. The chamber's interior racetrack profile, shown in Figure 8-21, is critical to undulator operation and function and remains unchanged from LCLS. Vacuum chamber height, straightness, and wall thickness must be carefully controlled during the manufacturing process. Vacuum chamber requirements are summarized in Table 8-9.

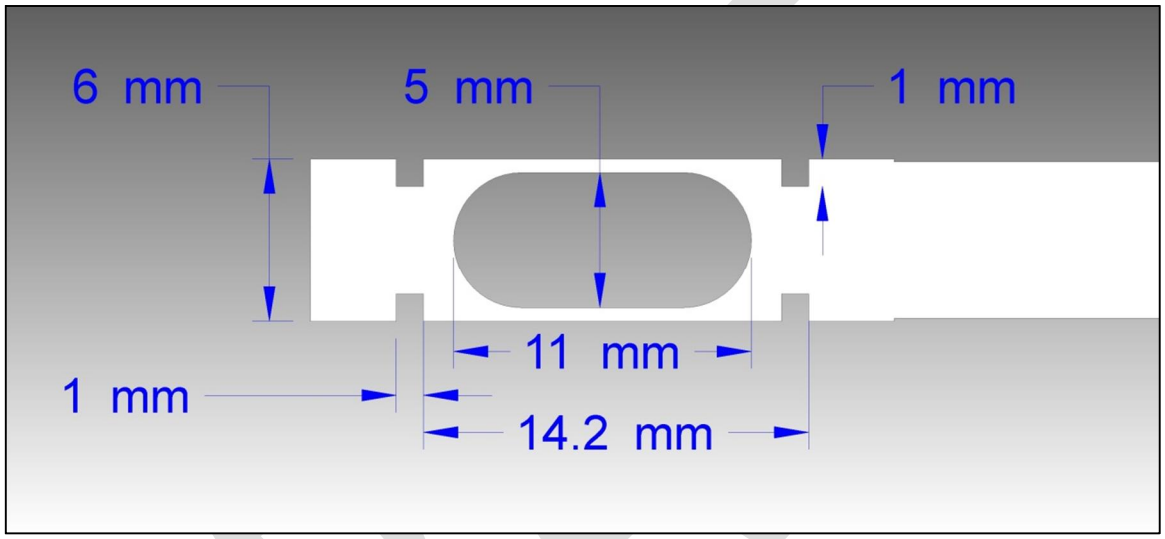

Figure 8-21. Typical vacuum chamber cross section (cooling water channels not shown). Note the four grooves in the vacuum chamber around the beam channel for insertion of earth field correction coil wires. (update with figure showing a colling channel too?)

Vacuum chamber height includes the inner aperture height and wall thickness. The chamber aperture is vertically centered between the undulator jaws and must fit between them in all operating conditions. The overall chamber height in the beam aperture region shall be 6.00 +0.15/-0.05 mm, while the chamber aperture height shall be 5.000 ±.08 mm. The nominal wall thickness and chamber aperture width are 0.5 mm and 11 mm, respectively. Vacuum chamber straightness is paramount in reducing impedance to the electron beam and shall be held to ± 100 μm in the vertical direction when installed.

The chamber shall maintain its 6 mm dimension over a minimum 3688 mm length (z-direction) in order to prevent interference with the undulator and phase shifter magnets. Beyond this length, transition regions are necessary at each end of the chamber to allow vacuum flange welding. Vacuum flanges shall be 1.33" diameter ConFlat Flange and use explosion bonding or similar technology to weld a stainless steel flange to the aluminum extrusion. The overall length of the welded vacuum chamber assembly shall be 3907.7 +1 / -0 mm, measured from each flange's mating surface.

The chamber shall include two machined grooves on both top and bottom chamber surfaces. These 1 mm x 1 mm grooves are used to route earth corrector coil wires and are located symmetric to the vertical beam axis. The chamber shall include cooling water channels designed to mitigate a 4 W/m heat load from wake fields, spontaneous radiation and ambient field coils.

Table 8-9 - Undulator Vacuum Chamber Specifications

Parameter	Value	Unit
Maximum vacuum pressure (N_2 equivalent)	$< 1 \times 10^{-6}$	Torr
Maximum outgassing rate after bakeout	$< 2 \times 10^{-11}$	Torr*l/s/cm^2
Chamber material	Al 6063	
Chamber inner cross section profile	Race track	
Nominal chamber aperture height	5 ± .08	mm
Nominal chamber height (OD) at aperture	$6\ ^{+.15}_{-.05}$	mm
Nominal chamber aperture width	11	mm
Chamber length, welded, flange-to-flange	$3907.7\ ^{+1}_{-0}$	mm
Installed vertical chamber straightness	± 100	μm
Vertical chamber adjustment precision	< 50	μm
Aperture rms longitudinal surface roughness slope, a_z	< 20 (average)	mrad
Aperture rms azimuthal surface roughness slope, a_θ	< 30	mrad
Beam stay-clear radius	2.3	mm
Operating temperature	20 ± 1	°C
Interspace girder horizontal motion range	± 1	mm
Interspace girder vertical motion range	± 1	mm

The chamber is supported by an extruded box beam strongback and is fixed to adjacent (upstream and downstream) interspace stands. The vacuum chambers will be aligned to the quadrupole centers and move with them. This ensures that during beam-based alignment the electron beam – which is centered on the quadrupole – is also centered on the undulator vacuum chamber. In order to facilitate alignment, the strongback assembly must be adjustable in six DOF. In addition, each interspace girder is supported by a mechanical positioning system capable of ± 1 mm x- and y-direction travel. The strongback assembly and adjustment mechanism must allow for maximum differential interspace motion.

8.5.3.2 Interspace Vacuum System

The interspace vacuum system connects adjacent undulator vacuum chambers and is necessary for a contiguous vacuum system. The system design and layout are identical to both undulator and SXR drift interspace assemblies, as shown in Figure 8-22.

Each interspace vacuum assembly consists of a quadrupole spool, one or two vacuum crosses (depending on application), and a bellows at each end. The vacuum crosses allow ion pump,

vacuum gage, and angle valve connections as needed. The upstream vacuum cross may be replaced by a pneumatic gate valve to facilitate vacuum section isolation. Every interspace assembly includes an ion pump, with a minimum of two gage pairs per isolated section. The quadrupole spool is copper plated and polished to minimize resistive wall wakefield losses. Similarly, the RFBPM comprises part of the interspace vacuum system and is manufactured as a copper cavity.

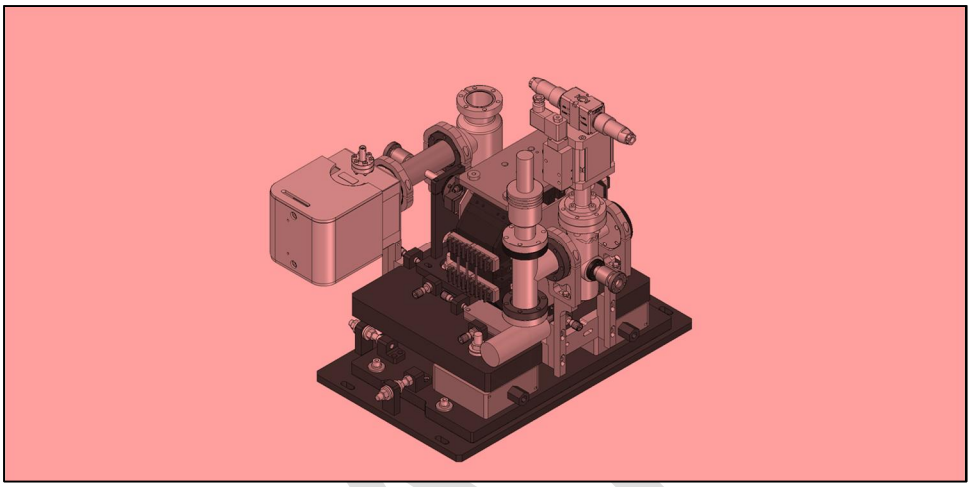

Figure 8-22. Interspace vacuum assembly, shown with pneumatic isolation valve

8.5.4 Quadrupole

LCLS-II reuses the LCLS quadrupole magnet design shown in Figure 8-23. The existing quadrupoles from LCLS will be reused without modification. and 26 additional ones will be fabricated. See chapter 5 and *0.433Q3.1 Quadrupole Magnet ESD*, LCLS-II-3.2-ES-0317, for the more complete description of this quadrupole.

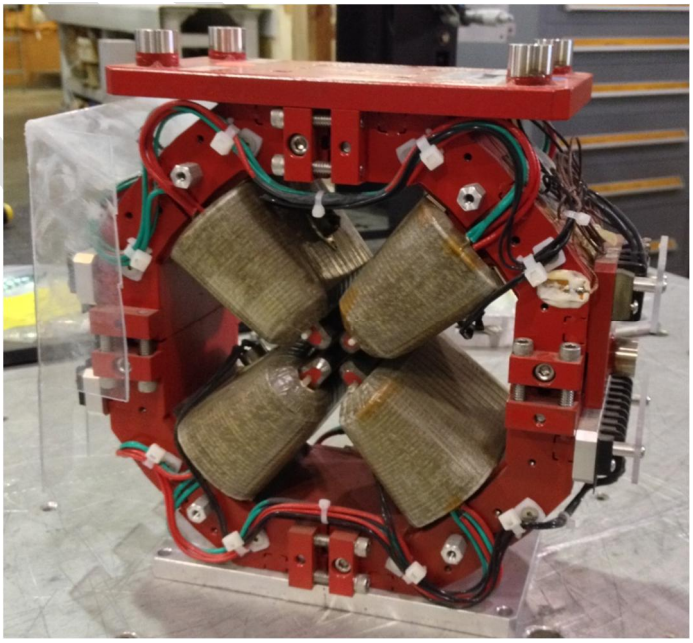

Figure 8-23. LCLS undulator quatrupole magent ready for installation.

8.5.5 BPM

The RFBPM design follows in large part the proven, successful design features of the LCLS undulator BPM developed by ANL. The requirements are defined in *RF Beam Position Monitor ESD*, LCLSII-3.2-ES-0049. A Cooperative Research and Development Agreement is in place with the Pohang Accelerator Laboratory, PAL, to develop a revised design. PAL is doing the design of the RFBPM body and SLAC is designing the electronics. The updated design incorporates a coaxial output and features fewer mechanical tuners. The system has been prototyped and testing has started on LCLS, see Figure 8-24.

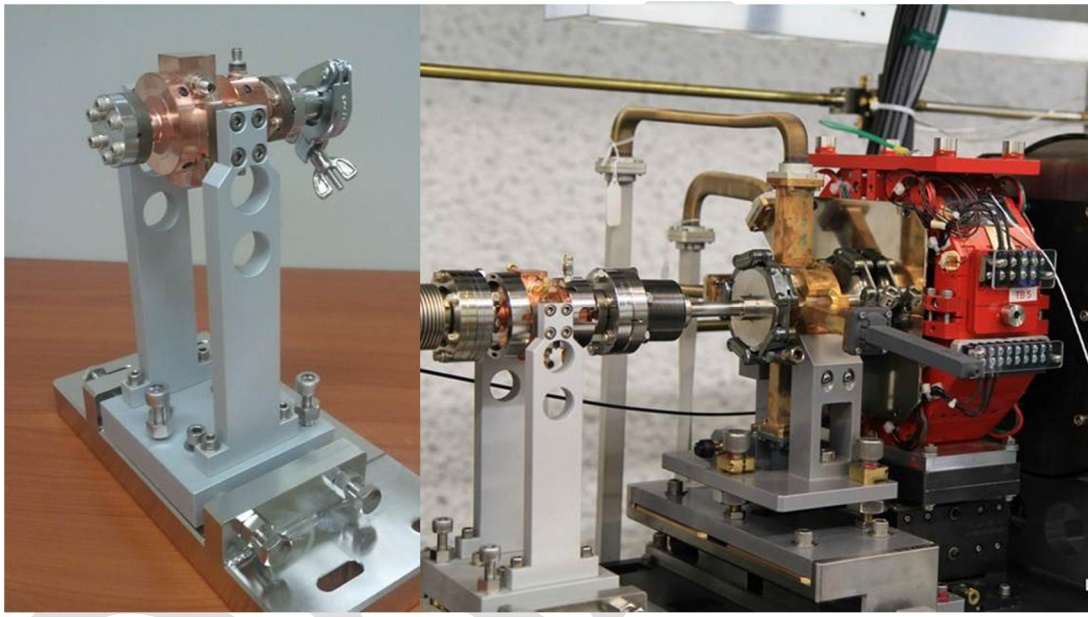

Figure 8-24. PAL RFBPM: Left, in its holder ready for installation. Right, installed on LCLS next to one of the ANL RFBPM's.

8.5.6 BLM

The LCLS-II Beam Loss Monitor (BLM) is constructed similarly to the LCLS device, with the radiation-detecting media coupled to a photomultiplier tube (PMT). The requirements are defined in *Undulator Beam Loss Monitor ESD*, LCLSII-3.2-ES-0180. Čherenkov detectors are located above and below the vacuum chamber and are coupled directly to the PMT face. The BLM is installed as part of the undulator vacuum chamber assembly and is located at the upstream end of each undulator. The BLM prototyped in Phase I of the Project is shown in Figure 8-25.

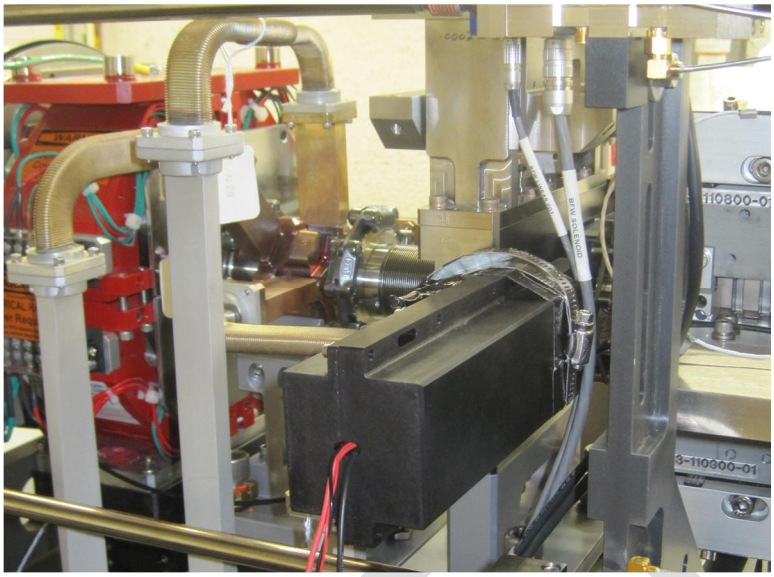

Figure 8-25. LCLS-II prototype BLM installed on LCLS Undulator System for testing.

8.5.7 Phase shifter

The undulator phase shifter is a variable gap, pure permanent magnet device used to maintain proper phase between the electron beam and the electromagnetic (radiation) field. A variable gap is necessary to tune the phase in relation to the variable gap undulators. The magnetic structure has been prototyped and tested in LCLS-II, Phase I. This magnet structure has been incorporated into phase shifter for the DELTA polarizing undulator on LCLS(see Figure 8-26), and is now in operation. The LCLS-II phase shifters will be built to SLAC specification *Undulator Phase Shifter FRD*, LCLSII-3.2-FR-0238, with the magnet structure to adhere to SLAC's designs.

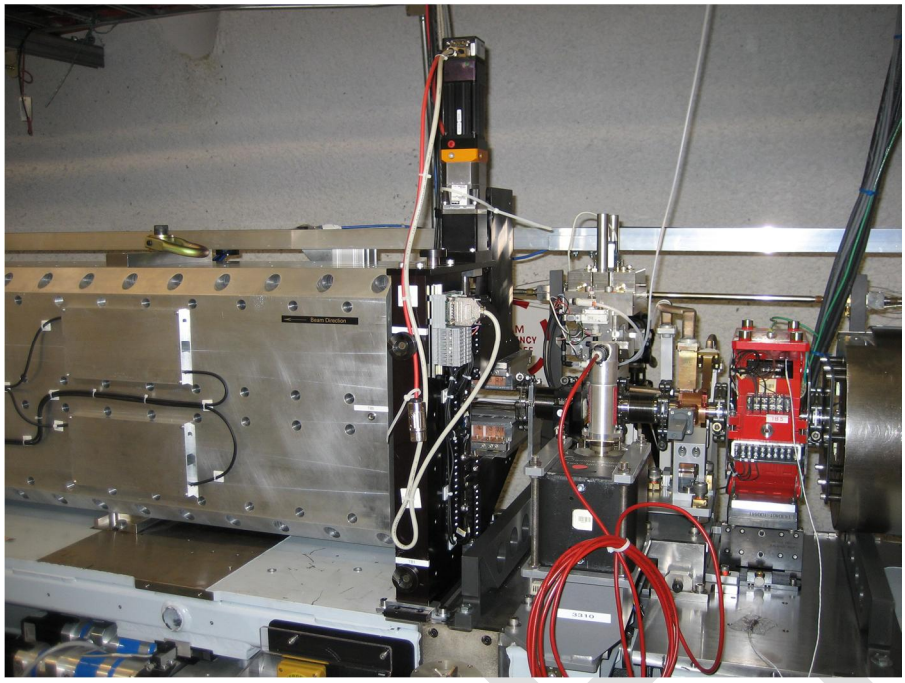

Figure 8-26. Phase shifter for DELTA polarizing undulator on LCLS. The the phase shifter is black structure at center of photo.

8.6 Self-Seeding

The LCLS-II will incorporate a self-seeding system in both the HXR and SXR undulator beamlines to significantly narrow the bandwidth beyond what is nominally produced in the standard self-amplified spontaneous emission (SASE) operational mode, and to ultimately produce Fourier transform-limited and longitudinally coherent FEL laser pulses. In general, a self-seeding FEL beamline consists of two undulators that are separated by a monochromator and a magnetic chicane. The SASE FEL process in the first undulator begins from shot-noise and is interrupted before saturation in the linear regime. In this way, the slice properties of the electron beam are preserved for an additional FEL process downstream. The SASE FEL X-ray beam is sent through a monochromator, which selects a narrow band of the radiation profile while the electron beam passes through the magnetic chicane. The physical principles governing the design and implementation of the monochromator are specific to the SXR and HXR beamlines and are discussed briefly below. The magnetic chicane serves the dual role of compensating for the delay introduced by the monochromator and destroying any residual electron beam microbunching from the first undulator. This is important because the narrow bandwidth radiation from the monochromator would have a transmitted power much less than the effective power of the microbunched electron beam. The monochromatized radiation and the demodulated electron beam then interact in a seeded FEL process in the second undulator, where the seed power dominates the electron beam shot-noise. The narrow bandwidth (much narrower than the SASE bandwidth) seed radiation is amplified to saturation, with the second undulator tuned such that the seed is resonant at the fundamental radiation frequency.

A brief description of both the SXR and HXR beamlines, including the self-seeding systems, is provided below. Details of the individual beamline components, including their operating parameters and tolerances, as well as initial comprehensive FEL performance studies, can be found in the *Soft X-ray Self-Seeding (SXRSS) System Requirements PRD*, LCLSII-3.2-PR-0101 and the *Hard X-ray Self-Seeding (HXRSS) System Requirements PRD*, LCLSII-3.2-PR-0102.

8.6.1 SXR Self-Seeding

The soft X-ray self-seeding system will operate in the photon energy range of 200 eV to 1.3 keV and is based on a concept originally developed at DESY [32] that was further improved to make a compact design at LCLS [33]. A rough schematic of the concept can be found inFigure 8-27. The first undulator section, which is responsible for the generation of the seed, consists of seven independent modules that are interspersed with strong focusing quadrupoles. The monochromator and chicane have a compact footprint and are designed to occupy the equivalent space of a single undulator module (U8 in Figure 8-27). The resolving power of the monochromator is nominally specified to be R = 5000, but upgrade paths to R > 10,000 are being explored.

The monochromator is based on the existing LCLS design [34] and consists of a toroidal variable line space (VLS) grating, a rotating plane mirror, a tangential cylindrical mirror, and a final plane mirror. The grating provides the sagittal focus of the light at the re-entrant point in the downstream seeded undulator and the tangential focus (in the dispersion plane) at the exit slit, while a focusing mirror downstream of the exit slit provides the final tangential focus. The total delay of the light with respect to the straight line path through the monochromator is less than one picosecond.

The four-dipole chicane creates a local horizontal electron trajectory offset so that the electrons can safely stay clear of the grating and mirrors of the monochromator. In addition, it destroys the microbunching that develops in the upstream SASE process and produces an adjustable delay line for the electrons that can be tuned to match the X-ray delay through the monochromator. The chicane can also act as an adjustable phase shifter if the SXR beamline is being used in the SASE mode of operation. This mode of operation allows the chicane to correct for phase errors that would nominally be introduced between the FEL light and the electrons due to the removal of the U8 undulator segment.

Since the X-rays and the electron beam are bent in different directions from their conventional straight line paths, a dedicated set of beam overlap diagnostics is needed to ensure sufficient spatial overlap in the seeded undulator (U9-U22). These diagnostics will be located at multiple positions downstream of the monochromator system and will consist of a combination of devices capable of detecting both the electron beam and the X-ray positions.

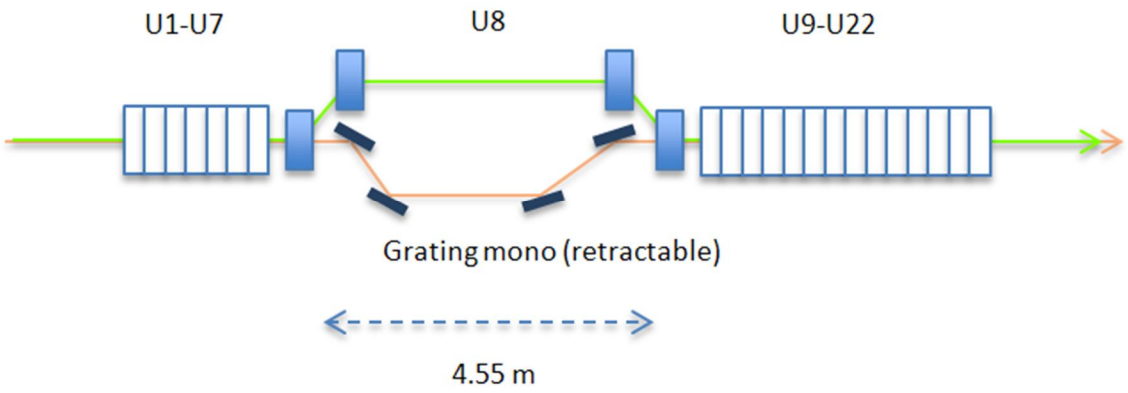

Figure 8-27. Schematic of the SXRSS beamline illustrating the first undulator (U1-U7), the chicane and monochromator (occupying the equivalent position of U8), and the second undulator (U9-U22). The electrons follow green path through the four dipole chicane while

8.6.2 HXR Self-Seeding

The hard X-ray self-seeding system will initially operate in the photon energy range of 4 – 12 keV using the electron beam coming from the CuRF linac and is based on the diamond single crystal wakefield seeding scheme [35], which has been successfully demonstrated on LCLS [36]. Operation between 1 and 3 keV and above 12 keV will require an additional upgrade that includes a grating monochromator system similar to the one described above for the SXRSS system. In addition, a two-stage diamond wakefield approach will be used to mitigate concern for crystal sample damage and for distributing the average thermal load when operating the system with the high rate electron beam from the SCRF linac. A rough schematic of the baseline concept can be found in Figure 8-28. The first undulator section, which is responsible for the generation of the seed, consists of 14 independent modules that are interspersed with strong focusing quadrupoles. The monochromator and chicane occupy the equivalent space of a single undulator at U15. The monochromatized radiation is overlapped with the electron beam in the downstream undulator (U16 – U33) and is amplified to saturation.

The seeding monochromator is a thin diamond single-crystal operating in the symmetric Bragg (004) geometry and will have a resolving power around R = 20,000. This crystal creates a reflected beam in the forward direction that has a temporal field distribution consisting of a main pulse similar to the noisy input signal and a number of time-delayed and highly monochromatic trailing satellite pulses of decreasing intensity. Seeding is initiated by properly delaying the electron beam to overlap with one of these satellite pulses in the second undulator.

Similar to the SXRSS chicane, the HXRSS four-dipole chicane deflects the electron beam around the monochromator crystal, destroys the microbunching from the upstream SASE FEL process that generates the seed, and provides the necessary delay to overlap the electrons with a monochromatic satellite pulse from the monochromator.

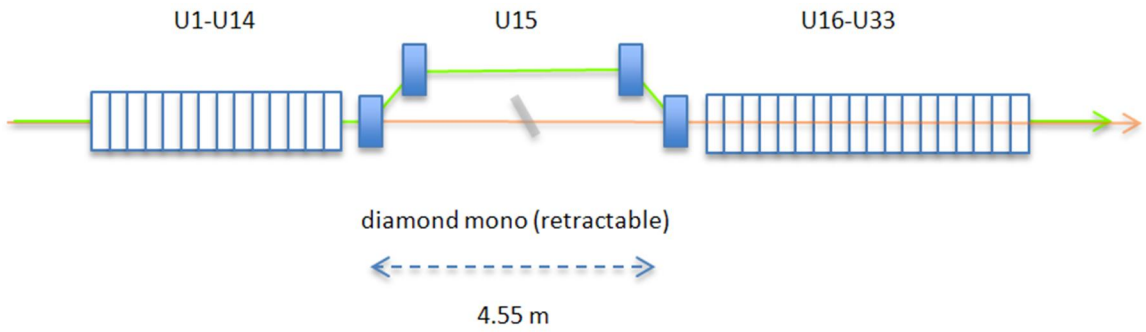

Figure 8-28. Schematic of the HXRSS beamline illustrating the first undulator (U1-U14), the chicane and diamond wakefield monochromator (occupying the equivalent position of U15), and the second undulator (U16-U33). The electrons follow green path through the four dipole magnets.

8.7 Undulator Transportation and Installations

Undulators system installation will take place over a 6-month period and encompass 53 undulator segments, all interspace assemblies, and the complete vacuum system. The interspace support stand and cam positioning assembly is preassembled and transported as a single unit. Interspace assemblies are pre-aligned and installed as a populated girder. Preassembly activities minimize alignment time and effort within the Undulator Hall.

Support stands are installed and aligned at the nominal operational height, then grouted in place. The base plate includes three holes patterns: two sets of thru holes used for floor anchors and a single set of threaded holes for leveling screws. The redundant thru holes provide flexibility for floor anchor placement, minimizing cutting of rebar.

Undulator installation takes place after the support stands are installed. Undulator transport entails driving each device from the MMF to the north research yard by truck. Undulators then enter the BTH at the north headhouse entrance, which requires removal of the plug wall. The undulator design incorporates various features to enable transport and installation. Rotatable, lockable caster wheels are located at each corner, enabling long-distance travel. Additionally, air casters are located beneath the undulator frame and are used for precision movements. An electric tugger is used to pull undulators, on their caster wheels, down the BTH and into the Undulator Hall. Once an undulator reaches its final longitudinal destination, the air casters are employed to move the undulator laterally into its final position. Compressed air valves are located along the length of the Undulator Hall and at the BTH entrance to facilitate air caster usage. Undulator installation begins at the east end of the UH and moves west, with HXR and SXR undulators installed concurrently. Effort will be made to minimize undulator exposure to the ambient air temperature during transportation.

SLAC personnel built and tested a mock undulator, including caster wheels, to simulate transport conditions. An electric tugger propelled the mock undulator throughout these tests, successfully demonstrated long-distance transport. Air casters were also investigated during the test sequence, and proved successful for shorter, precise movements.

Interspace assembly installation shadows the undulators, with the downstream interspace installed after its respective undulator. Similarly, each undulator vacuum chamber is installed once its two supporting interspace assemblies are in place, completing mechanical installation of an undulator cell. Once mechanical installation is complete, control and power cables are terminated to the undulator and interspace components.

The checkout process follows cable terminations and begins with mechanical inspection. Each beam line is then aligned, followed by vacuum system evacuation and leak check. Alignment is checked again, with final adjustments completed as necessary. After final alignment, the Undulator Hall is handed off to LCLS-II Operations.

8.8 References

1 H.-D. Nuhn, et al., "R&D Towards a Delta-Type Undulator for the LCLS," Proceedings of the 35th International Free Electron Laser Conference, New York, USA (2013)

2 LBNL Undulator Segments PDR, 30 October 2014.

3 J.C. Dooling, W. Berg, B.X. Yang, M.S. Leitner, A.S. Fisher, and H.-D. Nuhn, "Modeling the Optical Coupling Efficiency of the Linac Coherent Light Source Beam Loss Monitor Radiator," BIW 2010, JACOW (2010).

4 H.-D. Nuhn, G.L. Gassner, F. Peters, "Position Stability Monitoring of the LCLS Undulator Quadrupoles," Proceedings of the 33rd International Free Electron Laser Conference, Shanghai, China (2011)

5 K.L.F. Bane and G.V. Stupakov, "Resistive Wall Wakefield in the LCLS Undulator," *Proceedings of the 2005 Particle Accelerator Conference*, PAC2005.

6 H.-D. Nuhn, P.J. Emma, G.L. Gassner, C.M. LeCocq, F. Peters and R.E. Ruland, E"lectron Beam Alignment Strategy in the LCLS Undulators," *FEL2006 Proceedings*, Berlin, Germany (2006).

7. Z. Wolf, "Introduction to LCLS Undulator Tuning," LCLS-TN-04-7 (2004).

8. Z. Wolf, "Algorithms to Automate LCLS Undulator Tuning," LCLS-TN-06-8 (2006).

9. Z. Wolf, et al., "LCLS Undulator System Tuning and Magnetic Measurements," *Proceedings. Part. Accel. Conf*. Vancouver, BC (2009).

10. Z. Wolf, Y. Levashov, H-D. Nuhn, and I. Vasserman, "LCLS Undulator Test Plan," LCLS-TN-06-17 (2006).

11. Z. Wolf, "Requirements for the LCLS Undulator Magnetic Measurement Bench," LCLS-TN-04-8 (2004).

12. Z. Wolf, "Undulator Field Integral Measurements," LCLS-TN-05-22 (2005).

13. Z. Wolf and Y. Levashov, "Undulator Long Coil Measurement System Tests," LCLS-TN-07-3 (2007).

14. G. Bowden, "Roller Cam Positioners," LCLS-TN-05-28 (2005).

15. Z. Wolf and S. Kaplounenko, "Temperature Measurements in the Magnetic Measurement Facility," LCLS-TN-05-9 (2005).

16. Z. Wolf and Y. Levashov, "Undulator K Value Temperature Dependence," LCLS-TN-09-4 (2009).

17. Z. Wolf, et al., "LCLS Undulator Fiducialization Plan," LCLS-TN-07-2 (2007).

18. Y. Levashov and Z. Wolf, "Tests of Coordinate Transfer from Magnetic to Mechanical Reference for LCLS Undulator Fiducialization," LCLS-TN-05-10 (2005).

19. Z. Wolf, et al., "Girder Alignment Plan," LCLS-TN-08-3 (2008).

20. Z. Wolf, "A Vibrating Wire System for Quadrupole Fiducialization," LCLS-TN-05-11 (2005).

21. Z. Wolf, "LCLS Undulator Quadrupole Fiducialization Plan," LCLS-TN-07-7 (2007).

22. M. Levashov and Z. Wolf, "Commissioning a Vibrating Wire System for Quadrupole Fiducialization," LCLS-TN-07-8 (2007).

23. S. Anderson, et al., "Magnetic Measurement Results of the LCLS Undulator Quadrupoles," LCLS-TN-09-1 (2010).

24. Z. Wolf and S. Kaplounenko, "Temperature Measurements in the Magnetic Measurement Facility," LCLS-TN-05-9 (2005).

25. Y. Levashov and Z. Wolf, "Tests of Coordinate Transfer From Magnetic to Mechanical Reference for LCLS Undulator Fiducialization," LCLS-TN-05-10 (2005).

26. Z. Wolf and Y. Levashov, "Reference Undulator Measurement Results," LCLS-TN-09-3 (2009).

27. A. Fisher, H-D. Nuhn, and J. Welch, "Magnetic Measurements of the Background Field in the Undulator Hall with Ductwork and Cable Trays," LCLS-TN-08-4 (2008).

28. K. Hacker and Z. Wolf, "Earth's Magnetic Field Measurements for the LCLS Undulators," LCLS-TN-05-4 (2005).

29. A. Temnykh, Y. Levashov, and Z. Wolf, "I," *Nucl. Instr. and Meth. A* **622,** 650 (2010).

30. Z. Wolf, et al., "I," LCLS-TN-07-2 (2007).

31. Y. Levashov and Z. Wolf, "Tests of Coordinate Transfer from Magnetic to Mechanical Reference for LCLS Undulator Fiducialization," LCLS-TN-05-10 (2005).

32 J. Feldhaus et al., Opt. Comm., **140**, 341 (1997).

33 Y. Feng et al., *Proceedings of the 2010 FEL Conference*, Malmo, Sweden (2010).

34 LCLS Soft X-ray Self-Seeding (SXRSS) System PRD, SLAC-I-081-101-003-00-000.

35 G. Geloni et al., *Journal of Modern Optics*, **58**, 16 (2011).

36 J. Amann et al., *Nat. Photonics*, **6**, 693-698 (2012).

9 Photon Transport and Experimental Systems

TECHNICAL SYNOPSIS

The LCLS-II is designed to produce high-brightness, short-pulse X-rays from two parallel undulator systems in the existing LCLS undulator hall. Of these two undulators the one optimized for the soft X-ray range, 200 to 1300 eV, will be driven with electrons from the superconducting linac at rates up to 1MHz. The second undulator is optimized for hard X-rays, from 1-5 keV, when driven by the superconducting linac and from 1-25keV when driven by the lower rate existing roon temperature copper (CuRF) linac, at rate up to 120 Hz. This chapter describes the X-ray transport systems to deliver the beams to the experimental systems and the diagnostic systems to characterize them.

There are two separate beamlines for transport and diagnostics of the X-rays, one for each of the undulator systems. The soft X-ray system will deliver beam to a single experimental station optimized for high-fluence experiments. This beamline is laid out to accommodate eventual expansion to three branchlines with the addition of two monochromatic branchlines. The intermediate and hard X-rays will be delivered to the existing X-ray instruments in Hutch 3 of the Near Experimental Hall and the Far Experimental Hall at either high repetition rate from the superconducting linac or high pulse energy from the CuRF linac.

This chapter summarizes critical requirements for the beam transport and diagnostics for delivery and characterizing the FEL beams for optimization of operations and normalization of experimental data. Very low figure error mirrors will deliver the X-rays with minimal wave front distortion, which is critical for maintaining intensity in focal spots and uniformity when operating out of focus. The X-ray pulses will be manipulated by attenuation, aperturing and focusing. The pulse energy and spatial distribution will be characterized with energy monitors and imagers. Provisions for future monochromators and spectrometers are described.

9

9.1 Scope, Schedule and Design Status

9.1.1 XTES Scope

The X-ray Transport and Experimental Systems (XTES) for LCLS-II will deliver the FEL beams from the Hard X-Ray (HXR) and Soft X-Ray (SXR) undulator systems to experimental stations in the Near Experimental Hall (NEH) and the Far Experimental Hall (FEH). There will be two separate beamlines. The beam from the SXR undulator system will be delivered to a new experimental station in the NEH that will accommodate the existing LCLS SXR experimental end stations and detectors. The scope includes all the hardware, controls systems, electron beam safety systems and FEL beam containment systems for this beamline The data acquisition system for the SXR station is also included. The beam from the HXR system will be delivered to existing beamline at the west end of the NEH. On this beamline there are the four existing experimental stations, one in the NEH and three in the FEH plus fifth one under development. LCLS is responcible for upgrading these stations for high repetition rate operations

The XTES scope for both the HXR and SXR lines is illustrated inFigure 9-1. It starts just after the vertical magnents that bend the electron beams down into each of the two main electron dumps. On the SXR line the beam continues through focusing optics to one of the LCLS endstations in Hutch 1 of the NEH. On the HXR line, XTES will deliver the FEL beam to the existing X-ray channel in the NEH where the beam will be used by the existing LCLS hard X-ray instruments in the NEH and FEH. The SXR line is essentially all new equipment, though based largely on designs already employed at LCLS. Many components on the HXR line will be repurposed for use with the high rep-rate beam.

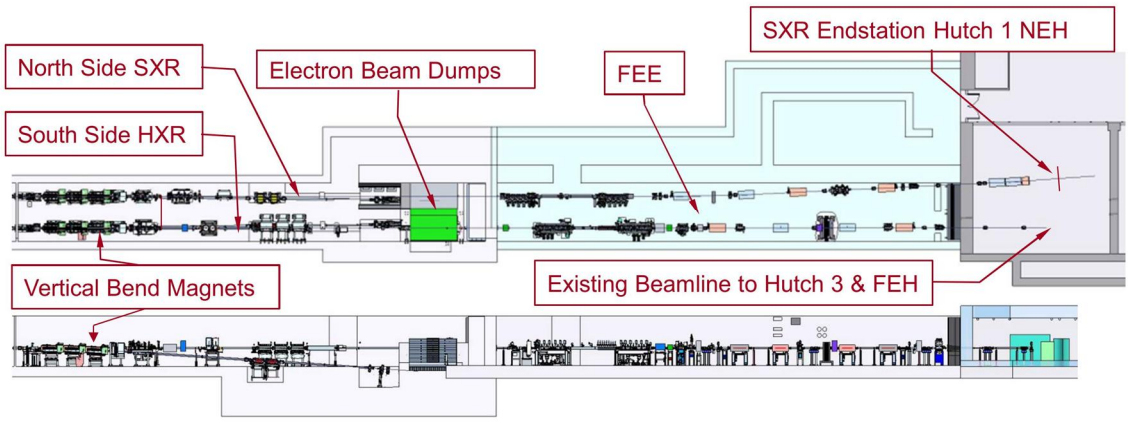

Figure 9-1: Layout of the X-ray transport systems from the vertical bend magnets to the electron dumps through to the Near Experimental Hall. The electron beam dumps are part of the Electron Systems scope.

9.1.2 Schedule

XTES activities are integrated into the LCLS-II P6 project schedule under WBS 1.03.05. The XTES schedule is composed of three main phases: Engineering and Design, System Procurement and Fabrication, and Installation. Individual activities for each component or subsystem fall within one of these phases. The XTES schedule, summarized in Figure 9-2, contains approximately 1,200 linked and resource-loaded activities.

The Engineering and Design phase, WBS1.03.05.05, contains the activities related to obtaining and documenting requirements, generating specifications for individual components and/or subsystems, engineering, design, and prototyping activities. The effort on this phase was started in April 2014. The completion of this phase and CD-3 aproval triggers the start of the procurements for each XTES element.

The System Procurement and Fabrication phase, WBS 1.03.06.06, contains the effort associated with procuring the XTES hardware, fabrication of components, assembly, and bench testing in preparation for field installation. The first of these activities is schedule to start in February 2016.

The Installation phase is comprised of the planning, coordination, and field installation effort needed to prepare the XTES system for commissioning. The planning effort starts in the last quarter of FY 17. All the XTES components in the dump area and FEE are to be installed and checd out during the planned twelve month long down in FY18. The installation of XTES components begins in the second quarter of FY18. The installation and checkout of components up to the front end enclosure will be completed by the end of FY18. The installations and checkouts of the NEH components are scheduled to be completed by the second quarter of FY19.

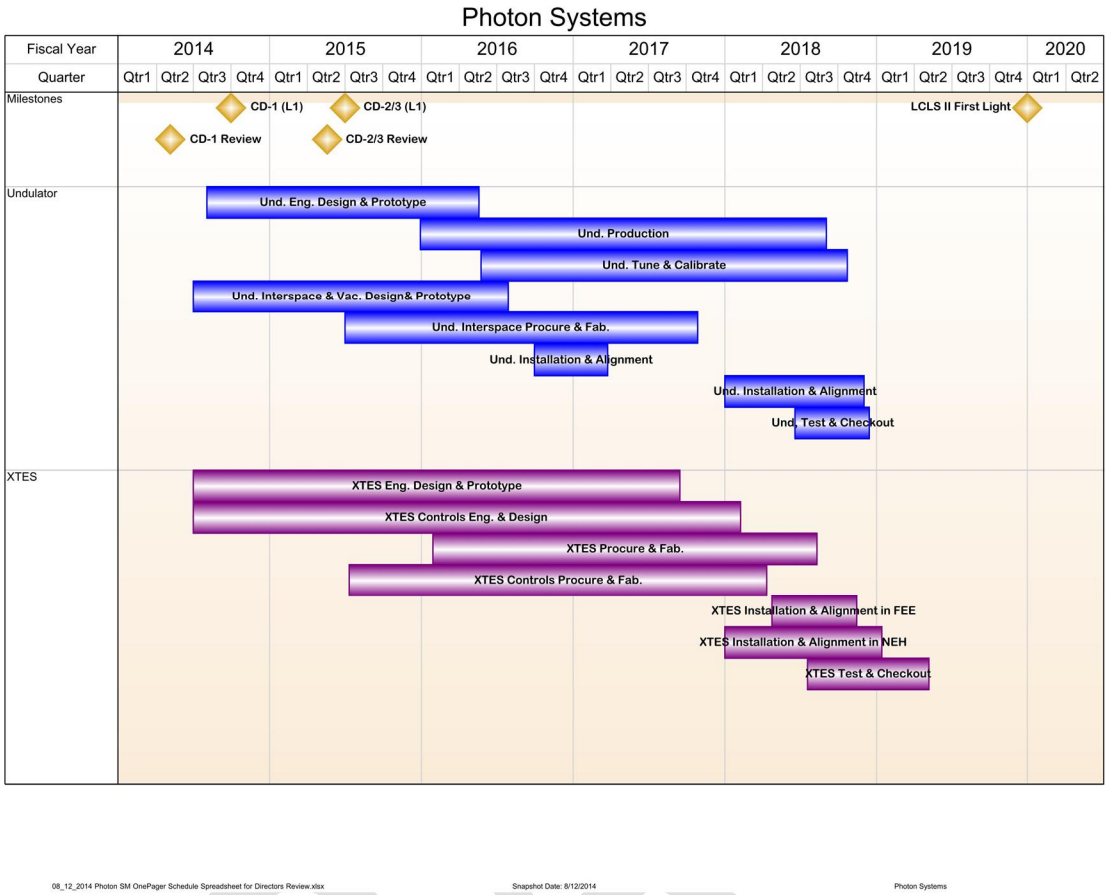

Figure 9-2. XTES Schedule Outline - Update with XTES specific schedule

9.1.3 Design Maturity

The LCLS-II Project Final Design Plan LCLSII-1.1-QA-0065 provides for a phased completion of the final designs for the LCLS-II facility. The plan ensures that designs are sufficiently mature to start procurements and construction, while enabling the most cost-effective schedule for constructing the facility and maximizing the technical capabilities of the facility at CD-4. Final design readiness at CD-3 recognizes that that not all subsystems will reach final design at the same time. Project-level requirements and interface control points between Accelerator Systems, Cryogenic Systems, Photon Systems and Infrastructure are defined at CD-3, which ensures that the phased procurements and construction are appropriate for the final design of the LCLS-II. Chapter 2, Project Overview, contains additional discussion of the approach to design completion. The Photon Systems design, described in Chapters 8, and this chapter is evaluated to be 65% complete. XTES on it own is at a preliminary design level, ~30% complete. Completing remaining design after CD-3 allows for coordination with developing designs for LCLS Operations upgrades to instruments.

9.1.3.1 Documentatation

The design for the XTES must start with setting the basic definition of the beam characteristics, boundaries, and the requirements of the beamline components. These basic beam definitions and requirements have been set in the *X-ray Transport and Experimental Systems PRD*, LCLSII-3.5-PR-0051. This document was originally released in March 2014 and revised in July 2014. Subsystem and components requirements have branched out of this PRD in the form of Functional Requirement Specifications, and Technical Notes. The requirements documents are listed inTable 9-1.

Table 9-1. XTES requirements documents

Title	Document Number
X-ray Transport and Experimental Systems PRD	LCLSII-3.5-PR-0051
LCLS-II Parameters PRD	LCLSII-1.1-PR-0133
Radiation Protection Requirements for XTES PRD	LCLSII-1.2-PR-0233
Electron Safety System – BCS PRD	LCLSII-3.5-PR-0111
XTES Imager FRS	LCLSII-3.5-FR-0132
XTES Flat Mirror FRD	LCLSII-3.5-FR-0067

Just as the beam parameter boundary conditions are outlined in the requirements documents, physical boundaries need to be aligned with other systems within the project to ensure they will work together on completion. These boundaries and interfaces have been outlined in various Interface Controls Documents (ICD) and Room Data Sheets (RDS). Table 9-2 lists these documents.

Table 9-2. Interface Control Documents and Room Data sheets between XTES and other areas of LCLS-II

Title	Document Number
XTES to Infrastructure Systems ICD	LCLSII-5.3-IC-0114
Electron to XTES ICD	LCLSII-3.5-IC-0116
XTES to Experimental End Stations ICD	LCLSII-3.5-IC-0112
XTES to Metrology Monuments ICD	LCLSII-3.5-IC-0113
Photon Beam Controls to Electron Beam Controls ICD	LCLSII-3.5-IC-0115
XTES Local Controls ICD	LCLSII-3.5-IC-0117

Front End Enclosure (FEE) and FEE Maze RDS	LCLSII-5.3-RD-0130
XTES in NEH RDS	LCLSII-3.5-RD-0013
Electron Beam Dump (EBD) RDS	LCLSII-5.2-RD-0193

9.1.3.2 Engineering and Design

Based on the given parameters and boundaries, engineering and design efforts have started to evaluate the modifications and changes necessary to the components of the existing hard X-ray line. Engineering and design efforts for the soft X-ray line are ongoing in parallel, in an effort to take advantage of design similarities to both LCLS and the LCLS-II HXR line. These beamlines will serve a wide range of applications and types of research; consequently finding the optimal design compromises is a challenging undertaking. The XTES team has taken steps to get the LCLS scientific staff and users involved at every stage of the design process to address the scientific goals of LCLS-II.

The layout of the beamlines has been coordinated and agreed upon in coordination with the LCLS operations group. CAD models have been created reflecting the latest understandings for the baseline and to accomodate expansion plans. Beamline Schematics for the SXR and HXR lines reflect these plans as well.

Design analyses of various components are ongoing. Some of these include: thermal analysis of the materials and cooling concepts for the distribution mirrors, solid attenuators, collimators, and photon stopper; gas injector upgrade concepts; and gas behavior simulations. Photon ray trace studies are in progress based on the latest beam parameters and component designs.

The work done on these analyses and simulations has helped put the distribution mirrors, photon collimators, and photon stoppers through their conceptual design reviews. The solid attenuator design has gone through its preliminary design review.

Vendors have been contacted to assess their capabilities and the manufacturability of the conceptualized distributions mirrors. Mirror coating test coupons have been acquired and test beam time has been scheduled for the first quarter of calendar year 2015.

The engineering and design activities performed have brought the XTES to the preliminary design level. Final designs will be developed and reviewed before proceding with procuremnets.

9.1.3.3 Management & Planning:

The activity start dates, durations, resources, and estimated cost have been loaded into the project P6 schedule. This is logically linked and ready for baselining.

Prototyping efforts during 2015 and first half of 2016 on the mirrors, gas attenuator, solid attenuator and collimator materials along with component reviews will propel the system to an FDR level by the summer of 2016.

9.2 Power Delivery Requirements

The X-ray transport system for both the HXR and SXR beamlines will need to handle operations up to 1 MHz and to cover the energy range from 0.2 to 1.3 keV for soft X-rays and from 1 to 5 keV for hard X-rays when operating with the superconducting (SCRF) linac, and to handle HXR operation from 1 to 25 keV at a maximum repetition rate of 120 Hz when operating with the CuRF linac. The XTES will handle the average FEL power delivery specified in *X-ray Transport and Experimental Systems PRD*, LCLSII-3.5-PR-0051. which also describes the required devices and components This document defines the stay-clear criteria, based on the designed FEL performances and including beam divergences and effective source locations. The designs of all devices and components are expected to preserve the X-ray beam characteristics to the greatest extent possible, including minimal wavefront distortions and minimal transverse coherence degradations. X-ray damage considerations will include both the single-shot as well as average thermal load and are discussed in the previously mentioned *X-ray Transport and Experimental Systems PRD*.

FEL beam will be delivered to the existing HXR stations in the NEH and FEH. Hard X-rays can be produced from the superconducting linac at up to 1 MHz from 1 to 5 keV and from the Cu linac at up to 120 Hz from 1 to 25 keV The project is responsible for ugrading the beam transport and diagnostics throught the Front End Enclosure (FEE). LCLS operations will upgrade the existing LCLS hard X-ray stations to handle higher repetition rates and high average FEL power operations as required by the scientific programs.

The new soft X-ray beamline and station, in NEH, will be designed to accommodate the existing LCLS SXR instruments. LCLS will upgrade these instruments as required by the scientific programs. The X-ray experimental system will be required to handle the SCRF linac operation at a maximum repetition rate of 1 MHz and to cover the energy range from 0.2 to 1.3 keV. The maximum average delivered FEL power for experiments is 20 W, while the safety systems will be designed for 200W. Both focused and unfocused FEL beams are required at the sample on the SXR instrument by using Kirkpatrick-Baez focusing mirrors working in and out of focus.

For both the new soft X-ray and existing hard X-ray instruments, the data acquisition and control systems will be upgraded to handle the high repetition rate operations from the existing LCLS systems.

9.2.1 Average power delivery

The average FEL power under the high repetition rate operation from 0.2 to 5 keV will be limited to a maximum of 200 W, per *LCLS-II Parameters PRD*, LCLSII-1.1-PR-0133, much higher than the 1 W with LCLS operation. The maximum required average power delivered to experiments is 20 W. The beam-intercepting components must survive maximum single-shot fluence defined by the per-pulse FEL energy (see Section 9.2.2). The diagnostics devices and beamline components for the LCLS-II FEE, unless otherwise noted, are required to operate only at the 20 W average power. Attenuators will limit the average power when it is not possible or

desirable to do so by modifying the energy per pulse and the pulse rate. In almost all cases, some form of cooling will be required. The mirror systems, are required to handle a maximum of 20 W FEL power with guaranteed optical performance. If more than 20 W FEL power is incident on the mirror systems, certain performance degradations will be expected and permitted. The mirrors will not be damaged, however, at the full 200 W average power. The X-ray safety systems, collimators and stoppers, will sustain the full 200 W incident average power.

9.2.2 Damage to Optical Systems

9.2.2.1 Normal Incidence

Single shot damage considerations: For low repetition FEL machines, the damage to optical systems is determined mainly by instantaneous damage mechanisms. The instantaneous damage problem has been studied extensively both theoretically and experimentally at the LCLS and other FEL facilities [see e.g. 1, 2, 3, 4]. The instantaneous damage happens in the time scale ranging from single femtoseconds to tens of picoseconds. The energy of femtosecond photon pulses is first absorbed in the electron system, which then thermalize with the lattice in the time scale of 1-50 ps. When the absorbed dose is larger than the heat of fusion (or a specific heat related to other phase transitions), melting and the subsequent damage occur. The typical heat of fusion scale is on the order of 1 eV/atom. Both thermal and non-thermal damage mechanisms have been reported in the literature. [2, 5]

Fatigue-related damage: Fatigue-related damage should also be considered in addition to instantaneous damage [6]. The theory predicts that fatigue-related damage could occur if the instantaneous absorbed dose is larger than a certain fraction of the heat of fusion [7], but this depends on the material being exposed. For example, in the case of B_4C no multi-shot damage was observed when a sample was exposed to 650 000 X-ray pulses depositing 0.16 eV/atom at the surface of the sample (the heat of fusion for B_4C is close to 0.7 eV/atom). However, the present theory [6] is directly applicable to ductile materials such as Be or Al. It is not clear how to extend the theory to materials that exhibit anisotropic yield strength. We currently use the lowest value of the yield strength, typically the tensile yield strength, to estimate the fatigue-related damage. In many cases the fatigue-related damage is a limiting factor that could diminish performance of the machine. Therefore, to mitigate the thermal fatigue risk, we are planning to perform multi-shot damage tests of materials that will be exposed to the LCLS-II beam and also to test prototypes of FEE components under repetitive thermal stresses.

Average power damage considerations: In the case of high repetition machines the situation is more complicated. The element under consideration can reach its melting temperature despite the fact that the instantaneous dose is much lower than the heat of fusion. The average temperature of the element depends on its geometry and its thermal resistance with respect to the environment.

In the steady state condition the maximum temperature at the surface can be estimated as:

$$T_{\max} \approx T_{ins} + P_{av} R_{th}(G, \sigma, k, h) \qquad \text{eqn. (1)}$$

where $T_{ins} = F_{inst} / C_v l_{abs}$ F_{inst} is the instantaneous fluence, l_{abs} is the absorption length, and Cv is specific heat. Here R_{th} denotes the thermal resistance, P_{av} is the average power, G stands for geometry of the element, σ is the rms photon beam size, k is the thermal conductivity, and h is the convective heat transfer. In practice the thermal resistance is modeled using finite element analysis (FEA). FEA also assesses an allowable thermal stress, similar to the process used at the existing synchrotron radiation sources.

9.2.2.2 Optical Surfaces

The problem of grazing incidence damage to optics is similar to the low frequency operation case when the instantaneous damage is the main concern. The average temperature of optical surfaces is small with respect to the instantaneous temperature because the absorbed beam power is spread over much larger surface than in the normal incidence case.

The key quantity that helps to assess the damage problem is the instantaneous absorbed dose per atom at the mirror surface. For the grazing incidence optics, this dose can be derived as presented in [7]. The absorbed dose can be used for calculating the maximum instantaneous temperature, which can be compared with the temperature of melting of fatigue related damage thresholds. Both the HXR and SXR mirrors will be operated below their damage threshold (see Figure 9-3

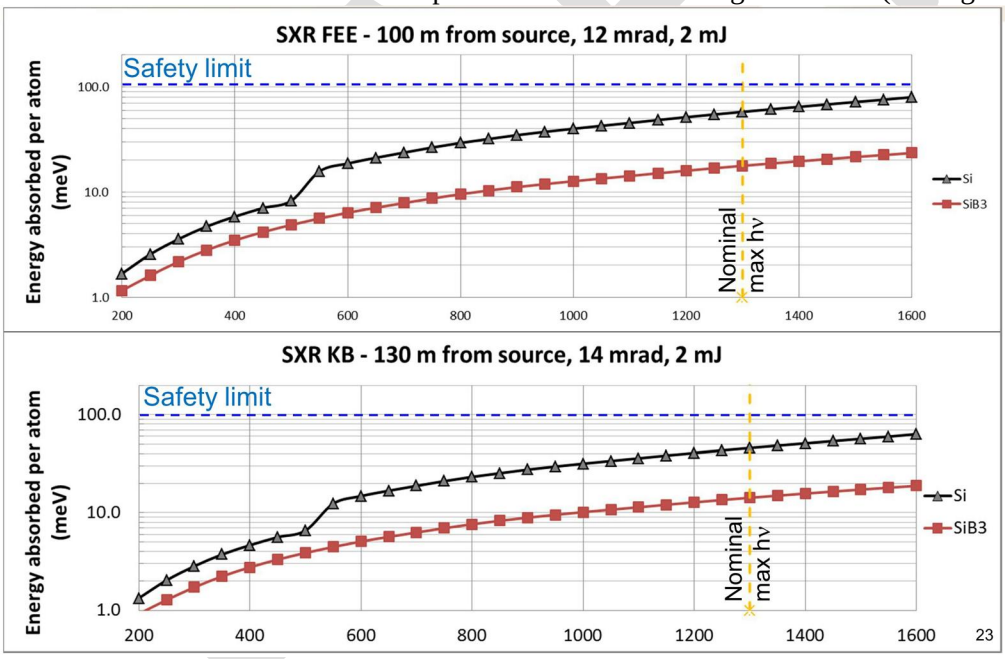

Figure 9-3).

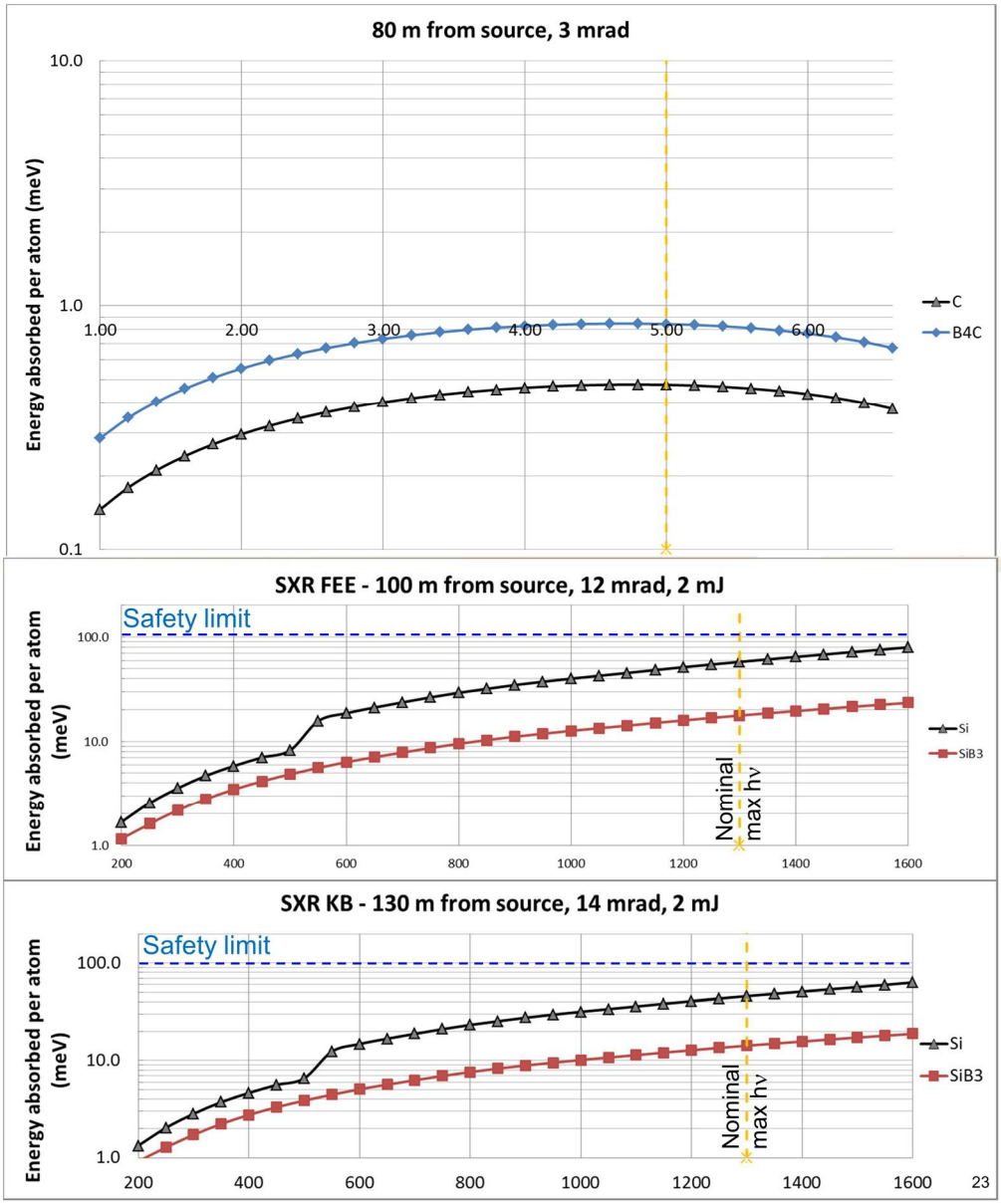

Figure 9-3. Absorbed dose in proposed HXR and SXR mirrors. Top: HXR mirror at 3 mrad in the FEE. Middle: SXR mirrors at 12mrad grazing angle in the FEE and Lower: 14 mrad at the focusing mirrors in the NEH

9.3 Mirrors

9.3.1 Wavefront preservation

The mirror suite of the photon transport system has to deliver the beam into the experimental chambers with a minimum loss of flux and preservation of the wavefront. The target imposed by the Project is that the mirrors shall be designed such that the intensity variation of the transmitted beam is less than 5% when used with a source power not larger than 20W This corresponds to a Strehl Ratio of 0.97 (see detailed description in chapter 11 of the *LCLS-II Conceptual Design*

Report, LCLSII-1.1-DR-0001). However, the mirrors should be able to sustain a source power as high as 200W while still providing a small focus into the experimental chambers (ideally a Strehl Ratio of 0.8 or larger). Preservation of the wavefront requires a geometrical acceptance of more than 2 FWHM, to avoid strong edge diffraction effects.

To collect more than 2 FWHM and to have good reflectivity, the following configurations are chosen. For the Front End mirror of the soft X-ray beamline, the angle of incidence will be of 12 mrad and for the focusing optics in the NEH the angle of incidence is 14 mrad. All these mirrors will have a minimum length of 800 mm with a Si or SiB_3 coating (both are viable solutions). For the hard X-ray mirrors, the angle of incidence is 3 mrad with a B_4C coating.

Chapter 11 of the *LCLS-II Conceptual Design Report*, LCLSII-1.1-DR-0001, provides a detailed description of requirements regarding shape error allowance. Here we report only the results. The shape errors for all the mirrors in the tangential direction must be below 0.4 nm rms in the central region in order to preserve the wavefront within the given tolerances, and can be "relaxed" to 1 nm rms over the entire length. These shape errors are to be achieved with the mirror is installed and under radiation power load. Therefore, the mechanically-induced and thermally-induced deformation are taken into account.

As stated in the CDR, the best available optics have a shape error of 0.3 nm in the central region and up to 1 nm rms overall for mirror 800 mm or longer. This is the starting point. All the other deformation must be such that the overall requirements are met.

The mechanically-induced deformation is minimized by using a mirror holder (Figure 9-4) that transfers all the deformation to the edge of the mirror, where the least demanding performance is required. A bender is also included in the holder to flatten the mirror to preserve the natural divergence of the beam. The bender is not included in the very first mirror of each beamline. This is because the first mirror is the one absorbing most of the radiation. Therefore, the first mirror is let free to expand in the tangential direction. This expansion produces a convex radius of curvature, increasing the divergence of the beam. This effect is compensated by the second mirror by using the bender to re-collimate the beam.

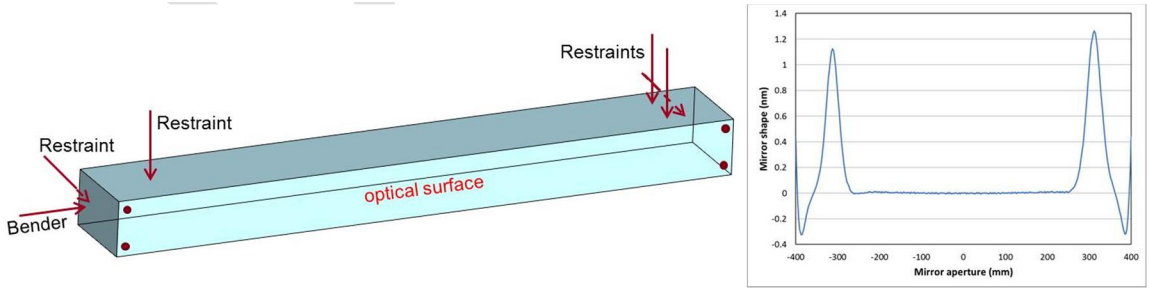

Figure 9-4: **Left: position of the mirror restraints and of the bender. The bender (longitudinal) will be used for the second mirror only. Right: Calculated effect of the restraints and bender on the mirror figure. The deformation is concentrated away from the central part of the mirror where the very high shape error tolerance is required.**

Handling the thermally-induced deformation is more complicated. Even if the power absorbed is only around 3-4 W for the 20 W incidence and 10 times larger for the 200 W incidence, lower than what is usually seen in a Synchrotron Radiation beamline, the tolerable maximum deformation is also very low. One of the main problems encountered is the higher harmonic contribution to the total deformation. While the deformation induced by the absorption of the fundamental has a profile very similar to the fundamental itself, the higher harmonics have a lower divergence. This produces a thermal bump in the center of the mirror that can potentially have a large impact on the wavefront itself. Another important aspect that is different from the Synchrotron radiation case, which drove the decision to adopt a two-part cooling scheme, is large variation of photon beam footprint on the mirror surface as a function of the wavelength..

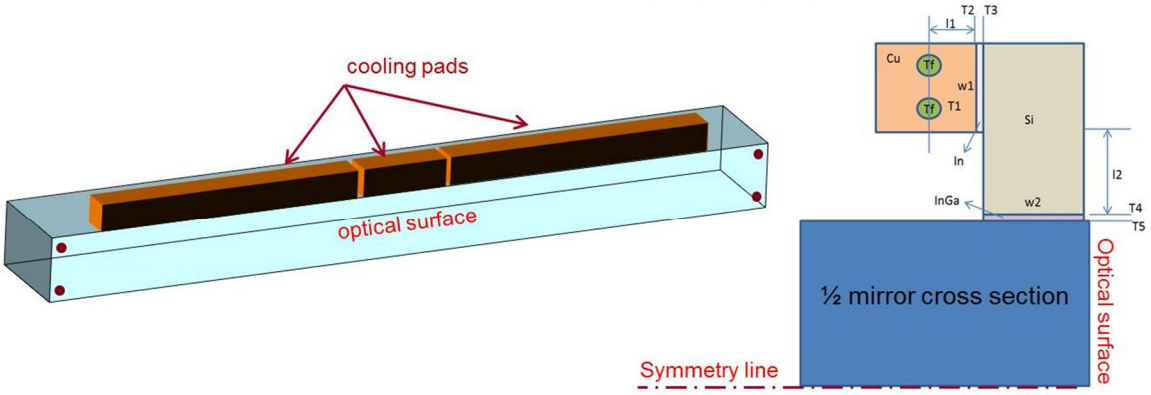

Figure 9-5: The mirrors will have two cooling lengths obtained by using all three or just the central one of the cooling pads shown on the left. The mirror cross section will be 70X50 mm with direct cooling obtained through a Copper-Silicon pad in thermal contact with the mirror via a GaIn eutectic. (right pannel with half of the system shown)

We adopted a side cooling scheme using water as a coolant in order to properly remove the heat load from the SXR and HXR mirrors. To optimize the cooling for the different photon energies, two cooling lengths are used, as shown in Figure 9-5. For the higher energy part of the range a 100 mm cooling length is adopted. For the lower part of the photon energy range the optimum cooling length is 700 mm. The different length is realized by using three independent copper pads, a central pad that is 100 mm long and two additional pads that are each 300 mm long, along with three independent water circuits. The circuit feeding the 100 mm pad will always be active, and the other two can be switched on or off depending on the need. The nickel plated copper pads are connected through a GaIn eutectic layer to a silicon bar. This silicon bar is then connected to the mirror side, again through the eutectic layer. The reason for this intermediate silicon bar is to avoid a strong bonding between the copper and silicon due to diffusion of Ga into the copper that could prevent the removal of the cooling system if needed. The silicon-silicon bonding via the GaIn eutectic is easily removable without risk of damage to the mirror itself.

For the 20 W case, the induced shape errors due to the thermal deformation, using the above described cooling scheme, are on the order of 0.2 nm rms for the higher photon energies and on the order of 1 nm rms for the lower energies. Figure 9-6 shows the expected different contribution to the shape errors, compared with that required to achieve the performance specifications.

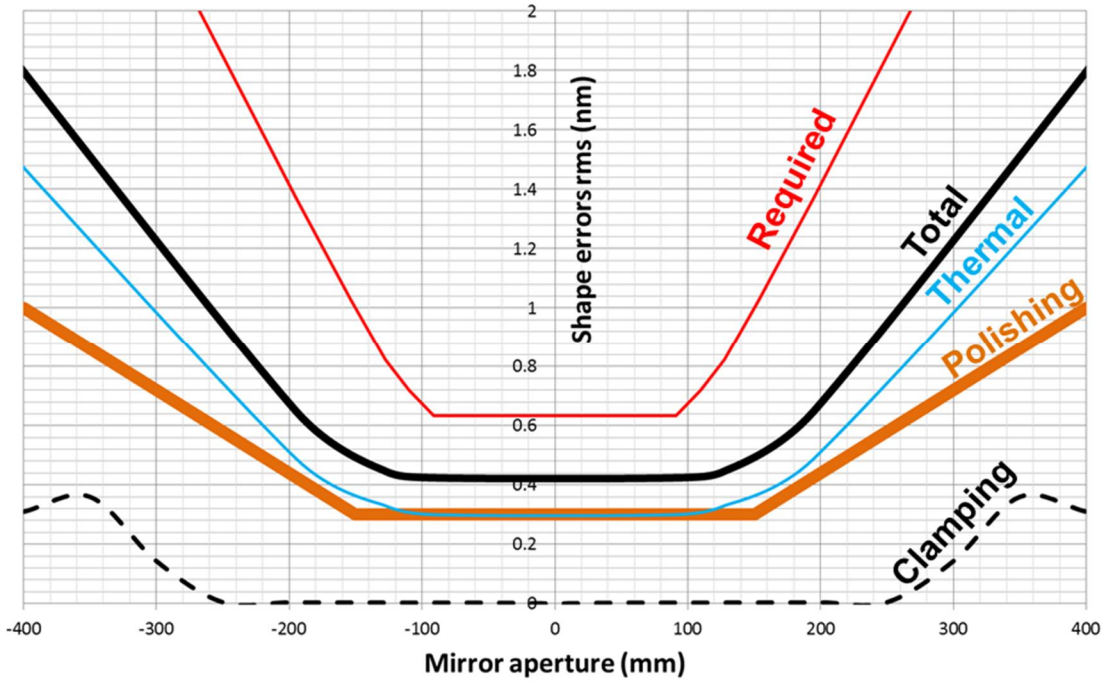

Figure 9-6: Shape error comparison. The red line is the required maximum shape errors to guarantee a Strelh ratio of 0.97. The thick orange line is the slope error of the mirror unclamped (state of the art polishing), the dashed black line represents the effect of the holder on the mirror figure, the light blue line the effect of the thermal deformation for the 20 W case (calculated for different photon energies) and the black thick line is the expected final shape error of the mirror.

9.3.1 Distribution mirrors

As mention above, there will be four distribution mirrors located into the FEE, two for the SXR beamline and two for the HXR beamline. The mirrors shall be as flat as possible to preserve the divergence. As stated above, the very first mirror in both beamlines will not have any bender, and the effect of the thermally induced convex radius of curvature on the first mirror will be compensated by a bender installed into the second mirror. This bender is an off center mono-directional bender that can only flatten the mirror starting from a convex radius of curvature (as shown inFigure 9-4). The second mirror must be convex to compensate for the increase of divergence due to the first mirror.

The native radius of curvature of the second mirror should be as low as necessary to compensate for the divergence of the beam in the case of an incidence beam of 100 W. For this beam power, the worst-case scenario is for the higher energy of both ranges, e.g., 1300 and 5000

eV for the Soft and Hard X-rays, respectively. The induced radius of curvature is 100-200 km for the SXR and 400-500 km for the HXR. Therefore, a different native radius of curvature (convex and near 200 Km for the SXR and 500 km for the HXR) is required.

Starting from these values, the bender is able to remove the unwanted divergence of the beam without increase appreciable the native shape errors of the mirror.

The two SXR distribution mirrors will have an angle of incidence of 12 mrad, both deflecting the beam in the same direction, away from the HXR beamline. With this angle and an uncoated silicon mirror, the reflectivity is above 90% for beam energy up to 1300 eV.

The HXR mirrors will have an angle of incidence of 3 mrad and will be offset from the beam, preserving its direction and providing good reflectivity (with a B_4C coating) up to 9 keV. This periscope system is coupled with the two existing LCLS mirrors working at 1.35 mrad to assure covering both the photon energy delivered by the LCLS-II superconducting linac and the energy delivered by the CuRF linac, up to 25 keV.

9.3.2 Focusing mirrors

The SXR beamline will be equipped with a pair of mirrors to focus the beam into two distinct longitudinal experimental chamber locations (Figure 9-7). The two mirrors will be oriented perpendicularly each other in the so-called Kirkpatrick-Baez (K-B) configuration. In this way the horizontal and vertical focus are decupled and one can obtain an almost aberration-free stigmatic spot as well as an astigmatic (or asymmetric) spot profile if needed. They are aimed to focus the photon beam into the two experimental station positions and to provide variable spot dimensions. The K-B mirror systems for LCLS-II will be therefore composed of two adaptive mirrors (to change the focal distance) and will include the side cooling system to dissipate the residual heat load left on the mirror by the photon beam.

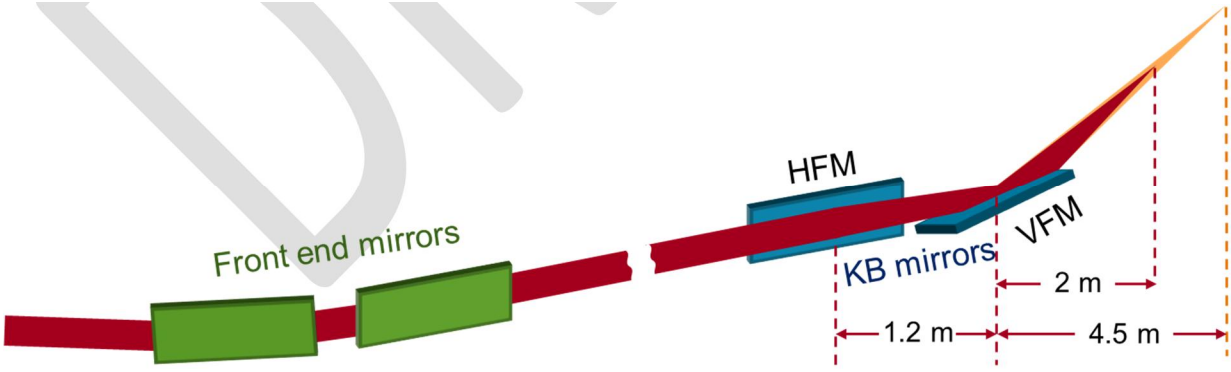

Figure 9-7: Schematic of the SXR beamline. The K-B mirror will be located in the NEH after the two flat mirrors. The relative distances of the mirrors and the distances to the focal spot are reported.

Two experimental chambers are located 2 and 4.5 m downstream of the center of the last K-B mirror (Figure 9-7). With these focal distances, the expected induced residual shape errors after bending are less then 0.1 μrad rms for the closest chamber and below 0.5 μrad for the farthest

one. The benders are optimized to produce the minimum possible spot in the first focal position. With this choice the spots are expected to be on the order of 1 μm diameter for the upstream position and less than 5 μm diameter for the down stream focal position.

The variable focal distance is obtained by applying two unequal moments at the end of the mirror substrate. The bending system is optimized by pre-shaping the mirror. In this case, we decided to use a mirror with constant thickness but variable width. The best solution found is the one implying a trapezoidal shape with the shortest edge toward the focus, as shown in Figure 9-8..

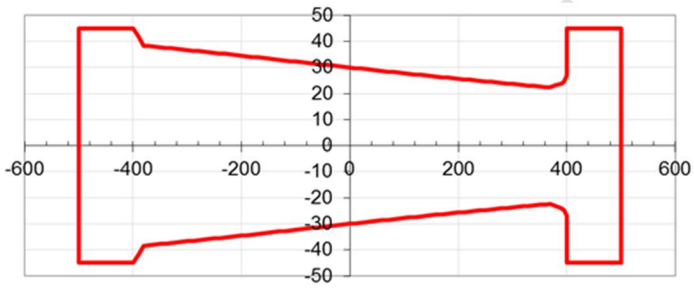

Figure 9-8. Shape of the adaptive focusing mirror. The shorter edge is toward the image. The profile is optimized to minimze the induced shape errors at the closest focal position.

The limited power density absorbed by K-B mirrors will be removed by indirect side cooling that guarantees the performance for the 20 W cases. A doubling of the effective spot area is expected for the 200 W case. The direct side cooling of the K-B mirrors, as described for the flat mirrors, would be very difficult to implemented due to the bending mechanisms. The K-B mirrors see a much lower power load so indirect side cooling with copper braids connected at one end to the mirror substrate and on the other side to a chilling reservoir to dissipate the heat load will be employed.

The K-B mirrors will have an angle of incidence of 14 mrad and a useful area of 800x25 mm^2. The 800 mm useful length guarantees the collection of 2 FWHM of the beam divergence down to 250 eV as required by the Project.

9.4 Diagnostics

9.4.1 Energy monitors

To measure the LCLS-II FEL pulse-to-pulse intensity fluctuations, single-shot energy monitors are required to help operators optimize the FEL lasing process and users to properly normalize their experimental data. For SCRF linac operation, the energy monitors must cover the energy range from 0.2 to 1.3 keV for soft X-rays and from 1 to 5 keV for hard X-rays; whereas for the CuRF linac hard X-ray operation, the range is from 1 to 25 keV. The monitors must be highly transmissive (> 95% transmission), introduce only minimal wavefront distortion or transverse coherence degradation, and capable of single-shot measurement at a maximum repetition rate of 1 MHz for the SCRF linac operation and 120 Hz for the CuRF linac operation.

The relative and absolute accuracy of the monitors must be better than 1% and 10%, respectively. Multipule gasses will be available so operating near the absorption edges of the interaction medium can be avoided.

9.4.1.1 Soft X-Ray Energy Monitor

The SXR undulator line using the SCRF linac and operating in the energy range from 0.2 to 1.3 keV will use two gas-based energy monitors. The first monitor will come from re-purposing an existing first-generation Gas-Monitor-Detector (GMD) originally developed by scientists at Deutsches Elektronen-Synchrotron (DESY) and currently installed on the LCLS Soft X-ray Materials Science (SXR) instrument. The second monitor will be a new built-to-specs second-generation GMD (or XGMD) also being developed at DESY and shown in Figure 9-9, which has an enhanced sensitivity and improvements for operating at shorter wavelengths. Two types of GMDs measure both the electrons and ions produced from the photoionization of a rare gas (Xe or Kr) by the incident FEL beam, and operate at relatively low pressures of $< 10^{-3}$ Pa, making them highly transparent. The low-pressure operation is very critical in ensuring measurement accuracy to minimize the gas heating effect, which is expected to occur when operating at high average FEL powers (c.f. discussion in Sec. 9.4.2.1), and in minimizing potential wavefront distortion and transverse coherence degradation.

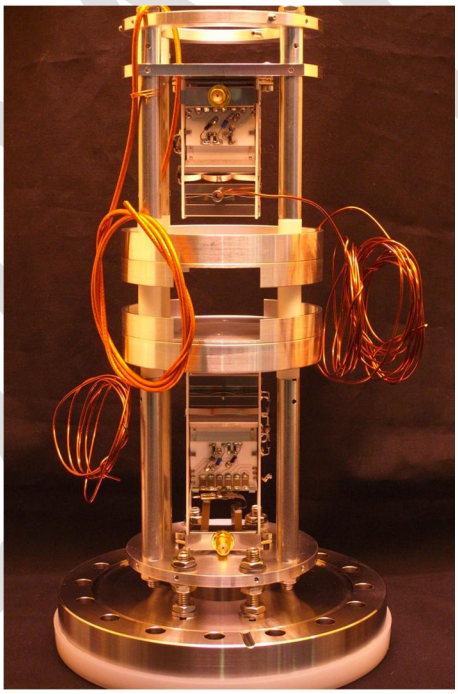

Figure 9-9. A prototype of second-generation Gas-Monitor-Detector (GMD) designed by scientists at DESY in Hamburg, Germany. The FEL beam passes through the middle opening, and the photoelectrons are detected in the bottom half and the ions in the top half of the device. Both electron and ion detections are enhanced by open multipliers.

The GMDs are in principle capable of operating on a shot-to-shot basis with a temporal resolution of less than 100 ns, allowing single-shot measurements at a maximum repetition rate of

over 10 MHz. The readout electronics of the existing GMD will be upgraded from the original 120 Hz operations to a maximum repetition rate of 1 MHz; whereas the new XGMD that has been developed for the XFEL project a DESY is specified for operations above 1 MHz. The existing GMD has an optional capability for position measurement, and a spatial resolution of less than 20 μm was achieved at the Free-electron LASer in Hamburg (FLASH). The original GMD has been demonstrated to perform well at low X-ray energies and can be calibrated absolutely at the PTB laboratory in BESSY-II, Germany to better than 10%. For shot-to-shot measurements, its relative precision accuracy was determined to better than 1%. The XGMD is expected to provide equally good absolute and relative accuracies to < 10% and 1%, respectively.

9.4.1.2 Hard X-Ray Energy Monitor

For the hard X-ray undulator line operating in the energy range from 1 to 5 keV using the SCRF linac at a maximum repetition rate of 1 MHz, or from 1 to 25 keV using the CuRF linac at a maximum repetition rate of 120 Hz, the two existing LCLS N_2 gas detectors shown schematically in Figure 9-10will be re-purposed with upgrades for LCLS-II. The N_2 gas detector was originally developed for LCLS to operate from 0.8 to 8 keV in single-shot mode at a maximum repetition rate of 120 Hz, and it measures the N_2 photoluminescence in the near ultraviolet (UV) produced by the incident FEL beam using photomultiplier tubes (PMT) and readout electronics based on charge-amplification and high-speed digitizers. The gas detector is typically cross-calibrated against the energy loss in the electron bunch for absolute accuracy, and its shot-to-shot relative accuracy depends on the gas pressure, with the best performance ever recorded at a level of ~ 1% towards lower energies.

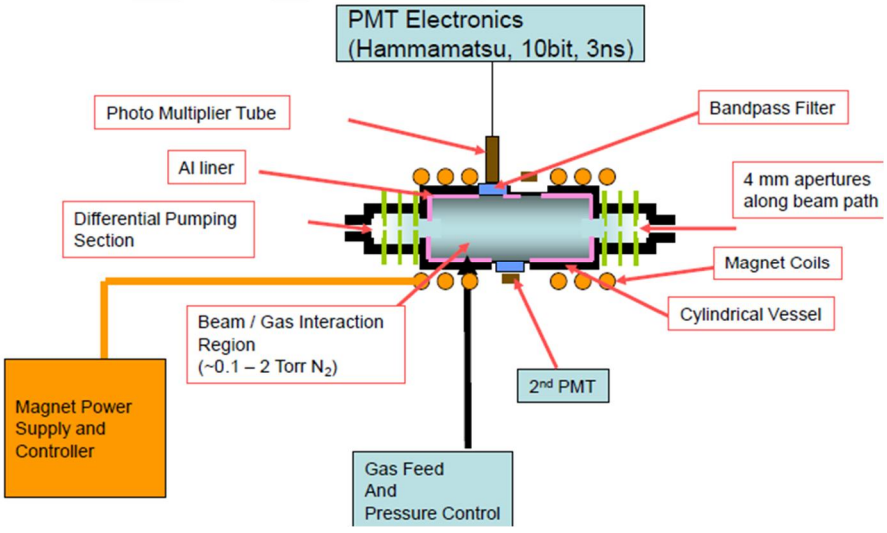

Figure 9-10. Schematics of the N_2 gas detectors currently installed and operating in the FEE of the LCLS, consisting of a N_2 gas vessel, a magnetic bottle, and two PMTs, and differential pumping and gas handling systems. The magnetic bottle enhances the signal but degrades the temporal resolution.

The natural lifetime of the N_2 photoluminescence was determined to be < 1 μs, thus making the gas detector feasible to be upgraded to > 1 MHz operations. The readout electronics upgrades will include faster PMTs and faster digitizers. Since the gas detector does not measure the direct products of the photoabsorption but rather the N_2 photoluminescence, whose cross-section is much lower, it therefore operates at a pressure anywhere from tens of millitorr to a few torr, many orders higher than that of GMDs or XGMDs. As such, the gas heating effect expected to occur at high average FEL powers (c.f. discussion in Sec. 9.4.2.1) will severely impact the measurement accuracies if the repetition rate changes frequently or the per-pulse energy fluctuates greatly. Remedies for the gas heating effect include frequent cross-calibration against electron bunch energy loss or using a separate co-located energy monitor.

To enable measurements for X-ray energies from 8 to 25 keV for the CuRF Linac operation, either more sensitive PMTs, or higher N_2 gas pressure will be used, as the gas heating effect will not be of concern due to the maximum average power limited to less than a few Watts by virtue of a maximum repetition rate of 120 Hz. An alternative solution for operating at high X-ray energies will be to use a solid-based energy monitor developed for the LCLS hard X-ray instruments, which is based on measuring the Compton back-scattered X-rays from an ultra-thin solid target and was demonstrated to achieve a best relative accuracy of 0.1%, only limited by the Poisson statistics of scattered photons.

9.4.2 Attenuator Systems

Attenuator systems are required to globally reduce the FEL per-pulse energy without altering the operation of the linac or the undulator. The attenuator system must be designed to minimize wavefront distortion or transverse coherence degradation to the greatest extent possible, and to avoid operating near the absorption edges of the attenuating medium. The attenuation factor should be either continuous or at least 3 steps per decade. The maximum attenuation factor should be 10^5 for soft X-rays while 10^3 attenuation of the existing system is retained for hard X-rays. The maximum power incident on the attenuator system for the SCRF linac operation will be limited to 200 W.

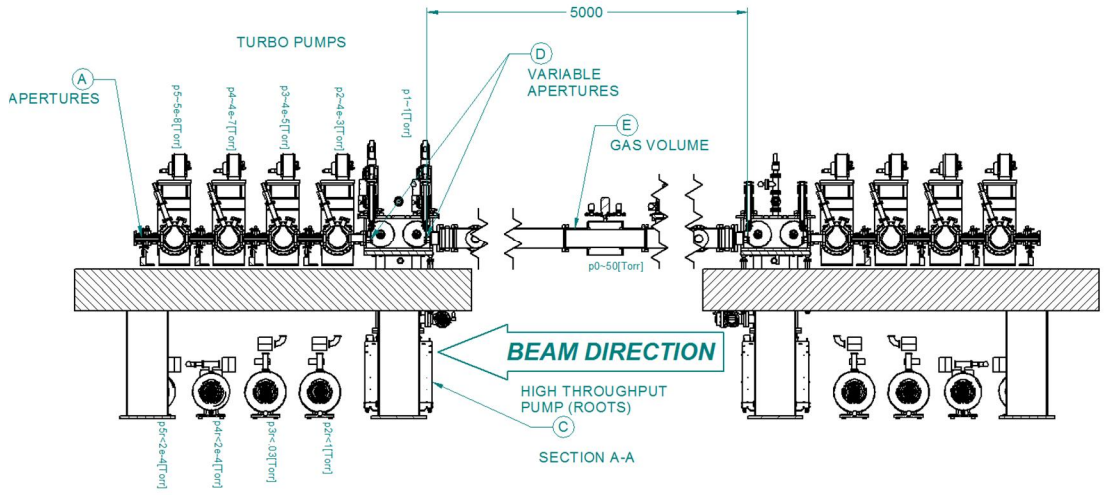

Figure 9-11. Schematics of the soft X-ray attenuator system, consisting of a 5m-long gas column book-ended by two multi-stage differential pumping stations with the two innermost apertures being variable in size.

9.4.2.1 Soft X-ray Attenuator System

For the soft X-ray undulator line using the SCRF linac and operating in the energy range from 0.2 to 1.3 keV at a repetition rate up to 1 MHz and a maximum power of 200 W, a new gas-based attenuator system will be built as shown schematically in Figure 9-11, consisting of a 5m-long Ar gas column sandwiched between two multi-stage differential pumping stations. The sizes of the two innermost apertures are designed to be variable to allow more efficient pumping. As the X-ray energy increases so does the required operating pressure for equal attenuation, while the FEL beam size decreases. The maximum operating pressure to achieve the maximum attenuation factor of 10^5 will be on the order of 10 torr.

When operating at high average FEL powers, the relatively poor thermal conductivity of gases has raised concerns over the potential filamentation effect observed in high-power visible laser systems, where energy deposition via photoabsorption was found to lead to local temperature elevation and correspondingly density depression [8]. Finite element analyses (FEA) were performed to derive the equilibrium state and transient behavior of the gas taking into account plasma (warm-dense matter) effects and the ensuing thermalization of the electronic degrees of freedom with the translational/rotational/vibrational of the gas molecules. This thermalization will occur at picosecond to nanosecond time scales. The gas thermal diffusion is the dominant heat conduction mechanism and an equilibrium constant pressure will be established throughout the entire gas volume. It was found that there exists a radial and axial temperature gradient in the gas volume and correspondingly a density gradient. As such, the otherwise very straightforward relation between attenuation and gas pressure becomes highly complex and thus requires a look-up table, which must come from the FEA, cannot easily be parameterized, and very much depends on the specific details the system. In the limit of small average power, the gas heating effect becomes negligible as in the case of 120 Hz LCLS

operations. The achieved attenuation must ultimately be determined by accurate energy measurements both before and after the attenuator system.

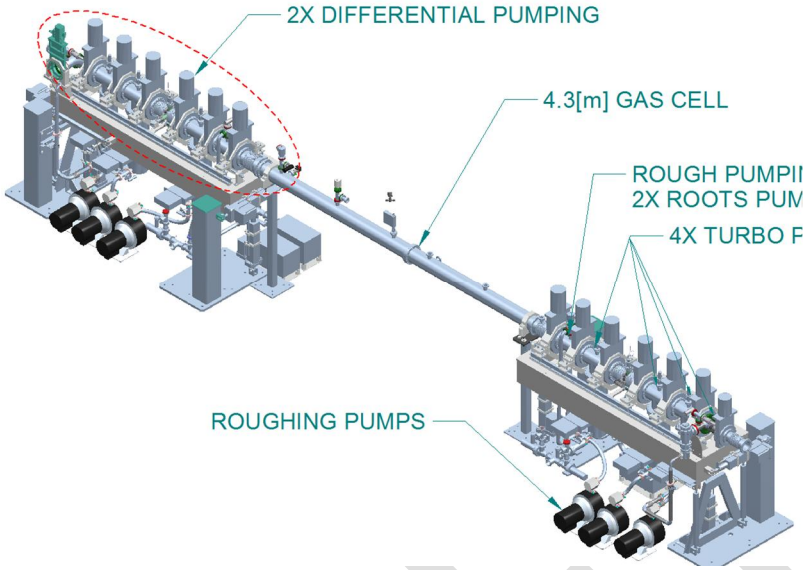

Figure 9-12. Schematics of the gas attenuator component of the hard X-ray attenuator system, consisting of a 4.3 m long N_2 gas column book-ended by two multi-stage differential pumping stations.

9.4.2.2 Hard X-ray Attenuator System

For the hard X-ray undulator line the existing LCLS N_2 gas attenuator (shown inFigure 9-12) will be re-purposed with upgrades for LCLS-II as well as a new solid attenuator component (Figure 9-13). The N_2 gas attenuator was originally developed for LCLS to operate for soft X-rays with a maximum attenuation of 10^3 at a maximum repetition rate of 120 Hz. Because of the high repetition rate operations, it has become difficult to conceive building an attenuator system using solid targets, especially for energies below 2 keV. The maximum operating pressure of the N_2 gas attenuator component is required to exceed 50 torr, and a gas heating effect similar to that described in Sec. 9.4.2.1 will also be present, thus calling for the need to establish a look-up table for the pressure-attenuation correspondence.

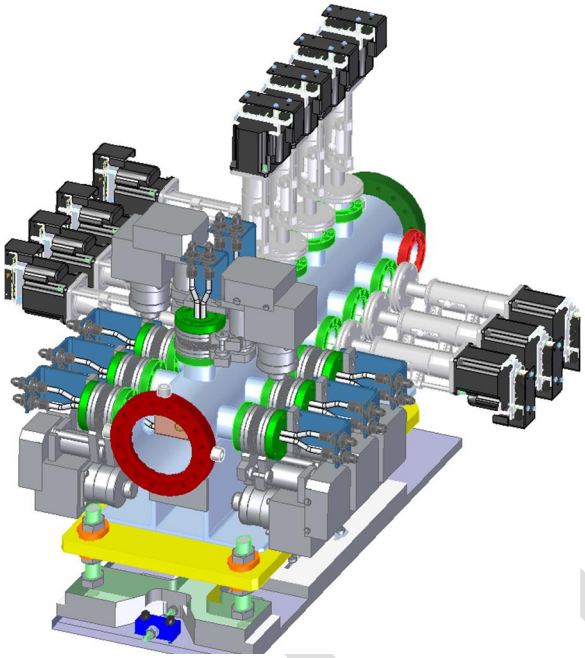

Figure 9-13. Schematics of the solid attenuator component of the hard X-ray attenuator system, consisting of diamond and silicon solid filters of various thicknesses.

For energies above 2 keV, a gas attenuator alone would not provide sufficient attenuation without using solids, which themselves must also be cooled to allow a maximum 200 W incident power. As such, the original uncooled solid attenuator component will be removed and replaced by a new solid attenuator component as depicted in Figure 9-13. The solid attenuator component will use single-crystal diamond and silicon plates with various thicknesses. Single-crystal samples are required to minimize potential wavefront distortion and transverse coherence degradation. The diamond filters are used because of their excellent thermal conductivity, but they will still be used in conjunction with gas pre-attenuation to avoid damage in high power operations, and the silicon filters will be used in conjunction with diamond pre-attenuation to avoid single-shot damages for energies above 5 keV at 120 Hz.

For energies from 5 to 25 keV at 120 Hz repetition rate, diamond and silicon filters do not require cooling due to the low power, but diamond pre-attenuation is always required to avoid single-shot damage in silicon.

9.4.3 Collimators, apertures, slits, stoppers

Control of the FEL beam requires collimators, apertures, slits and stoppers. These components must sustain not only single-shot FEL damages, but also be capable of dissipating the maximum allowable average FEL power of 200 W specified for the entire FEE. Both the stopper and collimator components have the same requirements for surviving FEL beam. The thermal and damage calculations have lead to a common deign and material selection for these systems.

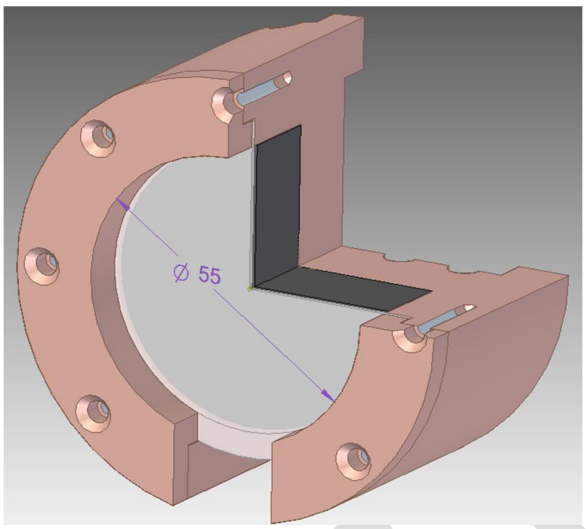

Figure 9-14. Design concept of the edge-cooled photon stopper, consisting of thin diamond disk backed by a thick SiC block attached to a Cu cooling block.

Figure 9-14 shows the edge-cooling concept of a photon stopper, consisting of a thin diamond disk backed a thick SiC block attached to a Cu cooling block. The front surface of the diamond is coated with a thin layer of beryllium to reduce the single-shot FEL fluence to the diamond disk to below its multi-shot damage threshold based on the tensile yield stress. To stop the hard X-rays up to 25 keV, an additional tungsten block will be positioned at the back after an active burn-through monitor (not shown). The same Be-diamond-SiC-W layered design will be used for the collimators, apertures, and slits.

The multi-shot damage mechanism for diamond under the FEL irradiation is not well understood, and only limited experimental data are available based on the history of diamond monochromator applications at synchrotron X-ray facilities around the world, in which the diamond samples have been exposed to similar average power of roughly 1 kW, but not the large amplitude thermal cycling encountered under the pulsed FEL illumination. Alternative designs have been explored to avoid relaying on diamond as the heat spreader. B_4C has been used and proven for the LCLS stopper/collimator/aperture/slits design where a very small average power (< 1 W at 120 Hz repetition rate operation) is incident on normal insidence absorbers. We have looked into an inclined B_4C absorber design which allows the average FEL power (200 W max) to be spread over a much large area to reduce the average temperature rise.

9.4.4 Imagers

Imagers are required to capture the FEL transverse intensity profile and help FEL operators tune the lasing process or steer the beam around. The imagers will intersept all of the FEL radiation and therefore will be inserted and withdrawing from the beam path as needed. The maximum power incident on the imagers for the SCRF linac operation will be limited to 20 W, thus requiring upstream attenuation either by the attenuator systems or by curtailing the FEL power by either reducing the repetition rate or producing less FEL energy per pulse. The imagers

will be designed to operate with variable field-of-view (FOV) from 2x to 20x of the beam full-width-at-half-maximum (FWHM), and correspondingly variable spatial resolution from 1% to 10% of the beam FWHM. The imagers should be capable of capturing single-shot images (although not continually) with the FEL operating at a maximum repetition rate of 100 kHz. At higher FEL rate, integration will be permitted.

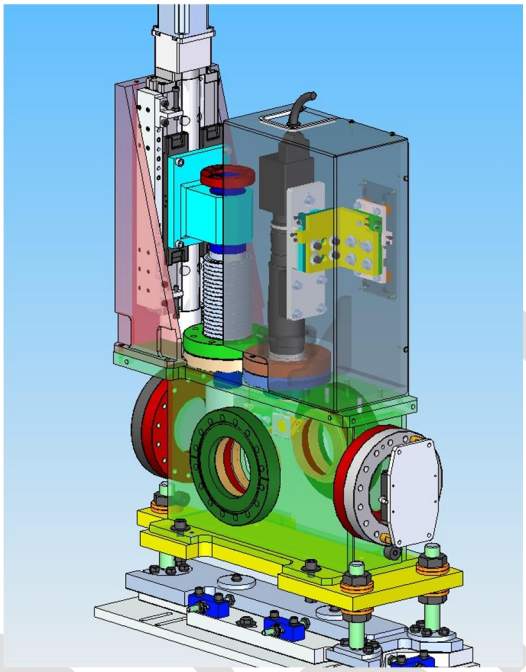

Figure 9-15. Design model for the single-shot imager for capturing the transverse intensity profile of the FEL beam. It is based on optical imaging of the X-ray scintillation image by the incident FEL beam onto a scintillation material of single-crystal YAG:Ce.

The imagers will be based on the same LCLS design shown in Figure 9-15 using optical imaging of the FEL beam impinging on an X-ray scintillation material, such as single-crystal Cerium-doped Yttrium Aluminum Garnet (YAG:Ce), which has shown to exhibit characteristics suitable for imaging high brightness light sources like the X-ray FEL. It has a very high melting temperature, though poor thermal conductivity, and is capable of sustaining unfocused FEL beam at normal incidence with moderate, 10x, attenuation. It is a fast scintillator with its maximum luminescence yield at 550 nm, which matches well with the quantum efficiency curve of a typical optical pixelated camera. Its scintillation image is not diffuse as for phosphor materials, thus a very high spatial resolution can be achieved and it is only limited by the numerical aperture of the lens and the pixilation of the camera. To achieve best spatial resolution, the YAG:Ce crystal is positioned normal to the incident FEL beam. The scintillation image is reflected into the optical camera by a 45° mirror positioned on-axis directly downstream of the YAG:Ce crystal.

Unlike in the LCLS design, cooling will be needed when the imagers are used at very high FEL repetition rate. The deposited thermal energy into the YAG:Ce crystal must be dissipated accordingly to avoid damage from overheating. Since the YAG single crystal has a relatively poor thermal conductivity, it must be attached to a transparent and yet highly thermal conductor

such as diamond to facilitate cooling from the edge. The YAG:Ce crystal must also be very thin to minimize thermal gradient within the crystal to below the melting temperature. The thermal conductor will then be attached to a Cu cooling block using GaIn eutectic liquid to promote thermal conduction. To avoid saturation in the optical camera, a neutral density filter not included in the LCLS design will be added.

9.4.5 Spectrometers and *k*-monochromator

9.4.5.1 *Hard X-ray transmissive single-shot spectrometer*

The spectral content of the SASE-based FELs exhibits shot-to-shot fluctuation. Ideally, the FEL operator uses single-shot spectrometers to help optimize FEL lasing or tailor the spectral distribution, or researchers use spectrometers to properly normalize their experiments. Due to limitations of experimental techniques, only a hard X-ray single-shot spectrometer has been demonstrated to show sufficient spectral range and resolution. As such, for the hard X-ray undulator line in the energy range from 5 to 25 keV using the CuRF linac at a repetition rate of 120 Hz, the existing LCLS bent crystal single-shot spectrometer shown in Figure 9-16 will be re-purposed for LCLS-II operations. The spectrometer uses an ultra-thin (10 to 20 μm) curved single crystal, which disperses a highly collimated polychromatic FEL beam onto a scintillator-based X-ray detector. The spectral range of this design can be as high as 1%, sufficient to capture the entire SASE FEL spectrum, and spectral resolution as high as 100 meV has been demonstrated using a Si (333) reflection at 8 keV, equivalent to a resolving power of 80,000. The transmissivity of the thin membrane is about 60% at 5 keV, and approaches 99% at 20 keV.

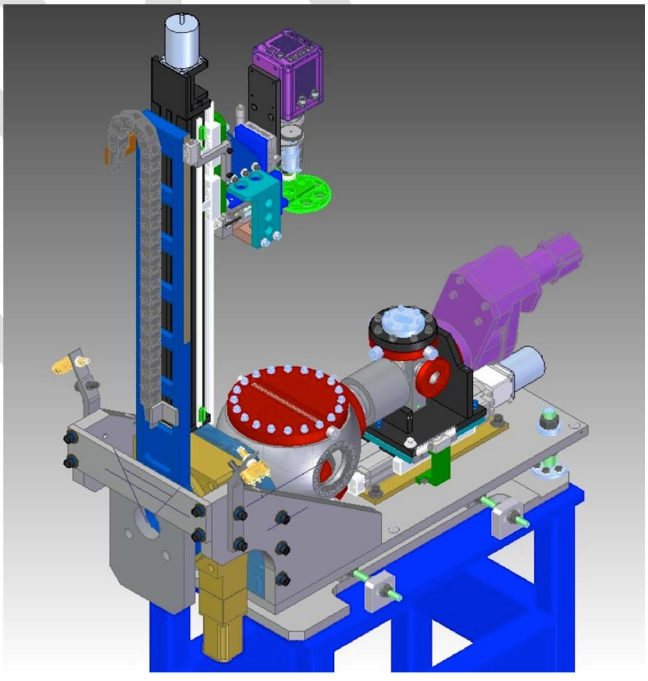

Figure 9-16. The LCLS single-shot hard X-ray spectrometer, consisting of a thin Si bent crystal and an X-ray scintillation-optical imaging system for capturing the spectrograph.

The operating energy range is from 5 to 25 keV. The maximum frame rate is 120 Hz.

9.4.5.2 *K*-monochromator

The LCLS-II undulators for both the soft X-ray and hard X-ray lines will be of the variable gap type, in contrast to the fixed-gap type of LCLS. As such, diagnostic tools are needed to make sure that the magnetic parameter *K* of each undulator matches that of all other undulators within a given tolerance of 0.015% to ensure the electrons stay on resonance as they traverse the entire undulator system. The concept of this diagnostic is based on the high precision measurement of the spectrum of the spontaneous emission from an individual undulator. By comparing the spontaneous emission spectra of two undulators, the relative difference in their *K* values can be extracted, which could in turn be used for matching. The spectrum is taken by scanning the electron energy while keeping the *K* fixed.

For the hard X-ray undulator line in the energy range from 1 to 25 keV, the existing LCLS *K*-spectrometer shown in Figure 9-17 will be re-purposed, as it was designed to work with spontaneous radiation from single undulators. This system uses a 4-bounce Si (111) single crystal monochromator operated at a fixed energy of 8.172 keV, with an angular acceptance of 32 μrad, matching the Darwin width of the Bragg reflection, which is equivalent to 1.2 eV. By varying the electron energy, the spectrum can be traced out and the relative *K* value of the undulator can be extracted.

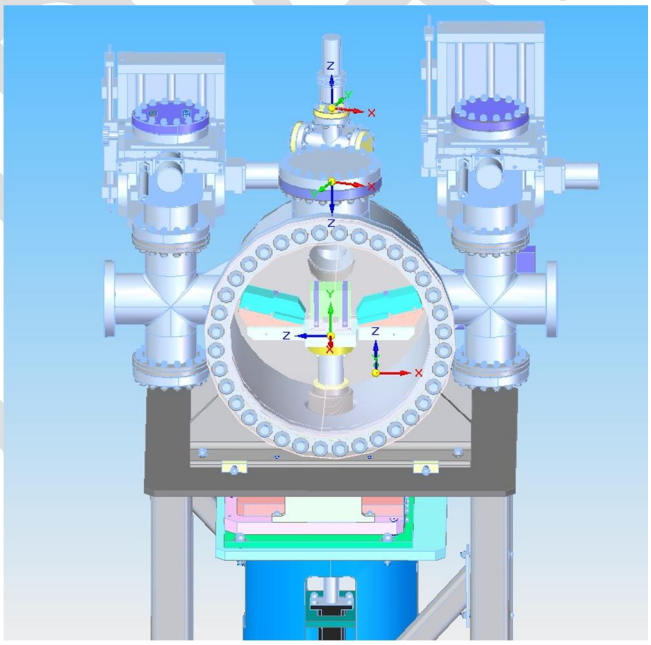

Figure 9-17. Schematics of the LCLS *K*-monochromator, consisting of a 4-bounce Si (111) monochromator working at a fixed X-ray energy of 8.127 keV.

9.5 Radiation Safety Systems

The radiation safety system for XTES is designed to provide a radiation-safe environment for personnel at designed accessible areas around XTES and is covered in detail in Chapter 13. Two issues that are related to the operations of the FEE and to XTES scope are discussed in further in the following sections.

9.5.1 Access to the FEE

The main radiation source affecting XTES is from the small fraction of the beam lost on the main bending dipole before the main dumps. The electron loss of 120 W, i.e. 0.1% of the full 120 kW beams, is assumed for the current design. The studies under these conditions showed an unacceptably high radiation level, >0.05 mrem/h, in the FEE, with electron beams going to the SXR or HXR dumps. Therefore access into FEE will not be available for LCLS-II.

With access to the FEE no longer permited with beam to the dumps, the access to the FEE will be moved to the dump maze at a point where there will only be one beam channel of the SXR line to impede access. The existing maze to the FEE will be modified as shown inFigure 9-18, making the space available for a rack room which will be accessible area during operations.

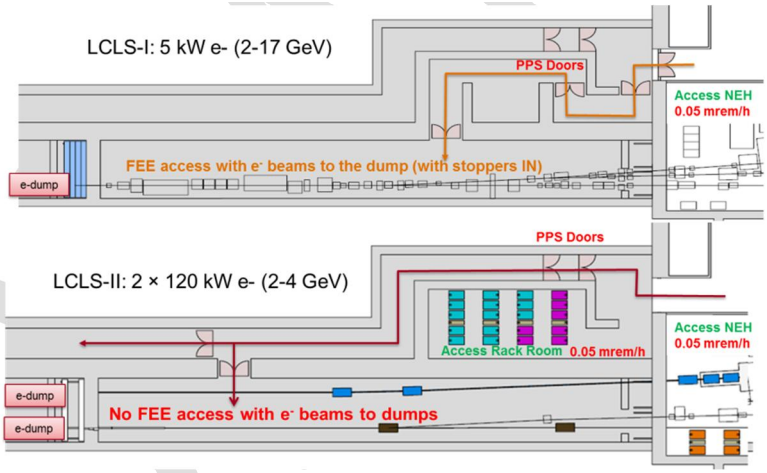

Figure 9-18. Change of accessible areas, showing configuration for LCLS (top) and LCLS-II (bottom)

9.5.2 Electron Safety Dumpline

Electron safety dumplines are required to prevent electrons entering FEE in credible accident scenarios and are therefore part of the XTES scope. The requirements for the two electron safety dumplines are defined in *Post-Undulator Safety Dump Lines PRD*, LCLSII-3.5-PR-0111. The safety dumplines are designed for an extended energy range of 2.0 to 20 GeV for HXR and 2.0 to 6.0 GeV for SXR to be compatible with possible future upgrades. Figure 9-19 shows the HXR safety dumpline, most of which reuses the existing LCLS safety dumpline. The SXR safety dumpline is similar but uses only one permanent magnet. The details of the locations and

dimensions of collimators are defined in the *Post-Undulator Safety Dump Lines PRD* and a Radiation Physics Note [9].

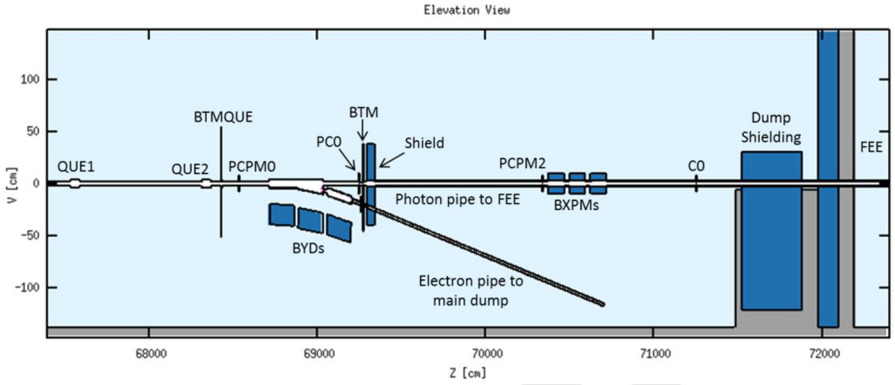

Figure 9-19 Elevation view (in rolled coordinates) of LCLS-II safety dumpline

9.6 Experimental Systems Implementation

9.6.1 Hard X-ray Beamline Delivery

At LCLS-II the hard X-ray undulator will deliver photons to five experimental stations:XPP, XCS, MFX, CXI and MEC. With the exception of MFX, which is currently under development, these stations have been commissioned and are currently operating at LCLS. While these instruments were developed for LCLS, they will continue to support science using both the high repetition rate and extended energy beams from LCLS-II.

Because these instruments receive beam only from the hard X-ray undulator, the beam delivery path is the same regardless of which accelerator is used to drive the undualtor. While upgrades to the optics, collimators, stoppers and diagnostics are required, the beam path for these instruments remains unchanged from LCLS.

The XPP (X-ray Pump Probe) instrument is the only hard X-ray instrument located in the Near Experimental Hall. Because the XPP instrument is closer to the X-ray source, it is the most suitable instrument for operation below 5keV at high repetition rate.

The MFX (Macromolecular Femtosecond Crystallography) instrument is currently under development and will be installed between hutches 4 and 5 in the Far Experimental Hall. The MFX instrument design takes future LCLS operations into account.

All five of the X-ray instruments will be able to operate at photon energies as high as 25keV (at 120Hz) because of the hard X-ray offset mirror upgrade currently underway.

In order for the X-ray instruments to realize their full operation capacity at higher repetition rate, several ancillary systems will require upgrades The upgrade options to data acquisition systems, detectors, pump lasers, controls, X-ray optics and sample delivery. are currently part of the LCLS facility development.

9.6.2 Soft X-ray Stations

Unlike the hard X-ray instruments, which will not change for LCLS-II, the soft X-ray instruments will move north within the Near Experimental Hall inline with the new soft X-ray undulator on the north side of the undulator hall. The soft X-ray design energy range of LCLS-II (200eV-1300eV) is lower than that of LCLS (800-2000eV). As a result the soft X-ray beamline optics and diagnostics must accommodate a much larger X-ray beam size much higher average power and thus require new and significantly modified components, see *X-ray Transport and Experimental Systems PR,* LCLSII-3.5-PR-0051.

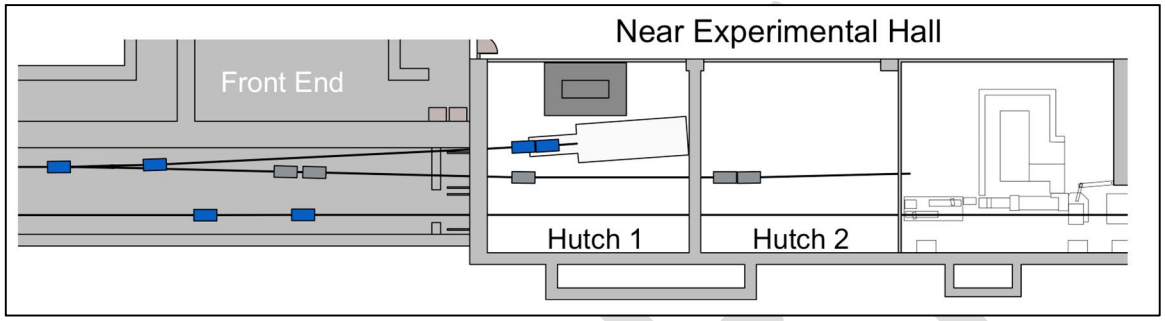

Figure 9-20: LCLS-II XTES Soft X-ray Instrument

A new soft X-ray beamline path will be introduced that is slightly different from that used by the current AMO and SXR instruments. The beamline is shown inFigure 9-20. Much of the current vacuum componentry and controls cabling will be moved or replaced. However, the key support utilities and infrastructure capacities are in place including: electrical power, process cooling water, bridge cranes, compressed air and HVAC.

The XTES soft X-ray beamline will require a new Beam Containment System (BCS), including collimators. Because the system will occupy Hutch 1 (the current location of the AMO instrument) the Hutch Protection System (HPS) can be modified and adapted to the LCLS Personnel Protection System PPS. Soft X-ray beam containment for radiation safety can be achieved with proper end station and beamline design without the need to isolate the equipment inside an interlocked hutch. This will be a design target for long-term end station installations. If needed, a personnel exclusion system will implemented.

Two mirrors will deflect the beam into Hutch 1 where a K-B mirror pair will focus the beam to a spot of 1µm x 1µm FWHM as discussed in Section 9.3.2. The K-B mirrors will be adaptive optics capable of translating the focal position and controlling the spot size. This beamline will also have a gas monitor detector diagnostic capable of measuring the number of photons in each arriving pulse.

In addition to the repurposed and new components, the soft X-ray beamline controls systems will undergo a substantial relocation and upgrade. While some of the current AMO servers and controls will be reused, the overall system will require a new cable plant. A new triggering system will also be installed to provide compatibility with the high repetition rate operating modes.

The DAQ will be upgraded to accommodate the data volume expected from high repetition rate detection. The DAQ upgrade will extend the current DAQ infrastructure to enable data capacities as high as 10GB/s. This is sufficient to readout a 20,000 channel (or pixel) detector at 100 kHz or a two megapixel area detector at 2 kHz.

The soft X-ray beamline will be multipurpose. Because it is optimized for transmission and high intensity it can be used for high field physics as well as imaging experiments. However, with self-seeding at LCLS-II this beamline will be able to be used for spectroscopy. The soft X-ray XTES beamline will reuse the LCLS experimental end stations such as the Resonant Soft X-ray Scattering (RSXS) and LAMP systems. Because the transport of soft X-ray photon beams require ultrahigh vacuum conditions, the beamline will end with a vacuum interface to which an experimental end station can be connected. To provide the greatest scientific capability, each end station can be used on any of the soft X-ray beamlines.

9.6.2.1 End Station Systems from LCLS

The end station area located downstream of the exit interface flange for the soft X-ray beamline will be designed with the intent to host different end station systems. The end stations described below have either been developed or are in development at the LCLS facility and are not within the scope of the LCLS-II Project. With upgrades to the detection systems they will be able to address the scientific objectives of LCLS-II.

The LCLS-ASG-Michigan Project (LAMP) end station provides soft X-ray coherent scattering capability for gas phase and solid samples. Its primary purpose is to study different types of ordering in condensed matter systems via diffraction, but it will also be used to perform imaging and fluorescence experiments. The design is based on the CFEL Advanced study group Multi Purpose (CAMP) endstation [10], which was used at LCLS from 2009-2011 in the AMO hutch. The LAMP design provides compatibility with existing components developed for CAMP such as injectors and spectrometers, but the functionality of the instrument has been further improved. The LAMP chamber features a compact differential pumping section that includes laser incoupling capabilities and X-ray beam diagnostics. The end station has two separable vacuum systems: the main interaction chamber hosts the sample injection systems as well as electron and ion imaging spectrometers, and the pnCCD detectors are housed in a downstream chamber. The pnCCD detectors consist of 1024 x1024 75um pixels that are sensitive to the full soft X-ray energy range of 200-1250eV. The LAMP vacuum chambers are fixed to a kinematic stand with six degrees of freedom and the capacity to support additional components such as sample injectors and large spectrometers.

This end station is dedicated to resonant diffraction with soft X-rays and is based on the RSXS chamber built at LBNL [11]. It will include an in-vacuum diffractometer, a 120Hz low noise CCD, a separate in-vacuum mounting station for long-wavelength optics for pump-probe measurements, and a cryostat with six degrees of freedom.

9.6.3 Build out concepts

While the single soft X-ray instrument serving the new soft X-ray undulator will provide revolutionary new soft X-ray capabilities and capacity, a total of three beamlines will result in the most efficient operation of the source. Figure 9-21 shows a possible build out scenario for three beamlines that expands the experimental capabilities and provides improved operational efficiency. All three instruments would be located in the NEH, but the wall between hutches 2 and 3 would be removed. Such a build out would likely be implemented in phases and is subject to further refinement as the scientific needs for LCLS-II become more clearly defined.

Assuming that soft X-ray seeding is not able to meet the scientific demands of high resolution spectroscopic techniques, a second monochromatic beamline is planned to occupy hutch 2. The second beamline will feature a grating monochromator system with a resolving power of greater than 20,000. This beamline will also have a gas detector system after the exit slit of the monochromator and a K-B focus mirror pair. The beamline will be multipurpose with emphasis on spectroscopy and may be configured to accommodate various end stations, similar to the implementation of the XTES soft X-ray beamline. It may also be designed to accommodate a high-resolution X-ray emission spectrometer, as shown inFigure 9-21. Such a spectrometer may span the space between hutches and 2 and 3 and would even require the removal of a structural pillar within the NEH.

A third beamline is envisioned for the soft X-ray undulator in a final build out phase. Here an additional branchline would share the soft X-ray monochromator system. This instrument would occupy hutch 3, as illustrated inFigure 9-21. As a result the XPP instrument would be displaced, but its functionally could be combined in hutch 4 with the XCS instrument. An alternative to a third soft X-ray beamline would be an instrument optimized for the tender X-ray energy range (2-5keV) and installed in hutch 3.

These new instruments would require upgrades to the DAQ, pump laser, controls, triggering and detector systems. Space to accommodate additional racks and laser tables is accounted for in the experimental floor layout.

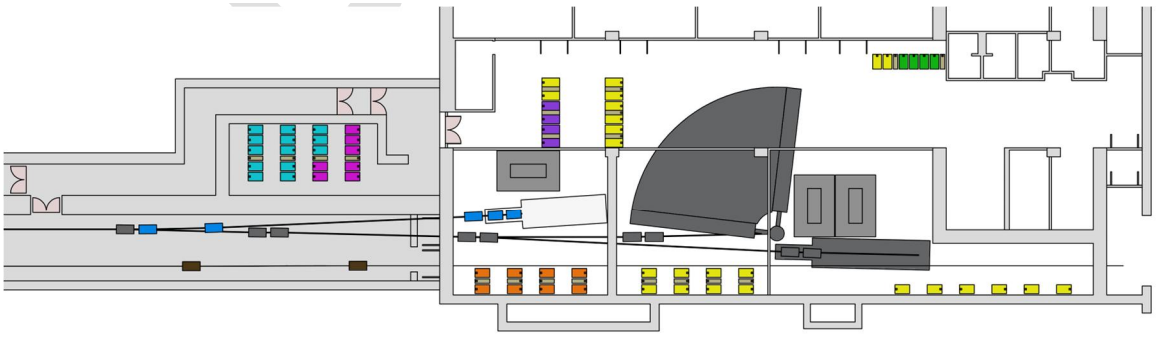

Figure 9-21. LCLS-II NEH Buildout Concept. (Add labels to the figure)

9.7 References

1 S. P. Hau-Riege et al., *Optics Express* **18**, 23933-23938 (2010).

2 S.P. Hau-Riege et al., *Appl. Phys. Lett.* **95**,11104 (2009).

3 B. Ziaja, et. al., *High Energy Density Phys.* **9**, 462 (2013).

4 S.P. Hau-Riege, LCLS note, LCLS-TN-06-5 (2006).

5 J. Gaudin, et al., *Phys. Rev. B* **88,** 060101 (2013).

6 D.D. Ryutov, *Rev. Sci. Instr*. **74**, 3722 (2003).

7 T.Koyama, et al.,, "Damage threshold investigation using grazing incidence irradiation by hard X-ray free electron laser," *Proc. SPIE* **8848**, 88480T, (2013).

8 Y-H. Cheng, et al, "The effect of long timescale gas dynamics on femtosecond filamentation " Opt. Express 4, 4740 (2013)

9 . S. Xiao, "Radiological Studies for the LCLS-II Post-Undulator Safety Dump Lines," RP-14-15, November 6, 2014.

10 L. Strüder, et al., *Nucl. Instrum. Meth. A* **614**, 483 (2010).

11 D. Doering, et al., *Rev. Sci. Inst.* **82**, 17620 (2011).

10 Controls and Safety Systems

TECHNICAL SYNOPSIS

The controls system for LCLS-II provides for the control, monitoring, operation, diagnostics, and performance optimization of the entire accelerator facility. Controls provides all of the necessary data acquisition and control hardware, software, networking, computing facility, safety systems and the Main Control Center (MCC) operations facility. The system scope and architecture spans from low-level interface and control of beamline components to high level automation and optimization.

Machine protection and radiation safety systems protect personnel and equipment from potentially dangerous or damaging radiation and beams. These systems couple together the control of many different accelerator systems and subsystems, such as the drive laser, gun RF, injector and accelerator RF, radiation monitors, personnel access gates, mirrors, stoppers, vacuum valves, insert-able diagnostics, and magnets. With the potential for MW-level beam power, these systems must be entirely reliable and robust, with very fast response times in some cases.

10

10.1 Control System Overview

The controls system for LCLS-II provides for the control, monitoring, operation, diagnostics, and performance optimization of the entire accelerator facility as well as interfaces to the photon controls system. Controls provides all the necessary data acquisition and controls hardware, software, networking, computing facility, safety systems and the Main Control Center (MCC) operations facility. The system scope and architecture spans from low-level interface and control of beam line components to high level automation and optimization. Figure 10-1, a screen shot of the LCLS-I top-level operator's display, presents an overview of the control functions provided for each region. LCLS-II will have an extensive operator's display package similar to that at LCLS-I.

Figure 10-1. LCLS-I Electron control systems main display and overview

Beamline devices are interfaced directly to the Experimental Physics and Industrial Control System (EPICS) input/output controller (IOC) front-ends, or indirectly to EPICS via

programmable logic controllers (PLCs). EPICS channel access (CA) over Ethernet provides the communication protocol for front-end computers and for mid- to upper-level control system elements. Many EPICS "soft IOCs" — processes running in servers — perform important control functions that require little hardware I/O. The distributed controls architecture has a backbone network supporting EPICS channel access, plus several dedicated networks for timing, feedback and machine protection. A data acquisition system separate from EPICS will be provided to handle the data rates required for recording diagnostics at the 1 MHz beam rate.

10.1.1 Documentation and Schedules

Controls Systems interfaces with nearly every accelerator and photon subsystem, hence the majority of the LCLS-II Physics Requirements Documents are relevant to control systems. Table 10-1 lists the high-level control systems design requirements, specifications, and interface documents.

Table 10-1 Control System High-Level Requirements and Specifications

Title	Document Number
Control System Requirements	LCLSII-2.7-PR-0066
LCLS-II Availability	LCLSII-1.1-PR-0163-R0
Electron Beam Diagnostic Systems	LCLSII-2.7-PR-0170
Beam Position Monitor Requirements	LCLSII-2.4-PR-0136
Phase Reference System	LCLSII-2.7-PR-0213
RF Power and LLRF Requirements	LCLSII-4.1-PR-0098
PPS Requirements (Electron Beamlines)	LCLSII-2.7-PR-0077
BCS Requirements (Electron Beamlines)	LCLSII-2.4-RP-0107
Electron Beam Controls to Accelerator Systems, Cryogenic Systems, Photon Systems and Infrastructure Systems	LCLSII-2.7-IC-0266
Photon Beam Controls to Electron Beam Controls	LCLSII-3.5-IC-0115
Radiation Safety Systems to Accelerator Systems, Cryogenic Systems, Photon Systems and Infrastructure Systems	LCLSII-1.2-IC-0278
Injector Laser to Electron Beam Controls	LCLSII-2.7-IC-0087
Machine Protection System to Accelerator Systems, Cryogenic Systems, Photon Systems and Infrastructure Systems	LCLSII-2.7-IC-0279
Low Level Radio Frequency (LLRF) to Accelerator Systems, Cryogenic Systems, Photon Systems and Infrastructure Systems	LCLSII-2.7-IC-0277
LCLS-II Vacuum Controls Requirements	LCLSII-2.7-ES-0344
SLAC Radiation Safety Systems Technical Basis Document, ESH Division	SLAC-I-720-0A05Z-002-R004
The Stanford Two-mile Accelerator, Chapter 2, Protection Systems, Section 3 Radiation Monitoring; Radioactive gas Monitor (GW)	

The schedule for major design reviews is given in Table 10-2. Table 10-3shows the overall schedule for control and safety systems.

Table 10-2 Control System Design Review Schedule

System	Component	Review	Date
Controls Systems	Basic Control Systems	Engineering Peer Reviews	April-May 2014
	Basic Control Systems	Preliminary Design Review	January 2015
	Basic Control Systems	Final Design Review	July 2016
Control Systems	High Performance Systems	Engineering Peer Reviews	May 2014
	High Performance Systems	Preliminary Design Review	September 2015
	High Performance Systems	Final Design Review	November 2016
Control Systems	Basic Control Systems	Specifications Released	February 2015
	High Performance Systems	Specifications Released	October 2016

Table 10-3 Control and Safety Systems Schedule

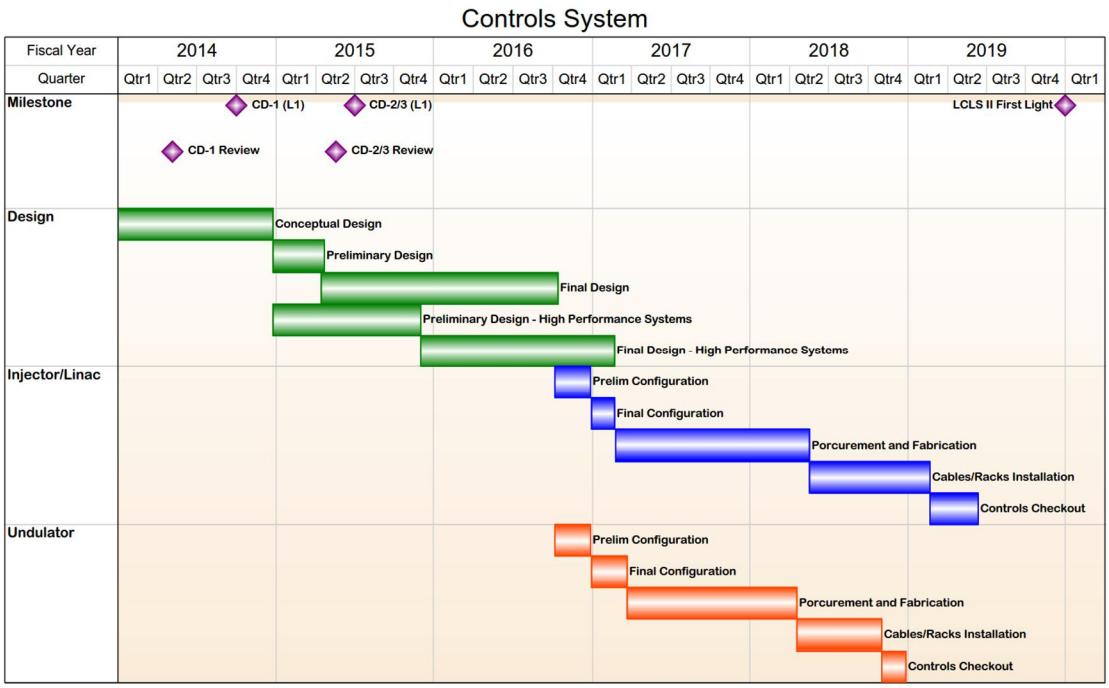

10.1.2 Controls Requirements

While some requirements for the LCLS-II controls system are nearly identical to those of the LCLS requirements, e.g. magnet and vacuum control, there are significant new requirements. The details can be found in the *Controls System Requirements Document*, LCLSII-2.7-PR-0066. The system is required to allow control and operation of the facility at up to 1 MHz, with beam-synchronized machine data available for diagnostics and automation.

LCLS-II includes a cryogenically cooled, superconducting CW linac. An entirely new cryogenic plant and distribution system will be installed, and will be controlled from a new cryogenic control room. The low-level RF system (LLRF) for this CW machine is completely different from that used for the pulsed linac of LCLS.

The design of the undulators for LCLS-II is significantly different from that of the LCLS undulators and requires new controls development. The Undulator Control section of this document gives an overview of the new design required for the LCLS-II undulators.

EPICS controls must be implemented for control of all newly-installed LCLS-II systems. As the capabilities of LCLS-II evolve over its many years of operation, the controls system has to be sufficiently extendable to support more than 100,000 I/O connections and several million EPICS process variables (PVs), as LCLS-II becomes the largest EPICS projects in the world.

10.1.3 Operations Requirements

Operations control of the LCLS-II linac and the electron beam will be carried out from SLAC's MCC. Operations control of the LCLS-II Cryogenic Systems will be carried out from a cryogenics control room, with a supplemental interface to the MCC. Necessary data for monitoring and control of the LCLS-II will be available to the operations in MCC, and all user interfaces will be clearly designated so that no confusion arises as to which machine is being controlled. The section on software describes plans for these additional requirements.

10.1.4 Reliability

Overall, the LCLS-II facilities must have an operational availability greater than 90 percent. Controls should contribute only a fraction of the down time, less than 2%. The reliability requirements for LCLS-II are detailed in the *Availability Document*, LCLSII-1.1-PR-0163-R0. The linac is typically operated about 6,600 hours per year for all purposes. In some cases, improvements of subsystem controls designs will be implemented to improve reliability, based on lessons learned during LCLS operations. These changes are described in the following sections of this chapter.

10.1.5 Design Maturity

The LCLS-II Project Final Design Plan LCLSII-1.1-QA-0065 provides for a phased completion of the final designs for the LCLS-II facility. The plan ensures that designs are sufficiently mature to start procurements and construction, while enabling the most cost-effective

schedule for constructing the facility and maximizing the technical capabilities of the facility at CD-4. Final design readiness at CD-3 recognizes that that not all subsystems will reach final design at the same time. Project-level requirements and interface control points between Accelerator Systems, Cryogenic Systems, Photon Systems and Infrastructure are defined at CD-3, which ensures that the phased procurements and construction are appropriate for the final design of the LCLS-II. Chapter 2, Project Overview, contains additional discussion of the approach to design completion. The Accelerator Systems design, described in this chapter, Chapters 4 and 5, is evaluated to be 65% complete. Much of the beamline hardware is quite advanced and based on existing components or existing designs while the control system design is less mature. Completing remaining design after CD-3 allows for potential upgrades to diagnostics and controls, using designs developed and proven by SLAC Operations.

10.2 Controls Architecture

10.2.1 Controls System Architecture

The controls architecture will be based on the standard three layer client/server architecture. This model has been very successfully implemented for LCLS, and the fact that it lends itself to incremental development will allow us to expand it relatively easily for LCLS-II. The system will be based on the proven EPICS toolkit with well-defined interfaces for both the client and server in order to enable fast integration and development. It will support the use of commonly available hardware and provide an extensive collection of ready-to-use applications software and device drivers.

10.2.1.1 Network Architecture

The LCLS-II controls network will be essentially an upgrade of the ones already in LCLS. It will consist of distribution switches located near the control system devices in each accelerator area. Controls devices will be connected to the distribution switches by CAT6 or fiber cables. The distribution switches will be connected to redundant large core routers in MCC by high-speed fiber optic links. A large number of fiber optic cables will be pulled to each accelerator area, and multiple fiber optic cables can be used for increased bandwidth or to isolate traffic, as needed. Redundant fiber links between the distribution switches and the core switches will allow immediate recovery from the failure of a single fiber link.

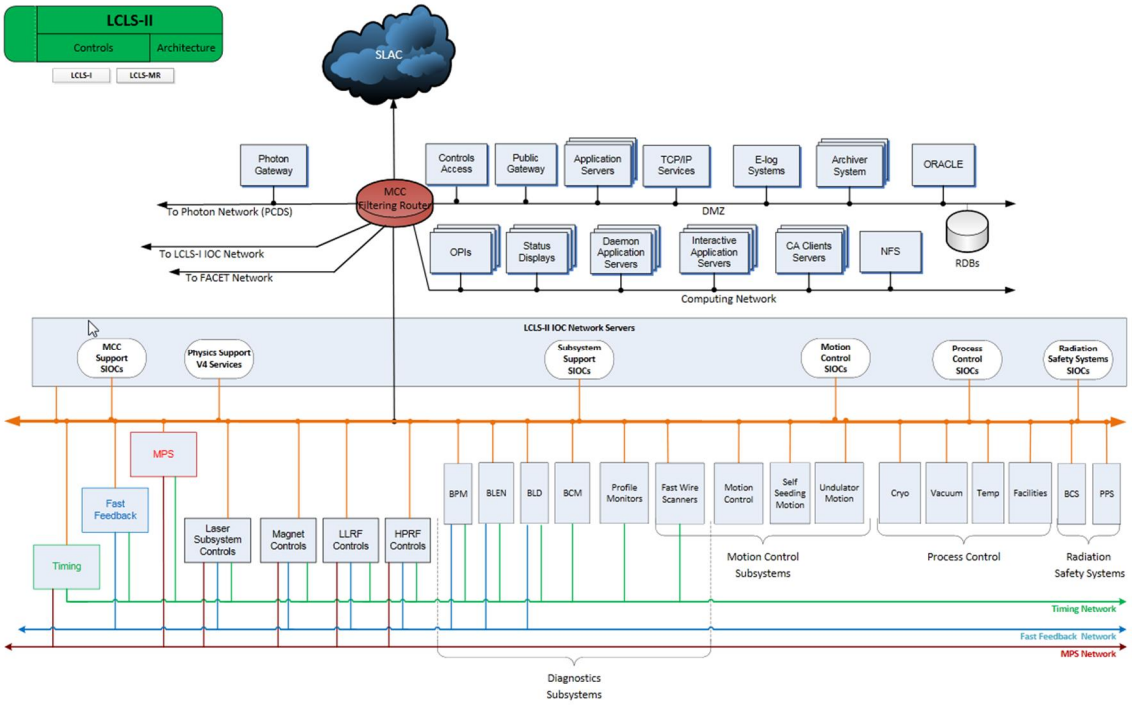

Figure 10-2 Network-based overview of the controls system

As indicated in Figure 10-2, the LCLS-II controls network will consist of many separate networks (VLANs), including computing, IOC, instrument, terminal, utility, video, and low latency for fast feedback and MPS. The low latency network will be separated from the other controls networks. The timing system network will use separate fiber links and connect directly to timing system devices. The intermediary network (often referred to as the DMZ), which will be shared between LCLS and LCLS-II, will allow limited and controlled access between the controls networks and other SLAC networks through dedicated and restricted servers on the DMZ network. The architecture of the switches allows all of these networks to be isolated from each other but to still share the same switches and fiber uplinks. Additional networks can be added when needed. Central redundant core routers will allow controlled connections between any of the LCLS and LCLS-II controls networks, as needed.

The LCLS-II controls network will be isolated from the rest of the SLAC public network. No accelerator control devices will be visible to SLAC campus or Internet networks. This avoids denial of service and reduces vulnerability to other types of hacker attacks from outside of the controls network. Read-only data access will be provided to SLAC public networks by an EPICS Process Variable (PV) Gateway on the DMZ network.

10.2.1.2 Controls Computing Infrastructure

The controls computing infrastructure provides services to controls applications from front-end IOCs, to mid-level software and upper-level operator interfaces (OPIs). The services include NFS, NTP, DNS, DHCP, TFTP, Oracle, Data Archiving, PV Gateways, Monitoring system, Message System, Controls Access, Status Displays, OPIs, and Application Servers. The

infrastructure will be hosted in a centralized fashion to support both LCLS and LCLS-II, as shown in **Error! Reference source not found.**.

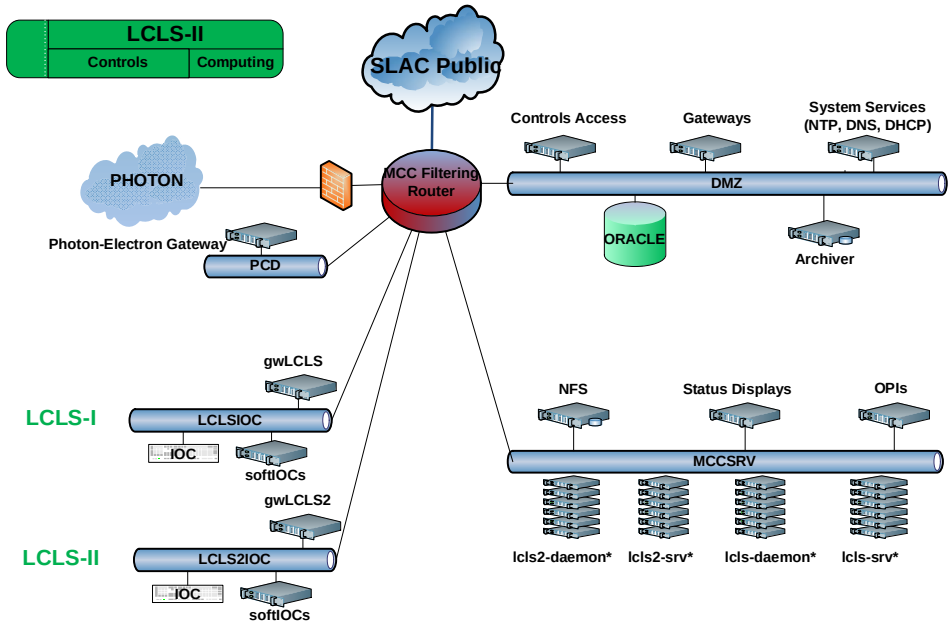

Figure 10-3 Controls Computing Infrastructure

IOCs (hard and soft) will be hosted on separated networks, one for LCLS (LCLSIOC) and another for LCLS-II (LCLS2IOC). The controls communication is mostly based on EPICS Channel Access network protocol. As shown in Figure 10-3, a pair of PV gateways (gwLCLS and gwLCLS2) will provide channel access traffic controls between LCLS and LCLS-II. As is the case with LCLS, limited and controlled access is provided to the SLAC public via dedicated servers on the DMZ. The channel access communication between photon and electron systems is controlled via PV gateways.

10.2.2 Controls Hardware Architecture

Some LCLS-II requirements for controls are largely the same as those for LCLS; thus implementations in those cases require copying existing systems. In some cases improvements in design or technology are implemented based on 1) change in requirements (e.g. 1 MHz beam rate, superconducting CW linac), 2) improving reliability, 3) increasing the level of standardization and maintainability of the systems (e.g., aligning the systems with new industry standards), 4) reducing costs either in the development or implementation phases, 5) taking advantage of commercial off-the-shelf hardware, or 6) replacing obsolete or unavailable components. The following sections will indicate where hardware differs from that of LCLS.

All subsystems will use EPICS, but different individual subsystems may use various hardware solutions such as Micro-TCA, crate-based IOCs, and PLC/soft IOC combinations.

10.3 Timing and Synchronization System

The role of the timing system is to provide pulse-to-pulse coordination (timing patterns) for beam control and data acquisition, and to remain synchronized with both the low-level RF phase reference distribution and the 360 Hz AC power line phase.

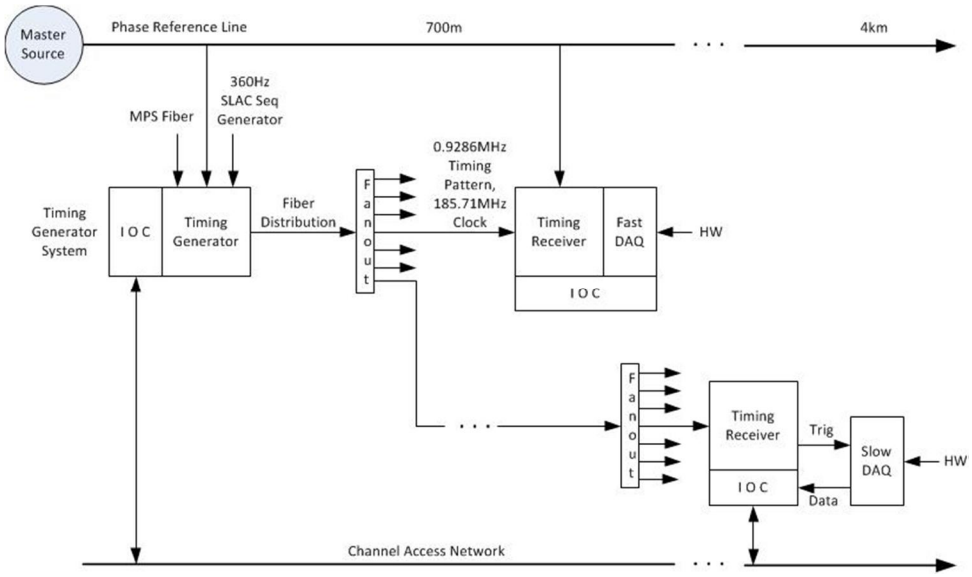

Figure 10-4 Timing system block diagram

The timing system architecture will have a master timing generator that will distribute timing patterns and a 185MHz clock over a dedicated fiber optic system to downstream timing receivers using fiber fanouts (Figure 10-4).

The RF phase reference line will provide a precise clock from which the 185MHz clock and maximum beam rate of approximately 1MHz is derived. The 360Hz AC power line phase will be provided by the SLAC sequence generator. Stability and jitter of timing for receivers without a connection to the RF phase reference line will be 1 ns and 30 ps, respectively. Stability and jitter for LLRF timing receivers will be 30 ps and 5 ps, respectively.

The master timing generator will provide a timing pattern on the fiber at 1MHz which will encode the following information:

- Beam rate (0 to 1MHz) and bunch pattern. Note that a beam rate at or below 360Hz can be synchronized with the power line.
- Pulse by pulse beam destination and kicker control.
- Unique pulse ID and power line time slot.
- Rate markers and flags for synchronous data taking and data fault array snapshot.

The transmitted timing pattern will be for 100 μs in the future, which is required by some applications to prepare for an upcoming pulse, allowing for either feed-forward or a long pre-

pulse trigger. The timing generator will receive rate and destination at 1MHz from the machine protection system (MPS) and will adjust the timing pattern so that the response to a change will be within 100 µs. When there is a machine fault or user request, a data array snapshot request is set in the timing pattern, which flags receivers to provide 1 second data value arrays per channel to the user. Other inputs to the timing pattern will be from the operator and the beam containment system. A 1 second timing pattern table, constantly adjusted based on inputs, will be played out continuously on the fiber at 1MHz. The user will set up and change the table for various start-up and recovery patterns to bootstrap the machine up to the CW operation mode.

Each timing receiver will receive the timing pattern at 1MHz and store it in an internal 100 µs pipeline. For each hardware or software trigger supported by the receiver, a triggering event is decoded from the appropriate pattern in the pipeline. The user will be able to specify the decoding algorithm, delay, pulse width, polarity, and enable/disable for each trigger channel.

The receivers for the HXR undulator devices that require timing will get both LCLS and LCLS-II fiber input and switch between the two modes based on user request.

A fiber length delay will be set programmatically for each timing receiver to account for the varying distances from the generator to the receivers down the linac.

Data acquisition will use the triggering timing pattern as follows:

1. Associate a pulse ID and power line time slot with each raw and processed data value.
2. Send each data value/pulseID to the IOC at rates at or below 360Hz so that data on the same pulse is available across all IOCs.
3. Freeze 1 second value/pulseID arrays on request and make available to the IOC for fault analysis.
4. For a small subset of devices, gather value/pulseIDs at the beam rate and periodically send blocks of data to the user at a rate <=360Hz.

10.4 Beam Diagnostic Systems

The LCLS-II diagnostics fall into two main categories: those that involve analog conditioning followed by a sampling analog to digital converter (ADC), and those that involve image acquisition. The next two sections cover these two cases. Detailed system requirements are spelled out in the *Electron Beam Diagnostic Systems Document*, LCLSII-2.7-PR-0170.

10.4.1 Sampling ADC based diagnostics

By far, most of the diagnostic devices are required to measure a beam quantity at 1 MHz. These fast diagnostic must make the data available in one of two ways:

1. Time stamped, buffered and transmitted to be stored and/or correlated with other data, or

2. Transmitted as rapidly as reasonably possible for use by MPS, BCS, or beam-based feedback.

All fast diagnostic devices will need to do the first method, while only a select fraction will need to do the second. The plan is to make all instances capable of doing both, but only connect the requisite communications fibers to those where the second method is required. The diagnostics that fall into this category are BPMs, relative bunch length monitors, halo monitors, beam current monitors, loss monitors, beam arrival time monitors, wire scanners in the main beam and halo secondary emission monitors.

All of these diagnostics are to be handled in a similar fashion. Each will have a front end that is designed for that diagnostic, followed by a sampling ADC that has a field-programmable gate array (FPGA) attached. The front end may also incorporate a signal source for calibrating the diagnostic, which can be triggered by a separate event code at convenient intervals. This allows for compensation of drift in the signal processing and continuous monitoring of the health of the system for high reliability. The FPGA will process some number of ADC readings to attain the properly calibrated diagnostic reading, buffer it to onboard memory, and send it out on a fiber if needed. We will strive to minimize the number of types of ADC boards and front ends. SLAC will likely produce two types of ADCs and five or six types of front ends.

Table 10-4shows what component types would be used for each diagnostic. The data can be buffered on the ADC board for several seconds if needed, and periodically read out and saved by a CPU running EPICS.

Table 10-4 Analog and Digital Processing for Diagnostic Systems

<table>
<tr><th>Diagnostic</th><th>Front end</th><th>ADC</th></tr>
<tr><td>L and/or S band cavity BPM</td><td>L and/or S band down mixer</td><td rowspan="4">125-250 MHz, at least 12 effective bits. May well be the same ADC used for LLRF.</td></tr>
<tr><td>X band cavity BPM</td><td>X band down mixer</td></tr>
<tr><td>Button BPM</td><td>Button down mixer</td></tr>
<tr><td>Stripline BPM</td><td>Stripline filter/attenuator</td></tr>
<tr><td>Relative bunch length monitor</td><td rowspan="3">Variable gain amplifier</td><td rowspan="3">At least 10 MHz ADC. (Perhaps same as above.)</td></tr>
<tr><td>Beam current monitor (toroid)</td></tr>
<tr><td>Wire scanner detector (PM)</td></tr>
<tr><td>Beam Loss Monitors (several types)</td><td>Filter / attenuator</td><td>At least 250 MHz QADC</td></tr>
</table>

While it is unlikely we will choose to save all the diagnostic data at 1 MHz, it is prudent to make sure the system is capable of doing this if it is necessary. Since the data are buffered and there are no hard real time requirements, this is simply a question of bandwidth. A rough calculation of the bandwidth needed for the linac diagnostics is the product of the following factors:

- Number of diagnostics; about 100

- Bunch rate of 1 MHz
- Six bytes per reading (two for x, two for y, one for status, one for overhead)

This calculation results in about 600 million bytes per second or about 5 gigabits per second. This performance is well within the reach of modern CPUs and networks, particularly as this is sourced from many CPU's.

10.4.1.1 Beam Position Monitors

The LCLS-II BPM system consists of three types: stripline BPMs, button BPMs, and cavity BPMs. Button BPMs are used in the cryogenic linac; cavity BPMs are used in the undulator region; stripline BPMs are used in the injector, transport, and diagnostic lines. The detailed requirements are listed in the *Beam Position Monitor Requirements Document*, LCLSII-2.4-PR-0136.

All BPMs are required to acquire data at the full beam rate (up to 1 MHz) and to be capable of providing data to the fast feedback and machine protection systems.

Depending on the frequency of the BPM signals, the front end electronics may be located in the beamline tunnel near the BPM or in the support building. For lower frequency signals, as from stripline BPMs, the front end electronics can be in the support building next to the sampling ADC. For higher frequency signals, as from cavity and button BPMs, the signal loss due to cable length is too great and down-mixer electronics must be located physically near the BPM. Long haul cables then transport the intermediate frequency to the ADC in the support building.

Stripline and button BPMs have online calibration systems used to compensate for thermal drift of the electronics. Cavity BPMs use a beam-based on-demand calibration scheme.

10.4.1.2 Relative Bunch Length Monitor

The LCLS-II Bunch Length Monitor system consists of two types; a pyro electric detector-based Relative Bunch Length Monitor (BLEN), and a Gap Monitor. The latter is used in regions where the electron bunch length is greater than 2 mm, such as the gun region. From the Controls perspective these are treated as the same since everything past the signal detector starting at the digitizer will be the same for both. Three relative BLENs are needed for longitudinal feedback, one after each bunch compressor (BC1, BC2, and BC3).

A mirror with a hole for the e-beam will be inserted into the beam line to reflect the radiation that is detected by the pyro detector. Each detector will provide two signals as inputs to the BLEN Controls.

The BLEN system will include, where necessary, remotely insert-able optical filters to properly attenuate or filter the radiation for the desired performance level. To compensate for the potential thermal drift in pyro detector sensitivity, temperature sensors are mounted close to the pyro element. These temperature readings will provide slow correction factor for the BLEN instrument. The BLEN system will have I/O support to read back these temperatures at a slow rate.

The BLEN controls must acquire the pyro detector waveforms at 1 MHz, and perform calculations on this waveform to derive the bunch length. The TMIT value of a nearby BPM will be used in the calculation. A fast digitizer will acquire the waveforms and an FPGA will perform the bunch length calculations. This information will be made available to feedback systems shot-by-shot.

Circular buffers that can hold a few million samples per snapshot will provide non-real-time diagnostics.

10.4.1.3 Beam Charge Monitors

The LCLS-II Beam Charge Monitor (BCM) system consists of two types: toroids, and Faraday cups. Faraday cups are low rate devices mounted in diagnostic lines, while toroids are high-rate and installed in the beam line. Toroids and Faraday cups will provide pulsed signals for beam charge measurement.

Signals from the commercial of the shelf (COTS) Toroid will be input to a Bergoz BCM RF receiver, which samples at a programmable rate. The output from this chassis will be input to a fast digitizer, which will digitize it. Bunch-by-bunch charge will be reconstructed inside the FPGA. This will provide the average beam current at a rate of up to 1 KHz. The toroid system can run at the full 1 MHz rate if needed. Calibration of the toroids via known charges is possible with the Bergoz chassis.

The BCM will use a picoammeter to read the average current from the Faraday cups. The picoammeter is controlled via network. The calibration pulses and trigger are provided by BCM controls for both Faraday cups and toroids.

10.4.1.4 Beam Loss Monitors

The LCLS-II machine protection system (MPS) will use several types of monitors to detect ionizing radiation. These detectors provide both a measurement of instantaneous loss, and a loss signal integrated over time. This allows the MPS to trip the beam immediately when a loss is over threshold, or to infer whether an integrated signal fault would be mitigated by lowering the beam rate.

Protection ion chambers (PICs) have been widely used at SLAC as MPS devices. They consist of a gas-filled can with a high-voltage electrode that draws current when struck by ionizing radiation. They are most often placed near collimators to detect beam losses that indicate an excursion in beam position or energy that may cause a problem further downstream if left unchecked. Cerenkov Detectors, called beam loss monitors (BLMs) at SLAC, are highly sensitive detectors that are positioned near the LCLS-II undulators, which can be damaged by a beam strike. The Panofsky Long Ion Chamber (PLIC) is used for detecting losses along extended beam lines where there are no discrete monitors installed. The amplitude of the loss pulse is measured within a timing gate with a gate length set to match the propagation time along the length of cable. This detector can provide both a measure of total loss along the cable length, and the location(s) of the loss.

The signals from these detectors are digitized and processed by the FPGA of an MPS Link Node (see Section 10.11.1 Machine Protection System). A QADC with a sampling rate of at least 250 MHz is required to digitize the waveform and produce diagnostic quality data.

10.4.1.5 Wire Scanner

The LCLS-II wire scanner system is the main diagnostic for projected beam size measurements of the high brightness electron beam for most of the accelerator. The wire scanner system consists of a linear motor driving a wire card with x, y and 45° wires. A 1 µm position encoder is attached to the linear motor and the waveform is digitized through a quadrature counter. Fast ion chambers and photomultiplier tubes (PMTs) are used for beam loss detection. A QADC is required to digitize the waveform. Depending on operating conditions and wire scanner location, the allowable beam rate for scans shall be between 10 Hz and 0.6 MHz.

During commissioning and rate changes, the electron beam will be delivered in a bunch train mode with variable duty cycle and full rate during the macro pulse and a much lower rate for the macro pulses. The motion control software will be capable of triggering the wire motion to enable interception of the beam with the wire during the time of the macro pulse.

10.4.2 Image Acquisition

Profile monitor images are gathered from insertable fluorescent yttrium aluminum garnet (YAG) crystals or optical transition radiation (OTR) screens. Light generated by these screens are directed to a vacuum window where a CCD camera is mounted. The YAG/OTR images are acquired at a reduced repetition rate, up to 120 Hz (The 1 MHz repetition rate is not supported by the profile monitor system). The x-band transverse cavity (XTCAV) profile monitor system at LCLS already performs at 120 Hz rate. The XTCAV installation is the basis for the LCLS-II profile monitor system, which be a similar system with improvements in the architecture.

10.5 Magnet Power Supply Controls

The LCLS-II magnet power supply systems will provide controllable, precise and stable excitation current to dipole, quadrupole, solenoid, corrector and kickers to generate the magnetic field required to steer the electron beam from the injector to the electron beam dump. The electron beam requires very tight magnetic field stability tolerances, which translates directly to current stability for the power supplies. The power supply design will be nearly identical to that of LCLS, which has proven stability performance. The user interface will be the same as at LCLS. The magnet control functions will include: trim, perturb, standardize, degauss, turn on power, turn off power and reset faults.

10.5.1 Power Supply Designs

The magnet power supply systems will be nearly identical to the LCLS design. Power supply types fall into four main categories: intermediate, trim type, bulk and high voltage modulator.

The power supply type for each magnet is selected based on the current and tolerance requirements. Refer to Chapter 5 for more detail.

10.5.2 Power Supply Controls

The LCLS-II power supply controls architecture system will largely use the same design as LCLS. The main difference in LCLS-II will be the interface to some of the power supply hardware, which include

- An upgrade in the low current power supply (trim type) slot-0 controller
- A serial links to the control that will be used monitor bulk power supplies
- An industrial PC with event receiver (EVR) to provide triggers for pulsed magnet power supplies.

The interface to the intermediate power supplies, an Ethernet power supply controller, will remain unchanged (Figure 10-6).

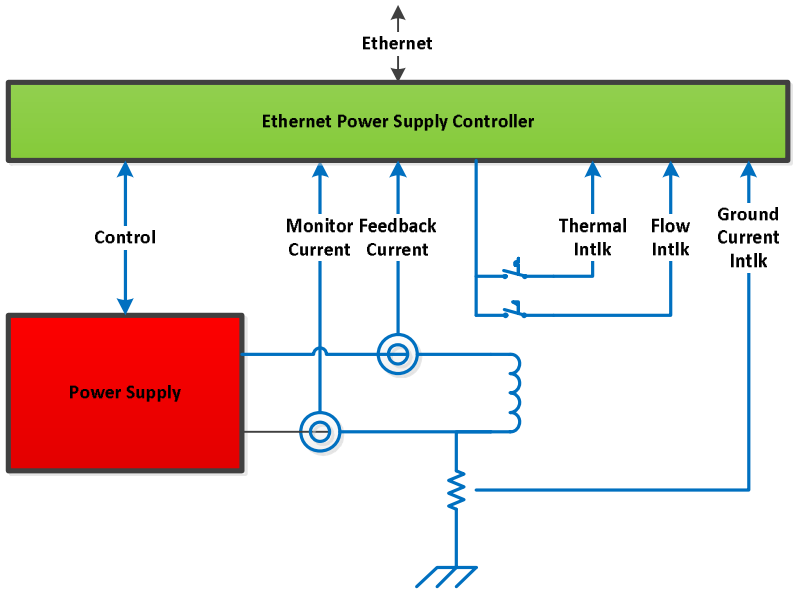

Figure 10-5 Intermediate power supply diagram

The low current power supply (trim type) MCOR system will use an upgraded slot-0 controller with an embedded PC, onboard digital and analog I/O and EVR, providing a timestamp with pulse ID and input triggers (**Error! Reference source not found.**). No output triggers will be available. The EMCOR slot-0 controller replaces the VME system used in LCLS for magnet power supply controls. The embedded CPU will run real-time Linux rather than the RTEM operating system. With a CPU on the slot-0 controller, signals available only off the backplane are now accessible. These signals include feedback current and fault status per channel as well as a crate-wide fault reset and MCOR crate voltages. The digital input signals will be used for

magnet interlock status, such as water flow and temperature faults, which in LCLS came from a PLC for low current trim type supplies.

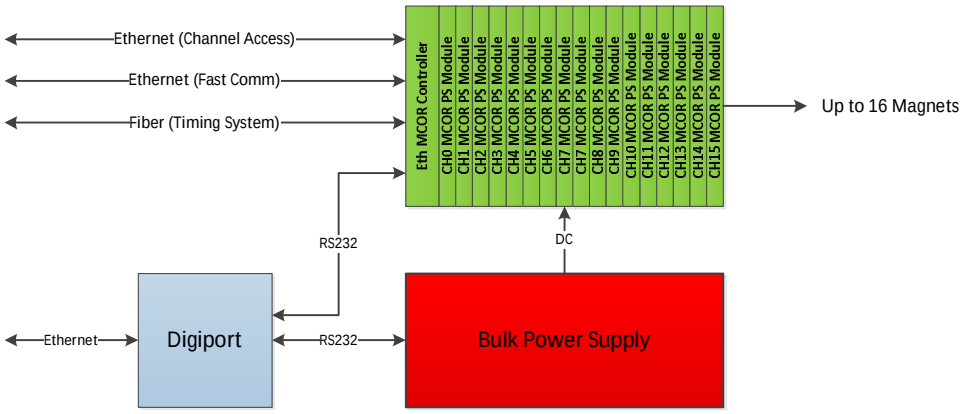

Figure 10-6 Trim type and bulk power supply diagram

The bulk power supplies used to provide power to the MCOR system will be monitored and controlled over a serial link, whereas LCLS used a programmable logic controller (PLC) with analog and digital I/O cards to turn on and off the supply ramp and monitor voltage, ground current and digital status.

The magnet power supply control system uses PLCs to monitor and control pulsed magnet power supplies (Figure 10-7). An EPICS soft IOC, running real-time Linux on an industrial PC, communicates over Ethernet to the PLC, which monitors the power supply voltage, current, and digital status, and performs control functions upon request. The control functions available to the users are turning on and off the high voltage power, setting the output current, and clearing software-latched interlock faults once the fault has been resolved. An EVR installed in the PC is used to provide output triggers to the modulator and to timestamp the data, which are collected once a second.

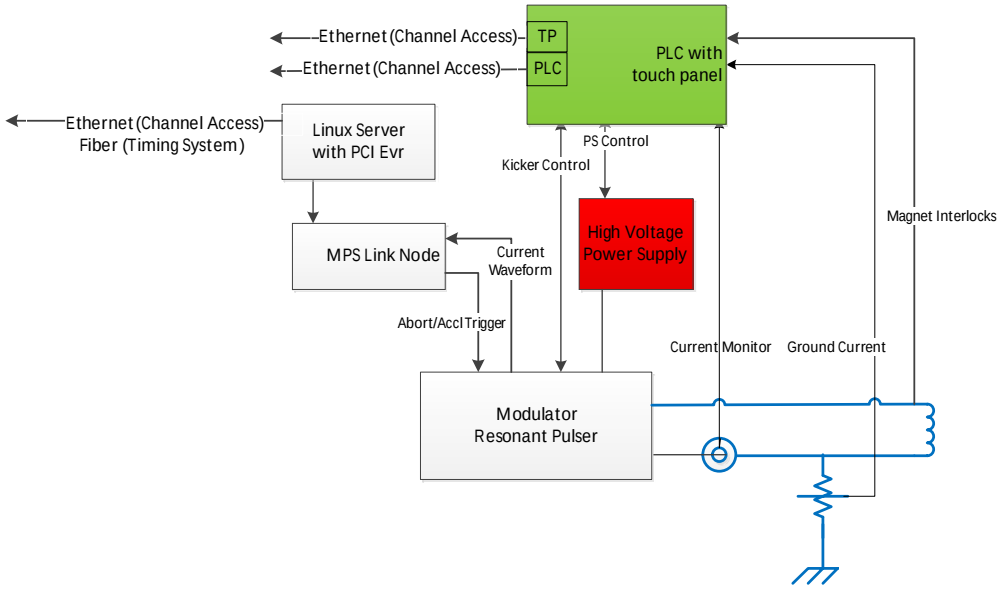

Figure 10-7 Pulsed power supply diagram

10.6 RF Controls, Low Level RF and Feedback

The low level RF (LLRF) system works to regulate the power couplings, RF field vector (amplitude and phase), and resonant frequencies of the superconducting cavities. The systems interface with the global phase/timing distribution system and the machine protection system, and include interlocks to protect the cavities. The linac will consist of four accelerating sections: L0, L1, L2 and L3. In all linac sections each cavity is powered by an individual solid state amplifier (SSA). The LLRF is structured around a four-cavity and SSA group that is described in detail in the following sections. In addition, there is a harmonic linearizer section composed of two cryomodules with eight 3.9 GHz superconducting cavities. Each of these cavities will be powered by its own klystron and controlled by LLRF stations set up the same as the 1.3 GHz sections. **Error! Reference source not found.** shows a block diagram of the installed LLRF systems. Reference and timing signal distribution is discussed in the *Phase Reference Requirements Document*, LCLSII-2.7-PR-0213

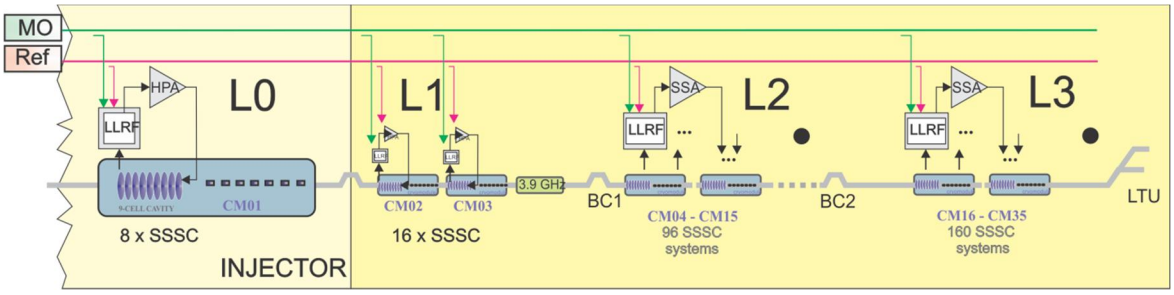

Figure 10-8 Schematic of the LCLS-II LLRF systems

The cavity field control specifications are determined by the beam qualities needed for the FEL. The amount and complexity of the field control are determined by the cavities and the environment in which they reside. The cavity and cryomodule parameters important for LLRF control are listed in Table 10-5.

Table 10-5 Cavity and Cryomodule Parameters

RF frequency	f_{RF}	1.3	GHz
Average RF gradient (powered cavities only)	E_{acc}	16	MV/m
Average electron current in linac	I_{av}	0.01–0.3	mA
Mean cavity quality factor (loaded)	Q_L	$4x10^7$	
RF power per cavity (average)	P_{cav}	3.8	kW
RMS. Microphonic Detuning		1.5	Hz
Peak Microphonic Detuning		10	Hz
Lorentz Detuning Coefficient		1.5	
RF phase of L1 linac	φ_1	-22.0	deg
RF phase of 3.9 GHz	$\varphi_{3.9}$	-160?	deg
RF phase of L2 linac	φ_2	-28.0	deg
RF phase of L3 linac	φ_3	0.0	deg

The phase and amplitude stability requirements for the cavities in L0, L1, L2, L3 and the 3.9 GHz cryomodules are shown in **Error! Reference source not found.**. The "close in"" field stability requirements (1 Hz to 100 kHz), are close to the state of the art but have been demonstrated at other laboratories (CEBAF and Cornell). An advantage of the single-source cavity control is that most driving noise terms are expected to be uncorrelated. Drifts below 1 Hz and slow field control errors will be adjusted by beam-based feedback. In addition, the LLRF system must support the precise timing/jitter requirements for the electron beam and the system will be closely coupled with the timing and synchronization system.

Table 10-6 Cavity Field Regulation Requirements

		Field Control without Beam Based Feedback Or 1 Hz High-pass		**Field Control Drift with Beam Based Feedback 1 Hz Low-pass**			
Parameter (rms)	**Symbol**	**Uncorrelated Errors**	**Correlated Errors**	**Uncorrelated Errors**	**Correlated Errors**	**N Cavities**	**Unit**
RF phase error in L0	$\Delta\varphi_0$	0.040	0.015	14	5**	7	deg L

RF phase error in L1	$\Delta\varphi_1$	0.039	0.010	14	5	15	deg L
RF phase error in 3.9 Ghz	$\Delta\varphi_H$	0.039	0.010	14	5	15	deg C
RF phase error in L2	$\Delta\varphi_2$	0.095	0.010	14	5	90	deg L
RF phase error in L3	$\Delta\varphi_3$	1.8	0.150	28	10	150	deg L
RF amplitude error in L0	$\Delta V_0/V_0$	0.026	0.010	***	***	7	%
RF amplitude error in L1	$\Delta V_1/V_1$	0.039	0.010	14	5	15	%
RF amplitude error in 3.9 GHz	$\Delta V_H/V_H$	0.039	0.010	14	5	15	%
RF amplitude error in L2	$\Delta V_2/V_2$	0.095	0.010	14	5	90	%
RF amplitude error in L3	$\Delta V_3/V_3$	0.12	0.010	28	10	150	%
Drive laser timing error on cathode	Δt_c	0.31	0.31	-	10?		ps

Because of the relatively high Q_L for matched cavities in LCLS-II, the cavity bandwidth approaches the microphonic detuning bandwidth of about 1.5 Hz rms and 10 Hz peak. The resulting large phase and amplitude variation of the cavity RF fields requires active feedback to maintain required stability. The effects of microphonics on field stability can be greatly reduced using RF electronic feedback, as demonstrated at CEBAF, Cornell and HZB, as long as the dynamic RF power headroom permits. In addition a fast piezo tuner (PZT) will be used on each cavity to control slow drifts and partially compensate the microphonic detuning. Tests at FNAL and HZB on long pulse and CW operation have demonstrated that cavity fields can be controlled close to the LCLS-II specification, albeit with different cavity and cryomodule configurations [1,2].

An additional challenge to cavity control is detuning due to the Lorentz force generated by the RF field. The cavity resonant frequency detunes by many cavity bandwidths as the electromagnetic force of the RF fields distort the cavity during turn on and fault recovery. A self-excited loop algorithm, in which the RF drive frequency is controlled to match the cavity resonant frequency, is used to maintain control of the cavity fields in these circumstances.

The LLRF system will be adaptable and easy to program, and will be able to quickly provide information and data, serve as a seamless interface to the EPICS global control system, and download digital firmware through the network. It will support cavity quench detection, beam-

based feedback and beam-based calibration. Calibration coefficients will be maintained both within the RF station and on the network. LLRF systems and cryomodule commissioning will be an integrated activity; each LLRF station will be programed to support Q_L and Q_o measurements, including calorimetry, and will provide local analog outputs for diagnostics and trouble shooting.

10.6.1 RF Control Stations

The LLRF system contains a number of subsystems, including cavity field control, resonance control (stepper tuner and PZT), and cavity/cryomodule interlocks. Peripheral subsystems such as cryomodule heaters and vacuum system may also be included.

10.6.1.1 Single Source Single Cavity Control (SSSC)

The technology for single-source systems has been demonstrated at CW SC linacs, most notably CEBAF [3]. The field control system maintains the cavity field through electronic feedback, typically a proportional-integral-derivative control algorithm. **Error! Reference source not found.** shows a block diagram of four LLRF stations, featuring single source single cavity control. The RF signals are converted down from 1.3 GHz or 3.9 GHz to an intermediate frequency (IF), ~ 20 MHz. The IF is digitized using a technique known as "near" IQ sampling. This technique has the benefits of removing ADC non-linearities and simplifying the reference system by using the local oscillator as the clock reference [4]. In order to enhance cavity field probe isolation and minimize drift, a set of four cavity probe signals are digitized along with the reference information in a precision receiver. The probe signal is then optically transported to the LLRF stations. Similarly, in the LLRF stations, the reflected and forward-power signals and "loop back" drive signals are digitized. FPGAs perform the signal processing and control algorithms. The power amplifier drive signal is converted to the IF frequency using a single DAC, and then the IF is converted back to RF (1.3 GHz or 3.9 GHz) using a mixer and image rejection filter. The cavity's resonance control algorithm (stepper motor and PZT) is also embedded in the LLRF FPGA.

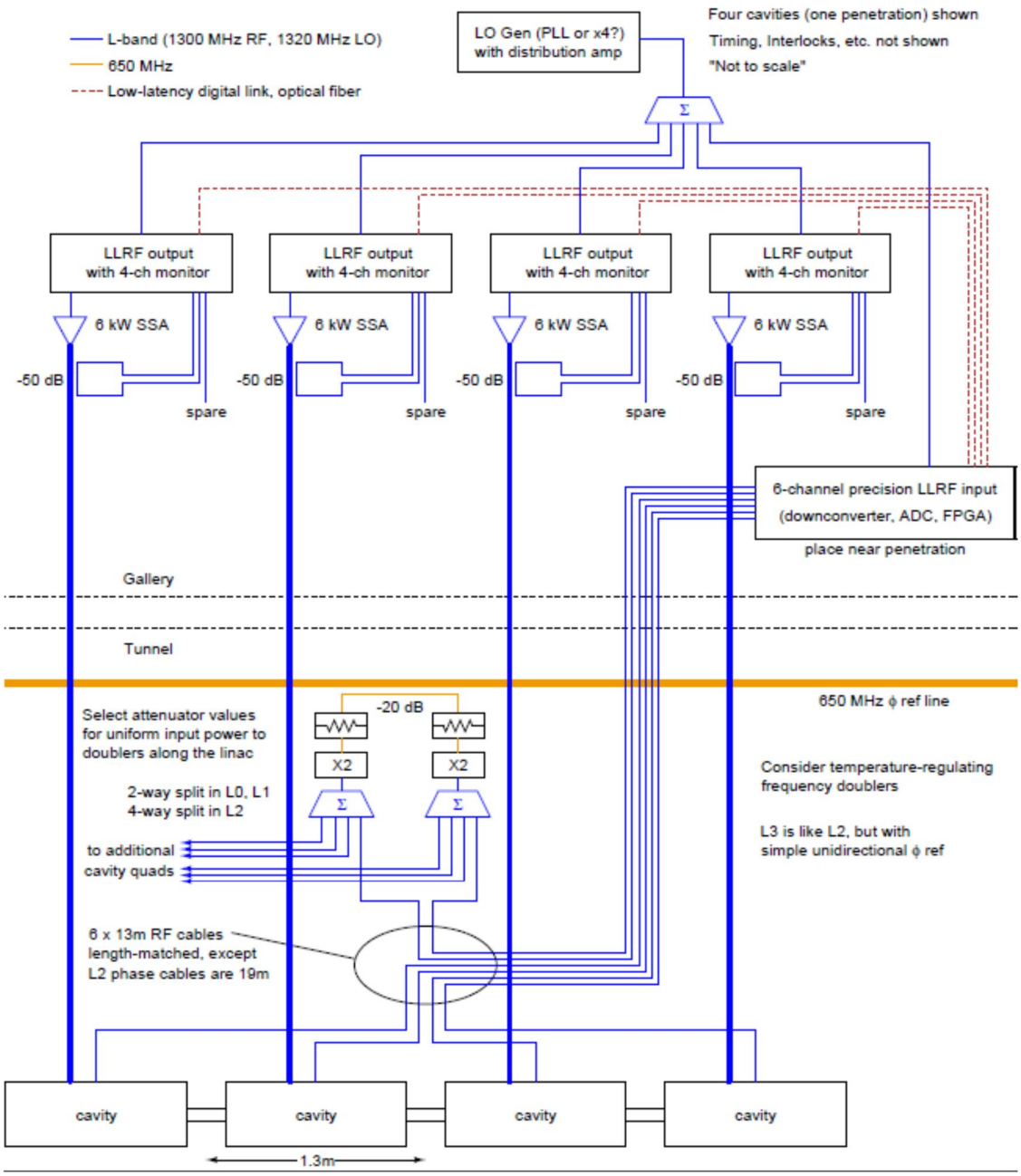

Figure 10-9 Block diagram of LLRF system showing four RF stations and the precision field probe receiver

10.6.2 3.9 GHz LLRF Systems

The LCLS-II linac will include two cryomodules of eight 3.9 GHz cavities each. The cavities will be operated under single-source, single-cavity control, similar to the process for the 1.3 GHz cavities.

Table 10-7 shows the important parameters for RF control of the 3.9 GHz cavities.

Table 10-7 3.9 GHz Cryomodule parameters

RF frequency	**3.9**	**GHz**
Total voltage available (16 cavities)	80	MV
Average operating gradient	14.5	MV/m
Coarse (slow) tuner range	750	kHz
Fine (fast) tuner range	~1	kHz
Lorentz detuning	≤0.6	$Hz/(MV/m)^2$
Number of cryomodules	2	-
Number of cavities per CM	8	-
Peak detune (with piezo tuner control)	30	Hz
Required cavity field amplitude stability†	0.01	% (rms)
Required cavity field phase stability†	0.01	deg (rms)
Q_{ext}	2.2×10^7	-
RF beam power per cavity (@300 μA load)	1.5	kW
RF power needed per cavity	1.0	kW

Field phase and amplitude stability requirements and LLRF systems will be similar to those of the 1.3 GHz cavities, with four times the sensitivity because the specifications are at 3.9 GHz. It is important that the 3.9 GHzsystems are not operated on-crest or 180 degrees out, but on-slope, thereby increasing the phase sensitivity.

10.6.3 Resonance Control

Cavity resonant frequency control is provided by a slow/coarse stepper motor and fast/fine piezo tuner (PZT). The stepper controller will consist of a chassis with eight stepper drivers. The PZT controller will be an eight channel amplifier. Communication with the cavity field control will be through a dedicated fiber link. Each LLRF station must process the individual cavity field and forward power signals to determine its detuning angle. An algorithm then determines a control signal to apply to the PZT (or stepper controller) to keep the cavity close to the reference frequency. This is critical for operations because of the very high Q_L of the cavities and the small power overhead of the SSAs. The controller and amplifier small signal bandwidth needed for resonance control needs to be ~400 Hz.

10.6.4 Cryomodule Interlocks

Table 10.1 shows the cryomodule and cavity interlocks for the LCLS-II cryomodule and the speed with which the RF must turn off to protect the machine.

Table 10.1 Cryomodule Interlocks

Interlock	RF Turn Off
Coupler arc	< 100 μs
Coupler Temperature	< 100 ms
Coupler e- pickup	< 100 μs
Coupler vacuum	< 1 ms
Beamline vacuum	< 1 ms
Quench	< 100 μs
He level	< 1 s
He pressure	< 1 s
Stepper Temperature	< 100 ms

10.7 Undulator Controls

The variable gap undulators will require an expansion and modification of the LCLS undulator control. The details of motor control for adjusting the undulators will be different from that used in LCLS, but the scope of the work is equivalent.

10.7.1 Undulator Motion Control

The LCLS-II undulator motion controls involve controlling the motion of the variable gap undulators, the interspace phase shifter, and the position of the interspace girders (Figure 10-10).

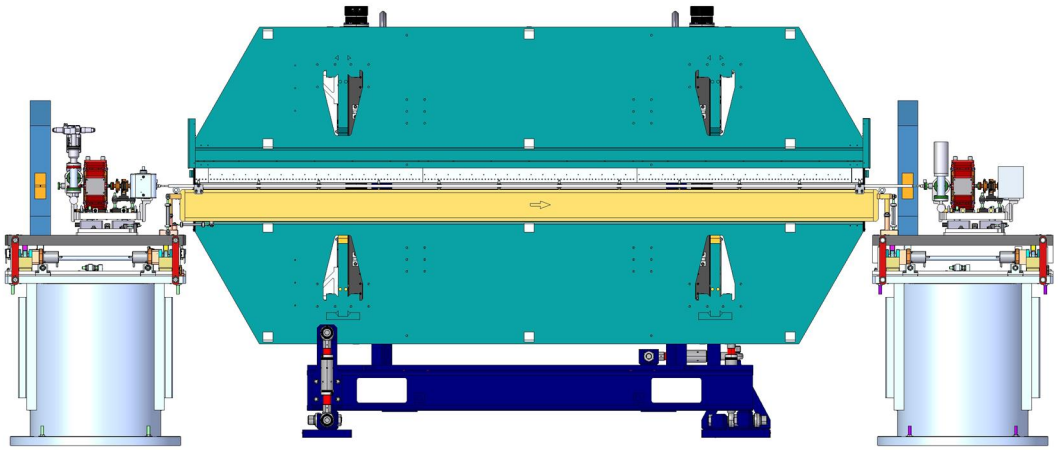

Figure 10-10 LCLS-II Undulator motion control components

The variable gap undulators use four motors and two position encoders to adjust their gap. The system uses end of travel and pitch limit switches. The system also uses linear position transducers between each undulator jaw and the undulator vacuum chamber. Finally, there are emergency stop buttons for the undulators.

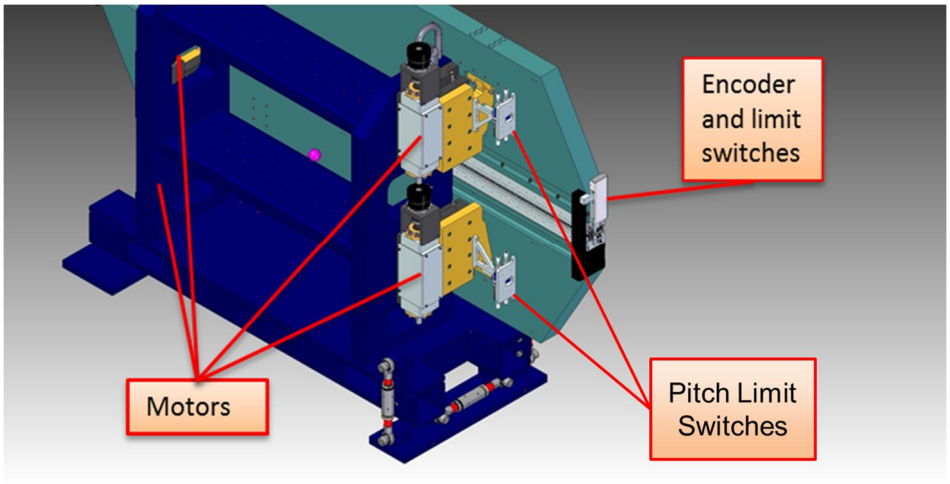

Figure 10-11 Variable Gap Undulator Motion Control Components (Vacuum chamber position transducers, emergency stop buttons not shown)

The interspace girders are adjusted using five cam motors, with position readback provided by 6 linear potentiometers and 5 rotary potentiometers.

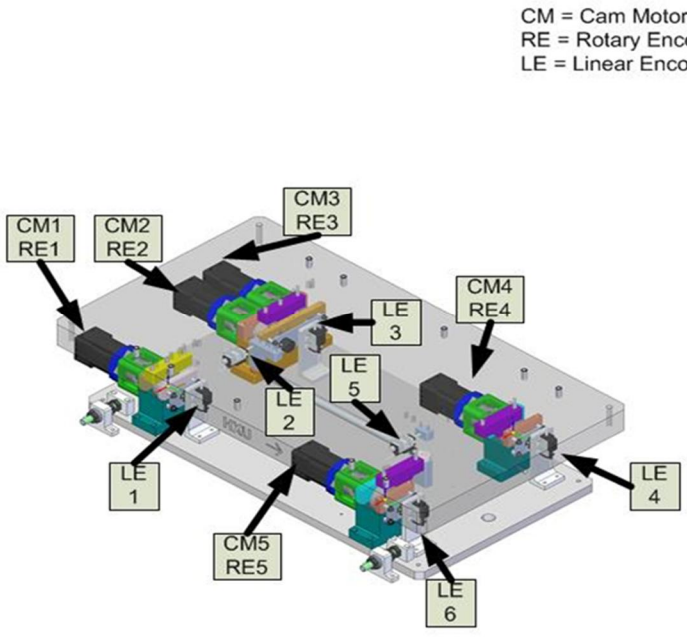

Figure 10-12 Interspace girder motion components

The interspace phase shifter motion components include a servo motor, absolute linear encoder and two limit switches.

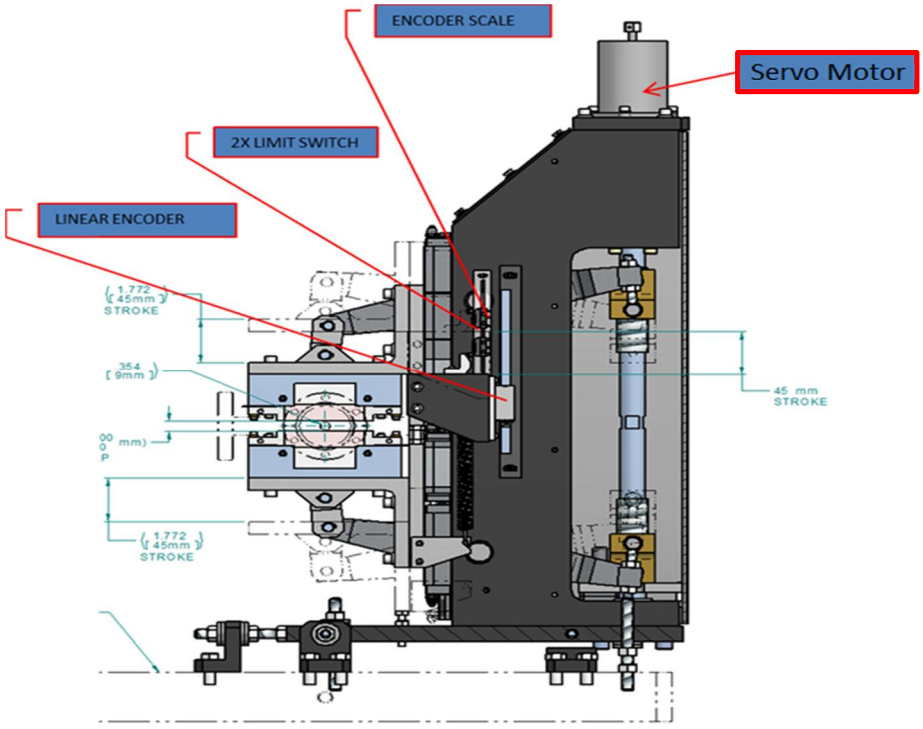

Figure 10-13 Phase Shifter Motion Control Components (Figure does not depict the final phase shifter design – mechanical components shown for reference only)

The controls for each undulator and interspace will be integrated into the EPICS control system. A temperature monitoring system will also be integrated into each undulator control chassis, which connects to sensors mounted on the undulator and interspace. An overview of the undulator controls architecture is shown in Figure 10-14

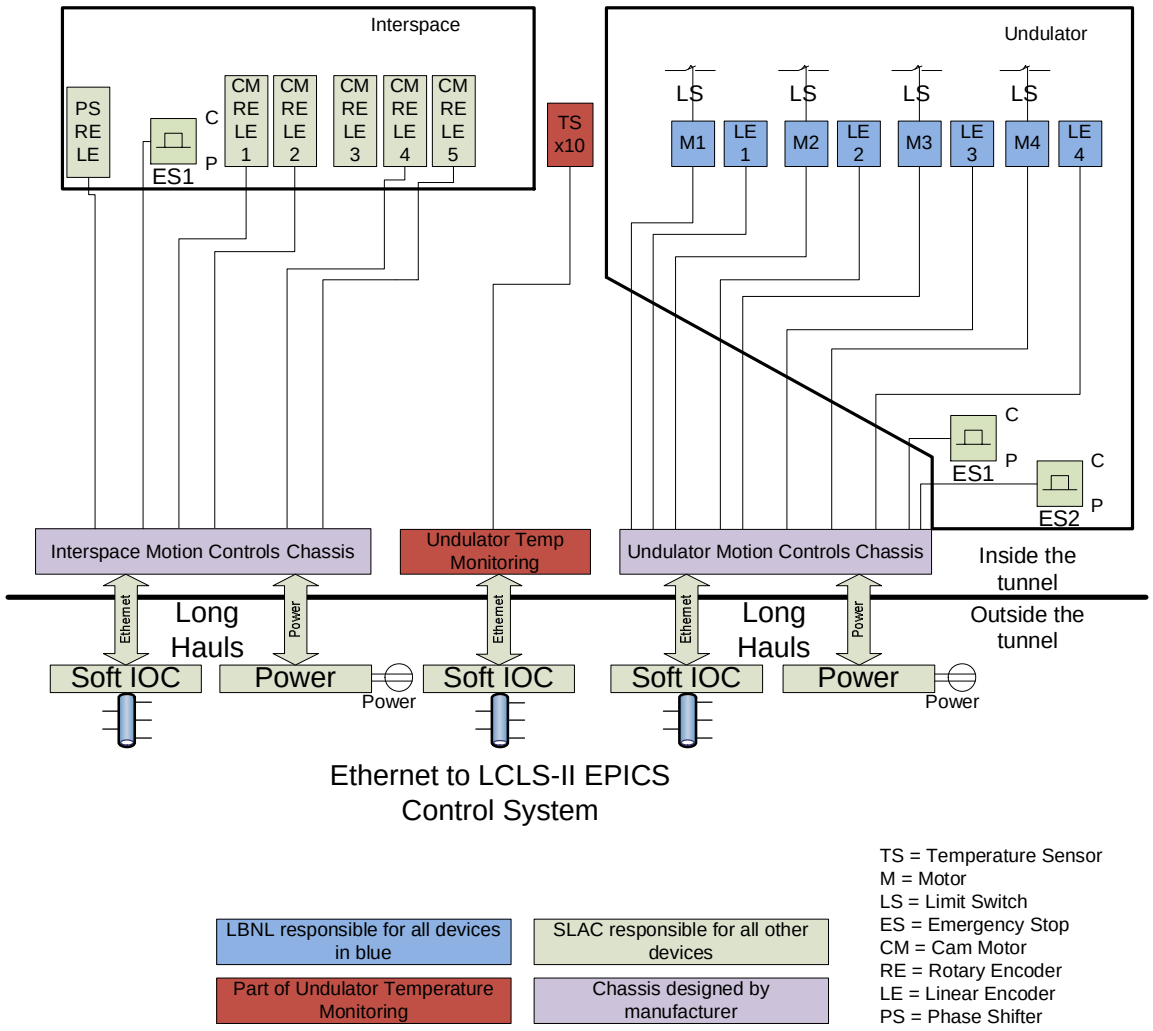

Figure 10-14 Undulator control system diagram

10.7.2 Undulator Temperature Monitoring

The temperature of each undulator segment must be monitored redundantly. The temperature monitoring must provide 0.1 °C accuracy and 0.05 °C resolution. The LCLS-II undulator temperature monitoring system will provide ten temperature sensors for each undulator and interspace cell. The location of the sensors is defined in the Undulator Engineering Specifications Document.

10.8 Beamline Instrumentation and Controls

The remaining beamline instrumentation and controls are described in the following sections. These include major subsystems such as the laser control system, cryogenic systems controls, and vacuum controls.

10.8.1 Laser Control Systems

The LCLS-II Injector laser system will largely use the same proven design in use at LCLS. The main difference is that LCLS-II will use separate oscillators for the drive laser and heater laser instead of deriving the heater IR off of the frequency doubling process used by the drive laser. Additionally, due to the high repetition rate of the beam, an acousto-optic modulator will serve as a fast shut-off, rather than the Pockels cell used in LCLS.

10.8.1.1 Laser Controls Architecture

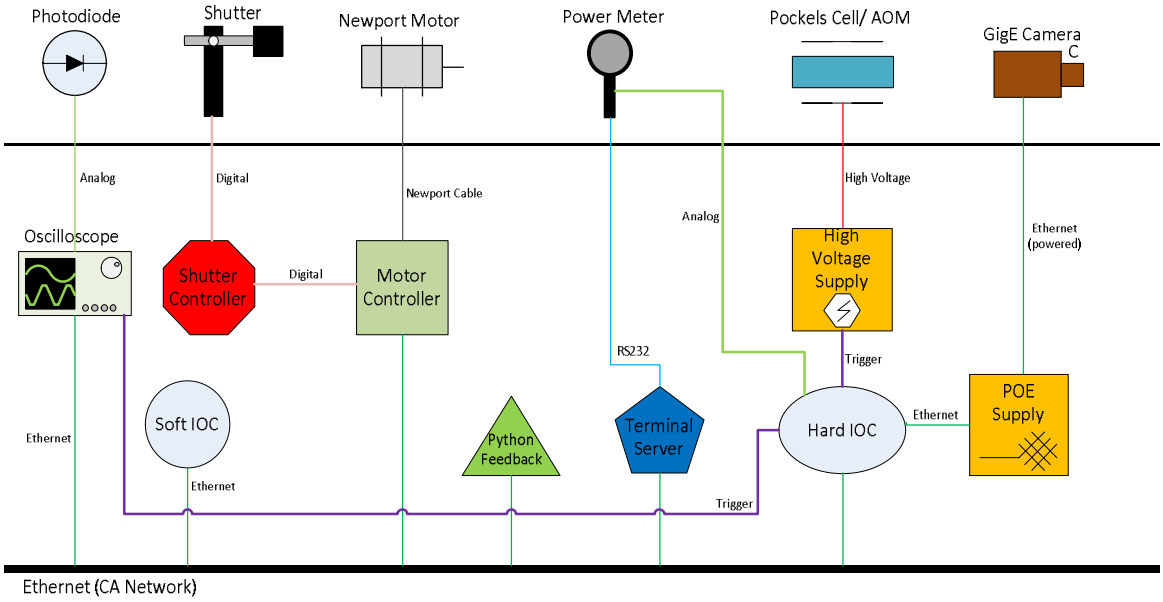

Figure 10-15 Laser Controls Architecture

The laser system will have controls for a variety of beam diagnostic devices for measuring and controlling the laser properties (position steering, timing, power measurements, etc.). Controls will be managed by a combination of hardware- and software-based (IOCs) running EPICS. The EPICS control system will communicate with cameras, motor controllers, and oscilloscopes via Ethernet, and will communicate serially with power meters and frequency counters using a terminal server. In addition, devices such as diodes, power meters, and shutters will use direct analog and/or digital signals into the Hard IOC for read back and control. Timing information will be provided by an EVR in the hardware-based IOC.

Controls will have similar features to those at LCLS, including operator interfaces, configuration save/compare/restore, data history, alarms and beam-synchronous data for power meters.

10.8.2 Vacuum Control System

The LCLS-II vacuum controls will use the same proven design used at LCLS. The LCLS vacuum system can be separated into two parts: mechanical vacuum devices and controls vacuum devices. Mechanical devices are those that are physically part of the beamline or waveguide: vacuum valves, vacuum gauges, and vacuum pumps. Controls devices are the remaining

hardware needed to build a complete vacuum system: controllers for the vacuum valves, gauges, and pumps; devices used to perform interlocking functions; and the vacuum portion of the EPICS control system.

The vacuum control system will automatically close vacuum valves in order to isolate beamline regions where vacuum pressures exceed allowable limits. Users will be able to modify allowable pressure limits, with capabilities for user bypasses should hardware become faulty. The system will report valve obstructions to the MPS in order to prevent beam from damaging vacuum equipment. The vacuum controls will have interlocks associated with the RF waveguides and will shut off klystron modulators when pressure thresholds are exceeded.

10.8.2.1 Vacuum Controls Architecture

The vacuum control system (**Error! Reference source not found.**) uses PLCs to monitor and control vacuum devices and to perform interlocking functions. An EPICS soft IOC performs auxiliary control functions and provides an interface to the LCLS global control system.

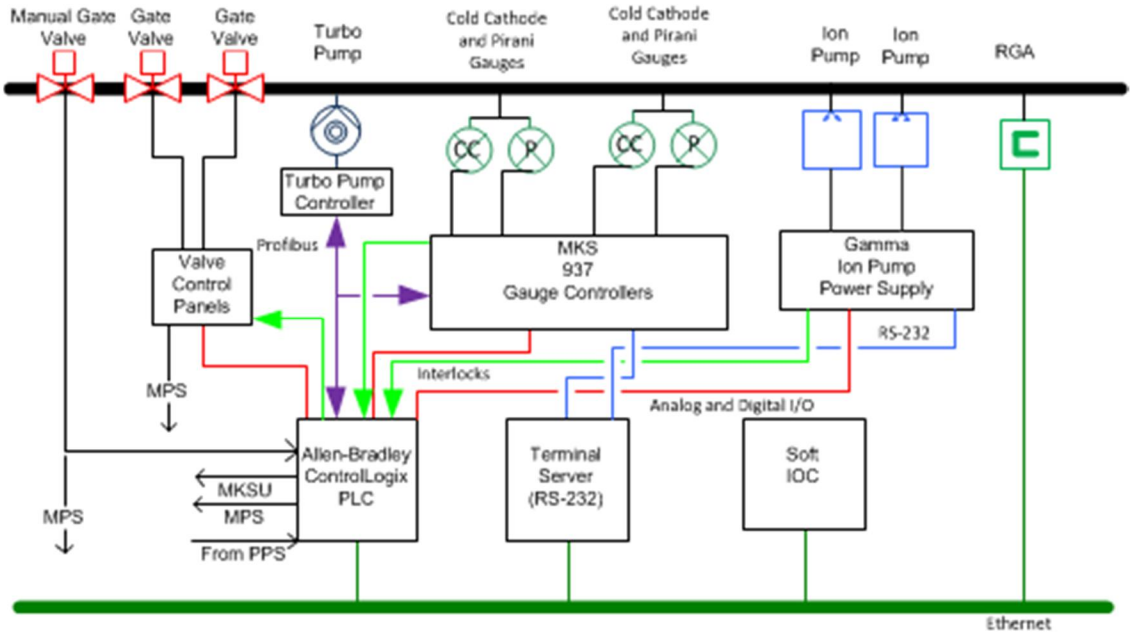

Figure 10-16 Block diagram of vacuum controls hardware

The IOC supervises the PLC, which enforces interlock functions. The vacuum PLC serves two purposes: it is the primary control system interface for status and control of vacuum controllers, and it performs vacuum interlock functions. The PLC communicates to the controllers using 24 V digital, 0-10 V analog signals, and Profibus. The PLC communicates to the EPICS control system via EtherNet/IP, an Ethernet industrial protocol. The soft IOC, a Linux process running on a centrally managed server, communicates with vacuum devices in two ways: 1) the IOC sends commands to and receives status from the PLC over the Ethernet using the EPICS Ether-IP driver and 2) the IOC communicates with some vacuum controllers via RS-232 serial links.

10.8.3 Cryogenic Control System

Cryogenic systems include three main subsystems: the cryogenic plant, the cryogenic distribution system and insulating vacuum, and the cryogenic modules.

The cryogenic plant will be delivered to SLAC with a dedicated PLC-based control system that can be fully controlled by local user interface panels. An EPICS controls system interface to the plant will be developed that will allow operators in the Cryogenics Control Room and the Main Control Center to control and monitor the cryogenic systems. The EPICS interface will be similar to that of the vacuum systems, with EPICS soft IOCs communicating with the PLCs via EtherNet/IP.

The cryogenic distribution system, insulating vacuum and cryogenic modules will also have a dedicated PLC-based control system, implemented at SLAC. The cryogenic distribution control system architecture is shown in **Error! Reference source not found.**.

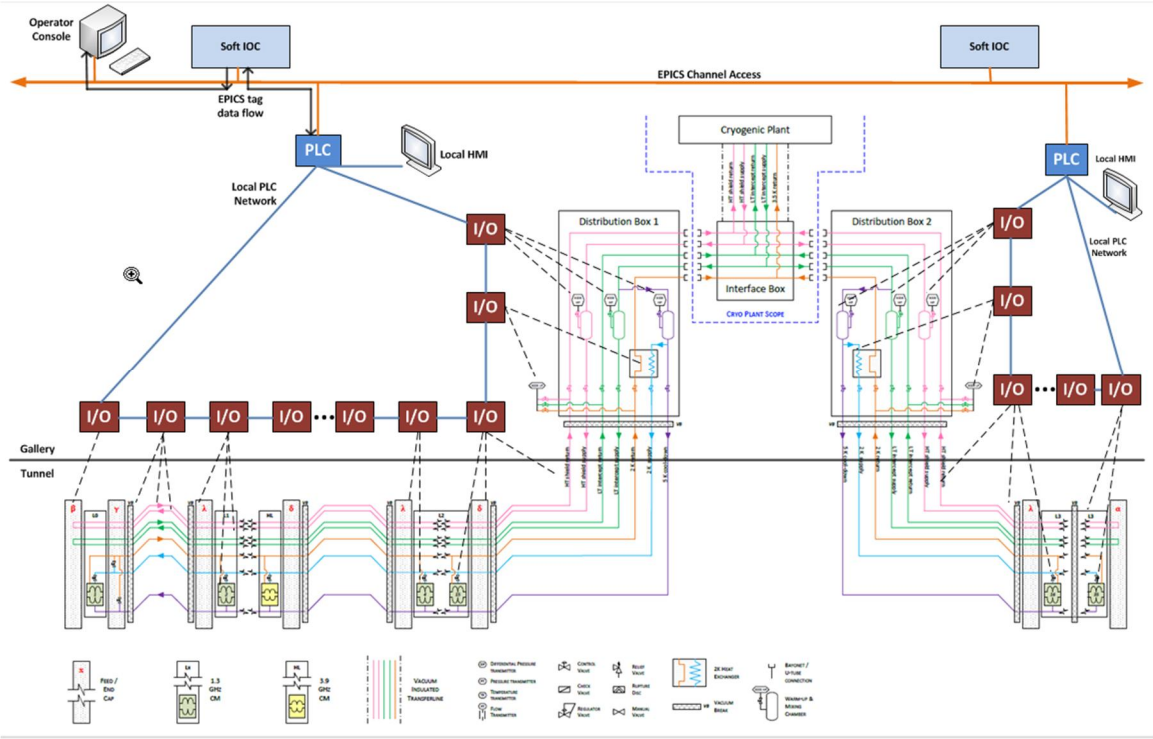

Figure 10-17 Cryogenic distribution control system block diagram

The cryogenic distribution is comprised of two sections, one upstream and one downstream of the cryoplant. These include a distribution box, a string of cryomodules, feed caps, bypasses, and an end cap. Each string will be individually controlled by a dedicated PLC. The control signals for the distribution system, insulating vacuum and cryomodules in each string are combined and serviced geographically by PLC I/O distributed along the gallery. As with the cryogenic plant, the distribution system and cryomodule control will include local control panels and an EPICS interface available to the Cryoplant Control Room and the Main Control Center.

10.8.4 Basic Motion Controls

Basic motion control for collimators and movable beamlines will be implemented with LCLS designs as much as possible. Motion control designs will limit accelerator tunnel hardware as much as possible to limit controller exposure to damaging radiation. Motor control will be handled by the same Aerotech Ensemble motion controllers used in the undulator system. LVDT signals will be converted by Daytronic 5M30 LVDT Conditioners for feedback.

Motion controls for wire scanners will be implemented with a new design, which decreases wire jitter and allows for increased scan speeds compared to the LCLS design. With the expected higher beam rate, it is important to carefully limit the time that the wire is within the beam. The wire position and speed will be reported to the machine protection system in order to prevent damage from the electron beam. See section 10.4.1.5 for more details on the wire scanner design.

10.8.5 Temperature Monitoring

Standard PLC industrial temperature monitor hardware will be used to monitor accelerator components. Resistance temperature detectors are the preferred sensors due to their increased accuracy over traditional thermocouples. Where necessary, temperature signals will be interlocked to the MPS to protect hardware from beam-induced temperature damage.

10.8.6 Controls System Interface to Conventional Facilities

The LCLS-II facilities controls is based on the same system deployed in LCLS. The facilities controls have three parts: facilities distributed control system, facilities HVAC system, and facilities EPICS interface (See Chapter 11). The hardware and primary control will be handled by the facilities HVAC and facilities distributed control systems. The EPICS controls interface will have read access to most of the system and in some cases have write access to facilities controls set points. The EPICS interface to the facilities control system will be based on standard PLC industrial protocols, such as EtherNet/IP, BACnet, and ModBus TCP/IP.

10.9 Controls Software

The software to operate the entire accelerator will mostly be based on the successful three-layer LCLS model. The basic low-level device control uses the distributed EPICS control system software, and standard EPICS clients to provide functionality for operator interfaces, IOC management and data archiving. High- level control of the accelerator has been implemented at LCLS, mostly using Java and MATLAB. A similar implementation is planned for LCLS-II, with the addition of the new functionalities of the emerging EPICS V4 services.

10.9.1 Operations Software

10.9.1.1 EPICS Software

LCLS-II will continue to use the EPICS software toolkit to host its distributed control system. It will also take advantage of some of the new service-layer application programming interfaces

(APIs) and tools becoming available in the next generation of EPICS, V4. LCLS-II will leverage the LCLS EPICS software IOC applications, EPICS modules, and EPICS client application codebases when possible and appropriate. LCLS currently has hundreds of EPICS IOCs networked together to allow communication between the IOCs and other EPICS-based client applications and to provide control and readback for machine devices. EPICS IOCs execute various I/O and local control tasks by setting, reading, and performing calculation with PVs. "Hard" VME or µTCA-based IOCs perform most of the lowest-level digital and analog I/O to accelerator hardware systems by converting set point PVs into analog or digital input that the hardware accepts and, conversely, by converting analog or digital read backs from the hardware into standard-format PVs. Process variables can be set or read back by any IOC or other EPICS client applications using the Channel Access network protocol.

The "soft" IOCs, hosted on Linux server machines, typically do not perform direct device I/O to accelerator hardware and contain standard EPICS IOC software. Additional operator workstations and servers provide higher level control and operator interfaces to the systems, as well as performing data logging, archiving, and analysis. LCLS is approaching 2 million PVs, a large number of which are being archived via the new EPICS archive appliance developed at SLAC.

10.9.1.2 EPICS Client Application Tools

LCLS Operations uses many EPICS Channel Access clients as well as SLAC-specific EPICS multi-facility client tools (Table 10-8). LCLS-II will utilize the same or enhanced applications, when appropriate.

Table 10-8 EPICS Tools used at LCLS

Category	Name
Display manager	LCLS-II will augment EDM for rapid development of control system graphical user interfaces (GUIs). A next generation of the manager is under evaluation.
Channel access gateways	Provides access security, name translation, and one connection from many clients to one server. An enhancement is planned to add more features required by EPICS applications.
Electronic logbooks	For operators, physicists and engineers
Machine state and analysis	Bumpless IOC reboot facility – auto-save
	Machine snapshot facility – save/compare/restore configurations.
	Archive appliance (up to millions of PVs) and archive viewers
	Message logging and message log viewer
	Alarm handling and alarm viewer
	Orbit display
	MPS status and history

Category	Name
	Strip tool and other PV diagnostic tools
	PV directory service
	Timing configurations
Model based applications	Model manager
	Linac energy manager
	Steering
Feedback framework	Slow transverse and 120Hz longitudinal feedback loops
	Fast 1 MHz beam-based feedback
MATLAB applications and toolkit	Support for physics group applications

10.9.2 Central Database

An Oracle Relational Database (Figure 10-3) hosts several databases in support of both operations and engineering teams, including snapshots of operational set points/read backs, machine model design lattice and model-run data, the operations electronic logbook, process variable metadata, device parameters, message log data, and machine fault history. Considerable engineering resources are required for management of EPICS-generated PVs and the numerous EPICS client application configurations, which need to incorporate them. PV configuration management automation will be enhanced to support the growing demands.

10.9.3 High Level Applications

As the EPICS software layer provides the infrastructure needed for individual device control and monitoring, high-level software is required for machine operation tasks involving multiple subsystems.

Most of this extensive set of high-level applications is fairly generic and will be used for LCLS-II, as it is not specific to the particular accelerator technology and the much higher beam rate. The main Java-based applications are SCORE (machine parameter save/restore function), LEM (energy dependent machine settings), and an XAL-based online machine model linked to an Oracle database. Plans are underway to replace XAL with a MAD-based online model using the MAD input deck as a single source for accelerator modeling. Furthermore, the new capabilities of EPICS V4 services will be used to better integrate higher level accelerator diagnostics and control functions requiring a hierarchical view of the accelerator with the existing EPICS control system.

The applications written in MATLAB cover most measurement and machine tuning tasks (e.g., beam size, emittance and bunch length measurements, undulator characterizations and settings, as well as accelerator configuration changes). They are highly automated to enable reproducible and fast machine characterization and optimization. They will be adapted for future use at LCLS-II. The MATLAB toolkit contains APIs for machine control functionality, including

set-point/readback control for PVs, beam-synchronous acquisition data, and PV allocation for computed physics data.

10.10 X-ray Transport and Experiment Systems Controls

Photon Controls and Data Systems (PCDS) provides all the computing capabilities needed to operate the front end enclosure (FEE) and the LCLS instruments and to acquire and analyze the science data generated by these instruments. These three activities correspond to the three core PCDS subsystems: controls, data acquisition (DAQ), and offline analysis.

This section describes the controls and DAQ systems for new photon instruments, diagnostics and detectors that will be located in the Electron Dump, FEE, and experiment hutches. The offline storage and analysis systems are not in the scope of LCLS-II and will not be described in this document.

The core computing services for the LCLS-II photon data systems will be provided by LCLS. These include:

- Network file system servers for the user home directories, instrument operator accounts, user groups, and disk-less nodes.
- Disk and tape backups.
- Timing services, naming services, host configuration services, authentication services, web authentication, and directory database.
- Experiment database, web server, electronic logbook, system monitoring, and logging services.

A simplified diagram of the photon systems networking is shown in **Error! Reference source not found.**. Each instrument has its own controls network and its own DAQ network. Network traffic between the different networks and with the accelerator is managed by the LCLS router in the NEH server room. Only one instrument is shown. The bold lines represent Infiniband-HDR connections.

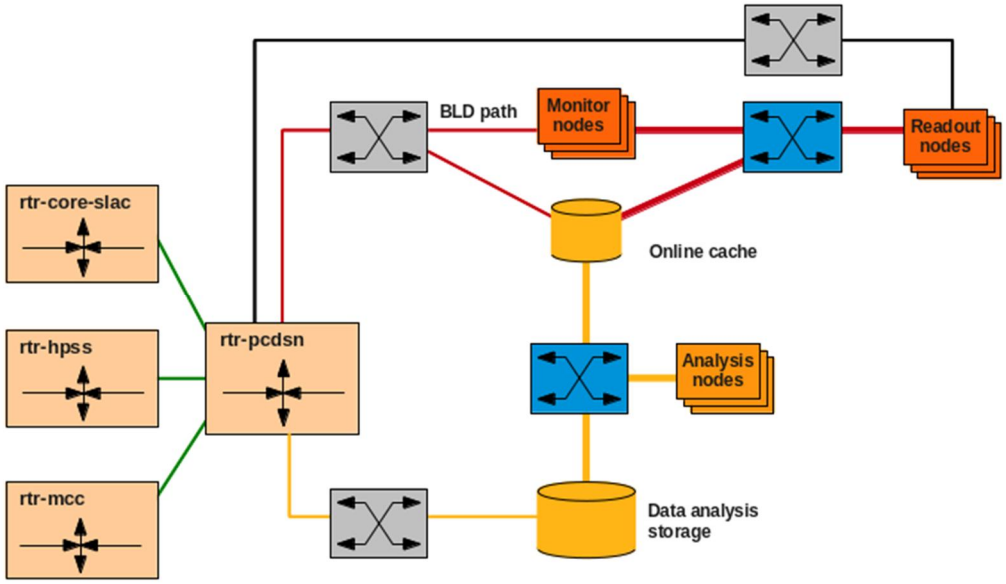

Figure 10-18 Simplified diagram of the photon systems networking, including Ethernet connections (thin lines), routers (beige boxes), IB-HDS switches (blue boxes), and layer-2 Ethernet switches (grey boxes)

10.10.1 Front End Enclosure

10.10.1.1 Instruments

FEE-II will reuse LCLS instruments where they match the requirements. Currently these include the gas energy monitors, gas and solid attenuators, spectrometers, and pop-in YAG cameras. There will be technical improvements based on LCLS experience, and where kHz-MHz readout is required (gas energy monitors and spectrometers). This incremental approach will significantly reduce engineering and cost risks.

The controls for the soft X-ray line and the hard X-ray line instruments are described in Table 10.2. Generous space will be provided for equipment racks throughout, keeping cable runs short. Thermocouples and pressure/temperature/flow transducers for nitrogen, water, and compressed air will be provided.

Table 10.2 FEE2 Instruments.

Instrument	Components	QTY SXR	QTY HXR	Comments
Slits	Motion	2	2	
Gas detector	HV; LV; pressure; gas handling; digitizer; pumping	2	2	PLC-based control 100 KHz readout
Gas attenuator	Pressure; gas handling;	1	1	PLC-based

	digitizer; pumping; motion			
Solid attenuator	Motion		1	
Flat mirrors	Motion	2	2	
K-B mirrors	Motion	1	-	
Spectrometer	Motion; 1D-Detector		1	100 KHz readout of a 1-dimensional strip detector
K-Monochromator	Motion		1	Possibly with added Piezos
Imagers	Motion; camera; illuminator	4	3	With zoom and focus lenses; 120Hz
Diagnostic chamber	Motion; detectors; vacuum	1	1	Multipurpose chamber for ad hoc use
Vacuum	Pumps/gauges/valves	1	1	PLC with EPICS monitoring

10.10.1.2 Machine Protection System

Two types of MPS inputs are foreseen for LCLS-II: fast signals (μs latency) and slow signals (ms latency). See Section 10.11.1 for details. The mitigation for photon system MPS faults is to turn off the e-beam, since there is no photon shutter that is fast enough. Photon controls will use a network of analog, digital, and position inputs, connected via EtherCat to a central PLC (one for the SXR beamline and one for the HXR beamline), to monitor the slow MPS signals and relay appropriate inputs to the MPS link-nodes. Fast signals will be input directly to the link-node. The increased beam power of the MHz machine will require water-cooling of all elements that may see beam, which includes slit blades, mirrors, YAG crystals, collimators, and stoppers). The MPS PLC will monitor a network of chilled-water flow meters and thermocouples in addition to slow valves, solenoids, position switches, and absolute encoders. The MPSs on the SXR and HXR beamlines will operate independently (wherever possible) so that a fault on one beamline does not prevent photon delivery to the other.

10.10.2 Data Acquisition

10.10.2.1 Overview

Architecture: The DAQ system will use an updated architecture based on the LCLS DAQ system. A diagram of this architecture is shown in **Error! Reference source not found.**. Each instrument will have a dedicated DAQ system with a dedicated network. Each of these systems will be built on an IB-HDR (Infiniband/high data rate) network. One or more console nodes will be installed in the control room, a set of readout nodes in the instrument hutch, and a set of data cache and monitoring nodes. The cache/monitoring nodes will be located within 10m of the readout nodes so as not to exceed the maximum practical IB range.

Data rate: The DAQ infrastructure will be scaled to accept the kHz-MHz data rate of LCLS-II. In addition to the network backbone upgrade to IB described previously, offline data storage and processing will require significant increases in both capacity and throughput.

Scope: The LCLS-II DAQ will be of sufficient capacity to read, process and monitor data from four 1-dimensional detectors (gas detectors, spectrometers, TOFs, etc.) for a total of ten

thousand elements at 100 KHz. The detector systems and DAQ system will be located in experimental hutch 1, AMO. The controls hardware currently in hutch 1 of the NEH for the AMO instrument will be relocated to accept beam from the new soft X-ray line. Four control racks will be relocated. Since the physical layout will be different, a new set of rack-to-instrument cables will be provided. The offline storage and analysis systems are not in the scope of this document.

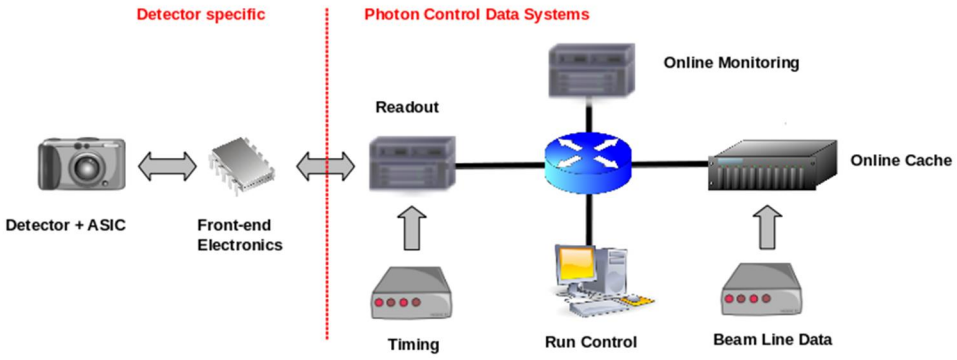

Figure 10-19 DAQ diagram: architecture of the data acquisition system

10.10.2.2 DAQ Elements

Online data cache: The data cache nodes store the components received from the different readout nodes in the local file system. These nodes form the online data cache, isolate the DAQ system from user operations and allow the experiments to take data even during outages of the offline system.

Offline data storage: The data files will be copied over high speed links from the online cache to the offline storage, where they are made available to the users for offline analysis and for offsite transfer.

Monitoring: Online monitoring is implemented by snooping on the multicast traffic between the readout nodes and the data cache nodes. Users will be able to augment the existing monitoring features by dynamically plugging in their code to the core-monitoring framework.

Controls system interface: The DAQ system will be able to interface to the control system in order to store user-selected EPICS process variables together with the science data and to control any device that can be used to perform a scan or a calibration run.

Timing system interface: The existing LCLS timing system will be reused (with modifications, see Section 10.3) in LCLS-II.

Beamline data interface: Beamline data (BLD) must be transmitted on every LCLS shot and archived together with the rest of the science data. The sources of the beamline data are the FEE gas detectors, the phase cavity, and the accelerator fast feedback system. The BLD contributions

of the latter system are the charge, energy and position of the electron beam. Scientists use these data to refine the energy and the precision of the beam arrival time on a pulse-by-pulse basis.

Time stamped beam information contained in User Datagram Protocol (UDP) packets is sent via multi-cast to MCC and to appropriate experiments. For LCLS-II there will be two sources of beamline data from FEE to describe the beam parameters, one for each beam-line (SXR/HXR). The same technique used at LCLS will be used to collect and package these beamline data.

:*RF Cavity Timing:* In order to provide timing to the instruments, an updated version of the RF cavity system currently in operation in the LCLS Undulator Hall (UH) will be provided for each line of LCLS-II's UH (see Chapter 9).

10.11 Machine Protection and Safety Systems

Two independent safety systems — the Personnel Protection Systems (PPS) and the Beam Containment System (BCS) — protect people from accidental exposure to high power beams and radiation. A third system, the Machine Protection System (MPS), is used to protect accelerator equipment from the high power beam. These systems exist for the present LCLS and linac configuration but will be substantially altered to accommodate the new beamlines and much higher beam power of LCLS-II.

Personnel safety and machine protection systems must respond to two main types of hazards. One occurs when beams go astray. Such beams can quickly damage equipment, and they can produce intense radiation fields that are not adequately shielded, thus endangering people outside the radiation area. The other type of hazard occurs when the beam power runs away. In this type of event, the beam may damage a dump and also produce more radiation than the shielding can safely attenuate. The necessary response time and action to be performed depend on the specific safety system and hazard.

Table 10.3 Response time requirements for the safety systems for controls.

System	Response Time	Type of Response
PPS	≤5 s for slowest response	Shut off all beams and the high power RF system, Insert beamline stoppers
BCS	As fast as ≤100 μs, otherwise < 600ms	Shut off all beams
MPS	<100 μs, (faster than BCS)	Limit beam power

Required response times and actions to be performed for the safety systems related to controls are given in Table 10.3. The response time is the time between when an event occurs and the time a response is performed by the appropriate devices. In the case of the PPS and BCS system, the response is to turn off all beams. In the MPS case, depending on the location and

severity, the response may be to reduce the beam power by dropping back to a less powerful beam mode, or turning off the beam in the most sensitive cases.

The required response time for the PPS system is relatively slow since it deals with access control and the insertion of physical beamline stoppers. The time it takes a person to traverse the shortest distance from outside the accelerator enclosure, through the maze or shaft, to a point where the dose is not meaningfully shielded is estimated to be around 5 seconds.

The BCS system has to deal with the cases where a kicker suddenly and erroneously puts a high-power beam precisely at one point on a protection collimator or erroneously sends a high power beam to a low power dump. In these situations, the collimators and dumps could be damaged by the highly concentrated thermal load, and the beam must be turned off quickly. A conservative estimate of the time to damage a copper collimator with a 1.2 MW LCLS-II beam and minimum beam size range is about 25 μs. This may be challenging to attain in all cases, particularly since the gun is roughly 3500 m from the main beam dump. Aluminum collimators or beam dumps would not be nearly as sensitive, and by the same estimate can withstand the worst case beam for at least 100 μs.

The response time of the MPS varies depending on the MPS fault and the components at risk. Where the hazard is accumulated radiation damage, speed is not an issue, but proper integration or averaging of the radiation levels is needed. Devices that require the fastest response time are those that might be exposed to misdirected beams, such as vacuum chambers, septa, or halo collimators. In these cases, the goal is for the MPS to respond before the BCS, to avoid a complete shutdown of the beam. In these cases MPS will require a response time less than 100 μs.

10.11.1 Machine Protection System

The role of the MPS is to turn off the electron beam or limit the average power by lowering the repetition rate of the beam when a fault is detected. This measure is not a life safety system, but is designed to prevent excessive losses of the electron beam, which would otherwise cause damage to sensitive machine components. Architecturally, LCLS-II MPS (**Error! Reference source not found.**) will be similar to that of the LCLS MPS, with an additional fast shut-off layer. The MHz pulse rate of LCLS-II requires the MPS to shut off the beam in sub-milliseconds in order to protect accelerator components during major faults (Table 10.3). Faults requiring sub-millisecond shutoff will be classified as Level 1; the rest will be classified as Level 2 faults.

The MPS takes input from many different devices, such as vacuum valves, beam charge monitors, beam loss monitors, protection ion chambers, and beam position monitors (see Chapter 5 for more detail). These inputs are fed into the MPS via dedicated custom electronics boards (link nodes). Based on the severity of the input signals, the MPS may either rate limit or completely shut off the beam. The mitigation devices include the gun laser acousto-optic modulator, the gun laser mechanical shutter and a downstream beam spreader kicker magnet located in the Beam Switch Yard (BSY). The beam spreader will either distribute the beam to the

soft X-ray and hard X-ray undulators or let the bunch pass straight through to the high power beam dump.

The choice of mitigation device to be used depends on the location of the fault, the type of mitigation desired (rate limiting vs. beam shut-off) and the fault level. Level 1 faults will be summarized internally in each MPS link node's internal FPGA, and a permit signal will be transmitted via a dedicated, fast connection to fast MPS supervisor FPGAs that collect the various MPS link node permit signals. The fast MPS supervisors relay the permit signal to the mitigation control link nodes. Two fast MPS supervisors will be implemented in order to minimize signal propagation times. One fast MPS supervisor will be located near the injector mitigation devices and one near the BSY's Beam Spreader kicker. Level 1 fault logic will result in a global zero rate beam inhibit. Level 2 faults will be interpreted by the MPS processor to determine the appropriate response. The MPS processor is capable of processing Level 2 faults in complex protection algorithms, and will determine the allowable beam rate for each destination. All MPS faults and rate transitions will be logged to a MPS history system for postmortem analysis.

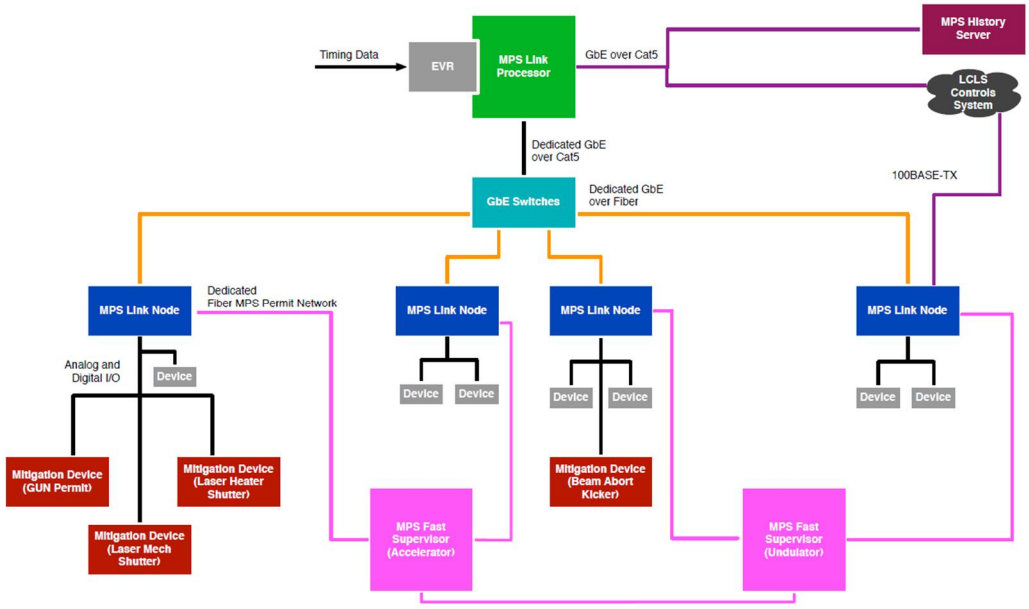

Figure 10-20 MPS system architecture

10.11.2 Personnel Protection System

The SLAC radiation safety system (RSS) (*SLAC-I-060-105-000-00*) protects personnel from prompt ionizing radiation due to accelerator operation. It is comprised of an access control system and a radiation control system (RCS), as modeled in **Error! Reference source not found.**.

The Personnel Protection System (PPS) for electron enclosures and Hutch Protection System (HPS) for photon enclosures are access control systems with some RCS safety functions. The RCS includes multiple sensor groups. Sensors inside the accelerator enclosure and along the beamlines are part of the first interlocked safety layer for radiation containment, the Beam

Containment System described in section 0. Sensors that provide the next interlocked safety layer to contain beam losses, such as Beam Shut Off Ion Chambers located outside of the beam enclosure, are part of the PPS or HPS.

The HPS interlocks the control of photon beamline stoppers to hutch access modes and sensors that verify beamlines are ready (Configuration Control Interlocks). The HPS systems are monitored by the PPS, which controls access to electron enclosures, interlocks the control of electron beamline stoppers, and permits the operation of the gun and accelerator radiation hazards.

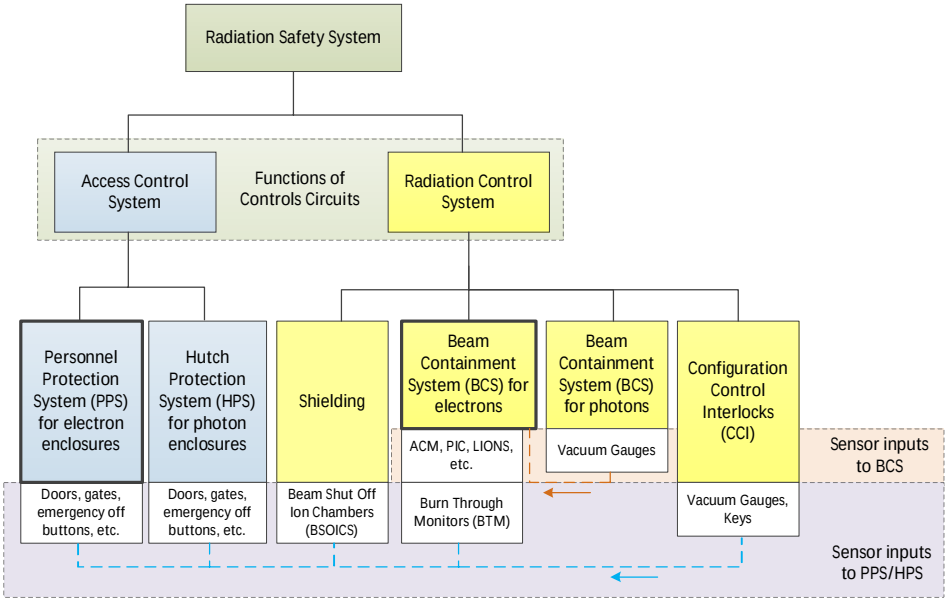

Figure 10-21SLAC radiation safety systems model for LCLS-II

Most of the PPS design concepts and hardware for the LCLS-II are already in place and in use by LCLS. Existing PPS and HPS hardware downstream of the LCLS-II SC linac will be reconfigured and expanded, while the first third of the accelerator will have new sensors, logic solvers (safety PLCs), and actuators (AC power contactors supplying hazard sources). The new installations will be integrated into the existing architecture using the system-level global interlocks (based on PLCs on a safety network or 20mA current loops) and local-level interlocks (based on PLCs or relay systems). The safety network extension (using redundant Siemens safety PLC remote I/O) and local access control system redundant PLCs (using PILZ) are shown in Figure 10-22. The Gun, L0B, L1B, L2B, and L3B segments have hazards interlocked to the PPS Global linac Logic PLC system. The Global LINAC system receives information from the local PLCs when the local areas have been searched, secured, and are ready for beam operations. The information passed between the system-level and local-level PLCs is discrete I/O, preserving the isolation of the PPS Safety Network from the EPICS IOC network. The operators remotely control access to the tunnel with EPICS HMI displays and a simultaneous hardwired signal to the remotely operated PLCs (hardwire signals not shown).

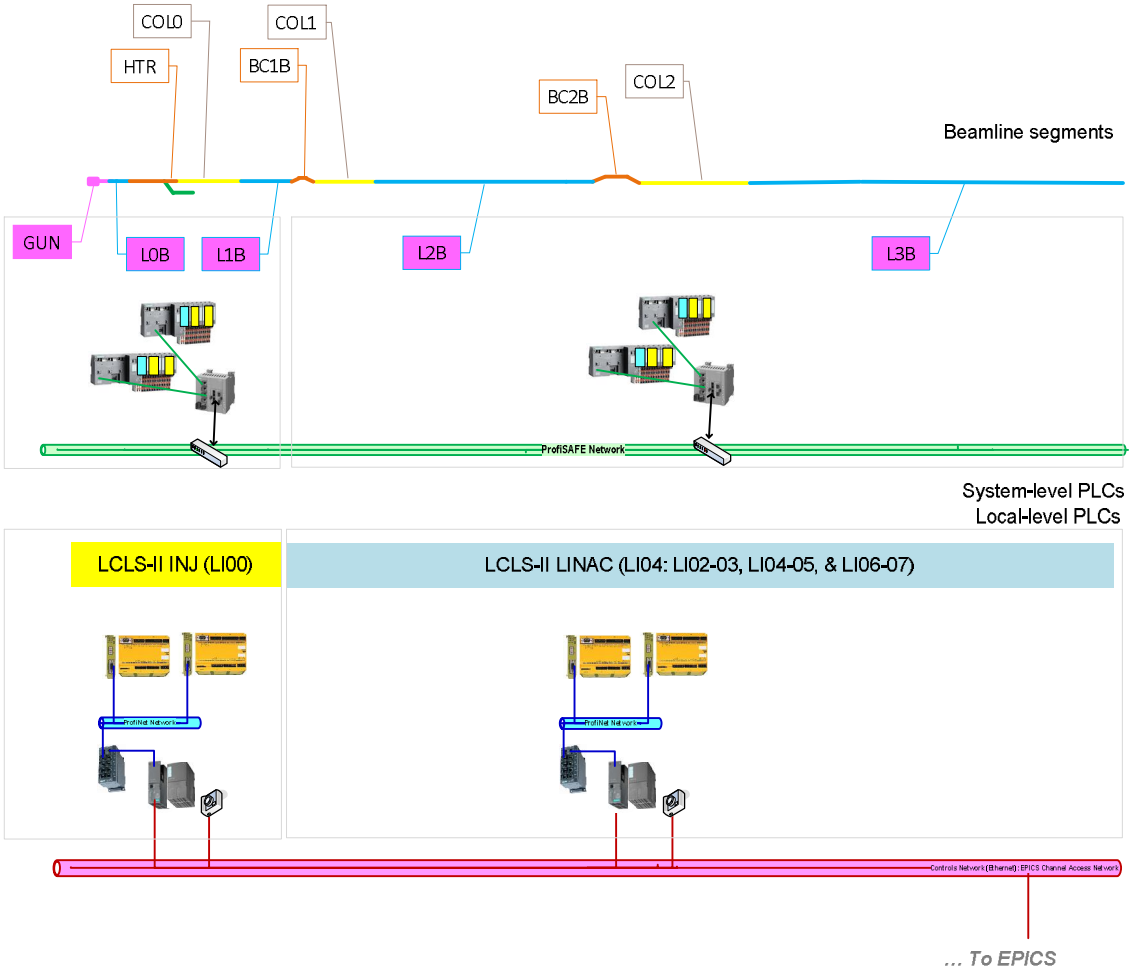

Figure 10-22 PPS system-level and local-level PLC systems

10.11.3 Beam Containment System

The BCS is a safety system that keeps potentially dangerous accelerator beams within their prescribed channels and within allowed power limits, and hence prevents the generation of excessive levels of radiation within occupied areas. The BCS also protects the integrity of safety-related beamline components. It performs this function by monitoring beam power and beam loss, and shutting beams down if a limit is exceeded.

A fault in the BCS will prevent delivery of all beams by three independent methods. The required shut off time is less than 100 μs.

The BCS for LCLS has been upgraded as part of a SLAC-sponsored project, and the upgraded designs will be incorporated into LCLS-II. Most notable is the introduction of networked programmable logic controllers (PLCs). As shown in Figure 10-23, the system has

both a fast as well as a "slow" shutoff path. A similar or modified system may be deployed for LCLS-II.

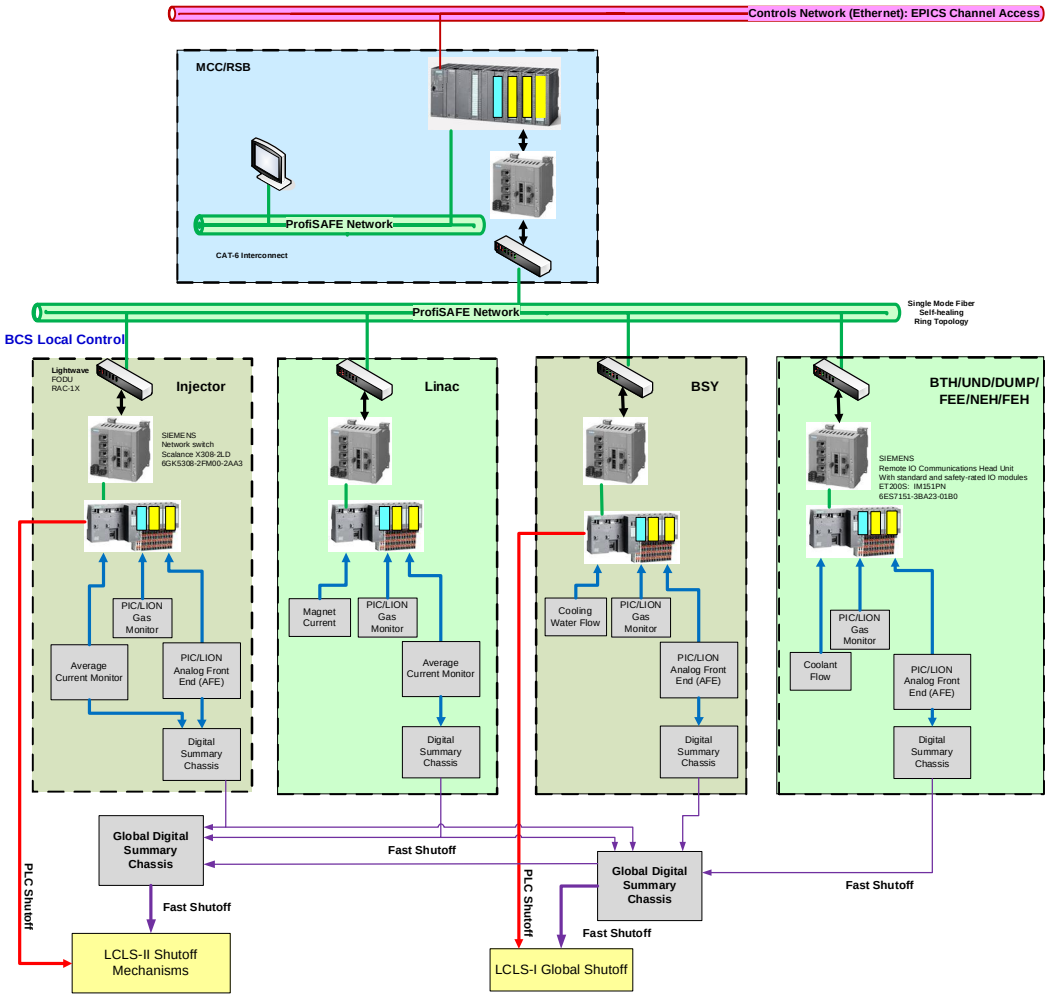

Figure 10-23 A model of a BCS networked PLC system

10.11.3.1 BCS Sensors

Currently BCS uses seven types of sensors. New types may be needed for LCLS-II.

1. Protection Ion Chamber (PIC): situated on or near the mechanical devices, such as PPS stoppers, that are to be protected. Some PICs will be installed for radiation dose control purpose.
2. Long Ion Chamber (LION): installed along the inside walls of the accelerator housings where shielding is inadequate.
3. Flow switch and transmitter: installed in cooling water systems for dumps, collimators, and slits.
4. Pressure switch and transmitter: installed in PIC and LION gas systems.
5. Micro switch: used to confirm the correct position of mechanical beamline components.
6. Current Transducer: used to monitor current in magnet power supply.

7. Toroid: current transformers that produce an output proportional to beam current.

10.11.3.2 BCS Shut-off Mechanisms

Beam shut off mechanisms comprise a key component in the BCS. There shall be three independent shut off mechanisms for the LCLS-II, which mirrors the requirements for LCLS as recommended in the *SLAC Radiation Safety Systems Technical Basis Document*:

1. A dedicated BCS Pockel Cell or acoustic optical modulator will stop laser light from striking the RF gun cathode, stopping the production of beam. These devices are fast acting and will make sure the BCS shutoff time can be met.
2. A dedicated mechanical laser shutter to block the laser light. These shutters will be situated as close to the production point of laser light as practicable. This device is slow, but it will completely block the laser to the gun cathode.
3. Gun RF will be inhibited once a BCS fault occurs. This will need careful analysis of the time it takes the VHF normal-conducting-radio-frequency (NCRF) gun to stop beam production. See chapter 5 for more information about the NCRF gun.

BCS fault will disable 3-way kicker in linac Sector 27 to protect against beam damage to protection collimators or PPS stoppers. In some cases a BCS fault in either LCLS or LCLS-II could require both systems to be shut off.

10.11.4 ODH Safety System

The LCLS-II superconducting cavities will use liquid helium. Potential failure modes of the cryogenic system could result in a discharge of helium to the tunnel. The helium would rapidly expand into a gas, displacing the air in the tunnel and support building above, causing an oxygen deficiency hazard (ODH).

The LCLS-II Linac and support building ODH safety systems will detect the displacement of oxygen and alert people to evacuate the area. Sensors will measure the level of oxygen and confirm proper ventilation where required. When oxygen levels drop to unacceptable levels, evacuation alarms and warnings lights will be used to notify personnel to evacuate the area.

10.12 References

1. Y. Pischalnikov et al, “Lorentz force compensation for long pulses in SRF cavities,” *IPAC 2012*, New Orleans, USA (2012).
2. A. Neumann et al., “Analysis and active compensation of microphonics in continuous wave narrow-bandwidth superconducting cavities,” *Phys Rev. Spec Topics- Accelerators and Beams* **13**, 82001 (2010).
3. C. Hovater et al., “Commissioning and Operation of the CEBAF 100 MeV Cryomodules,” *IPAC 2012*, New Orleans, USA (2012).
4. L. Doolittle et al., “Digital Low-Level RF Control Using Non-IQ Sampling,” *LINAC 2006* Knoxville, TN, USA (2006).

11 INFRASTRUCTURE and FACILITY PREPARATION

TECHNICAL SYNOPSIS

The LCLS-II project capitalizes extensively on the existing buildings and infrastructure of the SLAC linac and LCLS facilities, In order to support the new technical installation modifications are necessary, particularly in the first 1000 meters of the linac where the existing accelerator equipment will be removed and replaced with a new source and a superconducting Linac. The rest of the LCLS facility, including the Beam Switchyard (BSY), Beam Transport Hall (BTH), Undulator Hall (UH), Front End Enclosure (FEE), and Near Experimental Hall (NEH), Hutch 1, will also be modified to accommodate the new beamline and high current operation. These modifications, which are expected to be planned and installed over a period of 4 years, will be closely coordinated with the ongoing operations as well as the developing schedule of installation of technical components of LCLS-II. Detailed requirements derived from the Physics Requirements Document, (PRD), and technical systems provide the basis for the design of changes to the mechanical, electrical, and fire protection infrastructure for the Project. The standards and guidelines controlling changes to the infrastructure include SLAC and DOE specific standards, as well as local, statewide, and federal standards.

11

11.1 Scope

The LCLS-II infrastructure support systems scope is based on the requirements of the technical systems to be installed in each area, and as defined by the physical boundaries. Engineered design solutions will provide the infrastructure by taking advantage of the existing facilities at SLAC. Based on technical requirements linked in this document, the infrastructure systems to be provided include mechanical wet and dry side utilities, electrical power, compressed air, and specialized cooling systems to support new superconducting linac installations, electron beam dumps, and new beamline components.. The scope also includes removal of unnecessary linac and Klystron Gallery components in Sectors 0-10 prior to reconfiguration and installation work in these sectors of the Linac/Klystron Gallery. This report will describe the major portions of the work scope, schedule, and requirements as follows:

- Prior to Infrastructure and technical installations unnecessary accelerator equipment will be removed from the SLAC linac and Gallery Sectors 0-10, approximately 1,000 meters. This includes Klystrons, waveguide, accelerator structure, existing cooling lines, and associated electrical and controls installations. The equipment will be removed to planned areas. Final characterization, salvage, and disposal will be performed by others.
- A new site and building will be constructed at sector 4 along with gas storage pads and equipment areas to house the new cryoplant that supports the super conducting linac. A dedicated substation, power distribution and cooling is part of the scope.
- The cooling system and power in the existing laser room and injector area, referred to as Collider Injector Development(CID), will be reconfigured to support a new laser and injector that will be installed ahead of the superconducting RF cavities.
- The linac tunnel between Sectors 0 and 10 will be outfitted with piping, cabling, and ventilation to support new cryomodule installations and to meet the current building codes and federal requirements. The necessary existing infrastructure will be re-used wherever possible. Infrastructure that is replaced will comply with applicable codes. The reconfigured power and cooling systems will support the solid state amplifiers,(SSAs) control racks, bunch compressors and magnets located in linac Sectors 0-10.
- The Beam Switch Yard will be provided with necessary cooling system water for magnets and re-plumbing of the repositioned D-10 beam dump.
- The Beam Transport Hall (BTH) crosses the Research Yard (RSY) and connects to the Undulator Hall (UH) and will be reconfigured to support the new beamline components and include necessary radiation protection concrete shielding and access control fencing required due to increased beam power.
- The Undulator Hall (UH) extends under the ridge between the RSY and the Electron Beam Dump. The thermal barrier doors and mechanical systems will be reconfigured

to accommodate new undulators with larger dimensions for both beamlines. New control and convenience power will be installed for the new beamlines.

- The Electron Beam Dump (EBD) utilities will be reconfigured to accommodate new beamline configurations. A new isolated cooling system for the EBD will be installed to accommodate higher beam power and mitigate radiation issues.
- The Front End Enclosure (FEE) will have structural, mechanical and electrical reconfigurations to support Radiation Protection requirements, the new beamline components and rack space.
- The Near Experimental Hall (NEH) connects to the FEE and is where new experimental stations will be installed (See Figure 11-1**Error! Reference source not found.Error! Reference source not found.Error! Reference source not found.**). The scope for infrastructure and facilities includes system reconfiguration and the SLAC effort for commissioning the reconfigured infrastructure systems.

Figure 11-1. SLAC and LCLS II Infrastructure Work Locations

Figure 11-2. Cryoplant location at Sector 4

Figure 11-3. Accelerator Equipment to be removed from SLAC linac Sectors 0-10, 1,000 meters

The design and construction of the LCLSII Infrastructure is divided into 5 Construction Packages, (CP).

CP1 includes the Cryoplant building design and construction. The design has been awarded to an A&E moving towards design completion in May of 2015. Construction will follow a best value procurement and award strategy. Construction will be managed by Project Infrastructure staff.

CP2 includes the Laser/Injector area and Sectors 0-10, and BSY/LTU Infrastructure design and construction. We will use an IDIQ procurement competing prequalified Engineering firms. A similar procurement strategy is planned for construction subcontractors. Construction will be managed by Project Infrastructure staff.

CP3 includes the eastern end of the project, BTH, UH, EBD, and FEE design and construction. We will use an IDIQ procurement competing prequalified Engineering firms. A similar procurement strategy is planned for construction subcontractors. Construction will be managed by Project Infrastructure staff.

CP4 includes the NEH Hutch 1 modifications design and construction to support new experimental equipment configurations. We will use an IDIQ procurement competing

prequalified Engineering firms. A similar procurement strategy is planned for construction subcontractors. Construction will be managed by Project Infrastructure staff.

CP5 includes the Accelerator Equipment Removal technical document preparation for the RFP and subcontractor removal activities. We will use IDIQ procurement to competing prequalified Engineering firms to prepare the technical portion of the RFP. A similar procurement strategy is planned for subcontractors. Activities will be managed by Project Infrastructure staff.

11.2 Design Maturity

The LCLS-II Project Final Design Plan LCLSII-1.1-QA-0065 provides for a phased completion of the final designs for the LCLS-II facility. The plan ensures that designs are sufficiently mature to start procurements and construction, while enabling the most cost-effective schedule for constructing the facility and maximizing the technical capabilities of the facility at CD-4. Final design readiness at CD-3 recognizes that that not all subsystems will reach final design at the same time. Project-level requirements and interface control points between Accelerator Systems, Cryogenic Systems, Photon Systems and Infrastructure are defined at CD-3, which ensures that the phased procurements and construction are appropriate for the final design of the LCLS-II. Chapter 2, Project Overview, contains additional discussion of the approach to design completion. The Infrastructure Systems design, described in this chapter, is evaluated to be 35% complete. Completing remaining design after CD-3 allows for sufficient maturity of the technical systems requirements to ensure appropriate infrastructure is provided.

11.3 Schedule

The schedule is divided into five design and construction packages based on critical path support, available construction access times relative to laboratory operations, system integration, and geographic area, as shown in 4 and 5. Construction Package 1 (CP1) is the design and construction of the cryoplant building and infrastructure to support the critical path installation of the cryoplant components, (by JLAB). The activity is the first CP in order to have a facility available for cryoplant equipment installations in the Spring of 2017. Construction Package 2 (CP2) is the schedule for the design and construction of the Accelerator area infrastructure systems, Sectors 0-10 and Beam Switch Yard. This CP integrates with and supports Accelerator and Cryosystem installations in the West end of the Project. Construction package 3 (CP3) is the schedule for the design and support of the Photon System area infrastructure systems. This CP integrates with both Electron Beam transport and Photon systems in the eastern sections of the Project. Construction Package 4 (CP4) is the schedule for design and construction of the Near Experimental Hall Infrastructure systems supporting the new experimental hutch configuration in the NEH. Construction Package 5 (CP5) covers the planning, design, and removal of existing equipment in Sectors 0 thru 10 of the existing linac and gallery prior to the construction of CP2.

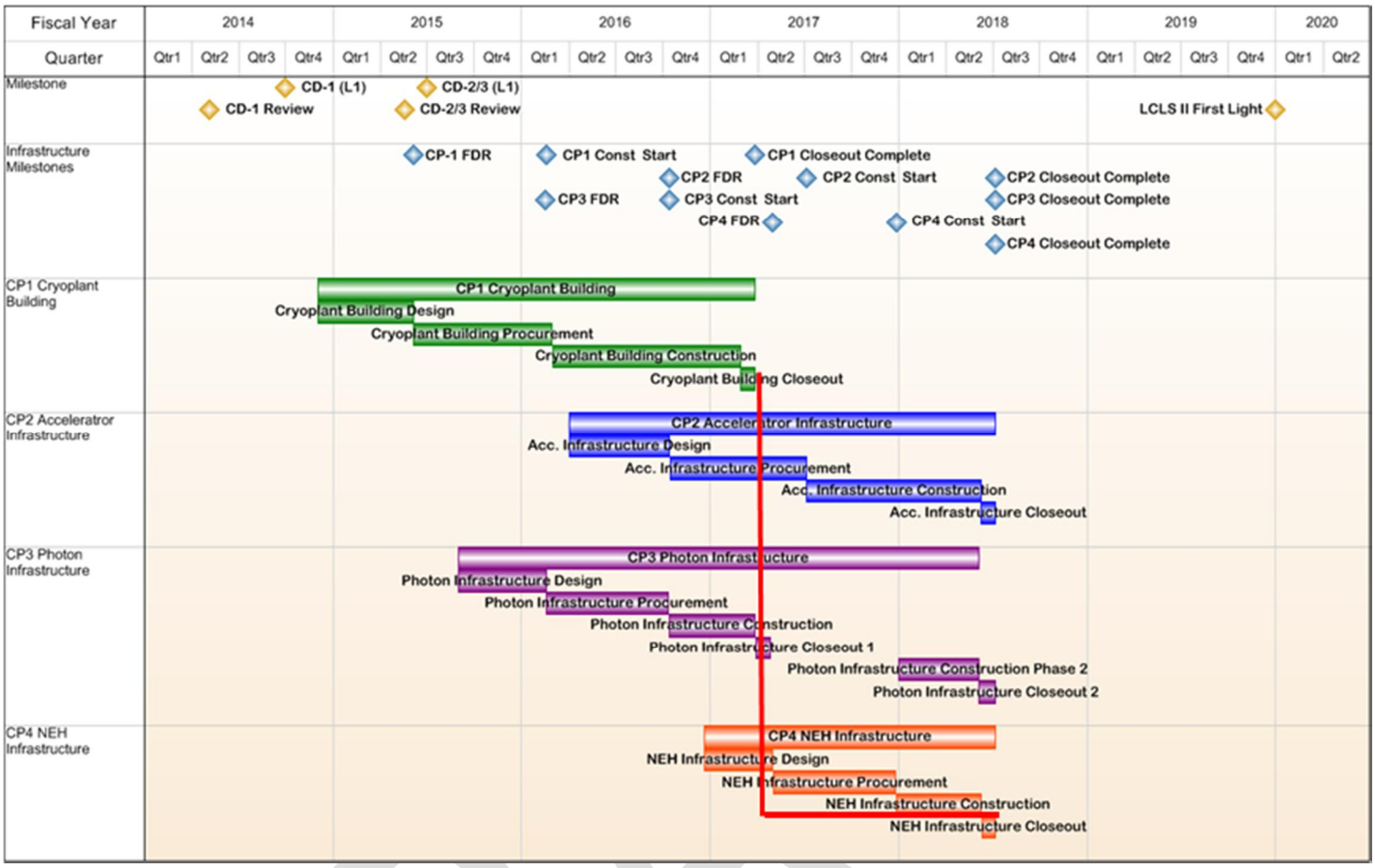

Figure 11-4 Construction packages 1,2,3,4 Schedule

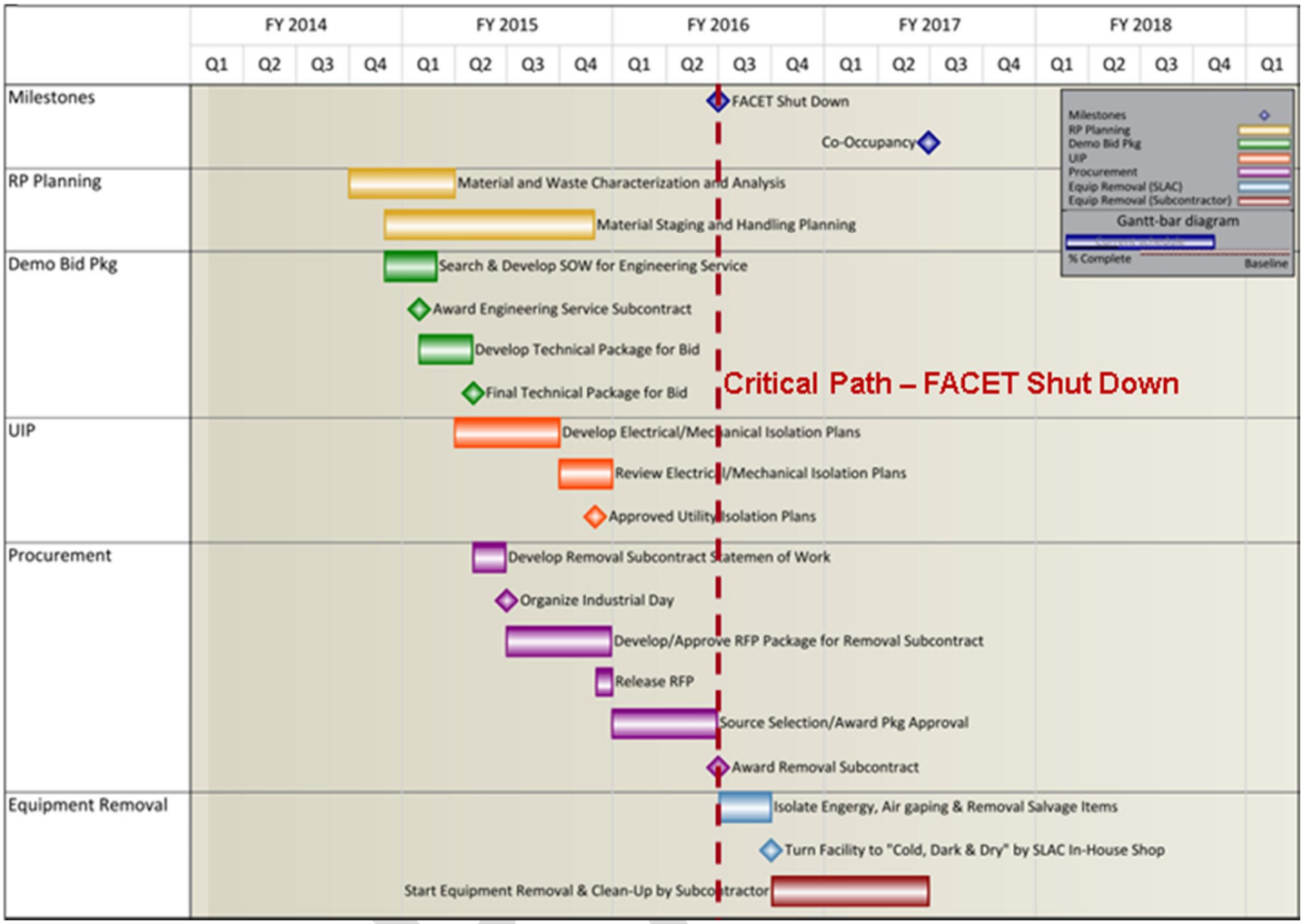

Figure 11-5 Construction Package 5, Equipment removal schedule

11.4 Infrastructure Requirements

This section describes the infrastructure requirements for the LCLS-II project for each affected area, starting from the laser and injector areas and proceeding to the experimental stations. Some documents may be applicable to more than one area and will be referenced in the appropriate section description. Table 11-1 lists the infrastructure requirements documents.

Table 11-1. Infrastructure Requirements Documents

Design/Construction Area	Requirements Document Type	Title	Document Number
Cryoplant Building and infrastructure, CP1	Room Data Sheet,(RDS)	Cryogenics Facility-Compressor Room	LCLSII-5.4-RD-0123(TBD)
Cryoplant Building and infrastructure, CP1	RDS	Cold Box Room	LCLSII 5.4-RD-0124
Laser/Injector/CID, Sector 0-10, Beam Switch Yard CP2, BTH,UH,EBD,FEE, CP3, NEH, CP4	Physics Requirements Document,(PRD)	Environmental Radiation Requirements	LCLSII-1.2-PR-0265
Laser/Injector/CID, Sector 0-10, Beam Switch Yard CP2, BTH,UH,EBD,FEE, CP3, NEH, CP4	PRD	Radiological Requirements for LCW Systems	LCLSII-1.2-PR-0211
Laser/Injector/CID, Sector 0-10, Beam Switch Yard CP2, BTH,UH,EBD,FEE, CP3, NEH, CP4	PRD	Requirements for Air Ventilation Controls for Protection of Workers and Public	LCLSII-1.2-PR-0160
Laser/Injector/CID, Sector 0-10, Beam Switch Yard CP2, BTH,UH,EBD,FEE, CP3, NEH, CP4, Existing Equipment Removal, CP5	PRD	Workplace Radiation Monitoring Requirements	LCLSII-1.2-PR-0153
All design and construction packages	Fire Hazards Analysis,(FHA)	Conceptual Project Fire Hazards Analysis	LCLSII-1.1-PM-0149
Laser/Injector/CID Sector 0-10, Beam	Interface Control Document,(ICD)	Accelerator to Infrastructure Systems	LCLSII-2.1-IC-0156

Switch Yard, CP2,			
Laser/Injector/CID, CP2	RDS	Laser Room	LCLSII-5.2-RD-0131
Sector 0-10, CP2	RDS	Klystron Gallery sector 0-10	LCLSII-5.2-RD-0144
Sector 0-10, CP2	RDS	Linac Housing sector 0-10	LCLSII-2.4-RD-0011
All secured beamline areas, CP2, CP3, CP4	ICD	PPS to Infrastructure Systems	LCLSII-2.7-IC-0247
Beam Switch Yard, CP2	ICD	Beam Switch Yard to Infrastructure	LCLS II-5.1-IC-0182
Beam Switch Yard, CP2	RDS	Beam Switch Yard,(BSY)	LCLSII-5.2-RD-0128
Beam Transport Hall,, CP3	PRD	Radiation Protection Requirements for the Beam Transport Hall	LCLSII-1.2-PR-0263
Beam Transport Hall, CP3	ICD	LTU to Infrastructure Systems	LCLS II-5.2-IC-0183
Beam Transport Hall,, CP3	RDS	Linac to Undulator,(LTU)	LCLSII-5.2-RD-0129
Undulator Hall, CP3	ICD	Undulator to Infrastructure	LCLS II-3.2-IC-0047
Undulator Hall, CP3	RDS	Undulator Hall	LCLSII-3.2-RD-0012
Electron Beam Dump	ICD	EBD to Infrastructure Systems	LCLS II-5.2-IC-0174
Electron Beam Dump, CP3	RDS	EBD TBD	
Front End Enclosure, CP3	ICD	XTES to Infrastructure Systems	LCLSII-5.3-IC-0114
Front End Enclosure, CP3	RDS	Front End Enclosure (FEE) and Fee Maze	LCLSII-5.3-RD-0130
Near Experimental Hall Hutch, CP4	RDS	XTES in NEH	LCLSII-3.5-RD-0013

11.4.1 Laser Room and Injector

In the CID area a new laser room will be constructed and a new injector installed. Existing utilities will be reconfigured to accept the new components. The scope includes reconfiguring the

existing utilities inside and surrounding the laser and injector facility, and preparing for connecting the new components.

Interface Control Document LCLSII-2.1-IC-0156, *Accelerator to Infrastructure Systems*, describes the interface between the Accelerator and Infrastructure Systems.

Room Data Sheet, LCLSII-5.2-RD-0113, *Laser Room*. LCLSII-2.4-RD-0011, _ Linac, and LCLSII-5.2-RD-0144, *Linac Housing sector 0-10*, contain detailed requirements for the reconfiguration.

11.4.1.1 Mechanical

The Laser/injector facility requires conditioned spaces and process cooling. The existing HVAC system will be modified as necessary to provide cooling for HVAC and process cooling water. The HVAC system will provide stable temperatures, positive pressure, and humidity control for the spaces. Cooling systems are required for, laser, injector, accelerator, waveguide, and bunch compressor systems.

11.4.1.2 Electrical

The available electrical power is adequate for the injector. Electrical systems will be cleaned, repaired and prepared for re-use. The new components will be connected to serviceable breakers, panel boards and motor control centers.

11.4.1.3 Fire Protection

The existing fire protection and detection systems will be preserved to the extent possible. Upgrades to the alarm system will be provided by SLAC. Fire extinguishers will be provided in accordance with NFPA 10 throughout the injector facility. The injector facility will meet current life-safety standards, including one-hour-rated barriers and fire-rated exit doors. The access and exit doors will include an interlock that is integrated into the existing Personnel Protection System (PPS). Exit signs will be edge-lit with concealed lamps and integral lettering on a clear lens. Where low-level exit signs are required, they will be backlit and set flush with the adjacent wall.

11.4.2 Cryogenic Plant Infrastructure-

The infrastructure requirements for the cryogenic plant are described in this section. A complete description of the cryogenics is presented in Chapter 7. Cryoplant and Distribution Interfaces between the plant and Infrastructure are described in ICD LCLSII-05.4-IC-0235, *Cryoplant to Infrastructure Systems*.

Detailed requirements are found in Room Data Sheets LCLSII 5.4-RD-0124, *Cold Box Room*, and LCLSII-5.4-RD-0123(TBD), Cryogenics Facility- Compressor Room.

11.4.2.1 Civil Site Work

The new cryogenic plant to be installed near Sector 4 of the Klystron Gallery is expected to be approximately 10,000 square feet in size, with roughly an additional 20,000 square feet of

equipment pads, tanks, storage, and parking and outdoor equipment to be installed at various locations (see Figure 11-6). Civil infrastructure requirements include the reconfiguration of the north access road, leveling and grading for the cryoplant building pad, installation of the cryoplant structure, site improvements, storm water retention features and site restoration.

Approximately 30,000 cubic yards of soil will be excavated to provide a level area on which to build the cryogenic plant and appurtenant features. To the extent possible, the excavated material will be placed nearby to shield the site visually and acoustically.

Sound level mitigation measures are required for the new facility, including the cryogenic plant. The specified sound level limit at the SLAC site boundary is 60 dB during normal business hours. During the evening hours, when traffic on the adjacent freeway is limited, the sound coming from SLAC is prominent; this will require special facility design considerations.

New domestic water and sanitary sewer line laterals will be installed from main lines near the Klystron Gallery.

Storm water collection drains and piping will be installed in the cryogenics plant area. Section 438 of the Energy Independence and Security Act (EISA) of 2007 requires the project to maintain or restore, to the maximum extent technically feasible, the predevelopment hydrology of the property with regard to the rate, volume, and duration of flow. This dictates that a storm water retention basin be installed down-gradient of the cryogenics plant installation to collect the flow. Overflow from the retention basin will drain to the existing storm drain system in the vicinity.

The new cryoplant building pad will match the existing road.

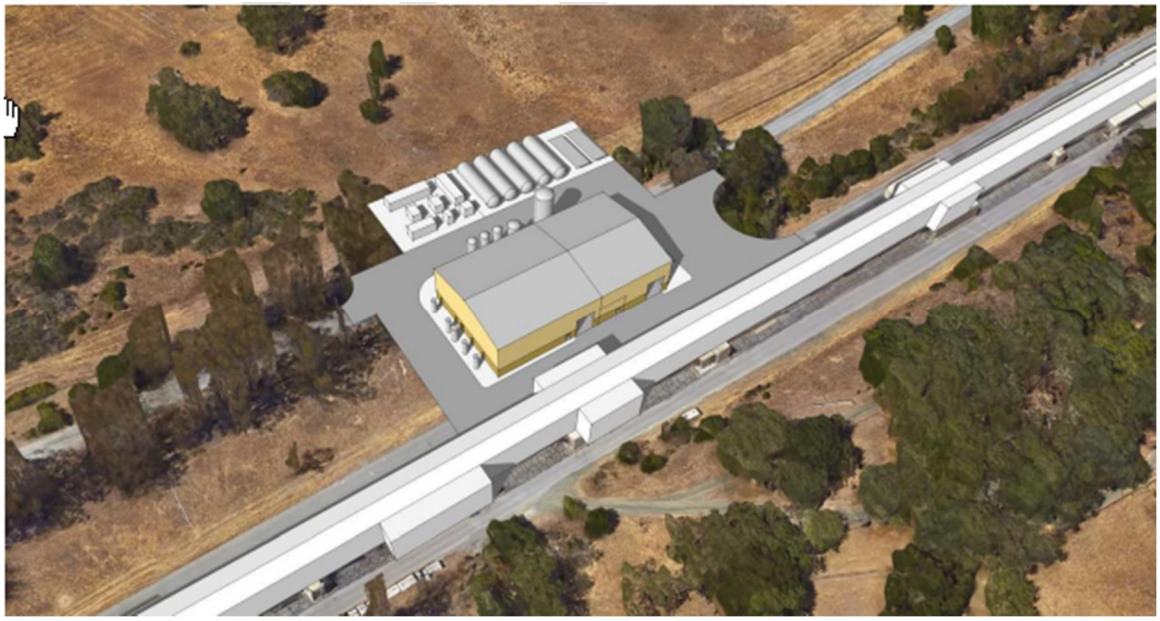

Figure 11-6 Cryoplant and building rendering (Courtesy HDR)

11.4.2.2 Mechanical

The cryogenic plant will require approximately 2800 GPM of cooling tower water (CTW) at 15 degree F temperature rise. The CTW will be supplied from the existing linac cooling tower 1201. Cooling tower water lines and valves will be provided within 5 feet of the new cryoplant building.

11.4.2.3 Electrical

Cryogenic plant power will be provided from existing services to a new double-ended, 12KV-rated main substation/switchgear, powered by dedicated 12KV feeders from the existing spare breakers located in the master substation at B016. Distribution of power for the warm compressors will come from the new 4160V-rated, double-ended unit substations powered by the main substation mentioned above. Power for the various small compressors, pumps motors, HVAC, and others will be provided from a new 480V distribution and motor control center, powered from the new 12KV rated, double-ended unit substation mentioned above.

Electrical power for the new cryogenic equipment house power, cold box room power, and the local cryogenics control room will be provided from a new 480V distribution switchboard. .

The A&E subcontractor has produced an Interim Design Report, Interim FHA, and drawings. Review was held November 17 thru 24, 2014. The drawings and reports are located at the review site.(See link)

11.4.3 Linac Housing and Gallery Sectors 0 through Sector 10

A large portion of the existing equipment in both Linac Sectors 0 to 10 Housing and the Klystron Gallery must be removed to make room for the LCLS-II installation. After removing old equipment, the affected areas will be appropriately cleared and ready for the installation of LCLS-II experimental equipment. Most of the building systems and equipment will remain in place for reuse. Interfaces between Accelerator systems and Infrastructure systems are described in ICD LCLSII-2.1-IC-0156, *Accelerator to Infrastructure Systems*. Detailed requirements are found in RDS LCLSII-5.2-RD-0144, *Klystron Gallery sector 0-10* and LCLSII-2.4-RD-0011, *Linac Housing sector 0-10*.

11.4.3.1 Linac Sector 0 to Sector 10 Housing Existing Equipment Removal

Prior to reconfiguration and new installations, the linac housing sectors 0 to sector 10 will be cleared of all experimental equipment starting from the CID shielding wall up to and including Linac Girder 10-6. At the conclusion of the removal activities, the housing will be cleared of all beamline experimental equipment, cable trays and cables. Existing cable trays and associated experimental equipment cables will be removed back to point where they enter the housing. Existing waveguides, water and air system piping, and vacuum manifolds will be removed back to the point where they enter the housing. All contents will be removed from penetrations.

11.4.3.2 Linac Sector 0 to Sector 7 Klystron Gallery Existing Equipment Removal

Prior to reconfiguration and new installations the Linac sector 0 to sector 7 of the Klystron Gallery will be cleared of all experimental equipment including electronic racks, power supplies, Fiat racks, Sub-boosters, Klystrons, modulator cabinets, the 480V bus duct and associated power panels for Fiat racks, and associated cables. The electronic racks and equipment with associated cables in I&C Alcoves on the North side of the Gallery will be removed. Existing site compressed air lines will be removed back to the last threaded fitting closest to the horizontal header and capped in place. Existing cables along the north and south walls will be removed from the existing cable trays. The north and south oriented cable trays will be remained in place for reuse.

11.4.3.3 11.3.3.2.1 Linac Sector 8 to Sector 10 Klystron Gallery Existing Equipment Removal

The Linac Sector 8 to Sector 10 Klystron Gallery will be removed from the cable trays. Both north- and south-oriented existing cable trays will remain in place for reuse

11.4.3.4 Mechanical

Existing mechanical systems in Sectors 0 through 10, including the Klystron Cooling System (KCS), Accelerator Cooling System (ACS), and Waveguide Cooling System (WCS) will be reconfigured to provide cooling to the linac RF solid state amplifiers, waveguide, injector and bunch compressors, and electronics. The Sector 10 HER extraction line cooling system will be upgraded. Detailed requirements are found in RDS LCLSII-5.2-RD-0144, *Klystron Gallery sector 0-10.*

Exhaust fans for all linac superconducting (SC) Sectors will use as much of the existing ventilation system as possible. for air distribution.

Controls for process systems (LCW, PCW, and CTW) will be available via the existing linac distributed control system. HVAC controls will be handled by the site-wide BACnet protocol DDC, integrated with EPICS for system monitoring.

Water cooling systems are required for the SSAs and for the injector and bunch compressors. Rack cooling will be provided in the Klystron Gallery. The waveguides will be temperature stabilized. Each sector has existing independent LCW cooling systems. The waveguide and klystron cooling systems will utilize the existing linac cooling tower water system. Cooling water will be provided for the injector and bunch compressors. The PEP-II HER transport line magnet cooling piping distribution system will be reused.

11.4.3.5 Fire Protection

The fire protection system includes an existing VESDA smoke detection and will require sprinklers in the linac housing for fire safety. A wet pipe system (NFPA 13) will be installed where required.

11.4.3.6 Oxygen Deficiency Considerations

Liquid Helium present in the cryoplant, helium distribution system and the superconducting cryomodules may cause an oxygen deficiency hazard if there are helium leaks or system ruptures. Requirements and scope to be added.

11.4.3.7 Electrical

All existing electrical systems will be reused to the greatest extent practical. Existing components and cables include: panels, lighting systems, controllers, transformers, disconnects, motor control centers, power distribution systems, unit substations and various other systems located in the gallery and the tunnel.

Any new lighting shall be designed in accordance with recommendations from the Illuminating Engineering Society (IES) and will be suitable for the gallery area application. No new lighting is anticipated.

The fire alarm and detection systems will integrate with the existing campus network. The fire alarm and detection systems will comply with NFPA 72 and all associated codes and regulations.

The existing telecommunication system will be used to support voice, data and low-voltage networks.

11.4.4 Beam Switch Yard

The BSY modifications include the use of an existing beam dump for the new beam. The dump will be serviced by an existing closed-loop cooling system. This effort will require modifications of the selected beamline to accept the new beam. Cooling systems will be provided for the transport line bend and quadrupole magnets.

Interfaces between Accelerator systems and Infrastructure systems are described in ICD LCLS II-5.2-IC-0183, *LTU to Infrastructure Systems*. Detailed requirements are found in RDS LCLSII-5.2-RD-0128, *Beam Switch Yard,(BSY)*.

11.4.5 Beam Transport Hall

The existing BTH is constructed of formed concrete. The project will install a second array of beamline components on the northern aisle of the BTH. Considerations for this second beamline were provided during the design and construction of the LCLS. These considerations primarily provide the space required to install a second beamline and to provide long-term utilities, ventilation, lighting, and power for two similar beamlines. The scope of work in the BTH will consist of installing utility distribution networks for the second beamline. The majority of the installations will consist of power, cooling water systems, and radiation safety systems. The existing ventilation consists of exhaust fans, with no air conditioning capability available for the BTH.

Interfaces between Accelerator systems and Infrastructure systems are described in ICDLCLS II-5.2-IC-0183, *LTU to Infrastructure Systems*. Detailed requirements are found in RDS LCLSII-5.2-RD-0129, *Linac to Undulator,(LTU).*

Due to the increased power of the electron beams, either additional local radiation shielding or administrative control is required around the BTH housing. The radiological requirements are described in Chapter 13, Radiological Considerations. During beam operations, access to the BTH and service buildings will be under Controlled Access protocol. To accomplish this fencing and access control will be installed around the BTH as part of the radiation protection requirement. Controlled access to the interior of the BTH includes two entrance mazes on opposite ends of the Research Yard. The west end of the BTH "head house" access points is currently plugged with removable panels. These panels may be removed for access to the facility. Local shielding to meet the radiological requirements of the higher energy beam may be required in specific areas.

11.4.5.1 Mechanical

The BTH has an existing ventilation system that is activated when the beam is off. The ventilation system provides more than two air changes per hour. A roof-mounted exhaust fan with ductwork provides the necessary ventilation. The fan is monitored and controlled by SLAC's Energy Management System. Relocation of existing chilled water piping will be required to accommodate distribution to the new undulators. Supplemental LCW supply and return piping with pressure gauges and isolation valves will be mounted on the north wall of the BTH.

Supplemental clean, dry compressed air at 100 psig will be provided along the length of the BTH. Compressed air piping is mounted along the south wall, with shut-off valves and pressure gauges. The compressed air piping will be extended to the north wall for the second beamline components. The compressed air piping system is connected to the SLAC site-wide compressed air piping. The estimated demand for two beamlines is 20 SCFM.

Modifications to the current fire water main line supports will be required to accommodate transportation paths of the new undulators.

11.4.5.2 Service Buildings 911, 912, 913

Service buildings are also included in the BTH section. There are currently three existing service buildings of varying size on top of the BTH. These service buildings were originally sized to hold the controls and power racks for two beamlines. Current air handling units (AHUs) are installed on the roof of the BTH, next to the service buildings. Air distribution ductwork (supply and return) is provided inside the building. The operation of the AHUs is controlled and monitored by SLAC's Energy Management System (EMS). Existing duct mounted smoke detectors were installed per California Mechanical Code (CMC).

The BTH service buildings have a wet fire sprinkler system. Zone control valves with supervisory and flow switches are provided where the piping system enters the building.

11.4.5.3 Electrical

The 480V or 120V/208V distribution panel boards will be installed to provide power to various systems located in the BTH and the I&C racks, power supply racks, and PPS racks in service buildings 911, 912, and 913. Low profile fluorescent lighting is provided in the entire length of the BTH.

Electrical power for the new BTH equipment and control racks will be provided as required by the existing and new panels located inside service buildings 911, 912, and 913, routing cabling through the existing penetrations to the I&C, PPS, and power supply racks.

Lighting will be in accordance with IES recommendations and suitable for the building application.

The fire alarm and detection systems will integrate with the existing campus network. The fire alarm and detection systems will be designed to comply with NFPA 72 and all associated codes and regulations.

The existing telecommunication system will be used to support voice, data and low voltage networks.

11.4.6 Undulator Hall

The UH is approximately 170 meters long and houses the electron beam and the undulators. The tunnel is in line with the BTH. The downstream part connects to the EBD in the vicinity of the existing service building 921.

The LCLS-II undulator requires stringent temperature control, which is provided by a dedicated HVAC facility near service building 921.

Interfaces between Photon Systems and Infrastructure are described in LCLS II-3.2-IC-0047, *Undulator to Infrastructure*. Detailed requirements are found in RDS LCLSII-3.2-RD-0012, *Undulator Hall.*

The utilities required in the tunnel for the LCLS-II are to support the technical systems for photon and electron beams. New utility resources are required, including new plumbing, wiring, and power.

Due to the configuration of the variable gap undulator magnets, the height of the utilities in the UH will have to be modified. The existing utilities are generally 8 feet above the finished floor. The variable gap undulators will require nine-foot clearance from the finished floor to the lowest utility. This will require that some existing utilities be rearranged within the tunnel envelope.

The UH is physically defined by two thermal barriers, which are located at the end of the BTH to the west and before the start of the EBD to the east. The UH is geometrically defined as a horseshoe tunnel with internal cross-sectional dimensions of 14'6"x14'10" (HxW). Service access through the existing thermal barrier into the UH will be modified to allow for taller variable gap magnets. This access point is from the BTH.

11.4.6.1 Mechanical

The existing UH HVAC system will be used to maintain space temperature and gradient inside the tunnel. The existing air handling units (AHUs) serving the UH are located at the ground surface east of the current UH Service Building 921.

The current AHUs have pre-heat coils, temperature control valves, supply and return fans, heating and cooling coils and economizers. Chilled water (CHW) and hot water (HW) piping are connected to the AHUs. The operation of the existing AHUs is monitored and controlled by SLAC's EMS. Duct-mounted smoke detectors are installed, per California Mechanical Code. . Air radiation monitoring will be installed in the HVAC system.

Relocation of existing chilled water piping will be required to accommodate transportation paths of the new undulators.

Supplemental insulated supply and return PCW piping with pressure gauges, isolation valves, and circuit setters will be mounted on the wall in the current UH, out of the stay clear zones established by technical systems. PCWS and PCWR connections for technical equipment will be spaced along the wall of the tunnel. The PCW system currently located inside the UH service building 921 at ground level will be upgraded to accommodate a second XTCAV system in the UH tunnel. PCW supply temperature is 65 °F, with stability of 0.1 degree F. and a total estimated demand of approximately 30 GPM. The operation of the current PCW system and equipment is controlled and monitored by SLAC's EMS. Existing chilled water pipes will be raised and new taps added to support the new beamlines. Supplemental clean, dry compressed air at 100 psig will be provided along the length of the UH tunnel. Compressed air piping will be mounted along the UH wall with shut-off valves and pressure gauges. The compressed air piping system will be connected to SLAC site-wide compressed air piping. The estimated demand for two beamlines is approximately 30 SCFM.

11.4.6.2 Fire Protection

The UH currently has a wet fire sprinkler system. Zone control valves with supervisory and flow switches are provided where the piping system enters the tunnel. Modifications to the current fire water main line's supports will be required to accommodate transportation paths of the new undulators.

Current sump pumps along the existing tunnel collect any accumulated water, and drainage piping routes the water to an existing outdoor storage tank located outside of the BTH. The storage tank drains into the sanitary waste piping once the water has been tested. A high-level indicator is connected to the SLAC Distributed Control System (DCS) network to monitor the water level. No modifications will be required.

11.4.6.3 Service Building 921

The current air handling unit (AHU) with cooling coils, economizer and chilled water piping and air filters provides conditioned air to the service building. The AHU removes the heat generated by the electronic racks.

In the service building, the current fire protection piping system is designed to meet NFPA 13 and Life Safety Code 101.

11.4.6.4 Electrical

Electrical power for the UH new equipment I&C, PPS and power racks will be provided from the existing and new panels, located inside the service building 921 and 913 routing conduits, through the existing penetrations in the floor on both the north and south side of the service buildings.

11.4.7 Electron Beam Dump

No modifications to the existing HVAC system serving the EBD will be necessary to accommodate the technical requirements for the new beamlines. Radiation air monitoring will be required per PRD LCLSII-1.2-PR-0265, *Environmental Radiation Monitoring Requirements.*

The existing outdoor exhaust fan serving the tunnel area between FEE and EBD removes any excess heat when the beam is off. Operation of the exhaust fans and AHU is interlocked, and all equipment is controlled and monitored by SLAC's EMS.

Modifications to the existing beam dump pits will be required to provide room for the beam pipes leading to the beam dump devices. The modifications resulting from the increase power of the beams will include the addition of iron shielding in strategic locations.

Utilities will be provided for both beamlines, which will require reconfiguring the existing utilities, minor structural modifications to the beam dump trench, and installing additional utilities for the second beamline.

Interfaces between Accelerator systems and Infrastructure systems are described in ICD LCLS II-5.2-IC-0174, *EBD to Infrastructure Systems* and LCLSII-5.3-IC-0114, *XTES to Infrastructure Systems*. Detailed requirements are found in RDS TBD.

11.4.7.1 Mechanical

An isolated LCW cooling system is required due to the increased beam power and potential cooling water activation. Supplemental LCW piping will be necessary to accommodate cooling requirements for the components of the new beamlines.

Supplemental clean, dry, compressed air at 100 psig will be installed along the length of the EBD tunnel. Compressed air piping drops from the existing CA system, with shut-off valves and pressure gauges will be installed. The compressed air piping system will be connected to SLAC site-wide compressed air piping. The estimated demand for the two beamlines is approximately 40 CFM.

Current sump pumps in the dump pits are routed to the UH drainage system. The current fire protection piping system for the EBD is designed to meet NFPA 13 and Life Safety Code 101. The EBD is classified as an Ordinary Hazard (Group I) facility.

11.4.7.2 Electrical

Electrical power for the EBD new equipment will be provided, as required, by the existing panels located inside the service building 921 routing conduits and by wires through the existing penetrations in building 921. Any electrical utilities located in the new beamline area will be relocated or removed as required to accommodate installation of the new equipment.

11.4.8 Front End Enclosure Add Figure

Modifications to the existing FEE structure will be required to provide for the additional beamlines. The modifications will include structural modificationsincluding a new entrance, and coring through the common wall leading into the experimental stations.

Utilities will be provided for both beamlines through a reconfiguration of existing utilities. Additional utilities will be provided for the second beamline.

Interfaces between Photon systems and Infrastructure systems are described in ICD LCLSII-5.3-IC-0114, *XTES to Infrastructure Systems.*

Detailed requirements are found in RDS LCLSII-5.3-RD-0130, *Front End Enclosure (FEE) and FEE Maze*.

11.4.8.1 Mechanical

The FEE tunnel is currently sharing a HVAC system with the EBD to provide ventilation and conditioned air. The AHU serving both FEE and EBD is located in basement mechanical room of the NEH. This system will be modified to address the structural changes and access changes in the FEE.

A supplemental supply and return PCW piping with pressure gauges and isolation valves will be mounted on the wall of the FEE tunnel. PCWS and PCWR connections for experimental equipment will be spaced along the wall of the tunnel. The PCW serving the FEE is currently being fed from an existing PCW piping system installed in the Central Utility Plant, and the current PCW system includes recirculating pumps, plate heat exchanger, control valves, temperature and pressure sensors, valves and piping. The current PCW system will be modified to accommodate the anticipated increase in loads in the FEE. Chilled water (CHW) piping from the Central Utility Plant is connected to the heat exchanger to remove the heat from the PCW system.

The operations of the current HVAC and PCW systems serving the FEE are both controlled and monitored by SLAC's Energy Management System.

11.4.8.2 Fire Protection

Minor modifications to the existing fire protection piping system serving the FEE will be required to accommodate installation of new science equipment supporting the new beamlines.

11.4.8.3 Electrical

New electrical power for FEE area equipment will be provided, as required, from both existing and new panels located inside the NEH and FEE area alcove. All electrical utilities

located on the north side of the FEE will be relocated or removed, as required, to accommodate installation of the new beamline equipment and any control racks.

Electrical distribution panel boards (480V or 120V/208V) will be installed to provide power to various systems, I&C racks, and PPS racks located in the FEE and maze alcove.

11.4.9 Near Experimental Hall

Modifications to the NEH will consist of reconfiguring the first experimental hutch, located at the sub-basement level within the NEH. The hutch will be converted for installation of new experimental end stations. Modifications will include relocating existing wall-mounted power, mechanical, ventilation, and cooling systems. Radiation protection for the existing experimental hutch includes lead-line soft (sheetrock) walls with multiple utility penetrations and access doors. All radiation protection will be restored during the utility reconfiguration.

Interfaces between Photon systems and Infrastructure systems are described in ICD LCLSII-5.3-IC-0114, *XTES to Infrastructure Systems*.

Detailed requirements are found in RDS LCLSII-3.5-RD-0013, *XTES in NEH*.

11.4.9.1 Mechanical

In order to accommodate the reconfigured experimental Hutch 1 and Hutch 2 and related support areas, the following upgrades and changes will need to be made:

- Modifications to the current HVAC system's chilled water piping, hot water reheat coils piping, conditioned air, and exhaust ductwork to meet user requirements
- Equipment upgrade and piping modifications to the current PCW system
- Installation of supplemental control points to the current energy management system
- Modifications to the current compressed air piping distribution system
- Minor modifications to the existing fire sprinkler system serving the sub-basement level

11.4.9.2 Electrical

All the hutches have existing electrical utilities (lighting, outlets etc.) and panel boards located inside and outside the hutches that support all the electrical requirements for the experimental areas, including controls and monitoring systems. Power to these panel boards inside and outside the hutches is provided by the main distribution panel located in the NEH electrical room. This panel is powered by the unit substation, located in the Central Utility Plant in building B950A.

11.5 LCLS-II Standards

All infrastructure systems will comply with the following LCLS-II system standards for new renovations or for modifications of existing infrastructure, including local code requirements LCLS-II Project Building Office Codes and Standards of Record and SLAC Building and Site-

Wide Design Guidelines, Binder 2, DS-018-000-01-R0, SLAC National Accelerator Laboratory, Menlo Park, California, 28 July, 2010.

11.5.1 Architectural Standards

Planning and development of new facilities at SLAC is guided by the SLAC Long Range Development Plan. The campus planning framework is summarized in the following [1]:

"SLAC's scientific and support facilities were constructed on a strongly conceived framework established in the General Development Plan (1961) and the Master Plan (1966). For nearly four decades SLAC grew within this original framework; however, over the years, many small support, storage buildings, and increased parking demands have crowded the core research areas and obscured the original circulation plan. This next stage of facilities development at SLAC cannot be accommodated by "filling in" parking and scarce open space. The Long Range Development Plan (LRDP) utilizes strategies that will make room for growth: redevelopment of low-density areas into high-density, expansion and intensification of existing facilities, and importantly, careful consideration of expanding into undeveloped areas.

The LRDP will gradually implement the replacement of small, outdated structures with more efficient and well-planned development, with the clear organizing principles of the original Master Plan will be restored and reinforced. The logic of well-planned development will make room for research program expansion and the human support systems (offices, parking, food service, short term lodging, and computer facilities) necessary to serve those programs. SLAC users and visitors will find their way safely and efficiently through an ordered campus system. All of this is compatible with the casual, naturalistic feeling of the SLAC landscape and will reserve areas for the creative work of enterprising scientists.

The LRDP was created by a group of dedicated experts, both the SLAC LRDP Working Committee and the professional land use, environmental and campus planners from the Stanford University Architect and Planning Office. The LRDP thus combines the entrepreneurial spirit, scientific knowledge, and working experience of SLAC employees with sound planning expertise to produce the LRDP. This effort will ensure that planned future development at SLAC will reflect the highest and best use of financial, land, and human resources to meet the Center's research goals."

Building on these principles, the project will select appropriate sites, layouts, exterior finishes and site lighting with consideration for the Long Range Development Plan, the local environment, existing facilities and structures, the safety of personnel, staff, visitors, and guests.

11.5.2 Structural Standards

Structural work includes assessing the existing condition of the structures proposed for structural modifications. The necessary modifications of the facilities will comply with current state codes, SLAC and DOE guidelines.

Structural Design Criteria

The selected structures will be evaluated against and conform to CBC 2013 requirements, as well as SLAC Building & Site-Wide Design guidelines (DS-018-000-01-R0) and Seismic Design Specification for Buildings, Structures, Equipment, and System (SLAC-I-720-0A24E-001-R003). Table 11-2 lists relevant design parameters.

Table 11-2. General Structural Design Parameters

Parameter	Value	Comment

Structure dead load	ASCE 7	Minimum loads
Structure live load	varies	As calculated
Floor live load	150 psf or equipment weight	Use greater value
Collateral dead load	5 to 10 psf or as calculated	Use greater value
Laser room, service building, HVAC deck live load	350 psf or equipment weight	Use greater value
Platform, stairs and corridors Live Load	100 psf	
Wind Load	ASCE 7, 85 mph, Exposure C	Basic "3 second gust"

Seismic Design

The structures which are identified for modification will be analyzed for seismic loads and deflection limits generated by strong ground motion during a seismic event, using parameters given in Table 11-3.

Table 11-3. General Seismic Design Parameters.

Parameter	Value			Comment
Occupancy category	II			Importance factor I=1.0, Ip=1.0 (Ip=1.5 for life safety systems)
Soil class	varies			Based on Geotechnical Report, Assume Class D
Seismic coefficients - CID				
Latitude:: 37.41230 deg.	Ss= 2.438g	S1=1.238g	SMS=2.438g	SDC=E (ASCE 7.05, article 11.6)
Longitude: -122.2397 deg.	SMI=1.856g	SDS=1.625g	SDI=1.238g	Fa= 1.0 Fv=1.5
Seismic coefficients - BTH				
Latitude:: 37.416928 deg.	Ss= 2.414g	S1=0.997g	SMS=2.414g	SDC=E (ASCE 7.05, article 11.6)
Longitude: -122.200955 deg.	SMI=1.495g	SDS=1.609g	SDI=0.997g	Fa= 1.0 Fv=1.5

Reference: Seismic Design Specification for Buildings, Structures, Equipment, and Systems: 2014, SLAC-I-720-0A24E-001

11.5.3 Mechanical Systems Standards

Occupied spaces and specific technical equipment installations will require process cooling water for various technical components. Technical components are housed in various areas, and as such, will require independent clean or general air conditioning zones to handle different temperature set points. for specific spaces A mechanical equipment plant will provide the infrastructure space for cooling and hot water needs.

Chilled Water System

The cooling plant consists of suitably-sized packaged, air-cooled chillers with associated circulating chilled water pumps to support the air handling system.

Heating Hot Water System

The heating hot water system consists of a boiler with associated circulating pumps and distribution piping for heating hot water.

Air Handling System

Air handlers and distribution systems will be sized to provide the required volume, temperature and pressures for the intended areas. Specific rooms may require additional, smaller package air handlers or fan coil units,(FCU). The air handlers will be a packaged fan-wall type, furnished with 30 percent pre-filter, 95 percent high efficiency filter, chilled water coils, hot water reheat coils, humidifier, HEPA filters where applicable, and associated variable frequency drive (VFD).

Ductwork and Air Distribution

The air flow delivery system consists of lined, rectangular or round, galvanized supply ducts. It returns ductwork extending from the air handler, located at the nearby mechanical equipment plant, and terminates inside the service areas. Supply air will terminate at engineered heights derived from installation stay-clear envelopes and equipped with Lami-Vent or equivalent supply air diffusers placed at equal distances throughout the service area.

EMS and Controls

The site WebCTRL Direct Digital Controls (DDC) System will be provided to monitor and control the mechanical systems and equipment, and it will be integrated with EPICS through BACnet protocol.

Cooling Water Systems

Cooling water systems will include CTWLCW systems and PCW systems. Cooling is required for the injector components, klystrons and modulators, bunch compressors, and electronics racks. Each sector will have independent LCW cooling systems.

Fire Protection System

The fire protection piping system will be a wet type fire sprinkler system per NFPA 13, for Ordinary Hazard (Group 1). The sprinkler system is connected to the nearby existing riser sprinkler main. Sprinkler system is designed per NFPA 13 at 0.10 GPM/FT^2, with heads rated to 155 degrees Fahrenheit. Each head is spaced to cover a maximum of 130 square feet. Each single zone includes a zone control valve with supervisory and flow switches where the system enters into the building. A fire department connection will be provided at the sprinkler system riser. Changes to sprinkler coverage will be installed as needed for new equipment configurations.

11.5.4 Electrical Systems Standards

The site electrical master substation systems provides 12.47KV underground power distribution system to the all the site buildings, including the new cryoplant building substation and existing gallery B002 substations. From there it will be distributed to various electrical

equipment, such as motor control centers and distribution panels that will provide power for all mechanical infrastructure and science support equipment in the gallery and the tunnel. Advanced metering will be provided for all installations, and meters will be connected to SLAC's metering system.

Unit Substation

An outdoor 12.47 KV 1,000 KVA unit substation will supply power to the new cryoplant building. The substation shall have a draw out main circuit breaker (MCB) primary section; outdoor, FRP3-based, 12KV to 480/277V oil-filled transformer and a secondary distribution section with an MCB and feeder breakers of the Magnum DS type. All unit substations will be installed on a concrete pad.

Motor Control Center (MCC)

The 1200A, 480V/277V rated MCC for the new cryoplant building will be furnished with a 100-percent-rated solid state main circuit breaker with LSIG trip unit, branch circuit breakers, starters, power monitoring, and metering instruments.

Power for the Sector 0 injector laser rooms, gallery and injector area I&C racks, power supply racks, SSA, and PPS racks will be provided from new electrical distribution panel boards fed from the above-mentioned MCC through step-down transformers.

Distribution Panel Boards

480V or 120V/208V distribution panel boards will be installed to provide power to systems and support equipment. Distribution panel boards will be dead-front, dead-rear, solid-state-type. Branch circuit breakers are group mounted, front-accessible, bolt-on thermal magnetic molded case type, with adjustable magnetic trip settings. Full-length busses are required for both voltage and 200 percent neutral bussing on 208V distribution panels.

Dry Type Transformer

The transformer will be NEMA TP-1 compliant, Energy Star labeled to step down voltage from 480V to 120V/208V, three-phase/four-wire, and K13 rated with 200 percent neutral and individual neutral wire for each of the phase wire.

Arc Flash Rating

For the 480V system, solid-state type breakers will be used for coordination selectivity to reduce fault-clearing time. For the 208V system, limit step-down transformers will be provided to 112.5 KVA.

Lighting System

An existing lighting system, consisting of industrial fluorescent and recessed fluorescent light fixtures, is provided for the existing enclosures, vaults, and tunnels. New installed lighting levels shall be designed in accordance with IES recommendations and suitable for the specific application. Fixtures shall be fluorescent type, with energy-saving T8 lamps, 3,500 Kelvin color

temperature with high efficiency electronic ballasts with 95 percent power factor, and total harmonic distortion (THD) of less than 10 percent. Lighting control will be designed to meet or exceed the requirement of Title 24 and other Project requirements. Exterior lighting at the entrances, landings, and equipment pad shall be LED, with photocell controls and bypass switch.

Grounding and Bonding System

Service grounding will be designed as required by the California Electric Code and the National Electric Code (NEC) requirements. All ground busses will be tied back to the area grounding. All systems and equipment will be bonded as per NEC and NFPA requirements.

Fire Alarm and Detection System

The fire alarm and detection systems will integrate with the existing campus network. The fire alarm and detection systems will be designed to comply with NFPA 72 and all associated codes and regulations. New fire alarm system installations will consist of, but not be limited to, a fire alarm control unit, alarm initiating devices, occupant notification appliances, and associated ancillary equipment for interfacing the new fire alarm system with the existing SLAC alarm receiving equipment. The fire alarm system will also communicate with other life safety systems and building system equipment, as applicable.

The fire detection system will be VESDA Air Sampling and Early Warning Smoke Detection. The VESDA system will consist of, but not be limited to, the sampling pipe network, , aspirators, filters, detector assembly network, and digital communication ports. The fire detection system will also communicate with other life-safety systems and building system equipment, as applicable.

Telecommunication System

The existing telecommunication system is provided to support the physical transmission facility for voice, data and low voltage networks. The system consists of, but is not limited to, the following:

- Telecommunication backbone pathways, which include a dedicated point-to-point (BDF to IDF) pathway system.
- Telephone and data structure cabling systems that comply with the requirements of EIA/TIA 569 Commercial Building Standard for telecommunications pathways and spaces. The cabling system will be upgraded to comply with pertinent codes, rules, regulations, and laws of the authorities having jurisdiction.

11.5.5 Site Utilities Standards

Site civil utilities improvements includes storm drainage, site sanitary sewer service, potable water service, and fire protection water service systems, and will conform with all current applicable codes and CBC 2013 requirements. Design guidelines set in SLAC Building & Site-Wide Design guidelines (DS-018-000-01-R0) will be considered. The following links are the reference requirements for survey control.

Horizontal and Vertical Control

Reference: Height Systems for LCLS-II Construction, LCLSII-1.1-TS-0015

Reference: LCLS-II Beamline Coordinates, LCLSII-1.1-TS-0034

Reference: Plane Coordinate Systems for LCLS-II Construction, LCLSII-1.1-TS-0014

Reference: Tunnel Finished Floor Elevations and Shield Wall Locations, LCLSII-1.1-TS-0016

Excavation and Grading - Site Earthwork

Earthwork will be designed in accordance with the recommendations provided in the project geotechnical report. Consideration will be given to the use of recycled roadway base and asphalt pavement as part of the site earthwork fill requirements for the site. Site grading design will be done to minimize the need for imported fill material. Existing asphalt, concrete, and soil to be excavated will be characterized by SLAC for possible contamination to determine disposal and/or reuse prior to start of work. **Parking Lot, Roadways and Sidewalks**

New parking lots will be provided at areas of new personnel concentration, such as the cryogenic plant. They will be provided with charging stations for government electric vehicles and with minimum lighting of 1 foot candle. Parking lots will have curbs and gutters, and the drainage system will be connected to groundwater recharge systems.

Primary roadways, as applicable, will be designed for H20-44 truck loading, fire truck loading, and FL-40 forklift loading (98,500 pounds for each front wheel and 9,500 pounds for rear wheels). Roadways will have curbs, gutters and catch basins where needed. Catch basins will be connected to existing drainage system. Rerouted roads will be constructed to match existing roads.

Domestic Water

The domestic and fire water service connections will be designed based on all applicable codes and on the sizing requirements for the building. Metering for the domestic service, backflow prevention, and valve control for services will be included. Approval for fire services will be under the direction of the SLAC fire marshal. All water connections — domestic, fire and irrigation — are supplied from one master source on the SLAC campus.

Pipe will have a minimum cover of three feet. A cover of less than three feet may be considered, but only if some other protection is provided and the proposed installation is approved by SLAC.

Sanitary Sewer System

Toilet and utility rooms will be provided with hot and cold domestic water and vent and sanitary-waste plumbing. The sanitary waste will connect and discharge to the existing sanitary sewer system. Additional loads to the existing sanitary sewer system will be evaluated for capacity, and modifications engineered and installed.

Sewer service for the new installations will be designed to provide capacity for the calculated sewer flows. The minimum slope for the pipe will be determined based on a minimum design velocity of 2.0 feet per second at peak flow and a minimum of four inches in diameter.

11.5.6 Environmental Standards

Storm Water Management

Section 438 of the Energy Independence and Security Act (EISA) of 2007 requires the final design, construction and maintenance of all projects with a footprint that exceeds 5,000 square feet in such a way that maintains or restores, to the maximum extent that is technically feasible, the predevelopment hydrology of the property with regard to the rate, volume, and duration of flow. Rainfall up to the 95th percentile rain event shall not enter the storm drain system, but be accommodated by one or more alternative methods, such as permeable pavements, landscaping or sediment basins. (A 95th percentile rainfall event is an event for which the measured depth of precipitation over a 24-hour period is greater than or equal to 95 percent of all 24 hour storms over a 30 year period.). The project will be engineered and installed in accordance with these requirements.

Construction and Operations Noise Mitigation

Reference noise reports for design of the cryoplant noise mitigations are linked below:

- Reference: Cryogenic Plant Construction and Noise Assessment, LCLSII-5.4-EN-0215
- Reference: Background Noise Measurements in First Ten Sectors of SLAC Linac, LCLSII-1.1-EN-0019

11.6 Sustainability Standards

SLAC, as a federal facility, is required to comply with Executive Order (EO) 13423, “Strengthening Federal Environmental, Energy, and Transportation Management,” dated January 24, 2007. The order sets goals in the areas of energy efficiency, acquisition, renewable energy, toxics reductions, recycling, renewable energy, sustainable buildings, electronics stewardships, fleets, and water conservation. In EO 13423, Section 2(f), federal agencies are required to ensure that new construction and major renovation of agency buildings comply with the Guiding Principles for Federal Leadership in High Performance and Sustainable Buildings set forth in the Federal Leadership in High Performance and Sustainable Buildings Memorandum of Understanding (2006).

The approach to be taken by the project toward this initiative includes:

- Meet High Performance and Sustainable Buildings practices for new construction and renovations in the conventional facilities scope for LCLS-II.
- Meet Leadership in Energy and Environmental Design (LEED) gold certification practices for new construction, as applicable.

For additional information, see http://www.fedcenter.gov/programs/greenbuildings/.

BES has concurred that the LCLS-II Project scope does not need to implement High Performance and Sustainable Building provisions because no federal buildings will be constructed. This fulfills the HSPB requirement for CD-1.

12 SYSTEMS INTEGRATION AND AVAILABILITY

TECHNICAL SYNOPSIS

The overall design authority and responsibility for ensuring that the design of the facility meets critical operational and safety requirements associated with the project resides with the LCLS-II Project Director. The Project Technical Director is responsible for the Project level technical integration of the facility. The LCLS-II Systems Engineering Manager is responsible for global engineering and design standards and system integration. Responsibility for system integration starts from the top with the Project Director, Project Technical Director, and System Managers and permeates through the entire organization. Each Control Account Manager and project line manager involved in project activities is responsible for the integration of their own work and that of their subordinates. The Systems Integration Team provides horizontal integration of systems to complement the vertical integration provided by the Work Breakdown Structure of the Cryogenic Systems, Electron Systems, Photon Systems and Infrastructure Systems.

12

12.1 Introduction and Overview

The LCLS-II Project team consists of members from institutionally and geographically diverse organizations and is managed by the project office at SLAC. The LCLS-II Project organizational and management structure is designed to accomplish the project's mission effectively and safely. The *LCLS-II Preliminary Project Execution Plan*, LCLSII-1.1-PM-0002, which will become the Project Execution Plan, describes the high level responsibilities and level of authority for personnel in key positions and provides descriptions of those positions. The Project Management Plan [1] defines the plans, organization, responsibilities and systems for managing the LCLS-II Project. The *LCLS-II Quality Assurance Plan*, LCLSII-1.1-PM-0007, provides requirements applicable to all project participants, encompassing all activities performed by or for the LCLS-II Project, from research and development (R&D) through facility acceptance. The *LCLS-II Project Systems Engineering Management Plan*, LCLSII-1.1-PM-0043, describes the Systems Engineering processes and related procedures to be used on the LCLS-II Project, to assure successful technical development and delivery of the LCLS-II facility. All Project functional line managers are responsible for the delivery of their respective systems and for actively managing interfaces with interconnected systems.

12.2 Systems Integration Team activities

The Systems Integration Team consists of individuals from specific disciplines required to support integration activities. The LCLS-II Systems Engineering Manager conducts regular Integration Team meetings with all affected integration support personnel. Overall responsibility for each functional area remains under the Project line management of the respective System Manager. After an assessment of the specific issue and the Project's requirements, the Systems Engineering Manager determines if Integration Team involvement is required, or whether a specifically designated Control Account Manager (CAM) or Responsible Engineer should be assigned. In making this determination, consideration is given to the issue complexity and visibility, requirements for cross-functional support, unusual technical requirements, whether the issue is a one-time anomaly or is ongoing, and other considerations. In the case of integration or installation work involving only a single functional LCLS-II system (e.g., late shipment of a procurement, missing or discrepant part or component), system personnel keep the Systems Engineering Manager apprised of the work through informal communications and, more formally, at regularly scheduled Project Status Meetings.

The LCLS-II Systems Engineering Manager facilitates the Integration and Coordination process for assigned issues or activities and maintains the project level Action Item List. The Systems Engineering Manager conducts regular meetings to identify and discuss project integration/installation requirements, issues and plans, and ensures that appropriate functional

areas are represented at these meetings. Action Items are assigned and resolution tracked to completion.

The following are examples of topics discussed and addressed:

- Technical interface requirements
- SLAC interface issues
- Procurement support requirements related to integration or installation activities
- Installation and/or integration documentation
- Engineering analysis and design review

12.3 Integration and Coordination with LCLS X-ray Operations

An LCLS Operations scientific leader for the development of upgrades to existing instruments has been designated to interface with the LCLS-II Project. Integration and coordination with LCLS Operations development of user requirements, experimental instrumentation and build-out plans is facilitated by communications at recurring meetings with the Project Management. Schedules for the project installation work are coordinated with facility users through the LCLS Operations scientific leader.

12.4 LCLS-II Project – Final Design Plan

The *LCLS-II Project Final Design Plan*, LCLSII-1.1-QA-0065, provides for a phased completion of the final designs for the LCLS-II facility. The plan ensures that designs are sufficiently mature to start procurements and construction, while enabling the most cost-effective schedule for constructing the facility and maximizing the technical capabilities of the facility at CD-4.

The *LCLS-II Project Systems Engineering Management Plan*, LCLSII-1.1-PM-0043, describes the Systems Engineering process and related procedures used on the LCLS-II Project, to assure successful technical development and delivery of the LCLS-II facility. This Systems Engineering approach ensures that safety, quality and integration are addressed from the requirements definition and design stage of the Project and controlled throughout the Project life cycle.

Final Design is defined as the completion of the design effort and production of all the approved design documentation necessary to permit procurement, construction, testing, checkout and turnover to proceed. The Final Design will include clear statements of testing requirements and acceptance criteria for the safety and functionality of all subsystems. Independent technical reviews are performed periodically during the design process. These reviews are called by the Project Director to evaluate design progress and provide expert advice on key technical design choices.

The Project's integrated, resource-loaded schedule provides the baseline scope, schedule and costs. It contains the design development and verification tasks to be performed, the resources required and the scheduled dates to perform the work. The status of work accomplished is provided by the Control Account Managers on a monthly basis and input to the Project's Earned Value Management System (EVMS).

Progress on final design is monitored on a monthly basis by Project management, at the control account level, using the Project's Earned Value Management System.

12.5 Availability

The LCLS-II X-Ray source is planned to be a user facility and therefore expected to operate with high availability. The approach used to set availability goals for systems and areas of the complex is described in the Physics Requirements Document (PRD), *LCLS-II Availability*, LCLSII-1.1-PR-0163.

Availability is defined as the percentage of time the facility is running and capable of supporting user operations when user operations are scheduled. Maintenance periods and scheduled outages are not included in the analysis. Availability goals are taken into consideration during the design, construction and operation of LCLS-II. The availability budget presented in the PRD represents the long term availability goal after three to five years of operations. The availability performance at the start of user operations may be less than this target.

LCLS-II availability target for user operations is 95%. This is the same target set for LCLS, which has demonstrated performance at or above the 95% level. Table 12-1 provides LCLS-II system availability targets and, where applicable, corresponding actual LCLS experience from recent operating runs. The target availability values are consistent with actual LCLS operating experience. The availability targets for the cryogenic systems are based on actual operating experience at JLAB and other existing facilities. While some components of the LCLS-II cryogenic systems incorporate newer technology than the existing facilities, the reliability of these components is expected to be consistent with the availability targets of the system.

Table 12-1. System Availability

System	LCLS-II Target Availability	LCLS Runs IV-VII Actual Availability
Lasers	99.73%	99.19%
Magnets	99.997%	100.00%
PS controllers	99.57%	99.03%
RF power sources	99.85%	
SCRF Linac	99.87%	
Vacuum	99.88%	99.74%
Tuning and Diagnostic	99.16%	98.85%

Water system	99.77%	98.74%
AC power	98.96%	96.90%
Cryogenics Plant	98.62%	
Controls	99.62%	99.32%
Photon Controls	99.89%	99.78%
All	95.00%	94.66%

12.5.1 System Availability Targets

LCLS-II can be divided into the following systems: Magnets, Power Supply Controllers, RF Power Sources, SCRF Linac, Vacuum, Tuning and Diagnostics, Water, AC power, Cryogenics Plant, Controls, Photon Controls, and Lasers.

For many of the systems where a relatively accurate, one-to-one, comparison can be made between LCLS and LCLS II; LCLS availability performance is used to predict LCLS-II performance. For systems where there is no LCLS experience, reliability numbers for similar systems at other facilities (CEBAF and LHC) are used to establish expected availability performance.

12.5.2 Reliability Availability Maintainability and Inspect-ability

A complete availability program needs to take into account reliability, maintainability and inspect-ability, as well as availability.

Reliability is the probability that an item will survive to a specified operating age, under specified operating conditions, without failure. In addition to maximizing availability, systems are designed to minimize the Mean Time To Repair (MTTR) and maximize the Mean Time Between Failure (MTBF).

The concept of maintainability takes into account the time of recovery from an event. A system can have a long downtime event in a single week, while still achieving its availability goals. LCLS users have beam time allocated to them on a week-to-week basis. Long outages in a single week would severely affect that user group. Systems typically need to operate with unplanned outages of at most 2-4 hours in a given week. Systems are designed with input from operations personnel to meet the desired maintainability.

Inspect-ability refers to the ability of an availability program to monitor systems in-situ in order to predict and remedy imminent faults before they occur. This leads to increases in the MTBF.

Setting targets for availability is based on documented operating experience at existing facilities with similar systems. Where appropriate, the LCLS operating experience is utilized. The cryogenics plant availability target is derived from CEBAF and CERN performance. The

cryomodule availability is derived from ILC and XFEL simulations, as used in the MATLAB based simulation program *AvailSim* [2]. LCLS-II Project technical experts work with SLAC Operations representatives to provide input to *AvailSim*, for components and systems that are new to SLAC. The *AvailSim* program takes as input a list of components, their quantities, mean time between failures, mean time to repair, and the effect of their failure. It then simulates the failure and repair of components, while tracking important machine parameters such as energy overhead and time available to users. *AvailSim*'s output can then be used to predict expected replacement cycle(s) of critical components such as cryomodules. The simulation output will also assist in predicting the need for spare inventory, as well as planning and scheduling of long maintenance downtimes.

12.6 References

1 "LCLS-II Project Management Plan"

2 T. Himel, *et al*., "Availability and Reliability Issues for ILC", Particle Accelerator Conference (PAC 07), Albuquerque, NM, USA, June 2007.

13 RADIOLOGICAL CONSIDERATIONS

TECHNICAL SYNOPSIS

This chapter describes the radiological impact of the LCLS-II beam operations and covers radiation protection measures and controls needed to mitigate them. Experience with LCLS=I and previous high-power beam operations at SLAC and peer laboratories provided an excellent basis for the development of the requirements needed for shielding, the Beam Containment System (BCS), the Personnel Protection System (PPS) and other systems required to protect personnel, public and the environmental. Every effort is made to use existing infrastructure, especially existing accelerator housing and dumps. Changes to the existing protection systems are required to account for the new beamlines and faster response times needed for beam mis-steering events. Shielding modifications in some places, and new area and environmental radiation monitoring systems are required to accommodate the much higher beam power compared with LCLS.

13.1 Requirements and Reviews

13.1.1 Design Requirements

LCLS-II is designed to ensure that radiation doses above background received by workers, the public, and the environment are As Low As Reasonably Achievable (ALARA), as well as to prevent any person from receiving more radiation exposure than is permitted by SLAC's radiation safety requirement.

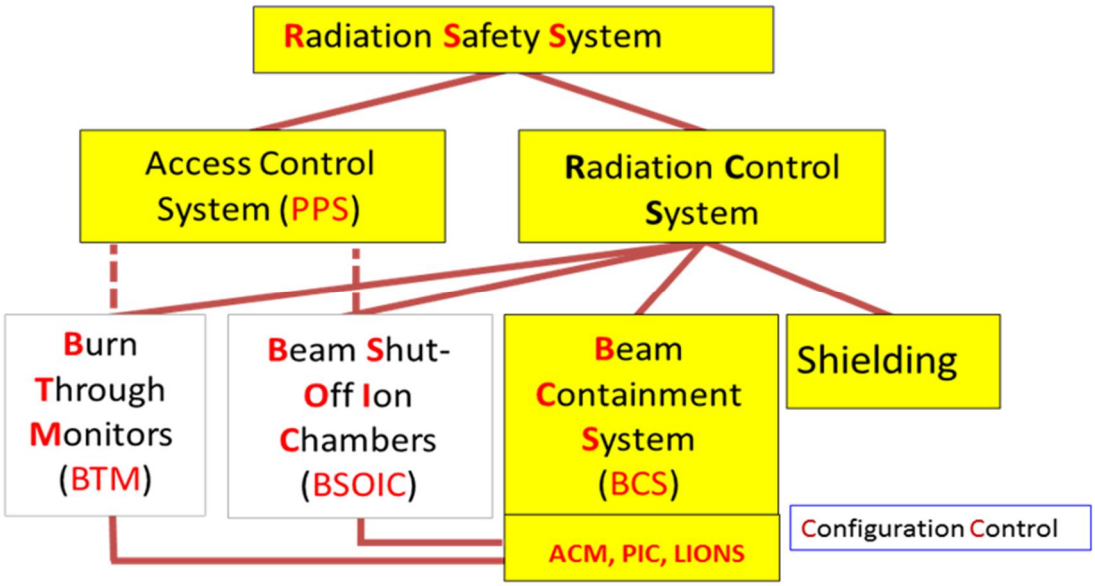

Figure 1. Overview of the LCLS-II radiation safety system (BCS components tied to PPS are in white boxes).

Several technical, operational, and administrative systems were taken into account to implement the radiation safety program for LCLS-II, as described in the SLAC Radiological Control Manual [1] and the Radiation Safety Systems Technical Basis Document [2]. These systems are part of the SLAC Radiation Safety System (RSS); a combination of active and passive safety systems used to protect personnel from prompt radiation. Figure 1 shows an overview of the RSS components used in LCLS-II. The primary components of the SLAC RSS include shielding to attenuate radiation (explained extensively in section 13.4) and several active systems, which are described below:

13.1.1.1 PPS system at SLAC

At SLAC, a Personnel Protection System (PPS) is a combination of devices and interlock systems that include access control and warning systems and beam stoppers. The PPS prevents access to secured areas when beam is possible or present [2].

The interlock system must be operated, maintained, and tested in accordance with a set of documented administrative procedures, which ensure that such activities as setting access states, searching the beam enclosures, and testing the interlocks are carried out safely and thoroughly.

At SLAC, the PPS primarily serves an access control function. In the following description, PPS will be used because of its widespread and long-standing use at SLAC, and because the system does perform radiation monitoring and safety functions other than controlling personnel access. PPSs also provide the logic and the hardwired connections to beam-shutoff devices, which operate in response to signals from Beam Shut Off Ion Chambers (BSOICs) and Burn Through Monitors (BTMs) and may provide input to or control for other safety functions. These devices are described in separate sections under the heading, "Beam Containment System" (BCS). In addition, the PPS will ensure that beam stoppers are in place to prevent prompt radiation exposure to personnel located inside beam enclosures, prevent entry into beam enclosures while beams are operating, and to turn off beams when a security violation is detected. Beam-shutoff devices operating in response to signals from BTMs and BSOICs may also be integrated into the PPS.

While the main function of the PPS is to prevent entry into radiation enclosures when beams are operating, and to turn off the beams when a security violation is detected, there are several other important functions that the logic circuits must also accomplish. These include:

- The provision of administrative assistance interlocks for orderly searching of an area before beam turn-on
- Interlocks for setting up the various entry states, such as Controlled and Restricted Access
- Provision for emergency beam shut-off
- The operation of annunciator signs, audio warning systems, and other indicators and warnings
- Controlling access to exposed electrical hazards in legacy tunnel areas — specifically, uncovered magnet terminals operating at 50 V and above.

Specific requirements for LCLS-II PPS are described in section 13.5.1

13.1.1.2 Hutch Protection System at SLAC

Like PPS, the Hutch Protection System (HPS) prevents personnel from entering areas with dangerous radiation levels and burn-through, in this case for X-ray beam lines.

13.1.1.3 BCS at SLAC

SLAC's BCS policy[2], requires beams to be contained in prescribed channels and the beam power and beam losses to be limited to prevent excessive radiation within occupied areas. The BCS is implemented through a system of redundant fail-safe electronic and mechanical devices, which are subject to strict administrative controls. A typical BCS consists of mechanical devices (such as collimators, magnets, electron beam stoppers, beam dumps) and active devices (average current monitors, magnet current monitors, protection ionization chambers (PIC), long ionization chambers (LION)) that shut off the beam when they detect out-of-tolerance conditions. The

specific BCS configuration required for a particular experiment or mode of operation is described in the corresponding Beam Authorization Sheet.

The BCS for the linac typically uses average current monitor to limit the incoming average beam power, PICs and LIONs to limit abnormal beam losses, protection collimators to limit the range of trajectories of mis-steered beams, and ion chambers and flow switches to protect collimators, stoppers and dumps. The particular configuration depends on the experimental program and specific beam requirements.

It should be noted that the BCS is distinct and separate from the Machine Protection System (MPS). The BCS protects personnel against elevated radiation levels in occupied areas. The MPS protects beamline components that do not have a personnel safety function from damage due to high-power beams. The MPS uses many of the same protection techniques and instruments as the BCS, but there is less redundancy and less-rigid administrative control, compared to the BCS.

Functions of the BCS include monitoring and limiting the beam power in a beam line to the allowed value, limiting the losses along a beam line, protecting safety-related beam line components from damage, and shuting off the beam if excessive radiation levels are detected or can be generated in occupied areas.

Specific requirements for the LCLS-II BCS are described in section 13.5.2.

13.1.1.4 BTMs and BSOICS

Other safety systems, such as BTMs and BSOICs' active area monitors, are also integrated into the SLAC RSS. BTMs are pressurized systems located near shower maximum that are designed to rupture when the device being protected absorbs greater than its allowed beam power, thus detecting the onset of damage to mechanical protection devices, such as collimators, beam stoppers, and beam dumps. BSOICs are interlocked radiation detectors that are used to detect prompt radiation and terminate accelerator operation if excessive radiation is detected within potentially occupied areas. BSOICs' trip limits are typically set at 10 mrem/h or 100 mrem/h, depending on the location of the detector and the occupancy of the area.

13.1.2 Radiological impacts and review process

SLAC has operated high-power beams in the past. However LCLS-II's anticipated beam power presents several additional challenges: the use of superconducting RF cryogenic modules for accelerating electron beams, the transport of high-power beams through the Beam Transport Hall (BTH), the undulators at forward angles with respect to the LCLS Experimental Hall (bremsstrahlung production points at experimental halls) and longer periods of beam operations (increased use factor).

Potential radiological impacts to the public and the environment include: 1) direct prompt radiation dose to the public, 2) doses to the public due to the production and release of airborne radioisotopes, 3) activation or release of radioisotopes to groundwater, 4) activated Low Conductivity Water (LCW) systems, and 5) storm-water pollution. The environmental impacts

from LCLS-II operations mainly come from high beam loss points, such as main dumps. Requirements from regulations (e.g., from DOE and EPA) and SLAC radiological environmental protection program, including the ALARA principle, are satisfied for LCLS-II by appropriate safety system design and operational controls. This is described in more details in section 1713.6.

Thorough and independent reviews of assumptions, techniques, results and requirements of radiation safety systems are planned and are already underway. Reviews of radiation safety systems are being performed by the Radiation Safety Committee (RSC) and ALARA committee at SLAC, as well as by subject matter experts from peers' laboratories, in both the US and abroad. Documents and actions generated from these reviews will be tracked to resolution by the LCLS-II project QA. These reviews cover the:

- beam parameters and beam losses,
- BCS and PPS specifications and the beam containment at the dump line and along the ray-traces,
- shielding and Monte Carlo calculations,
- radiological impact,
- design and retrofit of dumps and stoppers, photon beam lines, and
- operation radiation protection.

The PPS and BCS systems are subject to design reviews and technical implementation reviews by experts from within and outside SLAC. These systems are implemented with hardware redundancy and are subject to configuration control requirements as defined in SLAC Guidelines for Operations [3]. As part of the configuration control program, these systems are subject to access-driven inspections and check out. Further, these systems undergo rigorous annual certification as defined in SLAC Guidelines for Operations. LCLS-II is required, prior to checkout and operations, to perform an Accelerator Readiness Review where the operating parameters are captured in the Accelerator Safety Envelope, Safety Analysis Document, etc. The BCS will be designed to those parameters and to be in compliance with the governing documents.

13.2 Criteria for Radiation Protection Systems

13.2.1 Shielding and Radiation Safety Systems

The SLAC Radiological Control Manual specifies an administrative control level of 500-mrem total effective dose (TED) per year and a dose-management "ALARA Level" for radiological workers of a maximum of 360 mrem TED per year above natural background levels.. The actual dose that the majority of personnel at SLAC typically receive is well under these levels. This will continue to be the case for LCLS-II operations, with very little to no doses expected from prompt radiation generated during beam operations.

The following radiation dose criteria have been used in the design of the LCLS-II radiation safety systems:

1. The effective dose to personnel working inside and around the experimental halls should not exceed 100 mrem in a year (2000 work hours) for normal beam operation. The users of the LCLS-II who will be working in the experimental halls are not classified as radiological workers and therefore cannot be exposed to higher dose levels.

2. During normal operations, the LCLS/LCLS-II electron beam enclosures are shielded to an average dose rate of less than 0.5 mrem/h in accessible areas of the accelerator and research yard and to 0.05 mrem/h in general public areas (where yearly occupancy by non-radiological workers is potentially high).

3. The maximum effective dose rate in accessible areas at 30 cm from the shielding or barrier should not exceed 400 mrem/h for mis-steering conditions, defined as conditions that are comprised of infrequent or short-duration situations in which the maximum allowable beam power, limited by Beam Containment System (BCS) devices, is lost locally or in a limited area.

4. The effective dose-rate in the event of the Maximum Credible Incident (MCI) should not exceed 25 rem/h [2], and the integrated effective dose should not exceed 3 rem [2]. The MCI, which considers the unlikely scenario of failure of safety systems, is defined as the highest beam power that the accelerator can deliver to a point, assuming that all the BCS devices that limit beam power have failed.

5. In addition to shielding (bulk and local), the LCLS-II radiation protection systems have a BCS and PPS in the tunnel, and the HPS in the X-ray beam lines.

13.2.2 Radiological Environmental Protection

DOE/EPA [4][5][6][7], state and local regulatory limits, as well as SLAC administrative limits, and are to be maintained ALARA. The DOE Order 458.1 imposes an annual dose limit to the Maximum Exposed Individual (MEI) of a general public member of 100 mrem/y from all exposure pathways, including skyshine, radioactive air effluent, contaminated groundwater, release of potentially contaminated materials. The exposures must also be kept ALARA, thus measure may need to undergo a formal optimization process.

1. For the air pathway, the annual EPA/DOE dose limit for the MEI is 10 mrem/y. A continuous air effluent monitoring system is required for the release point that is expected to create MEI dose exceeding 0.1 mrem/y [8][9]. The annual dose to the MEI and the collective dose to the population living up to 80 km from SLAC needs to be evaluated and reported every year.

2. LCLS-II beam operations may not impact groundwater [10][11]. To meet this requirement, the groundwater cannot have detectable radioactivity due to LCLS-II operation. For

example, the EPA-required detection limit of ^{3}H in drinking water is set to 1000 pCi/L. The ALARA principle should be followed for soil and groundwater protection.

3. Storage, radiological monitoring and analysis, and discharge of wastewater (e.g. activated LCW) into sanitary sewer are managed per various requirements [12] to satisfy the regulatory discharge limits (e.g., 5 Ci/y of ^{3}H and monthly concentration limits in wastewater permit from the South Bayside System Authority) [13] and SLAC radiological environmental program requirements.

13.3 LCLS-I and LCLS-II Beam Distribution System

The electron beam distribution system for the LCLS/LCLS-II complex involves multiple destinations for each source, different modes of operation, and several high- and low-power beam dumps. The scheme and the parameters for the dumps are chosen to provide the flexibility of more or less arbitrary bunch distributions to be sent to either the SXR or HXR undulators independently. Moreover, a lower-power diagnostic line "steals" a few pulses that are characterized and used for feedback to maintain high beam quality.

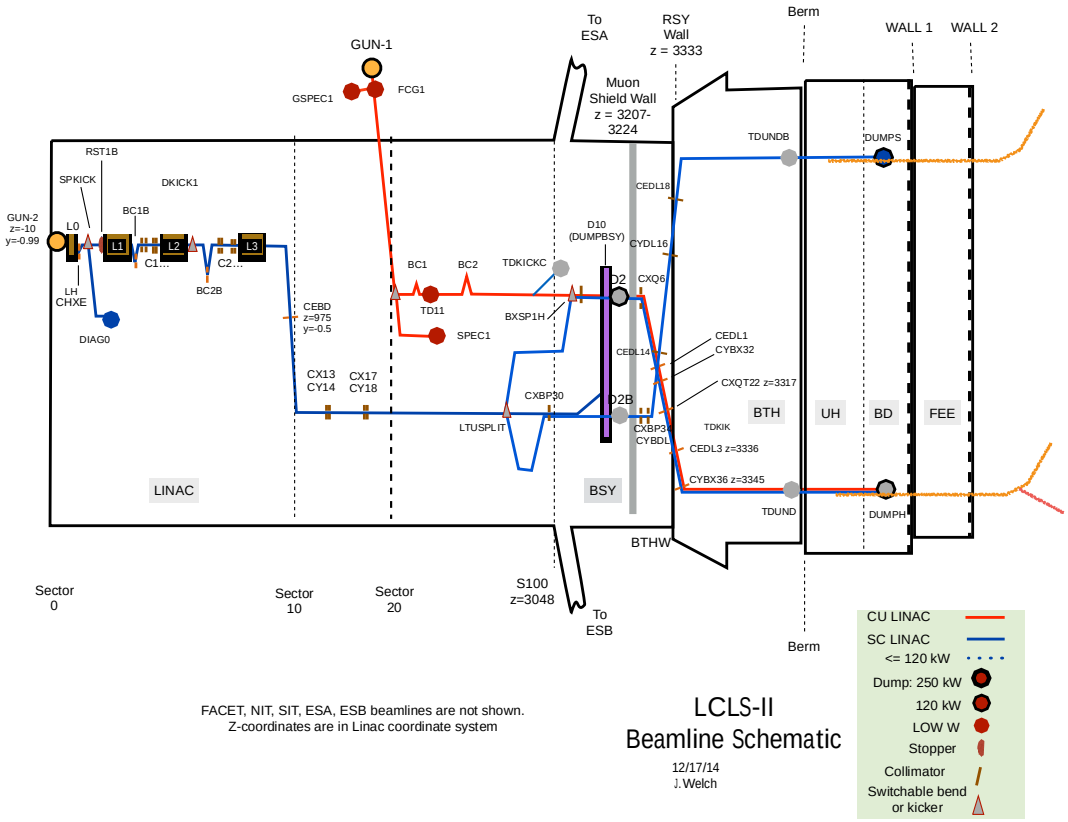

Figure 2. Overview of LCLS and LCLS-II electron beam sources and dumps.

A schematic showing both electron guns and all dumps is given in Figure 2. Following the solid blue line representing the high-powered CW beam, a dump labeled DIAG0 is located at the end of a diagnostic line used to measure the laser heater energy spread. Continuing along the main Continuous Wave (CW) line, the beam passes through two more chicanes and one dogleg before reaching LTUSPLIT, where two overlapping pairs of fast-kicker/septum magnets direct bunches to either the HXR or SXR undulator lines; or by not kicking, allow the beam to proceed to the high-power dump labeled both D10 and DUMPBSY. In the event of a fault, these systems can very quickly inhibit the kickers at the LTUSPLIT and direct all pulses to DUMPBSY before the BCS or MPS systems have had time to shut off the gun.

Beam that is directed toward the SXR undulator passes by two insertable low-power dumps, labeled D2B and TDUNDB, before it passes through the undulator magnet, where it generates x-rays, and is terminated on the final high-power dump labeled DUMPS. Beam kicked toward the HXR line joins the existing LCLS beam path at the DC “merge magnet” BXSP1H and passes by two insertable low-power dumps, labeled D2 and TDUND. Finally, the CW HXR beam passes through HXR undulator magnet and is terminated in the high-power dump labeled DUMPH. Both DUMPS and DUMPH are located in the same shielded area and are installed in existing pits, side

by side. The shielding on top of and down beam of the dump is modified to be commensurate with the higher average beam powers.

Beams that start with the LCLS gun see the same dumps that are in operation prior to LCLS-II, but they will be terminated on a much higher-power dump (DUMP), which will replace the current 5 kW LCLS dump. When the operating mode is sending CW beam to both undulators, the Cu Linac can be run by directing a low-power beam to the tune up dump labeled TDKICKC. This tune-up dump and its associated magnets were moved from their pre-LCLS-II location downstream of the merge magnet.

13.3.1 Dump Performance Parameters

Basic parameters for the three high-power dumps are listed in Table 1. DUMPH can receive beam from either the SC or Cu Linac, so two beam energies are listed. The beam power from the Cu Linac is negligible compared with the beam power from the SC Linac. "Max Beam Power" refers to the beam power consistent with the "Functional Requirements" stated in the project global requirements document LCLSII-1.1-GR-0018-R0. Shielding and dumps should be capable of transporting and absorbing the Max Beam Power, so each dump must be rated at a power no lower than the Max Beam Power in Table 1. Due to the available space for shielding and to its thermal capabilities, beam power to DUMPBSY is limited by the BCS to 240 kW, even though the Linac is designed with the capability of 1.2 MW beams. Similarly, the BCS system will limit power to the other main dumps to 120 kW.

"Average Beam Power" is a design value for the overall time-average power the dumps are expected to absorb. It is expressed in terms of MW-hours per calendar year. 'Max Power' values are used to design the shielding of dumps for prompt and residual radiation, while 'Average Power' values are used to determine shielding needed to protect the environment from long-term operations.

Estimates of the time-averaged dump powers were made based on 5000 hours of operation during one calendar year, and are comfortably below the Max Beam Power entries in Table 1. The estimates were made by taking, for each accelerator mode of operation, the power going to each dump and the percentage of time the accelerator is in that mode, and calculating the weighted average of the power. The following assumptions were also made:

- FEL X-ray beam power is limited by mirror distortion to 20 W per beamline. Beams up to 200 W are possible, but they will not contribute significantly to the overall usage.
- FEL X-ray beam will be delivered to experimental stations either as 1 W for tuning up the experiment.
- The experimental program requires a seeded beam for the majority of the experiments, and seeded-beam pulse energies will be around 100 µJ/per pulse.

- A negligible number of experiments will require harmonic operation (~1 µJ/per pulse at maximum beam power).
- 1 kW of beam power is always maintained on a high-power dump for MPS/BCS reasons and diagnostic purposes.
- The Linac is tuned up at 80 kW x 2 + 1 kW and maintained at this current. Current in excess of that going to the SXR or HXR lines is sent to DUMPBSY (80 kW is derived from 4 GeV × 100 pC × 20 W / 100 µJ, seeded operation).
- The LCLS beam is 5 kW. This is a conservative simplification with little impact to the overall dump average.
- Operational time when beam is scheduled to be delivered to users is estimated to be 5000 hours per year.

Table 1. Design parameters for LCLS-II electron beam dumps.

Symbol	Beam Energy [GeV]	Max Beam Power [kW]	Average Beam Power [MW-h/y]
DUMPH	4 or 15	120	135
DUMPS	4	120	239
DUMPBSY	4	240	607

Note that for most photon wavelengths it is possible to deliver self-amplified spontaneous emission (SASE) pulse energies of 1 mJ or more with as little as 8 kW of electron beam power. However, for the Average Beam Power estimates it was assumed that effectively all of the delivered beam is seeded and has a pulse energy of only 0.1 mJ. With this assumption it takes 80 kW of electron beam to reach the mirror limit. Maximum beam power, 120 kW, is required only when the FEL efficiency is extremely low, such as when generating harmonics. Another assumption used to determine average power estimates is that the DUMPBSY dump takes remainder of 80 kW beam in the Linac that is not sent to DUMPS or DUMPH. This arrangement insures independent operation of two beamlines. When one beamline changes repetition rate or even turns off their beam entirely, the other is not affected. Lastly, a minimum beam of 1 kW to DUMPBSY is always maintained to keep the controls system feedbacks active and to verify that the beam path is viable in case of an MPS fault.

Table 1 was the starting point for the design of shielding for prompt and residual dose rates (typically designed for the Max Beam Power, MCI) as well for environmental protection (based on Average Power). These and all other loss sources along with their potential radiological impacts have been systematically identified and cross-linked [14].

13.3.2 Upgrade Scenarios

The beam distribution system for LCLS-II is designed with the expectation of adding beamlines in future upgrades. With additional RF source power, the SC Linac is capable of 1.2 MW beam power and could support 10 or more beamlines. For the baseline only, 240 kW is required, and this will be the operations safety envelope. For dumps, there are two basic options for upgrading to more beamlines. One option is to upgrade the DUMPBSY dump to 1.2 MW. This option is attractive due to the simplicity of all unused beam going to one location that can be well-shielded. A few megawatt-class dumps already exist at SLAC and could be employed. The near-term disadvantage is the additional cost to the project. The other option is to add ~300 kW class dumps as new beam lines are incorporated. This option gives more flexibility to locate the new beamlines. A combination of the two options is also possible.

13.4 Radiation Safety System Design

This section presents the shielding design for most relevant LCLS-II systems and components, from the injector to XTES. Detailed analysis is presented in the linked Radiation Physics notes (RP-YY-##) and in the Physics Requirement Documents.

13.4.1 Prompt radiation at the injector

The LCLS-II injector [LCLS-II-1.1-DR-0001-R0], which is going to be installed in Sectors 0-1, is designed to provide a continuous-wave electron beam with an energy up to 98 MeV for the superconducting RF Linac. The high gradient of the gun generates dark current, which may significantly increase the radiation levels not only inside the tunnel enclosure, but also in neighboring areas, such as the Laser Room and the Klystron Gallery. The injector radiation source term has two main components: the dark current produced by the gun and the dark current generated by field emission from the cavities (see section 13.4.4). We expect that the dark current due to field emission will dominate, and we conservatively estimate that a total dark current close to the gun might be about 1 W [15].

13.4.1.1 Prompt radiation at the Klystron Gallery above the injector

The injector system is located below the Klystron Gallery and it is accessible through an existing maze with a PPS secured entry. A detailed description of the maze shielding is given in [16]. The injector enclosure is connected with the ground level by several penetrations, which were constructed for klystron wave-guides and another supporting services, and by a wide shaft used for material transport. Calculations show that during injector operation, the radiation levels above the unshielded penetrations and transport shaft are very low (below 0.05 mrem/h) and thus any additional radiation protection mitigation measures are not required. Nevertheless, if the radiation source will be placed closer or right below the penetration, an additional shielding, local or inside the penetration, should be considered.

13.4.1.2 Shielding requirements for the area upstream from the injector

The injector system is accessible through an existing maze equipped with a sliding door connected to PPS. Thus the area upstream from the maze might be occupied during the linac operation. Calculations show that expected radiation levels in this area are about a factor 10 above its current classification, and hence it is required to enclose an opening between the maze and the tunnel ceiling with adequate shielding material and to install additional shielding on the maze door or other areas close to the dark current source. Specific shielding requirements for the injector are described in LCLSII-2.7-PR-00##-R0

13.4.1.3 Prompt dose due to penetrations utility shaft

There is one dump at the DIAG0 diagnostic line (see Figure 2). This dump is planned to work at 120 Hz only and will receive beams from an upstream kicker, so the beam pulse rate can be controlled by the kicker. Since a few watts (~4 W) of beam may be parked on this dump, shielding for residual activity will be designed according to the expected use factors, average beam powers, and access requirements [17, 18] and will range between 4inches and 8inches of iron or cold-rolled steel.

The dark current is another source of radiation in the LINAC. It is estimated [19] that ~10 μA of dark current will be generated at the LCLS-II gun, of which only 1 μA will reach the first cryomodule. The 9 μA dark current lost at that stage is at low energy (~1 MeV), and thus carries a low power level (~9 W). The sweeper magnet will then reduce the dark current that is propagated downbeam the LINAC by another factor of 10. The remaining 0.1 μA dark current will be accelerated and lost on several collimators at various energies. These collimators will be locally shielded (not only for dark current, but also for primary beam as well). Dark current from field emission in the SRF cavities is mainly localized, and simulations performed at Cornell show that only a relatively small current (pA level) travels appreciably far from its (where? “its source?” (Give a reference for the simulation?).

Other sources of beam loss have also been modeled (e.g. beam gas, Touschek) and found to be in the 100 pA level.

13.4.2 Klystron Gallery

During beam operation, the Klystron gallery, which is 27 feet above the Linac, is accessible. Thus the general 100 mrem/year limit [2] applies to that zone. Since occupancy of the Klystron gallery is expected to be low (at least 10 times less than in office spaces), the corresponding dose rate limit for 2000 h work hours/year can be increased from 0.05 mrem/h to 0.5 mrem/h.

Radiation fields in the Klystron gallery will mainly be generated in the Linac, and be transmitted up through the penetrations. The Klystrons themselves are other potential sources of radiation. Moreover, it has been identified [LCLSII-2.7-PR-0079-R0] that some failure scenarios could lead to up to 2 MW beams through the Linac. Dose rates derived from brief operation and eventual loss of such beams shall not exceed 25 rem/h in any accessible area (i.e., Klystron Gallery and injector vaults), and any such event shall not integrate to more than 3 rem [2]. Local shielding on top of the collimators and shielding along penetrations between the Klystron gallery and the Linac should ensure those limits are met.

13.4.2.1 LINAC Penetrations

The 25 feet of soil/concrete between the Linac and the Klystron Gallery provide attenuation for losses in the accelerator, including accident scenarios, where up to 2 MW are lost at a point. Penetrations from the gallery to the Linac are used for cables and helium lines, and must be shielded. The amount and design of this shielding depends on the distance between penetration and the beam-line and the number and arrangement of conduits passing through the penetrations.

For example, the penetrations near the cryomodules will require 3 inches of iron shielding on top of the cryomodule in the direction of the penetration, plus 4-5 feet of gravel filling the lower end of the penetration between conduits. Moreover, the 2-foot perimeter around the penetration in the gallery would need to be fenced from floor to ceiling. In any case, the roof of the Klystron gallery shall not be accessible.

Details about the shielding requirements for the penetrations are described in [LCLSII-2.7-PR-00##-R0].

13.4.2.2 SC cooling penetrations

Helium lines (20-24 inches in diameter) from the heat exchanger will feed the cryomodules through two new penetrations from the Klystron Gallery into the Linac. Among the various designs of 36-50-inch penetrations, the most challenging for radiation protection are vertical penetrations aligned with the beam axis. If the maximum credible beam (MCB) were lost below such penetrations, dose rates in the gallery would be above the SLAC limit of 25 rem/h. Thus, such configuration must incorporate the following shielding (or an equivalent arrangement): 10 cm of iron above the beam-line, 1 foot of concrete enclosing the penetration elbow at the Linac (see Figure 3-left), and 1 foot of concrete above the penetration in the Klystron Gallery (some of this shielding could be substituted by self-shielding provided by the heat exchanger). Moreover,

the space between the penetration and its inner conduit should be filled with borated polyethylene (or equivalent material) for the full height of the penetration. Also, a 5-foot control area shall surround the penetration. Figure 3-(left) shows the elevation dose map [rem/h] at beam and penetration plane for a 1 MW beam loss. The subfigure on the right illustrates in a Z-cross section, how the potential dose would be lower, even with less shielding, if the penetration was placed away from the beam plane.

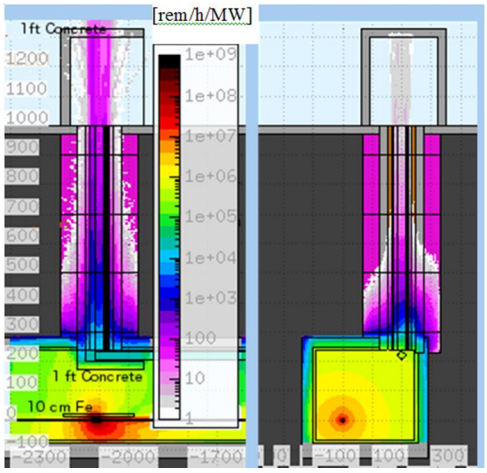

Figure 3. Dose rate maps [rem/h] for 1 MW beam loss. Left) below a shielded penetration (10 cm Fe + 1 ft. concrete + 1 ft. concrete), or Right) to the left of an unshielded penetration

13.4.2.3 Klystrons

Most of LCLS-II will use solid-state amplifiers, except for the 3.9 GHz klystrons in L0, which are expected to emit negligible radiation due to their low voltage (8.5 kV).

13.4.3 Halo collimators

13.4.3.1 Basis of Requirements and Assumptions

A small fraction of the radiation generated at the collimators will escape the surrounding local shielding and the LINAC enclosure, and will irradiate the soil near that section of the Linac and the water table located below the Linac. Isotopes such as ^{3}H (tritium), ^{7}Be or ^{22}Na, will be formed mainly via spallation reactions induced by mid- and high-energy neutrons. Movement of percolating moisture and the water table (at a speed close to 1 m/year) will limit the exposure time window for any given water sample (to 3-4 years), leading to an effective tritium concentration reduction factor of about 5 with respect to the saturation activity[1]. Following SLAC's commitment to not radiologically impact the environment, the resulting radioisotope concentrations resulting from irradiation and water motion, but neglecting dilution, should be very low, allowing not only that the water be drinkable, but also making such isotope traces undetectable. This translates into activity limits of 1,000 pCi/dm^3 for ^{3}H and ~100 pCi/dm^3 for ^{7}Be or ^{22}Na.

[1] That factor is smaller for shorter-lived isotopes, but their production cross section is smaller and so is their leacheability into water

It is desirable that the Linac will be accessible no later than one hour after the beam is turned off (cool-down time). Thus, residual dose rates inside the Linac should not exceed 5 mrem/h at that time unless a zone is identified and as a Radiation Area. Shielding on top of and on the aisle side of the collimators should be thick enough to limit the residual dose in the Linac.

In [LCLSII-2.7-PR-0079-R0] four different materials are considered for the jaws of each collimator: Al, Ti, Cu and W. (For a few collimators Cu is ruled out.) Each of these collimators is made of two opposed jaws of 15 radiation-lengths (in the Z axis), with 1 Molière radius transverse width (each jaw), and measuring 2 Molière radii in the third axis. For the purpose of this study, electron beams of 98 MeV, 250 MeV, 1.6 GeV or 4 GeV were simulated irradiating cylinders of 1 Molière radius and 15 radiation lengths. Results and requirements are re-scaled to the halo loss power levels identified in [LCLSII-2.4-PR-0095-R0], and consider a ~57 % duty factor. The distance of each collimator to floor, ceiling, south wall and north wall, as well the thickness of each (see table 1). From all collimator materials, the most conservative configuration is chosen to determine the shielding needs (typically aluminum).

Details on models are explained in dedicated physics notes [RP-14-17][20].

13.4.3.2 Local Shielding Around Generic Collimators

Table 2 (below) has the shielding requirements for all halo collimators except CEDOG, which is addressed in the 13.4.3.4. Shielding thicknesses on both sides of, on top of, and below the collimators are expressed in [cm] of iron. Alternatively, for the north and down directions, concrete shielding is also proposed. This suggested concrete is alternative to the iron, NOT in addition to it. In some cases, there is not enough space below the collimator or between the collimator and the north wall to accommodate the recommended concrete shielding.

The lateral shielding should extend upstream and downstream of the collimators so that any rays emitted by the jaws at angles between 20-160 degrees (with respect to the beam axis) are intercepted by the shielding. Moreover, collimators marked with one star in table 2 (CEBC1, CEBC2, CY21) are near penetrations and therefore must have 10 cm-thick end caps to prevent streaming neutrons from escaping into the penetrations.

Table 2: Iron (or concrete) shielding required around the LCLS-II halo collimators

Collimator name	Energy [GeV]	Z [m]	Intercepted [W]	Iron local shielding thickness [cm] *North*	South	*Below*	Above	Alternative concrete [cm] *North*	*Below*
HXR									
CEHTR	0.098	6.681	10	shielding required	5		5	No shielding required	
CY01	0.098	24.102	2	No shielding required					
CX01		36.132	2						
CY02		48.162	2						
CX02		60.192	2						
CEBC1*	0.25	121.42	182	8	17	4	17	17	7
CY11	0.25	142.59	5		4		4		
CX11		150.66	4		3		3		

CY12		158.72	4		3		3		
CX12		166.78	3		3		3		
CEBC2*	1.6	353.26	287	Fill all	34	Fill all	34	Not enough Space!!	
CY21*	1.6	395.34	29	8	11	8	11	21	20
CX21		407.33	26	6	10	6	10	15	15
CY22		419.32	23	4	10	4	10	10	10
CX22		431.31	21	3	9	3	9	5	5
CEDOG	4	967.38	1036	See dedicated PRD				See dedicated PRD	
CX13*	4	1249.7	104	22	27	14	38	50	31
CY14		1351.3	93	20	25	12	36	45	26
CX17		1656.1	84	18	23	10	34	41	22
CY18		1757.7	76	16	23	10	32	37	17
CXQ6	4	3177.8	306		39	4	39		7
CEDL1	4	3264.8	187		30	32	30		72
CYBX32		3275.6	19		9		9		
CXQT22		3317.8	17		9		9		
CEDL3**		3336.4	15	8	8				
CYBX36**		3345.3	14	8	8				
SXR									
CXBP30	4	2972.3	68	6	17		17	5	
CXBP34		3198.8	61		15		15		
CYBDL		3218.1	275	40	45	31	55	82	63
CEDL14		3269.4	138		27	25	27		38
CYDL16		3295.2	14		8		8		
CEDL18*		3320.4	62	15	15	15	15		11

13.4.3.3 Special Requirements for CEBC2

There is not enough space to shield CEBC2 on the wall side. The entire space between the collimator and the wall should then be filled with lead, and the jaws of CEBC2 should NOT be made of aluminum, but rather of a heavier component, preferably tungsten.

13.4.3.4 Shielding of CEDOG

The CEDOG collimator is located in Sector 10 (S10), which is upstream of the Linac transfer line. Due to expected high losses (>1 kW) and space constrains inside the accelerator housing, we designed an optimized multi-layer shielding for this collimator. We tested several shielding configurations for different shielding andcollimator materials and compared their basic radiological characteristic to each another. Details of the shielding optimization are given in [RP-14-18], and radiation protection requirements are summarized in [LCLS-II-1.2-PR-0260-R0]. We designed the proposed shielding for a tungsten collimator, which requires less shielding and therefore also less space than one made of aluminum. The proposed shielding consists of cast iron as the innermost shielding material, surrounded by a layer of 5%-borated polyethylene. The lower part of the shielding is made of concrete, which reduces induced activation of the soil below the tunnel enclosure and also serves as a supporting structure. The overall dimensions, including the concrete structure, are 175 x 165 x 182 cm^3 (length x width x height), which enables the shielding to fit within the allocated space.

Predicted residual dose rates allow access to the collimator area after ~1 hour after beam shutdown. The prompt radiation at the location accessible during Linac operation, i.e. Klystron Gallery, S10 injector, and positron vault, complies with the RCA classifications of those areas.

We estimate the groundwater activation to be low. The conclusions for potential air activity released into the atmosphere during operation are provided in section 1713.6.4.

In summary, the proposed shielding provides adequate protection of personnel as well as of the environment, and thus fulfills the radiation protection requirements.

13.4.3.5 Shielding of Halo Collimators in Head House and BTH

According to [LCLSII-2.4-PR-0095-R0], the last two halo collimators in HXR and the last one in SXR are within the Head House (HH) and Beam Transport Hall. All other collimators are in BTHW, BSY or Linac. These collimators are centered in the HH, thus they need shielding on both sides (north and south) to reduce the residual dose rate for access times. These collimators are placed higher (from the floor) than Linac collimators, and therefore residual dose shielding is not required on top of them, provided that the lateral shielding is tall enough to intercept all decay gammas from the collimators. hHwever, additional shielding is required on the top of CEDL18 to restrict prompt dose rates through the roof , which would otherwise contribute excessively to the skyshine.

13.4.3.6 LIONs and PICs

LIONs and PICs will be installed by the collimators in the Linac and BTH (East) to ensure the loss rates assumed in the shielding design ing are not overly exceeded. Details of these components are provided in [LCLSII-2.7-PR-0077-R0] and [LCLSII-2.4-PR-0107].

13.4.3.7 Minimum Cool-down Time to Access Linac areas near collimators

The minimum cool-down time to access nearby collimators will be no less than 1 hour. Also, depending on how much radiation actually leaks through collimators (PRD [LCLSII-2.7-PR-0079-R0] foresees up to 10 W/m), radiological measures to access collimator areas may be increased (e.g. longer cool-down times and/or RA posting).

13.4.4 Superonducting Radio Frequency (SCRF) Cavities

The strong electromagnetic fields in the SCRF cavities lead to substantial field emission. Electrons emitted at the surface of the niobium cavities are accelerated to some degree until their trajectory is intercepted by an iris between cells or by another aperture. A small fraction of these emitted electrons may be extracted out of the eight cavities that compose each cryomodule. We used Track3P code [21] to simulate the starting coordinates (position, time, etc.), and extraction/impact properties (location, vector velocity, time, etc.) of field-emission electrons in LCLS-II cavities at 16 MV/m. We wrote subroutines to feed such events into Fluka Monte Carlo Code, which then tracked those particles and their respective showers through a realistic 3D model that included, as shown below, cavities, helium lines and all relevant components in the cryomodules and in the surrounding area.. We neglected the effects of cavity RF fields in this step. We includedquadrupoles in between cryomodules in the model, with fields corresponding to those in the last cryomodules. Results were normalized to the current at the exit of the quadrupole, which, according to measurements [22], could amount to 10 nA.

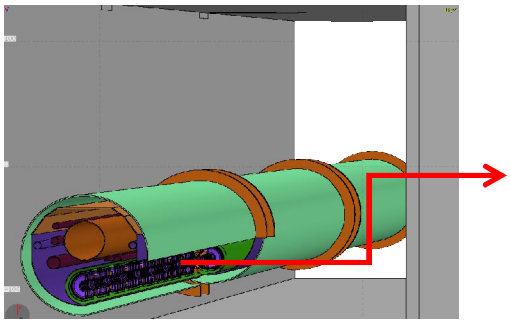

Figure 4. A detailed model of cryomodules and cavities has been implemented to perform radiation transport simulations with FLUKA Monte Carlo code

13.4.4.1 Radiation Levels in the vicinity of the SCRF

Figure 5A is a dose rate [mrem/h] map at the cryomodule vertical plane for a string of five cryomodules, each with 10 nA captured current. As expected, the quadrupoles, which are set for ~4 GeV beams, deflect most of the ~100 MeV electrons, leading to a radiation peak in the front end of the next cryomodule and a smaller radiation peak at the end of the previous cryomodule. The asymmetry in the dose map is a consequence of the asymmetric placement of quadrupoles between cryomodules. Dose-rate levels are high (up to 1,000 rem/h on contact), and thus access to the tunnel requires that all cryomodules be OFF and fully de-energized.

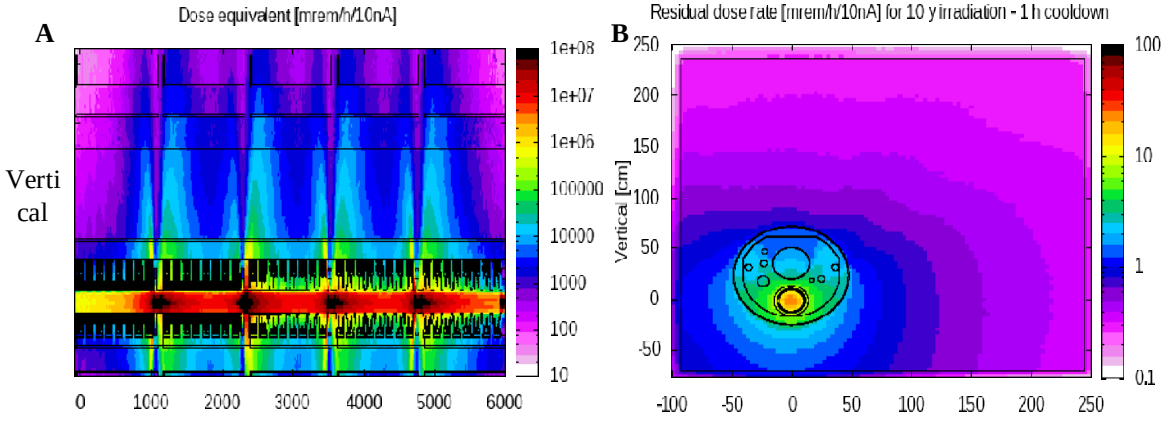

Figure 5. Dose rate map [mrem/h] for 10 nA field emission in each of the last few cryomodules (A) elevation view during op

The high radiation fields near the cryomodules may also damage and activate components, and generate radioisotopes in effluents, such as air and helium (see 13.4.4.4). More on radiation damage to components can be found in [RP-14-22].

13.4.4.2 Radiation to upstream and downstream components

Most of the field emission electrons are low energy, and even the highest energy tail will not exceed ~110 MeV. This means that for the most part, electrons will be swept away at the quadrupoles in between cryomodules, leading to local radiation peaks in those areas, as shown in the previous section. The small amount of remaining dark current may make it to the next/previous cryomodule, but not all electrons will be in the right phase to be accelerated

towards the end of that neighboring cryomodule. However, although that fraction may be small, efforts are being carried out to estimate its value and its potential radiological implications.

13.4.4.3 Residual dose rate by the SCRF

Even if SCRF (and the LCLS-II gun) are powered OFF, radiation near the cavities may exist due to activation of components, especially near the quadrupoles. Figure 5. Dose rate map [mrem/h] for 10 nA field emission in each of the last few cryomodules (A) elevation view during operation, (B) cross section after 1 h cool-down-B, shows the residual dose rate after a long run with 10 nA captured current. The map is a cross section just downstream of a quadrupole. Residual dose rates seem to be in the order of 1 mrem/h and therefore special access requirements to the area are not expected. However, due to the uncertainty on field emission, radiation surveys will be carried out before allowing access. Moreover, up to two residual radiation detectors will be installed near the SCRF to monitor the levels of radiation prior to access.

13.4.4.4 Activation of Helium

Helium will leak out of the cooling systems thereby requiring periodical refills.. Thus, radioisotope production rates in He (and any subsequent spills) need to be limited. The main isotope of concern that can be generated in He near SCRF is tritium, which is the product of $^{4}He(\gamma, p)^{3}H$ reactions. Tritium production rates from field emission in the different supply/return pipes into was simulated with FLUKA. In order to obtain reliable results, the density of He in each of the 9 domains was set to the corresponding phase state, leading to 6 different values, ranging from 145.7 to 1.008 Kg/m^3, and alsto to two volumes where there are mixed phases.

Results of simulations, normalized to 10 nA captured current, lead to a production rate of 1.74E6 [^{3}H-atoms/s/cryomodule], i.e. ~6E7 ^{3}H-atoms/s for the 35 cryomodules (if losses are equal). Annual He losses are estimated at 1/5th of the total volume, and therefore the average residence time of any given He atom in the system is ~3.5 years (assuming an exponential law for leaks). Thus, for the total volume of 15000 liters of He, the average ^{3}H $T_{1/2}\,^3H = 12.3\ y$) activity density built before leakage is $A_{3H} = 6E7 * (1-e^{-3.5/12.3})/15000 = 716$ [Bq/liter] = *19300* [pCi/liter] (below drinking water limit). The average annual ^{3}H activity discharge would then be close to 0.1 mCi/year.

13.4.5 BSY

The Beam Switch Yard (BSY) contains the highest dump power in LCLS-II. Extensive Radiation Protection (RP) studies for this area have therefore been carried out, as shown below. The RP shielding and PPS/BCS design is based on the BSY beam-line design described in [LCLS-II-2.4-PR-0080-R0].

13.4.5.1 BSY penetrations

The BSY enclosure has many penetrations, some of which are unused and filled with material, while some others are cable or ventilation shafts and thus provide relatively unobstructed path for the air to escape outside the facility, and therefore constitute a path for radiation leakage. With the

introduction of a high power beam electron dump in the BSY (D10 placed inside the muon shielding) the level of radiation escaping through the nearest concerned penetrations is currently being estimated to assess the need for additional local shielding at those locations. Despite the fact that the muon shielding was put in place during previous high-power and high-energy operations at SLAC, this shielding was not intended to be a primary electron beam stopper, but rather a massive attenuator for muons generated upstream. Having instead the electron beam stopped inside the muon shielding generates a radiation field of different nature and spectrum, which may have a consequence on the amount of necessary shielding for the cable and ventilation penetrations. This sort of shielding has typically no civil engineering footprint (e.g. borax bags inside the LINAC Klystron gallery penetrations), but is essential to meet the dose rate limit requirements.

13.4.6 DUMPBSY (D10)

With beam powers of hundreds of kilowatt, the electron beam dumps and their associated shielding are a major aspect of the LCLS-II facility. In addition, LCLS-II includes several beam dumps and stoppers of different power and energy ratings, as indicated in Table 1. This section covers the dump taking the highest peak beam power, 240 kW, i.e., DUMPBSY.

SLAC has several dumps in stock that can take beams of 240 kW: D10 (250 kW), SL10 (500 kW) and D-400 (2.2 MW). Considering its relatively compact size the existing D10 dump in its current position at BSY C-line was initially retained as DUMPSY.

Based on the radiation levels resulting from 240 kW of electron beam power hitting a stopper, the shielding requirements around D10 in its current location were given in [LCLS-II-1.2-PR-0232-R0]. The amount of iron to add to the existing concrete structure to provide adequate shielding (mainly driven by environmental protection and residual dose blockage during access) as well as its implementation proved to be infeasible. Thus, an alternative layout was found in which D10 is placed about 33 m downstream from its current location, inside the already existing BSY muon shielding, a massive structure made of iron blocks that is a legacy from past high-power and high-energy operations at SLAC.

To determine the required shielding dimensions, the assumed conditions for prompt and residual radiation were **250 kW of beam power with the 4 GeV LCLS-II beam** and **5 kW of beam power for the 17 GeV LCLS beam**, while for the mitigation of the impact to the groundwater activation (for environmental protection), **90 kW of average power over 10 years of operation** [LCLSII-2.7-PR-0079-R0] were taken. This contains a safety factor of about 2 in the foreseen average of 51 kW.

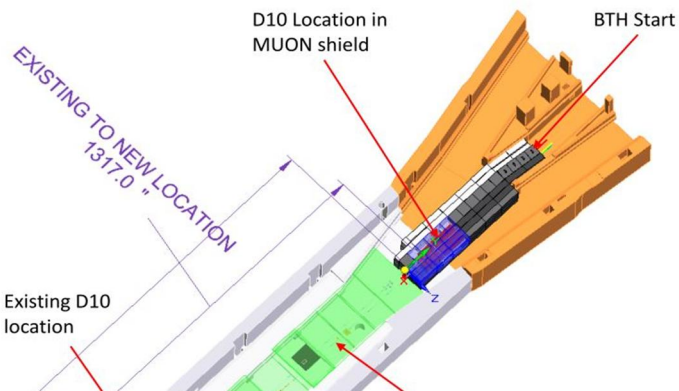

Figure 6. BSY model showing the relocation of D10 from its current original position to the inside of the BSY muon shielding.

Figure 6 shows the layout of the BSY muon shielding with D10 relocated from its original location to the front part of the muon shielding, with shielding dimensions shown in Figure 7. To provide flexibility for the accelerator physicists in the choice of beam line layout, the shielding requirements were given in [LCLSII-1.2-PR-0261-R0] for two options: one with D10 inserted in the center of the BSY muon shielding width, and another where the D10 location is shifted towards the south side. The difference is that in the later case, there would be a lack of iron shielding on this particular side that would need to be compensated with the addition of 4 ft. of iron.

In both cases, the shielding is designed so that the prompt dose rate limits are met outside the BSY enclosure, including directly above the muon shielding on the hill or on top of the roof of the BTH HH more than 100 meters downstream. For residual dose rates, it was assumed that the D10 area would need to be accessible as a Radiologically Controlled Area (RCA) only one hour after beam shut-off. The dimensions of the shielding surrounding D10 were therefore set such that the residual dose rates were at most 5 mrem/h at 30 cm during access [2], both on top and on the sides of the BSY muon shielding.

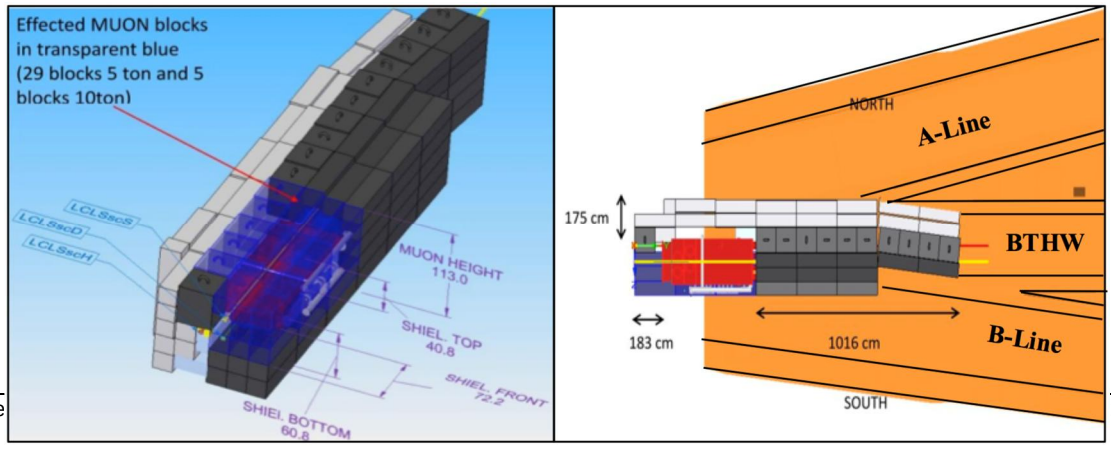

Figure 7. Shielding dimensions (iron) with D10 inserted off–center inside the muon shielding.

A large part of the massive amount of iron needed around D10 for its shielding is due to the need to prevent, as much as possible, activation of the soil and groundwater. This requirement comes from the presence of ^{3}H (tritium), ^{7}Be, and other radionuclides that will be formed in the soil and water mainly via spallation reactions induced by high-energy neutrons in silicon and oxygen nuclei. Part of these radionuclides are directly generated in groundwater as a result of the radiation coming from beam hitting D10, which explains the need for iron below the dump, and part of these radionuclides will be generated in the surrounding soils, slowly migrate and eventually reach the groundwater table, thought to be located just underneath the BSY enclosure at the D10 location. This explains the need for iron shielding on the top and sides of D10.

In SLAC's commitment to not radiologically impact the environment, the activity concentrations of these radionuclides in groundwater should be very low and below the EPA-required detection limits, e.g., 1000 pCi/dm^3 for ^{3}H. Iron is among the most effective shielding material against high-energy hadrons and to meet such low levels of activation in water while at the same time operating as high as 240 kW of beam power, several meters of shielding thickness are required and lead to such size for the D10 shielding.

13.4.7 Head House, BTH, Undulator and Roof Buildings

The Head House (HH) and the BTH are the structures built for LCLS-I to link the BSY complex and the Undulator tunnel. Those buildings cross the Research Yard (RY), which is accessible to personnel but does not belong to the general public accessible area. The general 100 mrem/year limit [3] applies to the RY. Since occupancy close to the BTH is expected to be low (at least 10 times less than in office spaces), the corresponding dose rate limit can be increased from 0.05 mrem/h to 0.5 mrem/h everywhere in the RY except in buildings with regularly used offices. Shielding, distance and occupancy factors should limit the yearly dose of personnel to 100 mrem for normal beam losses. In the case of shielding, this is provided by the walls and roof of the BTH, as well as by local shielding on collimators or other specific areas.

The previous statements refer to direct radiation fields and showers into the RY. However, there are other paths to radiation. A small fraction of the neutrons leaking through the roof will be scattered by atmospheric atoms in different directions and will reach areas that can be potentially occupied by public for long periods of time. Among those areas, the Maximum Exposed Individual (MEI) marks the location where yearly dose rates could be highest. SLAC [2] and the EPA limit that annual dose to 5 mrem for each facility (and 10 mrem/year for all SLAC). Minimized beam losses and BTH shielding should ensure compliance with that limit.

BTH was designed so that LIONs would allow continuous losses of up to 0.1 % (1 ‰) of the 5 kW LCLS-I beam (i.e. $\leq$ 5 W) to occur anywhere in the LTU, and resulting normal dose rates

would stay below 0.5 mrem/h in the accessible areas (Research Yard and service buildings) and below 3 mrem/h on the roof. This led to 6 ft. thick concrete walls and 4 ft. thick roof (except below service buildings, where it is also 6 ft. thick). Moreover, in case of LCLS-I accidental loss of its 150 kW MCI, the 25 rem/h SLAC limit would not be exceeded. For LCLS-II, the design needs to be revised, as normal beam losses are higher than those of LCLS-I and MCI may reach 2 MW.

13.4.7.1 Shielding and fence requirements for BTH

It has been identified [LCLSII-2.7-PR-0079-R0] that failure scenarios could lead to up to 2 MW beams through BTH. Dose rates derived from brief operation with those beams should not exceed 25 rem/h in any accessible area (per SLAC RSS), and any such event could not integrate more than 3 rem [2]. That scenario dictates either an increase of the BTH wall thicknesses or of the minimum accessible distance to the BTH walls. In particular, the walls will need to be increased by 32" (concrete) on the outside face of BTH *or* a PPS fence should be installed at 18 feet from the BTH outside walls, as shown in

Figure 8. Details about the PPS interlock features for this fence are provided in [LCLSII-2.7-PR-0077-R0]. Hybrid solutions that reduce the minimum distance of the fence and the necessary shielding supplement are possible, e.g. 20" additional concrete and a fence 13' from the shielding. The fence could be installed in some areas, while shielding could be installed in some others (e.g. to preserve access to buildings that would otherwise fall inside the fenced perimeter).

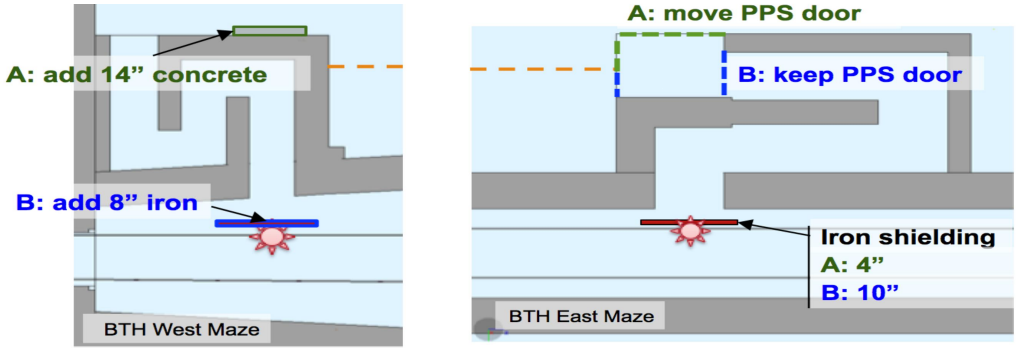

Figure 8. Shielding alternatives for the BTH mazes.

It is recommended (ALARA) that some shielding be installed in the southeast end of the BTH, so that normal operation dose rates to building 211 are reduced.

There are two locations where a point loss of the MCB entails specials requirements. Those are the interfaces between the each of the two mazes and the HH or BTH.

The lateral wall at the first leg (from the HH) of the BTH West maze is only 50" thick. If MCB were lost by the maze exit, dose in RY would exceed the 25 rem/h limit. Two alternatives solutions are proposed:

Add 14'' of concrete outside of the maze, as shown in

A. Figure 8-(left), covering the entire width of the maze aperture and 1 foot in each direction. This is the preferred solution.

B. Add local shielding to the beamlines: SXR should be shielded by 8" iron and HXR by 5". This shielding could be removable but it would be padlocked to adequate anchors and would be part of the configuration control and listed as a safety item in the Beam Authorization Sheet (BAS) checklist.

The lateral wall at the first leg (from the BTH) of the BTH East maze is only 60" thick and the PPS KeyBank is at just 12 ½ feet from the BTH wall, thus closer than the proposed 18 feet PPS fence to the sides of BTH. If MCB were lost by the maze exit, dose in RY would exceed the 25 rem/h limit. In this case, shielding cannot be easily added to the maze wall, as it would reduce the maze aisle width. The default solution is to eliminate the possibility of a mis-steering loss in front of this maze. This means that during ray-trace design, protection collimators should be set such that any mis-steered beam is intercepted either upbeam or downbeam of that coordinate. As mentioned earlier such collimators may require some local shielding. With this solution no additional shielding is required at the East maze. In the event that this condition could not be ensured, two alternative shielding solutions have been proposed in LCLSII-1.2-PR-0263-R0.

In the current design, the last two halo collimators in the HXR and the last one in the SXR are within HH-BTH. All other collimators are in BTHW, BSY and LINAC. CEDL3 and CYBX36 in HXR will take 15 and 14 W, respectively. This means that they will require *3" iron local shielding* to keep residual dose rates around them below 5 mrem/h at 1 h access time. As for CEDL18, it could intercept up to 62 W. Thus, its local shielding should be *6" iron with at least 2" on the top*. The shielding should be as snug around the collimator as possible, to reduce the production of activated air and ozone.

Due to their thin dimensions, insertion of wire scanners, even at full rep-rate, does not lead to sufficient electro-nuclear generation, and thus dose rates in the research yard should not see a direct increase of neutrons from that mechanism. However, small distortions of the electron beam traversing the wires (e.g. dpx, dx'…) and how those may lead to increased beam losses in the HH dogleg and in downstream components should be investigated as those could lead to additional dose rates in the research yard.

13.4.7.2 Access requirements for BTH and nearby areas

Service buildings on top of BTH *(911, 912 and 913)* and buildings 406 and 407 to the North of BTH and within the 18' fence, and building 209 in the South of BTH *will have the same PPS access conditions as the fenced area*. Also, the utility tunnel below BTH will be gated, and access controlled through the same PPS logic as the BTH fence (MCB loss just above could lead to ~360 rem/h, scaling results from [RP-14-15]).

It is desirable that BTH will be accessible after one hour cool-down time. Thus, residual dose rates inside BTH should not exceed 5 mrem/h at that time unless this zone is posted as a Radiation Area. For the settings of the LIONs described below, after 20 min cool-down, the residual dose rate in BTH should be less than 5 mrem/h at 30 cm distance from the beam-line. The actual minimum cool-down time will depend on measured dose rates and on whether this zone has separate access conditions.

13.4.7.3 Setting of BCS in BTH

On average, up to 1 W/m could be lost along the BTH [LCLSII-2.7-PR-0079-R0]. Thus, in any of the seven ~35 m long sections covered by LION pairs, up to 35 W could be lost on certain occasions. The LIONs should be set so that beam is not tripped in such cases. *This means that each LION should be set to trip at ~35 W* (exact setting adjustments may depend on calibration procedure and overhead provisions). With such a beam loss, radiation at the 18' fence is just below the 0.5 mrem/h design limit.

It is expected that the above beam losses will not constant or uniformly distributed, spraying different areas of the beam-lines, and LIONs will be set so that operation is possible under those circumstances. Upon activation measurements performed during commissioning, if a given zone/component is found to be a significant contributor to beam showers, local shielding in that location may be installed.

Multiple considerations (e.g. dose to personnel, undulator damage) preclude such a loss density (1 W/m) to extend along the entire length of the BTH. In particular, in order that RY buildings other than 209, 206 and 407 be accessible without major restrictions, total losses in BTH should be limited to 75 W, i.e. $SUM(LIONs)_{north} < 75$ W and $SUM(LIONs)_{south} < 75$ W. This setting may be raised, but then several buildings would need to be posted as RCA. This condition also satisfies the skyshine limit.

13.4.8 Undulator tune-up dumps

Each undulator will be preceded by a diagnostic tune-up dump similar to TDUND in LCLS-I, which can take a beam-power no larger than 200 W. Thus, the existing shielding for LCLS-I TDUND should be used for HXR tune-up dump. Such shielding [RP-08-08-r2] is composed of an inner layer of tungsten (to break the EM showers), borated polyethylene (to moderate and absorb neutrons) and outer panels of marble facing accessible areas, to shield from gammas. Moreover a downstream lead collimator shielding is necessary to protect the undulators from showers developed at the stopper and at upstream locations. For SXR, a mirror-image shielding of TDUND-HXR should be designed unless lower beam powers are planned to be intercepted, in which case solutions similar to those described in sections 13.4.3.2, 13.4.3.3 could be adopted. Protection ion chambers will be installed by each tune-up dump to control the amount of beam power deposited on those.

13.4.9 Main Dumps, DUMP/DUMPB

Radiation Physics requirements for the main dumps and detailed analysis can be found in [LCLSII-1.2-PR-0100-R0] and [RP-14-13], respectively.

Normal beam power at each of the main dumps, DUMP and DUMPB will typically range between 40-120 kW (delivered by superconducting Linac), or, for DUMP, also ≤ 5 kW (delivered by the copper Linac). In particular, as shown in Table I, total beam power in the dump hall will peak at 240 kW, while power averaged over calendar years is not expected to exceed 42 kW. These power levels exceed the present capacity of the LCLS-I dump and its enclosure (dump pits), both of which were designed for an average beam power of 5 kW.

This section describes the shielding solution for the main dumps that preserves the integrity of the main dump hall concrete structure. Figure 9 and Figure 10 show the LCLS-II shielding design for DUMP and DUMPB, in which the dump lines have been raised and bent inwards, and top iron and concrete shielding has been added to compensate for the increased beam power and for the elevated location of the dumps.

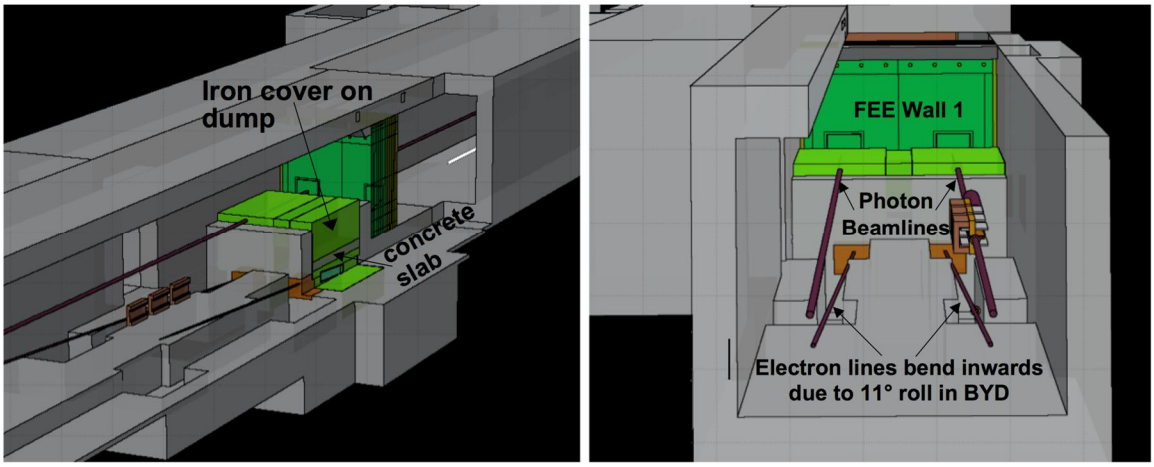

Figure 9. 3D rendering of the model used for LCLS-II main dump hall simulations, where the BYD bends are rolled by 11° and the strengh of the kick has been reduced to 3.9°. A 1 ft thick concrete slab (gray) and 5 ft iron (green) are stacked on top of the dumps providing also photon collimation, and supplementing FEE Wall 1 shielding.

13.4.9.1 New Design for DUMP and DUMPB Stoppers

A design for the main dump stoppers is been produced to cope with the higher power requirements [23] [LCLSII-2.5-EN-0313-R0] [RP-14-19]. The new stoppers are cylinders made of 146 cm (16.5 radiation lengths) aluminum alloy 1100 (of high thermal conductivity), backed with 16.5 cm tungsten (47 radiation lengths). A radius of 6 inches is sufficient to maintain maximum peripheral energy flux leakage below 2 W/cm^2 while keeping moderate temperature gradients between the axis and the cooling water coil.

13.4.9.2 Shielding of Groundwater Below DUMP & DUMPB Against Radioisotope Contamination

Radiation escaping the dump pits may either reach occupied areas or activate equipment and the environment. In the latter case, the main concern is the generation of radioisotopes in soil, which could eventually reach the groundwater, located about 30 ft. below the dump pits. LCLS-I shielding was designed to conservatively mitigate this risk. In order to compensate for the higher average power on LCLS-II (with respect to LCLS-I), the shielding inside the DUMP and DUMPB pits has been redesigned while leaving the outside enclosure unaltered. By raising the dumps, relative to the dump pits, (by reducing the vertical bend of the main bends to 3.9°) and to bringing the dumps closer together towards the center of the tunnel (by adding an 11° roll to the bends) provided the space needed for the required additional shielding. The space vacated below (51 cm) and to the sides (31 cm) of the dumps is filled with iron to further attenuate the high-energy neutron fields, which are mainly responsible for generation of radioisotopes in soil (Figure 9).

Simulated radioisotope production rates [24], coupled with a conservative, build-up/decay hydrogeological model for an hypothetical groundwater column trajectory, dropping from the surface towards the water table (located about 30 ft. below the pits) at constant speed, show activation values that in the *worst* case (for speeds of 2 ft./year instead of the presumed 3.3 ft./year), and for this high estimate of the average power, would reach 1200 pCi/L for ^{3}H and ~100 pCi/L for ^{22}Na. These values would be well below the EPA drinking water limits (20000 pCi/L and 400 pCi/L, respectively), but they are just slightly above the detection limits of 1000 pCi/L, and 86 pCi/L (see 13.4.9.2). However, considering other factors such as lateral diffusion towards less-irradiated areas, it is expected that the actual radioisotope concentrations in the dripping water before it gets diluted into the volume of the ground water table would be minimal, and certainly undetectable. To further assure that assumption remains true, a geomembrane, will be installed covering the dirt berm over the dumps. This area will be periodically inspected to verify the reduction in the direct rainwater flow near the dump area.

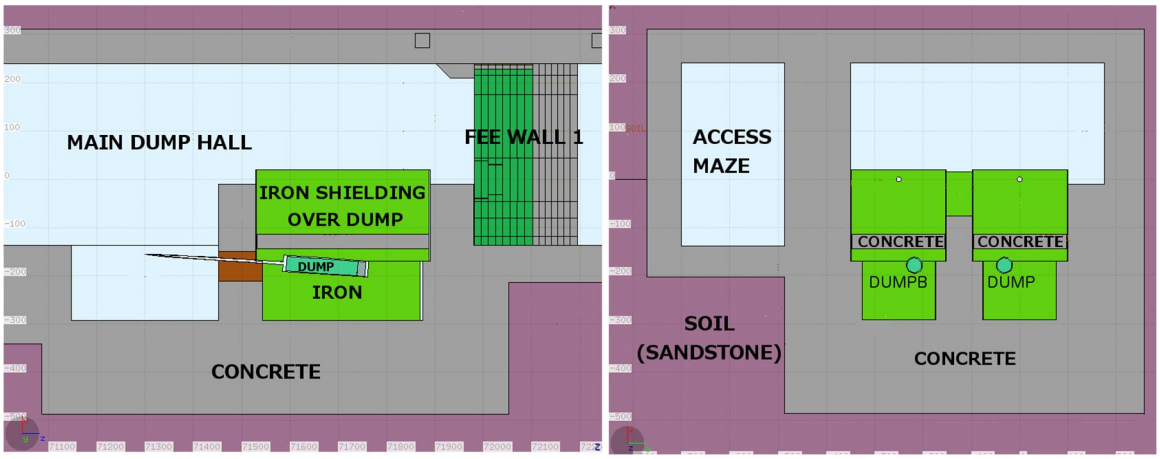

Figure 10. Elevation and transverse sections of the main dump pits showing the position of DUMP and DUMPB as well as the concrete cover plates (gray) on top and the iron (A36 steel) shielding (green) on top and in the dump pit. The grid is at 1 m intervals.

In the longitudinal direction, for LCLS-I, the soil was shielded by 25.92 of copper and 1.23 cm of tungsten (18 & 3.5 radiation lengths) in DUMP, followed by 146 cm of A36 steel (~83 radiation lengths) shielding in the pit. Also included are 150 cm of air and 6 ft. of pit concrete. For LCLS-II, after filling the entire length of the pit with iron (steel A36), as shown in Figure 10(left side), the longitudinal direction will be shielded by the 146.8 cm of aluminum and 16.5 cm of tungsten (16.5 & 47 radiation lengths) in the DUMP/DUMPB stoppers, followed by about 110 cm of steel A36 (62.6 radiation lengths) before the 6 ft.-thick concrete pit. The latter shielding is equal to that in the vertical direction, which in the preceding paragraphs was considered sufficient to shield radioisotope production in soil from high-energy neutrons generated in electronuclear showers in the dump area. For high-energy beams, the dominant dose at small angles is due to showers induced by photo-muons. These will be drastically reduced in LCLS-II because at 4 GeV their production is very low, as evidenced by comparing Figure 11(left side) to Figure 12. The relocation of the main dumps by ~1 foot represents a net attenuation rate in the production of radioisotopes in soil of about a factor of six. This alone is not sufficient to offset the increase of average beam power from LCLS-I to LCLS-II.

A study was then carried out to investigate whether the radioisotope activities in neighboring soil elements near the dump pits would decay sufficiently during their transport towards the lower aquifer. Simulated radioisotope production rates were coupled with a build-up/decay hydrogeological model for a hypothetical groundwater column trajectory, dropping from the surface towards the water table (located about 30 ft. below the pits) at constant speed and grazing the tunnel structure in the descendant trajectory. The results of the study showed isotope concentrations exceeding detection limit by just a factor of two. This means that if lateral diffusion (present, but difficult to quantify) was considered, concentrations would be undetectable.

13.4.9.3 Shielding of the DUMP and DUMPB for Prompt Radiation Fields to Occupied Areas

During operation, low intensity high-energy neutron fields will reach the upper ground surface where the general public can access, while dose to the experimental areas will be dominated by high-energy muons and the associated showers.

With the configuration shown in Figure 10, consisting of an immediate cover of 15-20 cm iron (A36 steel), followed by 30 cm concrete and topped by a 135 cm tall A36 steel block, and with the indicated front shielding, the prompt radiation field at 4 GeV with 2 x 120 kW on the main dumps is shown in Figure 11. At those power and energy levels, radiation fields to the NEH (or even FEE) are very small and, as advanced earlier, irradiation of the downstream soil is moderate. As for vertical neutron streaming *both peak and yearly average dose rates in the upper ground exceed the instantaneous dose rate limit* (~0.3 mrem/h and ~0.08 mrem/h, instead of 0.05 mrem/h) with the initially designed shielding. Thus, 4 inches of iron were added to the starting design, leading to a shielding configuration with 15-20 cm A36 steel, 30 cm concrete, and 135 cm A36 steel.

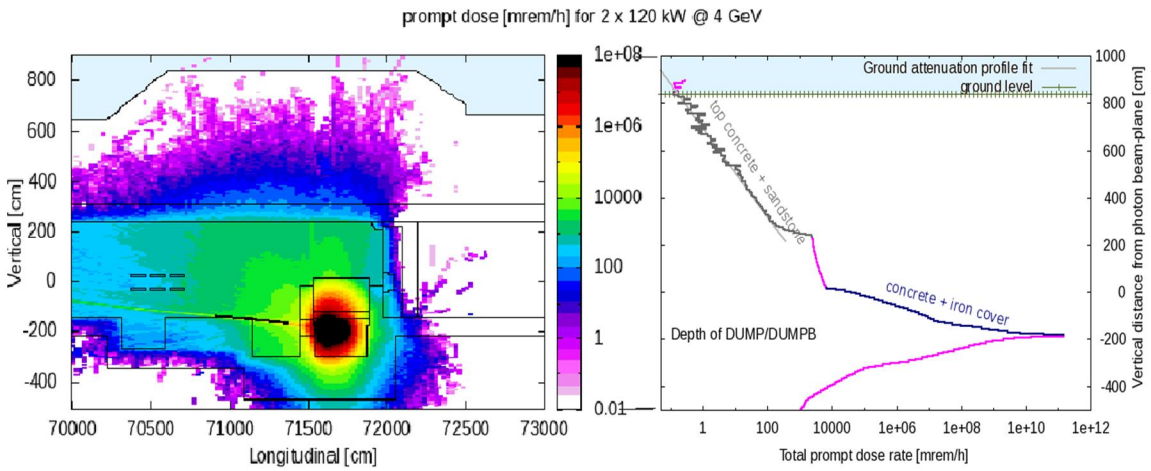

Figure 11. 2D prompt dose rate plot [mrem/h] and 1D projection to the vertical direction above the dump pits for 120 kW @ 4GeV simultaneously for each of DUMP and DUMPB.

The initial design of the dumps included 16.5 cm of iron in the back. For such design, if the superconducting Linac was upgraded to provide 240 kW 10 GeV beams, then peak dose rates in NEH could reach ~0.8 mrem/h (Figure 12), which is above the reference value of 0.05 mrem/h. The current design proposal for the dump substitutes that thickness by tungsten, which also helps reduce the irradiation of the downstream soil. This configuration should be included at the beginning of operations, even if beam energies are limited to 4 GeV, as upgrade work in the dump would be unfeasible once it has been irradiated.

Prompt dose to the areas on top of the dump, with the dump shielding/position described above will be below 0.05 mrem/h, with the current coverage of 530 cm of earth on top of the Electron Beam Dump (EBD) structure. Because the computed values (0.03 mrem/h) are not far

from the limit, and given that other radiation sources (BYD losses) will simultaneously contribute to the exposure in that zone, *the soil coverage above the EBD should be kept to a minimum of 530 cm*.

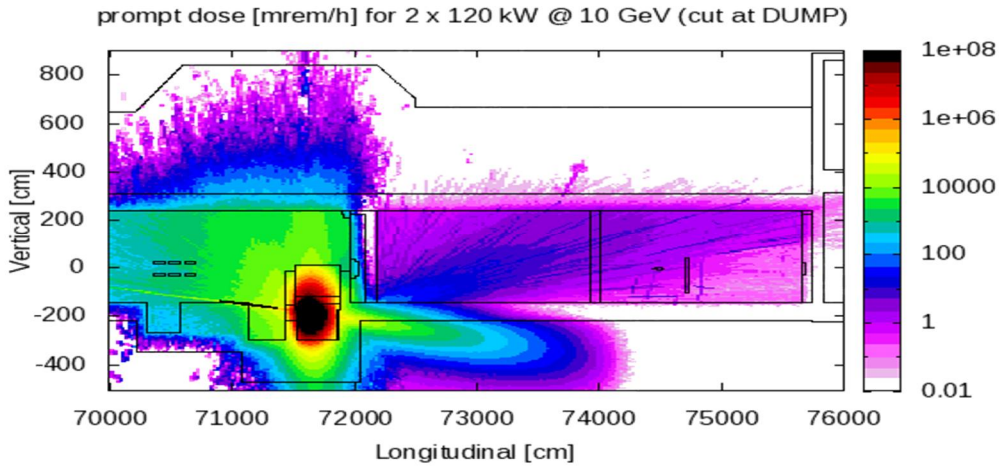

Figure 12. 2D prompt dose rate plot [mrem/h] for 10 GeV upgrade option (2 x 120 kW on DUMP/DUMPB), prior to dump redesign that includes 47 radiation lengths or tungsten.

13.4.9.4 Residual Dose Rates in the Main Dump Hall

When beams are off, access to the LCLS/LCLS-II complex will be through the maze that connects the beam dump hall with the Front End Enclosure (FEE) and Near Experimental Hall (NEH). It is therefore important to ensure that shielding around the dumps minimizes the residual dose rates in this area.

For that reason, a plate of 30 cm concrete (see Figure 10) has been included as part of the shielding that covers the main dumps. The purpose of this component is to reduce low energy neutron fluence to the tunnel walls, which is responsible for ^{24}Na activation decays. In previous LCLS-II studies, residual dose rates at typical access times (within one to few hours of beam off) were an order of magnitude smaller after application of this intermediate shielding component. On top of the concrete plate, a thick (135 cm) A36 steel cover will shield prompt high-energy neutrons (that activate other decay mechanism in the concrete and beam-lines) and it will also attenuate decay-gammas from the activated dump and concrete slab. These two components (concrete+iron covers) were already introduced as part of the shielding for the prompt dose to the upper ground. *A ray going vertically front the front face of the dump would cross the 15 cm of aluminum in the dump, followed by about 13 cm of steel, then 30 cm concrete and finally 135 cm steel.*

The front face of the dump (except along the beam-pipe) should be shielded by at least 40 cm of steel in the pit, plus additional 91.5 cm iron in the front, at the current location of the so-called 'RORO' front plug. *This shielding configuration captures the photon beam pipes, which are 20 cm below the top-shielding surface.*

Figure 13 shows the simulated residual dose rates [mrem/h] after the first day of irradiation at 2 x 120 kW and one hour cool-down. Note how residual dose rates at accessible areas near the dump remain below 5 mrem/h, except for on top of the simulated 1 cm gap for tolerance between the dump pit and the iron plates and in the diagnostic pits in front of the dump pits (~10 mrem/h). Activities from short-lived isotopes will have saturated after 1 day of operation while the longer-lived isotopes will continue to build up during days and months or irradiation.

Figure 14 shows the equivalent plots after the first full year at 2 x 120 kW. For that case it is observed how dose rates are just slightly higher, and this seems mostly due to radioisotopes from components inside the pit (dump+shielding) rather than from the beam dump hall.

In summary, the described shielding in place is adequate to allow access through the FEE maze after one hour cool-down. Radiation Area barriers to the dump area may be put in place as activities build up, based on radiation surveys and readings from area monitors. Additionally, shutters could be installed to suppress gamma-leakage from the irradiated dump during beam-off. Moreover, like for other high-loss areas, the second half of the main dump hall should be painted adequately to minimize the production of loose-contamination from concrete/shotcrete dust.

Due to residual radiation back-leakage from the front of the dump through the electron beam-pipe, the *RORO pits in front of the dumps should be posted as Radiation Areas.* This condition could be waived if shutters were installed during access to shield that radiation or if low residual dose rates were systematically measured at those locations.

To minimize activation and *contamination*, the main dump hall should be cleared of all unnecessary equipment, and the walls and floors and/or any element prone to release rust or dust should be *painted with epoxy* or by equivalent means.

In general terms, access to the EBD should not occur before a 1 hour cool-down. A *residual dose rate monitor* shall be used to monitor the radiation levels prior to accessing that area. As for the FEE, that area could be accessed earlier, provided the PPS creates a separate access path for that zone.

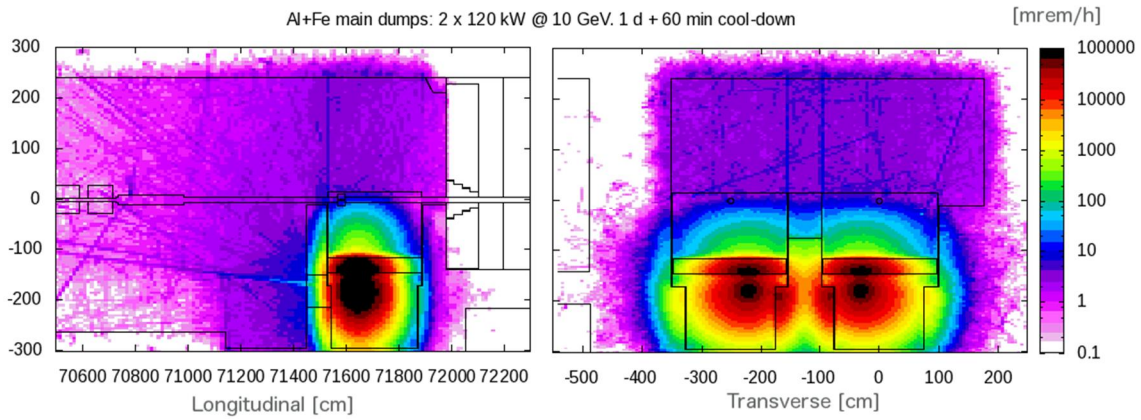

Figure 13. Elevation and cross section residual dose rate maps [mrem/h] for *1 day* of operation at 2 x 120 kW, and 1 hour cool-down.

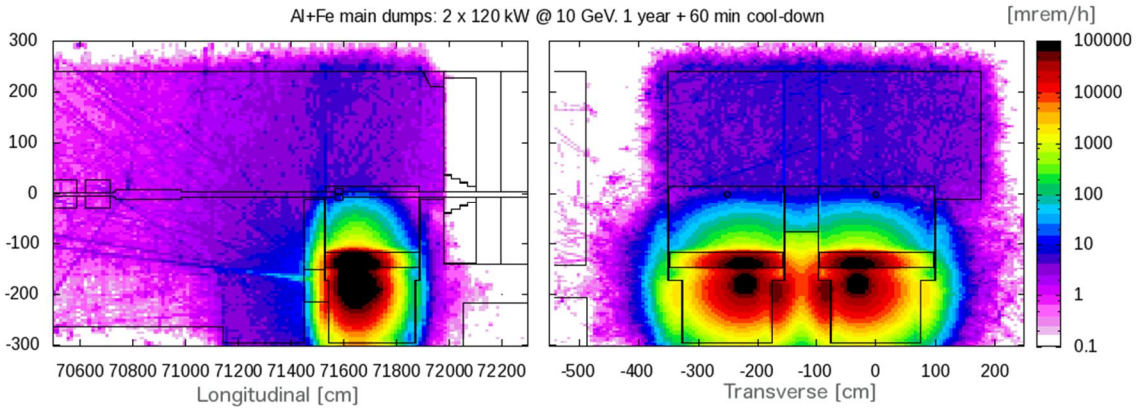

Figure 14. Elevation and cross section residual dose rate maps [mrem/h] for *1 year* of operation at 2 x 120 kW, and 1 hour cool-down.

13.4.9.5 Service of the Main Dumps

Due to the high residual dose rates around the main dumps, interventions, repairs, accesses etc. should be studied to best decide how to stack and install shielding around the dumps. These dumps will be very hot, with contact dose rates in the order of 100 rem/h at access time and not decaying to less than 20 rem/h after one week cool-down. Thus, removal of (at least) inner shielding layers should be done remotely (e.g. using cranes) and fast/distant release mechanisms should be designed to unplug cooling circuits for extraction of the dumps. Thickly shielded iron/lead containers or bunkers should be used to store the activated dumps. Finally, spare dumps should be fabricated to avoid long down periods, as repairing used dumps would be difficult due to the high residual activity of those.

13.4.9.6 Dose to electronics from DUMP/DUMPB

Simulations of the prompt dose leaking from the main dumps to the MDH suggest that annual neutron fluence will range from 10^9 to 10^{12} [n/cm^2/y] (depending on location), while 1-MeV neutron equivalent fluence in silicon will be an order of magnitude lower. Without local shielding,

these fields, which show a 50-100 increase factor with respect to current LCLS-I values, may induce some damage to electronic devices with bipolar components, while semiconductors and CMOS may be spared.

As for electronic devices installed in the Front End Enclosure (FEE), which is separated by from the MDH by a thick steel and concrete wall, those will not be damaged by radiation. More on dose to electronic devices in the EBD can be found in [RP-14-06] [RP-14-11]

13.4.10 X-ray Transport and Experiment Systems (XTES)

The X-ray Transport and Experiment Systems (XTES), east of the EBD, is located in the FEE. It consists of Free Electron Laser beam delivery, collimation and diagnostic components. The radiation safety system for XTES provides a radiation-safe environment to personnel at designed accessible areas around XTES. For LCLS-II, the FEE will not be accessible during electron beam operation. The FEE maze will be modified as shown in Figure 15 and the rack room will be a new accessible area during operations. The primary source of radiation in these accessible areas is due to electron beam losses on the main vertical bend magnets (BYDs).

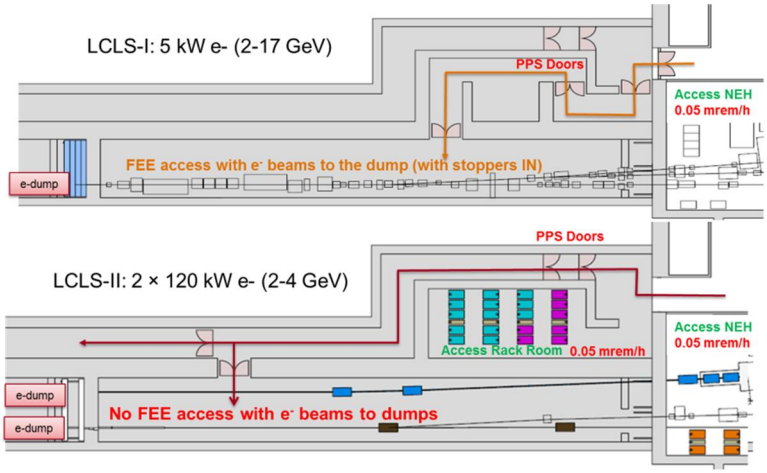

Figure 15. Changes in FEE access from LCLS-I to LCLS-II

13.4.10.1 Radiation sources for XTES

In normal operations, electrons will be sent to the main electron dumps without entering the FEE, and an electron safety dumpline with permanent magnets will be deployed for each FEL beam line to prevent electrons from entering the FEE in credible accident scenarios. According to the simulations shown before (Figure 11), prompt radiation from the main beam dumps located in the existing LCLS-I pit locations does *not* contribute to dose rates in NEH.

However, before being sent to the main dump, electrons generate bremsstrahlung radiation through collisions with residual gases (called “gas bremsstrahlung”), or when intercepted by thin diagnostic components, and a small fraction of that radiation will also be lost at BYDs. The gas bremsstrahlung power at pressures as high as 10^{-6} Torr represents 1.7×10^{-9} of the total beam power (0.2 mW at 120 kW beam). LCLS-II will use wire scanners to diagnose electron beam profiles at different locations [25]. Electrons interacting with wire scanners will generate forward-

focused bremsstrahlung, and the electrons whose enegies and/or trajectories are changed during the interaction with the scan wire may be lost afterwards and generate secondary radiations. No wire scanner should be operated at high repetition rate.

The main radiation source affecting XTES is from the small fraction of the beam lost on the main bending dipole before the main dumps. As a conservative assumption, an electron beam loss of 120 W, i.e. 0.1% of the full 120 kW beam power, is used for the shielding design. Combined losses in BYDs should not exceed 24 W (0.01 %). This will help avoid additional shielding around BYD that would be required for the excessive prompt dose (towards the groundwater and to the upper campus) and the residual dose (in the dump hall).

13.4.10.2 Ray-trace studies for electron safety dumplines

The electron ray-trace studies for the safety dumplines define the number, locations and dimensions of the collimators necessary to prevent electrons from entering the FEE in credible accident scenarios. Two magnet failures are considered here: first, BYD magnets may lose current or mismatch with the electron energy or the magnet may have the opposite polarity; second, mis-wired QUE magnets will act as a dipole and give undesired bending of the electron beams. Also, we assume that more than one failure at a time is not a credible scenario. The safety dumpline is designed for an extended energy range of 2 – 20 GeV for HXR and 2 – 6 GeV for SXR; beyond LCLS-II base line prameters (2 – 15 GeV for HXR and 2.0 – 4.2 GeV for SXR [26]) to be compatible with possible future upgrades. Figure 16 shows the HXR safety dumpline, which reuses the existing LCLS-I safety dumpline. The SXR safety dumpline is similar but use only one permanent magnet. The FLUKA code was customized with user subroutines to track electrons and to cover the full phase space. Figure 17 shows the ray-trace for the SXR safety dumpline. The detail locations and dimensions of collimators are defined in the safety dump line PRD [27] and RP Note [28].

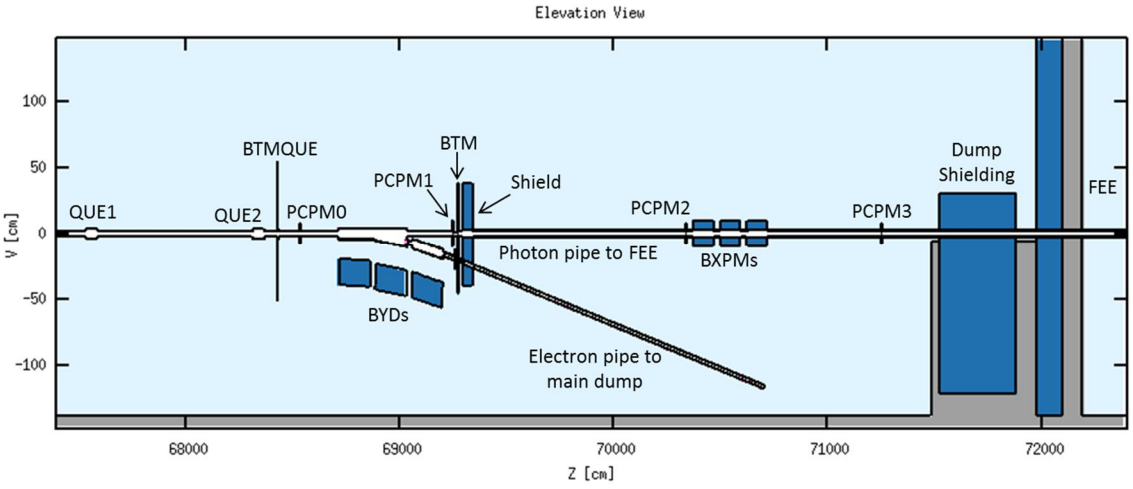

Figure 16. Elevation view (in rolled coordinates) of LCLS-II safety dumpline

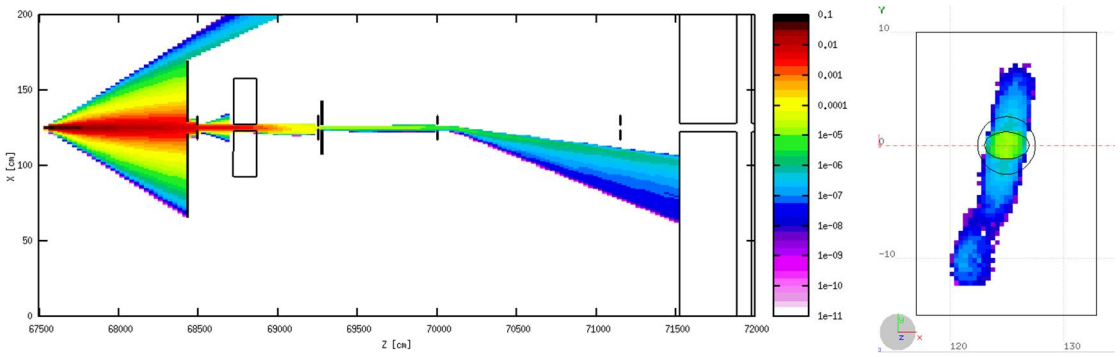

(a) Top view at the beam height (b) BEV at PCPM2

Figure 17. SXR safety dumpline ray trace for 2.0-6.0 GeV electrons

With 2 MW MCB on the safety dump, the dose rates in the NEH and the rack room are several mrem/h [28], well below the limit of 25 rem/h. Also electrons may hit the beam pipe when they are bent toward the safety dump by the permanent magnets. Secondary particles generated from this interaction will propagate to the FEE and enter the penetrations from the FEE to the rack room if there are open spaces. Studies [28] show that the any open space in cable penetrations must be filled with sand bags or other suitable material and that the air duct penetration needs to have a maze design to prevent any direct view to FEE.

13.4.10.3 Prompt radiation through the ground above BYD magnets

There are about 3.4 – 5.3 m soil on top of the 70-cm thick concrete ceiling of the EBD. With 120 W electron losses at the 1st BYD, the dose on top of the soil is up to 0.28 mrem/h considering the simultaneous losses on both SXR and HXR lines [29]. Thus the area on top of BYD magnets must be classified as “Radiological Controlled Area” or more soil/shielding to be added. On the other hand, studies show also the dose on top of the soil for 2 MW MCB is up to 13 rem/h, which is acceptable [28].

There is an existing penetration from the EBD roof to the surface, in the middle of the SXR and HXR lines at the Z-location between the 1st and 2nd BYD magnets. There is concrete shielding on top of the penetration and the penetration is locked in a fenced area. Although the dose underneath the shielding can reach 20 mrem/h for 120 W losses, the dose beside shielding is only 0.6 mrem/h and reduces to 0.2 mrem/h at 30 cm [29]. Thus the existing shielding will still be enough for LCLS-II and the fenced area will be kept and classified as “Radiation Area”.

13.4.10.4 Prompt radiation to NEH and rack room

There are two radiation pathways to NEH: direct penetration through the walls between the dump hall and NEH and leakage along beam pipes. The existing Wall 1 (4’ steel and 3’ concrete, separating the dump hall and FEE) and Wall 2 (3’ steel and 3’ concrete, separating the FEE and the NEH) plus the 40 cm-thick steel bremsstrahlung shielding on each beam line is enough to reduce the direct penetration [30]. As for the radiation along beam pipes, leakage can be reduced by a set of bremsstrahlung collimators with enough thickness (e.g. 8 cm tungsten or 40 cm steel)

[30]. The most important difference and improvement from LCLS-I is that the 1st collimator after BYDs (PCPM1, in the EBD) will be rebuilt with a small aperture and enough thickness. This will reduce radiation entering the FEE significantly. Inside the FEE, SXR will have one collimator before the 1st mirror, one between the 1st and 2nd mirror, and two after the 2nd. HXR collimators are like those of SXR except for the one after the 2nd mirror, which is not needed in HXR due to the proximity of the 2nd mirror to Wall 2 and the smaller collimator. Also each beam line will have one collimator in the NEH.

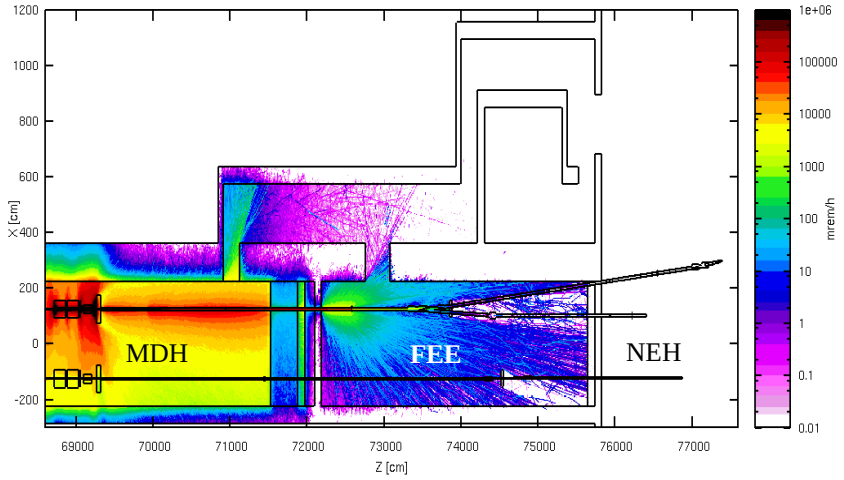

Figure 18. Prompt radiation doses toward NEH for 120 W losses on SXR BYD

13.4.10.5 Residual radiation around BYD magnets

Beam losses at BYD magnets will activate components and leave residual radiation after the beams are shutdown. Though beam losses can reach up to 120 W, the long-term average are estimated lower, at 48 W for SXR and 27 W for HXR (scaled as the average beam powers on the main dumps in Table 1). Figure 19 shows the elevation view of residual radiation after 300 days of 75 W beam losses on the 1st BYD, and 1-hour cooling [29]. The studies include two scenarios: the beam losses happen at a single point (called "point losses") or when they are uniformly distributed in the 1st BYD (called "linear losses"). The residual doses are similar in the two scenarios. The dose reaches 2 mrem/h at the tunnel center and 3 mrem/h at 30 cm beside BYDs. However the dose in the space between the last BYD magnet and PC0 shield can reach 15 mrem/h at 30 cm from beam pipe and 10 mrem/h at 60 cm, and the dose at PC0L, the collimator on the electron beam line toward main dump, can reach 100 mrem/h on contact, 30 mrem/h at 30 cm and 10 mrem/h at 60 cm. *Therefore, shielding around these hot spots should be considered.*

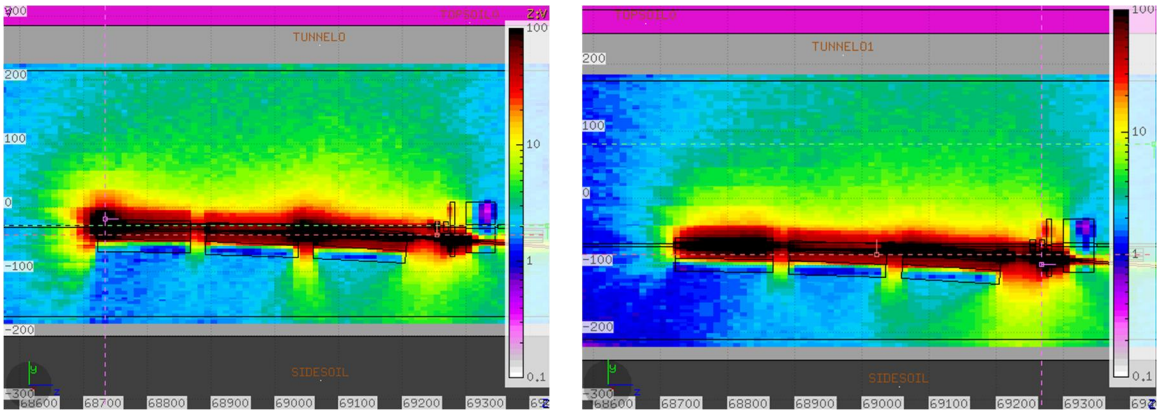

(a) Point losses (b) Linear losses

Figure 19. Elevation view of residual radiation after 300-day 75 W beam losses on the 1st BYD and 1-hour cooling

13.4.10.6 Radiation damage to electronics

Besides radiation safety considerations, some studies have been performed to help understand radiation damage to electronics in XTES [31]. Studies show that the ionization damage is the primary damage mechanism, and the displacement damage is secondary. Collimators on photon beamline (PCPM1) and electron beamline (PCPM1L) will reduce radiation levels by a factor of 10. Since the ionization damage dominates, local shielding can be an effective way to mitigate damage. Studies show that 2" lead can reduce the ionization damage by a factor of 10.

13.4.10.7 Experimental Systems and Hutches

The LCLS-II baseline will include one Soft X-Ray (SXR) beamline to Hutch 1 in NEH and one Hard X-Ray (HXR) beamline. The high rep-rate FEL (up to 1 MHz) will be 200 – 1250 eV for SXR and 1 – 5 keV for HXR, also hard x-ray FEL of 1 – 25 keV will be delivered at low rep-rate (up to 120 Hz). Although beam diagnostics are designed for 20 W FEL beams, the front end mirrors, FEL collimators and beam line shutters are designed for 200 W FEL. The FEL ray trace defines the number and locations of FEL collimators. The SXR beam line will reconfigure the existing end stations and operate without hutch exclusions. The HXR experimental systems and hutches are not included in the baseline.

The studies in previous sections define the radiological requirements to limit radiation from electron losses in order to protect personnel in NEH. However, the undulators will generate spontaneous radiation together with the desired FEL. The SXR mirrors in the FEE will have low cutoff energies and will remove the high-energy spontaneous radiation, such that the SXR beam enclosures (e.g. beam pipes, chambers, etc.) are still expected to have enough radiological protection. But the HXR mirrors cutoff energy will be higher and there may be a noticeable amount of high-energy spontaneous radiation after the mirrors. Increasing the electron beam power (from 5 kW to 120 kW) may also increase the power of spontaneous radiation (the operating parameter of undulators is another factor). Also increasing the FEL power and energy (up to 25 keV) will also increase the penetration of FEL beams. All these factors bring the

necessarity of re-evaluating the hard X-ray hutches shielding requirements, but the study is not included in the baseline.

13.5 PPS and BCS Requirements

13.5.1 PPS Design Requirements for LCLS-II

The PPS for LCLS-II will prohibit access to the shielded accelerator enclosure from the LCLS-II injector through the FEE during electron beam or RF operation. The prohibited areas include LCLS-II injector, LINAC, North Damping Ring (NDR) and South Damping Ring (SDR_, BSY, and BTHW to FEE. Beam from the gun, including gun dark current and dark current from all RF devices, must be shut off before access is permitted. In the event of PPS fault, interlock shut-off time must be less than 5 seconds (it includes the time for PPS stoppers "IN" or magnets "OFF" if it is required). Areas in LINAC tunnels that may be accessed during LCLS-II beam operations, include Sector 10 Vault, Positron Vault at sector 19 and LCLS-I injector vault. In the LCLS-II baseline, there are no changes for access to areas adjacent to BSY, which includes SLC South ARC (SARC), SLC North Arc (NARC), PEP-II Rings, End Station A (ESA) and End Station B (ESB).

In the current configuration, FEE access is allowed with LCLS-I FEE PPS stoppers ST1 and ST2 "in" during LCLS-I operations. The LCLS-II project will block the present FEE maze and access will be via the new dumpline maze. In the new configuration, access to FEE will require BTH PPS stoppers "in" during LCLS-I operation.

For access to NEH and FEH hutches, the PPS stoppers inside the FEE are required to be inserted until the corresponding beam line (SXR or HXR) is authorized for operations.

For the LCLS-I project; the beam losses in HH and BTH are limited to 5 W by BCS LIONs. For the LCLS-II project, the beam losses in HH and BTH are limited to 35 W by BCS LIONs. These LIONs will be set to trip individually for 35 W or as a summation of a group of seven LIONs for 75 W for LCLS-II. RP requires either adding 32 inches additional concrete on side walls or installing fences at 18 feet from the outside of existing concrete walls. RP requires either shutting off LCLS-II entirely or stopping the LCLS-II beam on D10 (DUMPBSY) before granting access to the following fenced areas:

- BTHW HH roof or BTH roof, including BTH Service Buildings, B911, B912, and B913.
- B406, B407 in the research yard.
- Partial of B209 and B211 in the research yard.
- Fenced areas around BTH HH and BTH.
- The existing utility tunnel in the research yard passing under BTH

Before access to the above areas, LCLS-II beam must be stoppered in the DUMPBSY by PPS. Also, the beam power must be limited to be less than 6 kW by BCS and BTH LIONs trip point must be reduced to 5 W.

It is required to install eight Beam Shut Off Ion Chambers (BSOICs) in the areas located upstream of BTH. Trips of these BSIOCs (except LCLS-II injector BSOIC) will cause the injector PPS stopper to insert ("in") *and* all RF devices OFF. Trip of LCLS-II injector BSOIC will cause gun RF power supply OFF, injector PPS stopper IN and all RF devices OFF.

An additional 20 BSOICs must be installed in the areas located around and downstream of BTH. Trips off these BSOICs will cause the LCLS-II beam to stop in the DUMPBSY, beam power to be reduced <6 kW and BTH LIONs trip set reduced to 5 W.

BSOICs with both photon and neutron probes are required to detect radiation levels outside most enclosures except S10 Injector Vault, Positron Vault, S20 Injector Vault and area inside BTHW before muon shield wall.

Detailed PPS requirements for are listed in [LCLSII-2.7-PR-0077-R0].

13.5.2 BCS Design Requirements for LCLS-II

The LCLS-II Beam Containment System (BCS) monitors and limits the beam power and beam energy from LINAC to the dumps, ensuring that it is within the allowed limits, and limiting beam losses in these areas. Additionally, BCS protects safety-related beam line components from damage due to excessive beam power deposition in them. BCS will shut off the beam if excessive radiation levels are detected or can be generated in occupied areas, or limits set in BCS sensors are exceeded.

LCLS-II Beam Containment System (BCS) must be redundant and fail-safe since high power beams could quickly burn-through collimators, beam pipes, dumps, and then strike the shielding enclosure, thereby generating high radiation doses outside of the enclosure. Fast BCS beam shut-off time is essential to protect the radiation safety components. To protect safety-related beam line components from melting by high power beam up to 300 kW, the BCS response time should be equal to or less than 100 micro-second [32]. Burn-through monitors (BTMs) are designed to shut-off the beam for burn-through scenarios that assume BCS failure.

For each area 1) Injector 2) LINAC, 3) BSY, 4) BTHW, BTH HH and BTH, 5) Undulator, 6) Dumpline, 7) FEE and NEH, detailed ray-trace studies need to be performed to ensure that all mis-steered beams are contained by BCS collimators. These BCS collimators are protected by fast shut-off BCS devices (except collimators in the FEE and NEH for FEL only). Average current monitors will limit the beam power that is delivered to each area. The currents of all dipole magnet (located downstream of sector 10) will be monitored by BCS magnet current monitors. The measured magnet current will be compared with Sector 10 dogleg magnet current by PLC safety system to make sure that all dipole magnet setting matches the delivered electron beam energies.

BCS beam loss monitors such as protection ion chambers and LIONs as well as comparators, are critical BCS devices to protect the personnel outside shielding enclosure, especially for the BTH. LIONs require radiation sources for a function check and calibration of losses. Furthermore, the existing HH and BTH LIONs will be repurposed to trip individually for 35 W beam losses and as a group for 75 W beam losses during LCLS-II operation.

Except for the main dump line, each beam line (SXR and HXR) needs also to have a safety dump line with permanent magnets [LCLSII-3.5-PR-0111-R0], [RP-14-15]. The safety dump line will be similar to the existing LCLS-I safety dump line [RP-14-15]. Each safety dump line will need 6 BTMs and 7 pairs of PICs for collimators and safety dumps.

The FEL BCS collimators and PPS shutters inside the FEE and NEH are different than the electron BCS collimators and stoppers along the machine. FEL collimators and stoppers will be designed for up to 200 W FEL power and will be built with BTMs. The 1st FEL collimator inside the FEE for each of SXR and HXR lines needs a pair of PICs. The bremsstrahlung shadow wall in the FEE requires a BTM in front (west end) for FEL burn through. Meanwhile the flow of cooling water for FEL mirrors, collimators and shutters will be interlocked as a part of the BCS. Also a set of fast vacuum sensors will be deployed to the KB mirrors and end station chambers in the NEH and be interlocked as a part of BCS.

BCS requirements for LCLS-II are described in detail in [LCLSII-2.4-PR-0107] and Radiation Protection Requirements for XTES [S. Xiao, "Radiation Protection Requirements for XTES", LCLSII-1.2-PR-0233-R1, *to be issued*].

13.6 Radiological Environmental Issues

13.6.1 Introduction

Operation of the high-power LCLS-II can generate radiation hazards affecting the public and environment (e.g., air, soil, and groundwater). Radiation Protection (RP) Department provides the support for radiation hazard evaluation and controls for the protection of the public and the environment.

In this section potential radiological impacts to the public and environment from radiation and releases of radioactive materials due to LCLS-II operations are described. The requirements and issues are identified, mitigation measures, and monitoring of the radiological hazards are described.

The impacts to the public and environment include: 1) direct radiation (mainly skyshine radiation of neutrons and photons) dose to the public, 2) protection of groundwater, and 3) radioactive air effluent and its resulting dose to public. The impacts and their mitigation and monitoring shall satisfy the DOE/EPA regulatory requirements [4][6][7], state and local requirements [11][33][13], and SLAC requirements [1][2][34], and are to be maintained ALARA [4].

The impacts from LCLS-II are similar to those considered for past high power beam operations at SLAC. The radiation sources creating the impacts includes high normal electron beam loss points such as the beam dumps (D10 in BSY and 2 main dumps in Beam Dump Hall) as listed in Table 1 and the Linac collimators (e.g., the dogleg collimator in S10). As shown in sections below, extensive local shielding will be used near high beam loss points to reduce impacts to potential activation of groundwater (the dictating factor), production of radioactive air and ozone, and the residual dose rates in accelerator components. Radiation monitoring will also be provided near these beam loss points.

13.6.2 Direct Radiation to Public

Potential sources for direct radiation to the public are skyshine radiation and leakage of x-rays from the klystrons in the LINAC Klystron Gallery. Skyshine radiation is caused by neutrons and photons transmitted through the accelerator housing roof, scattering off air molecules, and returning to the ground. High-energy neutrons (> 20 MeV) dominate the skyshine radiation from LCLS-II accelerators, shielding is the main measure to reduce the skyshine impact. SLAC shielding design guideline for skyshine radiation is an annual dose of no more than 10 mrem/y to the Maximum Exposed Individual (MEI) from all facilities at SLAC and 5 mrem/y from any single facility [2].

Since Linac, BSY, undulators and main dumps (EBD) are covered with thick earth shielding (~ 30 ft.); the annual doses to public from the beam loss points in these areas are negligible. The other skyshine source is from normal beam losses in BTH, where the roof is only 4-6 ft. concrete, which gives 4 mrem/y at site boundary if 450 W is lost along the BTH (calculated with the SKYSHINE analytic code [reference]). Mitigation options include: limiting BTH beam losses to no more than 100 W, adding local shielding to identified beam loss points, or relocating beam loss points.

The skyshine neutron/photon radiation will be continuously monitored using sensitive, passive dosimeters placed at SLAC site boundary. Active Perimeter Monitoring Stations (PMSs) will also be upgraded to monitor neutron and photon radiation at site boundary [34][LCLS-II-1.2-PR-0265].

13.6.3 Groundwater Protection and Soil Activation

High-energy neutrons produced from electron beam losses are the most penetrating and are the main cause for radioisotope production in environment media (soil and groundwater) outside accelerator shielding walls surrounding the beam loss points. The main radioisotopes of concern in soil are ^{3}H (12.3-year half-life) and ^{22}Na (2.6-year half-life). For groundwater protection, ^{3}H is the main radionuclide of concern due to its high leachability (nearly 100%) from soil to groundwater.

Past high beam power ESA operations have resulted in detectable ^{3}H in groundwater wells located very close to the beam dump D400. This issue was anticipated during the design of the project and the situation has been addressed and regularly monitored to satisfy an EPA Order

[11].

Regulation requires that groundwater may not be impacted [7][11], which in practical terms means that the groundwater cannot have detectable radioactivity due to LCLS-II operation. Therefore, the groundwater activation (both evaluation and measurement) should be less than the EPA-required detection limit of 1000 pCi/L for ^{3}H in drinking water. The ALARA principle should also be followed for soil and groundwater protection [4].

The safety design for the LCLS-II high loss points includes extensive and thick shielding to minimize the impact to soil and groundwater surrounding the beam loss points. In many cases, the shielding required for a beam loss point is dictated by groundwater protection, which helps reduce the air activation and reduce residual dose rates to workers.

For example, compared to existing LCLS-I 5-kW beam dump, extra shielding (by at least a factor of 100 or more attenuation) should be incorporated for two LCLS-II main dumps to compensate for the increase in total beam power such that the potential activation for the water reaching the groundwater table below the dumps is insignificant (i.e., non-detectable). The shielding design for Linac S10 dogleg collimator, D10 dump in BSY or Muon Wall location, and 2 main dumps have been optimized in geometry and size with Monte Carlo calculations [LCLS-II-1.2-PR-0260-R0][LCLS-II-1.2-PR-0232-R0][LCLSII-1.2-PR-0261-R0][LCLSII-1.2-PR-0100-R0]. A generalized shielding design tool to estimate shielding requirements for Linac collimators has also been developed [LCLS-II-1.2-PR-0259]. A geo-membrane may be considered to further reduce the impact to groundwater in certain locations.

Additional groundwater monitoring wells will be installed for areas near the high loss points such as Linac, BSY, and 2 beam dumps [LCLS-II-1.2-PR-0265].

13.6.4 Radioactive Air Effluent

Radioisotopes will be generated in the ambient air surrounding beam loss points and then released to environment during accelerator operation and during access after beam is off. These radioactive air releases can produce potential dose to the MEI. The annual EPA/DOE dose limit for the MEI is 10 mrem/y, and a continuous air effluent monitoring system is required for the release point that is expected to create a MEI dose exceeding 0.1 mrem/y [4][9].

The main radioisotopes of concern include the short half-life ^{11}C, ^{13}N, ^{15}O and ^{41}Ar. The method of public dose evaluation includes the following steps [8]. Bremsstrahlung yields from beam loss targets, reasonable air paths surrounding the target, and beam loss scenarios are used to calculate airborne radionuclide yields. Conservative accelerator operational scenarios and reasonable air exchange rates for accelerator housing are then used to estimate the annual release of airborne radioactivity. The EPA approved code CAP88-PC is then used to calculate the annual dose to the MEI and the collective dose to the population up to 80 km from SLAC.

The MEI and population doses will be evaluated at least annually to ensure that the regulatory limits are not exceeded. The Air Monitoring Stations (AMSs) outside accelerator housing will be

upgraded so that the airborne radionuclide yields in air zones of Linac, BSY, BTH and the main dumps enclosures can be periodically measured [34][35].

For the high-power LCLS-II operation, the production of airborne radioisotopes and ozone are minimized by adding local shielding, and thus reducing the air paths. Engineered and/or administrative controls are required to control the forced effluent and ventilation systems. During accelerator operations, the air effluent system should not discharge air from the accelerator housing to the environment (e.g., no forced air effluent in Linac, BSY and Beam Dump Hall when beam is on) [LCLS-II-1.2-PR-0160].

Radioisotopes such as ^{3}H and ^{7}Be can also be produced in the air, but with activities 2 orders of magnitude lower than the above inert-gas radioisotopes. Their dose impacts to the public MEI are minimal, but they may present contamination impact to the workers entering accelerator enclosures and impact to groundwater, which are addressed by operational radiation protection program and controls as needed.

13.7 Operational Radiation Protection Issues

13.7.1 Introduction

For worker protection, the operational radiation protection issues that will be encountered at high beam power levels of LCLS-II include: 1) increased level of air activation and ozone production, 2) higher levels of residual activity (and dose rate) at beam loss locations, 3) high radioactivity in LCW system components, and 4) increased radioactive material and waste, as well as increased Radiological Areas. The impacts to workers and their mitigation and monitoring shall satisfy the DOE and SLAC requirements, and are to be maintained ALARA [36][1].

13.7.2 Exposure to Radioactive Air and Ozone

Airborne radionuclides inside accelerator housings present a worker exposure concern when accessing the housing after machine shutdown. Venting of these radionuclides from accelerator housing areas to working areas (e.g., from Electron Beam Dump to the NEH) can potentially also create external exposure to workers.

Ozone can also be produced from the high-power electron beam hitting beam line components during operations and from synchrotron radiation at or past the undulators. Potential hazards from ozone include lung and eye irritation, which presents a worker protection issue but does not present an air effluent issue for public exposure protection.

For worker protection, local shielding is added, particularly for high beam loss pints, to reduce the production of airborne radionuclides and ozone (design goal is no more than 1-DAC for radionuclides and OSHA 29CFR1910.1000 Permissible Exposure Limit of 0.1 ppm for ozone). A cooling period of at least one hour is needed for accelerator housing with high beam loss points after beam operation ceases before access or the air should be discharged prior to access to accelerator housing (which helps mitigate the ozone hazard also) [LCLS-II-1.2-PR-

0160]. In addition, air ventilation systems are designed such that there is no forced air flow from the accelerator housing with potential air activation to working areas during beam operation.

Extensive sets of active detectors are required for in-situ monitoring of airborne radionuclide and ozone concentrations and an area which has airborne concentration of 1 DAC or more should have airborne radiation monitoring [LCLS-II-1.2-PR-0153].

13.7.3 Exposure to Residual Radiation from Accelerator Components

Worker exposure to residual radiation from accelerator components is one of the main concerns. The beam-line components should be chosen such that activation and generation of radioactive materials and mixed (hazardous and radioactive) waste is minimized. Beam line components should be designed and installed in such a way that they can be extracted quickly from the beam-line for repairs, or they can be maintained *in situ* with minimum exposure to residual radiation.

Local shielding has been designed around high beam loss points (e.g., Linac halo collimators, S10 dogleg collimator, D10 and 2 main dumps) to reduce the residual radiation fields [LCLS-II-1.2-PR-0260-R0] [LCLS-II-1.2-PR-0232-R0] [LCLSII-1.2-PR-0261-R0] [LCLSII-1.2-PR-0100-R0] [LCLS-II-1.2-PR-0259]. Active detectors will be installed to monitor residual dose rate at these locations [LCLS-II-1.2-PR-0153]. Monitoring personnel for contamination when exiting accelerator housing will follow the present SLAC process.

For maintenance and repair activities associated with during routine operations; cool-down times and optimum work control plans will be utilized to keep doses ALARA [1]. Intervention to components that may result in high doses to personnel will be assessed to ensure that the ease of potential repairs and maintenance have been considered.

13.7.4 LCW Systems and Waste Water Management

The LCLS-II high-power dumps and collimators require LCW for cooling, thus the LCW connected to these systems will get activated. The main radionuclides produced in the LCW are ^{3}H, ^{7}Be and ^{15}O in LCW itself and radionuclides of ^{22}Na, ^{54}Mn, ^{57}Co and ^{60}Co in corrosion and wear products. These radionuclides may accumulate in various LCW system components, e.g., LCW coolant, resin tanks, and filter tanks. The operation and maintenance of LCW systems can potentially create radiological impacts to workers and environment, particularly for those systems associated with high beam losses.

The LCLS-II LCW systems will follow the following main radiological design and operational considerations, which are prescribed in a detailed in [LCLS-II-1.2-PR-0211]:

- The production of radionuclides in the LCW systems should be evaluated and minimized by reducing the amounts and time periods of the beam losses / dump usage,
- Resin tanks and filter tanks should be located, such that their exchange, maintenance and repair, and waste disposal can be conducted efficiently,

- The LCW systems, particularly for those with large amount of water in the cooled device (such as D10), should have hydrogen sensors and recombining equipment, i.e. D10 and Main Dumps both need a hydrogen recombiner
- Potential LCW leakage should be accumulated in a sump for discharge to sanitary sewer, and
- Any LCW leakage should be captured and accumulated in a storage tank where it is tested before possible discharge into the sanitary sewer
- Independent LCW systems for D10 and two main dumps.
- Storage, monitoring and discharge of wastewater into sanitary sewer are managed to satisfy the regulatory limits and SLAC requirements.
- Protection of storm water from potential spill of the LCW systems and possible leakage to the soil and storm drains is considered both in the design and for operation.

13.7.5 Management of Radioactive Material/Waste and Radiological Areas

Key issues related to high-power LCLS-II operation include management of increased radioactive material and waste, as well as increased Radiological Areas (e.g., Radiation Area and Contamination Area). These issues are be addressed by SLAC operational radiation protection program [1].

These include a program to ensure that activated material is not removed from accelerator housing without proper surveying and labeling, and processes and procedures that designate locations for storing radioactive materials on site, transport of radioactive materials to machine shops for disassembly and repair, as well as radioactive waste disposal.

Typical sources for contamination in the accelerator enclosure include dust, flaking or peeling paint, beam-line components, spilled water from closed loop cooling systems for dumps and collimators, flaking or peeling paint chips and liquids created when activated material or equipment is machined or refurbished or otherwise damaged. Removal of excess components and legacy beam lines in the accelerator, especially in the BSY, and taking strong measures to control the dust (e.g. using paint to seal the enclosure) and debris reduces the magnitude of the contamination problem.

13.7.6 Radiation Damage Fields to Beam-Line Components

Potential radiation-induced damage to sensitive components like electronics and permanent magnets will continue to be studied through measurements and simulations. The on-going program of investigating radiation environment in LCLS-I undulator (synchrotron radiation, Bremsstrahlung losses) will continue and potential damage to LCLS-II undulators can be simulated and mitigated.

13.8 References

1. SLAC ES&H Division, Radiological Control Manual, SLAC-I-720-0A05Z-001-R005, SLAC National Accelerator Laboratory, Menlo Park, CA, 2010
2. SLAC ES&H Division, Radiological Safety Systems, SLAC-I-720-0A05Z-002-R003, SLAC National Accelerator Laboratory, Menlo Park, CA, 2010
3. SLAC Guidelines for Operations SLAC-I-010-001-000-00
4. DOE-2011: Radiation Protection of the Public and the Environment, DOE Order 458.1, Feb. 2011.
5. EPA-1987: U.S. EPA, "National Pollutant Discharge Elimination Systems (NPDES)", 40CFR122, 1987.
6. EPA-1989: U.S. EPA, "National Standards for the Emission of Radionuclides Other Than Radon from Department of Energy Facilities (NESHAPs), 40CFR61, Subpart H, 1989.
7. EPA-1992: U.S. EPA, "National Primary Drinking Water Regulation (NPDWR), Environmental Protection Agency", 40CFR141, 1992.
8. RE-022: SLAC National Emission Standards for Hazardous Air Pollutants (NESHAPs) Program Technical Manual", Radiation Protection Department, RE-022.
9. EPA-1989: U.S. EPA, "National Standards for the Emission of Radionuclides Other Than Radon from Department of Energy Facilities (NESHAPs), 40CFR61, Subpart H, 1989.
10. EPA-1992: U.S. EPA, "National Primary Drinking Water Regulation (NPDWR), Environmental Protection Agency", 40CFR141, 1992.
11. RWQCB-2009: California Regional Water Quality Control Board (RWQCB), San Francisco Bay Region Order No. R2-2009-0072, 2009.
12. RE-019: Approving Sanitary Sewer Release of Water Containing Radioactivity: Rationale and Process, Radiation Protection Department, RE-019, SLAC-I-760-2A16Z-000.
13. SBSA-2011: South Bayside System Authority (SBSA), Mandatory Wastewater Discharge Permit WB 111216, 2011.
14. M. Santana, "Response to LCLS-II (2013) CD1 Directors Review Recommendation to RP", RP Memorandum, RP-RPG-140109-MEM-01, January 2014.
15. J. Welch, Private Communication
16. W. R. Nelson and A. Kulikov, CID Radiation Protection - Revised Figure, SLAC Memorandum, September 1991.
17. S. Xiao, M. Santana and S. Mao, "Shielding Studies for Prompt and Residual Radiation from LCLS-II Injector Dumps", RP Note RP-12-04, 2012.
18. S. Xiao, M. Santana and S. Mao, "Linac Sector 10-20 Radiation Shielding Analysis for LCLS-II Operations", RP Note RP-12-05-R1, 2013.
19. Christopher Mayes, Cornell University, personal communication.
20. RP-RPG-140807-MEM-01, Air activation and ozone production due to beam losses on LCLS-II halo collimators (reference case and CEDOG collimator)
21. L. Ge1, C. Adolphsen, L. K. Ko, Lee, Z. Li, C. Ng, G. Schussman, F. Wang, "Multipacting Simulations of the TTF-II Power Coupler Components ", Proceedings of PAC07, Albuquerque, New Mexico, USA
22. H. Weise, 2004

23. D. Waltz, "Investigation of 100 kW SLC FF Extraction Dump for Use in LCLS-II", SLAC Memorandum, October 30 2013.

24. M. Santana, "First radioisotope production evaluations for DUMP/DUMPB of LCLS-II MHz project", Radiation Physics Note, RP-13-22.

25. H. Loos, "Injector/Linac Wire Scanner System Requirements", LCLSII-2.4-PR-0099-R0, 2014.

26. T. Raubenheimer, "LCLS-II Parameters", LCLSII-1.1-PR-0133-R0, 2014.

27. P. Emma and S. Xiao, "Post-Undulator Safety Dump Lines", LCLSII-3.5-PR-0111-R0, 2014.

28. S. Xiao, "Radiological Studies for the LCLS-II Post-Undulator Safety Dump Lines", RP-14-15, 2014.

29. S. Xiao, "Radiological Studies for Beam Losses on LCLS-II BYD Magnets: Prompt, Residual Radiation and Environment Impact around Dump Area", RP-15-01, 2015.

30. S. Xiao, "Radiation Shielding for Prompt Radiation to NEH and Rack Room", RP-15-02, 2015.

31. S. Xiao, "Radiological Studies for Beam Losses on LCLS-II BYD Magnets: Damage to Electronic Components", RP-14-11, 2014.

32. M. Santana, "Minimum estimated time to damage LCLS-II MHz beam components during accidental mis-steering: reference response time for BCS and MPS design", RP-RPG-140506-MEM-02

33. California Code of Regulation (CCR), Title 17, Public Health, Division 1, Chapter 5, Subchapter 4, Group 3, Article 5, Section 30287, 1994

34. Radiation Protection Department (RPD), "SLAC Radiological Environmental Protection Program Manual", RE-200, 2012

35. Radiation Protection Department (RPD), "Environmental Radiation Monitoring

36. Department of Energy (DOE), "Occupational Radiation Protection", DOE 10 CFR 835, 2011

14 ENVIRONMENT, SAFETY, HEALTH

TECHNICAL SYNOPSIS

SLAC is committed to the success of the mission objectives of the LCLS-II Project and to the safety of its users, staff and the public. It is our vision to construct LCLS-II with zero incidents or injuries. Worker safety is integrated into the Project at all levels, from the design, fabrication, and construction through to commissioning and operation. The SLAC Worker Safety and Health Program will be the primary vehicle for the LCLS-II Project to meet that vision, and is therefore essential to the safety of the workers as well as the successful completion of the project. ES&H has completed a Hazards Analysis Report, describing a variety of potential hazards that the LCLS-II Project may encounter or generate, and has made plans to mitigate these hazards. LCLS-II Management will communicate these hazard mitigations, to personnel working on or for the project, through daily meetings, design reviews, and management walkarounds.

14.1 Introduction and Overview

It is SLAC's policy to integrate safety and environmental protection into its management and work practices at all levels and to achieve its scientific mission while protecting the worker, the public and the environment. To achieve this policy, SLAC has developed and implemented a Worker Safety and Health Plan (WSHP) [1]. SLAC's WSHP was developed to be compliant with 10 CFR 851 [2] and with DOE's Integrated Safety Management System (ISM). SLAC has taken the additional step of combining ISM and the DOE's Environmental Management System [3] into one integrated system: the Integrated Safety and Environmental Management System (ISEMS) [4]. Supporting this process is the SLAC institutional Environment, Safety and Health (ES&H) Manual that addresses ES&H risks relevant to SLAC's mission, including construction and routine operations of Accelerator Facilities.

To align with SLAC's policy and ensure that all aspects of the design, manufacturing, installation, testing, operational, and decommissioning phases of the project are reviewed and consistent with that policy, LCLS-II has adopted SLAC's WSHP. This action meets the Critical Decision 1 requirement for the Project to have an integrated safety management system. The LCLS II project director is responsible for implementing the SLAC policy for the project through the adoption of the SLAC WSHP. Supporting the project director in this effort are the project's representatives for ES&H. The representatives advise the project director and the project staff on ES&H aspects of the project, helping to ensure LCLS-II meets both its DOE and SLAC ES&H requirements. The *LCLS-II Project Management Plan* LCLS-II-1.1PM-0109-R0 will describe high level responsibilities and authorities and position descriptions that define their ES&H responsibilities.

SLAC will follow existing, mature programs to ensure that all aspects of the design, decommissioning, installation, testing, and operational phases of the project are reviewed to meet regulatory requirements and SLAC's policies and procedures. SLAC's *Project Review Procedure* [5] provides a systematic, streamlined, and effective review of technical, infrastructure, and other projects to ensure the ES&H aspects are adequately identified and mitigated before authorization and release of project activities. It also describes the thresholds and applicability determination for reviews and the experimental project review and conventional project review processes. LCLS-II has taken an additional step by creating a controlling document that expands on the *Project Review Procedure*. This document, the *Project Design and Review Procedure*, LCLSII-1.1-QA-0009-R0, defines the roles and responsibilities for LCLS-II reviews. It elaborates on the review process and describes how to capture, address, and close comments, and finalize a design for construction, fabrication, and installation.

The hazards and selected mitigations will be identified through the hazards analysis process, as described in Section 14.2. SLAC has several decades of experience operating electron accelerators, free-electron lasers (FELs), and their accompanying user facilities. Engineered safety systems, policies, and procedures have been developed to control the hazards and risks

associated with them. Upon completion of the installation activities, the hazards and mitigations will be included in the LCLS-II Safety Assessment Document (SAD).

The LCLS-II Project will not generate new hazards that have not already been identified and addressed at SLAC or across the DOE complex. The potential hazards that have been initially identified can be mitigated through established SLAC ES&H policies and procedures. Additionally, LCLS-II will use the experience, hazard analysis, documentation, and Lessons Learned from partner labs and other DOE laboratories in order to evaluate our mitigation efforts against potential and identified hazards. The LCLS-II Project is shown **Error! Reference source not found.**schematically in Figure 14-1**Error! Reference source not found.**.

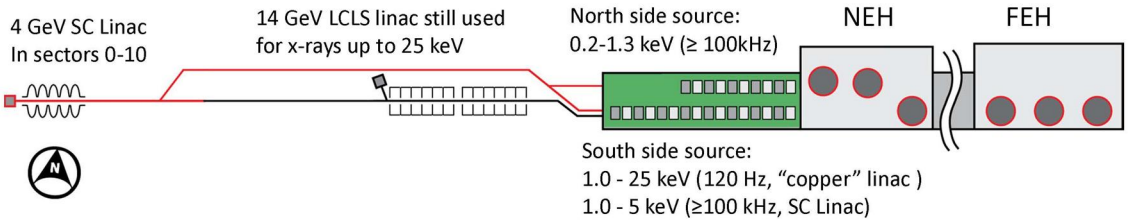

Figure 0-1. The LCL- II Project is shown schematically above.

14.2 Hazards Analysis Report (HAR)

A principal component of an effective ES&H program is to ensure that all hazards have been properly identified and controlled through design and mitigations (policies and procedures). To ensure that these issues are understood at the final phase, the preliminary hazards analysis has been updated into a Hazard Analysis Report (HAR). This process has been conducted to identify the hazards that will be encountered during the various phases of the project. In addition, some sections of the HAR were also used to meet the safety requirements defined in DOE Order 420.2C, "Safety of Accelerator Facilities" [6].

Generally, all hazards and risks anticipated to be encountered at LCLS-II, as identified in the HAR, are well known to SLAC, LCLS-II, and across the DOE complex. This institutional knowledge has been used to generate well-defined design criteria and controls to eliminate and/or control these risks.

Table 0-1 summarizes the hazards. The sections following Table 14-1 describe the hazards in more detail and list design and operational factors that will mitigate these hazards.

Table 0-1. Project Hazard Analysis Identifier and Hazard List.

PHA Identifier and Category	Hazard List
LCLS II – PHA-1 **Construction**	Demolition and decommissioning Welding Asbestos Nuisance dust Work at elevations (e.g.; steel erection, roofing) Material handling Utility interfaces, (electrical, steam, chilled water) Noise exposure Powered tools Slips/trips/falls Weather-related conditions Scaffolding Transition to Operations Radiation generating devices
LCLS II – PHA-2 **Natural phenomena hazards**	Seismic Flood Wind Precipitation (snow, ice and rain) Lightning Landslide
LCLS -II – PHA-3 **Environmental hazards**	Construction impacts Operations impacts Storm water discharge (construction and operations) Soil and groundwater activation/contamination Air activation Cooling water activation (HVAC and machine) Oils/chemical leaks or spills Discharge/emission points (atmospheric/ground)
LCLS-II – PHA-4 **Waste hazards**	Construction phase Facility maintenance Experimental operations Industrial Hazardous Radiological

LCLS-II – PHA-5 **Fire hazards**	Facility occupancy classification Construction materials Storage of flammable /combustible liquids Flammable gasses Egress/access Electrical Lightning Hot work: welding/cutting/grinding Personnel smoking
LCLS-II – PHA-6 **Electrical hazards**	Facility Experimental Equipment built by SLAC/Partner Labs Low Voltage/High Current High Voltage/High Power Maintenance activities Arc flash Electrical shock Cable tray overloading/mixed utilities Stored energy (capacitors & inductors) Beryllium compounds in contactors
LCLS-II – PHA-7 **Noise/vibration hazards**	Powered hand tools Machine shop tools Industrial vehicles Drilling, cutting, grinding Pressure/vacuum vessels & lines High temp equipment (bakeout) Compressors/turbines
LCLS -II – PHA-8 **Cryogenic hazards**	Oxygen deficiency Thermal Cryogenic distribution system Pressure LN_2/liquid He vent/spill/leak Use of inert gases (nitrogen, helium) Experimental specialty gases
LCLS -II – PHA-9 **Confined space hazards**	Hazardous gases Oxygen deficiency Hot work Limited egress Electrical
LCLS-II – PHA-10 **Ozone hazards**	Toxic Irritant Mutagen

LCLS-II – PHA-11 **Chemical/hazardous material**	Toxic Extremely toxic Compressed gas Carcinogens, mutagens, teratogens Combustibles Explosives Flammable gases Lead (shielding)
LCLS-II – PHA-12 **Accelerator/Beamline hazards**	Vacuum/Pressure Cooling water Compressed gas Electrical Heavy equipment handling Magnetic Cryogenic mechanical (e.g.; moving shutters, valves and actuators)
LCLS-II – PHA-13 **Ionizing radiation hazards**	Prompt radiation (scatter, neutrons, bremsstrahlung) Radioactive contamination Activation (equipment) Radioactive material (experimental)
LCLS-II – PHA-14 **Non-ionizing radiation hazards**	RF & microwave Magnetic fields (> 3 kHz) Laser
LCLS-II – PHA-15 **Material handling hazards**	Overhead cranes/hoists Fork trucks Manual material handling Delivery area distribution Manual movement of materials Vehicle and traffic

LCLS-II – PHA-16 **Experimental operations**	Electrical equipment Transportation of hazardous materials Biological materials Chemicals (corrosive, reactive, toxic, flammable) Nanomaterials (particulates) Elevations Darkroom hazards Clean room hazards Ionizing radiation Ozone production Slips, trips, falls Machine tools/hand tools Stray static magnetic fields Research gasses (corrosive, reactive, toxic, flammable)

14.3 Construction Hazards (LCLS-II PHA – 1)

SLAC has a mature construction safety program, with recent experience in constructing the LCLS Project, the Research Support Building (65,500 square feet) the Sector 10 injector facility, and other projects. Lessons Learned from these projects, as well as from other construction projects within the DOE complex, will help establish the controls necessary to minimize the risk associated with installation and construction activities for the LCLS-II Project. SLAC's Work Planning and Control (WPC) process is the mechanism used communicate the construction safety program to the workers. It identifies the tasks and work steps to understand the scope of work, identify qualified workers, identify hazards and mitigations, and communicate hazards and mitigations to all the workers, employees and subcontractors. The typical installation and construction hazards anticipated for the LCLS-II Project include the following:

- Demolition and decommissioning
- Welding
- Asbestos
- Nuisance dust
- Work at elevations (steel, roofing, MEP)
- Utility interfaces, (electrical, steam, chilled water, compressed air)
- Noise
- Powered tools
- Slips, trips, and falls
- Crushing
- Vehicle contact; backing, traffic
- Hoisting and rigging

- Access and egress
- Animals and insects
- Weather-related conditions
- Transition to operations

14.3.1 Construction Hazards – Mitigating Factors (Design)

- Engineered and approved excavation systems
- Engineered and approved fall-protection systems
- Permanent fall-protection systems incorporated into facility's roof and elevated work surfaces (for future maintenance)
- Modern code-compliant construction equipment with the required safety controls (e.g., backup alarms, seatbelts, load capacity readouts, emergency shut-offs)

14.3.2 Construction Hazards – Mitigating Factors (Operational)

- Strict adherence to 29 CFR 1926, OSHA Construction Standard
- Integrated Safety Management and the contractor required Health and Safety Plan (contractually flowed down to subcontractors) through SLAC's WSHP.
- Review of contractors and subcontractors based on their Safety Plan, Experience Modification Rate, Days Away, Restricted, Transfer rate, and Total Recordable Case rate
- Periodic evaluation of construction safety program
- Dedicated onsite construction safety professionals
- Hazards analysis for high-risk activities (e.g., site clearing, work at elevations), are captured in the subcontractor documentation (SOW, SSSP, JSA, plans and permits). Reviewed and authorized by the required Project personnel
- Frequent ES&H communication with the general/prime subcontractor and lower-tier subcontractors at a plan-of-the-day (tool box) meeting.
- Major construction equipment inspected on arrival at site

14.4 Natural Phenomena Hazards (LCLS-II PHA-2)

Natural phenomena hazards (NPHs), including winds, floods, earthquakes, precipitation, and lightning are considered in the design and operation of LCLS-II. The LCLS-II design will follow DOE-STD-1020-2012 [7] and the California Building Code (CBC) 2013 at the time of its construction and installation.

LCLS-II is categorized as Seismic Design Category 1 (SDC-1) per DOE-STD-1020-2012, which is Risk Category II per ASCE 7-10 [8], except where some systems may require a higher risk categorization (e.g., high-powered beam dumps; Risk Category IV). Note that Table 3-1 of DOE-STD-1020-2012 is used in conjunction with ASCE 7-10 to determine the response modification coefficient to be utilized for design.

LCLS-II areas will contain only some quantities of activated materials during equipment removal, decommissioning, and demolition. Some hazardous chemical materials may be used during the Project installation and operation. If a NPH were to cause significant damage, the impact would be mission-related and would not pose a hazard to the public or the environment.

DOE O 420.1C [6] requires structures and facilities to be evaluated for the effects of seismic hazards every decade. This evaluation assists the contractor in determining what, if any, actions are required to update the affected structures or facility. The SLAC Seismic Study [9] confirmed that accelerator facilities at SLAC were built to the appropriate national consensus codes and standards at the time of their construction and have a seismic performance rating consistent with Life Safety (ASCE 31-03)[10] or better.

14.4.1 NPH Mitigating Factors (Design)

- Seismic design follows DOE-STD-1020-2012 and ASCE 7.
- Strict conformance to California Building Codes
- Wind design: 110 mph (with 3-second gust)
- Lightning protection per NFPA 780Pitched roofs on structures to preclude localized flooding/roof leaks
- Site drainage designed to shed and channel water

14.4.2 NPH Mitigating Factors (Operational)

- Limited and controlled quantities of hazardous materials
- SLAC Site Emergency Plan
- Construction site emergency plan
- Emergency drills

14.5 Environmental Hazards (LCLS-II PHA 3)

Installation of LCLS-II requires the removal of some hardware (magnets and vacuum chambers) and the installation of new components (cryomodules, electrical distribution and cooling systems) suited to the Project. . Removal of these materials and the subsequent installation activities will produce quantities of nonhazardous, hazardous, and radioactive waste that will be managed through SLAC's defined processes. Past operating experience indicates that normal operation of the accelerator does not typically produce significant quantities of waste, but some hardware may have induced radioactivity associated with its proximity to the beam. Other components may contain hazardous materials as part of their design (e.g., mineral oil in electrical components, or radioactive contamination from the low conductivity water (LCW) system).

All material removed from the accelerator and gallery will be surveyed for residual radioactivity or contamination, labeled, and appropriately disposed of as defined in the SLAC

Radiological Control Manual [11] and The SLAC Radioactive Waste Manual [12]. Items that show residual radioactivity or contamination will be stored onsite until ultimately disposed of offsite.

Component manufacturing and system installation may also produce hazardous wastes, such as spent solvents from degreasing baths or spent cutting fluids. These wastes are managed and controlled routinely during operations at SLAC, in full compliance with its policies on the management of hazardous materials and waste minimization. The LCLS-II partner laboratories will produce wastes from their manufacturing and assembly work. They will follow their own approved Environmental Management Systems requirements for minimizing the generation of wastes and collecting and disposing of those wastes safely.

14.5.1 Environmental Hazards – Mitigating Factors (Design)

- Recirculating (closed-loop) cooling systems
- Minimal need for the regeneration of filter beds, through the use of water-treatment chemicals and disposable pre-filters
- Handling and storage facility for control of waste water
- Design to CBC (secondary containment) requirements

14.5.2 Environmental Hazards – Mitigating Factors (Operational)

- Implementation of an environmental management program designed to minimize chemical use through review and less hazardous chemicals and processes are substituted where possible. Controls are based on the following:
- Process Assessments
- Annual environmental reports Work Planning and Control
- Experimental Safety Reviews
- Training/qualification
- LCLS-II Environmental Assessment
- Air quality policies and procedures

14.6 Waste Hazards (LCLS-II PHA-4)

Waste-related hazards from LCLS-II include the potential for releasing waste materials (oils, solvents, chemicals, and radioactive material) to the environment and personnel contact or injury. Typical initiators would be transportation accidents, incompatible materials, insufficient packaging/labeling, failure of the packaging, and natural phenomena.

During the installation and operation phases of LCLS-II it is anticipated that minimal quantities of hazardous materials will be used. Such materials include paints, epoxies, solvents, oils and lead in the form of shielding. There are no current or anticipated activities at LCLS-II that would expose workers to levels of contaminants (dust, mists or fumes) above permissible levels.

The ES&H Industrial Hygiene Group provides program management and guidance to SLAC and subcontractor employees who are subject to waste-related hazards. Their staff identifies workplace hazards at the earliest stages of the project, assists with identifying controls, and monitors the implementation. Industrial hygiene hazards will be evaluated, identified, and mitigated as part of the hazard assessment process.

Site- and facility-specific procedures are in place for the safe handling, storing, transporting, inspecting and disposing of hazardous materials. These are contained in the *SLAC ES&H Manual*, Chapter 17, "Hazardous Waste" [13] which describes minimum standards to maintain for compliance with Title 40, Code of Federal Regulations.

The field construction manager and project manager have responsibilities for subcontractors' use of chemicals and other materials that can become hazardous waste. They ensure subcontractor personnel are aware of, and remain in compliance with *SLAC ES&H Manual* Chapter 40, [14], Chapter 52 [15], and Chapter 53 [16]. They also keep affected SLAC personnel informed of hazardous material usage and the associated hazards and risks.

14.6.1 Waste Hazards – Mitigating Factors (Design)

- Materials alternative review
- Designated waste accumulation areas

14.6.2 Waste Hazards – Mitigating Factors (Operational)

- Periodic inspections
- Planned county/state facility inspections
- Hazardous Waste Generator training
- Experimental Safety review process
- Work planning and control
- Facility-Specific safety orientation
- Tritium sampling program for accelerator's cooling-water systems
- Waste reduction, pollution prevention, and recycling
- HazMat transportation procedures per DOT and SLAC policies and procedures

14.7 Fire Hazards (LCLS-II PHA – 5)

The probability of a fire at LCLS-II is very low, similar to that for present operations, as accelerator and beamline components are primarily fabricated out of nonflammable materials and combustible materials are kept to a minimum. Operational experience at SLAC and at accelerators throughout the DOE complex has demonstrated that most fires in accelerator facilities are electrically initiated, typically by component failure. All other potential sources of fire are also considered in the design of the LCLS-II facility and installation. They include the combustibility of building construction materials, the accumulation of combustible materials by occupants during installation and operation, the use of pyrophoric or reactive materials, improper storage or use of flammable materials and gasses, lightning storms, and static discharge.

14.7.1 Fire Hazards – Mitigating Factors (Design)

- Design to CBC and appropriate NFPA standards
- Fire Hazards Analysis
- Noncombustible construction throughout facility
- Early-warning fire-detection systems (e.g., smoke detectors, rate-of-rise detectors)
- Automatic fire suppression (e.g., sprinkler system)
- Emergency power supply for essential systems
- Hazardous material storage areas: rated, vented, alarmed
- Grounding systems

14.7.2 Fire Hazards – Mitigating Factors (Operational)

- Manual fire suppression provided by required portable fire extinguishers
- Alarm systems to alert occupants and summon fire department (e.g., fire alarm bells/strobes, manual pull stations connected to local fire department)
- SLAC emergency response organization together with local fire departments on going inspection program to minimize combustibles and ignition sources
- Ignition-source control programs (cutting/welding permits, no smoking policy)
- Experimental Safety Review to minimize fire hazards of experiments by design features
- Fire evacuation drills

14.8 Electrical Hazards (LCLS-II PHA – 6)

LCLS-II will have subsystems that either produce or use high voltage or high current, either of which can present an electrical hazard to personnel. Since LCLS-II will operate similarly to

other accelerators at SLAC, control and work procedures for electrical subsystems and entry into the accelerator housing are well understood. Mitigations for these hazards consist of deenergizing equipment, placement of barriers, PPE, and the use of Lockout and Tagout (LOTO) procedures as specified in *SLAC's ES&H Manual*, Chapter 51, Control of Hazardous Energy [17].

The design, upgrade, installation and operation of electrical equipment will be in compliance with the National Electrical Code, Title 29 Code of Federal Regulations, Parts 1910 and 1926 (as applicable) and SLAC's policy on electrical safety, *SLAC ES&H Manual*, Chapter 8 [18]. Entry into the accelerator housing requires the mitigation of electrical hazards through either the lockout of power supplies or selective use of mechanical barriers, interlocked to further reduce the risk of exposure to electrical shock. Various levels of electrical safety training and LOTO training are provided by SLAC for all personnel who may work on or near potential electrical hazards.

14.8.1 Electrical Hazards – Mitigating Factors (Design)

- Design to NFPA 70 and 70 E and National Electric Code
- Adequate power distribution (beamlines and laboratories)
- Segregated power and utility distribution (cable/utility trays)
- Electrical and mechanical equipment rooms adequately sized
- Electrical distribution/disconnect equipment located in unobstructed areas (physically marked to provide clear access)
- NRTL-certified equipment

14.8.2 Electrical Hazards – Mitigating Factors (Operational)

- Non NRTL-certified equipment inspected and accepted per SLAC's Electrical Equipment Inspection Program
- Engineering and beamline design reviews
- Operation of equipment at <50 volts where feasible
- Electrical safety training
- Operational procedures to keep electrical equipment unobstructed
- Ongoing inspection program

14.9 Noise and Vibration Hazards (LCLS-II PHA – 7)

Hazards from noise and vibration can result in permanent hearing loss, also known as Permanent Threshold Shift. In addition, vibrations at various frequencies can affect personnel (fatigue), the surrounding area and community, and equipment and machinery operations.

LCLS-II will incorporate a wide variety of equipment that will produce a wide range of noise and vibration. Both support equipment for cooling water circulation, compressed air, air handling and exhaust fans and equipment that compresses gases into cryogenic liquids, contribute to the ambient and point source noise levels. The majority of LCLS-II areas will be below the OSHA noise threshold. Certain areas however, could exceed that requirement and will require periodic monitoring, postings, and personal protective equipment. [19]

14.9.1 Noise and Vibration – Mitigating Factors (Design)

- Separate mechanical/utility areas from work areas
- Isolate operations and experimental process equipment (e.g., pumps); utilize service chase concept, hutches, or individual equipment enclosures
- Use low-noise fans in HVAC systems
- Incorporate sound-absorbing materials into structure (wall and ceiling panels, baffles)

14.9.2 Noise and Vibration – Mitigating Factors (Operational)

- Baseline and periodic area noise surveys
- Personnel noise dosimetry as required
- Noise-exposure medical protocol where required
- New equipment reviews for noise and vibration levels as part of review and procurement process

14.10 Cryogenic and Oxygen Deficiency Hazards (LCLS-II PHA – 8)

Large volumes of liquid helium will be used to cool the superconducting linac (SCRF). In addition, liquid nitrogen will be used for precooling the cryogenic plant, cooling experimental samples and cooling beamline components and detectors. The use of these cryogens will include the potential for oxygen-deficient atmospheres in the event of catastrophic failure of the cryogenic systems, thermal hazards (cold burns) from cryogens or cryogenic components, and pressure hazards. Initiators could include the failure or rupture of cryogenic systems from overpressure, failure of insulating vacuum jackets, mechanical damage or failure, magnet quenching, deficient maintenance, or the use of improper procedures.

The extreme low temperatures of cryogenic liquids and gases have a significant adverse effect on the human body, as well as on inanimate objects. These effects range from destroying human tissue to altering the physical characteristics and properties of materials, such as size, strength and flexibility of metals and other materials.

14.10.1 Cryogenic Hazards – Mitigating Factors (Design)

- Design piping systems and pressure vessels per ASME codes or equivalent and SLAC policies and procedures.
- Lessons learned from partner Laboratories
- Required ODH analysis for all affected areas
- Installation of appropriate ODH monitoring and alarm systems, with interfaces to access control and ventilation systems as necessary
- High volume relief mechanisms in all piping and dewar systems piped external to buildings
- Personnel refuge areas

14.10.2 Cryogenic Hazards – Mitigating Factors (Operational)

- Review process for ODH analysis and design
- Operational readiness reviews
- Hazard training
- ODM system
- Forced ventilation

14.11 System Confined Space Hazards (LCLS-II PHA – 9)

Hazards from confined spaces could result in death or injury due to asphyxiation, compressive asphyxiation, smoke inhalation, or impact with mechanical systems. Initiators would include failure of the cryogenic systems releasing liquid, the release of gas, fire, or failure of mechanical systems.

The LCLS-II facility will have several types of confined spaces. They include those associated with the facility's support and maintenance, and typically include sump pits and HVAC plenums that can only be accessed by facilities maintenance personnel or escorted vendor personnel. An additional confined space will be the beam dump or dump pits. Other confined spaces can be created by the experimental programs and may include vessels or chambers.

14.11.1 Confined-Space Hazards – Mitigating Factors (Design)

- Definition of confined space criteria for designers – "design out," where possible
- Design of multiple means of egress
- Adequately size mechanical enclosures to allow maintenance
- SLAC policies and procedures for equipment access and egress

14.11.2 Confined-Space Hazards – Mitigating Factors (Operational)

- Identification of all confined spaces
- Facility-specific safety orientation for identified spaces
- Work Planning and Control program
- SLAC database of confined spaces maintained and updated as required.

14.12 Ozone Hazards (LCLS-II PHA-10)

Beamlines can generate radiation if the beam comes into contact with beamline components during operations. Resulting electromagnetic cascades deposit some of the beam energy onto the surrounding air, leading to ozone production. During the design and review phases of the project this hazard will be further evaluated and mitigated.

14.12.1 Ozone Hazards – Mitigating Factors (Design)

- Direct the beam path through evacuated or inert gas atmosphere containing pipes
- Minimize beam's horizontal and vertical dimensions
- Install ozone monitoring at potential problem areas

14.12.2 Ozone Hazards – Mitigating Factors (Operational)

- Experimental and beamline review program
- Delay personnel entry time to allow ozone to degrade

~~14.13~~ Chemicals and Hazardous Materials (LCLS-II PHA – 11)

The LCLS-II Project anticipates a minimal use of chemical and hazardous materials, based on the construction of LCLS and its subsequent operations. Exposure to these materials could, however, result in injury or in exposures that exceed regulatory limits. Initiators could be conventional and technical installations, experimental operations, transfer of material, failure of packaging, improper marking/labeling, failure of fume hood or glove box, reactive or explosive events, improper selection of or lack of personal protective equipment, or natural phenomena.

As explained in Section 16.6, SLAC has site- and facility-specific policies and procedures for the safe handing, storing, transporting, use, and disposal of these materials. These materials are managed throughout their life-cycle from purchase to removal/disposal.

14.13.1 Chemical and Hazardous Material Hazards – Mitigating Factors (Design)

- Dedicated Chemical Storage Area with segregation, ventilation, fire-protection system, flammable, and oxygen monitors and access control

- Defined Chemical delivery areas
- Vented chemical storage cabinets in Project areas
- Gas cabinets for flammable, toxic and highly toxic gasses, individual venting and purging capacity and exterior access
- Double-wall stainless tubing for distributing toxic and highly toxic gasses
- Dedicated storage for biological- and infectious-materials
- Bulk gas (liquid nitrogen, gaseous nitrogen, air) piped in, limiting number of individual bottles
- Appropriate controls for automatic shut-off on the bulk system where applicable (eg. nitrogen delivery into the building)
- Exhausted fume hoods in laboratories, (specialized hoods, e.g., HEPA where necessary)
- Utility exhaust available throughout for pump exhausts and other applications
- Safety showers and eyewashes in designated facilities
- All lead material encapsulated/painted
- Hutches with exhaust ventilation to exterior of building

14.13.2 Chemical and HazMat Hazards – Mitigating Factors (Operational)

- Chemical Management System (CMS) for purchasing and chemical inventory
- Lab standard Hazard Communication Training
- HazMat transportation per DOT and SLAC policies and procedures

14.14 Accelerator/Beamline Hazards (LCLS-II PHA – 12)

Hazards from the accelerator and beamlines include activated cooling water, chemicals, compressed gas, electrical systems, material handling and magnetic/cryogenic/radiation, access and egress, falls, and walking and working surfaces.

The accelerator and beamlines will have medium- and high-voltage electrical equipment and associated power supplies. High-power equipment includes RF, vacuum pumps, vacuum gauges, detectors, and beam position monitors (higher voltage-biased system).

Access and egress from the linac tunnel is limited by its location. Fixed ladders provide the access and egress from the tunnel at all locations (sectors) with some sectors having stair access. Ladder hazards include falls, hand or feet slipping, hard contact with the ladder, and muscle strain.

14.14.1 Accelerator/Beamline Hazards – Mitigating Factors (Design)

- Engineered safety-systems in place will protect the ring and beamlines from vacuum, cooling-water flow, extreme temperatures, and compressed air faults
- Vacuum faults will cause the accelerator's interlock systems to close the sector and front-end valves, thus dumping beam; beamline interlocks will close a beamline valve and/or a front-end valve; insertion device beamline interlocks will close the fast valve and dump RF
- Any reduced flow of cooling water is sensed, causing the accelerator's interlocks to dump RF and the beamline interlocks to close the safety shutters
- Elevated magnet temperature sensors will turn off the magnet's power supply. If sensed on ring components, RF will be dumped. If sensed in the pump room water, RF and magnet power supplies will be dumped.
- Loss of primary compressed air supply from the SLAC system will activate the SLAC backup supply and alert the control room

14.14.2 Accelerator/Beamline Hazards – Mitigating Factors (Operational)

- Safety Analysis Document and Accelerator Safety Envelope
- Operational procedures
- Systems design review

14.15 Ionizing Radiation Hazards (LCLS-II PHA – 13)

Potential hazards from ionizing radiation include prompt radiation (X-rays, neutrons, bremsstrahlung) produced during machine operation; induced activity in machine components; and radioactive material (use and storage). Typical initiators of radiation exposure would include operating machines, maintenance work, and the use of radioactive materials. Accidental exposure could result from failure of an interlock or other protective system, inadequate design or control of shielding, or an inadequate procedure.

To address these issues, the LCLS-II design will incorporate the requirements specified in 10 CFR 835 and the accelerator-specific safety requirements as set by DOE Order 420.2C, "Safety of Accelerator Facilities." The facility will be designed and operated in a manner to maintain radiation exposure to staff, users, and the general public within DOE and SLAC dose limits and control levels [20] [21].

14.15.1 Ionizing Radiation – Mitigating Factors (Design)

- Shielding for accelerators and beamlines to reduce dose to design levels
- Redundant interlock systems for accelerator enclosures and beamline hutches

- Redundant radiation safety critical devices (e.g., transfer line beam stops, beamline safety shutters)
- Real-time beam loss monitoring systems for injection and storage-ring operation
- Routine area monitoring of dose levels by passive dosimeters for neutrons and gammas on the experimental floor

14.15.2 Ionizing Radiation – Mitigating Factors (Operational)

- Radiological protection program incorporating requirements of 10 CFR 835 SLAC Radiological Control Manual
- Strict configuration control of shielding systems
- Radiological safety training (e.g., GERT, Radiation Worker I)
- Facility-specific Safety Orientation and ES&H Orientations
- Work control procedures ensuring adequate planning and ALARA reviews before work authorizations

14.16 Non-Ionizing Radiation (LCLS-II PHA – 14)

Non-ionizing radiation will be comprised of RF and microwave radiation and magnetic fields and lasers at LCLS-II. SLAC's policies and procedures, Lessons Learned, and safety measures based on present operations will provide the controls to address these hazards.

The LCLS-II RF systems will produce radio frequency radiation which, when not controlled, could have an adverse health effect on personnel working on or near the system.

LCLS-II will use equipment and devices that generate magnetic fields. The concern with these devices is the strength and extent of the fringe fields and how they may affect people and equipment in their vicinity. Fringe fields in excess of 5 gauss are of particular concern because they could affect medical electronic devices (pacemakers), while fields over 600 gauss could impact ferromagnetic implants (artificial joints) and other materials (tools).

The LCLS-II operations and experimental programs using Class 1, 2, 3R, 3B, and 4 lasers can present hazards to personnel. Direct exposure of laser radiation can adversely affect human skin or eyes if it exceeds certain levels. In addition, Class 4 lasers intensity can exceed the combustibility thresholds of some materials. Laser-target interactions may produce laser-generated air contaminants and hazardous plasma radiation at very high intensities.

14.16.1 Non-Ionizing Radiation Hazards – Mitigating Factors (Design)

- Equipment designed with integral shielding and interlocked systems, as needed
- Laser interlock systems

14.16.2 Non-Ionizing Radiation Hazards – Mitigating Factors (Operational)

- Baseline and routine surveys for stray magnetic fields, RF, and microwave
- Training for static magnetic fields, RF, microwave, and laser hazards
- Equipment ES&H review during installation
- Laser Safety Officer reviews
- Personnel protective equipment

14.17 Material Handling (LCLS-II PHA – 15)

A wide variety of equipment and material must be removed and installed during the decommissioning, deconstruction, installation, and operational phases of the LCLS-II Project. Hazards associated with these moves and material handling include vehicle impact with building or personnel, back strain or injury, being caught in a pinch point, the striking of body parts against equipment, cuts and bruises, as well as slips, trips, and falls. Additional material handling hazards from forklift and tow cart operations include injury to the operator or personnel in the area and contact with equipment or structures. Cranes and hoists will be used during fabrication, testing, removal, and installation of equipment. The hazards associated with this type of work include irregular shaped loads, awkward load attachments, limited space, obscured sight lines, and poor communication. Lessons learned for these hazards, from across the Complex, have been evaluated and incorporated into the design and operational mitigations.

14.17.1 Material-Handling Hazards – Mitigating Factors (Design)

- Hoists and attach points designed to ASTM/ANSI standards
- Piped-in gasses to reduce material handling of cylinders
- Incorporating lessons learned from SLAC and DOE Complex
- Equipment designed per applicable standards.

14.17.2 Material-Handling Hazards – Mitigating Factors (Operational)

- Routine inspection and maintenance of all material-handling equipment
- Only trained and qualified personnel are allowed to use equipment
- Equipment is locked to prevent unauthorized use
- Pre-use and inspection as required by supervisors to assure proper condition of equipment.

14.18 Experimental Operations (LCLS-II – PHA-16)

Based on existing experimental facilities, operational hazards and how they affect personnel and equipment are well understood at SLAC. Initiators would include the release or unexpected

reaction of hazardous material, protective systems failures, laser hazards, the use of radioactive and biological materials, operator error, lack of training, poorly designed or installed equipment, equipment failure, and unexpected chemical reactions. Many of the anticipated hazards are discussed in the specific hazard analysis sections in this document (e.g., ozone, non-ionizing radiation). Various inert and flammable research gases will be used in experiments. Inert gases include nitrogen, helium, and argon. Flammable gasses can include hydrogen, propane, and butane. Various toxic gases may be used in small quantities at the experiment. Small-scale use of oxygen and halogens is also is anticipated. Liquid nitrogen and helium will be used to cool experimental samples such as protein crystals.

14.18.1 Experimental Hazards – Mitigating Factors (Design)

- Each experiment is evaluated for ESH concerns after the proposal is submitted.
- Laboratories are designed based on anticipated use and possible future use (user input in design process, historical inventories/hazards considered).
- Chemical fume hoods installed in laboratories will be appropriate to experimental work, (based on the design programming).
- HEPA filtered hoods used for work with nanomaterial particulate and radiological dispersible materials
- An adequate power supply designed into the laboratories to support anticipated equipment needs and future growth
- Provisions for adequate chemical storage
- Outdoor-vented cabinets for storing flammable gasses
- Laboratories designed for easy access/egress, process flow, and ease of cleaning
- Laboratories located near beamlines, reducing movements of experimental materials
- Facility and laboratories designed to meet OSHA 1910 (walkways, stairs, egress)
- Safety shower and eye washes
- Equipment grounding system installed in experimental areas

14.18.2 Experimental Hazards – Mitigating Factors (Operational)

- Experimental safety review program for all scheduled experiments.
- Chemical Management System (CMS) for purchasing and chemical inventory
- Hutches with dedicated exhaust systems to connect up process and experimental equipment
- ES&H support staff actively reviewing and providing oversight of experimental activities

- Adequate beamline staffing
- Area, hazards, and experiment specific training

14.19 NEPA and NHPA

The LCLS-II Project is required by the National Environmental Protection Act (NEPA) to perform an evaluation of its potential environmental impacts during construction and operation of the project. DOE Order 451.1B Change 3 [22] provides the directive for complying with NEPA. The Project performed an Environmental Assessment, which included a detailed analysis of potential environmental impacts and the safety and health hazards identified during the design, construction, and operating phases of LCLS-II. A Finding of No Significant Impact was issued.

The Project is also required to comply with the National Historic Preservation Act (NHPA), 36 Code of Federal Regulations, Part 800. The details contained in the Project's scope will describe in narrative form the Project's potential effects on historic buildings. The potential effects include the modifications of buildings and change-out of technical systems. To comply, the project performed a Section 106 process that evaluates the buildings and structures for historic significance against National Register criteria [23].

14.20 References

1. SLAC-I-720-0A21B-001-R006, "SLAC Worker Safety and Health Program."
2. PART 851—Worker Safety and Health Program.
3. SLAC-I-750-0A03H-002-R4, "Environmental Management System Description."
4. ISEMS contract clause from the DOE Acquisition Regulations [DEAR], specifically DEAR 970.5204.-2, "Integration of Environment Safety and Health into Planning and Execution."
5. SLAC-I-720-0A24C-001-R006, "Chapter 1: General Policy and Responsibilities ESH: Project Review Procedure."
6. DOE Order 420.2C, "Safety of Accelerator Facilities."
7. DOE-STD-1020-2012, "DOE STANDARD Natural Phenomena Hazards Analysis and Design Criteria for DOE Facilities."
8. ASCE/SEI 7-10, "Minimum Design Loads for Buildings and Other Structures".
9. 10 YEAR SEISMIC STUDY FOR SLAC, July 2011.
10. ASCE/SEI 31-03, "Seismic Evaluation of Existing Buildings."
11. SLAC-I-720-0A05Z-001-R007, "Radiological Control Manual."
12. SLAC-I-7602A08Z-001-R002, "Radioactive Waste Manual."
13. SLAC-I-720-0A29Z-001-R023, SLAC ES&H Manual, Chapter 17 "Hazardous Waste".
14. SLAC-I-730-0A09L-004-R000, "SLAC ES&H Manual, Chapter 40, Chemical Lifecycle Management".
15. SLAC-I-730-0A09L-003-R000, "SLAC ES&H Manual, Chapter 52, Hazardous Materials and Waste Transportation."

16. SLAC-I-730-0A09L-005-R000, “SLAC ES&H Manual, Chapter 53, Chemical Safety”.
17 SLAC-I-720-0A29Z-001-R000 SLAC ES&H Manual, Chapter 51 “Control of Hazardous Energy”.
18. SLAC-I-720-0A29Z-001-R007, SLAC ES&H Manual, Chapter 8 “Electrical Safety”.
19. SLAC-I-720-0A29Z-001-R023, SLAC ES&H Manual, Chapter 18 “Hearing Conservation”.
20. SLAC-I-760-0A05S-003-R001, “Radiological Safety, Facility Design and Operation Requirements”.
21 SLAC-I-760-0A05B-001, “Classification of Radiological Areas”.
22. DOE O 451.1B Admin Change 3, National Environmental Policy Act Compliance Program.
23. 36 CFR part 63, “National Register criteria”.

15 QUALITY ASSURANCE

TECHNICAL SYNOPSIS

SLAC is committed to the success of the mission objectives of the LCLS-II Project. To that end, we developed a Quality Assurance Program to assure the development of items, systems and services that meet or exceed the specification requirements of the machine. The Quality Program has been implemented across the entire LCLS-II project at SLAC, and the contributing partner labs.

15.1 Introduction and Overview

The LCLS-II Project has developed a formal Quality Assurance Program. The LCLS-II Quality Plan defines program requirements, and a *Quality Procedures Manual,* a series of web-linked documents, describes the specific instructions for QA program implementation in LCLS-II. A Graded Approach has been established to apply the appropriate level of QA commensurate with the risks when acquiring items systems and services.

15.2 Quality Roles and Responsibilities

Quality professionals are in place, at SLAC and the partner labs, to assure the effective implementation of the LCLS-II Quality Program. The Quality Representatives interface with scientists, engineers and management to develop an effective strategy for applying the appropriate quality practices. Quality Representatives interface with LCLS-II staff within the following project activities:

- Selecting the appropriate Quality Grade and determining QA actions
- Developing designs and specifications
- Qualifying vendors and performing source surveillance
- QC planning and developing of an Acceptance Strategy for items, systems and services
- Conducting inspection and testing
- Managing change and nonconformance
- Collecting and verifying QA documents
- Performing internal assessments
- Conducting QA training

15.3 Quality in the Design Review Process

Quality Representatives interact with design activities and are instrumental in developing the Quality aspects within a given design. Quality Representatives also assist in the creation of formal specifications and work instructions. QA participation in the design process is essential in the planning of Quality activities to assure that the specification requirements are ultimately achieved.

All LCLS-II Project components, systems and installation activities are subject to the project technical design review process. The primary objective of the *Technical Design and Milestone Review Program*, LCLSII-1.1-QA-0009, is to enhance the probability of success by identifying

potential or actual design problems associated with design, installation or construction, and operations in a timely fashion to minimize the impact on cost, schedule and performance.

15.4 Vendor Qualification and Surveillance

A Vendor Qualification program is in place to evaluate the Quality programs of potential vendors and suppliers. Evaluation criteria for suppliers have been created, and a formal vendor evaluation processes has been established. The Quality Representatives work close with the Technical Leads and the LCLS-II procurement staff during the entire qualification process. All events and interactions are documented and reviewed by Project QA Representatives.

15.5 Inspection Planning and Verification Strategy

Quality Representatives assure the development of Acceptance Criteria Strategies (ACSs) when acquiring items, systems and services. This ACS defines all the Quality requirements associated with a given acquisition, and assigns responsibility to individuals for carrying-out all the established Quality actions. A central database of ACS documents has been established on the LCLS II website to provide ongoing visibility into QA planning activities performed at SLAC and the partner labs.

15.6 Testing, Verification and Validation

Systems were developed to perform inspections and validations. Designated individuals are assigned responsibility for performing established verification tasks and confirming compliance. A formal non-conformance process was established to manage discrepancies and perform corrective action. Formal records of tests, validations and any non-conformance are generated to provide objective evidence that the Quality requirements have been addressed, and that the items and services meet specifications.

15.7 Internal Assessments

The LCLS-II facilities, including SLAC and the partner labs, perform routine internal assessments to confirm the effective implementation of the Project's QA program. Opportunities for improvement are identified and implemented to assure that the highest condition of Quality is reflected within LCLS-II items and services.

15.8 Partner Lab Integration

Partner lab QA systems provide local oversight of the Quality processes used throughout their facilities. A cross-walk exercise has been performed at each contributing partner lab to assure QA program compatibility with the central LCLS-II Quality system. Partner labs will utilize the QA practices that were previously determined to be similar to, and meet the intent of, the central LCLS-II Quality Program. Partner lab QA practices that do not meet the expectations

of the central LCLS-II QA program have been fortified or enhanced to achieve compatibility with the missions of the central QA program. The LCLS-II Project Quality group at SLAC will perform routine oversight of the partner labs' QA practices by performing assessments as the Project continues to evolve and grow.

15.9 Documents and Records

The LCLS-II Project operates and maintains a central computer repository of all project management documents, physics and engineering requirements documents, interface control documents, procurement technical specifications and design standards and guidelines, as outlined in Figure 15-1. These documents are available by the partner labs via the LCLS-II Project Controlled Document Site. Definitions for LCLS-II Technical Requirements Documents are delineated in the *LCLS-II Project Systems Engineering Management Plan*, LCLSII-1.1-PM--0043. The process for the development, review and approval of project documents is described in *Quality Procedure, Document Control*, LCLSII-1.1-QA-0196. Project drawings and 3D models are produced by various methods and at different sites. Irrespective of the method and site of production, all drawings and 3D models will be archived in the appropriate SLAC system. Quality records associated with project deliverables will be submitted to SLAC and archived in the applicable SLAC database. Examples of quality records may include, but are not limited to, QA travelers, inspection and test reports, engineering calculations, and material certifications.

Supplier and Manufacturer's documents and records will be captured by the project. Quality Representatives at SLAC and the partner labs will assure that these documents are not only captured, but fulfill their intended requirements.

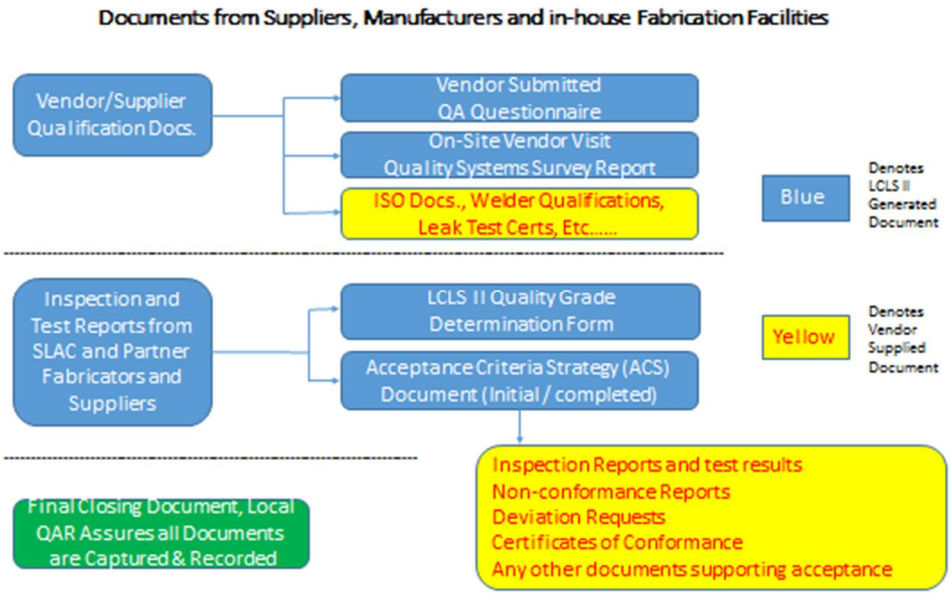

Figure 15-1: Documents from Suppliers, Manufacturers and in-house Fabrication Facilities

15.10 References

DOE Order 414-1D, Quality Assurance.

LCLS-II Preliminary Project Execution Plan, LCLSII-1.1-PM-0002.

LCLS-II Project Management Plan, LCLSII-1.1-PM-0109.

LCLS-II Project Systems Engineering Management Plan, LCLSII-1.1-PM-0043.

DOE G413.3-2 Quality Assurance Guide for Project Management.

10 CFR 830, Subpart A, "Quality Assurance Requirements".

ANSI/ASQ Z1.13 "Quality Guidelines for Research".

DOE G 414.1-2B, "QA Program Guide".

DOE G 414.1-4, "Safety Software Guide".

DOE O 243.1B, "Records Management".

SLAC Policies and Procedures.

DOE P 450.4A, "Integrated Safety Management Policy".

DOE G 414.1-3, "Suspect/Counterfeit Items Guide".

16 R&D PROGRAM

TECHNICAL SYNOPSIS

The design of LCLS-II is based on existing technologies. There are a few areas where advances to that technology, or where possible design changes, need development work which the Project is performing: raising the superconducting cavity Q_0, determining the suitability of a DC electron source, and evaluating the possibility of an undulator that produces vertically polarized X-rays. These programs are described in this chapter.

16.1 Introduction and Overview

The design of LCLS-II is based on existing technologies. However, there are a few areas where advances to that technology, or alternatives, need development work that the Project is pursuing: raising the superconducting cavity Qo, evaluating the suitability of a DC electron source and exploring the possibility of an undulator that produces vertically polarized X-rays.

The main contribution to the cryogenic load from the accelerator system is RF losses in the accelerator cavities. Recent results from Fermilab [1] have shown that superconducting niobium accelerating cavities can achieve very low losses, with high values of cavity quality factor Q_0 at 2 Kelvin, by doping the interior surface of the cavities with nitrogen. LCLS-II makes use of this new process to reduce heat loads, and thus significantly reduce the cryogenic plant size. A Q_0 value of greater than 2.7×10^{10} is used in the design. Preservation of high Q_0 in the installed cryomodules is required. This places requirements on ambient magnetic fields and on the cool-down rate of the superconducting accelerator cavities.

The LCLS-II baseline design uses as the electron injector source the RF gun under development at LBNL for the APEX project [2,3]. APEX is a separately funded project which will demonstrate its performance at high energy in mid-FY15. As a back-up plan, LCLS-II is funding tests at Cornell University on high voltage performance of an existing DC gun. The tests, described below, involve operating the gun at 400 kV and measuring beam performance at high energy. There is currently no plan to adopt the DC gun into LCLS-II scope. A change from the baseline RF gun to a DC gun could be done if there were to be a major problem with the baseline plan.

The undulator magnets in the LCLS-II baseline are of a conventional design modeled after undulators produced at LBNL and XFEL. A proposal from ANL for a new novel design is being investigated. The Horizontal Gap Vertical Polarization Undulator (HGVPU) would produce vertically polarized X-rays, which might be advantageous for monochromation and beam splitting. As described below, prototype HGVPUs are being fabricated and tested at ANL. If the user community requires an undulator with vertical polarization, the new design could be adopted.

16.2 Development of High Performance Superconducting Cavities – High Q_0 R&D Program

Total cryogenic design load has a large influence on project design factors, principal of which is cryoplant design. The LCLS-II project therefore seeks to maximize confidence in design performance specifications of the Superconducting RF (SCRF) accelerator cavities, particularly those that determine the realized cryogenic load under operating conditions. Rather than simply adopt the state-of-the-practice standards used for other recent large SCRF accelerator projects,

LCLS-II seeks to exploit newly emerging technology that offers the prospect to reduce the 2.0 K cryogenic plant load by approximately a factor of two compared with the status quo.

Recent work [**Error! Bookmark not defined.**] has demonstrated a novel cavity surface preparation technique that results in as much as a three-fold improvement of mid-field Q_0 for conventional bulk-niobium superconducting cavities at 2.0 K; related work is therefore labelled 'High Q_0'. Fermilab has developed a repeatable processing recipe that yields high Q_0 ($>3.0 \times 10^{10}$) values in 1.3 GHz cavities at the 16 MV/m operating gradient of LCLS-II at a vertical test temperature of 2.0 K, making possible the construction of a practical CW superconducting RF linac with resonator-loss of 10 W per meter-long cavity at an acceleration gradient of around 16 MV/m, (2.0 K). Because the technique used only differs from the current internationally recognized standard method by the addition of a few process steps, it appears reasonable to fast-track its refinement and incorporation into the production baseline for LCLS-II within one year.

The goal is confident, reliable performance of the SCRF cavities in LCLS-II with $Q_0 \geq 2.7 \times 10^{10}$ at 16 MV/m and 2.0 K, which corresponds to ≤ 10 W dynamic load from each cavity at the design operating acceleration gradient. The High Q R&D program, documented in the *High Q_0 R&D Plan* LCLSII-8.2-PM-0052-R0 and excerpted here, proceeds through a progression of increasingly more complex and time-consuming platforms: (A) single-cell cavity work, (B) bare 9-cell cavity work, and (C) horizontal "dressed" cavity cryogenic RF testing. The program seeks to quickly build sufficient confidence in the new cavity process performance that the project can proceed with its baseline cryoplant specification, while subsequently reducing any remaining technical risk as may be appropriate.

Additional technical details can be found in LCLS-II technical note *High-Q Development Plan and Choice of Q_0* LCLSII-4.5-EN-0216.

16.3 Development of an Alternate Injector Source – DC gun

The goal of the Cornell injector R&D collaboration was to demonstrate that their source could meet the requirements for the proposed LCLS-II Injector, listed in Table 16-1. Performance for 20 pC and 100 pC bunches had nearly been demonstrated earlier [4], but there was no previous demonstration of the 300 pC requirements in a gun capable of operating up to 1 MHz repetition rate.

Table 16-1: LCLS-II beam specifications for the injector

Bunch Charge	95% emittance	Peak Current
20 pC	0.25 µm	5 A
100 pC	0.40 µm	10 A
300 pC	0.60 µm	30 A

16.3.1 Simulations

Detailed beam simulations of the injector have been done using the code General Particle Tracer (GPT), and cavity field models [6]. The GPT runs multi-objective genetic optimizations, minimizing both the x and y projected normalized emittance and the RMS bunch length at the measurement location for each bunch charge. The model also includes variation of the initial laser shape. The transverse profile is a truncated Gaussian with variable truncation fraction and diameter. The longitudinal profile uses a realistic model of the shaping crystals used in the injector laser system. The cavity voltages and magnet settings can also be varied within realistic ranges.

For three values of bunch charge, Figure 16-1 shows the optimizer found injector settings that meet the emittance and peak current targets with a beam energy of roughly 9.5 MeV. In addition, the plot shows that the asymmetric effect of the couplers on the emittance in both planes can be mitigated.

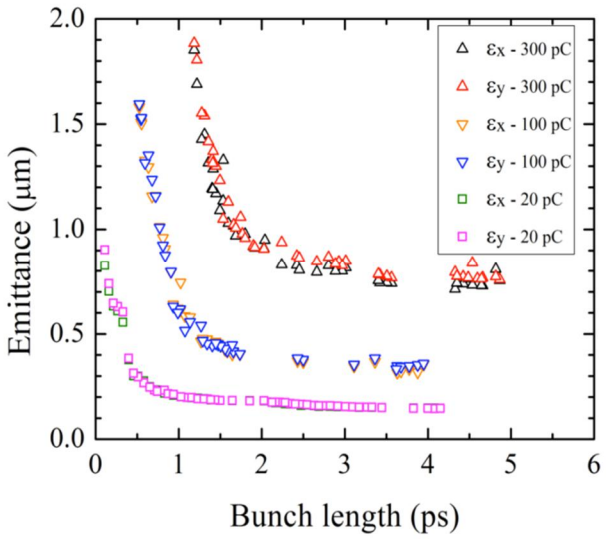

Figure 16-1: Optimized emittance vs. bunch length for 20, 100, and 300 pC bunches

16.3.2 Measurements

Previous measurements [**Error! Bookmark not defined.**] on the Cornell single insulator DC gun have been performed with the gun operating at 350 kV. For the LCLS-II measurements the gun high voltage (HV) was processed up to 440 kV in order to run reliably around 400 kV. This was checked by operating the gun continuously at 400 kV for 48 hours, during which time no HV trips occurred. All measurements reported here were conducted at 400 kV.

The Cornell Injector emittance measurement system was rebuilt for these measurements and therefore required recalibration. Measuring the emittance to low bunch charge and comparing that to thermal emittance measured for the cathode provides a sensitive check of the calibration as

well as the beam alignment through the injector. Figure 16-2 shows the comparison of these data to GPT predictions, indicating proper alignment.

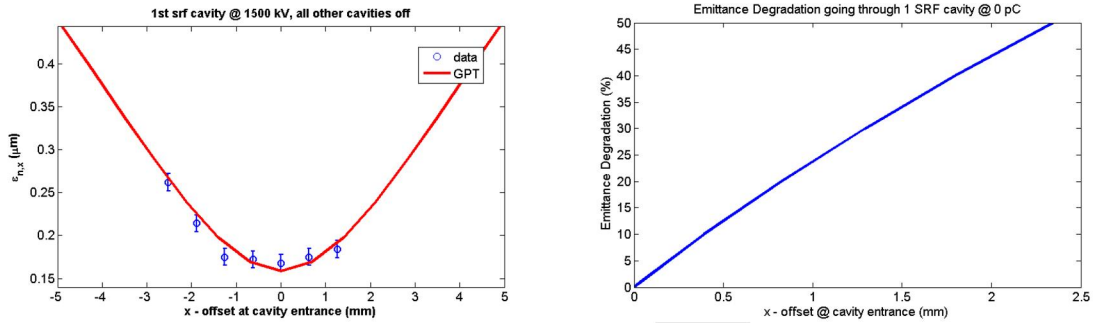

Figure 16-2: Emittance at zero bunch charge vs. offset in first SCRF cavity (left), and emittance degradation vs. x-offset in first cavity (right)

A 2D scan of both solenoid currents versus both the x/y emittances was performed at both 20 pC and 100 pC. Figure 16-3 shows the measured phase spaces for both 20 pC and 100 pC with a Cs_2Sb cathode (180 meV mean transverse energy).

Longitudinal profiles were also measured and Figure 16-4 shows the horizontal phase space and longitudinal profile with a NaKSb cathode (140 meV mean transverse energy). Results with both cathodes at all three charges are summarized in Table 16-2.

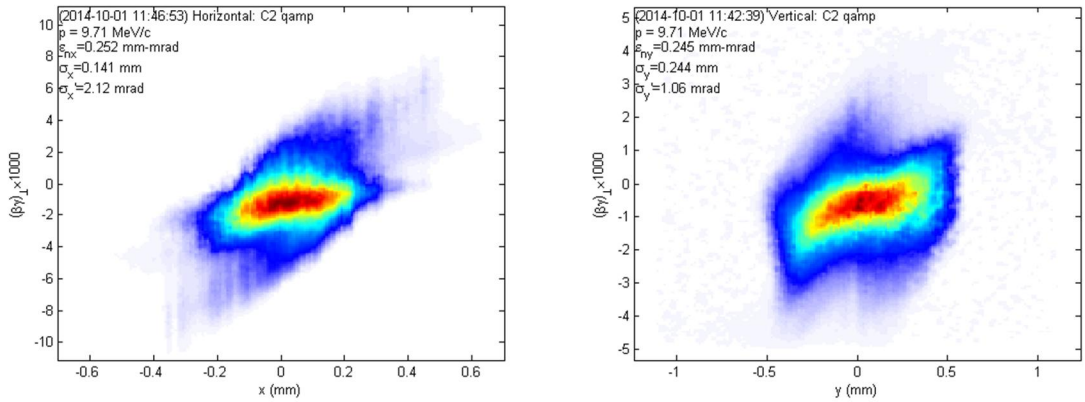

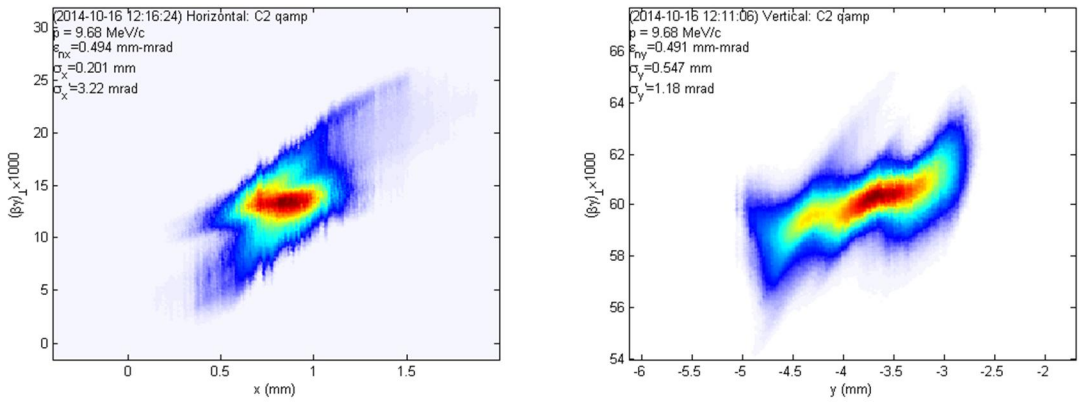

Figure 16-3: Measured transverse phase space at 20 (top) and 100 (bottom) pC with Cs_2Sb cathode. Horizontal phase space is shown on the left and vertical on the right

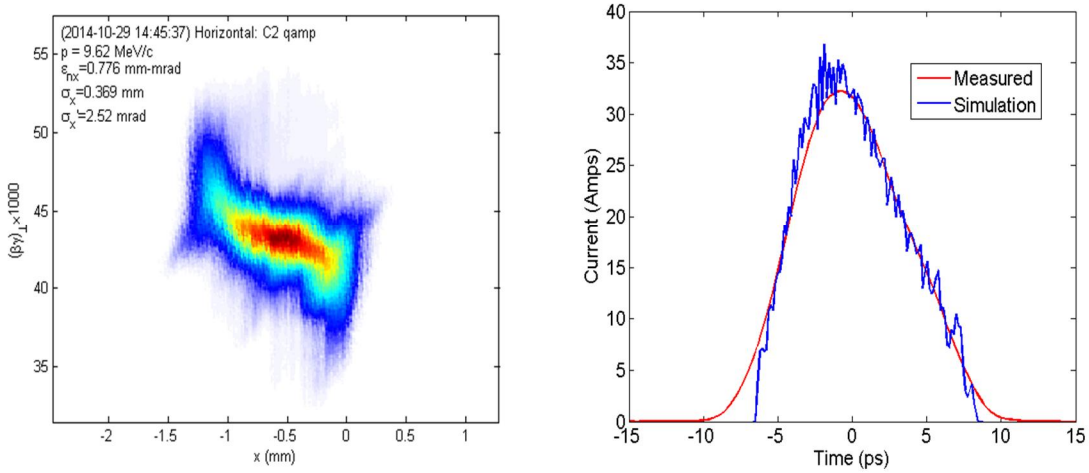

Figure 16-4: Examples of horizontal phase space (left) and longitudinal current profile (right) at 300 pC for the NaKSb Cathode

Table 16-2: Emittance and peak current results for NaKSb and Cs2Sb cathodes.

NaKSb Cathode			
Bunch Charge	$\varepsilon_{n,x}$(95%)	$\varepsilon_{n,y}$(95%)	I_{peak}
20 pC	0.18µm	0.19 µm	5.0 (A)
100 pC	0.30 µm	0.32 µm	11.5 (A)
300 pC	0.62 µm	0.60 µm	32.0 (A)

Cs_2Sb Cathode			
Bunch Charge	$\varepsilon_{n,x}$ (95%)	$\varepsilon_{n,y}$ (95%)	I_{peak}
20 pC	0.20 µm	0.21 µm	5.0 (A)
100 pC	0.39 µm	0.40 µm	10.2 (A)

300 pC	0.67 µm	0.66 µm	31.0 (A)

Comparing Table 16-2 to Table 16-1, it is clear that the measurements done with the NaKSb cathode meet all of the specifications except the vertical emittance at 300 pC, which is within 4%. Similarly, the measurements using the Cs_2Sb cathode all meet the specification with the exception of the emittances at 300 pC. In this case, both x/y emittances are within 12% of the specification.

The new Cornell segmented gun has been processed up to a maximum (unstable) conditioning value of 550 kV in vacuum. The conditioning process lasted for more than 140 hours [5]. A low current beam has been demonstrated at 400 kV. Both the transverse emittance measurement system and deflecting cavity on the segmented gun diagnostic beam line have been commissioned and calibrated at low charge.

16.4 Development of an Alternate Undulator Design – Horizontal Gap Vertical Polarization Undulator (HGVPU)

The majority of insertion devices on synchrotrons are constructed with the magnetic field oriented vertically and the X-ray beam polarized horizontally. This is due to the large asymmetry of the electron beam stay-clear in storage rings. A number of variable polarization devices have been built, using either electro-magnets, combinations of electro-magnets with hybrid magnets, or pure permanent magnets [6, 7, 8, 9]. They all require longer periods than the equivalent Halbach hybrid undulator structure [10].

The electron beam in an FEL, in contrast with that in a synchrotron, is nearly circular with a symmetrical stay-clear, so the orientation of the magnet is not driven by accelerator requirements. In LCLS-II the performance requirements drive an undulator design that has a high magnetic field and a short period, criteria that are most easily met with the hybrid design. The basic vertical field, horizontal polarizing, hybrid undulator design is well understood, with variations having been built for 30 years by institutions and commercial vendors around the world, and therefore the baseline LCLS-II undulator design follows this approach. There is not sufficient space in the LCLS tunnel to turn the basic design on its side.

Argonne National Laboratory proposed a novel HGVPU design that is very compact (see Figure 16-). It is based on the concept of distributing force-compensating springs along the length of the magnetic structures, thus eliminating the need for deep beams to carry the magnetic loads between the undulator jaws and small gaps. LCLS-II has been supporting ANL's effort to develop the concept. The motivation for LCLS is:

- Ability to deliver vertically polarized X-rays
- Compact design compatible with the existing mechanical support and control systems

- Lower cost from simplified fabrication and assembly and reuse of existing supports and controls.

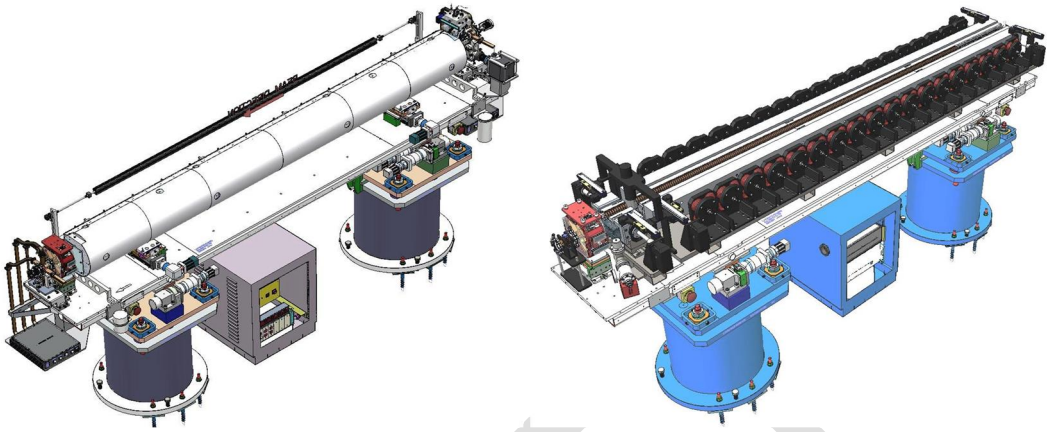

Figure 16-5: Left, LCLS fixed gap undulator on supports with control rack. Right, proposed HGVPU design on the same support system.

ANL first built a short 0.85 m prototype from existing magnetic arrays to prove the basic concept [11]. This prototype was completed in September of 2013. It was quite successful in demonstrating that motion and gap control could be achieved on a small scale. ANL, with LCLS-II support, proceeded with a larger 3m prototype. This prototype, shown in Figure 16-, was designed to LCLS-II requirements with a 26mm period and completed in September 2014. This prototype exhibited mechanical problems that prevented it from fully meeting the LCLS-II requirements. The location of the compensating springs allows for small moments to be generated by the drives, and the drives are not properly located to balance the friction in the stages. The team at ANL has identified fairly straightforward solutions to these issues that will be incorporated in the next prototype. This is to be a full 3.4 m magnetic array that meets all the LCLS-II undulator requirements and should be able to demonstrate that the ANL concept can be made to work on a full-scale system. It will also be used to demonstrate production methods and develop procedures for tuning the undulators efficiently for large production runs. ANL has developed a cost and schedule for the next prototype with completion at the end of FY2015.

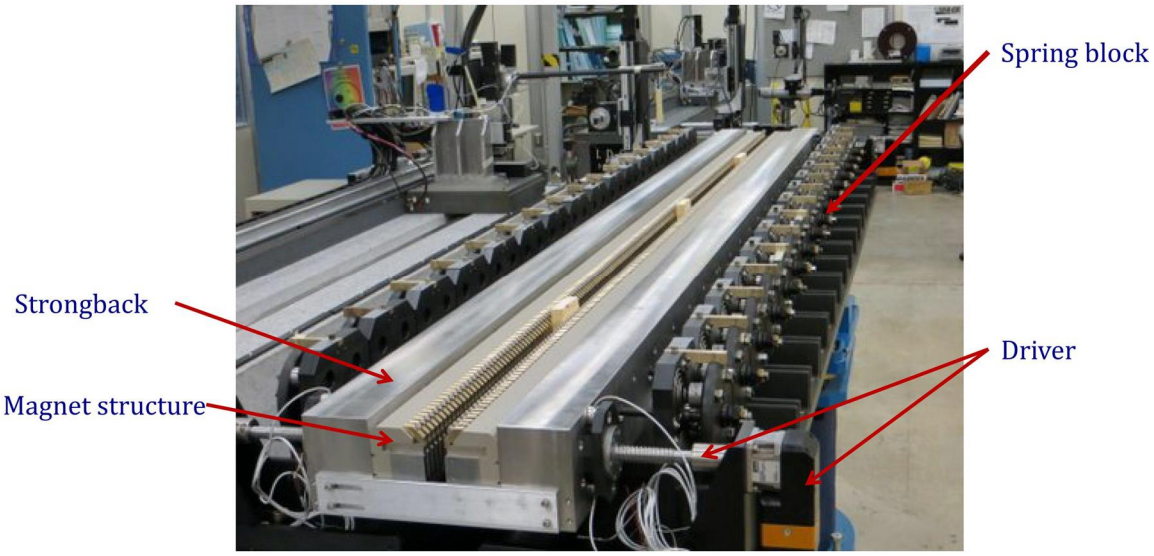

Figure 16-6: 3 m HGVPU prototype at ANL. It is supported on a LCLS girder and support system.

16.5 References

1 A. Grassellino, et al., Superconductor Science and Technology 26, 102001 (2013)

2 F. Sannibale, et al., PRST-AB 15, 103501 (2012)

3 F. Sannibale, et al., Proceedings of IPAC2014, Dresden, Germany MOPRI054, 797.

4 C. Gulliford, et al., Phys. Rev. ST Accel. Beams 16, 073401 (2013).

5 J. Maxson, et al., Rev. Sci. Instrum. 85, 093306 (2014).

6 R.P. Walker, B. Diviacco, "Studies of Insertion Devices for Producing Circularly Polarized Radiation with Variable Helicity in Elettra," Review of Scientific Instruments 63, 332 (1992).

7 P. A. Montano, et al., "Elliptical Multipole Wiggler Facility at the Advanced Photon Source," Review of Scientific Instruments 66, 1839 (1995).

8 S. Sasaki, "Analyses for a planar variably-polarizing undulator," Nucl. Instrum. Methods A 347 (1994) 83-86.

9 R. Carr and S. Lidia, "The Adjustable Phase Planar Helical Undulator," SPIE 2013, 56 (1993).

10 K. Halbach, "Permanent Multipole Magnets with Adjustable Strength," IEEE Trans. Nuclear Science 30, 3323 (1983). PERMANENT MULTIPOLE MAGNETS WITH ADJUSTABLE STRENGTH, IEEE TRANSACTIONS ON NUCLEAR SCIENCE Volume: 30 Issue: 4 Pages: 3323-3325 Published: 1983

11 N. Strelnikov, et al., "Vertically polarizing undulator with the dynamic compensation of magnetic forces for the next generation of light sources," Review of Scientific Instruments 85, 113303 (2014).

17 FUTURE UPGRADE OPPORTUNITIES

TECHNICAL SYNOPSIS

The LCLS-II is designed to meet several baseline requirements with two separate FELs driven by a new superconducting CW linac. Although the baseline design is clear, it is useful to envision future expansion concepts and enhanced performance so that present design decisions will not exclude these avenues. This chapter briefly describes some of these future expansion ideas, including energy upgrades of the SCRF or CURF linacs, expanded FEL facilities, external laser seeding with HGHG, HHG and EEHG FEL designs, short bunch generation, two-color generation, an increased bunch repetition rate, and several other concepts.

17.1 Introduction and Overview

This chapter describes several upgrade or expansion schemes that are being envisioned and considered at the present time. These may provide extended wavelength range, higher X-ray power, a higher pulse rate, narrowed bandwidth, and additional user capacity. Where practical, baseline design decisions will be made in order to preserve these possibilities.

17.2 Photon Energy upgrades

The electron energy of the new SCRF linac was chosen to be 4 GeV, including some small operational margin, which will allow the generation of 5 keV photons. Enhanced FEL performance and a wider spectral tuning range are possible with an increase in electron energy. The CuRF linac is able to deliver a compressed beam with an energy of 15 GeV which would provide photons with energies greater than 25 keV. There are various options to increase the CuRF linac energy and thereby increase the photon wavelength range. There is also an option of connecting the CuRF linac to the SXR undulators, which could provide beams with higher peak currents and energies of up to 10 GeV (the maximum design beam energy for the SXR beamlines). Finally, operating at harmonics of the fundamental energy also is another possible method to increase the photon energy reach.

17.2.1 SCRF Linac Beam Energy

The 35 cryomodules included in the baseline design extend from the beginning of the existing SLAC linac tunnel to about midway along Sector 6 (101.6 m/sector). This stretch constitutes about 650 m of accelerator length, accommodating the injector, bunch compressors, and several beam collimation sections. The available (unused) tunnel length leading up to the start of the bypass line in Sector 10 is then about 250 m. This empty tunnel might be filled in the future with up to an additional 19 cryomodules (12.2-m period). There are two ways in which this upgrade might be adopted. First, using only the baseline cryoplant where the total heat would not be allowed to grow, the acceleration gradient could be decreased inversely with the square-root of the accelerator length allowing a final electron energy in Sector 10 of about 5.2 GeV with a 12.5 MV/m average gradient. Second, with an additional cryoplant comparable in power and scale to the initial LCLS-II system, the gradient could be maintained at 16 MV/m, reaching a final energy in excess of 6.5 GeV. This upgrade would allow the full CW, high-rate operation of the SXR and HXR FELs with a significantly extended wavelength range into the hard X-rays, approaching 8-10 keV in the HXR FEL. Further expansion is possible using Sectors 10-19 of the SLAC linac, ultimately allowing for >15 GeV beams from the SCRF linac if fully populated.

17.2.2 CuRF Linac Beam Eenergy

The beam energy of the existing copper linac could also be extended from 15 GeV in a few different ways. First, a large number of existing RF stations will be removed from Sectors 0 through 10 during the preparation for the LCLS-II SCRF linac installation. Many of these could

be used to increase the CuRF linac energy [1] and could increase the maximum compressed beam energy from 15 GeV to ~19 GeV, allowing access to photon energies well in excess of 40keV from the HXR undulator. Alternately, a new injector could be installed in the Sector 11 Stub and the twenty sectors of the SLAC linac could be used to achieve compressed beam energies in excess of 28 GeV at 120 Hz with corresponding photon energies in excess of 50 keV. Alternately, the linac could be retuned to operate the twenty sectors at 360 Hz with a compressed beam energy greater than 18 GeV and photon energies in excess of 40keV from the HXR undulator. Such an injector was designed and construction was started as part of the LCLS-II Phase 1 project; the hardware has now been set aside awaiting a future program. The design of the LCLS-II SCRF Dogleg and Bypass -- see Chapter 4 -- has been optimized to allow such an installation in the future.

17.2.3 CuRF Linac Connection to SXR Undulator

In the baseline LCLS-II design, the CuRF linac can supply beam to the HXR Undulator but not to the SXR Undulator while the SCRF linac can supply beam to either undulator. It is possible to add a beamline to connect the CuRF linac to the SXR Undulator as well as the HXR Undulator. This will increase the photon tuning range from the SXR and will increase the X-ray peak power, possibly enabling X-ray imaging applications. Connecting the CuRF linac to the SXR Undulator could also allow optimization of the operation schedule. For example, when the SCRF linac shuts down for extended upgrades, beam could continue to be delivered to both the HXR and the SXR.

17.2.4 Nonlinear Harmonic Generation

Strong bunching at the fundamental wavelength near saturation can drive substantial bunching and power levels at the harmonics in a high-gain FEL [2,3,4]. As a result of this nonlinear harmonic interaction, the gain length, transverse profile, and temporal structure of the harmonics are determined by those of the fundamental. In addition, the power levels of the harmonics are subjected to larger fluctuations than the fundamental, while the relative spectral bandwidth is the same.

Typical power levels of the third harmonic produced in this way can be on the order of 1-2% of the fundamental for large values of the undulator parameter (K) [5,6] but can fall off quite dramatically if K is small (K<~1.5) or if emittance or energy spread effects become dominant. Therefore, small power levels can be expected from nonlinear harmonic generation at 7-8 keV photon energies where K<1.5. No modifications to the beamline are needed to leverage these photons, but attenuation of the fundamental is necessary to isolate the harmonics, which could limit the maximum delivered power.

17.2.5 Harmonic Lasing

Harmonic lasing in FELs, where the collective electron beam and radiation instability of odd harmonics in a planar undulator evolve independently of the fundamental resonant radiation, has

generated much recent interest and potentially offers many benefits over nonlinear harmonic generation [7,8,9]. Some of these benefits include a more intense, stable, and narrow-band radiation pulse. Harmonic lasing can also be a relatively efficient way of extending the photon energy tuning range of a particular FEL beamline.

The performance of harmonic lasing schemes is contingent on the successful suppression of the fundamental radiation. In this way, incoherent energy spread that is associated with the growth of the fundamental does not interrupt linear growth of the target harmonic, allowing it to reach full saturation. A variety of methods have been proposed to suppress the fundamental radiation including, but not limited to: introducing periodic phase shifts between the field and the electron beam such that the fundamental experiences a non-integer 2π phase shift while the desired harmonic experiences an integer 2π shift; periodically filtering the fundamental with a spectral attenuator while allowing the desired harmonic to pass and simultaneously debunching the electron beam in a bypass chicane; using a combination of detuned/retuned undulators such that the desired harmonic is resonant at different harmonic numbers (third, fifth, etc.) for contiguous undulator sections.

These schemes have been explored in the context of LCLS-II using numerical particle simulations with an ideal electron beam, where the slice parameters are specified by the nominal LCLS-II 100 pC electron beam. The results of these simulations are reported in [10]. Initial investigations suggest that both the SXR and HXR beamlines would benefit greatly from these concepts. The high end of the HXR beamline tuning range, for instance, could potentially extend to ~7 keV with an appropriate distribution of phase shifters and spectral attenuators. Performance with lower bunch charges (and lower beam emittances) will likely be better and will be studied.

17.3 Polarization control

The LCLS-II is designed to generate linearly polarized, intense, high-brightness X-ray pulses from planar, variable-gap undulators. While the planar undulator design is well understood and expected to be tunable within tight FEL tolerances, it lacks polarization control, which is of great importance for soft X-ray experiments. The design provides space to add polarization control with APPLE or DELTA type polarizing undulator segments. The polarization control undulator segments will work as so-called “afterburners,” producing right or left circular, elliptically polarized FEL radiation from the micro-bunched electron beam generated by a few of the regular LCLS-II SXU undulator segments. Switching between right and left polarized radiation will be achieved via row position adjustment in the added polarizing undulator segments. The linearly polarized radiation produced by the regular SXU undulator segments during the micro-bunching process will be a small background component, keeping the total degree of polarization slightly below 100 percent. With 12 m of polarizing undulators for the 39 mm SXU period, polarization degrees above 90 percent are expected at millijoule-pulse-energy levels for the 250–1250 eV photon energy range. The pulse-to-pulse fluctuations of the polarization degree should be below

the 1 percent level. Increasing the number of polarizing undulator segments will further enhance both the intensity and the degree of the polarized radiation.

In addition, vertically polarizing undulators (VPU) are being developed at Argonne National Laboratory as part of the LCLS-II R&D program – see Chapter 16. Using a combination of VPU's and the baseline horizontal polarizing undulators, described in Chapter 8, would provide some polarization control over much of the HXR photon energy range where the full undulator length is not necessary for saturation.

17.4 Superconducting Undulators

Superconducting undulators (SCUs) might be installed in place of the permanent magnet undulators (PMU) in the HXU system to significantly increase the undulator magnetic field. Figure 17-1 shows the average X-ray power at 300 kHz and 100 pC per bunch for the PMU (blue) and two different SCU technologies: Nb_3Sn (red) and NbTi (green). The three curves are plotted for a 140-m HXU system (baseline plan). A much shorter SCU can also be installed with only a 77-m system length, still producing up to 5-keV photons (similar to the PMU curve in Figure 17-1) with an undulator length almost two-times shorter than the PMU. The details for the SCU parameters are described in Ref. [11].

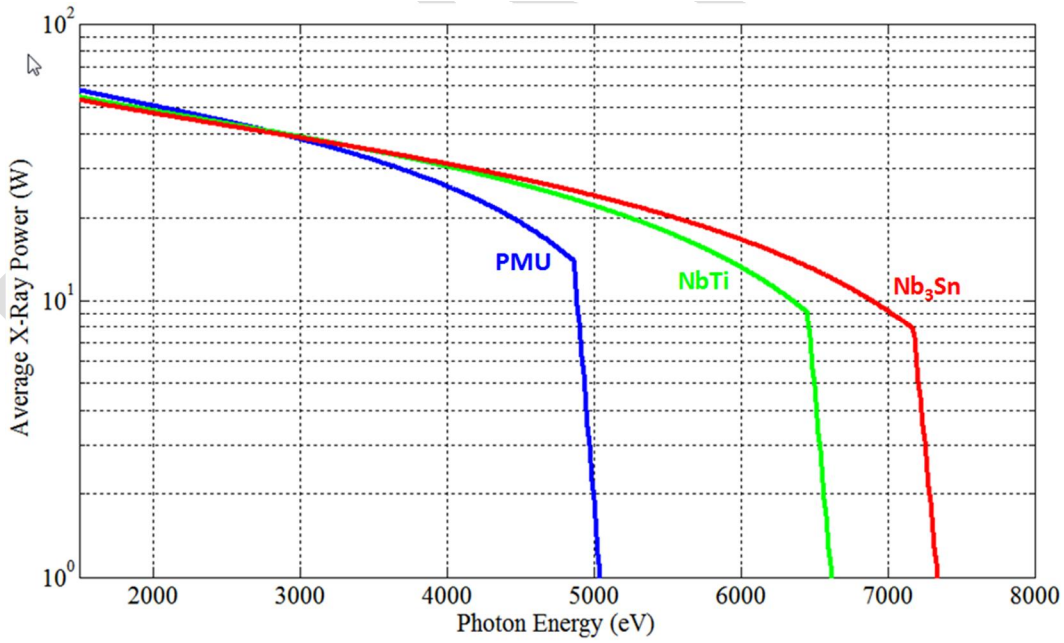

Figure 17-1. Average FEL X-ray power (at 300 kHz and 100 pC per bunch), as a function of photon energy, when driven by the SC-linac for the PMU (blue), NbTi (green), and Nb_3Sn (red) technologies. The undulator periods are 26 mm, 20 mm, and 18 mm, respectively, and the full vacuum aperture is 5 mm (7.3-mm full magnetic gap). Beam parameters are taken at the 100-pC configuration.

17.5 Additional FEL Lines

The LCLS-II baseline project includes two FELs feeding six experimental stations. Operationally, such a configuration is useful because it allows each FEL to supply X-rays to one or two stations while the other stations modify their experiments for another user but presents significant limiations in overall experiment capacity and capability. Of course, the SCRF linac is capable of supplying beam to many additional FELs, and the SLAC site could support this expansion. The original LCLS project, constructed in 2009, anticipated two paths for subsequent expansion:

1) Installation of a second undulator in the existing tunnel.
2) Construction of a new beamline and tunnel on either the north or south sides of the existing Beam Transport Hall (BTH) and tunnel that could support long undulators.

The first path is described in this Final Design Report. The second path was developed to the point of readiness to receive DOE approval for construction (CD-3). In addition, other facilities exist on the SLAC site, such as End Station A (ESA) and End Station B (ESB), which might be modified to support short, soft X-ray FELs. These options are illustrated in Figure 17-2.

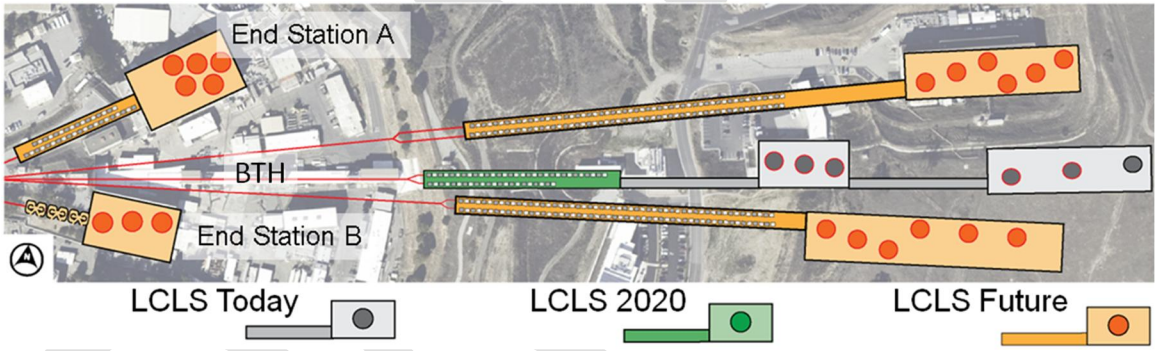

Figure 17-2 Options for future expansion of the LCLS FEL complex. The existing LCLS and the new LCLS-II (referred to here as LCLS-2020 and described in this FDR) are indicated in gray and green. Future expansion possibilities are indicated in orange and include a new tunnel proposed for an earlier version of the LCLS-II to the South of the existing tunnel, as well as a new tunnel to the North as described in Section 18.3.1. In addition, the SLAC facility has existing tunnels to two of the original SLAC End Stations, End Station A to the north of the existing LCLS, and End Station B to the south as described below.

17.5.1 End Stations A and B

The SLAC Beam Switchyard (Figure 17-3) includes several tunnels for transport of electrons and/or positrons to several destinations. Most of these tunnels were put to use in support of SLAC's high energy physics research program. The "A Line" and End Station A are still in operation for R&D supporting LCLS and for high energy physics detector tests.

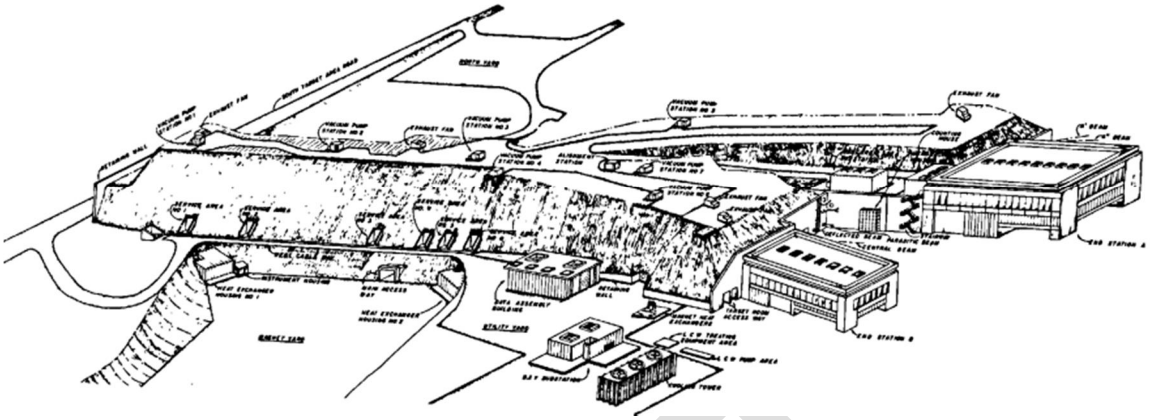

Figure 17-3. Illustration of SLAC Beam Switchyard conventional facilities, excerpted from the SLAC "Blue Book" [12]. ESA is at upper right and ESB at lower right.

Several of these facilities could be repurposed to support new X-ray laser sources. For example, a concept was developed for the "A Line" and End Station A [13,14] as a location for a soft X-ray source with extremely high single-pulse power, using 14 GeV electrons from the LCLS linac. Work is underway on a concept for a high repetition rate soft X-ray source located in the A-Line. It is expected that End Station B could be similarly repurposed to support a high repetition rate soft X-ray FEL and these two facilities could provide a fast, relatively inexpensive path to increasing the breadth of soft X-ray experimental stations driven by LCLS-II.

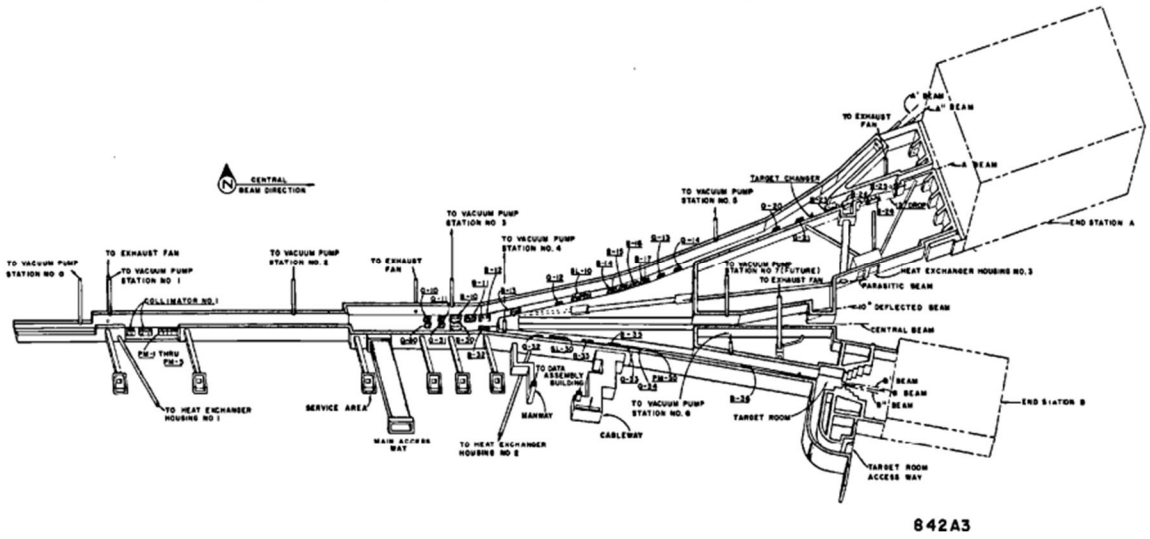

Figure 17-4. Cutaway view of the Beam Switchyard. ESA is at upper right and ESB at lower right while the LCLS tunnel continues straight between the two end stations.

17.5.2 LCLS-II Phase 1

As of September 2013, the LCLS-II Project proposed to build a new tunnel and experiment hall on the south side of the existing facility, as shown in Figure 17-5. This design was

documented in a Preliminary Design Report prepared to support approval of CD-2 for the project. Elements of this project, ranging from the tunnels and experimental facilities to the normal conducting linac in Sectors 11-20, could be resurrected as a follow-on upgrade of the LCLS and LCLS-II facility. The long tunnel of the original LCLS-II project is ideally suited for long undulators that would be heavily tapered and generate intense hard X-ray pulses in a 'TeraWatt' configuration [15].

This earlier LCLS-II Project was designed to provide the following facility enhancements:

- A hard X-ray undulator source (2,000-13,000 eV).
- A soft X-ray undulator source (250-2,000 eV).
- A dedicated, independent electron source for these new undulators, making use of Sectors 10-20 of the SLAC linac. All components of the off-axis injector for source have been fabricated.
- Construction of an annex to the Klystron Gallery to house a laser for the photocathode gun. This annex is now complete and in use as a laser laboratory.
- Modifications to sectors 10-20 of the SLAC linac, primarily to install two bunch compressor chicanes.
- Adaptation of an existing beam transport line to carry electrons past the LCLS linac through the existing Beam Switchyard.
- Expansion of the existing LCLS Beam Transport Hall in the SLAC Research Yard to house new transport lines to the new undulator sources.
- A new shielded enclosure that is roughly 300 meters in length for the two new undulator sources, beam dumps, and X-ray front ends.
- A new experiment hall capable of accommodating at least four experiment stations.
- A high-field physics experiment station served by the soft X-ray undulator.

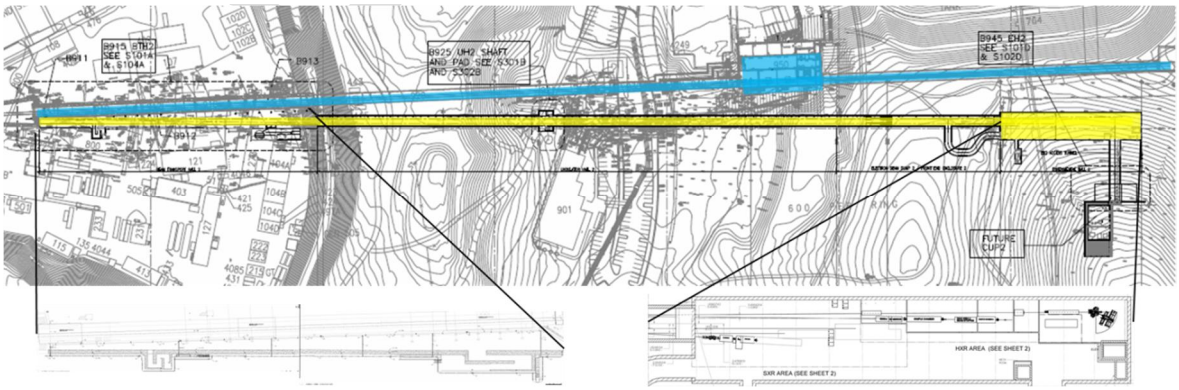

Figure 17-5. Layout of LCLS and an earlier version of LCLS-II. Items tinted blue are existing LCLS facilities. Items tinted yellow are possible new LCLS-II facilities. Blowups of the Beam Transport Hall extension and the new Experiment Hall are shown below the site layout.

Table 17-1 lists sample operating parameters for the LCLS-II Phase 1 SXR and HXR beamlines, illustrating the range of photon energies, beam energies, bunch charges, peak currents, and possible parameter sets for the HXR and SXR. Self-seeding configurations are labeled as SXRSS and HXRSS.

Table 17-1. Sample operating parameters for the LCLS-II Phase 1 SXR and HXR beamlines.

Parameter	"Earlier" LCLS-II Operational Configurations									
Undulator line	SXR	SXR	SXR	SXR	SXR	HXR	HXR	HXR	HXR	HXR
Operational mode	SASE	SASE	SASE	SASE	SXRSS	SASE	SASE	SASE	SASE	HXRSS
Photon energy [keV]	2.0	1.0	0.50	0.25	1.0	13	13	5.0	3.7	8.3
Final electron energy [GeV]	13.5	13.5	10.0	10.0	10.0	13.5	13.5	10.0	10.0	13.5
Laser pulse length (FWHM) [ps]	3.0	3.0	3.0	3.0	3.0	3.0	3.0	3.0	3.0	3.0
Laser iris diameter [mm]	0.6	1.0	1.0	1.2	0.8	0.6	1.0	1.0	1.2	0.6
Bunch charge [pC]	20	150	150	250	150	20	150	150	250	40
Slice emittance ε_n [μm]	0.19	0.41	0.41	0.51	0.41	0.19	0.41	0.41	0.51	0.23
Bunch length (rms) [μm]	0.58	4.3	4.3	11	6.5	0.58	4.3	4.3	14	0.87
Undulator K []	5.4	7.8	9.0	9.9	4.8	2.5	2.5	2.6	3.5	3.3
Undulator period [mm]	63	63	63	63	63	32	32	32	32	32
Undulator gap [mm]	14.6	10.0	8.3	7.2	16.2	10.2	12.2	10.1	7.6	8.1
Magnetic undulator Length [m]	50.1	50.1	50.1	50.1	63.4[§]	67.8	67.8	67.8	67.8	109[§]
$<\beta_{x,y}>$ [m]	20	20	15	15	15	20	20	15	15	20
Peak power [GW]	70	68	70	37	>190	62	34	56	18	580
Pulse duration (FWHM) [fs]	6.7	50	50	125	75	6.7	50	50	167	10
Waste size (FWHM) [μm]	23	32	32	43	38	19	23	26	34	16
Beam divergence. (FWHM)	12-	17-	30-61	49-98	17	2.7-	2.2-	5.0-	5.6-	4.0
Photons per fs [$\times 10^{10}$]	22	43	88	94	119	3.0	1.7	7.0	3.0	43
Pulse intensity [mJ]	0.47	3.4	3.5	4.7	14	0.41	1.7	2.8	2.9	5.8
Photon bandwidth [$\times 10^{-4}$]	16	17	22	22	1.0	10	9.3	13	12	0.5
Peak brightness [$\times 10^{33}$]*	0.29	0.14	0.051	0.016	12	1.5	1.1	0.37	0.11	630

* Ph/(s×mm^2×mrad^2×0.1%BW). Peak brightness occurs at saturation in non-seeded mode.

§ The SXRSS case uses four extra undulator segments that are in the baseline. The HXRSS case assumes 12 additional undulator segments.

† In non-seeded mode, smallest divergence occurs at saturation; post-saturation divergence has been measured up to two times larger.

The undulator sources were designed to produce spatially coherent plane-polarized X-rays by self-amplified spontaneous emission (SASE). They were designed to be compatible with future upgrades, to include full temporal coherence (*i.e.*, seeding) and polarization control. The undulator designs developed for the earlier version of LCLS-II will require some relatively minor modifications to meet the present LCLS-II requirements. Such long sources would provide very intense hard X-ray pulses.

This earlier version (Phase 1) of the LCLS-II Project was designed to reuse Sectors 10-20 of the SLAC linac; therefore the new sources would have been limited to operation at 120 Hz. The conventional facilities for the project were designed to support upgrades permitting the highest possible *peak* X-ray power and brightness to make best use of the SLAC linac capabilities (high energy electrons at low repetition rate). In order to support future increases of peak power to about 1 TW at up to 13 keV, the LCLS-II undulator hall was specified to be 302 m in length — that is, 132 m longer than of LCLS. This length was chosen to provide ample space for future upgrades, such as self-seeding systems. The Phase 1 experimental hall was designed to accommodate up to six experiment stations.

17.6 Longitudinal Coherence

The baseline LCLS-II design will implement self-seeding in the SXR and HXR for X-ray wavelengths between 0.2 and 1.3 keV and from 4 to about 12 keV, as described in Chapter 8. These self-seeding insertions will be similar to those that are being developed for the LCLS. An R&D program will develop self-seeding techniques for the intermediate range between 1.3 keV and 4 keV. Space is available in the SXR and HXR undulators to accommodate this planned upgrade, which is also described in Chapter 8.

In addition, external seeding might be implemented for further photon pulse control in the soft X-ray region, and various alternate approaches could improve the longitudinal coherence by making changes to the undulator sources. These are all discussed below.

17.6.1 Self-seeding upgrades

Both soft and hard X-ray schemes require upgrades for achieving better performance in terms of handling higher repetition rate, operating in a wider energy range, and producing seeds with narrower bandwidths for potentially increasing spectral brightness.

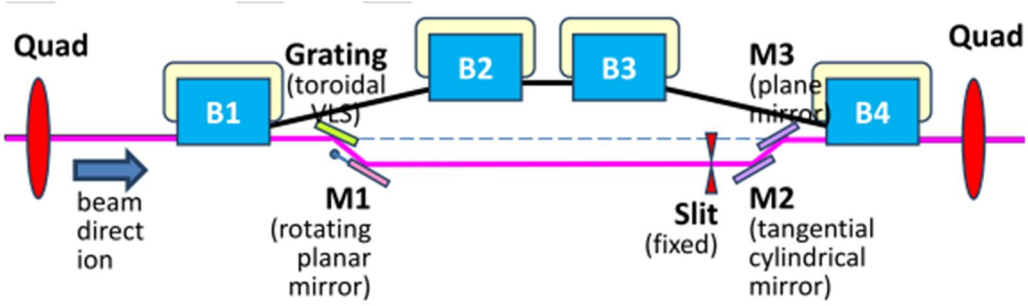

Figure 17-6. Schematic of LCLS Soft X-ray Self-seeding installtion.

17.6.1.1 Self-seeding for the Soft X-ray Undulator

The baseline design based on the LCLS SXRSS system shown in Chapter 8 and illustrated in Figure 17-6 is limited to a resolving power of 5,000, and is not optimized in the overall system throughput due to the mode of operation not being “fixed-focus” when tuning the X-ray energy,

thus producing an enlarged image of the source at the interaction point and reducing the overlap with the electron beam. These characteristics were results of compromises made to minimize design complexities and meet other non-technical requirements. The LCLS SXRSS system has been installed and was commissioned over the last year.

Potential upgrades to the system include higher resolving power in the range of 10,000 to 20,000 or higher, and "fixed-focus" mode of operation to maximize X-ray-electron overlap. The more efficient overlap between the X-rays and electrons is especially important for the high repetition rate operation because of increased concern over the thermal loading on the optics.

Achieving higher resolving power will require a higher line density for the VLS grating and a longer distance to the exit slit. To operate in the "fixed-focus" mode, the grating and the M1 mirror will need to rotate. As such, the sagittal focusing function of the grating must be taken up by either the M2 or the M3 mirror.

17.6.1.2 Self-seeding for the Hard X-ray Undulator

For the hard X-ray undulator, the baseline seeding scheme only covers the energy range of 4 to 12 keV at 120 Hz, using the diamond wake-field monochromator that has been operating on LCLS and is shown in Chapter 8. To extend beyond 12 keV, Si in either (333) or (440) reflection should be considered. These two reflections have a Darwin width comparable to that of diamond (400) at 8 keV, and the lateral shift of the forward Bragg diffracted beam is comparable to that of diamond (400) at 8 keV.

To seed high-rate beams from the SCRF linac, a two-stage diamond wake-field approach [16] will be used to mitigate the concern about sample damage due to the average thermal loading on the small seeding crystal. In such a scheme, the first stage is designed to take less incident power and will pre-seed the beam before the quasi-seeded beam proceeds to the second stage for enhanced seeding performance. In addition, when seeding below 5 keV, the diamond (400) crystal should be replaced by a diamond (111) crystal in the symmetric Bragg geometry to minimize absorption. This would extend the X-ray energy down to slightly above 3 keV.

Between 1 and 3 keV, a grating-based system would be more feasible due to the increasing absorption by either diamond or silicon crystals, although the efficiency of the grating tends to drop off dramatically towards higher X-ray energies, especially when higher resolving power is required to produce transform-limited pulses of equal duration at lower energies. The complete system for the hard X-ray undulator from 1 to 20 keV is shown in Figure 17-7.

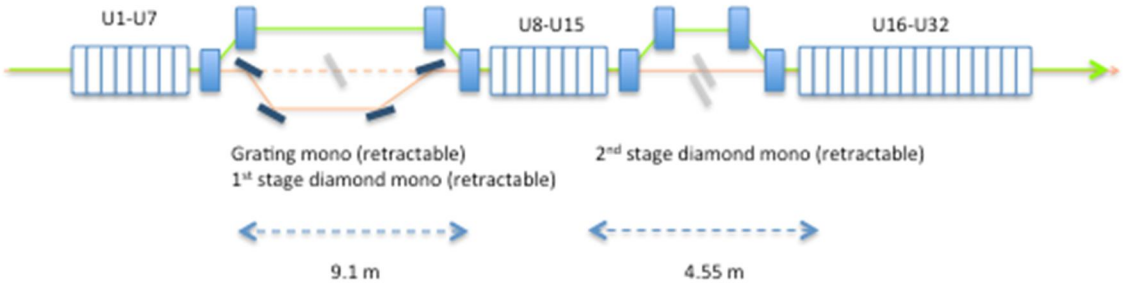

Figure 17-7: Schematics of the complete self-seeding system for the hard X_ray undulator with beams from the CuRF or SCRF linacs, consisting of a two-stage diamond wake-field monochromator seeding section, and a grating monochromator seeding section. For seeding above 3 keV, the grating system is retracted, while both the 1st and 2nd diamond systems are retracted for seeding below 3 keV. Between 3 and 5 keV, both the 1st and 2nd diamond monochromators are in and use (111) crystals, and above 5 keV, only the 2nd diamond monochromator using a (400) crystal is inserted and ererything else retracted.

17.6.2 External seeding

External seedingcould be able to offer many advantages over self-seeding, including better synchronization with an external laser signal for pump-probe experiments, detailed control of the temporal and spectral properties of the output pulses, and shorter total undulator lengths to reach the same saturated power levels. Over the past year, the externally-seeded FERMI FEL at Trieste [17] has produced transversely and longitudinally coherent output pulses at the 10 microjoule energy level down to 5 nm wavelength, utilizing the fresh bunch technique in a two-stage, High-Gain Harmonic Generation (HGHG) configuration. FERMI's near-term goal is to reach the carbon K-edge at 280 eV with its 1.5 GeV electron beam. Reaching even shorter output wavelengths (*e.g.*, 2 nm or shorter) with good longitudinal coherence is very challenging but may be feasible with the brighter and more energetic LCLS-II electron beams. A preliminary design of a two-stage HGHG [18] satisfies the following criteria:

- Nearly transform-limited soft X-ray pulses over an initial range of 250 eV to 600 eV photon energy (5 nm to 2 nm radiation wavelength).
- Length of the entire FEL line of less than 80 m, allowing placement in the existing End-Station A (ESA) tunnel.
- Highly stable output pulse timing, spectral bandwidth, and central FEL wavelength.

Upgrade options might also allow possible HHG seeding (High Harmonic Generation) or reconfiguration to an EEHG design (Echo-Enabled Harmonic Generation) in order to reach output photon energies of 1.2 keV or greater. A design concept using the EEHG scheme is described in Ref. [19]. An ongoing R&D program will make detailed studies of these different approaches to external seeding to understand the detailed implications.

17.6.3 Improved Coherence with iSASE and pSASE

Various techniques can use the undulator system itself to control the spectral properties of a SASE FEL. For example, LCLS scientists recently performed a proof-of-principle experiment on reducing the SASE bandwidth using the "improved SASE", or *iSASE*, scheme [20,21]. The *iSASE* technique should be readily applicable to the LCLS-II.

The *iSASE* technique uses a method that effectively increases the cooperation length. The concept is to introduceadditional slippage (*i.e.*, localized shifts of the electron bunch) in the FEL undulator, which is divided into modules separated by a break, by repeated delays of the electron beam with respect to the radiation field. The shifts are introduced with small magnetic chicanes at the end of each module. A delay of the order of the cooperation length introduces a correlation between the electromagnetic field phases and amplitudes of the spikes, in effect increasing the slippage length and the longitudinal coherence. The most important parameters in the mixing process are the electron delay (δ), the cooperation length (L_c), the number of delays introduced, and the gain in each module.

With a geometrically increasing series of 5 or 6 delays, the bandwidth reduction is about a factor of ten, and for some X-ray wavelengths the resulting pulse is nearly transform-limited. Combing *iSASE* with a tapered undulator, the X-ray peak power and brightness can be significantly increased by one or two order of magnitude.

The main advantages of *iSASE* are as follows:

1. It can operate at any repetition rate, since it does not require external lasers or monochromators which are subject to thermal effects at high repetition rate.
2. It is completely tunable over the entire LCLS-II energy range, even in the 1 to 5 keV range where the efficiency of self-seeding monochromators is not optimal.

Implementing *iSASE* in the LCLS-II, however, requires 5 or 6 small chicanes, with a maximum length of about 60 cm. These might be able to be inserted in the LCLS-II undulator breaks, but a careful assessment is needed to determine whether the break lengths allow this addition.

Another scheme called *pSASE* (purified SASE) has also been proposed to potentially improve the temporal coherence of a standard SASE FEL [22]. The *pSASE* configuration consists of three undulator sections (U1, U2 and U3), with U1 and U3 being resonant at the target FEL wavelength, λ_0, and U2 resonant at a sub-harmonic wavelength, $n\lambda_0$. In U2 the average longitudinal velocity of the electrons is reduced, which effectively increases the FEL slippage length, allowing the radiation fields to communicate phase information over larger portions of the electron beam to improve the FEL temporal coherence. Simulation using realistic beam and undulator parameters shows that this method can be readily used to enhance the temporal coherence and spectral brightness of a SASE FEL by a factor of 5 with U2 tuned to $7\lambda_0$. When combined with tapering, *pSASE* may enhance the spectral brightness by two orders of magnitude compared with standard SASE, as reported in a recent study from the European XFEL [23].

It is worth pointing out that the implementation of *pSASE* at the LCLS-II over a large wavelength range is straightforward and no additional hardware changes are needed. All that is required is reducing the gap of a few (2 to 3) undulator sections where FEL is in the middle of the exponential growth regime to increase the resonant wavelength to $n\lambda_0$. This system will be straightforward to apply on the SXR for photon energies between 0.75 and 1.25 keV, where the variable gap undulators have a large tuning range. It may also be useful for producing narrow-bandwidth radiation at 4 to 5 keV where the monochromators required in the self-seeding schemes have limited efficiency. However, the bandwidth narrowing may be limited to a factor of 3 to 4 since the tuning range for the HXR undulator is only a factor of 5. The full range of applicability for this option is being studied.

17.7 Short Pulse Operation

In its baseline configuration, the LCLS-II generates X-ray pulses with a duration of several tens of fs. While this meets the specifications of many experiments, there is an increasingly growing request for fs-level pulses, especially in the soft X-ray region, for time-resolved studies of atomic and molecular processes. Several options are being considered for short pulse operation.

17.7.1 Low charge

Pulses of several fs duration can, in principle, be obtained with low charge (few pC) bunches. This option has been extensively studied in the FEL scientific literature (e.g. Ref. [24]). Use of a few high-resolution rf BPM's in addition to the LCLS-II bsaeline strip-line BPM's would allow the SCRF linac to operate down to a charge of 3 pC per bunch, making this option technically feasible. However, the considerable beam dynamics challenges associated with this method are still being addressed.

17.7.2 Emittance Spoiler Foil

The next possibility is using an emittance spoiler [25] in the second bunch compressor. This technique is currently in use at LCLS and allows the generation of pulses as short as 4-5 fs. The emittance spoiler consists of a thin metal foil (typically aluminum) with a slot that lets a small fraction of the electrons through. If placed in a high dispersion region, such as the middle of the second bunch compressor, BC2, the foil leaves a short region of the electron bunch unspoiled while suppressing the lasing process in the rest of the bunch. The resulting X-ray FEL pulse is significantly shorter than the duration of the bunch itself. Preliminary calculations indicate that a thin aluminum foil can withstand the thermal load from the MHz-level LCLS-II beam [26]. While this option is the most reliable from the beam-dynamics point of view, it presents several technical challenges that are currently being studied, such as the additional load on the downstream collimators due to a larger beam halo.

17.7.3 Laser Heater Spoiler

An alternative to the emittance spoiler is using a laser heater pulse with a fast rise-time stepped profile. Similar to the emittance spoiler, the aim of this technique is to suppress the lasing process in most of the electron bunch, allowing only a short fraction of the beam to lase. In this case, however, the lasing process is suppressed by selectively increasing the slice energy-spread well beyond the FEL tolerance.

17.7.4 Chirped beam

Finally, as first proposed in [27], a time-energy chirped bunch together with a monochromator configuration could generate X-ray FELs with pulse duration much shorter than the electron bunch length. This chirped beam can be achieved by operating the accelerator and bunch compressor in an over-compression mode. With the planned self-seeding mode at LCLS-II, this scheme could be applied directly to LCLS-II by using the grating-based monochromator. In this configuration, the chirped beam is sent to the first stage FEL undulator to generate wide-bandwidth SASE FELs with expected power of about 100 MW. Then, the SASE signals pass through the grating monochromator, creating a narrow bandwidth seed, and at the same time the electron beam microbunching structure is smeared out after passing through the chicane. The chicane is also used to align the seed with the chirped bunch so that only a fraction of the time-energy chirped electron bunch will be amplified by the seed where the beam energy matches the resonance condition. In this way a fully coherent, short X-ray pulse at the seed wavelength could be generated.

The X-ray seed pulse duration σ_t right after the monochromator with rms bandpass σ_m is given by [28]

$$\sigma_t{}^2 = \frac{\sigma_\omega{}^2 + \sigma_m{}^2}{u^2} + \frac{1}{4\sigma_m{}^2},$$

where $u = \Delta\omega/\Delta t$ is the X-ray frequency chirp and σ_ω is the rms SASE bandwidth. After the second stage amplifier, the final pulse duration σ_{tf} is dominated by the SASE bandwidth,

$$\sigma_{tf} = \frac{\sigma_\omega}{u}.$$

For example, with a typical SASE bandwidth at soft X-ray wavelength about 0.2%, and an electron bunch chirp of 1% in 30 fs (corresponding X-ray chirp of 2%), the final achievable X-ray pulse length would be 3 fs rms. The electron bunch chirp would be the main variable to control the final pulse duration, and superradiance might also help further shorten the duration. Since only a fraction of the bunch is actually used after seeding section, it would be possible to produce a second color X-ray pulse from other fresh part of the bunch. To facilitate this approach, the operational bandwidth downstream of the linac has been specified to be greater than ±1.5%.

17.8 Two-Color Generation

FELs that can deliver two X-ray pulses of different photon energies with a variable delay are among the most recent and exciting developments in X-ray FELs. Two color FELs have a wide

range of applications in time resolved X-ray pump/X-ray probe experiments as well as advanced imaging techniques such as multiple-wavelength anomalous dispersion imaging.

The two color operating modes for LCLS-II have been described in *the LCLS_II Two-Color Operation Physics Requirements Document*, LCLSII-2.1-PR-0106. There are two main schemes that could be implemented with modest modifications to the hardware, involving either a split undulator or a double bunch.

In the split undulator scheme [29], the undulator is divided in two parts tuned to two different photon energies. A magnetic chicane in the middle of the undulator delays the electrons with respect to the X-rays, thus delaying the second X-ray pulse by the same amount. This scheme can operate across the whole spectral range of the two undulators (namely 250 eV to 1200 eV for the soft X-ray undulator and 1 keV to 5 keV for the hard X-ray undulator). A magnetc chicane with a variable delay between 0 and 1 ps can fit in the space of one undulator section (see the LCLS soft-X-ray self-seeding project), minimizing the impact of the two-color mode on the standard FEL operation.

The double bunch scheme [30] relies on the generation of two electron bunches of different energies and with a variable time separation. The two bunches are generated by stacking the cathode laser with a split-and-delay system and radiate independently in one undulator, maximizing the output power of the two-color FEL. The time delay is typically variable between 0 and 100 fs, while the maximum energy separation is limited by chromatic effects to between 1 and 2%.

These schemes are currently operational at LCLS and routinely delivered to user experiments at soft and hard X-ray energies. While there are no conceptual limitations that will prevent them from being applied to LCLS-II, it will likely take time to make them fully operational with the new accelerator systems and, in some cases, modifications will be required such as a new chicane in the SXR.

17.9 Four-Wave Mixing Configuration

A pathway for producing FEL pulses suitable for four-wave mixing (FWM) experiments from a single electron beam was recently proposed [31] and was studied in the context of LCLS-II [31,32]. Those studies used a process of selective amplification employing a strongly chirped electron beam and a tapered undulator to isolate the gain region of a SASE FEL, allowing for a single longitudinally coherent pulse to amplify to saturation [33,34,35]. The taper also serves to suppress gain outside the chirped region, leaving the electron beam capable of producing additional radiation in a downstream FEL process. This energy modulation and undulator taper combination can be repeated in multiple stages to produce the three independent FEL pulses necessary for FWM experiments if a broad tuning range is necessary. Alternatively, a grating and mask can be used to split one of these large bandwidth pulses if two nearby frequencies are sufficient.

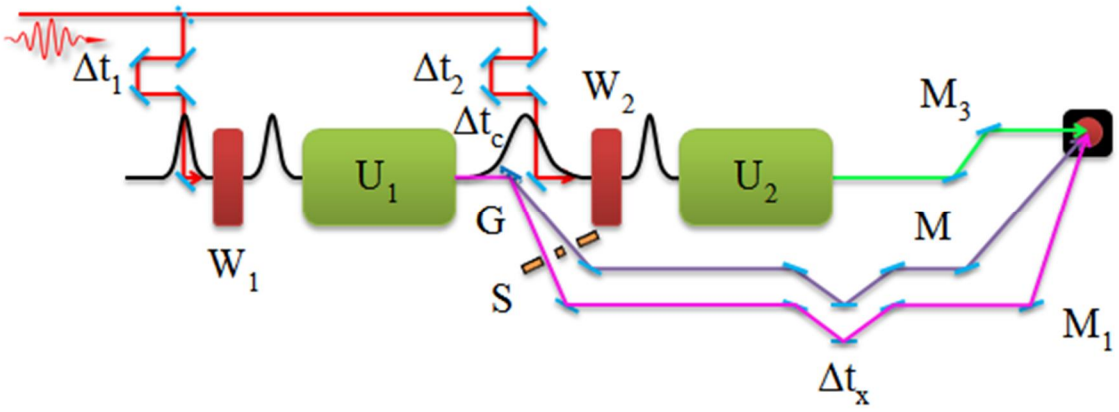

Figure 17-8. A possible beamline for a FWM FEL: W_1 and W_2 are modulators, U_1 and U_2 are undulators, Δt_1 and Δt_2 are seed laser delay stages, Δt_c is the electron beam chicane delay, Δt_x is the X-ray delay line, G is the grating, S is the slit, and $M_{1,2,3}$ are adjustable X-ray mirrors.

There is sufficient room along the SXR undulators beamline to implement this scheme as shown in Figure 17-8. Additional hardware beyond what is included in the baseline, including chicanes, wigglers, a mid-IR laser, and various optical components are required to fulfill the full beamline potential.

17.10 Beyond 1 MHz

The maximum beam rate in the linac is limited by the average beam power on the electron dump. A working limit of 120 kW has been set on each electron dump at the end of each FEL. For example, 300 pC of charge per bunch, 4 GeV, and a 100 kHz bunch rate per FEL results in an average beam power of 120 kW per dump. A reduced bunch charge of 30 pC would allow a 1 MHz bunch rate in each FEL simultaneously. This could be carried to an extreme with 10 pC per bunch and a 3 MHz rate per FEL, or possibly even lower charge levels, but the 10 pC bunch charge has been selected as the present lower limit for operations. However, a bunch rate up to 10 MHz, or perhaps higher, is not excluded as long as the beam power is within practical limits (less than 120 kW). The diagnostic kickers have a fast enough rise and fall (less than 200 ns), and the response time of the machine protection system is fast enough to shut down the beam before damaging components. Note also that for a constant peak current over the electron bunch, the bunch length will need to be reduced linearly with a lower charge. The much shorter bunch may not be well matched to a two-stage HGHG scheme, where a fresh-bunch manipulation may not function well.

17.11 Other Operating Modes

As has been observed with LCLS, it is fully expected that the flexible design of the LCLS-II will enable new operating modes to be developed which will enable the generation of novel X-ray

pulses. While these are not fully defined at this time, further exploration using LCLS will be critical in developing these new concepts. The LCLS-II design has been specified to operate over a broad range of bunch characteristics to ensure future flexibility.

17.12 References

[1] J. Sheppard, et al, "LCLS-I Linac Energy Increase," LCLSII-TN-14-10 (2014).

[2] Z. Huang, et al., *Phys. Rev. E* **62(5)**, 7295 (2000).

[3] Z. Huang, et al., *Nucl. Inst. Meth. Res. Sect. A* **475**, page # (2001).

[4] E. L. Saldin, et al., *Phys. Rev. ST Accel. Beams* **9**, 030702 (1006).

[5] A. Tremaine, et al., *Phys. Rev. Lett.* **88**, 204801 (2002).

[6] D. Ratner, et al., *Phys. Rev. ST Accel. Beams* **14**, 060701 (2011).

[7] B. W. J. McNeil, et al., *Phys. Rev. Lett.* **96**, 084801 (2006).

[8] E. A. Schneidmiller, et al., *Phys. Rev. ST Accel. Beams* **15**, 080702 (2012).

[9] E. A. Schneidmiller, et al., *Nucl. Instr. Met. Phys. Res. Sect. A* **717**, 37 (2013).

[10] G. Marcus, et al., LCLS-II-TN-14-12 (2012).

[11] P. Emma et al, 2014 FEL Conference {add location}.

[12] R. B. Neal, ed., *The Stanford Two-Mile Accelerator*, (1968) W. A. Benjamin Inc.; Library of Congress Catalog Card Number 68-24364; also available online at the SLAC website.

[13] H. Geng, et al., "Optics Design for a Soft X-Ray FEL at the SLAC A-Line," *Proceedings of PAC09*, Vancouver, BC, Canada, WE5RFP043, available at http://www.JACOW.org.

[14] H. Geng, et al., "Design of a Soft X-ray FEL in the SLAC A-Line," *Proceedings of FEL2009*, Liverpool, UK, WSEPC63, available at http://www.JACOW.org.

[15] G. Geloni, V. Kocharyan and E. Saldin, "Scheme for generation of fully coherent, TW power level hard X-ray pulses from baseline undulators at the European XFEL", DESY 10-108 (2010).

[16] G. Geloni, V. Kocharyan, and E. Saldin, "A Cascade Self-seeding Scheme with Wake Monochromator for Narrow-bandwidth X-ray FELs", DESY 10-080 (2010), http://arxiv.org/abs/1006.2045.

[17] E. Allaria, et al., "Highly Coherent and Stable Pulses from the FERMI Seeded Free-electron Laser in the Extreme Ultraviolet," *Nature Photon*. **7**, 913 (2013).

[18] Z. Huang, et al., "An HGHG Seeding option for the LCLS-II SXR," LCLSII-TN-14-13 (2014).

[19] G. Penn, "EEHG Seeding for the LCLS-II," LCLSII-TN-14-12 (2014).

[20] J. Wu, A. Marinelli, C. Pellegrini, "Generation of longitudinally coherent ultra-high power X-ray FEL pulses by phase and amplitude mixing," *Proc. of FEL2012*, Nara, Japan, TUPD07 (2012).

[21] J. Wu, et al., "X-ray spectra and peak power control with iSASE," *Proc. of IPAC2013*, Shanghai, China, WEODB101 (2013).

[22] D. Xiang, Y. Ding, Z. Huang and H. Deng, "Purified self-amplified spontaneous emission free-electron lasers with slippage-boosted filtering," *Phys. Rev. ST Accel. Beams* **16**, 010703 (2013).

[23] S. Serkez, V. Kocharyan, E. Saldin, I. Zagorodnov and G. Geloni, "Purified SASE undulator configuration to enhance the performance of the soft X-ray beamline at the European XFEL," DESY 13-135; see also arXiv:1308.0172.

[24] J. B. Rosenzweig, *NIM-A* **593**, 39–44 (2008).

[25] P. Emma, et al., *Phys. Rev. Lett*. **92**, 074801 (2004).

[26] C. Fields, private communication (2014).

[27] C. B. Schroeder, et al., *J. Opt. Soc. Am. B* **19**, 1782 (2002).

[28] S. Krinsky and Z. Huang, PRSTAB 6, 050702 (2003).

[29] A. A. Lutman, et al., *Phys. Rev. Lett.* **110,**134801 (2013)

[30] A. Marinelli, et al. *Nature Communications*, to be published (2014).

[31] G. Marcus, et al., *Phys. Rev. Lett*. **113**, 024801 (2014).

[32] G. Marcus, et al., in *Proc. 36th Int. Free-Electron Laser Conf.*, Basel, 2014, TUP033.

[33] E. L. Saldin et al., *Phys. Rev. ST Accel. Beams* **9**, 050702 (2006).

[34] L. Giannessi, et al., *Phys. Rev. Lett.* **106**, 144801 (2011).

[35] G. Marcus, et al., *Appl. Phys. Lett.* **101**, 134102 (2012).

Appendix A: LCLS-II Key Parameters

Dec. 15, 2014

Table 1. Electron beam operational parameters at SRF linac end, including rms stability goals.

Electron Beam Parameters	**symbol**	**nominal**	**range**	**units**
Final electron energy (operational)	E_f	**4.0**	2.0-4.14 [a]	GeV
Max. upgrade energy (or if reduced duty factor) [b]	E_{max}	**7**	-	GeV
Electron bunch charge (limited by beam power)	Q_b	**0.10**	0.01-0.3	nC
Max. bunch repetition rate in linac (CW) [c]	f_b	**0.62**	0-0.93	MHz
Average electron current in linac	I_{av}	**0.062**	0-0.3 [d]	mA
Average electron beam power at linac end (limit)	P_{av}	**0.25**	0-1.2 [e]	MW
Norm. rms transverse slice emittance at undulator	$\gamma\varepsilon_{\perp\text{-}s}$	**0.45**	0.2-0.7 [f]	μm
Final peak current (at undulator)	I_{pk}	**1000**	500-1500	A
Final rms bunch length (at undulator)	σ_{zf}	**8.3**	0.6-52	μm
Final estimated useable bunch duration (FWHM)	$\Delta\tau_f/\tau_f$	**50**	-	%
Total magnetic compression (cathode to undulator)	C_T	**85**	25-150	-
Final slice energy spread (rms, with heater)	σ_{Es}	**500**	125-1500	keV
Estimated RMS Beam Stability Goals:				
Relative rms electron energy stability (at und.)	$(\Delta E/E_f)_{rms}$	**< 0.01**	-	%
Relative rms peak current stability (at und.)	$(\Delta I/I_{pk})_{rms}$	**< 5**	-	%
Bunch arrival time stability (rms, at und.)	$(\Delta t_b)_{rms}$	**< 20**	-	fs
Transverse centroid stability (rms, at und., 100 pC)	$\Delta x_{rms}/\sigma_x$	**< 10** [g]	-	%

[a] Upper limit is with all 1.3-GHz RF gradients at 16 MV/m, nominal phasing for 100 pC, and 6% of cavities off.
[b] All transport lines are designed for up to 7 GeV for a linac upgrade or low duty-cycle operations.
[c] BSY dump steals pulses at 20 kHz as a keep alive and to limit the linac beam power to 240 kW.
[d] The average current is limited to 0.1 mA with the present RF amplifiers (0.3 mA with upgrade).
[e] The linac is designed to 1.2 MW of beam power although more FEL lines are needed to operate there.
[f] The transverse emittance varies with approximately the square-root of the bunch charge.
[g] Defined as the rms variation of the position or angle centroid normalized to its rms size.

Table 2. Accelerator, lattice, and compression parameters at nominal bunch charge.

Accelerator Parameters	**symbol**	**nominal**	**range**	**units**
Injector cathode	-	CsTe	-	-
Drive-laser pulse length (FWHM)	τ_{DL}	**33**	20-70	ps
Laser heater-induced energy spread (rms) [a]	σ_E	**5-6**	0-20	keV
RF phase of L1 linac	φ_1	**−21.0**	−30-0	deg
RF phase of L2 linac	φ_2	**−21.0**	−30-0	deg
RF phase of L3 linac	φ_3	**0.0**	−10-10	deg
BC1 R_{56}	$\lvert R_{56\text{-}1}\rvert$	**55**	0-75	mm
BC2 R_{56}	$\lvert R_{56\text{-}2}\rvert$	**37**	0-75	mm
Electron energy at Laser Heater	E_{LH}	**100**	90-120	MeV
Electron energy at BC1	E_{BC1}	**250**	200-300	MeV
Electron energy at BC2	E_{BC2}	**1600**	1400-1800	MeV
Length of full cryomodule with 8 cavities	L_{CM}	**11.99**	-	m
Active length of L0 linac (all cavities)	L_{L0}	**8.30**	-	m
Active length of L1 linac (all 1.3-GHz cavities)	L_{L1}	**16.6**	-	m
Active length of HL linac (all 3.9-GHz cavities)	L_{HL}	**5.54**	-	m
Active length of L2 linac (all cavities)	L_{L2}	**99.6**	-	m
Active length of L3 linac (all cavities)	L_{L3}	**166**	-	m
Bypass line length (RW-wake removes chirp)	L_{byp}	**2200**	-	m
Bypass line bore radius (stainless steel)	r_{byp}	**24.5**	-	mm

[a] Before bunch compression.

Table 3. Radio Frequency (RF) operational parameters, including rms stability goals.

RF Parameters (CW SRF Linac)	**symbol**	**nom. value**	**units**
RF frequency	f_{RF}	**1.3**	GHz
Max. avg. RF CW gradient (powered cavities) [a]	E_{acc}	**16**	MV/m
Max. RF gradient (low duty cycle)	E_{acc}	**18**	MV/m
Active length of 9-cell cavity	L_{cav}	**1.038**	m
Cryomodule length	L_{CM}	**11.919**	m
Installed 1.3 GHz voltage (all cavities at 16 MV/m)	V_{tot}	**4.65**	GV
Fraction unpowered cavities (operational reserves)	-	**6.5**	%
Mean cavity quality factor (unloaded)	Q_0	**> 2.7**	10^{10}
Nominal cavity external quality factor (loaded)	Q_L	**4.1**	10^7
Cavity operating temperature	T_{cryo}	**2.0**	K
No. of 9-cell cavities per cryomodule (1.3 GHz)	N_{cav}	**8**	-
Cavities per power amplifier in all linac sections	-	**1**	-
Total installed cryomodules (1.3 GHz)	N_{CM}	**35**	-
RF power per cavity (average at 100 μA) [b]	P_{cav}	**3.8**	kW
Total number of 3.9-GHz Cavities	-	**16**	-
Max. 3.9-GHz crest voltage (all cavities powered)	V_{39}	**75**	MV
No. installed 8-cavity CMs in L0	N_{CM0}	**1**	-
No. installed 8-cavity CMs in L1	N_{CM1}	**2**	-
No. installed 8-cavity CMs at 3.9-GHz (HL)	N_{CMHL}	**2**	-
No. installed 8-cavity CMs in L2	N_{CM2}	**12**	-
No. installed 8-cavity CMs in L3	N_{CM3}	**20**	-
Estimated RMS Stability Goals:			
RF phase stability (rms, pulse-to-pulse)	$(\Delta\varphi_{RF})_{rms}$	**0.01**	deg
RF amplitude stability (rms, pulse-to-pulse)	$(\Delta V/V_{RF})_{rms}$	**0.01**	%

[a] A round number here, with average gradients slightly less than 16 MV/m (100% duty cycle).
[b] At 0.1 mA maximum average current (ultimately 0.3 mA with an RF upgrade).

Table 4. SXR-Undulator operational parameters.

SXR Undulator Parameters (SASE/SS)	**symbol**	**nom. value**	**units**
Undulator type	-	**Hybrid PM**	-
Gap type	-	**variable**	-
Wiggle plane	-	**horizontal**	-
Full-height of magnetic gap (minimum)	g_m	**7.2**	mm
Undulator period	λ_u	**39**	mm
Undulator parameter (peak, maximum)	K	**5.5**	-
Magnetic field (peak, maximum)	$\|B_y\|$	**1.5**	T
Magnetic length of each und. segment	L_{seg}	**3.40**	m
Length of each break section (BPM, quad, etc)	L_{brk}	**1.0**	m
Total number of segments installed	N_{seg}	**21**	-
Total magnetic und. length	$L_{u,mag}$	**71.3**	m
Total und. beamline length (incl. breaks & chicane)	$L_{u,bl}$	**91.4**	m
Average beta function in undulator	$\langle\beta_{x,y}\rangle$	**16**	m
Monochromator location (after N_1 segments)	N_1	**7**	-
Monochromator length (e^- chicane)	L_{mono}	**< 4**	m
Monochromator resolving power (FWHM)	R_{res}	**5000**	-
Monochromator efficiency (not incl. BW reduction)	M_{eff}	**2**	%

Table 5. HXR-Undulator operational parameters.

HXR Undulator Parameters (SASE/SS)	**symbol**	**nom. value**	**units**
Undulator type	-	**Hybrid PM**	-
Gap type	-	**variable**	-
Wiggle plane	-	**horizontal**	-
Full-height of magnetic gap (minimum)	g_m	**7.2**	mm
Undulator period	λ_u	**26**	mm
Undulator parameter (peak, maximum)	K	**2.4**	-
Magnetic field (peak, maximum)	$\|B_y\|$	**1.0**	T
Magnetic length of each und. segment	L_{seg}	**3.40**	m
Length of each break section (BPM, quad, etc)	L_{brk}	**1.0**	m
Total number of segments installed	N_{seg}	**32**	-
Total magnetic und. length	$L_{u,mag}$	**108**	m
Total und. beamline length (incl. breaks & chicane)	$L_{u,bl}$	**140**	m
Average beta function in undulator	$\langle\beta_{x,y}\rangle$	**16**	m
Monochromator locations (after N_1 & N_2 slots)	N_1, N_2	**7, 15**	-
Monochromator lengths (e^- chicane) × 2	L_{mono}	**< 4** / each	m
Monochromator resolving power (FWHM)	R_{res}	**15000**	-
Monochromator efficiency (not incl. BW reduction)	M_{eff}	**2**	%

Table 6. Baseline SXR FEL (SASE/SS[§]) operational parameters driven by the SC linac, including rms stability goals. Values are for a constant 4-GeV electron energy and 100 pC bunch charge.

SXR FEL Parameters (SASE/SS[§])	**symbol**	$E_{r,min}$	$E_{r,max}$	**units**
Photon energy (tuning range, fund., 4 GeV) [a]	E_r	**0.25**	**1.3**	keV
X-ray pulse length (FWHM)	$\Delta\tau$	**60**	**60**	fs
FEL peak power (fundamental, SASE)	P_{FEL}	**18**	**16**	GW
Photons per pulse (fundamental, SASE)	$N_{ph,SASE}$	**20**	**2.2**	10^{12}
FEL pulse energy (fundamental, SASE)	$E_rN_{ph,SASE}$	**810**	**470**	µJ
Photons per pulse (fund., with PostSat taper)	N_{ph}	**44**	**7.9**	10^{12}
FEL pulse energy (SASE, with PostSat taper)	E_rN_{ph}	**1,800**	**1,600**	µJ
Peak brightness (SASE)	$B_{pk,SASE}$	**9.4**	**47**	$\times10^{30}$ [b]
Peak brightness (Self-Seeded)	$B_{pk,SS}$	**140**	**670**	$\times10^{30}$ [b]
Average brightness (max delivered, SS[§]) [c]	B_{av}	**21,000**	**120,000**	$\times10^{20}$ [b]
Power gain length (3D, magnetic)	L_G	**1.3**	**2.3**	m
FEL parameter (3D, SASE)	ρ_{3D}	**1.4**	**0.80**	10^{-3}
Bandwidth (FWHM, SASE)	BW_{SASE}	**0.77**	**3.5**	eV
Bandwidth (FWHM, SS[§])	BW_{SS}	**0.03**	**0.06**	eV
Photon source size (rms)	σ_s	**23**	**19**	µm
Photon far field divergence (FWHM)	$\Theta_{FWHM,x,\infty}$	**40**	**10**	µrad
Bunch rate in this FEL (20 kHz in BSY dump)	f_{FEL}	**ss[†]-300** [d]	**ss[†]-300** [d]	kHz
Avg. electron beam power in this FEL (max.)	P_e	**120**	**120**	kW
Avg. x-ray beam power <u>delivered</u> in this FEL	P_e	**> 20** [e]	**> 20** [e]	W

[†] single shot
[§] self-seeded

[a] The energy of 0.2 keV is accessed by lowering the electron energy from 4.0 GeV to 3.6 GeV.
[b] Photons per second, per mm^2, per mrad^2, per 0.1% bandwidth.
[c] At up to 300-kHz repetition rate. Rate is adjusted to keep x-ray beam power below 200 W.
[d] A 930-kHz rate is possible, but at a proportionally lower bunch charge to limit the average power.
[e] 20 W when in focus, with a maximum power of 200 W.

Table 7. Baseline HXR FEL (SASE/SS[§]) SC Linac operational parameters, including rms stability goals; the values are for a constant 4-GeV electron energy and 100 pC bunch charge.

HXR FEL (SC-Linac) Parameters (SASE/SS[§])	**symbol**	$E_{r,min}$	$E_{r,max}$	**units**
Photon energy (tuning range, fund.)	E_r	**1.5**	**5.0** [a]	keV
X-ray pulse length (FWHM)	$\Delta\tau$	**60**	**12**	fs
FEL peak power (fundamental, SASE)	P_{FEL}	**18**	**16**	GW
Photons per pulse (fundamental, SASE)	$N_{ph,SASE}$	**20**	**2.2**	10^{12}
FEL pulse energy (fundamental, SASE)	$E_rN_{ph,SASE}$	**420**	**2.4**	μJ
Photons per pulse (fund, with taper)	N_{ph}	**9.5**	**0.049**	10^{12}
FEL pulse energy (fund., with taper)	E_rN_{ph}	**2,300**	**40**	μJ
Peak brightness (SASE)	$B_{pk,SASE}$	**54**	**120**	$\times10^{30}$ [b]
Peak brightness (SS[§])	$B_{pk,SS}$	**800**	**1,800**	$\times10^{30}$ [b]
Average brightness (max delivered, SS[§]) [c]	$B_{av,SASE}$	**150,000**	**65,000**	$\times10^{20}$ [b]
Power gain length (3D, magnetic)	L_G	**1.6**	**5.8**	m
FEL parameter (3D, SASE)	ρ_{3D}	**0.72**	**0.21**	10^{-3}
Bandwidth (FWHM, SASE)	BW_{SASE}	**1.2**	**1.6**	eV
Bandwidth (FWHM, SS[§])	BW_{SS}	**0.075**	**0.25**	eV
Photon source size (rms)	σ_s	**16**	**14**	μm
Photon far field divergence (FWHM)	$\Theta_{FWHM,x,\infty}$	**10**	**3.2**	μrad
Beam rate in this FEL (20 kHz in BSY dump)	f_{FEL}	**ss[†]-300** [d]	**ss[†]-300** [d]	kHz
Avg. electron beam power in this FEL (max.)	P_e	**120**	**120**	kW
Avg. x-ray beam power <u>delivered</u> in this FEL	P_x	**> 20** [e]	**> 20** [e]	W

[†] single shot
[§] self-seeded

[a] Parameters at 5 keV with 100 pC nominal charge gives poor performance – 5-keV values are listed for a 20 pC bunch charge, which has a much smaller transverse emittance.
[b] Photons per second, per mm^2, per mrad^2, per 0.1% bandwidth.
[c] At a 300-kHz repetition rate.
[d] A 0.93-MHz is possible, but at a proportionally lower bunch charge to limit the average power.
[e] 20 W when in focus, with a maximum power of 200 W.

Table 8. Baseline HXR FEL (SASE/SS[§]) Cu Linac operational parameters, including rms stability goals. The values are for 2.5 - 15 GeV electron energy and 130 pC bunch charge.

HXR FEL (Cu-Linac) Parameters (SASE/SS[§])	**symbol**	$E_{r,min}$	$E_{r,max}$	**units**
Photon energy (tuning range, fundamental)	E_r	**1.0**	**25**	keV
X-ray pulse length (FWHM)	$\Delta\tau$	**43**	**43**	fs
FEL peak power (fundamental, SASE)	P_{FEL}	**31-7**	**28**	GW
Photons per pulse (fundamental, SASE)	$N_{ph,SASE}$	**1.5-3.3**	**0.080**	10^{12}
FEL pulse energy (fundamental, SASE)	$E_rN_{ph,SASE}$	**240-500**	**320**	μJ
Photons per pulse (fund., with taper)	N_{ph}	**8.3-21**	**0.30**	10^{12}
FEL pulse energy (fund, with taper)	E_rN_{ph}	**1300-3300**	**1200**	μJ
Peak brightness (SASE)	$B_{pk,SASE}$	**57-90**	**1500**	$\times10^{30}$ *
Peak brightness (SS[§])	$B_{pk,SS}$	**500-880**	**13,000**	$\times10^{30}$ *
Average[+] brightness (max delivered, SS[§])	$B_{av,SASE}$	**26-42**	**680**	$\times10^{20}$ *
Power gain length (3D, magnetic)	L_G	**1.4-2.5**	**5.0**	m
FEL parameter (3D, SASE)	ρ_{3D}	**0.48-0.83**	**0.24**	10^{-3}
Bandwidth (FWHM, SASE)	BW_{SASE}	**0.63-0.89**	**20**	eV
Bandwidth (FWHM, SS[§])	BW_{SS}	**0.05**	**1.2**	eV
Photon source size (rms)	σ_s	**17-19**	**9.8**	μm
Photon far field divergence (FWHM)	$\Theta_{FWHM,x,\infty}$	**12-14**	**1.0**	μrad
Beam rate in this FEL	f_{FEL}	**ss[†]-0.120**	**ss[†]-0.120**	kHz
Avg. electron beam power in this FEL (max.)	P_e	**0.5**	**0.3**	kW
Avg. x-ray beam power <u>delivered</u> in this FEL	P_x	**0.05-0.35**	**0.18**	W
Polarization purity (linear horizontal)	$\langle P \rangle$	**100**	**100**	%

* photons per second, per mm^2, per mrad^2, per 0.1% bandwidth

[†] single shot

[§] self-seeded